Bond Activation and Catalysis by Nontrigonal Tricoordinate and Tetracoordinate Phosphorus Compounds

by

Yi-Chun Lin

M.Sc., Chemistry, 2006
National Tsing Hua University

Submitted to the Department of Chemistry
in Partial Fulfillment of the Requirements for the Degree of

DOCTOR OF PHILOSOPHY
IN INORGANIC CHEMISTRY

at the

MASSACHUSETTS INSTITUTE OF TECHNOLOGY

September 2017

Signature redacted

Signature of author__ _____
Department of Chemistry
August 16th, 2017

Signature redacted

Certified by ____ _____
Alexander Radosevich
Professor of Chemistry
Thesis Supervisor

Signature redacted

Accepted by _____ _____
Robert W. Field
Haslam and Dewey Professor of Chemistry
Chairman, Departmental Committee on Graduate Students

This doctoral thesis has been examined by a Committee of the Department of Chemistry as follows:

Signature redacted

Professor Christopher C. Cummins: ___ _____
Chairman

Signature redacted

Professor Alexander T. Radosevich: _ _____
Thesis Advisor

Signature redacted

Professor Mircea Dincă: __ _____
Department of Chemistry

Bond Activation and Catalysis by Nontrigonal Tricoordinate and Tetracoordinate Phosphorus Compounds

by

Yi-Chun Lin

Submitted to the Department of Chemistry in Partial Fulfillment of the Requirements for the Degree of Doctor of Philosophy in Chemistry

ABSTRACT

Molecular distortion has a profound impact on the electronic structure and reactivity of molecules. This dissertation describes studies on E-H bond activation and catalytic reactivity of σ^3- and σ^4-phosphorus compounds with distorted nontrigonal structures. Specifically, a rare example of N-H oxidative addition to a planar, C_{2v}-symmetric P(III) center is described in Chapter 2. The kinetics and computational studies implicate a noncanonical, phosphorus-based electrophilic pathway for this transformation. As detailed in Chapter 3, a C_s-symmetric phosphorous triamide and its P–N cooperative reactivity are presented. B-H activation and catalytic imine hydroboration are achieved via the combination of the electrophilic phosphorus center and the basic anilide ligand moiety of this C_s-symmetric phosphorus compound. Finally, Chapter 4 extends the study of distorted phosphorus compounds to σ^4-phosphorus molecules. Iminophosphoranes bearing constrained ligand platforms are synthesized and their distortion-induced B-H, B-O and Si-H bond activation reactivity are presented. This research provides insight into the influence of molecular symmetry on the reactivity of σ^3- and σ^4-phosphorus compounds and represents an initial step toward the discovery of new chemistry in other distorted phosphorus molecules.

Thesis Supervisor: Alexander T. Radosevich
Title: Associate Professor of Chemistry

Acknowledgements

I never expected that my life as a graduate student would be completed here when I first came to the United States, but now I have arrived at the end of this fascinating journey after so many challenges and difficulties. I am so grateful to all the people who helped me along the way and I could never do this without their help.

I can never thank Professor Alex Radosevich enough. Alex, thank you for reintroducing chemistry to me with your extraordinarily broad knowledge and guiding my research with the creative ideas. Thank you for always been supportive and patient, and willing to tolerating and encouraging me when I was at my low points in life. I have learned a tremendous amount of knowledge in both science and life through the interactions with you and I would bring it forward to my next step. I would also like to thank Professor Cummins and Professor Dinca for their valuable advice and suggestions on my research and thesis.

I was blessed to be in the Radosevich group and had the pleasure to work with all members of the group. Kyle Reichl, Nicole Dunn, Wei Zhao, Eric Miller, Ajay Sathe, Shi Liu, Ryan Byrne and Rixin Wang, we learned a lot together and did so many unforgettable and stupid things together during those early days at Penn State. Samantha Damiano, Charlie Lai, Nick Fastuca and Allen Pistner, thank you for bringing so much laugh into the lab. Jared Mattos, Trevor Nykaza and Tyler Harrison, we did an incredible job moving the lab to here and I want to thank you for helping me much here in Boston. Avipsa Ghosh, Ayan Maity, Greg Cleveland, Connor Gilhula, Hye Won Moon and Akira Tanushi, knowing you is one of the best things from the lab relocation, and I will miss all those smart and not-so-smart ideas we generated together. Wishing you all the best in your future endeavors.

Finally, I would like to give my thanks to my family. Mom and dad, thank you for all the supports and encouragements. My little brother, thanks for taking care of mom and dad when I was away. Pin-Hua, thank you for always being there for me no matter what. This thesis never would have happened without your support.

Yi-Chun

August 22, 2017

Table of Contents

List of Figures

List of Tables

Chapter One. Geometrical Distortion of σ^3-Phosphorus and σ^4-Phosphorus Molecules as a Route to Non-canonical Reactivity

Chapter One

Geometrical Distortion of σ^3-Phosphorus and σ^4-Phosphorus Molecules as a Route to Non-canonical Reactivity

This dissertation presents investigations on geometrically deformed phosphorus molecules and their unique reactivity in stoichiometric and catalytic transformations. Organophosphorus molecules, especially tricoordinate phosphorus compounds, have long been known for their roles as synthetic reagents in chemical synthesis and ligands in organometallic chemistry. The well-known reactivity of tricoordinate organophosphorus molecules results predominately from the Lewis basic nature of the phosphorus lone pair, giving rise to nucleophilic applications. However, geometric distortion of organophosphorus molecules away from local threefold pseudosymmetry reconstructs their orbital diagram and unleashes their potential for non-canonical phosphorus-mediated transformations. This dissertation discusses the structural distortions of several tricoordinate and tetracoordinate organophosphorus molecules and their resulting non-traditional chemical behaviors, in both biphilic reactivity and E-H bond activations. Chapter 1 provides an overview of how geometrical modifications impact the bonding and reactivity of molecules, with several examples of these influences in organophosphorus chemistry.

1.1 The Influence of Geometrical Distortion on Molecular Electronic Structure and Chemical Behavior

Discovery of unprecedented reactivity is a major thrust that drives the understanding of chemistry forward. The reactivity of a molecule in a particular transformation can be controlled by a range of external variables, but the electronic structure of a molecule is the most crucial determinant that shapes how it interacts with other molecules.[1] Whereas electronic energy has been frequently invoked to rationalize ground state (equilibrium) molecular geometry,[2] the deliberate perturbation of molecular geometry distortion[3] as a means to access desired electronic structure (and consequently reactivity) is comparably less investigated and practiced.

Molecular distortion and the resulting change in molecular symmetry have profound consequences upon the energy level, shape and localization of molecular orbitals, and this phenomenon can be exemplified by even the simplest molecules. The imaginary molecule H_4 serves as an illustrative example,[4] where three possible molecular geometries can be considered (**Figure 1.1**): linear ($D_{\infty h}$), square (D_{4h}) and tetrahedral (T_d). The square planar H_4 molecule can be considered a geometric distortion from the linear H_4 molecule. Similarly, the tetrahedral H_4 molecule can be imagined as the result of the flexing of the square planar H_4 structure. The significant change in the electronic structure of H_4 upon distortion from linear to tetrahedral geometry is demonstrated by qualitative molecular orbital analysis (**Figure 1.1**). During the distortion from linear to square planar geometry, the $1\sigma_u$ and two σ_g MOs of the original $D_{\infty h}$ molecule approach each other in energy and eventually become the degenerate e_u MOs in the D_{4h} molecule.

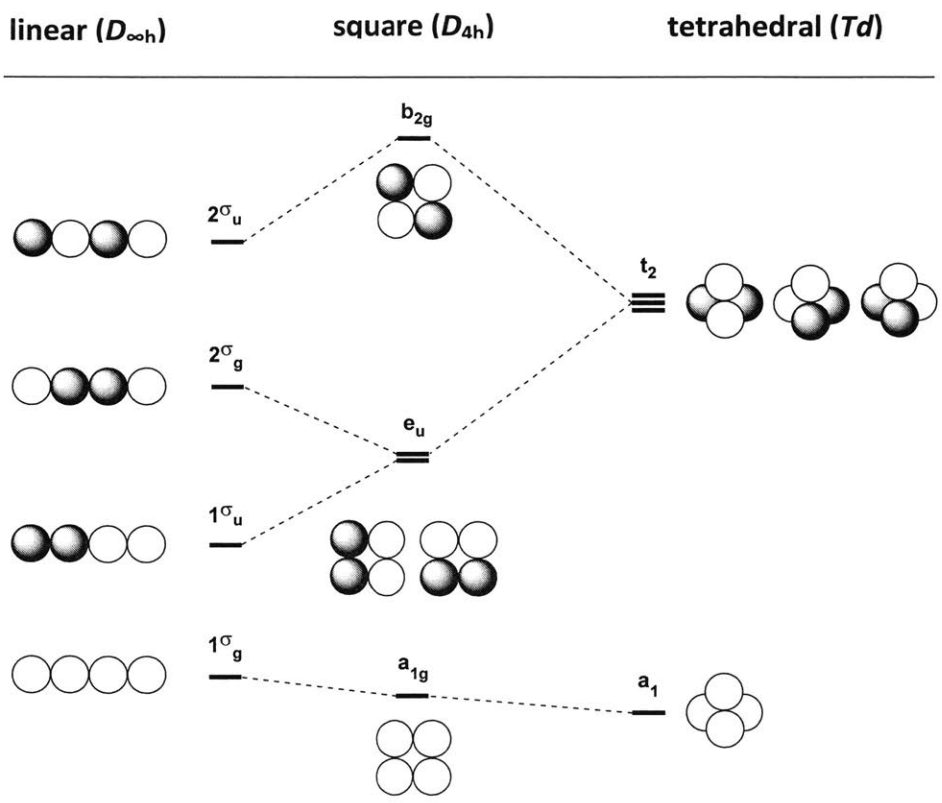

Figure 1.1. Qualitative MO correlation diagram for linear and square planar H4 molecule.

While the a_{1g} MO of D_{4h} molecule is only slightly stabilized due to the in-phase interaction of terminal hydrogen *s* orbitals, the transition from $D_{\infty h}$ $1\sigma_u$ to D_{4h} e_u rises significantly in energy level because of the out-of-phase interaction of terminal hydrogen *s* orbitals. Based on this qualitative MO analysis, a neutral H_4 molecule which contains four valence electrons would have a rising HOMO and therefore suffer a loss in stability during the linear to square planar distortion. With the same concept, HOMO (e_u) orbitals of neutral square planar H_4 transform into the high energy t_2 orbitals of tetrahedral H_4 and result in an even higher HOMO amid the D_{4h}-T_d distortion. Taking into account the strong Jahn-Teller effect in the t_2 orbitals, distortion of a neutral H_4 molecule to

tetrahedral geometry would transform the molecule to a more reactive species with better electron affinity and lower ionization energy.

The impact of geometry distortion demonstrated by the imaginary H_4 molecule can also be witnessed in real and more elaborate molecules. For instance, the molecular orbitals of a typical AH_3 molecule are constructed from the *s* orbitals of the central A atom and three peripheral hydrogens and *p* orbitals of the A atom. Due to the directional nature of *p* orbitals, molecular geometry exerts even more influence on the resulting AH_3 molecular orbitals (**Figure 1.2**).[5] With eight valence electrons, PH_3 is a pyramidal (C_{3v}) compound and has $2a_1$ and $3a_1$ orbitals as its HOMO and LUMO. Upon distortion from its original pyramidal to planar (D_{3h}) geometry, PH_3 gradually loses bonding interaction in its HOMO $2a_1$ orbital and becomes less stable as the hydrogen atomic *s* orbitals move into the central nodal surface of the orbital. On the other hand, the original C_{3v} LUMO $3a_1$ orbital would be stabilized and become more accessible due to the decreasing AO antibonding interactions. Necessarily, PH_3 undergoes a HOMO-LUMO energy gap contraction after the transition from pyramidal to planar geometry and affords better nucleophilicity and electrophilicity at the same time. Further PH_3 deformation from the planar geometry would likely make the compound even more reactive. Considering the desymmetrization from planar to T-shaped (C_{2v}) geometry, the original $1a_2$" HOMO transforms into the $1b_1$ orbital with no stabilization change because no interaction exists between phosphorus and hydrogens in both orbitals. In contrast, the original $2a_1$' LUMO is gradually stabilized and eventually turns into the $3a_1$ orbital due to the bonding interaction between two basal hydrogens and axial hydrogen. Therefore, the resulting T-shaped PH_3 molecule has an even more energetically accessible LUMO than D_{3h} PH_3

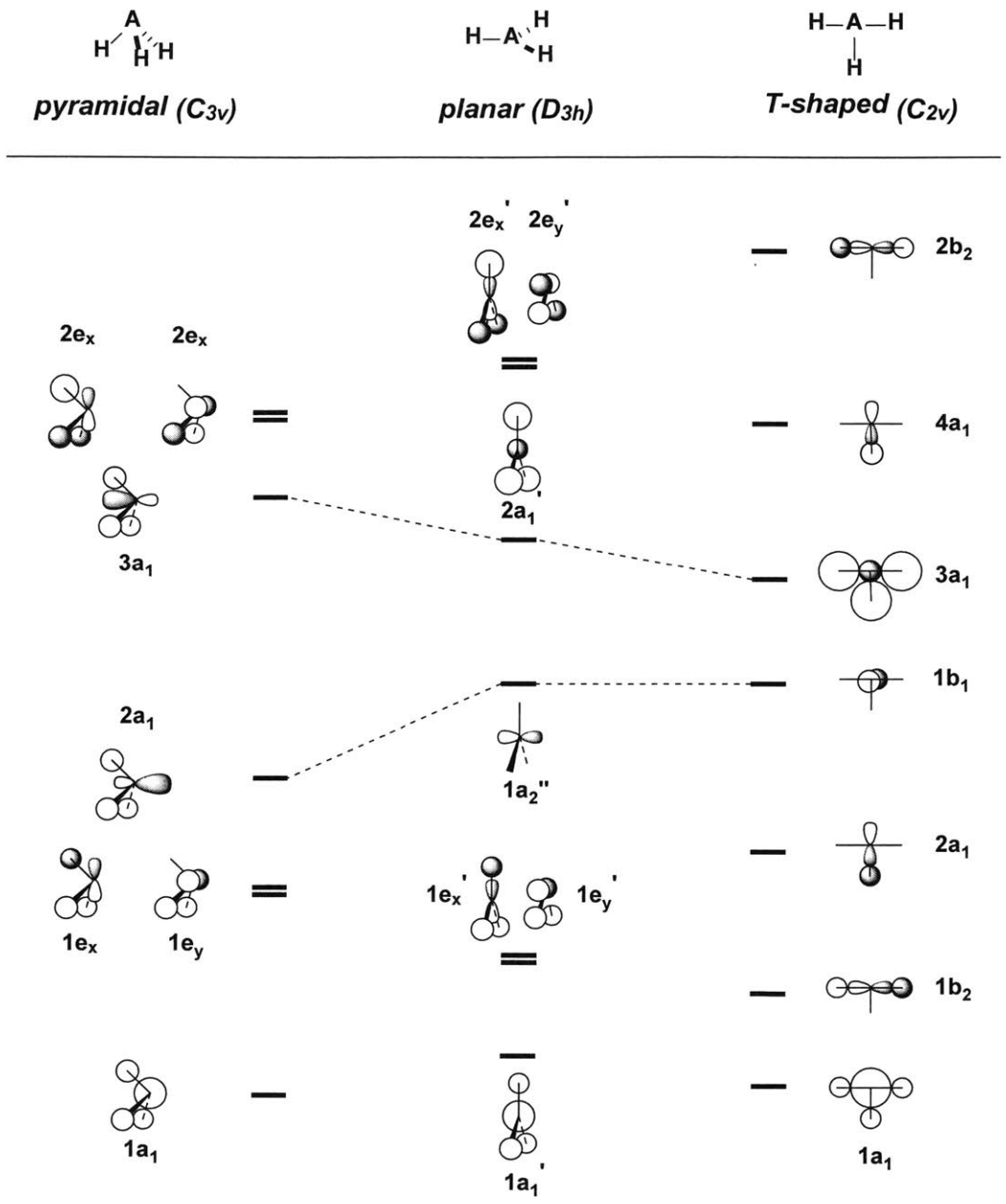

Figure 1.2. Qualitative MO correlation diagram for pyramidal, planar and T-shaped AH_3 molecules.[5]

after distortion and may endow the phosphine compound with noncanonical electrophilic reactivity. The geometry induced rearrangement of AH_3 molecular orbitals also explains the preference of planar geometry for species which contain less than seven valence

electrons in the ground state, such as BH_3 or CH_3^+. In contrast to PH_3, HOMO-LUMO energy gap contraction happens when these molecules distort their geometry from their planar structure to pyramidal geometry.

Molecules with a central atom permitting various coordination numbers can be more versatile in their molecular geometries and thus offer even more possibilities to access unusual electronic structures and reactivity. Depending on the valence electron count of the molecule, tetracoordinate AB_4 molecules can adopt a variety of geometries including tetrahedral (T_d), planar (D_{4h}) and C_{2v} geometries. Similar correlations between molecular geometry and electronic structure of tetracoordinate AB_4 molecules can be demonstrated again with the qualitative MO diagram (**Figure 1.3**).[6] Consider again a molecule with an eight valence electron count, PF_4^+ for example, LUMO stabilization and HOMO destabilization occur along the distortion from tetrahedral to planar to C_{2v} geometry because of the movement of ligands into the central nodal surface. Along with the geometrical versatility, the instability imposed by this mode of frontier orbital energy level contraction makes the AB_4 molecules valuable in the discovery of new reactivity.

In concert with the orbital considerations above, one might also consider the enthalpic impact of molecular distortions. Necessarily, the deviation from equilibrium geometry for a molecule results in an increase in overall energy that can be described as strain. Targeted release of this strain energy can serve as a driving force to enable otherwise nontypical reactions.[1] Such an approach is commonly utilized in a variety of synthetic procedures, as can be exemplified in ring-opening reactions of cyclopropanes,[7] epoxides,[8] aziridines,[9] including ring-opening metathesis polymerization.[10]

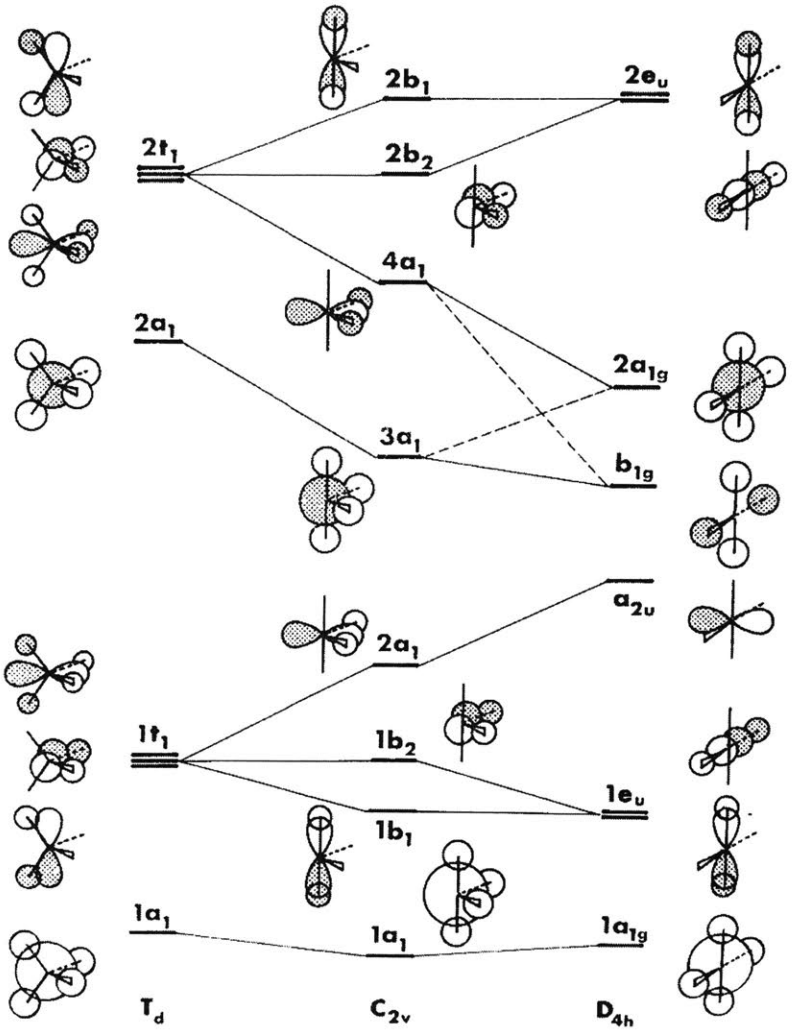

Figure 1.3. Qualitative MO correlation diagram for tetrahedral (T_d), C_{2v} and planar (D_{4h}) AB_4 molecules. Reproduced with permission from *J. Am. Chem. Soc.* **1978**, *100*, 2340.

The foregoing 'ground state destabilization' notion for altering reaction thermodynamics has a kinetic corollary. By enforcing a structural and energetic similarity between reactant and transition state, the required energy input for structural reorganization from starting species to transition state would be minimized, thereby speeding reactivity. It has been postulated that certain enzymatic catalysts operate in this

fashion, in which the supporting protein structures distort active metal centers into reactive "entatic states" and facilitate the enzymatic transformations.[11] Several theoretical and experimental investigations of similar strategies can also be found in organic and main-group chemistry, including the reactivity studies of the distorted alkynes[12] and phosphorus compounds.[13]

As presented above, geometric deformation of a substrate, reagent or catalyst can result in drastic changes in reactivity through frontier orbital rearrangement, structural strain imposition or reorganization energy minimization. It is a motivating hypothesis within the Radosevich laboratory that these considerations are underutilized as design principles in main group reactivity and catalysis. Organophosphorus compounds, for instance, are widely employed in synthesis but are limited in the ways that they are used. With the powerful influence of geometric distortion on AB_3 and AB_4 electronic structure in mind, we aimed to discover novel reactivity of distorted σ^3-phosphorus and σ^4-phosphorus molecules by designing new deformed structures. In doing so, we have also revisited known molecules to unleash their unrealized potential (**Figure 2.4**).

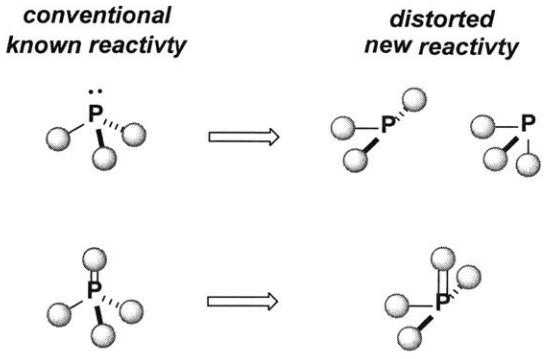

Figure 1.4. Molecular distortion of σ^3-phosphorus and σ^4-phosphorus molecules.

1.2 Geometry of Traditional σ^3-Phosphorus and σ^4-Phosphorus Molecules and Their Reactivity

The purpose of this section is to address the geometry and reactivity of traditional σ^3-phosphorus and σ^4-phosphorus molecules and use the information to discuss the potential reactivity changes of distorted phosphorus molecules. Traditional phosphines are tricoordinate molecules with pyramidal structure and a phosphorus-based lone pair. The lone pair is stereochemically active, pointing away from the three ligands of the pyramidal phosphines. The unhindered environment, along with the relatively large size and low electronegativity of the phosphorus atom, makes the lone pair easily susceptible to nucleophilic interaction with electrophiles. By consequence, the reactivity of pyramidal σ^3-phosphorus molecules results overwhelmingly from the nucleophilicity of this lone pair. In addition, phosphines are easily oxidized to the P(V) oxidation state and produce robust P=O bonds. The strong P=O bond makes phosphines capable reagents for mediating deoxygenative transformations.[14]

Because of their nucleophilic and oxophilic nature, phosphines are useful reagents in synthetic chemistry for constructing and modifying organic molecules. For instance, phosphines are used to catalyze the coupling of an activated alkene and an aldehyde in the Morita-Baylis-Hillman, proceeding via initial 1,4-nucleophilic addition of the phosphine to the conjugated alkene. [15] In stoichiometric phosphine-mediated transformations, such as Wittig,[16] Mitsunobu[17] and Appel[18] reactions, the nucleophilic interaction of the phosphine reagent and an electrophilic substrate generate a

phosphonium intermediate, which then further reacts through P=O elimination to afford the observed products.

In addition to their direct participation in chemical transformations, phosphines are also used as ancillary ligands in organometallic chemistry.[19] With the combination of their electron-donating nature, versatile substitution patterns and available π-accepting orbitals, phosphines make ideal ligands for transition metals and play a crucial role in catalysis. Furthermore, phosphines exhibit much a higher inversion barrier (30–40 kcal/mol) [20] than their nitrogen congeners (5-10 kcal/mol) [21] due to the lower electronegativity of the phosphorus atom, and thus can be prepared as P-stereogenic ligands for stereoselective metal-based catalysis such as asymmetric hydrogenation.[22]

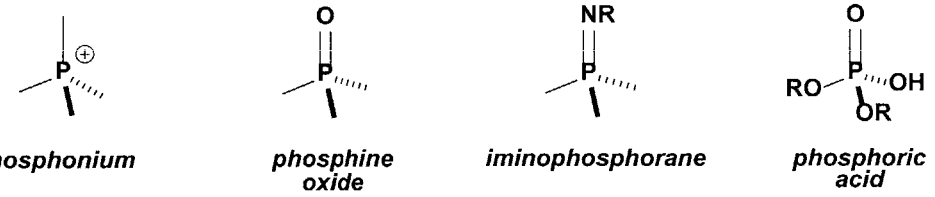

Figure 1.5. Tetracoordinate phosphorus compounds with traditional pseudo-tetrahedral geometry.

Tetracoordinate phosphorus compounds (**Figure 1.5**) are traditionally most stable in pseudo-tetrahedral geometry as predicted by VSEPR and AB_4 qualitative MO analysis. Without the nucleophilic lone pair on the phosphorus atom, σ^4-phosphorus compounds such as iminophosphoranes are generally less reactive and less frequently utilized in synthetic chemistry than σ^3-phosphorus compounds. Iminophosphoranes are σ^4-phosphorus molecules with double bonded nitrogen on the phosphorus atom. Without the lone pair, iminophosphoranes also have relatively unreactive phosphorus centers but can

still be useful reagents or precursors in the synthesis of amines,[23] amides[24] and heterocyclic compounds.[25] In particular, iminophosphoranes can be used in the aza-Wittig reaction to convert carbonyl compounds to imine molecules by utilizing the oxophilic nature of phosphorus atom.[26] The combination of the strong Lewis basic P=N nitrogen and low Lewis acidic phosphorus also makes iminophosphorane an ideal structural moiety for organic superbases and useful in Lewis-base-catalyzed transformations.[27] On the other hand, chiral phosphoric acids with chiral BINOL substituents are another example of σ^4-phosphorus molecules that have recently drawn attention for their applications in acid-catalyzed stereoselective transformations.[28]

1.3 Unusual Reactivity of Geometrically Constrained Phosphorus Molecules

As discussed above, the reactivity of σ^3-phosphorus compounds is mostly described by the nucleophilicity of their P-based lone pairs, and the reactivity of σ^4-phosphorus molecules usually arises from their P-substituents instead of the phosphorus center. However, several examples of distortion-induced nonconventional σ^3- and σ^4-phosphorus-based reactivity can be found in the literature and may provide information for designing new phosphorus compounds with novel reactivity.

Tris(dialkylamino)phosphine molecules exhibit unusual nontrigonal geometries as compared to other pyramidal σ^3-phosphorus compounds. The simple tris(dialkylamino)phosphine molecule $P(NMe_2)_3$ adopts a ground state C_s molecular symmetry due to the repulsions between N and P lone pairs and other unknown

intramolecular electronic interactions.[29] Further geometric deviation in the structures of other $P(NR_2)_3$ compounds give molecules of unusual reactivity. For instance, intramolecular N-H oxidative addition reactivity is observed by Richman and Atkins during their studies of cyclam derived phosphorus compounds (**Figure 1.6**).[30] Caged phosphorus compounds with small ring structures, such as compound **1.1a**, generated only σ^5-hydridophosphorane product **1.2a**. By contrast, larger ring analogues from **1.1c** prefer the tricoordinate structure **1.3c**. An explanation for this observation is that the undetectable phosphine intermediate **1.3a** is unstable due to the geometry deformation enforced by the small bicyclic ligand. With the inherent proximity of the phosphorus atom and the pendant N-H group, the phosphine intermediate is quickly intercepted by the pendant N-H through a non-nucleophilic mechanism and gives the formal intramolecular N-H oxidative addition product. With the expansion of the phosphabicyclic ring and the relieved molecular distortion, larger bicyclic phosphine products such as **1.3 b** and **1.3c** lose their intramolecular phosphorus-based N-H activation reactivity and thus can be observed as the P(III) isomeric form.

Along these same lines of reasoning, bicyclic O,N,O-phosphine **1.5** (**Figure 1.7**) was studied. Here, Wolf[31] and Denney[32] observed a P-hydridophosphorane compound **1.6** resulted from the N-H oxidative addition of Me_2NH to the phosphorus atom when diethanolamine **1.4** was mixed with $P(NMe_2)_3$.. Upon heating, the phosphorane **1.6** undergoes N-H reductive elimination and converts back to phosphorus compound **1.5**. By virtue of the apparent intermolecular N-H oxidative addition, O,N,O-phosphine **1.5** is presumably more reactive than the N,N,N-phosphine **1.1** in a similar distorted geometry.

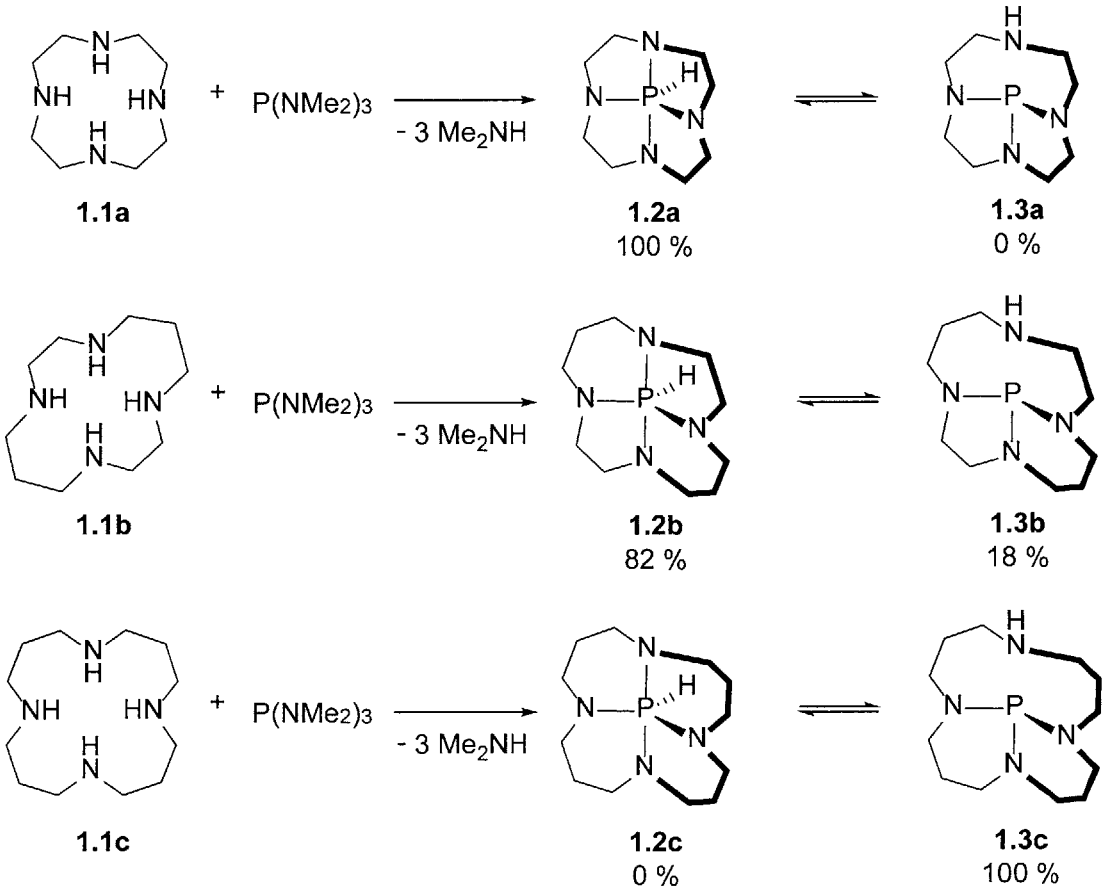

Figure 1.6. Synthesis of the cage tetra-aza-phosphorus compounds and the oberved P(III)-P(V) equilibrium.

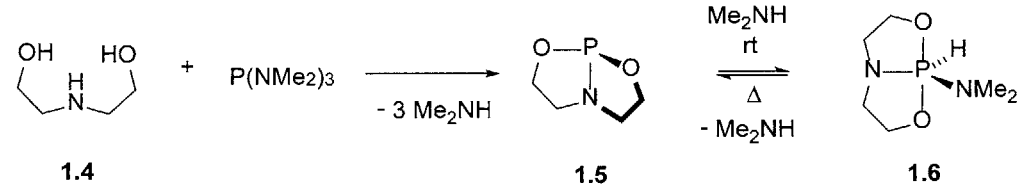

Figure 1.7. Synthesis of bicyclic O,N,O-phosphine **1.5** and its intermolecular N-H oxidative addition reactivity.

Bicyclic O,N,O-phosphine **1.5** is also reactive in oxidative addition of alcohol O-H bonds (**Figure 1.8**) and the resulting phosphorane product can be observed with ^{31}P NMR spectroscopy.[31a] Furthermore, a product equilibrium of the P-hydridophosphorane and a ring-opened species was observed when using phenol as the substrate alcohol in this transformation, indicating the mechanism involves an initial addition of nucleophilic –OH into the phosphorus center of **1.5** and a subsequent P(III)-P(V) tautomerization to afford the phosphorane product (**Figure 1.9**). In addition to O-H bonds, compound **1.5** also reacts toward a variety of nonpolar bonds including O-S and S-S and gives the formal oxidative addition products (**Figure 1.10**).[32] With a similar strained chelating structure, benzannulated O,N,O-phosphabicyclic compound **1.11** also shows intermolecular oxidative addition reactivity toward carboxylic O-H bonds (**Figure 1.11**), although the resulting P-hydridophosphorane **1.12** and ring-opened P(III) product **1.13** are fleeting intermediates that ultimately decompose to final product **1.15**.[33]

As a further an indication of the importance of ring size on reactivity at phosphorus, O,N,O-phosphabicyclic compound **1.17** – which has an expanded ring and

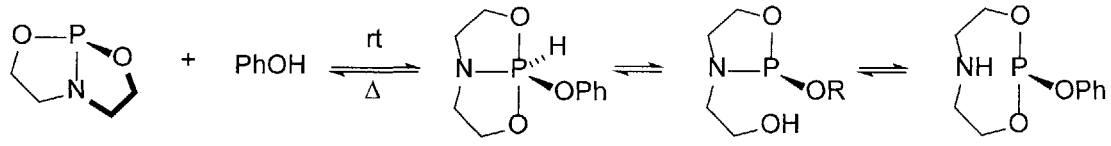

Figure 1.9. Reversible O-H oxidative addition of **1.5** toward PhOH and the product P(III)-P(V) equilibrium.

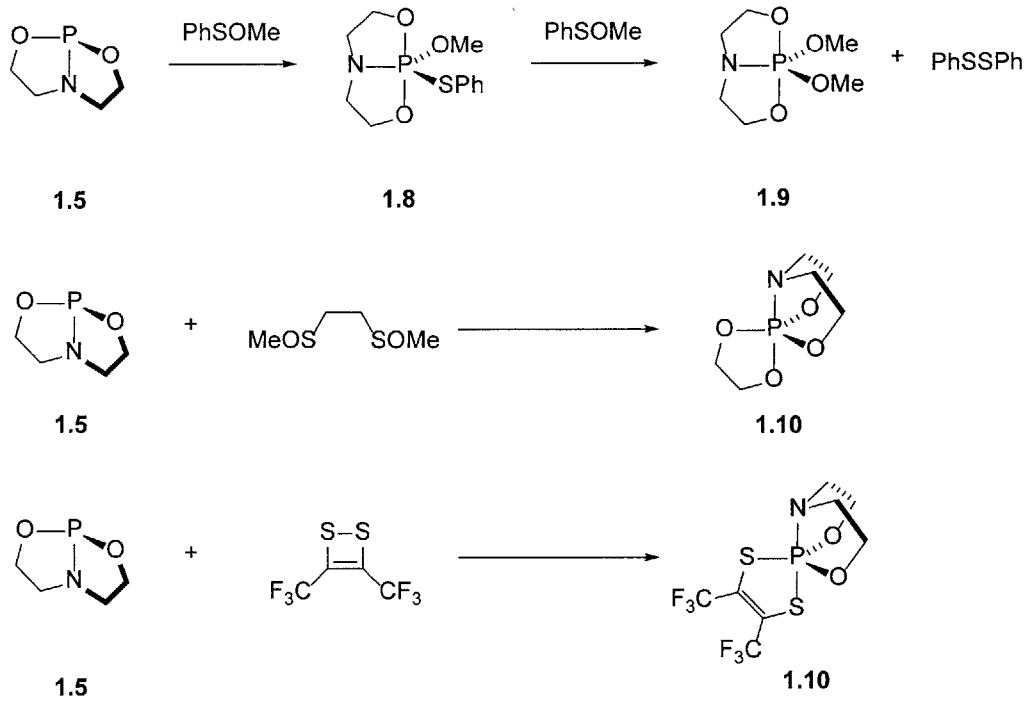

Figure 1.10. S-O and S-S oxidative addition of **1.5**.

less distorted structure – loses its N-H oxidative addition reactivity and gives no P-hydridophosphorane upon exposure to Me_2NH (**Figure 1.12**).[32]

With the above mentioned unusual bond activation reactivity of the deformed N,N,N- and O,N,O-bicyclic phosphines in mind, one can expect that further distortion of the phosphabicyclic structure to a planar geometry would cause even greater propensity for nonnucleophilic reactivity. O,N,O-bicyclic phosphine **1.18** synthesized by Arduengo[34] has a remarkable planar structure and a similar O,N,O-[3,3,0]-bicyclic binding motif as phosphines **1.5**, but the ethylene linkages in **1.5** are replaced by unsaturated ethenyl fragments (**Figure 1.13**). X-ray crystallography of compound **1.18** shows a planar T-shaped geometry with a large O-P-O angle (168.8°) and acute N-P-O

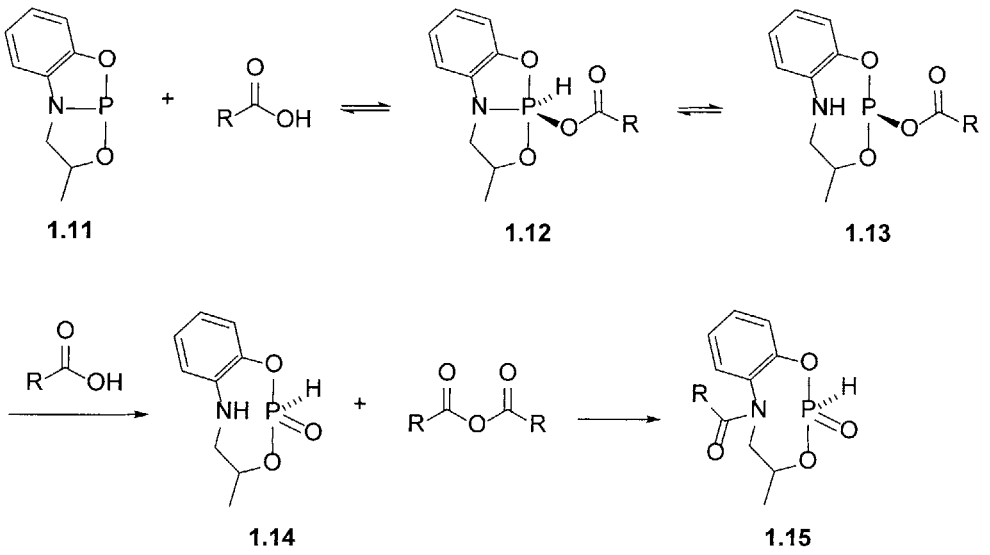

Figure 1.11. O-H oxidative addition of **1.5** toward carboxylic acid and the proposed product decomposition.

angles (84.0° and 84.9°). Several Lewis structural descriptions of the compound **1.18** have been proposed to explain its geometry (**Figure 1.14**). [35] The major factor contributing to the preference of planar geometry is the presence of the vinylic moiety which makes the O,N,O-ligand more electron rich and capable of donating electron density to the phosphorus atom. The extra electron density from the oxygen and nitrogen atoms and the strain imposed by the unsaturated ligand give phosphine **1.18** a formal ten valence electron count on the tricoordinate phosphorus center and subsequent T-shape planar geometry with apical oxygens and equatorial nitrogen. From the perspective of molecular orbital theory, lone pairs on the ligand nitrogen and oxygens donate electron density to the out-of-plane phosphorus p orbital, stabilizing the planar structure. In such a bonding arrangement, the stabilized out-of-plane phosphorus p orbital, the linear O-P-O bond and the rectangular N-P-O angles leave little p-character for the phosphorus lone

pair orbital and thus make the lone pair high s-character and significantly less nucleophilic.

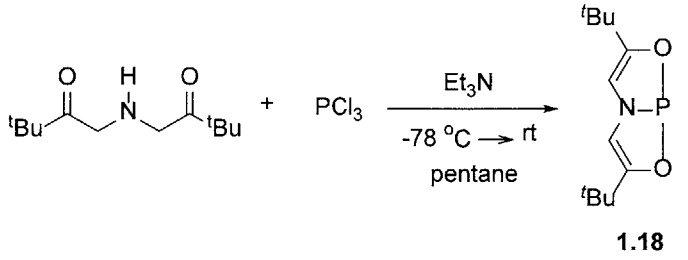

1.18

Figure 1.13. Synthesis of T-shaped O,N,O-phosphabicyclic compound **1.18**.

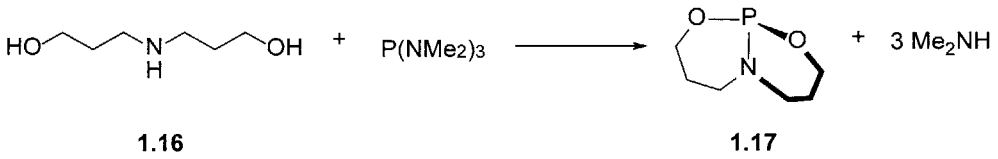

1.16 1.17

Figure 1.12. Synthesis of O,N,O-phosphabicyclic compound **1.17**.

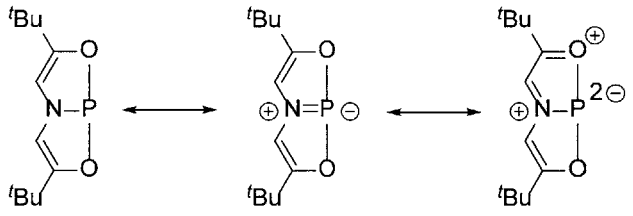

1.18

Figure 1.14. Resonance structures of compound **1.18**.

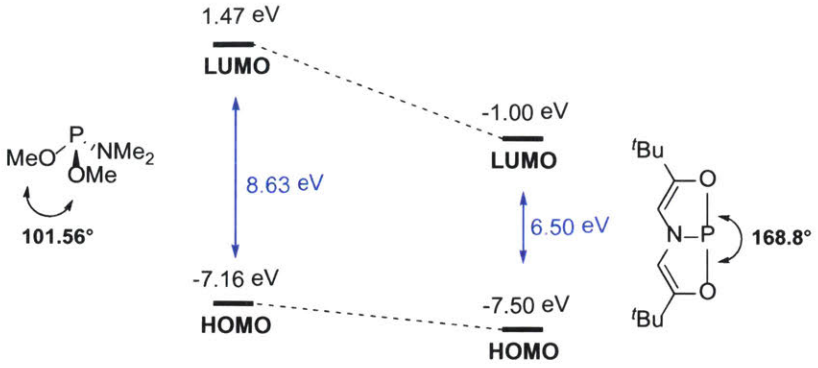

Figure 1.15. Reduced HOMO-LUMO gap of T-shaped phosphine **1.18**.

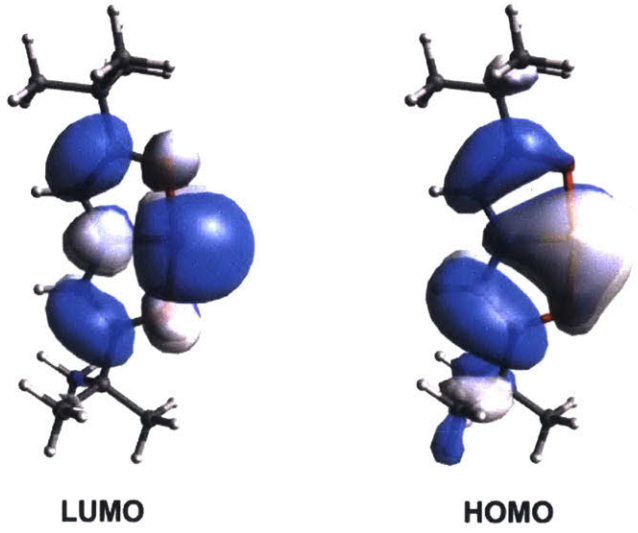

Figure 1.16. Visualized LUMO and HOMO of compound **1.18**.

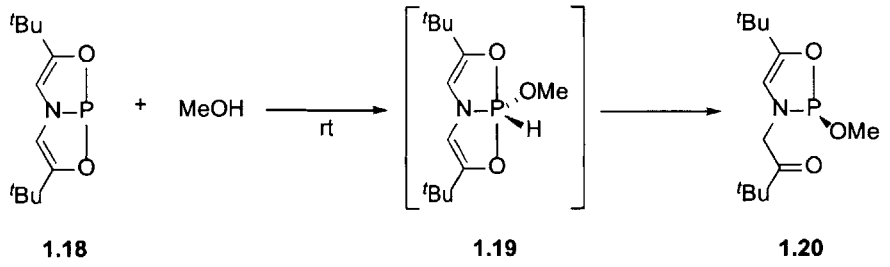

1.18 **1.19** **1.20**

Figure 1.17. Reactivity of compound **1.18** toward methanol.

In line with the predictions from qualitative MO analysis of distorted AB_3 molecules, calculations indicate that T-shaped compound **1.18** have a significantly stabilized LUMO as compared to $P(NM_2)(OMe)_2$. In effect, compound **1.18** has a much smaller HOMO-LUMO gap than a traditional C_{3v} phosphine (**Figure 1.15**). Furthermore, depictions of the LUMO of compound **1.18** (**Figure 1.16**) reveal that the orbital contains significant lobal density on the phosphorus atom. Similar to the distorted O,N,O-bicyclic phosphine **1.5**, when compound **1.18** is treated with methanol (**Figure 1.17**), a P-hydrido phosphorane intermediate **1.19** with a strong $^1J_{P\text{-}H}$ coupling can be detected by ^{31}P NMR spectroscopy. Following proton transfer and ligand tautomerization, final product **1.20** is generated. More recently, our group discovered that compound **1.18** can dehydrogenate ammonia borane to produce dihydridophosphorane **1.21** (**Figure 1.18**). [36] The dihydridophosphorane **1.21** can further be used to reduce azobenzene through a bimolecular mechanism with low activation barrier. By combination of the two stoichiometric transformations, compound **1.18** catalyzes transfer hydrogenation of azobenzene using ammonia borane as the terminal reductant (**Figure 1.18**).

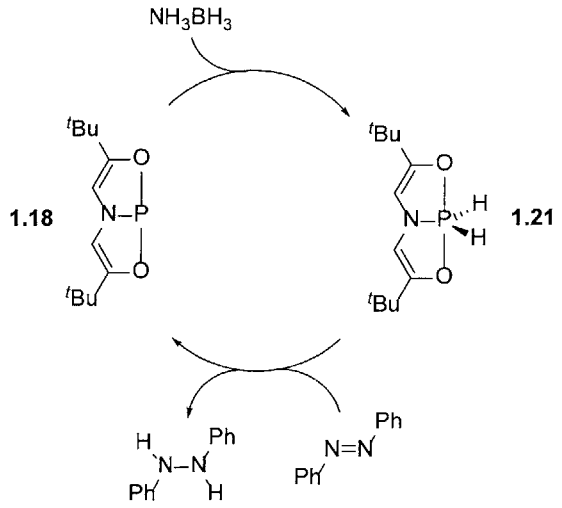

Figure 1.18 Transfer hydrogenation of azobenzene catalyzed by compound **1.18**.

Besides the distorted phosphabicyclic systems, several examples of geometry-induced non-traditional phosphorus-mediated chemistry have also been demonstrated by our group. Deformed phosphorus molecules with 4-membered phosphetane structures are shown to be efficient reagents or catalysts in transformations including deoxygenative condensation,[37] regioselective allylic reduction[38] and Cadogan-type N-N bond formation (**Figure 3.19**). [39] From mechanistic and computational studies, the unprecedented reactivity is unleashed by the stabilized LUMO of the deformed phosphetane molecules which facilitates the electrophilic interactions between the phosphorus centers and the incoming nucleophiles such as hydrides or silanes. In addition, the transformations are favored due to the minimized reorganization energy required for the conversions from

starting reagents to transition states because of the forced entatic geometries of the phosphorus intermediates.

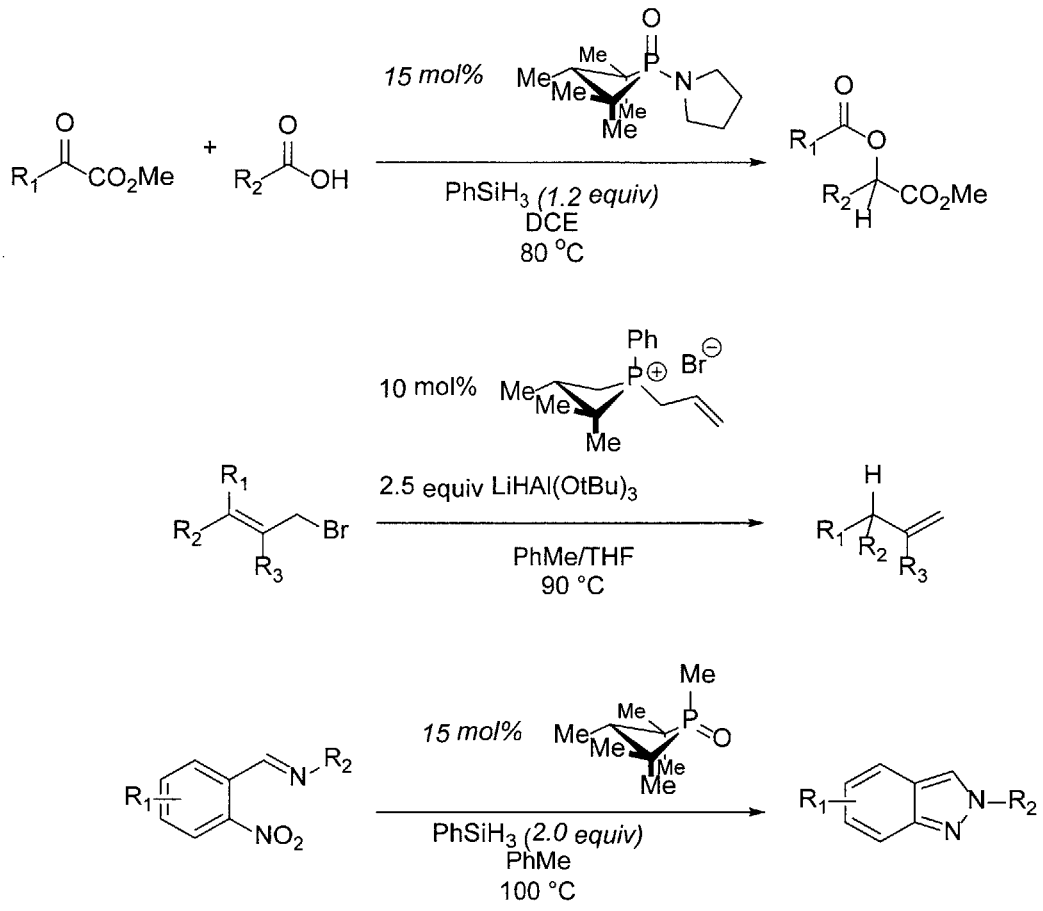

Figure 1.19. Catalytic reactivity of the phosphacyclic molecules with strained phosphetane structures.

1.4 Conclusion and Outlook

In view of the foregoing discussion of ring-constraint on the reactivity of tricoordinate phosphorus, it would appear that an as-yet-unrealized opportunity presents itself for the deliberate design of lower symmetry phosphorus compounds with nonnucleophilic reactivity. Through the research in this thesis, we hope to better understand the interplay between geometry and reactivity by studying nontrigonal σ^3- and σ^4-phosphorus compounds. The knowledge obtained in the research could help us to establish a general understanding of distortion-reactivity relationships, and thereby develop novel functionalization methods for synthetic chemistry.

1.5 References

[1] Carey, F. A.; Sundberg, R. J. In *Advanced Organic Chemistry: Part A: Structure and Mechanisms*; Carey, F. A., Sundberg, R. J., Eds.; Springer US: Boston, MA, 2007; pp 253–388.

[2] Albright, T. A.; Burdett, J. K.; Whangbo, M.-H. *Orbital Interactions in Chemistry*; Chichester : Wiley, 2013.

[3] Gimarc, B. M. *Molecular Structure and Bonding : The Qualitative Molecular Orbital Approach.*; New York : Academic Press, 1979.

[4] Gimarc, B. M. *J. Chem. Phys* **1970**, *53*, 1623.

[5] Gimarc, B. M. *J. Am. Chem. Soc.* **1971**, *93*, 593.

[6] Gimarc, B. M.; Khan, S. A. *J. Am. Chem. Soc.* **1978**, *100*, 2340.

[7] (a) Dieter, R. K.; Pounds, S. *J. Org. Chem.* **1982**, *47*, 3174. (b) DePuy, C. H. In *Three-Membered Rings*; Springer Berlin Heidelberg: Berlin, Heidelberg, 1973; pp 73–101.

[8] Parker, R. E.; Isaacs, N. S. *Chem. Rev.* **1959**, *59*, 737.

[9] Abramovitch, R. A. *Reactive Intermediates.*; New York : Plenum Press, 1980.

[10] Grubbs, R.; Tumas, W. *Science* **1989**, *243*, 907.

[11] (a) Vallee, B. L.; Williams, R. J. *Proc Natl Acad Sci U S A* **1968**, *59*, 498. (b) Williams, R. J. P. *Eur. J. Biochem.* **1995**, *234*, 363.

[12] Strozier, R. W.; Caramella, P.; Houk, K. N. *J. Am. Chem. Soc.* **1979**, *101*, 1340.

[13] (a) Westheimer, F. H. *Acc. Chem. Res.* **1968**, *1* (3), 70. (b) Hudson, R. F.; Brown, C. *Acc. Chem. Res.* **1972**, *5*, 204.

[14] Quin, L. D. *A Guide to Organophosphorus Chemistry*; John Wiley & Sons, Inc.: New York, N.Y., 2000.

[15] Basavaiah, D.; Rao, K. V.; Reddy, R. J. *Chem. Soc. Rev.* **2007**, *36*, 1581.

[16] Maercker, A. *Org. React.* **1965**, *14*, 270.

[17] Hughes, D.L. *Org. React.* **1992**, *42*, 335.

[18] Appel, R. *Angew. Chem. Int. Ed.* **1975**, *14*, 801.

[19] Hartwig, J.F. *Organotransition Metal Chemistry*; University Science Books: Sausalito, CA, 2010.

[20] (a) Baechler, R. D.; Mislow, K. *J. Am. Chem. Soc.* **1970**, 92, 3090. (b) Mislow, K.; Baechler, R. D. *J. Am. Chem. Soc.* **1971**, 93, 773. (c) Reichl, K. D.; Ess, D. H.; Radosevich, A. T. *J. Am. Chem. Soc.* **2013**, *135*, 9354.

[21] (a) Lambert, J. B.; Oliver, W. L., Jr. *J. Am. Chem. Soc.* **1969**, 91, 7774. (b) Rauk, A.; Allen, L. C.; Mislow, K. *Angew. Chem., Int. Ed. Engl.* **1970**, 9, 400. (c) Montgomery, C. D. *J. Chem. Educ.* **2013**, *90*, 661.

[22] (a) Knowles, W. S.; Sabacky, M. J. *Chem. Commun.* **1968**, 22, 1445. (b) Knowles, W. S.; Sabacky, M. J.; Vineyard, B. D. *J. Chem. Soc., Chem. Commun.* **1972**, 1, 10. (c) Knowles, W. S.; Sabacky, M. J.; Vineyard, B. D.; Weinkauff, D. J. *J. Am. Chem. Soc.* **1975**, *97*, 2567.

[23] (a) Murahashi, S.; Taniguchi, Y.; Imada, Y.; Tanigawa, Y. *J. Org. Chem.* **1989**, *54*, 3292. (b) Goldinga, B. T.; O'Sullivan, M. C.; Smith, L. L. *Tetrahedron Lett.* **1988**, *29* (50), 6651.

[24] (a) Lambert, P. H.; Vaultier, M.; Carrie, R. *J. Org. Chem.* **1985**, *50*, 5352. (b) Urpí, F.; Vilarrasa, J. *Tetrahedron Lett.* **1986**, *27*, 4623.

[25] Molina, P.; Vilaplana, M. J. *Synthesis* **1994**, *1994*, 1197.

[26] (a) Palacios, F.; Alonso, C.; Aparicio, D.; Rubiales, G.; de los Santos, J. M. *Tetrahedron* **2007**, *63*, 523. (b) Lambert, P. H.; Vaultier, M.; Carrié, R. *J. Chem. Soc., Chem. Commun.* **1982**, 21 , 1224. (c) Molina, P.; Alajarín, M.; Vidal, A. *J. Chem. Soc., Chem. Commun.* **1990**, 18, 1277.

[27] Ishikawa, T. *Superbases for organic synthesis : guanidines, amidines, phosphazenes and related organocatalysts.*; Chichester, UK : John Wiley & Sons, 2009.

[28] (a) Akiyama, T.; Mori, K. *Chem. Rev.* **2015**, *115*, 9277. (b) Parmar, D.; Sugiono, E.; Raja, S.; Rueping, M. *Chem. Rev.* **2014**, *114*, 9047. (c) Rueping, M.; Sugiono, E.; Azap, C.; Thiessman, T.; Bolte. M. *Org. Lett.* **2005**, *7*, 3781. (d) Hoffmann, S.; Seayad, A.; List, B. *Angew. Chem. Int. Ed.* **2005**, *44*, 7424. (e) Storer, R. I.; Carrera, D. E.; Ni, Y.; MacMillan, D. W.C. *J. Am. Chem. Soc.* **2006**, *128*, 84.

[29] (a) Mitzel, N.W.; Smart, B.A.; Dreihäupl, K-H.; Rankin, D.W.H.; Schmidbaur, H. *J. Am. Chem. Soc.* **1996**, *118,* 12673. (b) Cowley, A.H.; Dewar, M.J.S.; Goodman, D.W.; Schweiger, J.R. *J. Am. Chem. Soc.* **1973**, *95*, 6506.

[30] (a) Richman, J.E.; Atkins, T.J. *Tetrahedron Lett.* **1978**, 4333. (b) Atkins, T.J.; Richman, J.E. *Tetrahedron Lett.* **1978**, 5149.

[31] (a) Houalla, D.; Osman, F.H.; Sanchez, M.; Wolf, R. *Tetrahedron Lett.* **1977**, 3041. (b) Houalla, D.; Sanchez, M.; Wolf, R. *Tetrahedron Lett.* **1978**, 4675. (c) Wolf, R. *Pure Appl. Chem.* **1980**, *52*, 1141. (d) Bonningue, C.; Houalla, D.; Sanchez, M.; Wolf, R.; Osman, F.H. *J. Chem. Soc. Perkin Trans. 2* **1981**, 19. (e) Bonningue, C.; Houalla, D.; Wolf, R.; Jaud, J. *J. Chem. Soc. Perkin Trans. 2* **1983**, 773.

[32] Denney, D.B.; Denney, D.Z.; Hammond, P.J.; Huang, C.; Tseng, K-S. *J. Am. Chem. Soc.* **1980**, *102, 5073.*

[33] Terent'eva, S.; Pudovik, M.; Pudovik, A. *Izv. Akad. Nauk. SSSR* **1983**, 221.

[34] Culley, S.A.; Arduengo, A.J. *J. Am. Chem. Soc.* **1984**, *106*, 1164.

[35] Arduengo, A.J.; Stewart, C.A.; Davidson, F.; Dixon, D.A.; Becker, J.Y.; Culley, S.A.; Mizen, M.B. *J. Am. Chem. Soc.* **1987**, *109*, 627.

[36] Dunn, N.L.; Ha, M.; Radosevich, A.T. *J. Am. Chem. Soc.* **2012**, *134*, 11330.

[37] Zhao, W.; Yan, P. K.; Radosevich, A. T. *J. Am. Chem. Soc.* **2015**, *137*, 616.

[38] Reichl, K. D.; Dunn, N. L.; Fastuca, N. J.; Radosevich, A. T. *J. Am. Chem. Soc.* **2015**, *137*, 5292.

[39] Nykaza, T. V.; Harrison, T. S.; Ghosh, A.; Putnik, R. A.; Radosevich, A. T. *J. Am. Chem. Soc.* **2017**, *139*, 6839.

Chapter Two. N-H Oxidative Addition Reactivity of a T-Shaped Phosphorus Compound

A significant portion of the work described in this chapter has been published in:

McCarthy, S. M.; Lin, Y.-C.; Devarajan, D.; Chang, J. W.; Yennawar, H. P.; Rioux, R. M.; Ess, D. H.; Radosevich, A. T. *J. Am. Chem. Soc.* **2014**, *136*, 4640.

Chapter Two

N-H Oxidative Addition Reactivity of a T-Shaped Phosphorus Compound

With the aim of investigating the impact of geometric distortion on reactivity of tricoordinate phosphorus molecules, we present here the study of N-H oxidative addition reactivity of a geometrically unique T-shaped phosphorus compound.[1] Arduengo's C_{2v}-symmetric O,N,O-phosphabicyclic P(III) molecule was found to undergo N-H oxidative addition with ammonia and other primary amines to generate the corresponding P(V) products. The resulting phosphorane products from this transformation provide the first example of stable intermolecular phosphorus-based N-H activation products for isolation, spectroscopic characterization and in-depth mechanistic study.

2.1 Significance and Challenges of N-H Activation

Oxidative addition is an important elementary reaction type, with a crucial role that can be witnessed in the remarkable success of many transition metal catalyzed methods. The oxidative addition of N-H bonds is of considerable interest in connection with potential schemes for transforming nitrogen-based commodity feedstocks into value-added medicinal or consumer products. However, examples of N-H oxidative addition are rare by comparison to the many analogous E-H bond activations that

currently figure in large number of prominent transition metal-based catalytic functionalizations.[2] In particular, catalytic amination of aromatics and olefins with ammonia has been listed among the most valuable goals in industrial chemistry.[3]

The challenges associated with N-H bond activation and functionalization can be rationalized by several aspects. First, the high bond dissociation energies (90-110 kcal/mol) [4] and low acidity of N-H bonds (pK_a = 35-40) [5] make activation thermodynamically disfavored via both homolytic and heterolytic pathways. Second, late transition metals that are frequently used in E-H activations easily coordinate with the Lewis-basic ammonia and amine, forming stable Werner-type adducts. Despite these challenges, several examples of N-H oxidative addition to both transition metals and main group species have been reported, providing potential directions in the development of N-H functionalization methods.

2.2 Metal- and Main Group Element-Mediated N-H Oxidative Addition

Although recent N-H activation examples associated with bimetallic[6] and metal-ligand cooperative[7] systems have been reported, well-characterized studies of N-H oxidative addition to a single-site metal centers remain rare. Milstein et al.[8] first demonstrated in pioneering studies that some tetracoordinate iridium(I) compounds are reactive toward ammonia through oxidative addition and produce amido hydrido Ir(III)

complexes. A subsequent advancement was achieved by Hartwig with an aliphatic ligand-bearing iridium(I) P,C,P-pincer complex **2.1** (**Figure 2.1**).[9] With the relatively electron-donating aliphatic P,C,P-ligand, the pincer complex undergoes N–H oxidative addition with ammonia and gives an isolable terminal amido Ir(III) mononuclear complex without suffering from N-H reductive elimination and subsequent Ir-(NH_3) complex formation. The concept of the electron-donating pincer ligand was further utilized in the design of the reactive iridium P,Si,P-[10] and other similar pincer complexes.[11] In addition, Wolczanski et al. has demonstrated that early transition metal–mediated ammonia activation can be achieved with a trisiloxide tantalum(III) complex.[12]

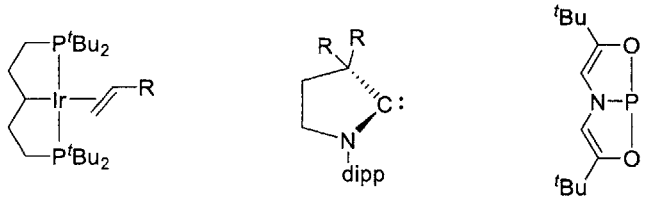

2.1 **2.2** **2.3**

Figure 2.1. Transition metal and main group molecules with N-H oxidative addition reactivity.

A well-characterized example of main group compound-mediated N-H oxidative addition was realized elegantly by Bertrand et al. with cyclic and acyclic (alkyl)(amino)carbenes **2.2** (**Figure 2.1**).[13] With orthogonally-oriented frontier orbitals of proximate energy, the (alkyl)(amino)carbenes behave react with dihydrogen H-H and ammonia N-H bonds through oxidative addition. In line with the high-lying HOMO of the (alkyl)(amino)carbenes, the oxidative addition transition state develops asynchronously with a leading nucleophilic contribution from the carbene carbon to the

N-H hydrogen giving significant negative charged accrual on the nitrogen atom in the transition state. The complementary interaction of the electron-rich nitrogen and the electron-deficient carbene carbon contributes to a lesser extent in the activation process en route to tetravalent products. Complementarily to the nucleophilic mechanism in Bertrand's study in (alkyl)(amino)carbenes, Bielawski et al. demonstrated that N-H oxidative addition could also proceed by an electrophilic process on an electron-deficient di(amido)carbene.[14] The di(amido)carbene in this study was designed to contain two electron-deficient amide N-substituents and consequently a lowerer LUMO energy.[15] The resulting electronic structure enables ambiphilicity of this carbene in N-H oxidative addition; depending on the precise identity of amine substrate, either electrophilic or nucleophilic reactivity can be discerned with this species.

In related fashion to the carbenes, the N-H oxidative addition reactivity of heavier divalent group 14 molecules has also been demonstrated by Roesky,[16] Power,[17] and others.[18] From the computational results, the oxidative addition transformations in these studies are most likely initiated by electrophilic interactions between the group 14 center and the lone pairs of ammonia nitrogen.

The prerequisites for successful N-H oxidative addition can be concluded from the above-mentioned studies in transition metal- and main group element-mediated transformations. Apart from a favorable reaction enthalpy, energetically and spatially accessible frontier orbitals are required for interaction with the N-H bonding and antibonding orbitals, and the consequent cleavage of N-H bonds. We envisioned that the

distorted O,N,O-phosphine **2.3** might exhibit N-H activation reactivity due to its electronic and steric properties (**Figure 2.1**).

2.3 Intermolecular N-H Oxidative Addition to the T-Shape O,N,O-σ^3-Phosphorus Molecule

As discussed in Chapter 1, O,N,O-supported σ^3-phosphorus compound **2.3** has a tricoordinating and electron-donating ligand which gives the molecule a planar T-shape geometry. As a result of this unusual geometry, the electronic structure of phosphine **2.3** contains an in-plane phosphorus-based lone pair in energetic proximity of the HOMO as well as a low lying LUMO with phosphorus-based pπ character. In effect, the electronic structure of phosphine **2.3** resembles the frontier electronic structure of carbenes and their heavier congeners. Distorted σ^3-phosphorus compounds have demonstrated reversible bond activation reactivity as discussed in Chapter 1, suggesting potential for catalytic applications. Specifically, the catalytic transfer hydrogenation reactivity of T-shape phosphine **2.3,** which involves formal transfer of dihydrogen equivalent to and from phosphorus, has been reported by our laboratory.[19] Although the mechanistic details in this system await a fuller accounting elsewhere, we hypothesized that this catalytic transformation might involve the oxidative addition of an N-H substrate to **2.3** (or its microscopic reverse – reductive elimination) at some stage of the catalytic cycle. In order to interrogate this hypothesis, we undertook a study of phosphine **2.3** with amine substrates including ammonia, alkyl and aryl amines.

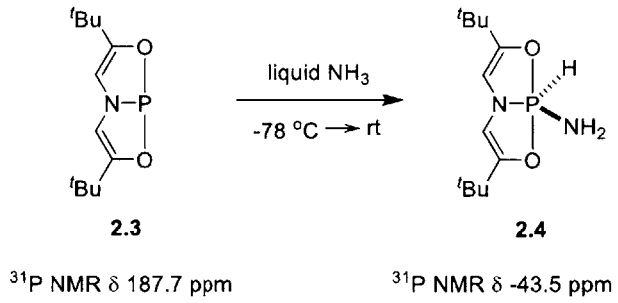

Figure 2.2. Ammonia N-H oxidative addition to phosphine **2.3**.

The N-H oxidative addition reactivity of compound **2.3** was first tested by treating a solid sample of **2.3** with liquid ammonia (this experiment was conducted by Sean McCarthy). Gaseous NH_3 was condensed onto a solid sample of **2.3** at −78 °C (**Figure 2.2**). The mixture was stirred at −78 °C for 30 min, and then warmed to room temperature. The excess ammonia was evaporated under a nitrogen stream and the crude product was characterized by NMR spectroscopy. ^{31}P NMR showed a clean conversion from **2.3** (^{31}P NMR δ 187.7 ppm) to a single product with a ^{31}P NMR signal centered at δ −43.5 ppm, suggesting that a pentacoordinate phosphorus product **2.4** was obtained.[20] The observed ^{31}P NMR signal (**Figure 2.3** *top*) presented as a large doublet with a coupling constant of J = 812 Hz, which is in the range of typical $^{1}J_{P\text{-}H}$ coupling and indicates the existence of a P-H bond. Based on previously reported correlations between P-H coupling and structure,[21] the large P-H coupling constant suggested the existence of equatorial hydrogen substituent within a trigonal bipyramidal structure. Smaller $^{3}J_{P\text{-}H}$ coupling (J = 1.1 Hz) resulting from the vinylic ligand protons and $^{2}J_{P\text{-}H}$ coupling (J = 10.2 Hz) from the addend amido were also evident.

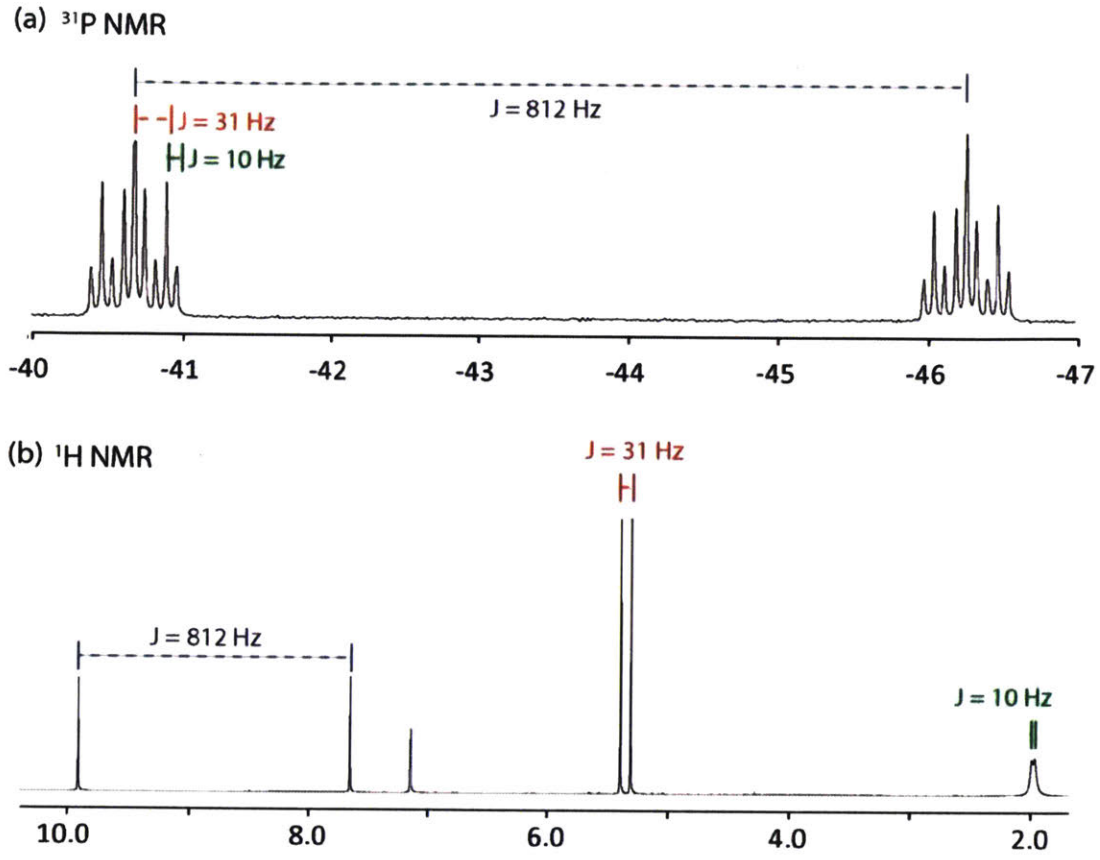

Figure 2.3. (a) Abridged annotated ^{31}P NMR spectrum for **2.4** in C_6D_6. Units are ppm relative to H_3PO_4. (b) Annotated ^{1}H NMR spectrum for **2.4** in C_6D_6. An additional signal for $-C(CH_3)_3$ is found at δ 1.06 ppm. Units are ppm relative to Me_4Si. Reproduced with permission from *J. Am. Chem. Soc.* **2014**, *136*, 4640.

The phosphorus-based N-H oxidative addition is further supported by the complementary coupling in the ^{1}H NMR spectrum (**Figure 2.3** *bottom*). A ^{1}H NMR doublet signal centered at δ 8.79 ppm with a very large coupling constant was observed and consistent with the P-H ^{1}J coupling (J = 812 Hz). Furthermore, the infrared spectrum of the product showed a diagnostic 2374 cm^{-1} absorption which was in line with a P-H stretching mode. Two other IR absorptions appearing at 3516 and 3411 cm^{-1} could be

assigned to the symmetric and asymmetric stretching bands of the terminal -NH_2 group. The spectroscopic evidence strongly suggests a successful transformation from σ^3-phosphorus molecule **2.3** to the σ^5-phosphorus product **2.4** through N-H oxidative addition.

In addition to ammonia, compound **2.3** is also highly reactive toward the N-H bond of primary alkyl amines (**Figure 2.4** *top*). When five equivalents of propylamine, isopropylamine, or benzylamine amine are added to a C_6D_6 solution of **2.3** in a sealed NMR tube at ambient temperature, complete consumption of **2.3** and quantitative conversion to hydrido amido phosphoranes **2.5a-c** is observed within 15 min by NMR spectroscopy (**2.5a**: δ −46.4 ppm, $^1J_{P\text{-}H}$ = 815 Hz; **2.5b**: δ −47.1 ppm, $^1J_{P\text{-}H}$ = 819 Hz; **2.5c**: δ −46.0 ppm, $^1J_{P\text{-}H}$ = 824 Hz). During the course of the reaction, no intermediates are observed in ^1H or ^{31}P NMR spectra. Pure phosphorane products for ^1H NMR, mass spectrometry and elemental analysis are obtained by reacting exactly one equivalent of the amines with **2.3,** or by removing the excess amine with distillation. Aryl amines including *p*-anisidine, 2,4,6-trimethylaniline and 2,6-diisopropylaniline also undergo oxidative addition to compound **2.3,** but with a slower reaction rate than alkyl amines. At room temperature, five equivalents of *p*-anisidine are observed to react with **2.3** in C_6D_6 and yield hydrido anilido phosphorane **2.5d** (δ −48.7 ppm, $^1J_{P\text{-}H}$ = 831 Hz) after 1 h. The reaction rate is further decreased with more sterically bulky anilines 2,4,6-trimethylaniline and 2,6-diisopropylaniline, but the transformations still give the corresponding adducts **2.5e** (δ −48.9 ppm, $^1J_{P\text{-}H}$ = 840 Hz) and **2.5f** (δ −51.4 ppm, $^1J_{P\text{-}H}$ = 841 Hz) respectively after 2 h at 55 °C (**Figure 2.4** *bottom*). The arylaminophosphorane

products can be purified by neutral alumina column chromatography under nitrogen atmosphere.

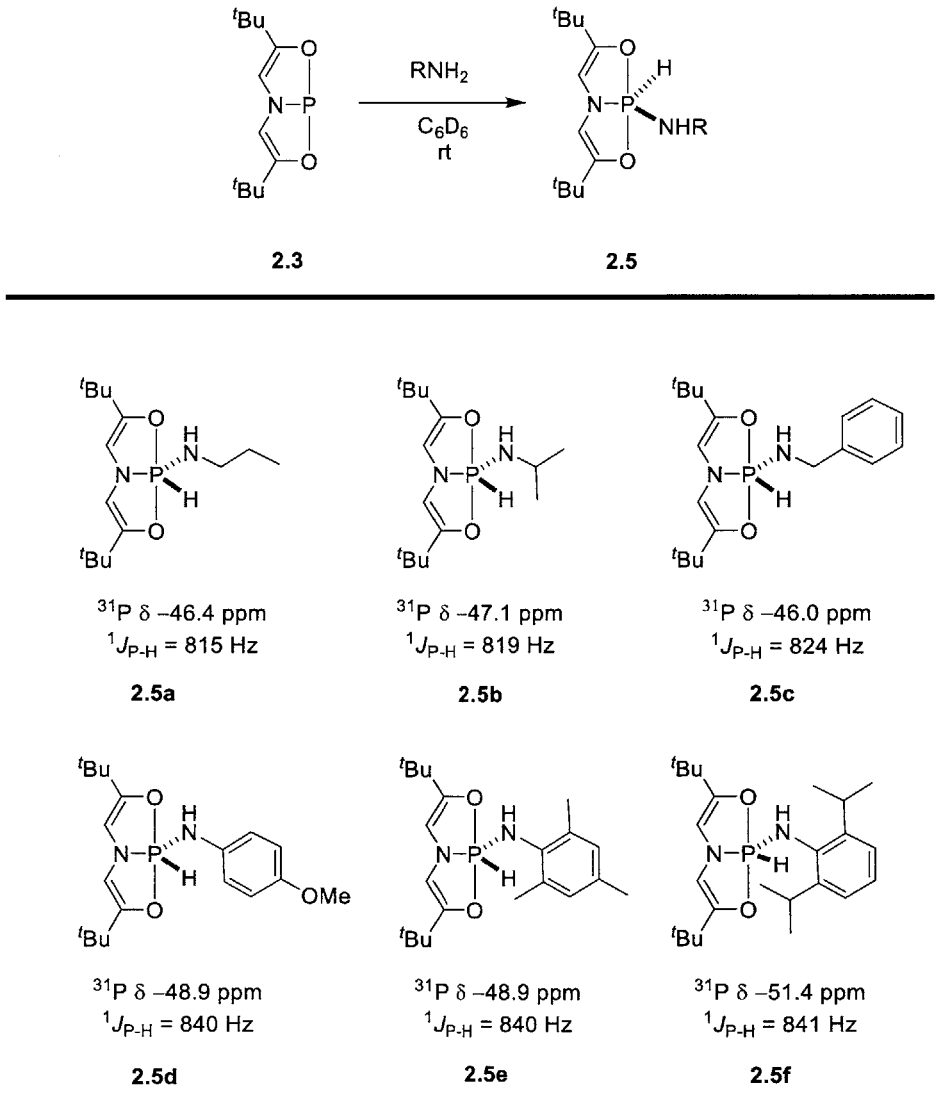

Figure 2.4. N-H oxidative addition of alkyl and aryl amines to phosphine **2.3**

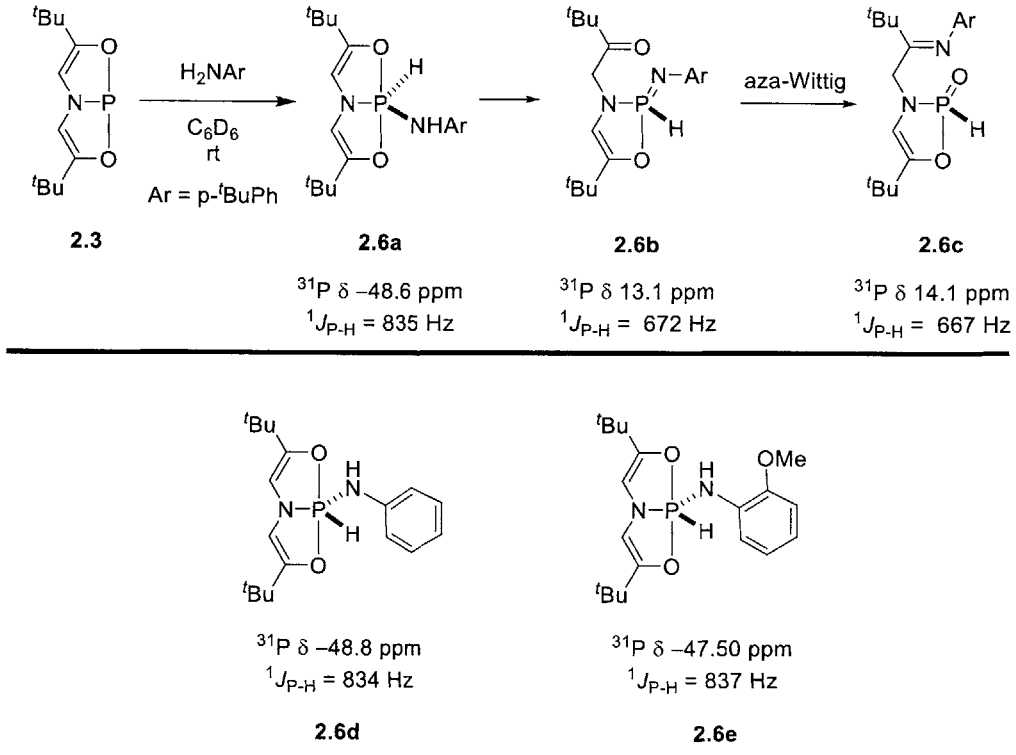

Figure 2.5. N-H oxidative addition of aryl amines to phosphine **2.3** and the resulting phosphorane adducts and by-product.

Reacting compound **2.3** with other aryl amines results in more complex product mixtures. For example, treating 4-*tert*-butylaniline to **2.3** gives the expected phosphorane N-H oxidative addition adduct **2.6a** (δ −48.6 ppm, $^{1}J_{P\text{-}H}$ = 835 Hz) along with two P-H bearing phosphorus by-products (δ 14.1 ppm, J = 667 Hz; δ 13.1 ppm, $^{1}J_{P\text{-}H}$ = 672 Hz). The by-products are tentatively assigned as ring-opened secondary iminophosphorane **2.6b** and secondary phosphine oxide **2.6c** (**Figure 2.5** *top*). The formation of the by-products probably involves an intramolecular proton transfer from the amido N-H to one of the electron-rich axial oxygens, followed by enol-keto tautomerization and

intramolecular aza-Wittig reaction. Attempts to synthesize **2.6d** and **2.6e** by independent synthetic routes were not successful.

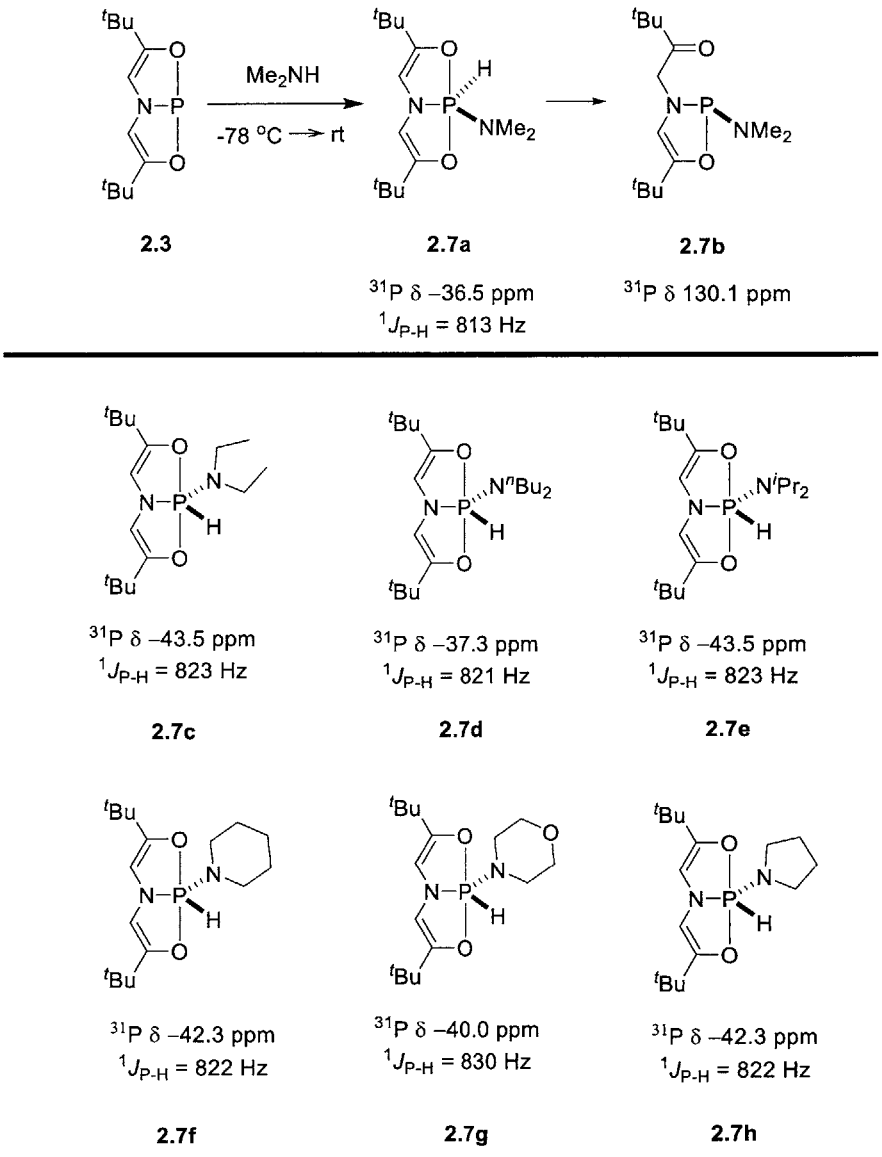

Figure 2.6. N-H oxidative addition of secondary amines to phosphine **2.3** and the resulting phosphorane adducts. Putative prototropic rearrangement product **2.7b** is depicted.

In contrast to the report by Arduengo,[22] reactions of **2.3** and secondary amines also give N-H addition products, albeit along with ring-opened by-products. After stirring a mixture of solid **2.3** and condensed dimethylamine at −78 °C for 30 min followed by evaporation of the excess amine at room temperature, phosphorane **2.7a** (δ −36.5 ppm, $^{1}J_{P\text{-}H}$ = 813 Hz) can be detected as a minor product. The major product is observed at δ 130.1 ppm in ^{31}P NMR spectra as singlet signal, presumably corresponding to prototropic rearrangement product **2.7b** (**Figure 2.6** *top*). Several other acyclic and cyclic secondary amines also undergo N-H oxidative addition with **2.3**, yielding comparable product and rearrangement product mixtures (**Figure 2.6** *bottom*). At this stage, we attribute the reactivity difference between primary and secondary amines to steric effects that favor the less hindered σ^3-product isomers over σ^5- isomers.

2.4 Structure of the N-H Oxidative Addition Product

The stability of certain N-H addition products of **2.3** allows a more in-depth study of the structures of these compounds. Specifically, a solid sample of 2,4,6-trimethylaniline adduct **2.5e** can be obtained after filtration of its C_6D_6 solution through neutral alumina under nitrogen atmosphere. The resulting solid sample was then crystallized from a concentrated pentane solution to provide diffraction quality single crystals. The X-ray crystallography of this sample provided the structure of **2.5e** as shown in **Figure 2.7** (the X-ray diffraction experiments was conducted by Dr. Hemant Yennawar). In line the information obtained from ^{31}P NMR chemical shift and coupling

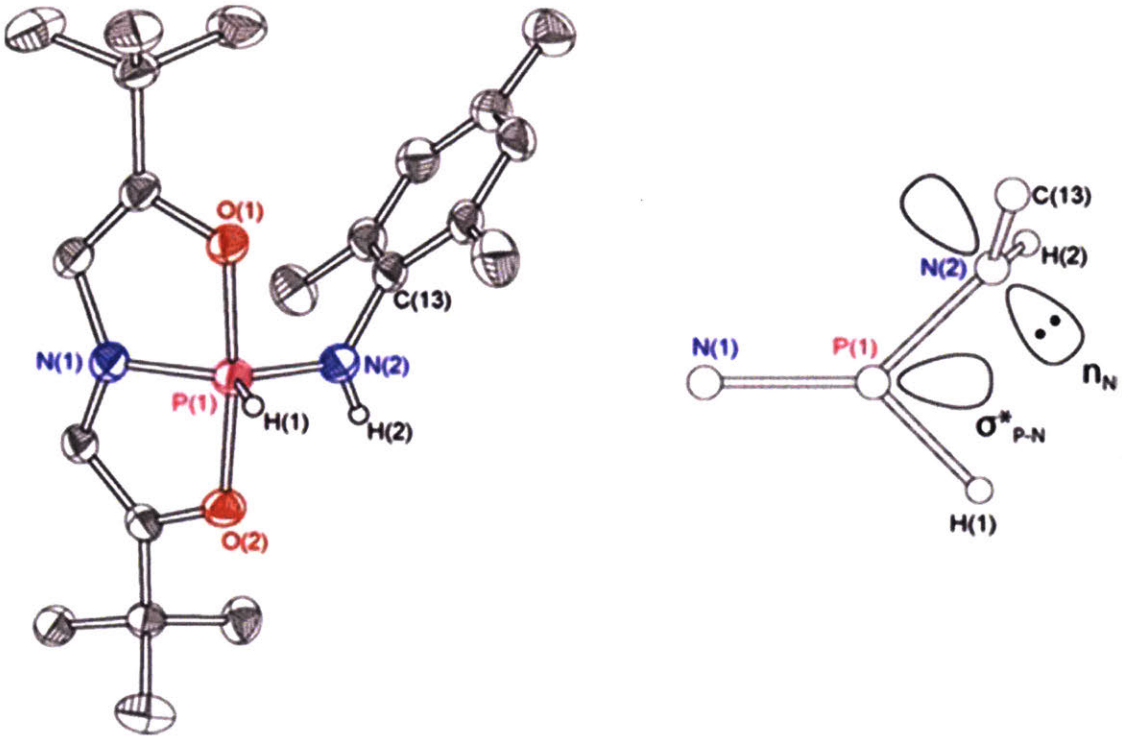

Figure 2.7. (Left) Molecular structure of **2.5e**. All hydrogen atoms on carbon are omitted for clarity. Thermal ellipsoids are shown at the 50% probability level. (Right) Top view of equatorial plane with schematic orbital representation of $n_N \rightarrow \sigma^*$ P–N interaction. Reproduced with permission from *J. Am. Chem. Soc.* **2014**, *136*, 4640.

constants, the phosphorane adopts an essentially trigonal bipyramidal structure at phosphorus with hydride and anilide group in equatorial positions. The O,N,O ligand retains a nearly planar arrangement spanning apical sites, with an O-P-O angle of 174.0(1)°. Given the higher phosphorus oxidation state, the P-O and P-N bond within the ligand framework are shorter in the phosphorane adduct than in T-shape phosphine **2.3,** as expected. Interestingly, the anilide nitrogen N(2) has a planar geometry and the coordination plane around N(2) oriented orthogonally to the phosphorus equatorial plane.

This structural arrangement suggests a possible stabilizing interaction between the N(2) lone pair and the P(1)-N(1) σ-antibonding orbital. This observation is in accordance with the established preference for π-donor substituents to occupy equatorial sites in pentavalent phosphorus molecules.[23] A computational NBO analysis provides additional support for the stabilizing hyperconjugative interaction.

2.5 Thermodynamic Analysis of the N-H Oxidative Addition Process

Thermodynamic studies of the reaction of **2.3** and *n*-propylamine has been conducted by Dr. Ji Woong Chang with isothermal titration calorimetry (ITC).[24] In a typical ITC experiment, a solution of **2.3** (1mM in C_6D_6, 1 mL total volume) was titrated with 6 μL aliquots of a solution of *n*-propylamine (12.5 mM in C_6D_6) under a nitrogen atmosphere. An isotherm for the addition of *n*- propylamine to **2.3** (top) and the measured integrated heats (bottom) are shown in **Figure 2.8**. An independent binding sites model (red line in **Figure 2.8**) was utilized to confirm a 1:1 stoichiometry as expected for the addition reaction. This model also provides a reaction enthalpy (ΔH_{rxn}) of -10.6 ± 0.1 kcal/mol and an equilibrium constant (K_{eq}) of $(3.03 \pm 0.17) \times 10^4$ M^{-1}.

Without reliable experimental P-N and P-H bond enthalpy data for comparable phosphoranes, computations were conducted to estimate bond strengths for comparison with the isothermal titration calorimetry results.[25] Using M06-2X/6-311++G(2d,2p) calculations, a reaction enthalpy (ΔH_{rxn}) of −7.4 kcal/mol is estimated, which is reasonably close to the experimental value of -10.6 ± 0.1 kcal/mol. Additionally, the P-H

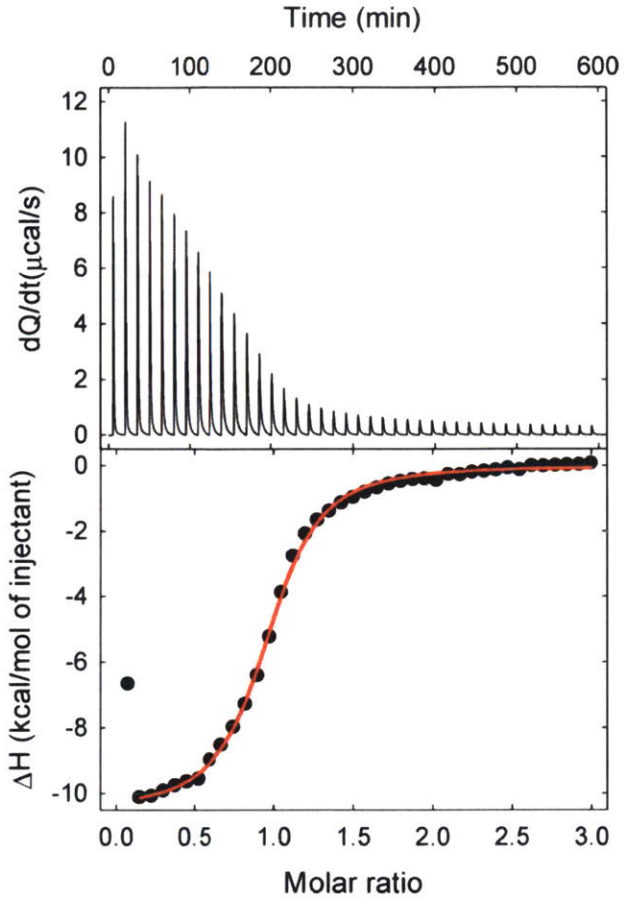

Figure 2.8. Thermochemistry of N-H oxidative addition of *n*-propylamine to **2.3**. (Top) ITC thermogram at 25 °C in benzene. (Bottom) Plot of integrated heat evolved with fitted model. Reproduced with permission from *J. Am. Chem. Soc.* **2014**, *136*, 4640.

and P-N bond dissociation energies of dimethylamine adduct **2.7a** were calculated for comparison with those of similar previously reported phosphorus species (**Figure 2.9**). The calculated P-H bond dissociation energy $D_{P\text{-}H}$ of 70.6 kcal/mol is consistent with the previously reported results of hydrogen radical abstraction of hydridophosphoranes with thiyl radicals.[26] The calculated P-N bond dissociation energy $D_{P\text{-}N}$ (68.3 kcal/mol) is also close to the reported experimental values in both σ^3-phosphorus ($D_{P\text{-}N}$ = 66.8 ± 0.8

kcal/mol in $P(NEt_2)_3$)[27] and σ^3-phosphorus ($D_{P\text{-}N}$ = 74.3 kcal/mol in $(Cl_3PNMe)_2$)[28] molecules.

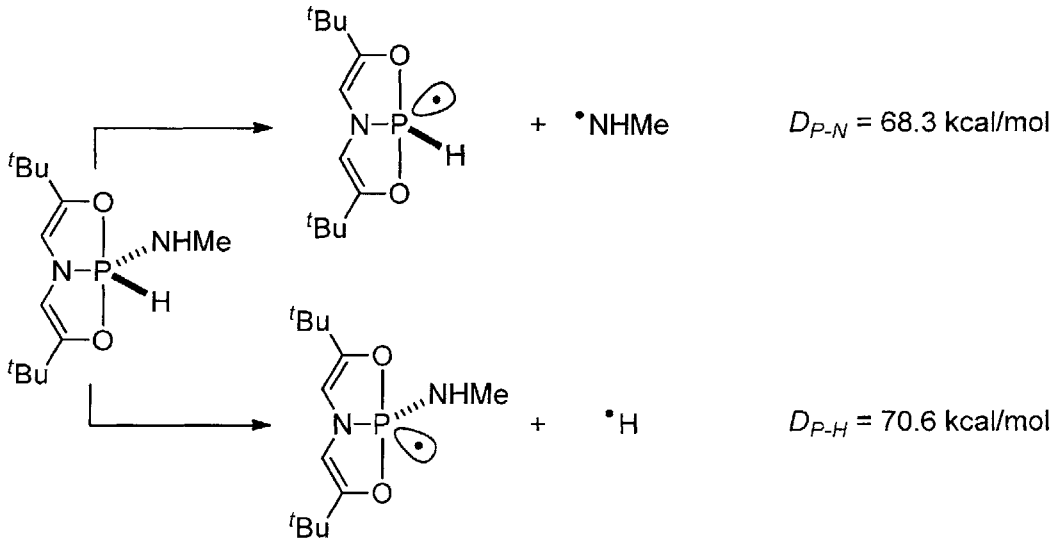

Figure 2.9. M06-2X/6-311++G(2d,2p) P–H and P–N bond enthalpies. Reproduced with permission from *J. Am. Chem. Soc.* **2014**, *136*, 4640.

2.6 N-H Elimination and Amine Exchange of the Phosphorane Adducts

Since the experimental reaction enthalpy ΔH_{rxn} of −10.6 ± 0.1 kcal/mol of the N-H oxidative addition process is large enough to inhibit the reversed transformation under proper conditions, the N-H reductive elimination reactivity of the obtained phosphorane adduct was investigated. Due to the low sublimation temperature (40 °C) of ammonia adduct **2.4** under reduced pressure (1 mmHg), phosphorane adducts **2.5a** – **2.5c** which

contain smaller amido substituents were heated to 100 °C *in vacuo* in attempts to facilitate reductive elimination of amine and regenerate phosphine **2.3**. Unfortunately, no regeneration of compound **2.3** was observed in any of these experiments. Heating heavier adducts such as 2,4,6-trimethylaniline adduct **2.5e** to 100 °C at 1 mmHg also failed to give the elimination transformation, and further heating to higher temperatures leads to nonspecific decomposition.

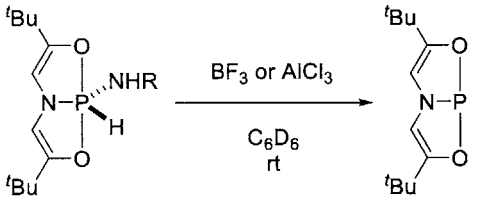

2.4 R = H
2.5a R = ^{n}Pr
2.5c R = Bn

2.3

Figure 2.10. N-H elimination of the phosphorane adducts.

Although no thermal N-H reductive elimination reactivity was observed for adducts **2.5**, treating phosphorane adducts **2.5** with Lewis acids gives the formal reductive elimination transformation (**Figure 2.10**). For example, adding five equivalents of boron trifluoride-diethyl etherate to a C_6D_6 solution of **2.4** results in the regeneration of **2.3** as the major product. The regeneration of **2.3** can also be observed in the reactions of **2.5a** and **2.5c** with boron trifluoride-diethyl etherate. Similarly, the reactions of aluminum trichloride and **2.4**, **2.5a** and **2.5c** result in conversion to **2.3** with little apparent decomposition.

In addition to Lewis acid-induced reductive elimination of amine, amine exchange was observed upon heating phosphorane adducts with an excess amount of an exogenous amine. In a sealed NMR tube, a C_6D_6 solution of 5 equiv of benzylamine and the propylamine adduct **2.5b** was heated at 80 °C for 24 h, during which time a complete conversion to benzylamine adduct **2.5c** was observed. In addition, the reverse reaction also gives complete conversion to **2.5b** when treating an excess amount of propylamine to **2.5c** under the same conditions (**Figure 2.11**). Although the mechanism of these exchanges has not been determined, the amine exchange of the phosphorane adducts is encouraging for the potential catalytic application of the N-H oxidative addition reactivity of **2.3**.

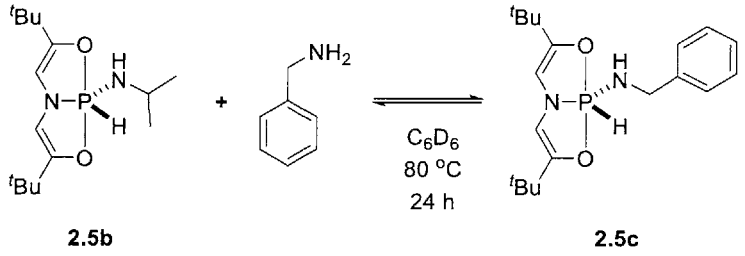

Figure 2.11. Amine exchange of the phosphorane adducts.

2.7 Mechanistic Analysis of the N-H Oxidative Addition Process[29]

Four possible mechanisms can be considered for the N-H oxidative addition to T-shape phosphine **2.3** (**Figure 2.12**). In the first possible mechanism, a phosphorus-ligand

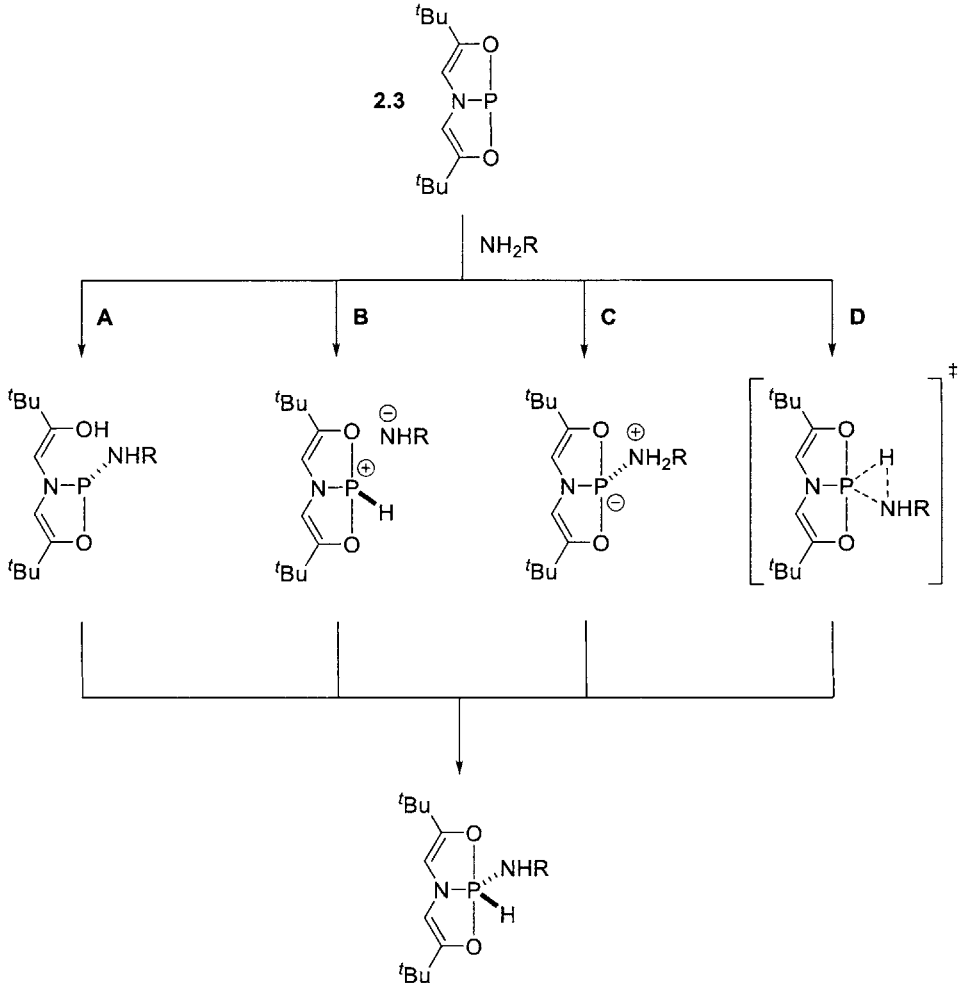

Figure 2.12. Possible Mechanisms for the N-H oxidative addition to phosphine **2.3**. (A) Ligand cooperative, (B) nucleophilic, (C) electrophilic, (D) concerted.

cooperative process (**Figure 2.12A**) proceeds through an initial N-H bond addition across the P-O bond and the resulting phosphacyclic intermediate. This phosphacyclic intermediate can then undergo an intramolecular O-H oxidative addition to yield the

phosphorane.[30] Metal-ligand cooperativity is generally accepted mechanism in bond activations by pincer-type transition metal species bearing similar O,N,O-ligand framework of **2.3**.[7, 31] Phosphorus-ligand cooperative mechanism appears to be a possible pathway due to the similar ligand structure with the pincer metal complexes and the detected phosphacyclic species in the oxidative addition of secondary amines. As discussed earlier in the chemistry of carbene-mediated N-H oxidative additions, stepwise mechanisms could involve either nucleophilic or electrophilic initiation steps. In an extreme case of the nucleophilic mechanism (**Figure 2.12B**), the nucleophilic phosphorus center might deprotonate the substrate N-H proton and generate a positively charged phosphorus center and an anionic amide. This ephemeral ion pair might then quickly collapse to the phosphorane product. However, with the low N-H bond acidity (pK_a = ~35-40)[5] and the reported poor nucleophilicity of the phosphorus center of **2.3**,[32] the nucleophilic mechanism seems unlikely for the N-H oxidative addition. The electrophilic mechanism (**Figure 2.3C**), on the other hand, is a more likely process because of the possible interaction of nucleophilic amine nitrogen HOMO with the distortion-induced low LUMO of T-shape phosphine **2.3**. In this electrophilic mechanism, the amine nitrogen might attack at the phosphorus center, producing a zwitterionic ammoniophosphoranide species with an acidified N-H proton. A following intramolecular proton transfer from nitrogen to phosphorus might then take place to give the formal oxidative addition product. In the last possible mechanism, a concerted three-centered mechanism (**Figure 2.12D**) involving the simultaneous cleavage of N-H bond and formation of the P-N and P-H bonds can be envisioned in analogy to well-established

reactivity in organometallic chemistry.[2] That said, this mechanism is more common for nonpolar substrates than for highly polarized bonds such as N-H. Therefore, the concerted mechanism is less likely to be involved in the N-H oxidative addition to phosphine **2.3** than other stepwise mechanisms.

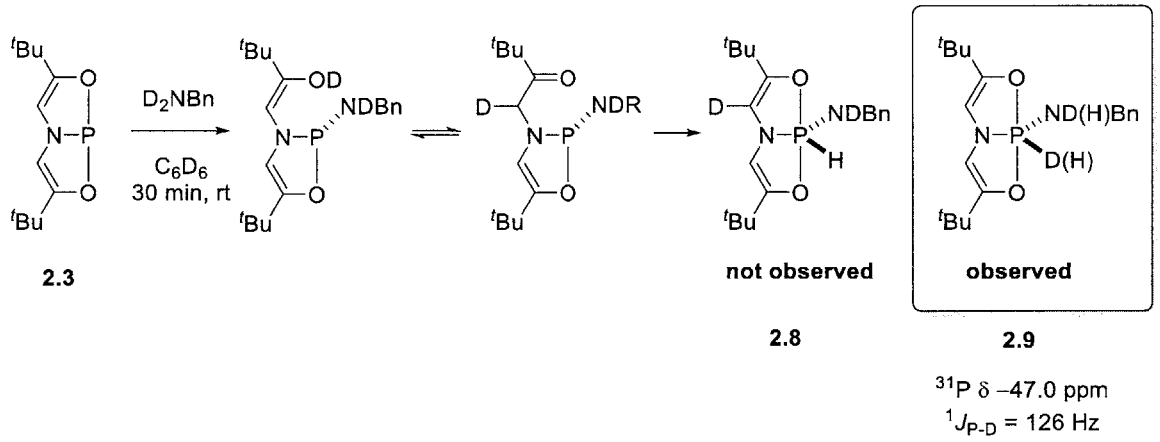

Figure 2.13. Oxidative addition of *N,N*-dideuterobenzylamine ($BnND_2$) to **2.3** without incorporation of the isotopic label at the vinylic position of the O, N, O-ligand backbone. Note: **2.9** is a mixture of isotopologues due to incomplete deuterium labeling of $BnND_2$.

2.7.1 Deuterium Labeling Study of N-H Oxidative Addition

Because of the observed phosphacyclic species in the oxidative addition of secondary amines (**Figure 2.6**), the phosphorus-ligand cooperative mechanism is considered a possible pathway for the N-H oxidative addition (**Figure 2.12A**). Due to the presumed enol intermediate and its rapid tautomerization in this mechanism, we

hypothesized that deuterium should be detected at the vinylic position of the O,N,O-supporting ligand in the P(V) adduct if a deuterium-labeled amine were used. Upon treatment of **2.3** to 5 equiv. of *N,N*-dideuterobenzylamine ($BnND_2$, 85% D) in C_6D_6, deuterium was detected only at phosphorus and nitrogen in the product **2.9** by ^{31}P and ^{2}H NMR (^{31}P δ −47.0 ppm, $^{1}J_{P\text{-}D}$ = 126 Hz; ^{2}H δ 8.95 ppm [1H, d, J = 824.7 Hz], 2.52 ppm [1H, s]) (**Figure 2.13**). Deuterium scrambling species (**2.8**) was not detected by ^{2}H NMR spectroscopy, indicating that the enol intermediate and phosphorus-ligand cooperative mechanism is not involved. Instead, a process with interactions localized only to the phosphorus center is more likely in the initial step of the transformation. Vanka[33] and Sakaki7 [34] recently investigated the phosphorus-ligand cooperative mechanism with computational methods. In their studies, a low energy pathway to formal oxidative addition with ligand assistance mechanism is suggested. However, we believe that a mechanism involving no ligand participation remains more convincing based on the direct experimental evidence presented above.

2.7.2 UV-Vis Spectra of Compound 2.3 and 2.5a for Kinetic Study

Due to the high reaction rate of the oxidative addition of *n*-propylamine to **2.3** (completed within 5 min. under pseudo-first order conditions), typical ^{1}H or ^{31}P NMR spectroscopy is not suitable methods for kinetic study. Therefore, UV absorption spectra of **2.3** and the *n*-propylamine adduct **2.5a** were recorded. Compound **2.3** exhibits UV absorption features at 313 nm ($\varepsilon = 7.9 \times 10^3$ $M^{-1}\cdot cm^{-1}$), 220 nm ($\varepsilon = 10.5 \times 10^3$ $M^{-1}\cdot cm^{-1}$),

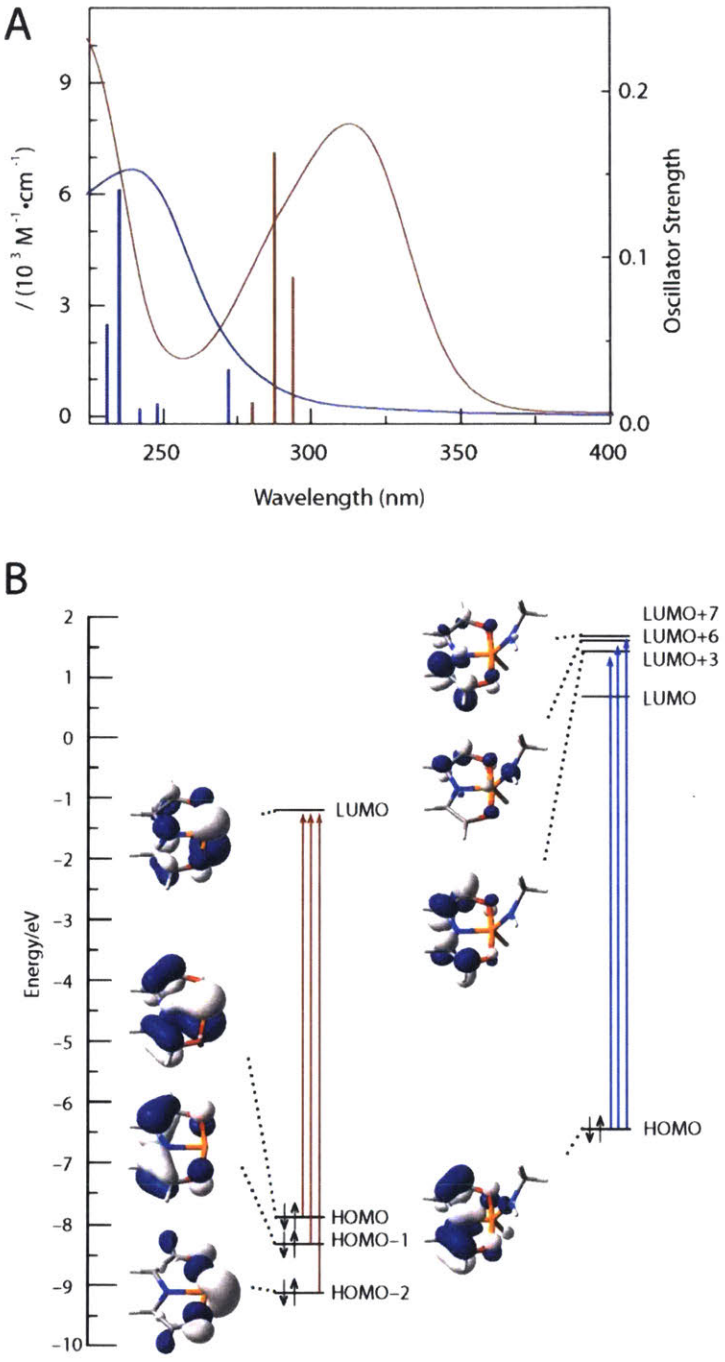

Figure 2.14. (A) Experimental absorption spectra for **2.3** (red line) and **2.5a** (blue line) superimposed with corresponding TDDFT (CAMB3LYP/6-311++G**) excited state transitions and oscillator strengths. (B) Molecular orbital isosurfaces and energies for models of **2.3** and **2.5a**. Reproduced with permission from *J. Am. Chem. Soc.* 2014, *136*, 4640.

and 207 nm (ε = 10.5 × 10^3 M^{-1}•cm^{-1}) (**Figure 2.14A**, red line). The oxidative addition product **2.5a** has a hypsochromically shifted lowest energy absorption at 239 nm (ε = 6.7 × 10^3 M^{-1}•cm^{-1}; **Figure 2.14A**, blue line) with minimal overlap with the lowest energy band of **2.3** centered at 313 nm. As a result, the progress of the reaction between **2.3** and *n*-propylamine could be followed by monitoring the decay of the absorption at λ = 313 nm. The excitation energies of **3.1** and **3.2a** could also be simulated with time-dependent DFT (TDDFT) calculations (CAMB3LYP/6-311++G**). The results indicate that the low energy band is dominated by $\pi \rightarrow \pi^*$ and nP $\rightarrow \pi^*$ electronic transitions and are in good agreement with the experimental UV absorption spectrum (**Figure 2.14B**).

2.7.3 Determination of Reaction Order in Phosphine 2.3 in Pseudo-First Order Condition

In order to obtain the reaction molecularity of **2.3** in the N-H oxidative addition transformation, kinetic studies were conducted under pseudo-first order conditions. A solution of **2.3** in pentane (0.27 M) was added to a septum-equipped screw top quartz cuvette sealed under inert atmosphere. Upon injection of a large excess of *n*-propylamine (2250 equiv.) at 25 °C, the reaction was completed within 60 s. A collection of spectra in the range 225 nm < λ < 400 nm every 5 s for 60 s shows clean conversion from **2.3** to **2.5a** without detectable intermediates or side products. An isosbestic point was found at λ = 272 nm (**Figure 2.15 A**), indicating that no secondary reactions are involved in the transformation.[35] Another experiment run under the same conditions using benzene as the

solvent while monitoring the decay at λ_{max} = 313 nm provided data for plots of [**2.3**] vs. time and ln[**2.3**] vs. time spectra consistent with pseudo-first order decay (**Figure 2.15 B**).

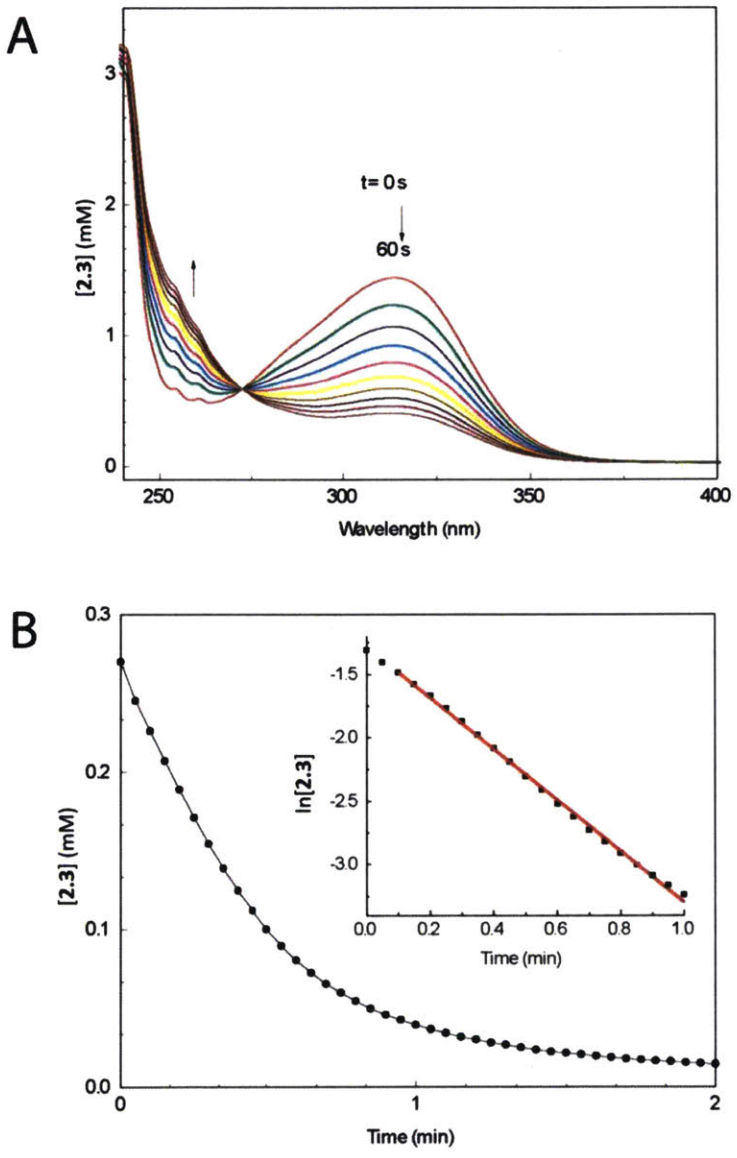

Figure 2.15. (A) Time stacked UV absorption spectra indicating consumption of **2.3** and formation of **2.5a** with time. An isosbestic point occurs at λ = 272 nm. (B) Plot of [**2.3**] vs time monitored at λ_{max} = 314 nm. (Inset) Plot of ln[2.3] vs time with linear least-squares fit. Reproduced with permission from *J. Am. Chem. Soc.* **2014**, *136*, 4640.

2.7.4 Determination of Reaction Order in Amine in Pseudo-First Order Condition

With the constant concentration of **2.3** in benzene (0.27 mM) at 25 °C, the reactions were monitored with various *n*-propylamine concentration in pseudo-first order conditions (14-2222 equiv. of *n*-propylamine). Surprisingly, plots of the observed rate constant k_{obs} vs. $[^{n}PrNH_2]$ and k_{obs} vs. $[^{n}PrNH_2]^2$ are both non-linear, suggesting a reaction rate law which is neither first nor second order in amine. However, the plot of k_{obs} against $[^{n}PrNH_2]^3$ exhibits a linear relationship (**Figure 2.16**, $R^2 = 0.9996$), indicating that a third order reaction in amine and an unusual rate law with high overall molecularity:

$$-\frac{d[\mathbf{2.3}]}{dt} = k_{obs}[\mathbf{2.3}] = k[\mathbf{2.3}][^{n}PrNH_2]^3$$

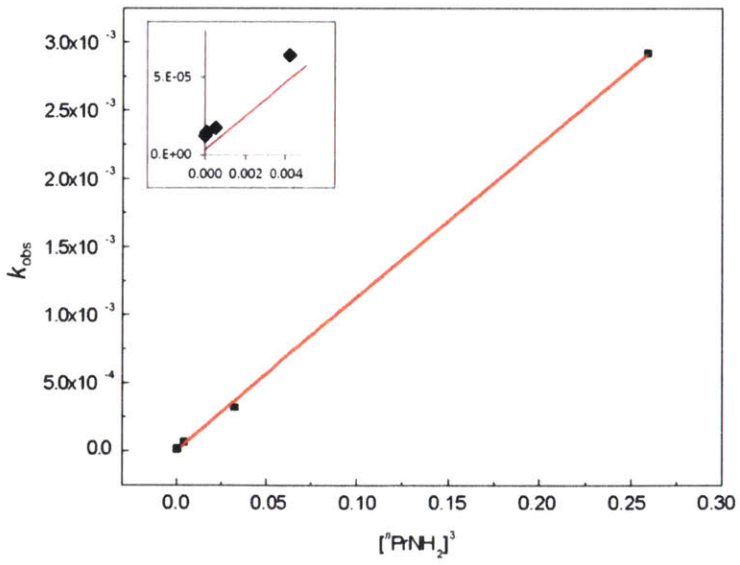

Figure 2.16. Plot of k_{obs} vs. $[^{n}PrNH_2]_3$ with linear least-squares fit (R^2 = 0.9996). Inset: Expansion of low concentration data points. Reproduced with permission from *J. Am. Chem. Soc.* **2014**, *136*, 4640.

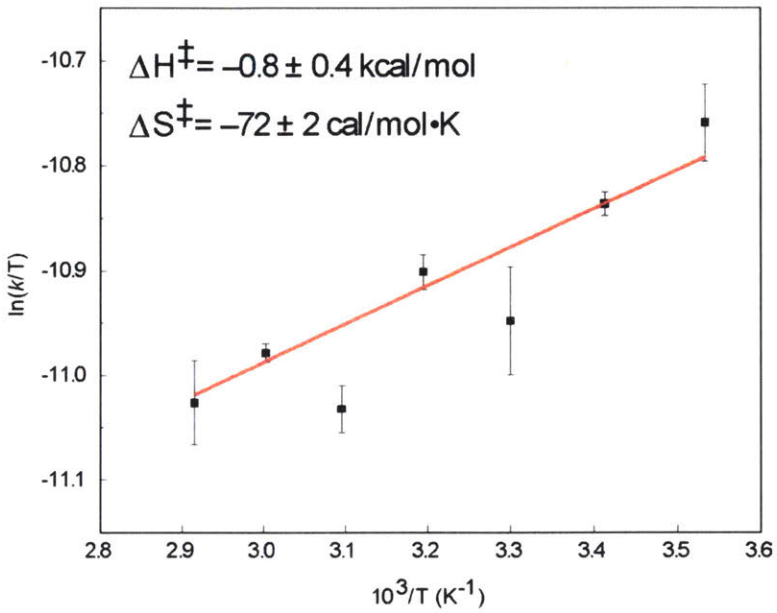

Figure 2.17. Eyring plot for kinetic data collected over the temperature range 10-70 °C. Reproduced with permission from *J. Am. Chem. Soc.* **2014**, *136*, 4640.

2.7.5 Eyring Plot for Activation Parameters

To find the activation enthalpy and entropy for the reaction, reactions between **2.3** (0.31 mM in benzene) and *n*-propylamine (2613 equiv.) were monitored at carried temperatures from 10 °C to 70 °C in 10 °C intervals. Interestingly, the observed reaction rate was found to decrease with increasing temperature. The Eyring plot derived from collected data provides activation parameters of $\Delta H^{\ddagger} = -0.8 \pm 0.4$ kcal/mol and $\Delta S^{\ddagger} = -72 \pm 2$ cal/mol•K (**Figure 2.17**). The highly negative activation entropy suggests the

existence of a high molecularity transition state which is agreement with the pseudo-first order experiments that a third order rate law in amine is involved. Although a reaction with a negative activation enthalpy is rare, examples of entropic-controlled transformations can be found in literature.[36]

2.8 DFT Investigation of the N-H Oxidative Addition[37]

The kinetic experiments discussed in the previous sections provide evidence for a high molecularity transition structure and large negative activation entropy, which confirm that a simple concerted mechanism for N-H oxidative addition to **2.3** is not involved in the transformation (**Figure 2.12 D**). To further assess the inviability of the concerted mechanism, DFT calculations were conducted to estimate the energetic barrier associated with the requisite three-centered transition structure (**Figure 2.18**). The calculated transition structure **TS-conc** (M062X, 6-311++G(2d,2p)) for the concerted N-H addition of methylamine to **2.3** was found to be significantly high in energy relative to the starting materials ($\Delta H^{\ddagger}$ = +50.1 kcal/mol). The magnitude of this barrier can be understood in the context of the valence bond configurational mixing framework,[38] where the large singlet-triplet gap for **2.3** (ΔE_{ST} = 62.6 kcal/mol) imposes a significant electronic barrier to direct, concerted oxidative addition. Together with the results from kinetics studies, these DFT calculations eliminate the concerted mechanism as a possible reaction pathway.

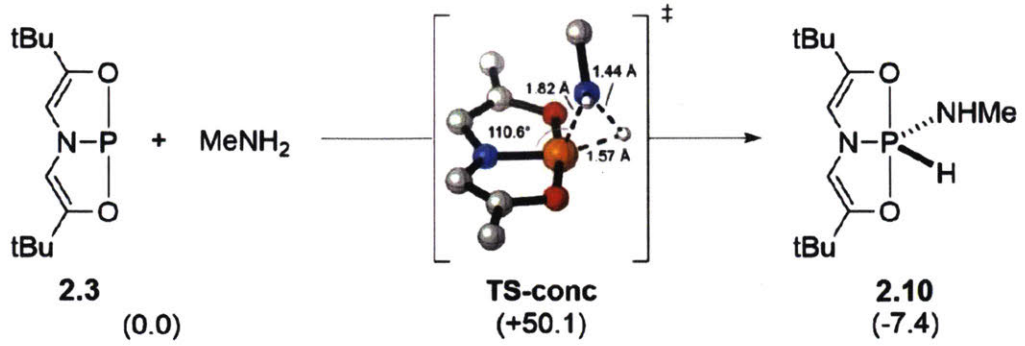

Figure 2.18. Concerted N-H oxidative addition to **2.3** with computed transition state structure. Computed enthalpies in parentheses in kcal/mol. Hydrogens and t-butyl methyl groups were omitted for clarity in TS-conc. Reproduced with permission from *J. Am. Chem. Soc.* **2014**, *136*, 4640.

DFT studies were also conducted for evaluating the proposed nucleophilic and electrophilic mechanisms (**Figure 2.12 B, C**). As discussed previously, the low N-H acidity of amines and the weak phosphorus nucleophilicity of **2.3** make the nucleophilic pathway (**Figure 2.12 B**) highly unlikely. Calculations performed on nucleophilic mechanism provide further confirmation that such a pathway is in fact energetically prohibitive. The relatively low energies of the occupied frontier orbitals of **2.3** (−7.5, −7.9, and −8.7 eV for HOMO, HOMO−1 and HOMO−2, respectively) as well as a large ionization potential (IP = 6.4 eV) suggest a high energetic barrier to phosphorus protonation. Additionally, a proton transfer from a single methylamine molecule is a prohibitively endothermic process (ΔH = 87.7 kcal/mol). This enthalpy decreases if additional amine molecules are included in the calculation, but not nearly enough to make

amine deprotonation thermodynamically viable. Based on these DFT calculation results, the nucleophilic mechanism may also be excluded from further consideration.

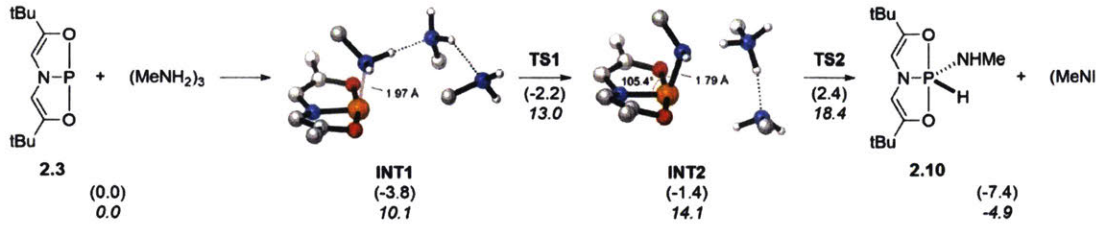

Figure 2.19. Calculated stepwise electrophilic reaction pathway for the N-H oxidative addition of methylamine to **2.3** (M06-2X/6-311++G(2d,2p)), with enthalpies in parentheses and free energies in italics in kcal/mol. Hydrogens and *t*-butyl methyl groups we omitted for clarity on INT1 and INT2. Reproduced with permission from *J. Am. Chem. Soc.* **2014**, *136*, 4640.

Compared to the nucleophilic mechanism, DFT calculations suggest that an initial nucleophilic interaction is a viable pathway in the transformation. Compound **2.3** is calculated to have a low lying LUMO (−1.0 eV) and a reasonably favorable electron affinity (EA = −2.2 eV), making the electrophilic interaction of the phosphorus center of **2.3** and the amine nitrogen possible (**Figure 2.12 C**). Indeed, a computed pathway initiated by amine attack at phosphorus center of **2.3** is found to be significantly more energetically favorable than the nucleophilic pathway. Attempts to locate a zwitterionic P-N adduct intermediate on the energy surface failed when using only one molecule of amine. However, the addition of two additional amine molecules allowed for the location of an adduct (**INT1**) with a P-N bond distance of 1.97 Å (**Figure 2.19**). Compared to

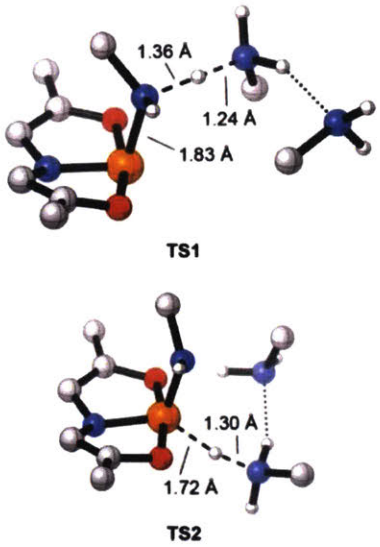

Figure 2.20. Transition structures along the stepwise electrophilic pathway for N-H oxidative addition to **2.3** with computed metrics. Hydrogens and *t*-butyl methyl groups were omitted for clarity. Reproduced with permission from *J. Am. Chem. Soc.* **2014**, *136*, 4640.

starting material **2.3**, **INT1** is 3.8 kcal/mol lower in enthalpy but the hydrogen bonding cluster of three amine molecules makes **INT1** 10.1 kcal/mol higher than **2.3** on the free energy surface. Amine-assisted deprotonation of the phosphorus-bound amine via **TS1** gives **INT2** as a phosphoranide anion and an amine-solvated proton. The energetic barrier to this initial step is relatively small, with $\Delta H^{\ddagger} = -2.2$ kcal/mol and $\Delta G^{\ddagger} = 13.0$ kcal/mol for **TS1**. Interestingly, the bond lengths found for P-N (1.83 Å) and N-H (1.36 Å) in **TS1** (**Figure 2.20**) are close to those calculated in the much higher energy **TS-conc** in the concerted pathway, suggesting that a significant stabilization from the assistance of the two additional amine molecules. Once **INT2** is formed, the ammonium cation pair undergoes a reorientation for the following protonation of the phosphoranide via **TS2**.

TS2 has a modest activation enthalpy of $\Delta H^{\ddagger} = 2.4$ kcal/mol, and is the maximum on the free energy surface with $\Delta G^{\ddagger} = 18.4$ kcal/mol. Therefore, this proton transfer step is the rate determining step in the transformation and its relatively high activation barrier is resulted from the entropic penalty associated with the organization of the amine hydrogen bonding network.

To conclude, the computed phosphorus-based electrophilic pathway for the N-H oxidative addition is consistent with the experimental kinetics study. From the calculation results, two additional amine molecules are needed for stabilizing the resulting positively charged species from the initial electrophilic interaction from phosphorus to amine, in good agreement with the observed third order molecularity of amine. Additionally, the highly ordered transition state structure rationalizes the entropy-dominated rate determining step derived from the Eyring plot. Although the calculated activation enthalpy is slightly positive ($\Delta H^{\ddagger}_{calc} = 2.4$ kcal/mol), this value is still reasonably close to the experimental value ($\Delta H^{\ddagger}_{expt} = -0.8 \pm 0.4$ kcal/mol).

2.9 Conclusion and Outlook

A rare example of well-characterized intermolecular N-H oxidative addition to a geometrically distorted phosphorus (III) center is presented in this chapter. The reactions of the T-shape phosphine and ammonia, alkyl and aryl amines through an unusual phosphorus-based electrophilic mechanism give stable hydrido amido phosphorane products. The stability of phosphorane products allows in-depth characterization via

NMR and X-ray diffraction for unambiguous confirmation of their identities and geometric structures. In addition to being a fundamentally interesting and largely unprecedented reaction, the discovered oxidative addition reaction provides important support for our hypothesis that geometry of phosphorus molecules can exert a strong influence on reactivity.

The experimental and computational results provide strong evidence for a highly unusual entropy-controlled mechanism for N-H oxidative addition to the T-shape phosphine. The mechanism involves a nucleophilic attack of amine to the tricoordinate phosphorus center followed by a rate determining proton transfer assisted by two additional amine molecules to give the product phosphorane. The direct N-H reductive elimination from the hydrido amido phosphorane was not observed even under forcing conditions, and the lack the reversibility of the transformation can be rationalized by the established reaction mechanism. Due to the necessity of proton shuttling by exogenous amine in the N-H oxidative addition, the principle of microscopic requires that reversed elimination reaction proceeds with the same pathway. Therefore, amine exchange of hydrido amido phosphorane can be achieved in the presence of exogenous amine while the reductive elimination from the isolated adducts is mechanistically prohibited. The understanding of this mechanism and the factors influencing this non-traditional P(III) reactivity should help future work both in leveraging the reactivity of the T-shape phosphine toward synthetically valuable transformations and more importantly, in the rational design of novel P(III) compounds capable of unprecedented reactivity.

2.10 Experimental

General Materials and Methods

All reagents were purchased through Sigma-Aldrich, Alfa Aesar, ACROS, TCI, or Oakwood Chemical, and used as received unless otherwise noted. Diethyl ether (Et_2O), methylene chloride (CH_2Cl_2), tetrahydrofuran (THF), and pentane were dried according to the method of Grubbs[39] as modified by Bergman[40] using a Glass Contour Solvent Purification System. Propylamine (99%) was purchased from Alfa Aesar and purified by vacuum distillation from zinc dust prior to use. Isopropylamine (≥99.5%) was purchased from Aldrich and purified by vacuum distillation from zinc dust. Benzylamine (98%) was purchased from Alfa Aesar and purified by vacuum distillation from zinc dust. 2,4,6-Trimethylaniline (98%) was purchased from Aldrich and purified by vacuum distillation from potassium hydroxide. 2,6-Diisopropylaniline (90+%) was purchased from Alfa Aesar and purified by vacuum distillation from potassium hydroxide. p-Anisidine (≥99%) was purchased from Aldrich and purified by recrystallization from ethanol. All glassware was oven-dried at 120 °C prior to use. All reactions were carried under dry nitrogen atmosphere (Schlenk line or glovebox) unless otherwise noted. NMR spectra were recorded on a Bruker AV-360 (360MHz), a Bruker AV-400 (400 MHz), a Bruker AV-500 (500MHz) or a VARIAN Inova-500 (500MHz) spectrometer. ^1H NMR chemical shifts are given in ppm with respect to solvent residual peak (C_6D_6, δ 7.16 ppm; $CDCl_3$, δ 7.26 ppm; CD_2Cl_2, δ 5.32 ppm), $^{13}C\{^1H\}$ NMR shifts are given in ppm with respect to $CDCl_3$ (δ 77.16 ppm), C_6D_6 (δ 128.06 ppm) or CD_2Cl_2 (δ 53.84 ppm). Coupling constants

are reported as *J*-values in Hz. High resolution EI and ESI mass spectra were obtained from the Mass Spectrometry Laboratory at the School of Chemical Sciences, University of Illinois at Urbana-Champaign.

Synthetic Procedures and Characterization Data

Phosphorus compound **2.3** was prepared by minor modification of the literature method according to the following sequence[22] (**Figure 2.21**):

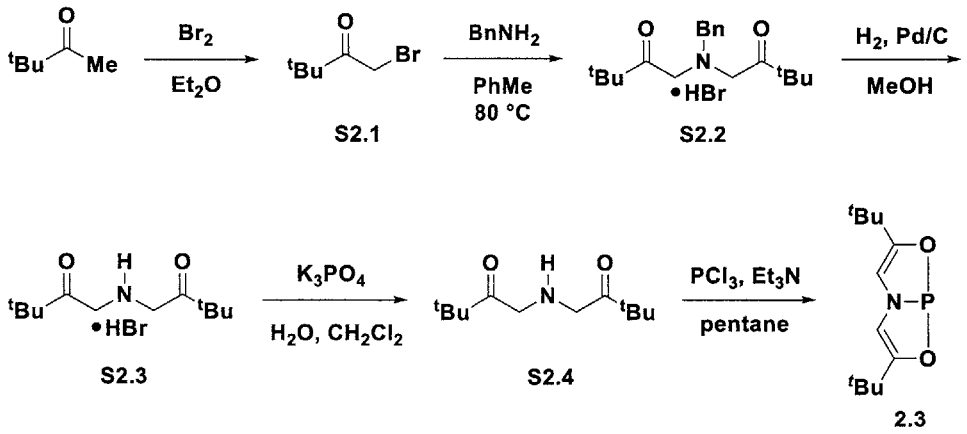

Figure 2.21. Multistep synthesis of phosphine **2.3**.

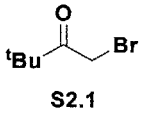
S2.1

To a ethyl ether of solution (80 ml) of pinacolone (50.0 g, 499 mmol) was added several drops of bromine at ambient temperature. The orange solution became colorless and was subsequently cooled in an ice bath. Bromine (26 mL, 499 mmol) was added dropwise over an hour, maintaining the internal temperature below 10 °C. The reaction mixture was stirred an additional 30 min, then 200 mL of water was

added and stirred for 15 min. The reaction mixture was warmed to room temperature and treated with solid sodium bicarbonate (42 g, 499 mmol) and the resulting phasic layers were separated. The ether layer was washed with brine (2x50 mL), dried (Na_2SO_4), and concentrated *in vacuo*. Purification by vacuum distillation yielded **S2.1** as a light yellow oil (78 g, 87%). ^{1}H NMR (300 MHz, $CDCl_3$): δ 4.18 (2H, s), 1.23 (9H, s) ppm.

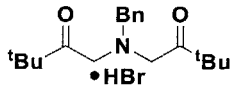

S2.2

To a toluene (900 ml) solution of **S2.1** (70.3 g, 393 mmol) was added benzylamine (43 mL, 339 mmol) in one portion. The reaction mixture was stirred at 80 °C for 48 h, during which time a voluminous white solid precipitated. The solid was collected on a Buchner funnel, washed with water (2x100 mL), and recrystallized in ethanol to give **S2.2** as a white crystalline solid (62 g, 82%). ^{1}H NMR (360 MHz, $CDCl_3$): δ 7.66 (2H, m), 7.46 (3H, m), 4.94 (2H, m), 4.72 (4H, m), 1.14 (18H, s) ppm.

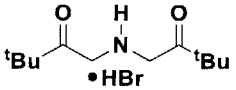

S2.3

To a suspension of **S2.2** (60.0 g, 150 mmol) in nitrogen-sparged methanol (500 mL) was added 10% palladium on carbon (600 mg, 0.6 mmol). The atmosphere was exchanged for hydrogen via three evacuation/backfill cycles. The heterogeneous mixture was stirred under H_2 (1 atm) for 24 hours. The reaction mixture was then filtered over celite and the filtrate was concentrated. Recrystallization of the crude solid product in ethanol gave **S2.3** as a white solid (40.5 g, 90%). ^{1}H NMR (360 MHz, $CDCl_3$): δ 4.31 (4H, s), 1.23 (18H, s) ppm.

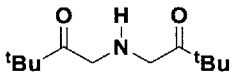

S2.4

A mixture of **S2.3** (30.0 g, 102 mmol), water (400 mL) and dichloromethane (300 mL) was cooled in an ice bath. An aqueous solution of tribasic potassium phosphate (26.0 g, 122 mmol, 270 mL, 0.46 M) was added dropwise over 30 minutes, then the solution was stirred for an additional 2 hours in an ice bath. The aqueous layer was extracted with dichloromethane (3x100 mL), then the dichloromethane extracts were washed with water (3x200 mL). The organic layer was dried (Na_2SO_4) and concentrated *in vacuo* to give **S2.4** as a yellow solid (16.0 g, 90%), which was stored at –30 °C prior to further use. ^{1}H NMR (400 MHz, $CDCl_3$): δ3.62 (4H, s), 2.83 (1H, br s), 1.15 (18H, s) ppm.

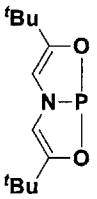

2.3

At –78 °C, a pentane solution (150 mL) of phosphorus (III) chloride (4.1 mL, 47 mmol) under nitrogen was added **S2.4** (10.0 g, 48 mmol) in pentane (130 mL) dropwise. After a pentane solution (100 mL) of triethylamine (20.5 mL, 147 mmol) was added dropwise, the resulting mixture was stirred at -78°C for 4 hours. The mixture was then warmed to room temperature and stirred for an additional 2 hours. The reaction mixture was concentrated to a residue *in vacuo* and transferred to a glovebox. The crude reaction residue was then triturated with pentane (200 mL) and filtered over celite. The filtrate was concentrated to give crude **2.3** and further recrystallization from pentane at –35 °C gives pure **1** as an yellow solid (4.6 g, 73%). ^{1}H NMR (400 MHz, $CDCl_3$): δ 7.40 (2H, d, *J*=9.6 Hz), 1.27 (18H, s) ppm. ^{31}P{^{1}H} NMR (145 MHz, $CDCl_3$): 187.7 ppm.

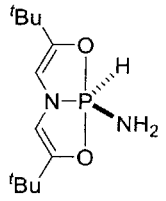

2.4

A nitrogen-flushed 25 mL round bottom flask equipped with a magnetic stirrer was charged with **2.3** (200 mg, 0.83 mmol). Ammonia (ca. 5 mL) was condensed into the flask cooled to −78 °C. The suspension was stirred at −78 °C for 30 min, and then warmed to room temperature to remove the excess ammonia, yielding **2.4** as a yellow solid (214 mg, 0.83 mmol, quantitative yield). ^{1}H NMR (360 MHz, C_6D_6) δ 8.79 (1H, d, J = 812 Hz), 5.35 (2H, d, J = 31 Hz), 1.98 (2H, d, J = 10 Hz), 1.12 (18H, s) ppm. ^{13}C NMR (90 MHz, C_6D_6): δ 149.6 (d, J = 3.6 Hz), 100.4 (d, J = 16.3 Hz), 31.9 (d, J = 3.6 Hz), 27.7 (s) ppm. ^{31}P NMR (145 MHz, C_6D_6): δ −43.5 (dtt, J = 813, 31, 10 Hz) ppm. HRMS (EI) calcd for [C12H23N2O2P]+, 258.14972; found, 258.15011. FT-IR (ATR): 3516, 3411, 3128, 2959, 2374, 1655, 1213 cm−1. Anal. Calcd (found) for C12H23N2O2P: C, 55.83 (55.68); H, 8.98 (8.71); N, 10.85 (10.51); P, 12.00 (12.35).

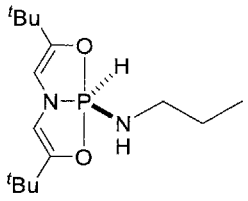

2.5a

To a solution of *n*-propylamine (85.0 μL, 1.05 mmol) in d_6-benzene (2 mL) was added **2.3** (50 mg, 0.21 mmol). The solution was transferred to a sealed J. Young NMR tube and allowed to stand at room temperature for 20 min. The volatile components were removed *in vacuo* to yield **2.5a** as a yellow solid (62 mg, 0.21 mmol, quantitative by NMR). ^{1}H NMR (300 MHz, C_6D_6) δ 8.87 (1H, d, J = 821.3 Hz), 5.42 (2H, d, J = 30.6 Hz) 2.82 (2H, qt, J = 7.3, 7.1 Hz), 2.22 (1H, dt, J = 12.5, 5.5), 1.24 (2H, ddt, J = 12.5, 7.1, 5.5 Hz), 1.16 (18H, s), 0.72 (3H, t, J = 7.3 Hz) ppm. ^{31}P NMR (146 MHz, C_6D_6): δ –45.85 (dtq, J = 821.3, 30.6, 12.5 Hz) ppm. ^{13}C NMR (91 MHz, C_6D_6): δ 149.4 (d, J = 3.6 Hz),

100.7 (d, J = 16.3 Hz), 43.5 (s), 32.1 (d, J = 2.6 Hz), 27.8 (s), 26.4 (d, J = 3.3 Hz), 11.2 (s) ppm. HRMS (ESI) calc'd for [C15H29N2O2P]+: 301.19667; found: 301.19580. FT-IR (ATR): 3436, 2959, 2871, 2372, 1655, 1215 cm-1.

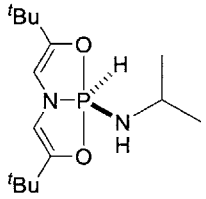

2.5b

To a solution of isopropylamine (85.0 μL, 1.05 mmol) in d_6-benzene (2 mL) was added **2.3** (50 mg, 0.21 mmol). The solution was placed in a sealed J. Young NMR tube and allowed to stand at room temperature for 20 min. The volatile components were removed in vacuo to yield **2.5b** (62 mg, 0.21 mmol, quantitative yield by NMR). Alternatively, compound **2.3** was dissolved in neat isopropylamine (2 mL) at ambient temperature for 1 h. Removal of the residual isopropylamine *in vacuo* yielded **2.5b** as a yellow solid. ^{1}H NMR (360 MHz, C_6D_6) δ 8.92 (1H, d, J = 819.0 Hz), 5.43 (2H, d, J = 30.6 Hz), 3.67 (1H, d septet d, J = 8.7, 6.3, 5.9 Hz), 2.14 (1H, dd, J = 11.2, 8.7 Hz) 1.17 (18H, s), 0.94 (6H, d, J = 6.3 Hz) ppm. $_{31}$P NMR (146 MHz, C_6D_6): δ –47.0 (dtdd, J = 819.4, 30.6, 11.2, 5.9 Hz) ppm. ^{13}C NMR (91 MHz, C_6D_6): δ 149.3 (d, J = 3.8 Hz), 100.5 (d, J = 16.4 Hz), 42.9 (s), 31.9 (d, J = 2.7 Hz), 27.6 (s), 25.9 (d, J = 5.6 Hz) ppm. HRMS (ESI) calc'd for [C15H29N2O2P]+: 301.19667; found: 301.19642. Anal. Calcd (Found) for C15H29N2O2P: C, 60.01 (59.61); H, 9.74 (9.68); N, 9.33 (9.26); P, 10.32 (10.83).

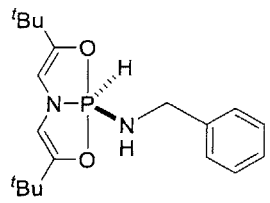

2.5c

To a solution of benzylamine (113.5 μL, 1.05 mmol) in d6-benzene (2 mL) was added **2.3** (50 mg, 0.21 mmol). The solution was transferred to a sealed J. Young NMR tube and allowed to stand at room temperature for 2 h. The volatile components were removed in vacuo to yield **2.5c** (72 mg, 0.21 mmol, quantitative yield by NMR). Alternatively, compound **2.3** was dissolved in neat benzylamine (2 mL) at ambient temperature for 1 h. Removal of residual benzylamine *in vacuo*, yielded **2.5c** as a yellow solid. ^{1}H NMR (360 MHz, C_6D_6) δ 8.95 (1H, d, J = 824.7 Hz), 7.18 (2H, dt, J = 7.0, 6.0 Hz), 7.11 (2H, t, J = 6.0 Hz), 7.01 (1H, t, J = 7.0 Hz), 5.44 (2H, d, J = 30.8 Hz), 4.12 (2H, dd, J = 12.7, 7.0 Hz), 2.52 (1H, dd, J = 13.3, 6.95 Hz), 1.09 (18H, s) ppm. ^{31}P NMR (146 MHz, C_6D_6): δ –46.4 (dttd, J = 823.6, 30.8, 13.3, 12.7 Hz) ppm. ^{13}C NMR (91 MHz, C_6D_6): δ 149.7 (d, J = 4.3 Hz), 142.3 (d, J = 4.5 Hz), 128.5 (s), 126.9 (s), 126.8 (s), 100.5 (d, J = 16.6), 45.7 (s), 32.1 (d, J = 3.1 Hz), 27.7 (s) ppm. HRMS (EI) calc'd for [C19H29N2O2P]+: 348.19667; found: 348.19721.

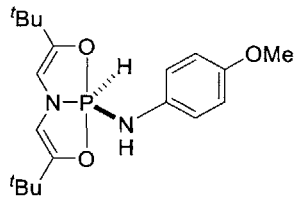

2.5d

To a solution of *p*-anisidine (258 mg, 2.10 mmol) in d6-benzene (2 mL) was added **2.3** (50 mg, 0.21 mmol). The solution was transferred to a sealed J. Young NMR tube and allowed to stand at room temperature for 12 h. Removal of the volatile components *in vacuo*, and purification by column chromatography under nitrogen atmosphere (neutral alumina, 12:1 pentane:CH_2Cl_2) yielded **2.5d** as an unstable solid. ^{1}H

NMR (360 MHz, C_6D_6) δ 9.08 (1H, d, J = 831.0 Hz), 6.92 (2H, d, J = 8.5 Hz), 6.65 (2H, d, J = 8.5 Hz), 5.45 (2H, d, J = 31.0 Hz), 4.14 (1H, d, J = 11.2 Hz), 3.26 (3H, s) 1.04 (18H, s) ppm. ^{31}P NMR (146 MHz, C_6D_6): δ −48.5 (dtd, J = 831.4, 31.5, 11.2 Hz) ppm. Instability precluded further characterization.

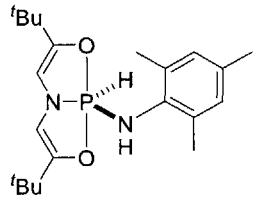

2.5e

To a solution of 2,4,6-trimethylaniline (106 mg, 0.78 mmol) in d_6-benzene (2 mL) was added **2.3** (200 mg, 0.83 mmol). The solution was transferred to a sealed J. Young NMR tube and heated to 55°C for 2 h. Removal of the volatile components *in vacuo*, and purification by column chromatography under nitrogen atmosphere (neutral alumina, 12:1 pentane:CH_2Cl_2) yielded **2.5e** as an off-white solid (110 mg, 35% yield). ^{1}H NMR (360 MHz, C_6D_6) δ 9.04 (1H, d, J = 839.0 Hz), 6.72 (2H, s), 5.41 (2H, d, J = 30.7 Hz), 3.43 (1H, d, J = 10.1 Hz), 2.27 (6H, s), 2.13 (3H, s), 0.97 (18H, s) ppm. ^{31}P NMR (146 MHz, C_6D_6): δ −48.7 (dtd, J = 839.3, 30.5, 10.2 Hz) ppm. ^{13}C NMR (91 MHz, C_6D_6): δ 150.0 (d, J = 4.0 Hz), 137.0 (d, J = 3.2 Hz), 135.5 (d, J = 3.7 Hz), 134.6 (d, J = 2.0 Hz), 100.2 (d, J = 15.5 Hz), 128.4 (s), 31.8 (d, J = 2.6 Hz), 27.3 (s), 20.7 (s), 19.0 (s) ppm. HRMS (ESI) calc'd for [C21H33N2O2P]+: 376.2358; found: 377.2351. Anal. Calcd (Found) for C21H33N2O2P: C, 67.04 (67.32); H, 8.84 (8.66); N, 7.45 (7.49); P, 8.23 (8.18).

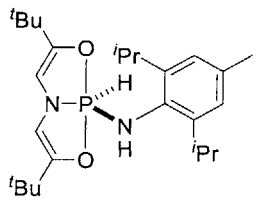

2.5f

To a solution of 2,6-diisopropylaniline (183 mg, 1.05 mmol) in d_6-benzene (2 mL) was added **2.3** (50 mg, 0.21 mmol). The solution was transferred to a sealed J. Young NMR tube and heated to 40°C for 16 h. Removal of the volatile components *in vacuo*, and purification by column chromatography under nitrogen atmosphere (neutral alumina, 12:1 pentane:CH2Cl2) yielded **2.5f** as an off-white solid (45 mg, 52% yield). ^{1}H NMR (300 MHz, C_6D_6) δ 9.11 (1H, d, J = 840.8 Hz), 7.03-7.16 (3H, m), 5.41 (2H, d, J = 30.7 Hz), 3.75 (1H, d, J = 9.7 Hz), 3.57-3.66 (2H, m), 1.20-1.37 (6H, m), 1.15 (6H, d, J = 6.8 Hz), 0.95 (18H, s) ppm. ^{31}P NMR (146 MHz, C_6D_6): δ −48.5 (dtd, J = 840.8, 30.6, 9.7 Hz) ppm. ^{13}C NMR (91 MHz, C_6D_6): δ 150.1 (d, J = 4.0 Hz), 147.7 (d, J = 3.2 Hz), 127.0 (d, J = 2.0 Hz), 123.4 (s), 123.1 (s), 100.5 (d, J = 15 Hz), 31.9 (s), 28.8 (s), 28.1 (d, J = 9.2 Hz), 27.3(s), 22.5(s) ppm. Anal. Calcd (Found) for C24H39N2O2P: C, 68.87 (68.95); H, 9.39 (9.10); N, 6.69 (6.72); P, 7.40 (7.57).

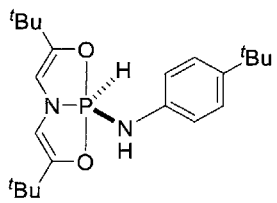

2.6a

To a solution of 4-*tert*-butylaniline (0.33 mL, 2.10 mmol) in d_6-benzene (2 mL) was added **2.3** (50 mg, 0.21 mmol). The solution was transferred to a sealed J. Young NMR tube and allowed to stand at room temperature for 12 h. Removal of the volatile components *in vacuo* yielded **2.6a** as an unstable solid (~50% conversion by ^{31}P NMR). 1H NMR (360 MHz, C_6D_6) δ 9.08 (1H, d, J = 831.0 Hz), 6.92 (2H, d, J = 8.5 Hz), 6.65 (2H, d, J = 8.5 Hz), 5.45 (2H, d, J = 31.0 Hz), 4.14 (1H, d, J = 11.2 Hz), 3.26 (3H, s) 1.04

(18H, s) ppm. ^{31}P NMR (146 MHz, C_6D_6): δ −48.6 (d, J = 835 Hz) ppm. Instability precluded further characterization.

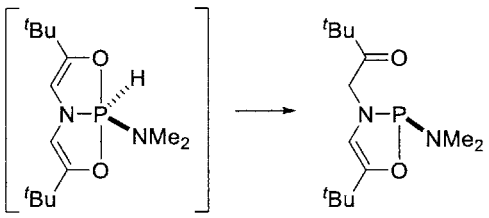

2.7a **2.7b**

A nitrogen-flushed 25 mL round bottom flask equipped with a magnetic stirrer was charged with **2.3** (200 mg, 0.83 mmol). Dimethylamine (ca. 5 mL) was passed through an anhydrous calcium sulfate column and condensed into the flask cooled to −78 °C. The suspension was stirred at −78 °C for 30 min, and then warmed to room temperature to remove the excess dimethylamine, yielding a mixture of crude **2.7a** and **2.7b** as a yellow solid (~80% total by 31P NMR). ^{31}P NMR (145 MHz, C_6D_6): δ −36.5 (d, J = 813 Hz) (**2.7a**); 130.1 (s) (**2.7b**) ppm. Instability precluded further characterization.

General procedure for Lewis acid-induced reductive elimination from adducts 2.4. To a solution of **2.4** (0.21 mmol) in d_6-benzene (2 mL) was added either boron trifluoride-diethyl etherate (0.13 mL, 1.05 mmol) or anhydrous aluminum trichloride (14 mg, 1.05 mmol). The solution was transferred to a sealed J. Young NMR tube and allowed to stand at room temperature for 30 m. In all cases, **2.3** was the only phosphorus-containing species detected by ^{31}P NMR after 30 m.

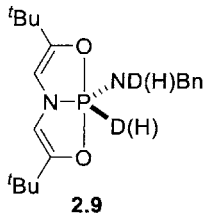

2.9

To a solution of *N,N*-dideuterobenzylamine (68.1 μL, 0.63 mmol, 83% deuteration) in d_6-benzene (2 mL) was added **2.3** (50 mg, 0.21 mmol). The solution was transferred to a sealed J. Young NMR tube and allowed to stand at room temperature for 2 h. The volatile components were removed in vacuo to yield **2.9** (72 mg, 0.21 mmol, 65% deuteration). ^{1}H NMR (360 MHz, C_6D_6): δ 7.18 (2H, dt, J = 7.0, 6.0 Hz), 7.11 (2H, t, J = 6.0 Hz), 7.01 (1H, t, J = 7.0 Hz), 5.44 (2H, d, J = 30.8 Hz), 4.12 (2H, dd, J = 12.7. 7.0 Hz), 1.09 (18H, s) ppm. ^{31}P NMR (146 MHz, C_6D_6): **2.9a** (**2.3**•[D][NDBn]) δ –47.0 (ttt, J = 125.8, 30.8, 12.6 Hz), **2.9b** (**2.3**•[D][NHBn]) (δ -46.87, tttd, J = 125.8, 30.8, 12.6, 13.3 Hz); **2.9c** (**2.3**•[H][NDBn]) (δ -46.50, dtt, J = 824.7, 30.8, 12.6 Hz); **2.9d** (**2.3**•[H][NHBn]) (δ -46.41, dttd, J = 824.7, 30.8, 12.6, 13.3 Hz), ppm. ^{13}C NMR (91 MHz, C_6D_6): δ 149.7 (d, J = 4.3 Hz), 142.3 (s), 128.5 (s), 126.9 (s), 126.8 (s), 100.5 (d, J = 16.6), 45.7 (s), 32.1 (d, J = 3.1 Hz), 27.7 (s) ppm. ^{2}H NMR (61 MHz, C_6D_6): δ 8.95 (1H, d, J = 824.7 Hz), 2.52 (1H, s) ppm.

Kinetics Experimental Procedures

All kinetics experiments were conducted on the oxidative addition reaction of *n*-propylamine to **2.3** (**Figure 2.22**). Compound **2.3** was recrystallized from pentane three times then stored in a nitrogen-filled glovebox before use. *n*-Propylamine was distilled twice from zinc dust then stored in a nitrogen-filled glovebox before use. Benzene and

pentane were dried by passage over an activated alumina column, stirring overnight over a mixture of K_2CO_3 and molecular sieves, and filtration through basic alumina.

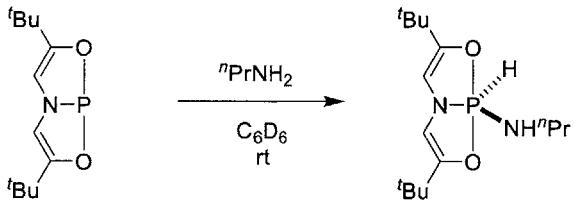

2.3 2.5a

Figure 2.22. Oxidative addition of *n*-propylamine to **2.3**.

Time-stacked UV-vis spectra (Figure 2.15 A). Measurements were performed on a Hewlett-Packard 8453 spectrophotometer with a Hewlett-Packard 8909DA peltier-thermostatted cuvette holder. A stock solution of compound **2.3** (3 mL, 0.27 mM in pentane) was added to a screw-top quartz cuvette (1 cm pathlength) fitted with a threaded septum. An initial UV-vis absorbance spectrum (225 nm < λ < 400 nm) was recorded. *n*-Propylamine (0.2 mL, 2250 equiv.) was then added via syringe and spectra were collected at 5 s intervals over the course of 1 min. The spectra (Figure 3.4) show the consumption of 1 (λmax = 313 nm) and an increase in absorbance at lower wavelengths consistent with the formation of **2.5a** (the absorbance maximum of **2.5a** (λmax = 239 nm) is obscured by the tail from the excess $^nPrNH_2$). An isosbestic point is evident at λ = 272 nm.

Pseudo-first order kinetics (Figure 2.15 B). Measurements were performed on a Hitachi Digilab U-3010 spectrophotometer equipped with a cuvette holder thermostatted

by a VWR 1140S water circulator. A stock solution of compound **2.3** (3 mL, 0.31 mM in benzene) was added to a screw-top quartz cuvette (1 cm pathlength) fitted with a threaded septum. The cuvette was placed in the temperature controlled spectrometer cell holder (25 °C) and allowed to thermally equilibrate for 10 min. Absorbance data were then collected at λ = 314 nm for ca. 15 seconds to establish a t = 0 baseline value. *n*-propylamine (0.2 mL, 2250 equiv.) was then added via syringe and spectra were collected at 0.2 s intervals over the course of 500 s.

Determination of reaction order in amine (Figure 2.16). Measurements were performed on a Hitachi Digilab U-3010 spectrophotometer equipped with a cuvette holder thermostatted by a VWR 1140S water circulator. A stock solution of compound **2.3** (3 mL, 0.31 mM in benzene) wasadded to a screw-top quartz cuvette (1 cm pathlength) fitted with a threaded septum. The cuvette was placed in the temperature controlled spectrometer cell holder (25 °C) and allowed to thermally equilibrate for 10 min. Absorbance data were then collected at λ = 314 nm for ca. 15 seconds to establish a t = 0 baseline value. *n*-Propylamine solutions of varying concentrations (0.2 mL, 0.06 to 10.33 M, 14 to 2222 equiv.) were then added via syringe and spectra were collected at 0.2 s intervals over the course of 500 s. The observed pseudo-first order rate constant (k_{obs}) was extracted from an average of three independent runs at each concentration. The raw data is available in Appendix A.

Eyring kinetics (Figure 2.17). Measurements were performed on a Hitachi Digilab U-3010 spectrophotometer equipped with a cuvette holder thermostatted by a VWR 1140S water circulator. A stock solution of compound **2.3** (3 mL, 0.31 mM in benzene) was added to a screw-top quartz cuvette (1 cm pathlength) fitted with a threaded septum. The cuvette was placed in the temperature controlled spectrometer cell holder and allowed to thermally equilibrate for 10 min to a series of temperatures (10 to 70 ^{0}C). Absorbance data were then collected at λ = 314 nm for ca. 15 seconds to establish a t = 0 baseline value. *n*-propylamine (0.2 mL, 2613 equiv.) was then added via syringe and spectra were collected at 0.2 s intervals over the course of 500 s. The observed pseudo-first order rate constant (k_{obs}) was extracted from an average of three to six independent runs at each temperature. The raw data is available in Appendix A.

2.11 References

[1] McCarthy, S. M.; Lin, Y.-C.; Devarajan, D.; Chang, J. W.; Yennawar, H. P.; Rioux, R. M.; Ess, D. H.; Radosevich, A. T. *J. Am. Chem. Soc.* **2014**, *136*, 4640.

[2] Hartwig, J.F. *Organotransition Metal Chemistry*; University Science Books: Sausalito, CA, 2010.

[3] Haggin, J. *Chem. Eng. News* **1993**, *71*, 23.

[4] (a) Bordwell, F. G.; Zhang, X. M.; Cheng, J. P. *J. Org. Chem.* **1993**, *58*, 6410. (b) Jursic, B. S. *J. Chem. Soc., Perkin Trans. 2* **1999**, 0, 369. (c) Wright, J. S.; Ingold, K. U. *J. Chem. Educ.* **2000**, *77*, 1062.

[5] Bordwell, F.G.; Drucker, G.E.; Fried, H.E. *J. Org. Chem.* **1981**, *46*, 632.

[6] Fafard, C. M.; Adhikari, D.; Foxman, B. M.; Mindiola, D. J.; Ozerov, O. V. *J. Am. Chem. Soc.* **2007**, *129*, 10318.

[7] (a) Gunanathan, C.; Milstein, D. *Acc. Chem. Res.* **2011**, 44, 588. (b) van der Vlugt, J. I.; Reek, J. N. H. *Angew. Chem., Int. Ed.* **2009**, 48, 8832. (c) van der Vlugt, J. I. Eur. *J. Inorg. Chem.* **2012**, 2012, 363. (d) Brown, R. M.; Borau Garcia, J.; Valjus, J.; Roberts, C. J.; Tuononen, H. M.; Parvez, M.; Roesler, R. *Angew. Chem., Int. Ed.* **2015**, 54, 6274. (e) Gutsulyak, D. V.; Piers, W. E.; Borau-Garcia, J.; Parvez, M. *J. Am. Chem. Soc.* **2013**, 135, 11776. (f) Chang, Y. H.; Nakajima, Y.; Tanaka, H.; Yoshizawa, K.; Ozawa, F. *J. Am. Chem. Soc.* **2013**, 135, 11791−11794. (g) Khaskin, E.; Iron, M. A.; Shimon, L. J. W.; Zhang, J.; Milstein, D. *J. Am. Chem. Soc.* **2010**, 132, 8542. (h) Kimura, T.; Arita, H.; Ishiwata, K.; Kuwata, S.; Ikariya, T. *Dalton Trans.* **2009**, 2912.

[8] (a) Casalnuovo, A. L.; Calabrese, J. C.; Milstein, D. *Inorg. Chem.* **1987**, 26, 971-973. (b) Koelliker, R.; Milstein, D. *Angew. Chem. Int. Ed. Engl.* **1991**, *30*, 707. (c) Schulz, M.; Milstein, D. *J. Chem. Soc., Chem. Commun.* **1993**, 3, 318.

[9] (a) Zhao, J.; Goldman, A. S.; Hartwig, J. F. *Science* **2005**, 307, 1080. (b) Huang, Z.; Zhou, J.; Hartwig, J. F. *J. Am. Chem. Soc.* **2010**, *132,* 11458.

[10] Morgan, E.; MacLean, D. F.; McDonald, R.; Turculet, L. *J. Am. Chem. Soc.* **2009**, 131, 14234.

[11] Sykes, A. C.; White, P.; Brookhart, M. *Organometallics* **2006**, *25*, 1664.

[12] Hulley, E. B.; Bonanno, J. B.; Wolczanski, P. T.; Cundari, T. R.; Lobkovsky, E. B. *Inorg. Chem.* **2010**, *49*, 8524.

[13] Frey, G.D.; Lavallo, V.; Donnadieu, B.; Schoeller, W.W.; Bertrand, G. *Science* **2007**, *316*, 5823.

[14] (a) Moerdyk, J.P.; Blake, G.A.; Chase, D.T.; Bielawski, C.W. *J. Am. Chem. Soc.* **2013**, *135*, 18798. (b) Hudnall, T.W.; Moerdyk, J.P.; Bielawski, C.W. *Chem. Commun.* **2010**, *46*, 4288.

[15] Hudnall, T. W.; Moorhead, E. J.; Gusev, D. G.; Bielawski, C. W. *J. Org. Chem.* **2010**, 75, 2763.

[16] (a) Jana, A.; Objartel, I.; Roesky, H.W.; Stalke, D. *Inorg. Chem.* **2008**, *48*, 798. (b) Jana, A.; Schulzke, C.; Roesky, H.W. *J. Am. Chem. Soc.* **2009**, *131*, 4600.

[17] Peng, Y.; Guo, J-D.; Ellis, B.D.; Zhu, Z.; Fettinger, J.C.; Nagase, S.; Power, P.P. *J. Am. Chem. Soc.* **2009**, *131*, 16272.

[18] (a) Kostina, S.S.; Singh, T.; Leigh, W.J. *J. Phys. Org. Chem.* **2011**, *24*, 937. (b) Protchenko, A.V.; Bates, J.I.; Saleh, L.M.A.; Blake, M.P.; Schwarz, A.D.; Kolychev, E.L.; Thompson, A.L.; Jones, C.; Mountford, P.; Aldridge, S. *J. Am. Chem. Soc.* **2016**, *138*, 4555.

[19] Dunn, N.L.; Ha, M.; Radosevich, A.T. *J. Am. Chem. Soc.* **2012**, *134*, 11330.

[20] Kühl, O. *Phosphorus-31 NMR Spectroscopy: A Concise Introduction for the Synthetic Organic and Organometallic Chemist;* Springer-Verlag: Berlin, 2008.

[21] Ross, M.R.; Martin, J.C. *J. Am. Chem. Soc.* **1981**, *103*, 1234.

[22] Arduengo, A.J.; Stewart, C.A.; Davidson, F.; Dixon, D.A.; Becker, J.Y.; Culley, S.A.; Mizen, M.B. *J. Am. Chem. Soc.* **1987**, *109*, 627.

[23] Hoffmann, R.; Howell, J.M.; Muetterties, E.L. *J. Am. Chem. Soc.* **1972**, *94*, 3047.

[24] In collaboration with Dr. Ji Woong Chang and Prof. Rob Rioux, Department of Chemical Engineering, The Pennsylvania State University.

[25] In collaboration with Dr. Deepa Devarajan and Prof. Dan Ess, Department of Chemistry. Brigham Young University.

[26] Bentrude, W. G.; Kawashima, T.; Keys, B. A.; Garroussian, M.; Heide, W.; Wedegaertner, D. A. J. *Am. Chem. Soc.* **1987**, *109*, 1227.

[27] Fowell, P.A.; Mortimer, C.T. *J. Chem. Soc.* **1959**, 2913.

[28] Fleig, H.; Becke-Goehring, M.Z. *Anorg. Allg. Chem.* **1970**, *376*, 215.

[29] All kinetic studies was conducted by Sean McCarthy.

[30] (a) Burgada, R.; Houalla, D.; Wolf, R. *C. R. Seances Acad. Sci., Ser. C* **1967**, *264*, 356. (b) Bernard, D.; Laurenco, C.; Burgada, R. *J. Organomet. Chem.* **1973**, *47*, 113. (c) Houalla, D.; Sanchez, M.; Wolf, R. *Tetrahedron Lett.* **1978**, 4675. (d) Wolf, R. *Pure Appl. Chem.* **1980**, *52*, 1141.

[31] Benito-Garagorri, D.; Kirchner, K. *Acc. Chem. Res.* **2008**, *41*, 201.

[32] Arduengo, A.J.; Stewart, C.A.; Davidson, F.; Dixon, D.A.; Becker, J.Y.; Culley, S.A.; Mizen, M.B. *J. Am. Chem. Soc.* **1987**, *109*, 627.

[33] Pal, A.; Vanka, K. *Inorg. Chem.* **2016**, *55*, 558.

[34] (a) Zeng, G.; Maeda, S.; Taketsugu, T.; Sakaki, S. *ACS Catal.* **2016**, *6*, 4859. (b) Zeng, G.; Maeda, S.; Taketsugu, T.; Sakaki, S. *J. Am. Chem. Soc.* **2016**, *138*, 13481.

[35] IUPAC. *Compendium of Chemical Terminology*, 2nd ed. Compiled by McNaught, A.D. and Wilkinson, A., Blackwell Scientific Publications, Oxford, 1997.

[36] (a) Kisalev, V.; Miller, J. *J. Am. Chem. Soc.* **1975**, *97*, 4036. (b) Turro, N.J.; Lehr, G.F.; Butcher, J.A; Moss, R.A.; Guo, W. *J. Am. Chem. Soc.* **1982**, *104*, 1754. (c) Turro, N.J.; Hrovat, D.A.; Gould, I.R.; Padwa, A.; Dent, W.; Rosenthal, R.J. *Angew. Chem., Int. Ed. Engl.* **1983**, *22*, 625. (d) Houk, K.N.; Rondan, N.G. *J. Am. Chem. Soc.* **1984**, *106*, 4293. (e) Kapinus, E.I.; Rau, H. *J. Phys. Chem. A.* **1998**, *102*, 5569.

[37] In collaboration with Dr. Deepa Devarajan and Prof. Dan Ess at Brigham Young University.

[38] Pangborn, A.B.; Giardello, M.A.; Grubbs, R.H.; Rosen, R.K.; Timmers, F.J. *Organometallics* **1996**, *15*, 1518.

[39] Pangborn, A. B.; Giardello, M. A.; Grubbs, R. H.; Rosen, R. K.; Timmers, F. J. *Organometallics* **1996**, *15*, 1518.

[40] Alaimo, P. J.; Peters, D. W.; Arnold, J.; Bergman, R. G. *J. Chem. Ed.* **2001**, *78*, 64.

Chapter Three. Phosphorus-ligand Cooperative B-H Activation and Catalytic Hydroboration by a C_s- Symmetric N,N,N-σ^3-Phosphorus Molecule

A significant portion of the work described in this chapter has been published in:

Lin, Y.-C.; Hatzakis, E.; McCarthy, S. M.; Reichl, K. D.; Lai, T.-Y.; Yennawar, H. P.; Radosevich, A. T. *J. Am. Chem. Soc.* **2017**, *139*, 6008.

Chapter Three

Phosphorus-ligand Cooperative B-H Activation and Catalytic Hydroboration by a C_s- Symmetric N,N,N- σ^3-Phosphorus Molecule

The investigation of the N-H oxidative addition reactivity of the T-shape O,N,O-phosphine discussed in the previous chapter offers valuable insight into the impact of geometric distortion on electronic structure and reactivity of σ^3-phosphorus molecules. The study demonstrates significant agreement with our hypothesis that a phosphine with low nucleophilicity and electrophilic reactivity can be obtained as its molecular symmetry transforms from traditional pyramidal to planar. However, it remained unclear whether the unique reactivity is limited only to the planar geometry or can also be realized with other geometries. As exemplified in Chapter 1 with simpler molecules, we envisioned that similar or more drastic electronic and reactivity changes might be associated with other modes of geometry distortion. Since the O,N,O-chelating framework appeared to be essential to the formation of the planar structure, substitution of chelating atoms may offer opportunities in creating phosphines with novel molecular structures and reactivity. To address these questions, our group has recently designed an N,N,N-chelated phosphine bicycle with C_s-symmetry and demonstrated its reactivity in reversible O-H and N-H activation.[1] Inspired by our study of the *Cs*-symmetric N,N,N-phosphine, this chapter will focus on the studies of distortion-induced B-H activation

reactivity of the *Cs*-symmetric N,N,N-phosphine and its application in catalytic hydroboration.

3.1 Geometry, Electronic Structure and Reactivity of the C_s-symmetric N,N,N-Phosphorus Molecule

Although the T-shape phosphine described in the previous chapter displays fascinating N-H oxidative addition reactivity through a non-canonical electrophilic mechanism, extending this reactivity to further synthetic applications is limited by the lack of reversible bond activation reactivity.[2] This lack of reversibility can be rationalized by the proposed mechanism that requires exogenous amines for proton shuttling. To overcome the challenge associated with reversible bond addition/elimination, a novel phosphine compound designed to operate bond activation via an alternative mechanism is required.

The intermolecular N-H oxidative addition reactivity of the T-shape phosphine compound **3.1** results from its unique structure (**Figure 3.1**). In addition to causing lowering of the LUMO energy level and significant perturbation in electronic structure, the planar structure can be viewed as a trigonal bipyramidal geometry with two equatorial vacant sites available for additional bonding. The *cis*-divacant trigonal bipyramidal structure minimizes the energetic penalty associated with the geometric reorganization

during the transformation from phosphine to trigonal bipyramidal σ^5-phosphorus molecules. For the similar reason, we imagined that if the planar geometry of a phosphine **3.1** were further modified and become closer to trigonal pyramidal geometry, the energy barrier of P(V) reductive elimination and P(III) formation may be reduced (**Figure 3.1**). Also, replacing the ligand oxygens of **3.1** with more basic nitrogen atoms might transform the E-H activation mechanism from the exogenous amine-assisted process to an intramolecular ligand-assisted pathway, in which the ligand nitrogens acting as the built-in proton shuttles and make the E-H elimination possible in the absence of exogenous amine.

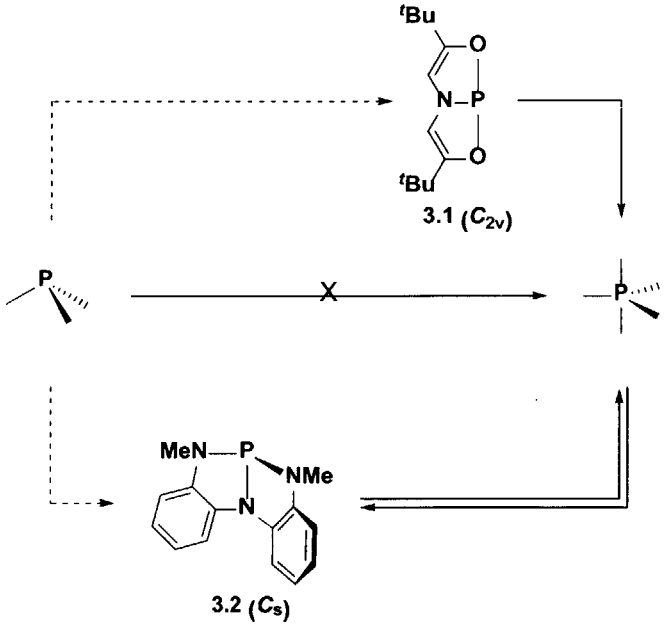

Figure 3.1. Design of phosphine **3.2** with fine-tuned geometry that benefits P(III) regeneration.

With this concept in mind, our group has recently reported the preparation and reactivity of geometrically deformed phosphorous triamide **3.2** (**Figure 3.1**, *bottom*). X-ray crystallography reveals that solid state structure of **3.2** has a significant folding along the central P-N axis (**Figure 3.2**) and the N-P-N bond angles between proximal nitrogens are nearly right-angled and roughly equivalent (∠N1-P-N2 = 90.51(6)°, ∠N1-P-N3 = 90.08(6) °). While the N-P-N angle between distal nitrogen atoms is much larger (∠N2-P-N3 = 115.21(7)°), the distal P-N bonds are nearly same in length (P-N2 = 1.7014(1) Å, P-N3 = 1.7190(1) Å) and shorter than the central P-N bond (P-N1 = 1.7610(1) Å). To conclude, X-ray crystallography indicates that the P(III) triamide **3.2** adopts a C_s-symmetric geometry which efficiently retains the beneficial low σ^3- σ^5 reorganization

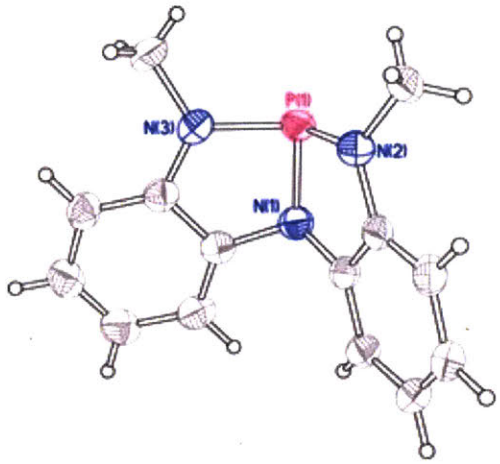

Figure 3.2. Molecular structure of phosphine **3.2**. Thermal ellipsoid plot rendered at 50% probability level. Reproduced with permission from *J. Am. Chem. Soc.* **2014**, *136*, 17634.

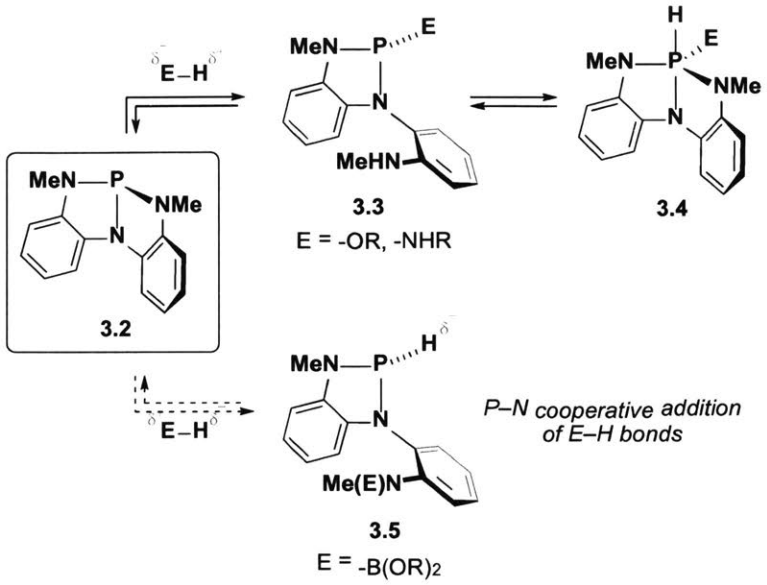

Figure 3.3. The reactivity of phosphine **3.2**. (Top) Phosphorus–ligand cooperative addition of protic E–H substrates to 1. (Bottom) Regioisomeric phosphorus–ligand cooperative addition of hydridic E–H to **3.2**.

barrier as phosphine **3.1** while having a less severe distortion from P(III) C_{3v} geometry.

Phosphine **3.2** was found to undergo rapid edge inversion through a C_2 symmetric planar transition state and an unusually low barrier, suggesting conformational flexibility between its bent ground state and a metastable planar geometry. In common with the previously studied planar O,N,O-chelated phosphine **3.1**, C_s-symmetric **3.2** also exhibits an anomalously low nucleophilic reactivity. Different from traditional phosphines, compound **3.2** demonstrates biphilic reactivity and reacts with E–H bonds (E = -OR, -NHR) on the phosphorus center with a reversible oxidative addition–reductive

elimination process. Mechanistically, we have shown that the formal oxidative addition process operates in a stepwise phosphorus–ligand cooperative mechanism (**Figure 3.3** *top*), wherein the protic E–H substrate reacts initially with one of the **3.2** axial P–N linkages to give a σ^3-phosphorus intermediate **3.3**, in which a new P–E bond is formed and the resultant proton is accommodated on a methylanilide nitrogen. Subsequent intramolecular $\sigma^3 \rightarrow \sigma^5$ ring–chain tautomerism then affords the overall oxidative addition product **3.4**.

Inspired by the previous studies, we envisioned the alternative reactivity from the same phosphorus–ligand cooperative activation but with formally hydridic E–H substrates such as boranes (**Figure 3.3** *bottom*). Inverted regioselectivity for the E–H addition to **3.2** could be expected due to the opposite substrate polarization, leading to the hydride-phosphorus interaction and the migration of attendant E^+ fragment to the ligand methylanilide nitrogen. This alternative mode of activation would result in the formation of a P-hydrido-1,3,2-diazaphospholene **3.5**, a class of compounds that Gudat [3] has reported to exhibit significant hydridic reactivity due to the strong electronic interaction between P-H σ^* orbital and the neighboring phosphacyclic nitrogen lone pairs. We aimed to investigate this phosphorus–ligand cooperative E-H activation reactivity and explore the potential catalytic E–H transfer results from the combination of the reactivity of intermediate **3.5** and subsequent E^+ group transfer from the pendant N-methylanilide.

In the following sections, we present the phosphorus–ligand cooperative reactivity for borane B–H addition to C_s-symmetric phosphine **3.2**. We also demonstrate

that the B-H activation can be further utilized to catalytic imine hydroboration. Through spectroscopic and kinetic analyses, the phosphorus–ligand cooperativity and the reversible addition and elimination across a reactive P–N linkage are confirmed. The study expands the scope of ligand cooperative catalytic reactivity in the main group chemistry and promises a broader opportunity for future design of phosphorus-based bifunctional and ligand cooperative catalysts.

3.2 Stoichiometric Phosphorus-Ligand Cooperative B-H Activation

Bifunctional reactivity resulting from the cooperative action of donor and acceptor functionalities placed within close structural proximity is a potent strategy for the modification of chemical bonds. The significance of cooperative bond activation is well exemplified in the literature of transition metal catalysis,[4] where activation of a substrate's covalent bond arises from the mutual participation and modification of both a reactive metal center and supporting ligand. Reported ligand-cooperative reactivities across diverse transition metals and ligand structures indicate its generality.[5]

Although attracting less attention, ligand cooperativity are also evident in the chemistry of the main group; recent stoichiometric examples from Groups 2,[6] 13,[7,8] 14,[9,10] and 15[11] are representative. These studies regarding main group element–ligand cooperativity contribute to current interest into the qualitative connections between the chemistry of transition metals and the main group.[12] In a compelling application of such stoichiometric reactivity to catalysis, Berben has demonstrated the cooperative

metal–ligand reactivity of aluminum-bis(imino)pyridine compounds in catalytic amine[13] and formic acid[14] dehydrogenation.

In transition metal chemistry, borane B–H activation via oxidative addition[15] and metal-ligand cooperativity [16] is well-studied and many catalytic hydroboration applications are based on these fundamental bond activation reactions.[17] Main group B–H activation such as 1,1-oxidative addition by carbenes[18] is also precedented. However, formally heterolytic reactivity modes are more common, for instance FLP-type activation[19] in the presence of Lewis bases or formally metathetical transformations across polarized σ-bonds[20] are found in catalytic applications.[21] In addition, although not rigorously involving B–H activation, the Corey-Bakshi-Shibata method is also an excellent example of bifunctional main group catalyzed hydroboration.[22]

To test our hypothesis that **3.2** would exhibit a bifunctional, phosphorus-ligand cooperative reactivity toward B–H bonds, a solution of **3.2** (0.13 M in C_6D_6) was treated with one equiv. of pinacolborane (HBpin) (**Figure 3.4**). Over the course of 12 h at 50 °C, ^{31}P NMR spectra indicated the complete consumption of **3.2** (δ 159.9 ppm) and formation of a major new phosphorus species **3.6** with a chemical shift δ 84.2 ppm (d, J= 146 Hz). Both the ^{31}P chemical shift and multiplicity are indicative of a tricoordinate phosphorus species with a direct P–H linkage. The presence of a P–H moiety is further supported by ^{1}H NMR spectra of compound **3.6**, which display a new doublet signal centered at δ 6.88 ppm with a complementary coupling (J = 146 Hz) to that observed in ^{31}P NMR spectra. Additionally, the ^{1}H NMR spectra show that compound **3.6** adopts a less symmetric

molecular geometry than phosphine **3.2**; the originally homotopic *N*-methyl groups from **3.2** transform into two distinct signals (δ 3.05, 2.55 ppm) in **3.6**. Only one of the *N*-methyl signals (δ 2.55 ppm) displays $^{3}J_{P-H}$ coupling (J = 15 Hz), suggesting the release of one *N*-methylanilide substituent from the phosphorus center of **3.2** upon reaction with HBpin. A ^{11}B NMR resonance at 24.2 ppm also confirms the existence of the boron nucleus in the structure of **3.6**.

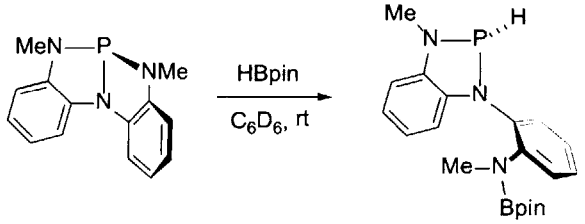

3.2 **3.6**

Figure 3.4. Activation of pinacolborane with **3.2** and resulting *P*-hydrido-1,3,2-diazaphospholene **3.6**.

3.3 Characterization of the P-Hydrido-Diazaphospholene Intermediate

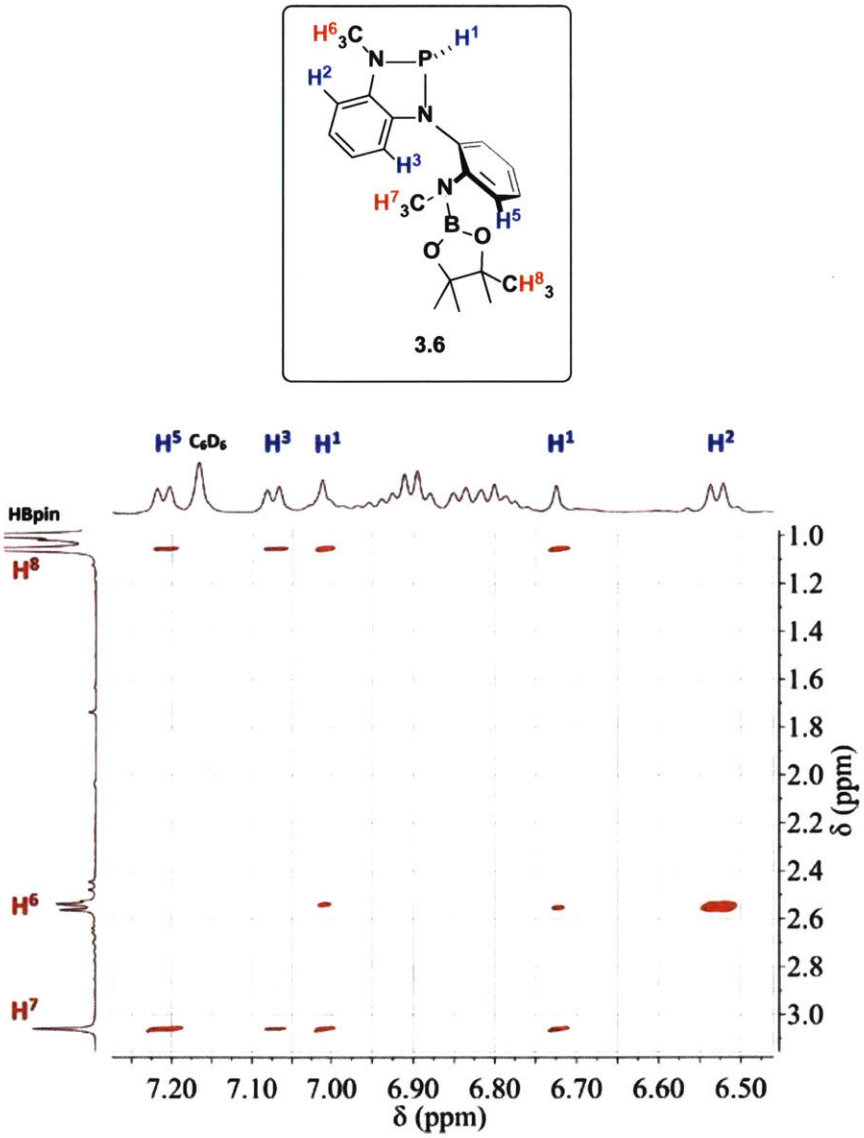

Figure 3.5. Annotated partial two-dimensional ^{1}H–^{1}H NOESY spectrum of **3.6** showing correlations between protons that share dipolar coupling (C_6D_6, 298 K, 500 MHz). Reproduced with permission from *J. Am. Chem. Soc.* **2017**, *139*, 6008.

Further information regarding the structure of **3.6** is obtained from two-dimensional NOESY spectra (**Figure 3.5**). Cross peaks indicate ^{1}H–^{1}H NOE correlation signals between H^{1} (i.e. P–H) and both H^{6} and H^{7} (*N*–methyl C–Hs), confirming the ring-opened structure of the ligand framework. Also, the correlation between H^{8} (pinacol methyl C–Hs) with both H^{1} and H^{7} confirm the presence of the Bpin moiety on the pendant N-methylanilide arm. Taken together, these spectral data are consistent with the identity of **3.6** as a *P*-hydrido-1,3,2-diazaphospholene arising from P–N cooperative activation of the B–H bond of HBpin. Potential atropisomeric diastereomers, which were previously observed in the analogous O-H activation intermediate **3.3**, are not resolved spectroscopically for **3.6** presumably due to the small size of the P–H moiety. Compound **3.6** is stable (0.12 M, 95 % NMR yield) in d_6-benzene solution but undergoes decomposition to a σ^5–P dihydridophosphorane upon prolonged standing in the presence of excess HBpin.

3.4 Hydridic Reactivity of the P-hydrido-diazaphospholene 3.6 toward Alkyl Halides and Imines

Inspired by the studies in the effects of endocyclic hyperconjugation on the reactivity of 1,3,2-diazaphospholenes,[23] the hydridic behavior of **3.6** was evaluated. Indeed, low NMR $^{1}J_{P-H}$ value (146 Hz) indicates a weak P-H bond and NBO charge analysis implicates a hydridic nature of the P–H moiety in **3.6** (atomic charge of –0.11). In agreement with these analyses, the addition of chloroform to a solution of **3.6** (78 mM

in C_6D_6) resulted in conversion over the course of 6 h to a new phosphorus species (^{31}P NMR δ 146.4 ppm) consistent with the assignment as *P*-chloro-1,3,2-diazaphospholene **3.7** (**Figure 3.6**). Compound **3.7** may also be obtained directly from treatment of **3.2** with HBpin in dichloromethane or chloroform solution for further identification of compound **3.7**. Surprisingly in this latter reaction, accumulation of P-hydrido-diazaphospholene intermediate **3.6** is not observed in the solution. This observation indicates that the reaction consuming intermediate **3.6** (with the halogenated substrate) happens more rapidly than the reaction generating **3.6** (from **3.2** by HBpin activation), consistent with the potent hydricity of *P*-hydrido-1,3,2-diazaphospholene **3.6**.

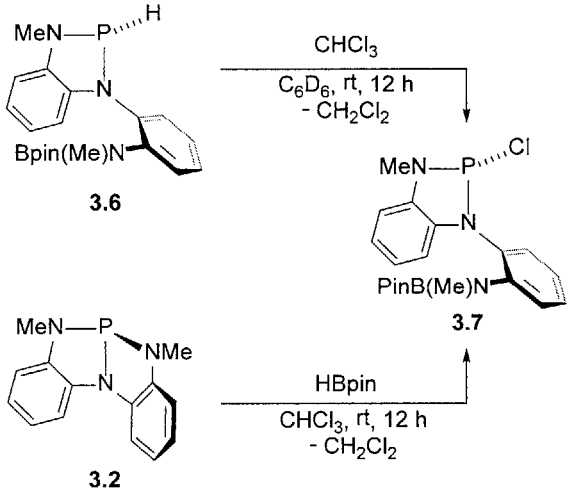

Figure 3.6. Hydrodechlorination of chloroform by **3.6** and formation of **3.7**.

Crystalline samples of **3.7** for x-ray crystallography were prepared by crystallization from CH_2Cl_2/pentane solution. The molecular structure (**Figure 3.7**)[24] unambiguously confirms the tricoordinate phosphorus local environment with pendant N(Bpin) moiety, supporting the analogous structural assignment for P-hydrido-diazaphospholene **3.6**. P-Cl compound **3.7** displays a small displacement (0.251 Å) of phosphorus from the C_2N_2 plane and a rather long P–Cl bond length (2.276(1) Å, compare 2.180(4) Å for $(Me_2N)_2PCl$[25]), indicative of hyperconjugative $n(\pi)\rightarrow\sigma^*$ overlap as has been reported in related compounds by Gudat. It is reasonable to assume that P-H compound **3.6** experiences similar electronic interactions that underpin its hydridic reactivity.

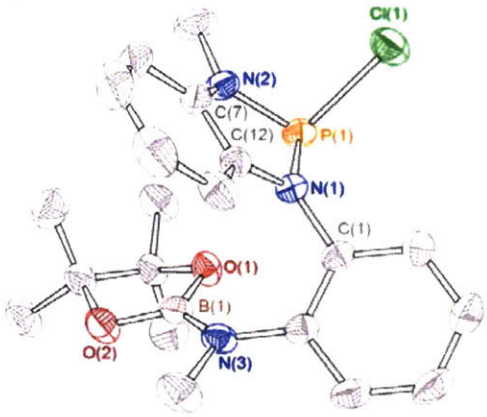

Figure 3.7. Molecular structure of **3.7** with 50% probability level rendered thermal ellipsoid plot. Reproduced with permission from *J. Am. Chem. Soc.* **2017**, *139*, 6008.

To further evaluate its hydricity with respect to organic substrates, treatment of P-H diazaphospholene **3.6** with *N*-tosylbenzaldimine at ambient temperature in benzene

(**Figure 3.8** *top*) resulted in complete conversion to a phosphorus species **3.8** with a ^{31}P NMR signal at δ 92.6 ppm. X-ray crystallography confirms the addition of **3.6** into the imine through a formal hydrophosphination and the formation of a phosphorus triamide with the Bpin moiety on a pendant *N*-methylanilide arm (**Figure 3.9**). As in the case of alkyl chloride reduction, compound **3.8** may also be accessed directly from C_s-symmetric phosphine **3.2** by treatment with *N*-tosylbenzaldimine and HBpin at ambient temperature (**Figure 3.8** *bottom*). The P-H diazaphospholene **3.6** is a presumed but unobservable intermediate in this preparation. Compound **3.8** is a stable species in both the solid state and solution; no decomposition is observed after heating a C_6D_6 solution at 60 °C for 48 h.

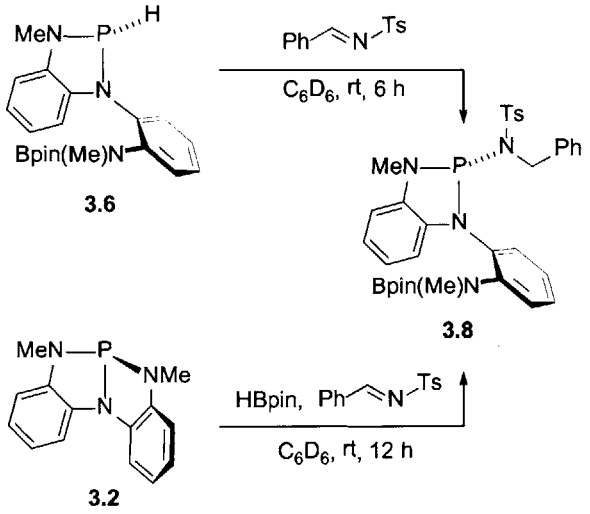

Figure 3.8. Reduction of *N*-tosylbenzaldimine and the formation of the triazaphospholene **3.8**.

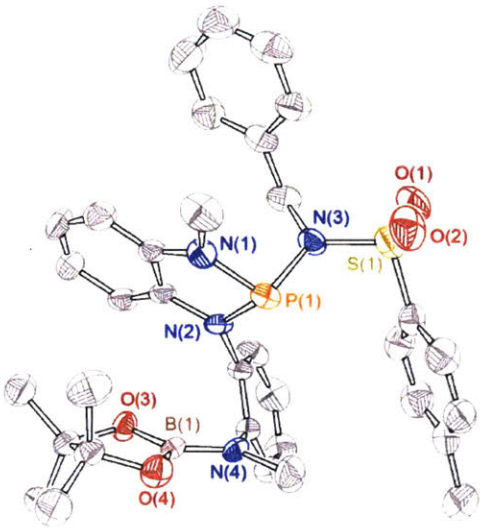

Figure 3.9. Molecular structure of **3.8** with 50% probability level rendered thermal ellipsoid plot. Reproduced with permission from *J. Am. Chem. Soc.* **2017**, *139*, 6008.

3.5 Cooperative B-N Elimination of the Triazaphospholene Intermediate

In contrast to the simple hydrophosphination of *N*-tosylbenzaldimine and the generation of stable triazaphospholene compound **3.8**, reaction of **3.6** with an *N*-alkyl benzaldimine results in a remarkably different outcome. Treatment of a C_6D_6 solution of **3.6** with *N*-benzyl *p*-methoxybenzaldimine (**3.9**) at ambient temperature resulted in the consumption of **3.6** and the unexpected generation of C_s-symmetric phosphine **3.2** (**Figure 3.10**). ^{1}H NMR spectra also confirm the concomitant formation of hydroboration product **3.11** under these conditions.

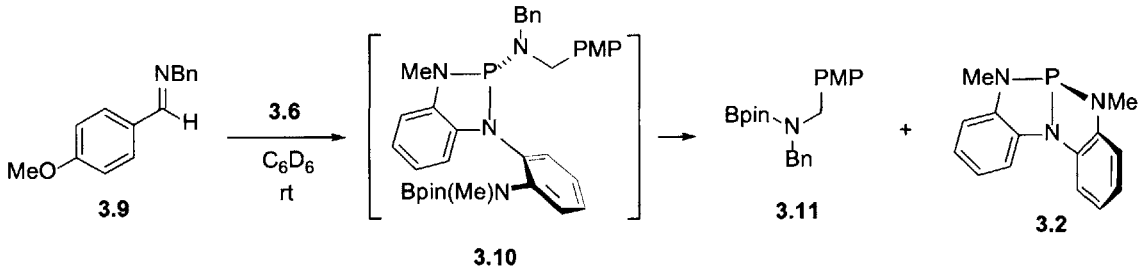

Figure 3.10. Reduction of imine **3.9** with P-H diazaphospholene 3.6 and the regeneration of **3.2**.

In situ ^{31}P NMR monitoring during the reaction provides additional insight of this transformation (**Figure 3.11**). In situ generated **3.6** in C_6D_6, was treated with imine **3.9**. As the reaction progresses (**Figure 3.11b** and **c**), the concentration of **2** decreased while the concentration of **3.6** was simultaneously observed to increase. Also observed in these spectra is the appearance of a transient minor peak δ 105.1 ppm. Based on the ^{31}P NMR chemical shift of this signal, we considered that this species might correspond to the phosphorous triamide **3.10** from hydrophosphination of imine **3.9** with P-H diazaphospholene **3.6**. Indeed, independent synthesis of **3.10** from treatment of P-Cl compound **3.7** with *N*-benzyl-*N*-(*p*-methoxyphenyl)methanamine (**Figure 3.12**) gives the same ^{31}P NMR signal δ 105.1 ppm. Consistent with the above observations, intermediate **3.10** is metastable in solution but not isolable. Instead, independently synthesized **3.10** decomposes cleanly to C_s-symmetric phosphine **3.2** within 60 h at ambient temperature (^{31}P NMR spectra, **Figure 3.13**). Correspondingly, ^{1}H NMR spectra confirm the formation of the N-borylamine product **3.11** by B–N elimination from **3.10**.

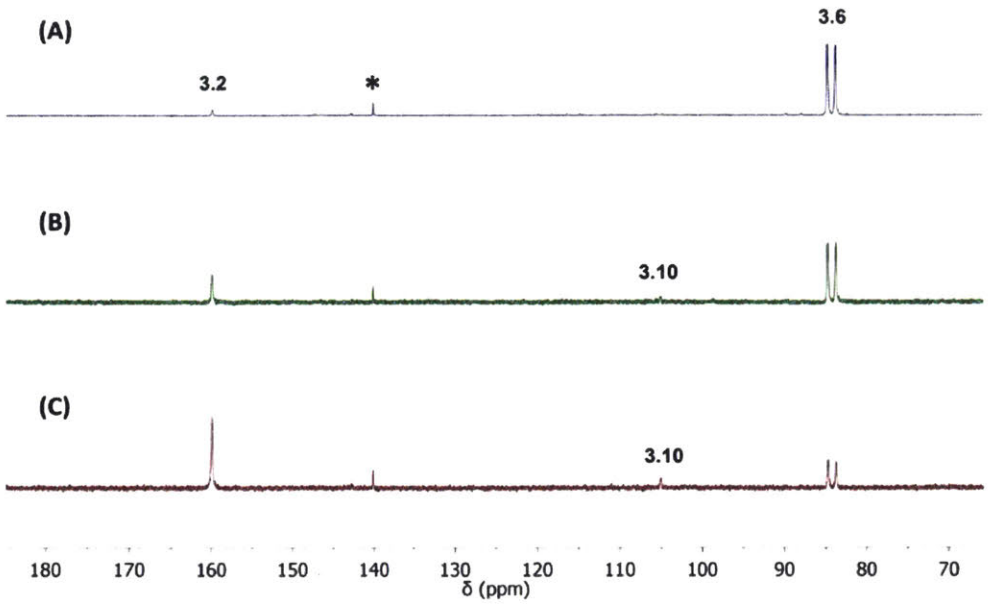

Figure 3.11. Representative time-stacked ^{31}P NMR spectra (C_6D_6, 145.79 MHz, 25 °C) for the reaction of **3.6** (δ 84.2 ppm) with imine **3.9** to give **3.2** (δ 159.9 ppm) via **3.10** (δ 105.1 ppm) at time points: (A) 10 min, (B) 30 min, (C) 12 h. Asterisk marks unidentified byproduct (δ 140 ppm).

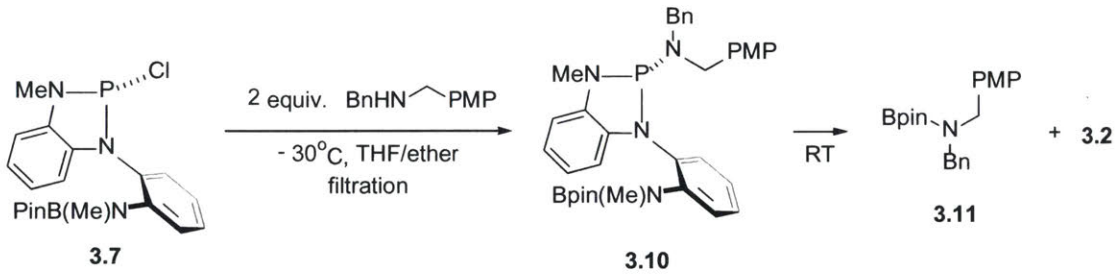

Figure 3.12. The independent synthesis of **3.10** and its elimination of the *N*-borylamine **3.11**. PMP=*p*-methoxyphenyl.

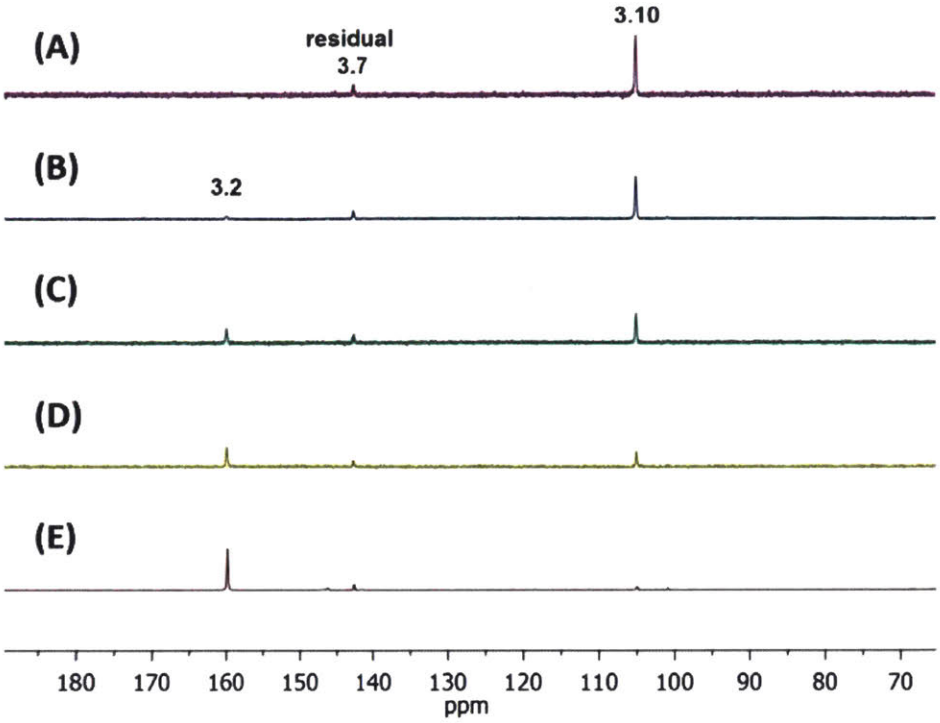

Figure 3.13. Time-stacked ^{31}P NMR spectra (C_6D_6, 145.79 MHz, 25 °C) for the conversion of **3.10** to **3.2** at time points (A) 10 min, (B) 3 h, (C) 12 h, (D) 36 h, (E) 60 h. Reproduced with permission from *J. Am. Chem. Soc.* **2017**, *139*, 6008.

Since compound **3.10** is not isolable, an analogous phosphorous triamide **3.12** (δ 91.3 ppm) was prepared by treatment of **3.7** with benzylamine for further structure confirmation (**Figure 3.14**). The composition of this compound was unambiguously proven by X-ray diffraction analysis of single crystalline samples (**Figure 3.15**). The similarity in ^{31}P NMR chemical shifts between isolable **3.12** and transient **3.10** supports the assignment of **3.10** as the phosphorous triamide depicted in **Figure 3.10**. In a further analogy to **3.10**, compound **3.12** can be directly converted to **3.2** upon heating (50 °C, 48 h) with liberation of *N*-boryl benzylamine **3.13**. Taken together, the experiments present

above demonstrates that the *N*-boryl benzylamines are generated from the phosphorous triamide intermediates via a ligand-phosphorus cooperative pathway.

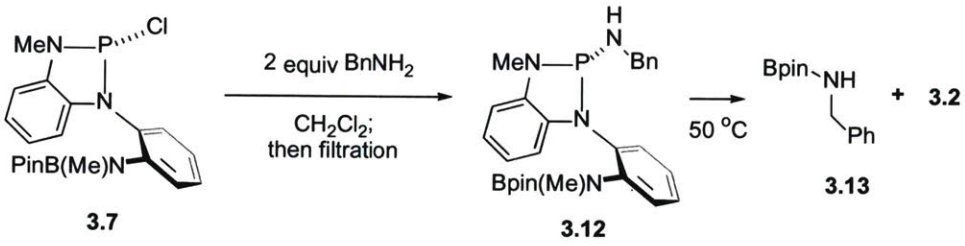

Figure 3.14. Synthesis of **3.12** and its conversion to **3.2**.

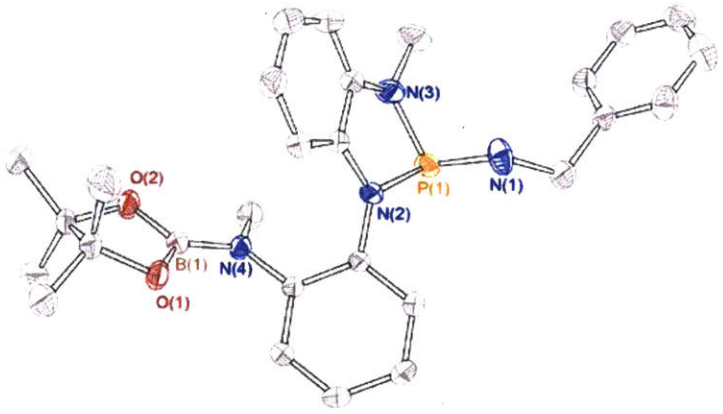

Figure 3.15. Molecular structure of **3.12** with 50% probability level rendered thermal ellipsoid plot. Reproduced with permission from *J. Am. Chem. Soc.* **2017**, *139*, 6008.

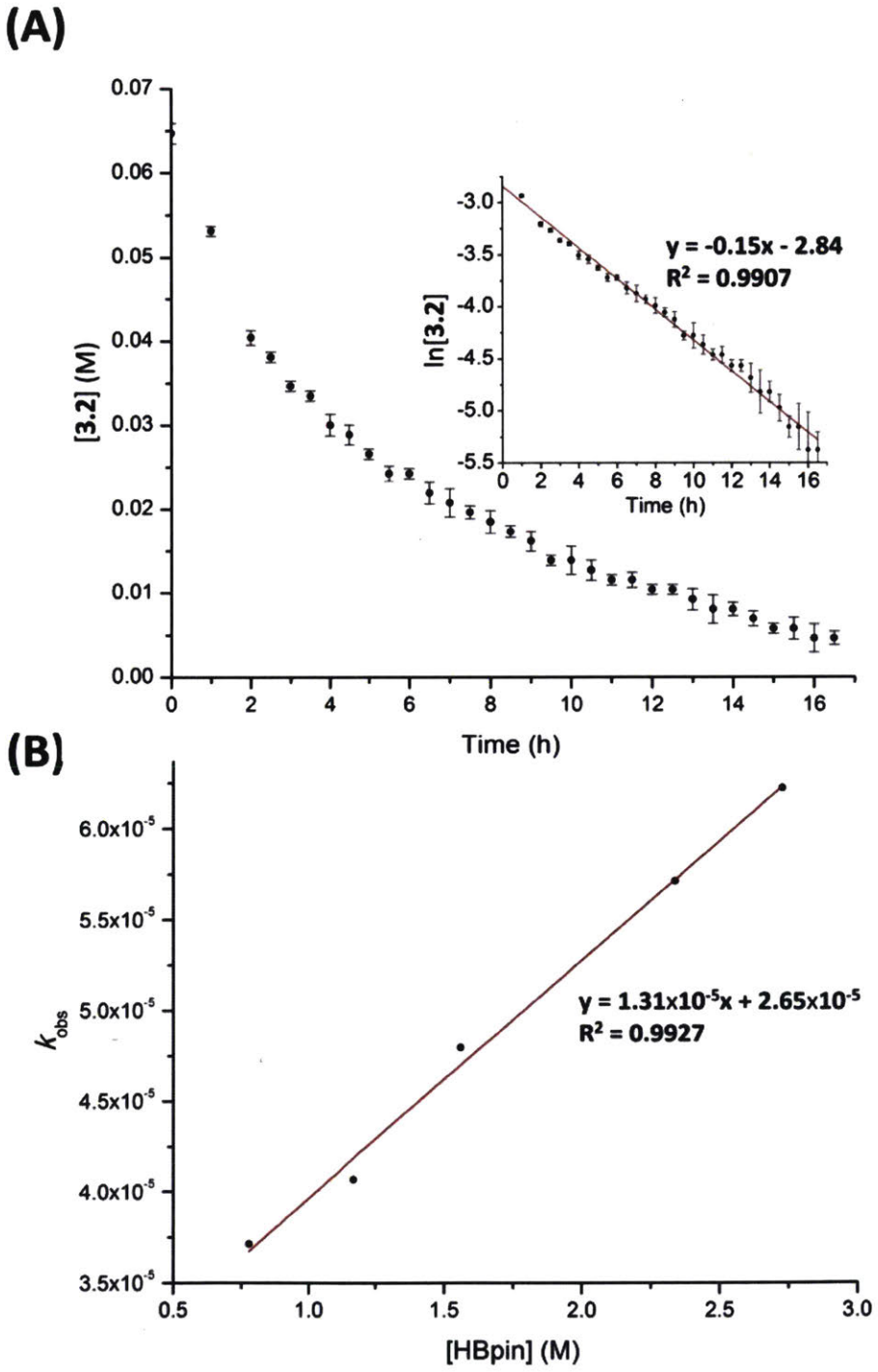

Figure 3.16. Kinetics experiments of the cooperative HBpin activation with **3.2**. (A) Plot of [**3.2**] vs time monitored ([**3.2**]$_o$ = 78 mM, [HBpin]$_o$ = 117 mM, C_6D_6, 297 K). (Inset) Plot of ln [**3.2**] vs time with linear least-squares fit. (B) Plot of k_{obs} vs [HBpin]$_0$ with linear least-squares fit. Reproduced with permission from *J. Am. Chem. Soc.* **2017**, *139*, 6008.

3.6 Kinetic Analysis of the Cooperative B–H Activation

Kinetic analyses were conducted to elucidate the reaction rate and molecularity of the phosphorus-ligand cooperative B-H activation. Using 1,3,5-trimethoxybenzene as the internal standard, the reaction of **3.2** (78 mM in C_6D_6) with excess HBpin (15 equiv.) was monitored via ^{1}H NMR as a function of time and the result reveals a pseudo-first order dependence on **3.2** (**Figure 3.16A**). Plots of k_{obs} vs. $[HBpin]_0$ (**Figure 3.16B**) demonstrate a linear relationship over the concentration range 0.78 M $\leq$ [HBpin] $\leq$ 2.73 M, thus establishing an overall second order reaction rate law for addition of HBpin to **3.2** (**eq 3.1**, k = 4.76 x 10^{-5} $M^{-1}s^{-1}$ at 25 °C) which in consistent with the direct bimolecular phosphorus-ligand cooperative activation of the B–H bond.

$$v = -k_{obs}[HBpin] = -k[\mathbf{3.2}][HBpin] \qquad \textbf{(3.1)}$$

3.7 Kinetic Analysis of the Cooperative B-N Elimination

The kinetic analysis was also conducted by NMR monitoring of the conversion from **3.10** to **3.2**. Compound **3.10** was in situ prepared in solution and purification by rapid filtration over celite to eliminate triethylammonium chloride. The decay of **3.10** was then monitored at ambient temperature by ^{1}H NMR spectroscopy to greater than 75% conversion (**Figure 3.17**). The linear relationship between ln[**3.10**] and time (**Figure 3.17** *inset*) demonstrates a first-order reaction kinetics as expected for a unimolecular

decomposition of **3.10**. The extracted rate constant (k = 0.04 s^{-1}) is independent of absolute concentration within the range 0.58 mM < [**3.10**] < 3.26 mM. These results are fully consistent with a ligand cooperative intramolecular transfer of the boryl unit from the *N*-methylanilide arm to the *N*-benzyl-*N*-(*p*-methoxyphenyl)methanamine fragment, elimination of *N*-borylamine **3.11**, and reconstitution of a P–N bond in the conversion of **3.10** to C_s-symmetric phosphine **3.2**.

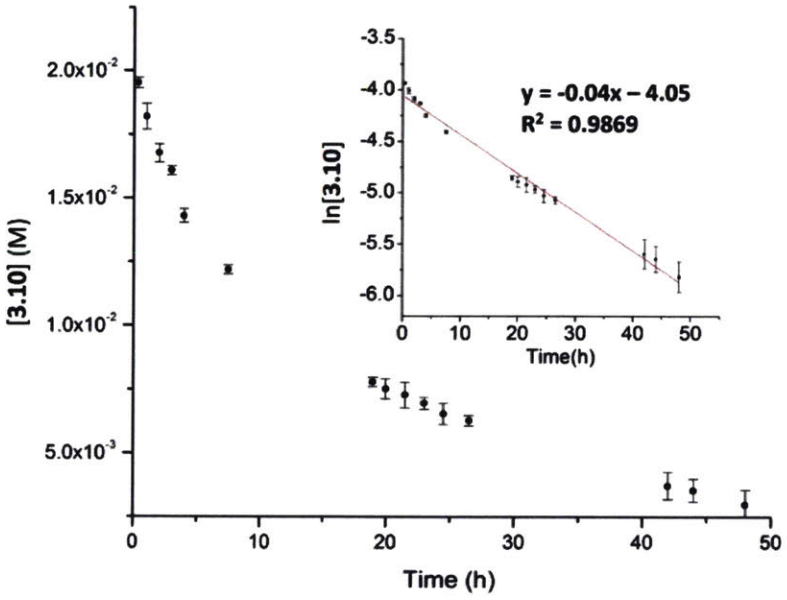

Figure 3.17. Kinetics experiments of the cooperative B–N elimination from **3.10**. Plot of [**3.10**] vs time monitored ([**3.10**]$_o$ = 3.3 mM, C_6D_6, 297 K). (*Inset*) Plot of ln [**3.10**] vs time with linear least-squares fit. Reproduced with permission from *J. Am. Chem. Soc.* **2017**. *139*. 6008.

3.8 Catalytic Reactivity toward Imine Hydroboration

With the stoichiometric reactivities in mind, we pursued investigations of hydroboration reactions catalyzed by C_s-symmetric phosphine **3.2**. In an initial attempt, a C_6D_6 solution of *N*-benzyl *p*-anisaldimine **3.9** (1 equiv.) and HBpin (1 equiv.) was exposed to 10 mol% of **3.2** at 50 °C. After 24 hours, imine **3.9** was completely converted to the hydroboration product **3.11** (**Figure 3.18** *top*). Control reactions between **3.9** and HBpin under identical reaction conditions without catalytic **3.2** show less than 15% conversion (**Figure 3.18** *bottom*), consistent with a transformation that is indeed under catalyst control.

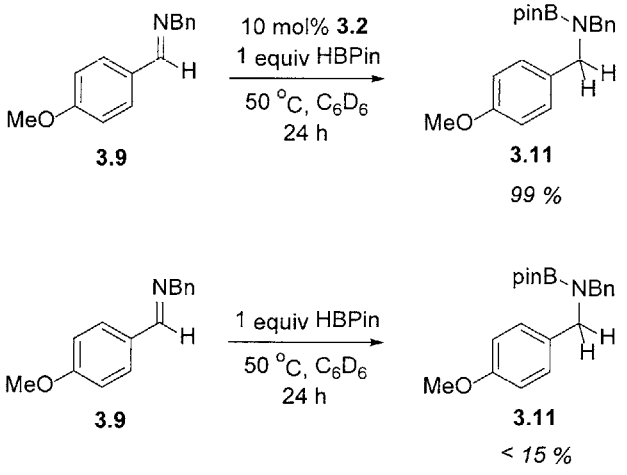

Figure 3.18. Catalytic imine hydroboration reactivity of **3.2**.

In situ NMR monitoring of the catalytic transformation was conducted to further substantiate the action of **1** during catalysis. After mixing of imine **3.9**, HBpin, and 10

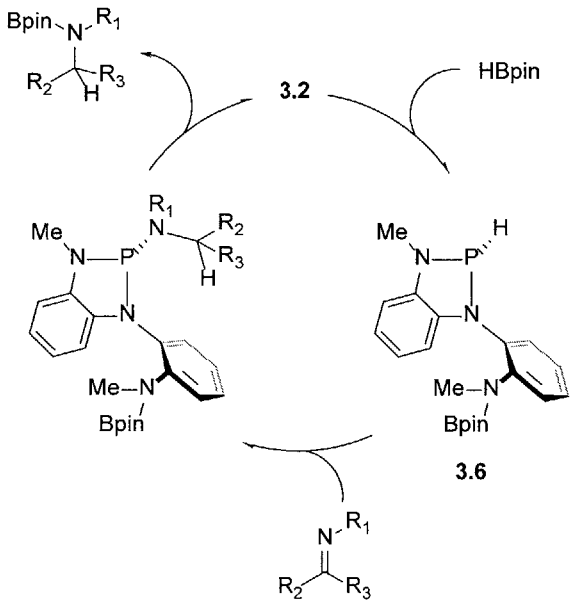

Figure 3.19. Catalytic imine hydroboration reactivity of **3.2**.

mol% **3.2** in C_6D_6 at 50 °C in a thermostatted probe, a ^{31}P NMR spectrum indicates the formation of small quantities of P-H diazaphospholene **3.6** at the expense of the initial concentration of **3.2**. At subsequent intermediate time points (time = 0.5-12 h), the concentrations of **3.6** showed no significant change. As the reaction progressed over the next 24 h, continued production of the corresponding hydroboration product **3.11** could be observed by ^1H NMR spectra. Catalyst **3.2**, although diminished, was never completely consumed. The existence of **3.2** during the entire course of catalytic reaction as opposed to its total conversion to **3.6** in stoichiometric reaction suggested again that the reduction of the imine by **3.2** leads to an ephemeral intermediate **3.10** which

decomposes to give **3.2** and the hydroboration amine product. The mechanism of phosphine **3.2**-catalyzed imine hydroboration is illustrated in **Figure 3.19**.

Under the same catalytic conditions, imines with varied substituents are reduced catalytically and produce the corresponding hydroboration products (**Figure 3.20**). Aldimines with *N*-aryl (**3.15**), *N*-alkyl (**3.16**), and electronically diverse (**3.18-3.23**) substitutions are tolerated. Ketimines are also reduced under the catalytic conditions (**3.26 – 3.28**) but with lower yields presumably caused by a steric effect.

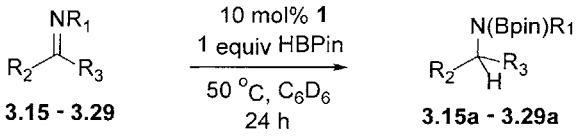

3.15	R_1=Ph	R_2=Ph	R_3=H	99 % y
3.16	R_1=Bn	R_2=*p*-BrC_6H_4	R_3=H	73 % y
3.17	R_1=*p*-MeC_6H_4	R_2=*p*-MeC_6H_4	R_3=H	88 % y
3.18	R_1=*p*-OMeC_6H_4	R_2=Ph	R_3=H	76 % y
3.19	R_1=*p*-OMeC_6H_4	R_2=*p*-FC_6H_4	R_3=H	94 % y
3.20	R_1=*p*-OMeC_6H_4	R_2=*1*-naphthyl	R_3=H	99 % y
3.21	R_1=*p*-OMeC_6H_4	R_2=*m*-$CF_3C_6H_4$	R_3=H	96 % y
3.22	R_1=*p*-OMeC_6H_4	R_2=*p*-OMeC_6H_4	R_3=H	64 % y
3.23	R_1=*p*-$CF_3C_6H_4$	R_2=*p*-OMeC_6H_4	R_3=H	99 % y
3.24	R_1=*p*-OMeC_6H_4	R_2=mesityl	R_3=H	77 % y
3.25	R_1=*p*-FC_6H_4	R_2=Ph	R_3=H	91 % y
3.26	R_1=Ph	R_2=Ph	R_3=Me	48 % y
3.27	R_1=Bn	R_2=Ph	R_3=Ph	64 % y
3.28	R_1=Bn	R_2=Ph	R_3=Me	94 % y
3.29	R_1= *p*-Ts	R_2=Ph	R_3=H	<5%y

Figure 3.20. Phosphine **3.2** catalyzed aldimine and ketamine hydroboration.

Our study of C_s-symmetric **3.2** and related distorted structures concerns the increased electrophilic character at phosphorus due to deformation from local threefold phosphorus center. Enthalpic (strain) arguments have been discussed in related systems that account for this observation[26] and this mode of reactivity is accentuated in the case of **3.2** due to the geometric constraint imposed by the triamide framework. In addition to our previous investigation of the increased electrophilicity at phosphorus of **3.2** and the resulting reactivity of **3.2** toward protic E–H substrates (E = OR, NHR), here we access a regioreversal by reaction with a hydridic E–H (E = Bpin) compound. In the transformation, the acceptance of a hydride at phosphorus occurs in a bimolecular pathway and accompanies with the boryl transfer to the pendant *N*-methylanilide with P–N cleavage. The regioselectivity of the B–H activation is unusual due to the ubiquity of phosphine-borane dative interactions, presumably both the weak *P*-nucleophilicity of **3.2** and weak *B*-electrophilicity of HBpin disfavor the common P→B Lewis acid-base interaction.

3.9 Conclusion and Outlook

C_s-symmetric σ^3-phosphorous compound **3.2** has been demonstrated to be a capable catalyst for the hydroboration of imines, and the mechanistic details of this transformation have been elucidated. The reactivity arises from the cooperative action of an electrophilic P(III) center and a proximal basic *N*-methylanilide nitrogen within a distorted molecular environment imposed by the triamide ligand. The bimolecular,

phosphorus-ligand cooperative mechanism is involved in both the initial B–H activation and the B–N elimination. The regeneration of the deformed phosphabicyclic structure of **3.2** happens with the concomitant formation of the hydroboration products. The ability of distorted phosphorous triamide **3.2** to catalyze B–H transfer through a P-N ligand cooperative mechanism promises further opportunity for targeted design of novel main group catalysts. On the basis of the described experimental results concerning the impact of geometry distortion on the reactivity of σ^3-phosphorus compounds, σ^4-phosphorus molecules with analogously constrained frameworks were also investigated and their potentials in activations of a range of E–H will be discussed in the following chapter.

3.10 Experimental

General Materials and Methods

All reagents were purified as described in the previous chapter. Pinacolborane was purified by vacuum distillation (60 torrs) and stored a nitrogen-filled glovebox. Benzylamine was purified by distillation from zinc dust and stored over 3 Å molecular sieves prior to use. All glassware was oven-dried at 120 °C prior to use. All reactions were carried under dry nitrogen atmosphere (Schlenk line or glovebox) unless otherwise noted. NMR spectra were recorded on a Bruker AV-360 (360MHz), a Bruker AV-400 (400 MHz), a Bruker AV-500 (500MHz) or a VARIAN Inova-500 (500MHz) spectrometer. ^{1}H NMR chemical shifts are given in ppm with respect to solvent residual peak (C_6D_6, δ 7.16 ppm; $CDCl_3$, δ 7.26 ppm; CD_2Cl_2, δ 5.32 ppm), $^{13}C\{^1H\}$ NMR shifts

are given in ppm with respect to $CDCl_3$ (δ 77.16 ppm), C_6D_6 (δ 128.06 ppm) or CD_2Cl_2 (δ 53.84 ppm). Coupling constants are reported as *J*-values in Hz. High resolution EI and ESI mass spectra were obtained from the Mass Spectrometry Laboratory at the School of Chemical Sciences, University of Illinois at Urbana-Champaign or Department of Chemistry Instrumentation Facility, Massachusetts Institute of Technology.

Synthetic Procedures and Characterization Data

Phosphorus compound **3.2** was prepared by minor modification of the literature[1] method according to the following sequence (**Figure 3.21**):

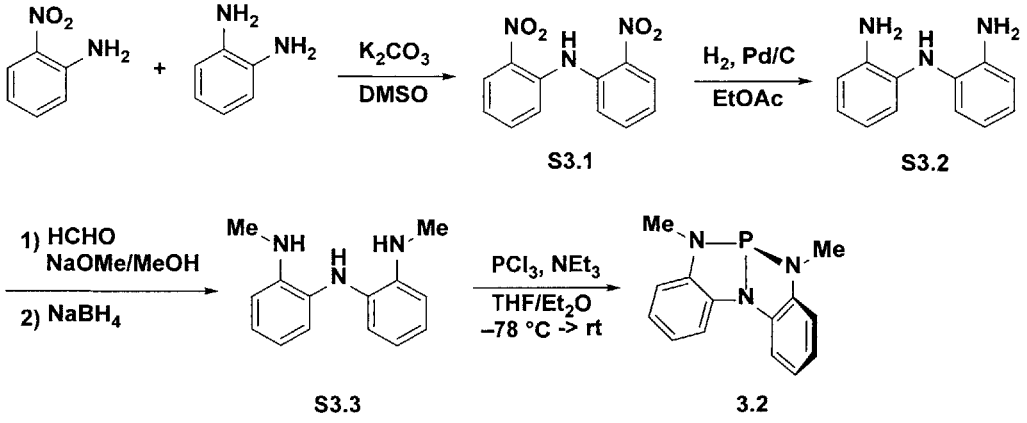

Figure 3.21. Synthesis of phosphine **3.2**.

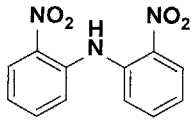

S3.1

Bis(2-nitrophenyl)amine (**S3.1**)**:** Synthesized according to literature procedure.[1] 1-Fluoro-nitrobenzene (20.0 mL, 190 mmol), 2-nitroaniline (26.2 g, 190 mmol) and K_2CO_3 (31.4 g, 228 mmol) were mixed in DMSO (300 mL). The reaction mixture was stirred at 120 °C for 36 h. H_2O was then added (300 mL), and the mixture was extracted with dichloromethane (3 x 500 mL). The combined organic layer was washed with a saturated aqueous solution of NaCl (6 x 300 mL, 15 %), dried over anhydrous magnesium sulfate and concentrated *in vacuo*. The product was obtained as an orange solid (46.5 g, 95 %) and was used for next step without further purification. ^{1}H NMR (360 MHz, $CDCl_3$): δ 10.98 (s, 1H), 8.16 (dd, 2H, J = 8.4 Hz, J = 1.3 Hz), 7.58-7.48 (m, 4H), 7.09-7.04 (m, 2H) ppm.

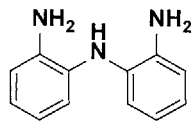

S3.2

Bis(2-aminophenyl)amine (**S3.2**): Synthesized according to literature procedure.[1] Bis(2-nitrophenyl)amine **S3.1** (10 g, 38.5 mmol) was suspended in EtOAc (100 mL). Palladium on carbon (790 mg, 10 wt%) was then added to the solution. The reaction mixture was transferred to a high pressure reactor, charged with hydrogen (400 psi), and stirred for 10 h. Upon completion, the solution was filtered through Celite and concentrated to a dark residue under vacuum, which was used in the next step without further purification (5.43 g, 94%). ^{1}H NMR (360 MHz, $CDCl_3$): δ 6.97-6.92 (m, 2H), 6.80-6.74 (m, 6H), 5.00 (br s, 1H), 3.74 (br s, 4H) ppm.

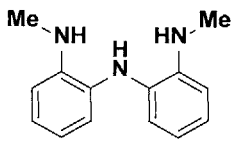

S3.3

Bis(2-methylaminophenyl)amine (**S3.3**): Synthesized via a modified literature procedure.[1] To a mixture of bis(2-aminophenyl)amine **S3.2** (10 g, 50.1 mmol) and paraformaldehyde (14.8 g, 494 mmol) in anhydrous methanol (500 mL) was added a solution of NaOMe in methanol (34.5 mL, 25 wt. %) slowly at 0 °C. The mixture was then stirred under reflux for 1 h. After being cooled to 0 °C, $NaBH_4$ (20.6 g, 545 mmol) was added in small portions. The solution was again stirred with heating to reflux for 1 h. The reaction mixture was then cooled to room temperature. To this mixture, 1 M NaOH (150 mL) was

added followed by extraction dichloromethane (3 × 300 mL). The combined organic phase was filtered after dried over magnesium sulfate. The crude mixture was concentrated under vacuum and flushed through a short column of silica gel with dichloromethane. After concentration, the resulting crude solid was recrystallized from ethanol to give the product as purple crystals (9.8 g, 87 %). ^{1}H NMR (360 MHz, $CDCl_3$): δ 7.07 (m, 2H), 6.77-6.71 (m, 6H), 4.91 (s, 1H), 3.76 (br s, 2H), 2.88 (s, 6H) ppm.

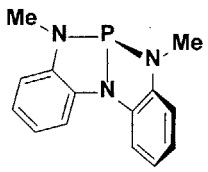

3.2

Compound ***3.2***. Synthesized via a modified literature procedure.[1] Phosphorus trichloride (1.15 mL, 13.2 mmol) was dissolved in ether (40 mL) and cooled to –78 °C. A solution of triamine **S3.3** (3.00 g, 13.2 mmol) in THF (10 mL) was added dropwise via syringe. Upon completion, an ether solution (36 mL) of triethylamine (5.60 mL, 40.2 mmol) was added slowly via syringe. The reaction mixture was stirred at –78 °C for 1h and then warmed to room temperature. After 4h of stirring at room temperature, all volatiles were solvent was removed *in vacuo* and the resulting solid mixture was moved into a nitrogen-filled glovebox. The solid mixture was stirred in pentane and filtered through Celite to remove all insoluble solids. Pentane was removed *in vacuo* and the resulting crude product was recrystallized with pentane in a freezer (ca. –35 °C) to yield **3.2** as light-pink crystals (2.5 g, 75 %). ^{1}H NMR (C_6D_6, 400 MHz): δ 7.38 (dd, 1H, J = 7.7, 1.3 Hz), 6.94 (td, 1H, J = 7.6, 1.2 Hz), 6.77 (td, 1H, J = 7.6, 1.3 Hz), 6.34 – 6.29 (m, 1H), 2.52 (d, 3H, J = 8.3 Hz). ^{31}P NMR (C_6D_6, 162 MHz): δ 159.8 ppm.

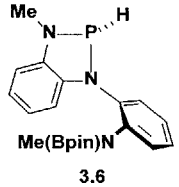

3.6

Compound ***3.6***. Under nitrogen atmosphere, pinacolborane (15 mg, 0.12 mmol) was mixed with a C_6D_6 solution (1 mL) of compound **3.2** (30 mg, 0.12 mmol) in a sealable threaded NMR tube. The mixture was kept at 50 °C for 12 h to afford crude **3.6** (NMR yield: 95 %). ^{1}H NMR (C_6D_6, 500 MHz): δ 7.29

(d, 1H, J = 7.8 Hz), 7.20 (d, 1H, J = 7.8 Hz), 7.07 (d, 1H, J = 7.7 Hz), 6.92-6.77 (m, 4H), 6.86 (d, 1H, $^{1}J_{P\text{-}H}$ = 146.3 Hz), 6.52 (d, ^{1}H, J = 7.8 Hz), 3.05 (s, 3H), 2.85 (d, 3H, J = 12.8 Hz), 1.05 (s, 12H) ppm. ^{31}P NMR (C_6D_6, 202 MHz): δ 84.2 (d, J= 146 Hz) ppm. MS (ESI) calcd for C20H27BN3O2P (M) 383.1934 submitted.

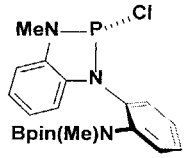

3.7

Compound ***3.7***. Under nitrogen atmosphere, pinacolborane (50 mg, 0.39 mmol) was added into a $CHCl_3$ solution (2 mL) of compound 1 (100 mg, 0.39 mmol) and the solution was stirred under room temperature. After 12 h, all volatiles were re-moved *in vacuo* and the remaining white solid was recrystallized in pentane to afford **3** as a white crystals (80 mg, 70 %). ^{1}H NMR ($CDCl_3$, 400 MHz): δ 7.64 (d, 1H, J = 8.0 Hz), 7.37-7.26 (m, 3H), 7.08 (t, 1H, J = 8.0 Hz), 7.01-6.97 (m, 2H), 3.39 (d, 3H, J = 16.0 Hz), 2.85 (s, 3H), 0.94 (broad s, 12H) ppm. ^{13}C NMR ($CDCl_3$, 100 MHz): δ 145.0 (d, $^{2}J_{PC}$ = 4.0 Hz), 136.9 (d, $^{2}J_{PC}$ = 12.0 Hz), 132.02 (d, $^{2}J_{PC}$ = 11.0 Hz), 129.51, 129.45, 128.81, 128.31, 125.71, 121.52, 121.05, 111.94, 110.00, 82.74, 37.20, 29.44 (d, $^{2}J_{PC}$ = 18.0 Hz), 24.15 ppm. ^{31}P NMR ($CDCl_3$, 145 MHz): δ 146.38 ppm. MS (ESI) calcd for $C_{20}H_{26}BN_3O_2P$ (M^+ -Cl) 382.1856 found 382.1859.

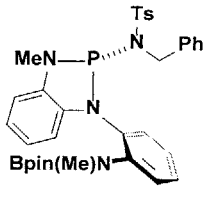

3.8

Compound ***3.8***. Under nitrogen atmosphere, a C_6D_6 solution of in situ generated **2** (1 ml, 0.24 M) was added *N*-tosyl-*1*-phenylmethanimine (64 mg, 0.24 mmol). The mixture was stirred at room temperature for 16 h, all volatiles were re-moved in vacuo and the resultinging white solid was washed with pentane (60 mg, 63%). The solid was then recrystallized in a 10:1 pentane/CH_2Cl_2 solution to obtain the samples for X-ray

crystallography. ^{1}H NMR (C_6D_6, 400 MHz): δ 7.80 (d, 2H, J = 7.9 Hz), 7.53-7.50 (m, 2H), 7.37 (d, 1H, J = 8.0 Hz), 7.20-7.07 (m, 5H), 6.93-6.69 (m, 5H), 6.65 (d, 1H, J = 7.4 Hz), 6.05 (d, 1H, J = 7.5 Hz), 4.51 (d, 1H, J = 15.9 Hz), 3.69 (d, 1H, J = 15.9 Hz), 2.93 (s, 3H), 2.38 (d, 3H, J = 11.8 Hz), 2.07 (s, 3H), 1.12 (s, 12H) ppm. ^{13}C NMR (126 MHz) δ 145.1, 141.6, 139.5, 137.9, 137.7, 137.7, 137.0 (d, $^{2}J_{PC}$ = 10.1 Hz), 134.1 (d, $^{2}J_{PC}$ = 12.6 Hz), 129.8, 129.3, 129.1, 128.1, 126.8, 126.8, 125.2, 124.2, 119.9, 118.5, 108.6, 107.8, 82.8, 47.9, 36.2, 36.2, 28.6, 28.4, 24.6, 24.4. ^{31}P NMR (C_6D_6, 145 MHz): δ 92.6 ppm. MS (ESI) calcd for $C_{34}H_{41}BN_4O_4PS$ 643.2679 (M^{+}+H) found 643.2685.

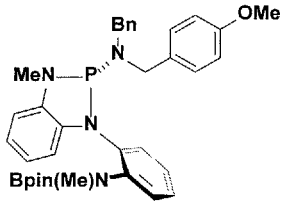

3.10

Compound ***3.10***. Under nitrogen atmosphere, a 1:1 THF/ether solution (2 ml) of **3** (10 mg, 2.39x10^{-2} mmol) and an ether solution (1 ml) of *N*-benzyl-1-(4-methoxyphenyl)methanamine (12 mg, 4.79x10^{-2} mmol) were both cooled to –30 °C and then mixed together. The resulting cloudy mixture was quickly filtered through Celite and all volatiles were removed in vacuo to afford crude **6**. (NMR yield 82 %). ^{1}H NMR (C_6D_6, 500 MHz): δ 7.56 (d, 1H, J = 11.0 Hz), 7.40 (d, 1H, J = 11.0 Hz), 7.23-6.80 (m, 12H), 6.80 (d, 2H, J = 11.5 Hz), 6.67 (d, 1H, J = 10.5 Hz), 4.25 (broad s, 2H), 3.70 (broad s, 2H), 3.45 (s, 3H), 3.20 (s, 3H), 3.04 (d, 3H, $^{3}J_{PH}$ = 13.8 Hz), 1.16 (broad s, 12H) ppm. ^{31}P NMR (C_6D_6, 145 MHz): δ 105.2 ppm.

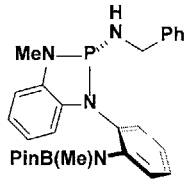

3.12

Compound ***3.12***. Under nitrogen atmosphere, benzylamine (26 mg, 0.24 mmol) was added into a CH_2Cl_2 solution of **3** (50 mg, 120 mM). The

resulting cloudy solution was quickly filtered through Celite and all volatiles were removed *in vacuo* to afford crude product. The crude product was recrystallized in a 1:5 dichloromethane:pentane solution to afford **8** as a white crystals. ^{1}H NMR (CD_2Cl_2, 360 MHz): δ 7.40-7.21 (m, 3H), 7.08 (d, 1H, J = 7.0 Hz), 6.83 (t, 1H, J = 7.3 Hz), 6.68 (t, 1H, J = 7.6 Hz), 6.61 (d, 1H, J = 7.5 Hz), 6.56 (d, 1H, J = 7.5 Hz), 3.72-2.64 (m, 2H), 3.07 (d, 3H, J = 10.3 Hz), 2.75 (s, 3H) ppm, 1.17 (s, 12H). ^{31}P NMR (CD_2Cl_2, 145 MHz): δ 91.34 ppm. ^{13}C NMR (CD_2Cl_2, 125 MHz): δ 144.48, 143.94, 140.89, 129.25, 128.96, 128.34 (d, $^{2}J_{PC}$ = 11.3 Hz), 127.41, 127.03, 126.76, 126.54, 126.18, 125.15, 118.74, 117.31, 105.99, 82.63, 46.41, 44.84, 35.86, 29.02 (d, $^{2}J_{PC}$ = 21.2 Hz), 24.33 ppm. MS (ESI) $C_{27}H_{35}BN_4O_2P$ (M^++H) calc'd: 489.2591; found: 489.2595.

Pseudo-first Order Kinetic Study of the B-H Activation Reaction

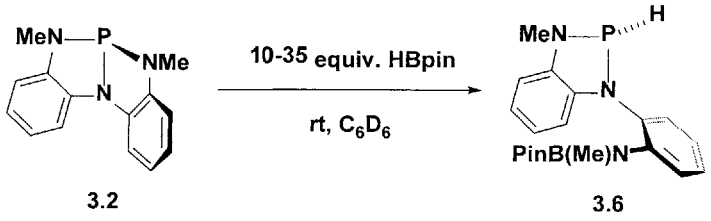

3.2 3.6

Figure 3.22. Kinetic Study of the B-H Activation Reaction of **3.2**.

Experiments were conducted with varying equivalent of HBPin with at least 10-fold excess. Measurements were performed on a Bruker AV-400 NMR spectrometer. A stock solution of compound **3.2** (0.6 ml, 13 mM in C_6D_6 containing 0.06 mmol 1,3,5-trimethoxybenzene as the internal standard) and HBpin were added to a volumetric flask

and the resulting mixture was diluted to 1 ml with C_6D_6. The diluted solution was then transferred to a J-Young NMR tube and the conversion of **3.2** to **3.6** was monitored with ^1H NMR at ambient temperature. The concentrations of **3.2** were obtained from the NMR signal integral ratios between **3.2** and the internal standard. The error bars on the plot are generated from variability of ^1H NMR integrals.

Kinetic Study of the B-N Elimination Reaction

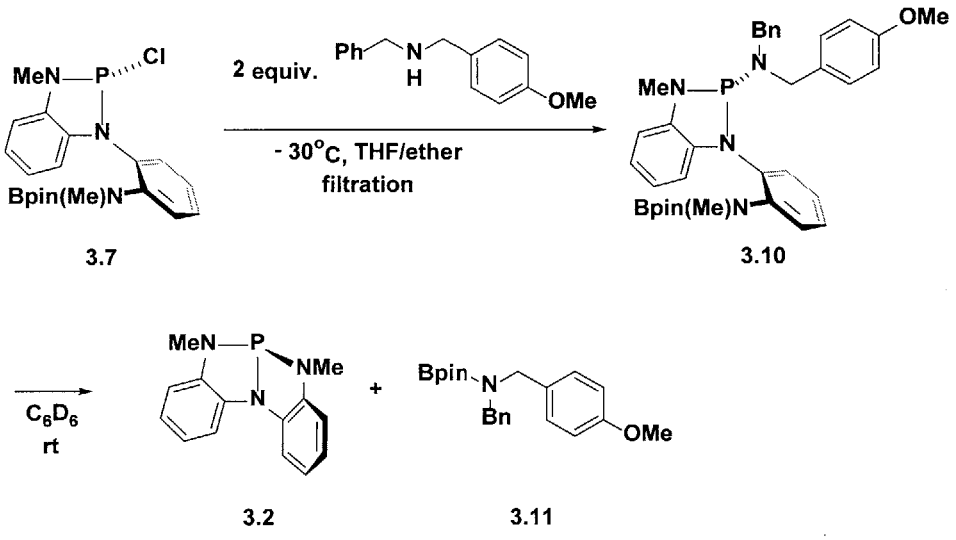

Figure 3.23. Kinetic Study of the B-N Elimination Reaction of **3.10**.

In a nitrogen-filled glovebox, a 1:1 THF/ether solution (2 ml) of **3.7** (10 mg, $2.39x10^{-2}$ mmol) and an ether solution (1 ml) of *N*-benzyl-1-(4-methoxyphenyl)methanamine (12 mg, $4.79x10^{-2}$ mmol) were both cooled to –30 °C and then mixed together. The resulting cloudy mixture was quickly filtered through Celite and all volatiles were removed in vacuo to afford crude **3.10**. (NMR yield 82 %). The

crude product was dissolved in 1 mL of C_6D_6 containing 1,3,5-trimethoxybenzene (2 mg, 1.9 x 10^{-2} mmol) and the conversion of **3.10** to **3.2** and the *N*-borylamine **3.11** was monitored by ^{1}H NMR spectroscopy, with the varying concentrations of **3.10** and **3.2** determined at regular time intervals by ^{1}H NMR integration relative to internal standard. The error bars on the plot are generated from variability of ^{1}H NMR integrals.

3.11 References

[1] Zhao, W.; McCarthy, S. M.; Lai, T. Y.; Yennawar, H. P.; Radosevich, A. T. *J. Am Chem. Soc.* **2014**, *136*, 17634.

[2] McCarthy, S. M.; Lin, Y.-C.; Devarajan, D.; Chang, J. W.; Yennawar, H. P.; Rioux, R. M.; Ess, D. H.; Radosevich, A. T. *J. Am. Chem. Soc.* **2014**, *136*, 4640.

[3] Burck, S.; Gudat, D.; Nieger, M.; Du Mont, W.-W. *J. Am. Chem. Soc.* **2006**, 128, 3946.

[4] (a) Khusnutdinova, J. R.; Milstein, D. *Angew. Chem. Int. Ed.* **2015**, *54*, 12236–12273. (b) Khusnutdinova, J. R.; Milstein, D. *Angew. Chem. Int. Ed.* **2015**, *54*, 12236.

[5] (a) Gunanathan, C.; Milstein, D. *Acc. Chem. Res.* **2011**, *44*, 588. (b) Zell, T.; Milstein, D. *Acc. Chem. Res.* **2015**, *48*, 1979. (c) Koren-Selfridge, L.; Londino, H. N.; Vellucci, J. K.; Simmons, B. J.; Casey, C. P.; Clark, T. B. *Organometallics* **2009**, *28* , 2085. (d) Schneider, S.; Meiners, J.; Askevold, B. *Eur. J. Inorg. Chem.* **2012**, *2012*, 412. (e) Hashiguchi, S.; Fujii, A.; Takehara, J.; Ikariya, T.; Noyori, R. *J. Am. Chem. Soc.* **1995**, *117* , 7562. (f) Fujii, A.; Hashiguchi, S.; Uematsu, N.; Ikariya, T.; Noyori, R. *J. Am. Chem. Soc.* **1996**, *118*, 2521. (g) Uematsu, N.; Fujii, A.; Hashiguchi, S.; Ikariya, T.; Noyori, R. *J. Am. Chem. Soc.* **1996**, *118*, 4916.

[6] (a) Arrowsmith, M.; Hadlington, T. J.; Hill, M. S.; Kociok-Köhn, G. *Chem. Commun.* **2012**, *48*, 4567. (b) Arrowsmith, M.; Hill, M. S.; Kociok-Köhn, G. *Chem. Eur. J.* **2013**,

19, 2776. (c) Arrowsmith, M.; Hill, M. S.; Hadlington, T.; Kociok-Köhn, G.; Weetman, C. *Organometallics* **2011**, *30*, 5556.

[7] (a) Dureen, M. A.; Stephan, D. W. *J. Am. Chem. Soc.* **2010**, *132*, 13559. (b) R. Cabrera, A.; S. Rojas, R.; Valderrama, M.; Plüss, P.; Berke, H.; G. Daniliuc, C.; Kehr, G.; Erker, G. *Dalton Trans.* **2015**, *44*, 19606. (c) Theuergarten, E.; Schlösser, J.; Schlüns, D.; Freytag, M.; G. Daniliuc, C.; G. Jones, P.; Tamm, M. *Dalton Trans.* **2012**, *41*, 9101.

[8] (a) Gellrich, U.; Diskin-Posner, Y.; Shimon, L. J. W.; Milstein, D. *J. Am. Chem. Soc.* **2016**, *138*, 13307. (b) Appelt, C.; Westenberg, H.; Bertini, F.; Ehlers, A. W.; Slootweg, J. C.; Lammertsma, K.; Uhl, W. *Angew. Chem. Int. Ed.* **2011**, *50* (17), 3925.

[9] (a) Li, J.; Li, B.; Liu, R.; Jiang, L.; Zhu, H.; Roesky, H. W.; Dutta, S.; Koley, D.; Liu, W.; Ye, Q. *Chem. Eur. J.* **2016**, *22* , 14499. (b) Yu, Y.; Li, J.; Liu, W.; Ye, Q.; Zhu, H. *Dalton Trans.* **2016**, *45*, 6259. (c) Freitag, S.; Henning, J.; Schubert, H.; Wesemann, L. *Angew. Chem. Int. Ed.* **2013**, *52*, 5640.

[10] (a) Xiong, Y.; Yao, S.; Driess, M. *Organometallics* **2009**, *28*, 1927. (b) Gau, D.; Rodriguez, R.; Kato, T.; Saffon-Merceron, N.; de Cózar, A.; Cossío, F. P.; Baceiredo, A. *Angew. Chem. Int. Ed.* **2011**, *50*, 1092. (c) Delawar, M.; Gehrhus, B.; B. Hitchcock, P. *Dalton Transactions* **2005**, 2945.

[11] Nifantiev, E. E.; Grachev, M. K.; Burmistrov, S. Y. *Chem. Rev.* **2000**, *100*, 3755.

[12] Power, P. P. *Nature* **2010**, *463*, 171.

[13] Myers, T. W.; Berben, L. A. *J. Am. Chem. Soc.* **2013**, *135*, 9988.

[14] W. Myers, T.; A. Berben, L. *Chem. Sci.* **2014**, *5*, 2771.

[15] (a) Keaton, R. J.; Blacquiere, J. M.; Baker, R. T. *J. Am. Chem. Soc.* **2007**, *129*, 1844. (b) Pun, D.; Lobkovsky, E.; J. Chirik, P. *Chem. Commun.* **2007**, 3297. (c) Chaplin, A. B.; Weller, A. S. *Angew. Chem. Int. Ed.* **2010**, *49*, 581.

[16] (a) Stahl, T.; Müther, K.; Ohki, Y.; Tatsumi, K.; Oestreich, M. *J. Am. Chem. Soc.* **2013**, *135*, 10978. (b) Anaby, A.; Butschke, B.; Ben-David, Y.; Shimon, L. J. W.; Leitus, G.; Feller, M.; Milstein, D. *Organometallics* **2014**, *33*, 3716.

[17] (a) Wilczynski, R.; Sneddon, L. G. *J. Am. Chem. Soc.* **1980**, *102*, 2857. (b) Wilczynski, R.; Sneddon, L. G. *Inorg. Chem.* **1981**, *20*, 3955. (c) Wilczynski, R.; Sneddon, L. G.

Inorg. Chem. **1982**, *21*, 506. (d) Davan, T.; Corcoran, E. W.; Sneddon, L. G. *Organometallics* **1983**, *2*, 1693. (e) Pender, M. J.; Carroll, P. J.; Sneddon, L. G. *J. Am. Chem. Soc.* **2001**, *123*, 12222. (f) Gridnev, I. D.; Miyaura, N.; Suzuki, A. *Organometallics* **1993**, *12*, 589. (g) Kaithal, A.; Chatterjee, B.; Gunanathan, C. *Org. Lett.* **2015**, *17*, 4790. (h) Burgess, K.; Jaspars, M. *Tetrahedron Lett.* **1993**, *34*, 6813. (i) Burgess, K.; Jaspars, M. *Organometallics* **1993**, *12*, 4197. (j) Yamamoto, Y.; Fujikawa, R.; Umemoto, T.; Miyaura, N. *Tetrahedron* **2004**, *60*, 10695. (k) Satoh, M.; Nomoto, Y.; Miyaura, N.; Suzuki, A. *Tetrahedron Lett.* **1989**, *30*, 3789. (l) Männig, D.; Nöth, H. *Angew. Chem. Int. Ed. Engl.* **1985**, *24*, 878.

[18] (a) Frey, G. D.; Masuda, J. D.; Donnadieu, B.; Bertrand, G. *Angew. Chem., Int. Ed.* **2010**, *49*, 9444. (b) Lastovickova, D. N.; Bielawski, C. W. *Organometallics* **2016**, *35*, 706.

[19] (a) Dureen, M. A.; Lough, A.; Gilbert, T. M.; Stephan, D. W. *Chem. Commun.* **2008**, 4303. (b) Eisenberger, P.; Bailey, A. M.; Crudden, C. M. *J. Am. Chem. Soc.* **2012**, *134*, 17384.

[20] Waterman, R. *Organometallics* **2013**, *32*, 7249.

[21] Hill, M. S.; Liptrot, D. J.; Weetman, C. *Chem. Soc. Rev.* **2016**, *45*, 972.

[22]. (a) Corey, E. J.; Bakshi, R. K.; Shibata, S.; Chen, C. P.; Singh, V. K. *J. Am. Chem. Soc.* **1987**, *109*, 7925. (b) Corey, E. J.; Bakshi, R. K.; Shibata, S. *J. Am. Chem. Soc.* **1987**, *109*, 5551. (c) Corey, E. J.; Helal, C. J. *Angew. Chem. Int. Ed.* **1998**, *37*, 1986.

[23] Gudat, D. *Acc. Chem. Res.* **2010**, *43*, 1307.

[24] All X-ray diffraction experiments were conducted by Dr. Hemant Yennawar.

[25] Snow, S. S.; Jiang, D. X.; Parry, R. W. *Inorg. Chem.* **1985**, *24*, 1460.

[26] (a) Greenhalgh, R.; Newbery, J. E.; Woodcock, R.; Hudson, R. F. *Chem. Commun.* **1969**, 22. (b) Hudson, R. F.; Brown, C. *Acc. Chem. Res.* **1972**, *5*, 204.

Chapter Four. Bond Activation Reactivity of Geometrically Constrained Iminophosphoranes

Chapter Four

Bond Activation Reactivity of Geometrically Constrained Iminophosphoranes

The studies of the noncanonical reactivity of the C_{2v} and C_s-symmetric phosphines presented in the previous chapters provide strong supports to our hypothesis that reactivity of σ^3-phosphorus molecules can be significantly altered by structural deformation. Bond activation reactivities arise from initial electrophilic interaction of phosphorus center and subsequent ligand-assisted or exogenous base-assisted transformation are realized as the geometry of phosphines distort away from a traditional pyramidal structure. In addition to providing valuable information about the impact of geometric distortion on the reactivity of σ^3-phosphorus molecules, the investigations also inspired us to leverage geometry manipulation beyond σ^3-phosphorus compounds by pursuing unprecedented reactivity in σ^4-phosphorus species. We present in this chapter the preparation and chemical properties of iminophosphorane compounds with constrained O,N,O– and N,N,N-frameworks. Additionally, reactivity studies of the geometrically deformed iminophosphoranes toward B-H, B-O and Si-H bonds are discussed in this chapter.

4.1 Synthesis and Characterization of the Iminophosphoranes with Constrained O,N,O Ligand Framework

As discussed in Chapter 1, iminophosphoranes are σ^4-phosphorus molecules with formally double-bonded nitrogen at the phosphorus atom that traditionally adopt pseudo-tetrahedral geometry. Although useful in the synthesis of amines, [1] amides [2] and hetrocyclic compounds, [3] the phosphorus center of iminophosphoranes is relatively unreactive due to the congested tetracoordinate environment and the energetically inaccessible phosphorus-localized frontier orbitals. Instead, the synergistic effect of low Lewis acidic phosphorus center and basic nitrogen in the structure of iminophosphorane makes the compound particularly useful in the chemistry of organic superbase and Lewis-base-catalyzed transformations.[4]

As can be rationalized by qualitative molecular orbital analysis, the electronic structure of tetracoordinate phosphorus molecules such as iminophosphoranes undergoes significant change upon geometry distortion (see **Figure 1.3**).[5] Most dramatically, the LUMO is lowered by molecular distortion of iminophosphorane from tetrahedral to C_{2v} geometry. Coupled with the increased steric accessibility of the phosphorus center in this lower symmetric state, new possibilities in iminophosphorane chemistry might be expected if such compounds are accessible. In light of the unique structures and the resulting reactivity of C_{2v}[6] and C_s[7]-symmetric phosphines, we were interested in the preparation of iminophosphoranes in the similar distorted O,N,O– and N,N,N-phosphabicyclic platforms (**Figure 4.1**).

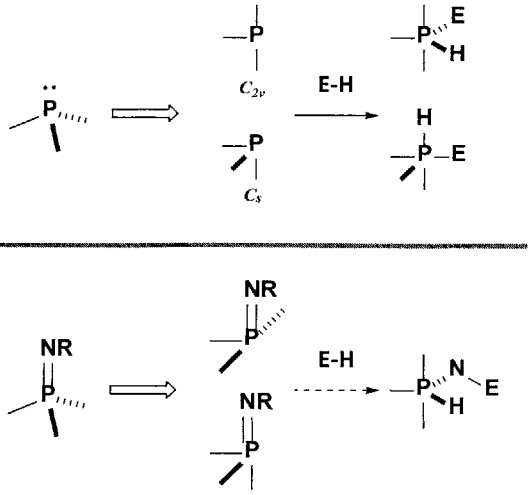

Figure 4.1. Geometry distortion and new reactivity of σ^3- and σ^4-phosphorus molecules.

Iminophosphorane **4.2** with constrained O,N,O–ligand was prepared from the C_{2v}-symmetric phosphine **4.1** with the Staudinger method [8] (**Figure 4.2**). Treatment of **4.1** with 1 equiv. of 2,6-diisopropylphenyl azide in C_6D_6 at 40 °C for 16 h resulted in a crude product mixture which showed a major ^{31}P NMR signal at 7.21 ppm. The chemical shift of the NMR resonance is consistent with compositionally related O,N,O–substituted iminophosphoranes in the literature.[9] All volatiles were removed *in vacuo* and the resulting residue was triturated with pentane. The crude product thus obtained after filtration was purified to a white solid by recrystallization from a 10:1 dichloromethane/pentane solution. Crystalline samples of **4.2** suitable for X-ray diffraction were prepared by slow crystallization from CH_2Cl_2/pentane solution. The molecular structure (**Figure 4.3**) confirmed that iminophosphorane **4.2** was obtained.

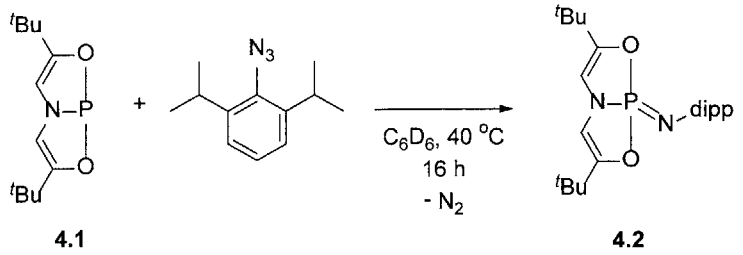

4.1 4.2

Figure 4.2. Synthesis of 4.2 from phosphine **4.1**. dipp = 2,6-diisopropylphenyl.

It warrants noting that the transformation from phosphine **4.1** to **4.2** requires harsher reaction conditions and longer reaction times than typical for Staudinger procedures. This observation can be rationalized on a mechanistic basis. Staudinger reactions are proposed to proceed in stepwise fashion by the initial addition of phosphine to an azide substrate. In the case of **4.1**, the initial nucleophilic interaction between the phosphine and azide is impeded due to the low nucleophilicity of the phosphorus center in **4.1.**

4.2 Synthesis and Characterization of the Iminophosphoranes with Constrained N,N,N Ligand Framework

Iminophosphorane **4.4** with the N,N,N-ligand backbone was similarly prepared from C_s-symmetric **4.3** and 2,6-diisopropylphenyl azide (**Figure 4.4**). Treatment of **4.3** with 1 equiv. of 2,6-diisopropylphenyl azide in C_6D_6 at ambient temperature for 12 h resulted in a crude product with a major ^{31}P NMR signal at 14.5 ppm. Following solvent removal *in vacuo*, the resulting crude product was recrystallized from a 10:1 dichloromethane/pentane solution to afford the

crystalline samples of **4.4**. X-ray diffraction (**Figure 4.5**) confirmed that N,N,N-iminophosphorane **4.4** was obtained as a monomeric iminophosphorane.[10]

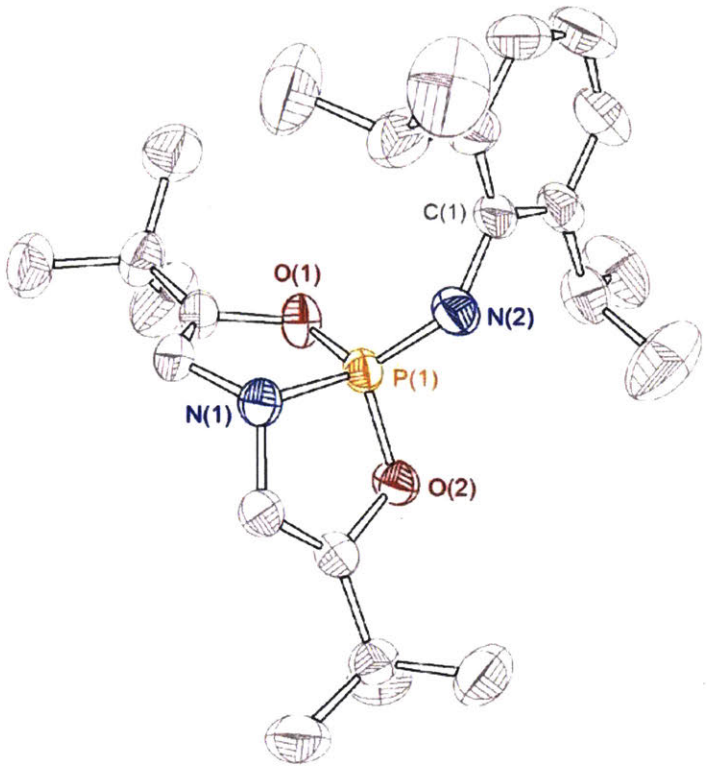

Figure 4.3. Molecular structure of **4.2** with 50% probability level rendered thermal ellipsoid plot. Selected bond lengths [Å] and angles [°]: P(1)–N(1) 1.690(1), P(1)–N(2) 1.507(1), P(1)–O(1) 1.604(1), P(1)–O(2) 1.596(1), C(1)–N(2) 1.399(2); O(2)-P(1)-N(2) 109.41(6), O(1)-P(1)-N(2) 115.31(6), N(1)-P(1)-N(2) 124.95(6), O(2)-P(1)-O(1) 112.61(5), O(2)-P(1)-N(1) 96.19(6), O(1)-P(1)-N(1) 96.68(5), P(1)-N(2)-C(1) 135.7(1).

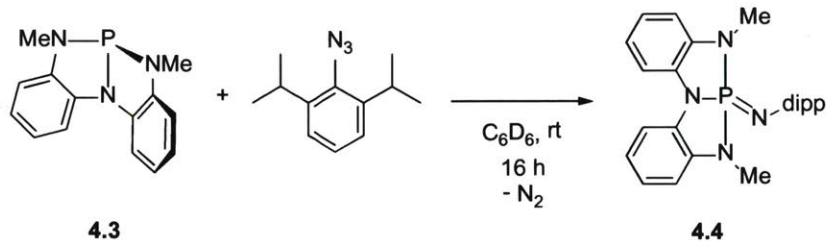

4.3 4.4

Figure 4.4. Synthesis of **4.4** from phosphine **4.3**. dipp = 2,6-diisopropylphenyl.

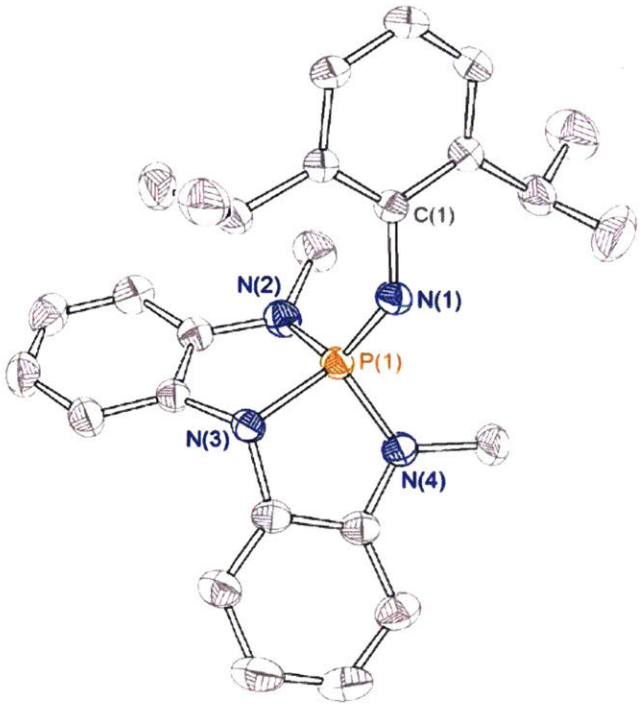

Figure 4.5. Molecular structure of **4.4** with 50% probability level rendered thermal ellipsoid plot. Selected bond lengths [Å] and angles [°]: P(1)–N(1) 1.531(1), P(1)–N(2) 1.673(1), P(1)–N(3) 1.710(1), P(1)–N(4) 1.659(1), C(1)–N(1) 1.402(2); N(1)-P(1)-N(2) 114.72(6), N(1)-P(1)-N(3) 129.23(6), N(1)-P(1)-N(4) 107.23(6), N(2)-P(1)-N(4) 119.73(6), N(2)-P(1)-N(3) 92.35(5), N(3)-P(1)-N(4) 92.84(5), P(1)-N(1)-C(1) 137.18(9).

4.3 Structural Analysis of the Constrained Iminophosphoranes

In order to understand the structural deformation imposed by the O,N,O- and N,N,N-phosphabicyclic frameworks in compounds **4.2** and **4.4**, iminophosphoranes with undistorted O,N,O- and N,N,N-substituents and the same *N*-dipp substituent were synthesized for comparison from phosphines **4.5** and **4.6** (**Figure 4.6**).

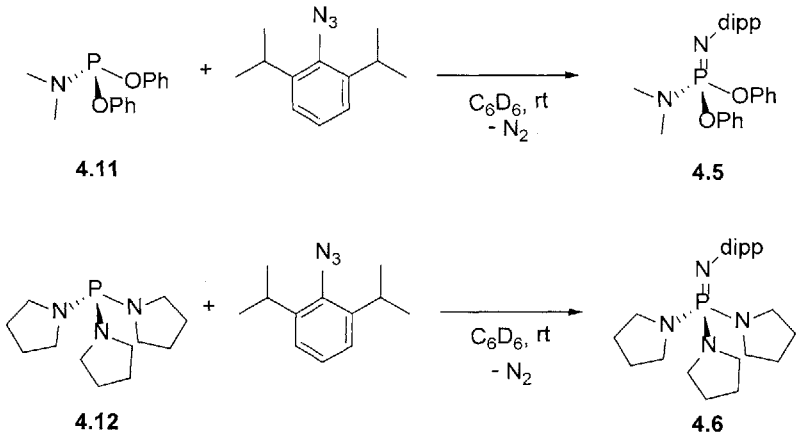

Figure 4.6. Synthesis of acyclic iminophosphorane **4.5** and **4.6**. dipp = 2,6-diisopropylphenyl.

The solid samples of iminophosphoranes **4.5** and **4.6** are obtained from crystallization in CH_2Cl_2/pentane solution and characterized by X-ray crystallography (**Figure 4.7** and **Figure 4.8**). To quantitatively evaluate the deviation of monomeric iminophosphorane **4.2** and **4.4** from tetrahedral geometry, geometry index parameter τ'_4 was calculated from the equation **4.1**:[11]

$$\tau'_4 = \frac{\beta - \alpha}{360^o - \theta} + \frac{180^o - \beta}{180^o - \theta} \qquad \textbf{(4.1)}$$

β and α are the two largest angles about the coordination center (β > α) and θ = 109.5°. Under this definition, a tetrahedral structure would result in τ'_4 = 1, whereas lower symmetry structures would have lower values (seesaw: τ'_4 = 0.36; square planar: τ'_4 = 0).

With the constrained O,N,O-phosphabicyclic framework, ∠O(1)-P(1)-N(1) (96.69(5)°) and ∠O(2)-P(1)-N(1) (96.19(6)°) of **4.2** are more contracted than the corresponding angles of acyclic **4.5** (107.1(1)° and 101.8(1)°) (**Table 4.1**). In addition, the angle between P=N and backbone P(1)-N(1) (124.95(6)°) in **4.2** is significantly larger than **4.5** (116.4(1)°), demonstrating a structure modestly distorted from conventional tetrahedral geometry toward the C_{2v} geometry with τ'_4 = 0.82 (compare τ'_4 = 0.87 for **4.5**). Similarly, O,N,O-phosphabicyclic iminophosphorane **4.4** has contracted endocyclic N(2)-P(1)-N(3) and N(3)-P(1)-N(4) angles (92.35(5)° and 92.84(5)°) and demonstrates an even more deviated structure with τ'_4 = 0.76 (compare τ'_4 = 0.90 for **4.6**) due to the larger angle (129.23(6)°) between P=N and backbone P(1)-N(3) (**Table 4.2**).

Compared to acyclic iminophosphorane **4.5** (d(P=N)=1.484(2) Å , ∠(P=N-C)=153.7(2)°), constrained O,N,O-iminophosphorane **4.2** has a longer P=N bond (1.507(1) Å) and a smaller P=N-C angle (137.18(9)°) (**Table 4.1**), presumably indicating a weaker P=N π-interaction. By contrast, distorted N,N,N-

iminophosphorane **4.4** has similar P=N bond length (1.531(1) Å, **Table 4.2**) and P=N-C angle (129.23(6)°) with acyclic N,N,N-iminophosphorane **4.6** (P(1)-N(1) = 1.526(3) Å, ∠P(1)-N(1)-C(1) = 137.1(3)°) and suggesting a stronger P-N π-bonding interaction and less reactive phosphorus center than its constrained O,N,O-congener **4.2**.

	4.2	**4.5**
∠O-P-N	96.69(5)°, 96.19(6)°	107.1(1)°, 101.8(1)°
∠N-P=N	124.95(6)°	116.4(1)°
d(P=N)	1.507(1) Å	1.484(2) Å
∠P=N-C	137.18(9)°	153.7(2)°

Table 4.1. Selected structural metrics for compound **4.2** and **4.5**.

	4.4	**4.6**
∠N-P-N	92.35(5)°, 92.84(5)°	104.4(2) °, 108.4(2) °
∠N-P=N	129.23(6)°, 114.72(6) °, 107.23(6) °	117.2(2) °, 115.0(2) °, 108.2(2) °
d(P=N)	1.531(1) Å	1.526(3) Å
∠P=N-C	129.23(6)°	137.1(3)°

Table 4.2. Selected structural metrics for compound **4.4** and **4.6**.

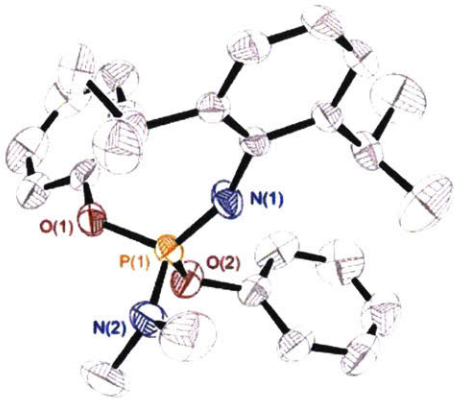

Figure 4.7. Molecular structure of **4.5** with 50% probability level rendered thermal ellipsoid plot. Selected bond lengths [Å] and angles [°]: P(1)–N(1) 1.484(2), P(1)–N(2) 1.613(2), P(1)–O(1) 1.606(2), P(1)–O(2) 1.600(2); N(1)-P(1)-N(2) 116.4(1), N(1)-P(1)-O(2) 112.3(1), N(1)-P(1)-O(1) 120.08(9), N(2)-P(1)-O(2) 107.1(1), O(1)-P(1)-O(2) 96.70(8), O(1)-P(1)-N(2) 101.8(1).

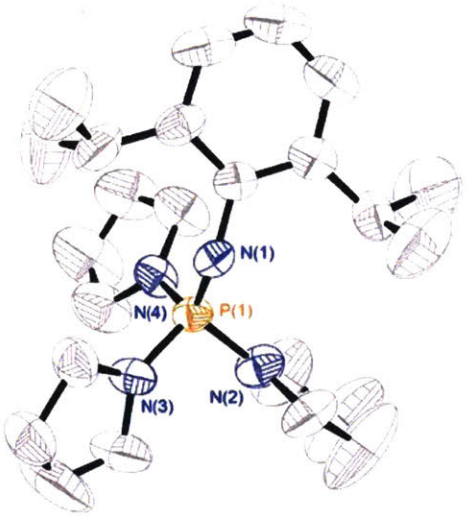

Figure 4.8. Molecular structure of **4.6** with 50% probability level rendered thermal ellipsoid plot. Selected bond lengths [Å] and angles [°]: P(1)–N(1) 1.526(3), P(1)–N(2) 1.649(4), P(1)–N(3) 1.633(4), P(1)–N(4) 1.638(3); N(1)-P(1)-N(2) 117.2(2), N(1)-P(1)-N(3) 115.0(2), N(1)-P(1)-N(4) 108.2(2), N(2)-P(1)-N(4) 102.6(2), N(2)-P(1)-N(3) 104.4(2), N(3)-P(1)-N(4) 108.4(2).

4.4 Dimerization of the Geometrically Constrained Iminophosphoranes

Interestingly, O,N,O-iminophosphoranes with imino N-substituents less sterically encumbering than 2,6-diisopropylphenyl undergo rapid dimerization at ambient temperature and can only be isolated in a dimeric form. In fact, even the deformed O,N,O-iminophosphorane **4.2** with bulky 2,6-diisopropylphenyl (dipp) N-substituent undergoes gradual dimerization at ambient temperature. The formal [2+2]-dimerization of iminophosphorane P=N units is known in the literature, occurring predominantly for iminophosphoranes bearing strong electron-withdrawing substituents, [12] or otherwise atypical structures. [13, 14] Consequently, the ready dimerization of O,N,O-iminophosphoranes **4.2** that lack strongly electron-withdrawing substituents is consistent with the hypothesis that a more Lewis acidic phosphorus center could be generated upon ligand distortion, facilitating the electrophilic interaction between the phosphorus centers and incoming electron donors such as the P=N nitrogen.

To differentiate the structural features between monomeric and dimeric iminophosphoranes in the constrained phosphorus ligation environment, the iminophosphoranes with N-substituted alkyl and aryl groups are prepared (**Figure 4.9** *top*). In a typical cyclophosphazane preparation, treatment of **4.1** with 1 equiv. of the azide in C_6D_6 at 60 °C (note elevated temperature compared to preparation of monomeric compounds above) for 24 h gave only dimerized iminophosphoranes with ^{31}P NMR signals in characteristic σ^5-phosphorus region (**Figure 4.9** *bottom*). The dimeric *O,N,O-*

iminophosphorane with N-2,6-diisopropylphenyl substituent could also be prepared from reacting **4.1** with the 2,6-diisopropylphenyl azide at 60 °C for 60 h. ^{31}P NMR signals of monomeric iminophosphoranes with N-dipp (**4.2**), N-tolyl (**4.7**), and N-mesityl (**4.8**) moieties can be detected as the reaction progresses. In contrast, iminophosphoranes with electron-withdrawing (**4.9** and **4.10**) and alkyl (**4.11** and **4.12**) N-substituents can only be observed in the dimeric forms. Single crystals of **4.2a**, **4.7a** and **4.8a** were obtained from benzene solutions and the X-ray diffraction patterns (**Figure 4.10**, **4.11** and **4.12**) confirmed a dimeric structure of the iminophosphoranes.

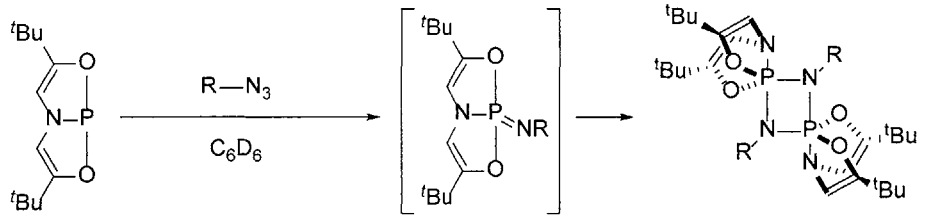

4.1 **4.2 - 4.12** **4.2a - 4.12a**

R =	^{31}P NMR	^{31}P NMR
4.2: 2,6-diisopropylphenyl	7.3	-26.9
4.7: *p*-tolyl	9.9	-45.7
4.8: mesityl	7.2	-50.1
4.9: 2-fluorophenyl	not observed	-42.9
4.10: 3,5-bis(trifluoromethyl)phenyl	not observed	-44.0
4.11: *n*-octyl	not observed	-36.3
4.12: cyclohexyl	not observed	-38.1

Figure 4.9. Synthesis of the dimerized *O,N,O*-iminophosphoranes.

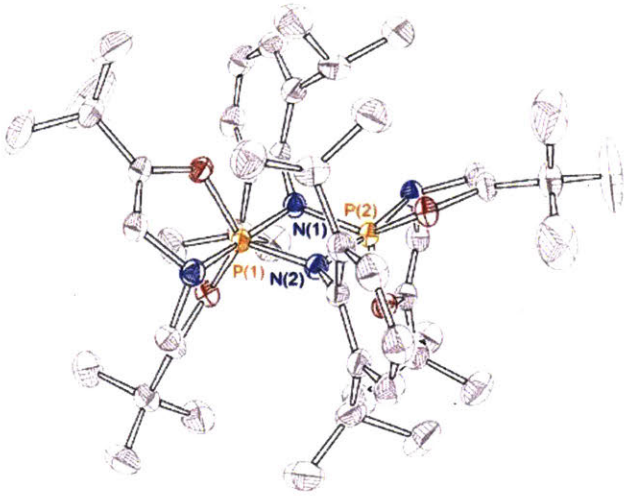

Figure 4.10. Molecular structure of **4.2a** with 50% probability level rendered thermal ellipsoid plot.

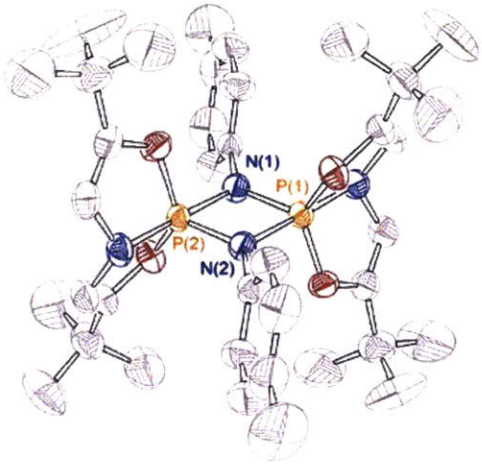

Figure 4.11. Molecular structure of **4.7a** with 50% probability level rendered thermal ellipsoid plot.

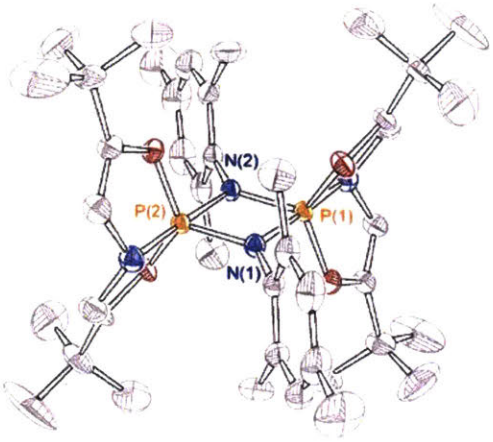

Figure 4.12. Molecular structure of **4.8a** with 50% probability level rendered thermal ellipsoid plot.

The axial P-N bonds are observed to be longer than the equatorial P-N bonds in the structure of dimeric iminophosphorane **4.2a**, **4.7a** and **4.8a**, in line with expectations for structures of typical pentacoordinate trigonal bipyramidal molecules. The P=N bond of monomer **4.2** (1.507(1) Å) is evolves on dimerization into the equatorial (1.664(2) Å) and axial (1.781(4) Å) P-N bonds in dimer **4.2a**, confirming the formation of covalently bonded four-membered cyclic structure in **4.2a** (as opposed to two closely packed monomers **4.2** in the solid state through the non-covalent interactions). Notably, the ^{31}P NMR resonance of dimer **4.2a** (-26.9 ppm) is significantly shifted down-field from the dimer **4.7a** (-45.7 ppm) and **4.8a** (-50.1 ppm). This ^{31}P NMR resonance shift to the less coordinate region can be explained by the existence of the bulkier N-dipp substituent and

the consequent larger separation between the two iminophosphorane sub-units in **4.2a**. The rationale is supported by the X-ray diffraction results, in which dimer **4.2a** displays longer bond length in both the axial P-N bond (1.781(4) Å) and the equatorial P-N bond (1.664(2) Å) than compound **4.7a** (axial P-N = 1.752(3) Å, equatorial P-N = 1.644(3) Å) and **4.8a** (axial P-N = 1.769(1) Å, equatorial P-N = 1.645(1) Å).

In accordance with larger separation between the two iminophosphorane sub-units in **4.2a**, dissolving the crystalline solid from the same sample used for X-ray diffraction of **4.2a** into C_6D_6 results in the regeneration of monomer **4.2** and a mixture with a 4:1 monomer/dimer ratio in ^1H and ^{31}P NMR spectra. In addition, after removing C_6D_6 from this solution mixture and storing the resulting solid at room temperature for 10 days, the redissolved sample in C_6D_6 gives no change in monomer/dimer ratio. Dissolving the crystalline sample of less bulky *N*-substituted **4.7a** and **4.8a** gave only dimer NMR signals and no monomer/dimer interconversion. This observation suggests that the dimeric forms of the constrained iminophosphoranes are predominate in the solid state for less steric demanding substituents, but in the most sterically hindered case of **4.2** /**4.2a**, monomer and dimer forms are interconvertible in the solution phase and exist as mixtures.

Further modifications of the N-substituents in the structure of deformed O,N,O-iminophosphoranes provide more information associated with the P=N [2+2] dimerization. No monomeric species were observed during the preparation of the N-electron-withdrawing group-substituted compounds (**4.9a** and **4.10a** in **Figure 4.9**), suggesting that a more electron-deficient phosphorus center further enhances the [2+2]

dimerization process by providing stronger interaction with the P=N nitrogen of second monomer. In addition to the aryl azides, alkyl azides were also used in the preparations of N-alkyl-O,N,O-iminophosphoranes. In the reactions of **4.1** with primary and secondary azides (**4.11a** and **4.12a** in **Figure 4.9**), ^{31}P and ^{1}H NMR monitoring showed exclusively the signals from dimerized iminophosphoranes, indicating that a less sterically hindered environment on the imine nitrogen again facilitated the dimerization process.

Inspired by the observation that the electron-deficient metal center of zirconium imido complexes can be coordinated by electron-donating species such as THF,[15] preparation of **4.2a** was attempted d_8-THF at 60 °C. In contrast to the reaction in C_6D_6, *in situ* monitoring of the transformation with ^{31}P NMR in d_8-THF showed that no dimerization happened during the process and the reaction eventually gave the pure monomeric product (^{31}P NMR δ 7.30 ppm in d_8-THF). Presumably, THF prevents the dimerization of **4.2** by interfering with the intramolecular interaction between the Lewis acidic phosphorus center and the imino nitrogen. However, the similarity of the observed ^{31}P NMR chemical shifts for **4.2** in both C_6D_6 and d_8-THF suggests only a weak solvation interaction between **4.2** and the donating solvent.

In contrast to the deformed O,N,O-iminophosphoranes, dimerization of the constrained N,N,N-iminophosphorane **4.4** was not observed under the same conditions, probably due to the less Lewis acidic phosphorus center and more congested environment around the P=N bond introduced by the N-methylanilide groups.

4.5 B-H and B-O Additions to Distorted Iminophosphorane

We were interested in the reactivity of iminophosphoranes **4.2** and **4.4** toward hydridic E-H bonds in order to probe reactivity of the P=N unit. Borane B-H bonds are excellent candidates for probing this potential reactivity because the Lewis-acidic boron atom can easily interact with the Lewis-basic iminophosphorane nitrogen and facilitate the hydride transfer from B-H to the phosphorus center. Indeed, even with the weakly hydridic pinacolborane, compound **4.2** undergoes an immediate B-H addition across the P=N bond (**Figure 4.13** *top*). The resulting ^{31}P NMR spectrum of this reaction shows a doublet of triplets centered at -43.7 ppm with a coupling constants $^{1}J_{P\text{-}H}$ = 837 Hz and $^{3}J_{P\text{-}H}$ = 33Hz, consistent with the formation of a pentacoordinate hydridophosphorane. Complementarily, the existence of a P-H moiety is confirmed by ^{1}H NMR spectroscopy, with a doublet centered at 9.37 ppm ($^{1}J_{P\text{-}H}$ = 837 Hz). N,N,N-iminophosphorane **4.4** similarly gives B-H addition with pinacolborane despite the lack of dimerization reactivity. To the best of our knowledge, no iminophosphorane has been previously reported to react with the borane B-H bonds to give the corresponding σ^5-hydridophosphorane. The reactivity of **4.2** and **4.4** toward B-H bonds demonstrate the hypothesized reactivity of the strained phosphabicyclic iminophosphoranes.

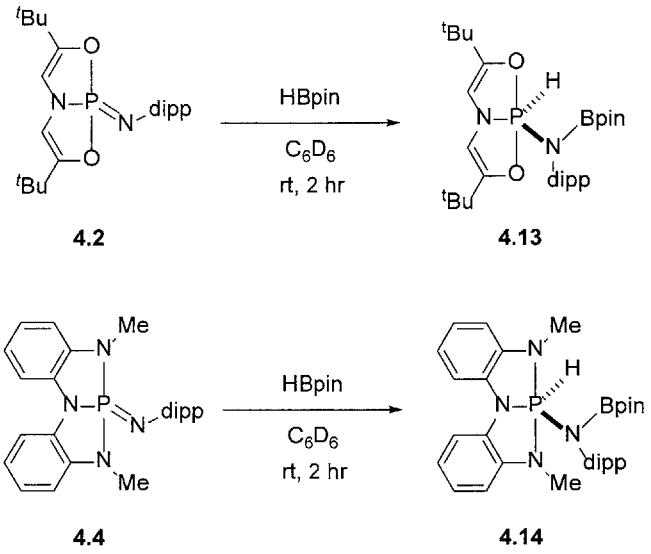

Figure 4.13. B-H additions to **4.2** and **4.4** with pinacolborane. dipp = 2,6-diisopropylphenyl.

With the distorted geometry, O,N,O-iminophosphorane **4.2** exhibits unusual Lewis-acidic reactivity toward B-O bonds of $B(OMe)_3$ and butoxy catecholborane (**Figure 4.14**). Reacting **4.2** with 1 equiv. of trimethyl borate produces a phosphorus species with a triplet at -41.2 ppm in ^{31}P NMR spectra ($J = 31$ Hz) (**Figure 4.14** *bottom*). ^{1}H NMR of this product also showed a doublet at 5.52 ppm ($J = 31$ Hz), corresponding to the ligand vinylic protons of the O,N,O-phosphobicyclic ligand. The characteristic ^{31}P NMR chemical shift and the small $^{3}J_{P\text{-}H}$ coupling of this product indicate that B-O addition across the P=N bond of **4.2** has occurred and the formation of a σ^5-phosphorus compound **4.15**. The reactivity of **4.2** toward B-O bonds is further demonstrated by reacting **4.2** with *n*-butoxy catecholborane (**Figure 4.14** *bottom*). Product **4.16** of this reaction again showed a triplet resonance centered at -31.4 ppm ($^{3}J_{P\text{-}H}$ =17 Hz) in ^{31}P NMR spectra. X-ray diffraction of the isolated **4.16** confirmed the σ^5-phosphorus

structure of this B-O addition product (**Figure 4.15**). The structure of **4.16** contains a *n*-butoxy group attached to the phosphorus center and a catecholboryl group on the amido nitrogen. The O,N,O-phosphabicyclic backbone of **4.2** has turned into part of the trigonal pyramidal structure and the phosphabicyclic nitrogen N(1) and the butoxy oxygen O(3) occupy the apical positions. The preference of placing the N(1) rather than two oxygen on the apical positions is probably due to the interaction between N(1) and the catecholboryl boron atom B(1), which renders N(1) even more electron-deficient than the phosphabicyclic oxygens. The N(1) - B(1) interaction can be confirmed by the short B-N distance (1.634(3) Å). These transformations demonstrated the first example of σ^4-iminophosphorane mediated B-O activation and provide further evidence for geometry-induced reactivity enhancement on the phosphorus atom.

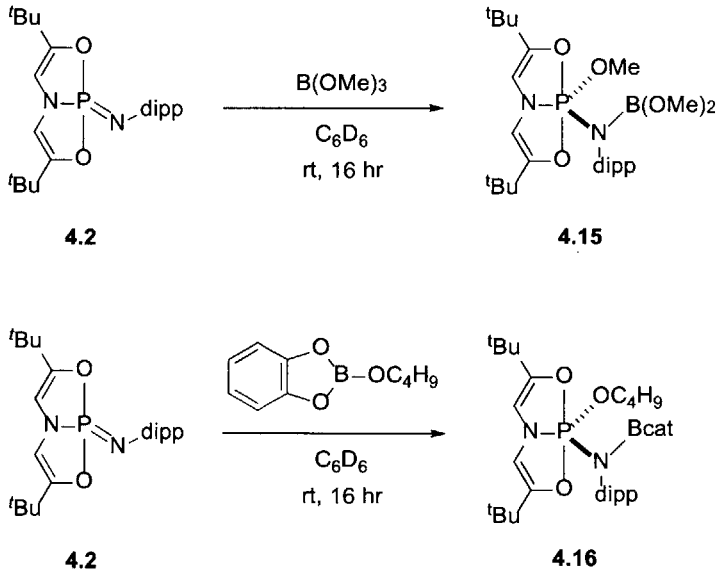

Figure 4.14. B-O additions to O,N,O-iminophosphorane **4.2**. dipp = 2,6-diisopropylphenyl.

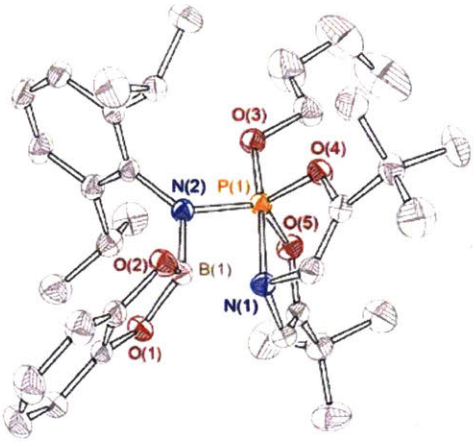

Figure 4.15. Molecular structure of **4.16** with 50% probability level rendered thermal ellipsoid plot.

4.6 Si-H Addition to Distorted Iminophosphoranes

Hydrosilanes are not generally as reactive as boranes due to the lack of non-bonding orbitals on the silicon atom with which to accept an incoming nucleophiles and increase hydricity. However, reacting phenylsilane with 1 equiv. of iminophosphorane **4.2** in C_6D_6 at 50 °C for 16 h (**Figure 4.16**) gives a phosphorus species **4.17** with a characteristic doublet resonance centered at 9.44 ppm in 1H NMR spectra exhibiting a large coupling constant ($^1J_{P\text{-}H}$ = 802 Hz), indicative of the existence of a P-H bond. Two other ^{1}H NMR doublet signals at 5.53 and 5.40 ppm represent P-H coupled vinyl protons and SiH_2 protons, respectively. The ^{31}P NMR spectra also show a doublet of triplets centered at -44.2 ppm with coupling constants of 803 Hz and 30 Hz. Taken together, the

product NMR spectra suggests that the silane Si-H bond has added across the P=N bond of **4.2** resulting in a hydridophosphorane with an N-silyl substituent. N,N,N-iminophosphorane **4.4** also reacts with phenylsilane but more slowly. The conversion of **4.4** and phenylsilane to hydridophosphorane **4.18** is completed after 48 hour of 80 °C heating in C_6D_6. The resulting ^{31}P NMR spectrum demonstrates again a signal centered at -29.1 ppm with a characteristic $^1J_{P\text{-}H}$ = 535 Hz, consistent with the structure of the σ^5-phosphorus Si-H addition product.

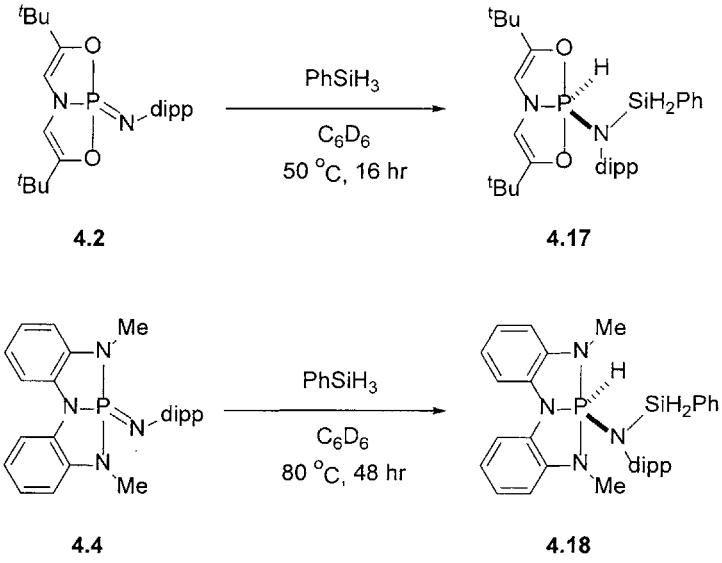

Figure 4.16. B-O additions to O,N,O-iminophosphorane **4.2**. dipp = 2,6-diisopropylphenyl.

In addition to the reaction with iminophosphorane **4.2** under mild conditions, phenylsilane also reacts with dimeric iminophosphorane **4.2a** to give complete conversion to the hydrophosphorane product, demonstrating again the monomer-dimer interconversion of **4.2/4.2a** in solution. Expanding the substrate scope to more sterically hindered silanes were attempted, but triethylsilane, triphenylsilane and diphenylsilane all gave no Si-H addition product even in refluxing toluene for several days. The low reactivity of **4.2** toward secondary or tertiary silanes may results from the steric hindrance of the *N*-dipp substituent. Attempts to react silanes with less bulky *N*-tolyl iminophosphoranes **4.7** were unsuccessful, likely because **4.7** dimerized to **4.7a** before reacting with the silanes and no monomer-dimer interconversion can regenerate monomer **4.7**. All other O,N,O-iminophosphoranes with less steric *N*-substituents behave the same as **4.7** and give no Si-H activation reactivity. The distorted N,N,N-iminophosphorane **4.4** demonstrates lower Si-H addition reactivity than **4.2** with higher reaction temperature (80 ^{o}C) being required for the transformation. Since **4.4** contains a more hindered structure around the phosphorus center and a similar P=N length with acyclic iminophosphorane **4.6**, the lower reactivity of **4.4** toward the Si-H bond is expected. Activation of Si-H bonds by **4.2** and **4.4** gives direct evidence for the distinctive chemical behaviour resulting from the molecular distortion of iminophosphorane and adds another example to our ongoing research of deformed phosphorus molecules.

4.7 Conclusion and Outlook

Geometrically distorted iminophosphoranes with the strained O,N,O- and N,N,N-phosphabicyclic frameworks are synthesized from the corresponding deformed phosphines. Their structures are characterized by X-ray diffraction and compared to acyclic iminophosphoranes without constrained structures. In line with the deviated molecular geometries and the modified electronic structures, these distorted iminophosphoranes display unusual reactivities such as rapid dimerization and hydridic E-H bonds additions. Intermolecular B-H, B-O and Si-H additions across the P=N bond of the iminophosphoranes are demonstrated and the resulting σ^5-phosphorus products are identified. Inspired by the significant property change induced by the molecular distortion in the iminophosphoranes, structure and reactivity of other σ^4-phosphorus compounds with similar deformed frameworks are currently under investigation.

4.8 Experimental

General Materials and Methods

All reagents were purified as described in the previous chapter. Pinacolborane was puridied by vacuum distillation (60 torr) and stored a nitrogen-filled glovebox. Benzylamine was purified by distillation from zinc dust and stored over 3 Å molecular sieves prior to use. All glassware was oven-dried at 120 °C prior to use. All reactions

were carried under dry nitrogen atmosphere (Schlenk line or glovebox) unless otherwise noted. NMR spectra were recorded on a Bruker AV-360 (360MHz), a Bruker AV-400 (400 MHz), a Bruker AV-500 (500MHz) or a VARIAN Inova-500 (500MHz) spectrometer. ^{1}H NMR chemical shifts are given in ppm with respect to solvent residual peak (C_6D_6, δ 7.16 ppm; $CDCl_3$, δ 7.26 ppm; CD_2Cl_2, δ 5.32 ppm), $^{13}C\{^{1}H\}$ NMR shifts are given in ppm with respect to $CDCl_3$ (δ 77.16 ppm), C_6D_6 (δ 128.06 ppm) or CD_2Cl_2 (δ 53.84 ppm). Coupling constants are reported as *J*-values in Hz. High resolution EI and ESI mass spectra were obtained from the Mass Spectrometry Laboratory at the School of Chemical Sciences, University of Illinois at Urbana-Champaign or Department of Chemistry Instrumentation Facility, Massachusetts Institute of Technology.

Synthetic Procedures and Characterization Data

Phosphine **4.1** and **4.3** were prepared by minor modification of the literature**Error! Bookmark not defined.** method as described in the previous chapters.

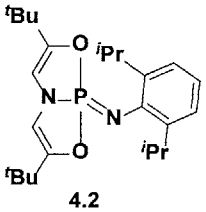

4.2

A C_6D_6 solution of **4.1** (100 mg, 0.42 mmol) was added 2,6-diisopropylphenyl azide (85 mg, 0.42 mmol) and the reaction was stirred at 40 °C for 16 h. All volatiles were removed *in vacuo* and the resulting residue was triturated with pentane. The crude product was obtained after filtration and pure **4.2** was isolated as a white solid by recrystallization from a 10:1 dichloromethane/pentane solution (131 mg, 75 % yield). ^{1}H NMR (C_6D_6, 400 MHz): δ 7.23-7.21 (m, 2H), 7.12-7.07 (m, 1H), 7.07 (d, 1H, J = 7.7 Hz), 5.49 (d, 2H, J =

28.8 Hz), 3.83 (hept, 1H, J = 6.9 Hz), 1.40 (d, 12H, J = 6.8 Hz), 0.91 (s, 18H) ppm. ^{13}C NMR (C_6D_6, 126 MHz): δ 154.19, 141.29 (d, J = 8.7 Hz), 123.03, 121.98, 112.43 (d, J = 10.1 Hz), 32.64 (d, J = 8.6 Hz), 29.35, 26.89, 23.75 ppm. ^{31}P NMR (C_6D_6, 162 MHz): δ 7.21 (t, J= 28.8 Hz) ppm. MS (ESI) calcd for C24H37N2O2P (M^+) 416.2593 found 416.2596.

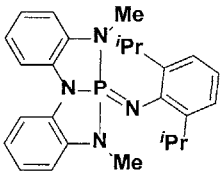

4.4

Treatment of **4.3** (100 mg, 0.39 mmol) with 1 equiv. 2,6-diisopropylphenyl azide (80 mg, 0.39 mmol) in C_6D_6 (1 ml) under ambient temperature for 12 h. The solvent was removed *in vacuo* and the resulting solid product was recrystallized from a 10:1 dichloromethane/pentane solution (121 mg, 72 % yield). ^{1}H NMR (C_6D_6, 400 MHz): δ 7.26 (d, J = 7.7 Hz, 2H), 7.16 (d, J = 7.4 Hz, 2H), 7.09 – 7.02 (m, 1H), 6.98 – 6.85 (m, 3H), 6.77 (d, J = 7.6 Hz, 3H), 6.23 (d, J = 7.7 Hz, 2H), 3.65 (hept, J = 6.9 Hz, 2H), 2.73 (d, J = 9.2 Hz, 6H), 1.22 (d, J = 6.9 Hz, 12H) ppm. ^{13}C NMR (C_6D_6, 125 MHz): δ 141.38, 141.00 (d, J = 11.7 Hz), 138.09 (d, J = 17.6 Hz), 134.58 (d, J = 13.0 Hz), 124.56, 123.26, 121.34, 120.14, 116.34 (d, J = 10.2 Hz), 108.66 (d, J = 10.0 Hz), 29.29 (d, J = 18.9 Hz), 23.75 ppm. ^{31}P NMR (C_6D_6, 162 MHz): δ 14.54 ppm. MS (ESI) calcd for C26H31N4P (M^+) 430.2286 found 430.2290.

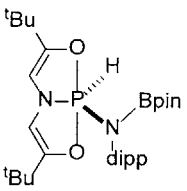

4.13

Treating **4.2** (30 mg, 0.07 mmol) with a C_6D_6 solution (0.3ml) of HBpin (9 mg, 0.07 mmol) at ambient temperature for 15 min. The solvent was

removed *in vacuo* to afford the crude product (37 mg, 95 % crude yield). ^{1}H NMR (C_6D_6, 500 MHz): δ 9.38 (d, 1H, J = 837.7 Hz), 7.27 – 7.25 (m, 1H), 7.08 – 7.04 (m, 2H), 5.49 (d, 2H, J = 33.2 Hz), 3.62-3.56 (m, 2H), 1.53 (d, 6H, J = 6.6 Hz, 1.45 (d, 6H, J = 6.6 Hz, 6H), 1.19 (s, 12H), 1.15 (s, 18H) ppm. ^{13}C NMR (C_6D_6, 126 MHz): δ 150.73 (d, J = 6.4 Hz), 147.14, 126.64, 124.52 (d, J = 4.4 Hz), 124.02, 123.42, 100.51 (d, J = 18.8 Hz), 82.52, 31.69, 28.25, 27.51, 24.66, 23.62, 23.26 ppm. ^{31}P NMR (C_6D_6, 203 MHz): δ -43.02 (dt, J = 837.0, 31.5 Hz) ppm. MS (ESI) calcd for C30H49BN2O4P (M-H$^+$) 543.3518 found 543.3523.

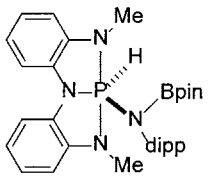

4.14

Treating **4.4** (35 mg, 0.08 mmol) with a C_6D_6 solution (0.3ml) of HBpin (10 mg, 0.08 mmol) at ambient temperature for 15 min. The solvent was removed *in vacuo* to afford the crude product (42 mg, 92 % crude yield). ^{1}H NMR (C_6D_6, 500 MHz): δ 7.44 (d, J = 7.5 Hz, 2H), 7.10 – 6.85 (m, 8H), 6.56 (d, J = 7.4 Hz, 1H), 6.36 (d, J = 578.8 Hz, 1H), 3.11 – 2.91 (m, 2H), 2.60 (d, J = 16.7 Hz, 6H), 1.15 (d, J = 6.9 Hz, 6H), 1.01 (d, J = 6.7 Hz, 6H), 0.83 (s, 12H) ppm. ^{13}C NMR (C_6D_6, 126 MHz): δ 147.97 (d, J = 5.0 Hz), 135.98, 134.16 (d, J = 12.9 Hz), 133.81 (d, J = 14.5 Hz), 126.90, 124.52 (d, J = 5.7 Hz), 123.11, 119.83, 118.86, 110.92 (d, J = 11.4 Hz), 108.55 (d, J = 7.2 Hz), 81.95, 28.15, 25.94, 24.61, 23.97, 23.07 ppm. ^{31}P NMR (C_6D_6, 203 MHz): δ -37.57 (d, J = 578.8) ppm. MS (ESI) calcd for C32H43BN4O2P (M-H$^+$) 557.3217 found 557.3212.

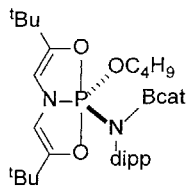

4.16

Treating **4.2** (60 mg, 0.14 mmol) with a C_6D_6 solution (0.3ml) of butoxy catecholborane (26 mg, 0.14 mmol) at ambient temperature for 1 hr. The solvent was removed *in vacuo* and the resulting solide product was recrystallized from a benzene solution (58 mg, 65 % yield). ^{1}H NMR (C_6D_6, 400 MHz): δ 7.15 (d, J = 1.5 Hz, 3H), 6.90 (dd, J = 5.6, 3.4 Hz, 2H), 6.67 (dd, J = 5.6, 3.3 Hz, 2H), 5.33 (d, J = 16.6 Hz, 2H), 4.05 – 3.90 (m, 2H), 3.84 – 3.71 (m, 2H), 1.52 (d, J = 6.8 Hz, 6H), 1.41 (d, J = 7.1 Hz, 6H), 1.24 – 1.10 (m, 4H), 1.04 (s, 9H), 0.87 (t, J = 7.4 Hz, 3H) ppm. ^{13}C NMR (C_6D_6, 126 MHz): δ 157.24, 151.97, 147.15 (d, J = 6.0 Hz), 134.07 (d, J = 8.2 Hz), 126.78, 124.02, 123.38, 119.33, 109.54, 109.33 (d, J = 4.7 Hz), 65.24 (d, J = 9.2 Hz), 32.56 (d, J = 10.1 Hz), 27.98, 26.40, 24.85, 18.46, 15.29, 13.34 ppm. ^{31}P NMR (C_6D_6, 203 MHz): δ -31.41 ppm. MS (ESI) calcd for C34H50BN2O5P (M^+) 608.3550 found 608.3555.

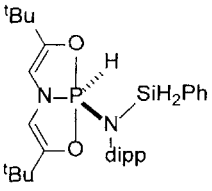

4.17

Treating **4.2** (60 mg, 0.14 mmol) with a C_6D_6 solution (0.3ml) of phenylsilane (16 mg, 0.14 mmol) at 50 °C for 16 h. All volatiles were removed *in vacuo* to afford **4.17** as colorless oil (74 mg, 98 % crude yield). ^{1}H NMR (C_6D_6, 500 MHz): δ 9.25 (d, J = 801.2 Hz, 1H), 7.85 (dd, J = 7.9, 1.7 Hz, 2H), 7.17 – 6.85 (m, 6H), 5.34 (d, J = 31.2 Hz, 2H), 5.22 (s, 2H), 3.63 (hept, J = 6.8 Hz, 2H), 1.29 (d, J = 6.9 Hz, 6H), 1.08 (d, J = 6.8 Hz, 6H), 0.85 (s, 18H) ppm. ^{13}C NMR (C_6D_6, 126 MHz): δ 150.26, 146.86, 140.12, 134.80, 129.54, 126.36, 123.82, 101.61 (d, J = 18.5 Hz), 31.85, 28.70, 28.22, 27.42 ppm. ^{31}P NMR

(C_6D_6, 203 MHz): δ -43.52 (dt, J = 801.8, 30.7 Hz) ppm. MS (ESI) calcd for C30H46N2O2PSi ($M+H^+$) 525.3061 found 525.3065.

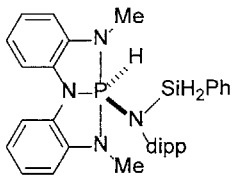

4.18

Reacting **4.4** (50 mg, 0.12 mmol) with a C_6D_6 solution (0.3ml) of phenylsilane (13 mg, 0.12 mmol) at 80 °C for 48 h. All volatiles were removed *in vacuo* to afford **4.18** as yellow oil (62 mg, 99 % crude yield). ^{1}H NMR (C_6D_6, 500 MHz): δ 7.32 (d, J = 7.1 Hz, 2H), 7.14 – 6.99 (m, 7H), 6.95 (t, J = 7.2 Hz, 3H), 6.87 (t, J = 7.7 Hz, 2H), 6.73 (t, J = 7.8 Hz, 2H), 6.37 (d, J = 7.5 Hz, 2H), 5.75 (d, J = 534.0 Hz, 1H), 5.05 (d, J = 5.8 Hz, 2H), 3.45 – 3.33 (m, 2H), 2.49 (d, J = 15.9 Hz, 6H), 1.15 (d, J = 6.8 Hz, 6H), 1.06 (d, J = 6.7 Hz, 6H) ppm. ^{13}C NMR (C_6D_6, 126 MHz): δ 148.30 (d, J = 5.8 Hz), 137.93, 135.77 (d, J = 10.4 Hz), 134.65 (d, J = 14.5 Hz), 134.25, 133.46, 129.01, 127.16 (d, J = 3.6 Hz), 123.90 (d, J = 4.0 Hz), 121.42, 119.38, 113.89 (d, J = 10.8 Hz), 108.72 (d, J = 7.6 Hz), 29.69 (d, J = 15.5 Hz), 27.61, 26.24, 23.84 ppm. ^{31}P NMR (C_6D_6, 203 MHz): δ -28.54 (dt, J = 534.5, 17.2 Hz)) ppm. MS (ESI) calcd for C32H40N4PSi ($M+H^+$) 539.2760 found 539. 539.2763.

4.9 References

[1] (a) Murahashi, S.; Taniguchi, Y.; Imada, Y.; Tanigawa, Y. *J. Org. Chem.* **1989**, *54*, 3292. (b) Goldinga, B. T.; O'Sullivan, M. C.; Smith, L. L. *Tetrahedron Lett.* **1988**, *29*, 6651.

[2] (a) Lambert, P. H.; Vaultier, M.; Carrie, R. *J. Org. Chem.* **1985**, *50*, 5352. (b) Urpí, F.; Vilarrasa, J. *Tetrahedron Lett.* **1986**, *27*, 4623.

[3] Molina, P.; Vilaplana, M. J. *Synthesis* **1994**, *1994*, 1197.

[4] Ishikawa, T. *Superbases for Organic Synthesis : Guanidines, Amidines, Phosphazenes and Related Organocatalysts.*; Chichester, UK : John Wiley & Sons, 2009.

[5] Gimarc, B. M.; Khan, S. A. *J. Am. Chem. Soc.* **1978**, *100*, 2340.

[6] McCarthy, S. M.; Lin, Y.-C.; Devarajan, D.; Chang, J. W.; Yennawar, H. P.; Rioux, R. M.; Ess, D. H.; Radosevich, A. T. *J. Am. Chem. Soc.* **2014**, *136*, 4640.

[7] Zhao, W.; McCarthy, S. M.; Lai, T. Y.; Yennawar, H. P.; Radosevich, A. T. *J. Am Chem. Soc.* **2014**, *136*, 17634.

[8] Gololobov, Y. G.; Zhmurova, I. N.; Kasukhin, L. F. *Tetrahedron* **1981**, *37*, 437.

[9] Kukhar, V. P.; Gilyarov, V. A., *Pure Appl. Chem.* **1980,** *52* , 891.

[10] All X-ray diffraction experiments were conducted by Dr. Hemant Yennawar.

[11] (a) Okuniewski, A.; Rosiak, D.; Chojnacki, J.; Becker, B. *Polyhedron* **2015**, *90*, 47. (b)Yang, L.; Powell, D. R.; Houser, R. P. *Dalton Trans.* **2007**, 9, 955.

[12] (a) Y. G. Shermolovich, A. V. Solov'ev, E. A. Danchenko and L. N. Markovskii, *Zh. Obshch. Khim.*, 1983, **53**, 2150. (b) A. P. Marchenko, V. V. Miroshnichenko, V. A. Kovenya, A. M. Pinchuk, A. N. Chernega, M. Y. Antipin and Y. T. Struchkov, *Zh. Obshch. Khim.*, 1988, **58**, 1758. (c) H. Rolland, E. Ocando-Mavarez, P. Potin, J. P. Majoral and G. Bertrand, *Inorg. Chem.*, 1991, **30**, 4095

[13] (a) Y. G. Gololobov, L. I. Nesterova, V. P. Kukhar and V. I. Luk'yanchuk, *Zh. Obshch. Khim.*, 1981, **51**, 477. (b) B. A. Arbuzov, É. N. Dianova and E. Y. Zabotina, *Russ Chem Bull*, 1981, **30**, 2192. (c) M. A. Pudovik, L. K. Kibardina, S. A. Terent'eva and A. N. Pudovik, *Zh. Obshch. Khim.*, 1991, **61**, 2470. (d) T. V. Kolodka and Y. G. Gololobov, *Zh. Obshch. Khim.*, 1983, **53**, 1013. (c) A. Schmidpeter, H. Tautz and F. Schreiber, *Z. Anorg. Allg. Chem.*, 1981, **475**, 211. (d) R. Francke and G.-V. Röschenthaler, *Z. Anorg. Allg. Chem.*, 1989, **572**, 135.

[14] (a) G. Bertrand, J.-P. Majoral and A. Baceiredo, *Tetrahedron Lett.* 1980, **21**, 5015. (b) J. Boeske, E. Ocando-Mavarez, E. Niecke, J. P. Majoral and G. Bertrand, *J. Am.*

Chem. Soc., 1987, **109**, 2822. (c) J. Boeske, E. Niecke, M. Nieger, E. Ocando, J. P. Majoral and G. Bertrand, *Inorg. Chem.*, 1989, **28**, 499. (d) V. D. Romanenko, A. V. Ruban, S. V. Iksanova and L. N. Markovskii, *Zh. Obshch. Khim.*, 1984, **54**, 313. (e) J. Vrána, S. Ketkov, R. Jambor, A. Růžička, A. Lyčka and L. Dostál, *Dalton Trans.*, 2016, **45**, 10343. (f) M. H. Holthausen and J. J. Weigand, *Dalton Trans.*, 2016, **45**, 1953. (g) O. Diallo, M. T. Boisdon, C. Malavaud, L. Lopez, M. Haddad and J. Barrans, *Tetrahedron Lett.* 1984, **25**, 5521. (h) O. Diallo, M. T. Boisdon, C. Malavaud, L. Lopez, M. Haddad and J. Barrans, *Tetrahedron Lett.* 1984, **25**, 5521. (i) N. Burford, T. S. Cameron, C. L. B. Macdonald, K. N. Robertson, R. Schurko, D. Walsh, R. McDonald and R. E. Wasylishen, *Inorg. Chem.*, 2005, **44**, 8058. (j) N. Burford, T. S. Cameron, K. D. Conroy, B. Ellis, M. Lumsden, C. L. B. Macdonald, R. McDonald, A. D. Phillips, P. J. Ragogna, R. W. Schurko, D. Walsh and R. E. Wasylishen, *J. Am. Chem. Soc.*, **2002**, 124, 14012. (k) J. Navech, H. Germa and S. Mathieu, *Phosphorus Sulfur*, **1988**, 35, 247

[15] Walsh, P. J.; Hollander, F. J.; Bergman, R. G. *J. Am. Chem. Soc.* **1988**, *110*, 8729.

Appendix A

Supplemental Data for Chapters Two

Table of Contents

I. Crystallographic Procedure and Data.

A colorless block shaped crystal of **2.5e** ($C_{21}H_{33}N_2O_2P$) with approximate dimensions 0.15 x 0.16 x 0.18 mm was prepared by crystallization from pentane at -30 °C used for the X-ray crystallographic analysis. The X-ray intensity data were measured at 173(2) K, cooled by Rigaku-MSC X-Stream 2000, on a Bruker SMART APEX CCD area detector system equipped with a graphite monochromator and a MoKa fine-focus sealed tube (l = 0.71073Å) operated at 1600 watts power (50 kV, 32 mA). The detector was placed at a distance of 5.8 cm from the crystal. A total of 1750 frames were collected with a scan width of 0.3° in w and an exposure time of 10 seconds/frame. The total data collection time was about 8 hours. The frames were integrated with the Bruker SAINT software package using a narrow-frame integration algorithm. The integration of the data using a Monoclinic unit cell yielded a total of 17228 reflections to a maximum q angle of 28.19° (0.90 Å resolution), of which 5154 were independent, completeness = 98.9%, R_{int} = 0.0303, R_{sig} = 0.0321 and 4342 were greater than 2s(I). The final cell constants: a = 14.8761(19)Å, b = 17.428(2)Å, c = 8.2778(10)Å, a = 90°, b = 99.402(2)°, g = 90°, volume = 2117.3(5)$Å^3$, are based upon the refinement of the XYZ-centroids of 7582 reflections above 20s(I) with 2.718° <q <28.172°. Analysis of the data showed negligible decay during data collection. Data were corrected for absorption effects using the multiscan technique (SADABS). The ratio of minimum to maximum apparent transmission was 0.7794. The structure was solved and refined using the Bruker SHELXTL (Version 6.1) Software Package, using the space group P2(1)/c, with Z = 4 for the formula unit, $C_{21}H_{33}N_2O_2P$. Hydrogen atoms on P1 and N2 were located from difference Fourier map and were refined isotropically. Rest of the hydrogen atoms were placed geometrically at chemically meaningful positions. The hydrogen atoms of the phenyl ring were allowed to ride at a distance of 0.93 Å from the parent carbons and their

thermal parameter were fixed at 1.2 times that of the parent atom. The secondary CH_3 hydrogen atoms were fixed at a distance of 0.96 Å from the parent atom and their thermal parameters were fixed at 1.5 times the parent atom. The final anisotropic full-matrix least-squares refinement on F^2 with 252 variables converged at R1 = 4.38%, for the observed data and wR2 = 12.71% for all data. The goodness-of-fit was 1.070. The largest peak on the final difference map was 0.460 e^- /Å^3 and the largest hole was -0.256 e^-/Å^3. Based on the final model, the calculated density of the crystal is 1.181 g/cm^3 and F(000) amounts to 816 electrons.

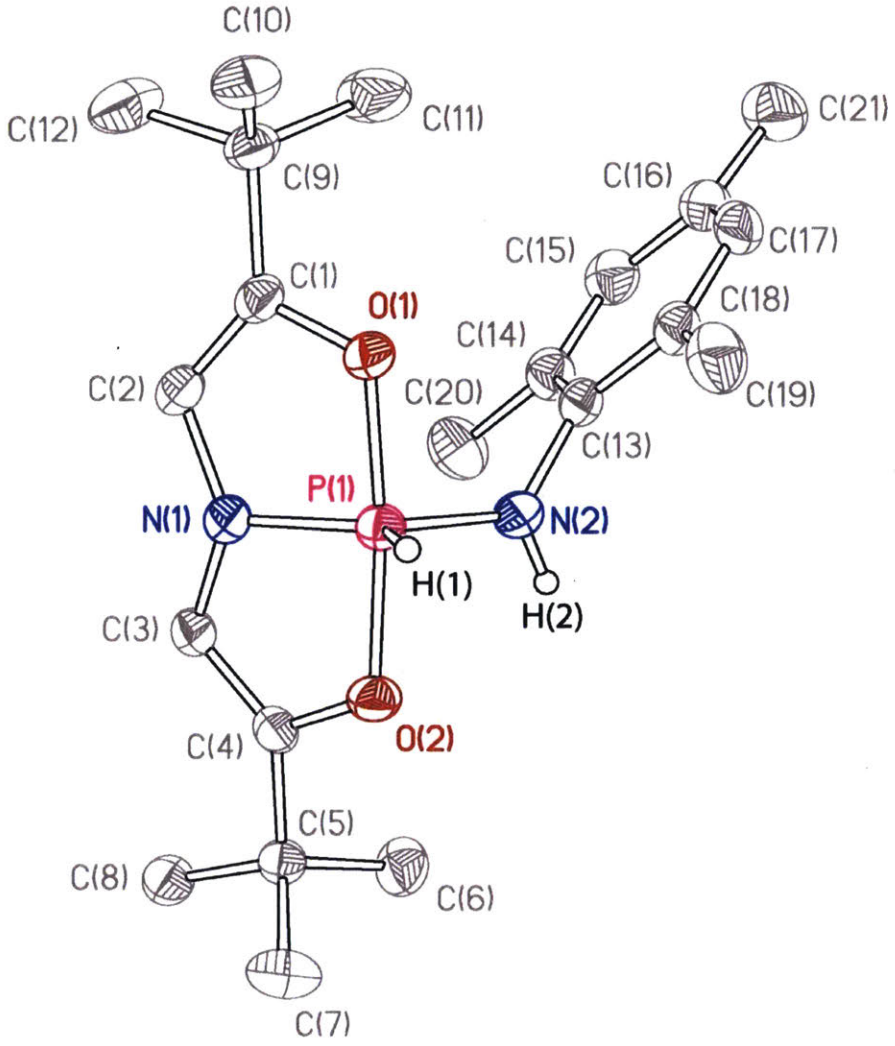

Table A1. Atomic coordinates and equivalent isotropic atomic displacement parameters ($Å^2$) for 2.5e.

	x	y	z	U(eq)
C1	0.15812(9)	0.57464(8)	0.59367(17)	0.0262(3)
C2	0.10507(10)	0.55892(9)	0.45289(18)	0.0311(3)
C3	0.10878(10)	0.46369(8)	0.22472(17)	0.0287(3)
C4	0.16041(9)	0.40464(8)	0.19712(16)	0.0244(3)
C5	0.16401(9)	0.35813(8)	0.04551(16)	0.0255(3)
C6	0.25579(11)	0.37178(11)	-0.00946(19)	0.0378(4)
C7	0.15342(13)	0.27298(9)	0.0833(2)	0.0397(4)
C8	0.08786(11)	0.38265(9)	-0.09111(18)	0.0338(3)
C9	0.15736(10)	0.64008(8)	0.71189(17)	0.0289(3)
C10	0.14560(12)	0.60875(10)	0.87942(18)	0.0368(4)
C11	0.24734(14)	0.68385(11)	0.7268(3)	0.0529(5)
C12	0.07786(14)	0.69363(10)	0.6501(2)	0.0463(4)
C13	0.38335(9)	0.54608(8)	0.51022(18)	0.0275(3)
C14	0.38142(10)	0.60952(9)	0.40661(19)	0.0329(3)
C15	0.43678(11)	0.67217(10)	0.4589(2)	0.0370(4)
C16	0.49436(10)	0.67222(10)	0.6085(2)	0.0365(4)
C17	0.49337(10)	0.60882(10)	0.70958(19)	0.0347(3)
C18	0.43881(10)	0.54511(9)	0.66320(18)	0.0302(3)
C19	0.43977(12)	0.47719(11)	0.7748(2)	0.0416(4)
C20	0.32236(13)	0.60991(11)	0.2414(2)	0.0454(4)
C21	0.55909(13)	0.73832(12)	0.6549(3)	0.0502(5)
N1	0.13168(8)	0.48975(7)	0.38717(15)	0.0292(3)
N2	0.33035(8)	0.47974(8)	0.45321(16)	0.0297(3)
O1	0.22435(7)	0.51941(6)	0.63630(11)	0.0265(2)
O2	0.22161(7)	0.38466(5)	0.33444(12)	0.0271(2)
P1	0.22908(2)	0.45294(2)	0.48714(4)	0.02322(11)

Table A2. Selected bond lengths (Å) for 2.5e.

C1-C2	1.325(2)	C1-O1	1.3814(17)
C1-C9	1.5041(19)	C2-N1	1.4058(19)
C2-H2	0.9300	C3-C4	1.326(2)
C3-N1	1.4075(17)	C3-H3	0.9300
C4-O2	1.3798(16)	C4-C5	1.5023(18)
C5-C8	1.5253(19)	C5-C6	1.527(2)
C5-C7	1.530(2)	C9-C10	1.527(2)
C9-C12	1.528(2)	C9-C11	1.528(2)
C13-C18	1.394(2)	C13-C14	1.397(2)
C13-N2	1.4350(19)	C14-C15	1.393(2)
C14-C20	1.500(2)	C15-C16	1.386(2)
C15-H15	0.9300	C16-C17	1.387(2)
C16-C21	1.510(2)	C17-C18	1.392(2)
C17-H17	0.9300	C18-C19	1.500(2)
N1-P1	1.6744(12)	N2-P1	1.6447(13)
N2-H2N	0.81(2)	O1-P1	1.7028(10)
O2-P1	1.7265(10)	P1-H1P	1.314(15)

Table A3. Selected bond angles (°) for 2.5e.

C2-C1-O1	112.21(12)	C2-C1-C9	131.48(13)
O1-C1-C9	116.30(12)	C1-C2-N1	110.66(13)
C1-C2-H2	124.7	N1-C2-H2	124.7
C4-C3-N1	111.00(12)	C4-C3-H3	124.5
N1-C3-H3	124.5	C3-C4-O2	112.13(12)
C3-C4-C5	131.55(12)	O2-C4-C5	116.31(11)
C4-C5-C8	110.16(12)	C4-C5-C6	108.70(11)
C8-C5-C6	109.11(12)	C4-C5-C7	109.49(12)
C8-C5-C7	109.54(12)	C6-C5-C7	109.82(13)
C1-C9-C10	109.50(12)	C1-C9-C12	109.45(12)
C10-C9-C12	109.00(13)	C1-C9-C11	109.36(13)
C10-C9-C11	109.52(14)	C12-C9-C11	110.00(15)
C18-C13-C14	121.14(14)	C18-C13-N2	120.05(14)
C14-C13-N2	118.74(13)	C15-C14-C13	118.54(14)
C15-C14-C20	120.55(15)	C13-C14-C20	120.91(14)
C16-C15-C14	121.72(16)	C16-C15-H15	119.1
C14-C15-H15	119.1	C15-C16-C17	118.18(15)
C15-C16-C21	120.19(17)	C17-C16-C21	121.56(16)
C16-C17-C18	122.16(14)	C16-C17-H17	118.9
C18-C17-H17	118.9	C17-C18-C13	118.22(14)
C17-C18-C19	120.87(14)	C13-C18-C19	120.91(14)
C2-N1-C3	127.36(13)	C2-N1-P1	114.39(10)
C3-N1-P1	113.80(10)	C13-N2-P1	129.94(10)
C13-N2-H2N	113.3(14)	P1-N2-H2N	115.9(14)
C1-O1-P1	113.64(8)	C4-O2-P1	112.58(8)
N2-P1-N1	123.34(7)	N2-P1-O1	94.48(6)
N1-P1-O1	87.87(5)	N2-P1-O2	91.25(6)
N1-P1-O2	87.44(5)	O1-P1-O2	173.98(5)
N2-P1-H1P	112.9(7)	N1-P1-H1P	123.7(7)
O1-P1-H1P	89.6(7)	O2-P1-H1P	89.9(7)

Table A4. Torsion angles (°) for 2.5e.

O1-C1-C2-N1	0.15(19)	C9-C1-C2-N1	-178.98(14)
N1-C3-C4-O2	0.41(18)	N1-C3-C4-C5	-178.67(14)
C3-C4-C5-C8	-5.4(2)	O2-C4-C5-C8	175.51(12)
C3-C4-C5-C6	114.07(18)	O2-C4-C5-C6	-64.98(16)
C3-C4-C5-C7	-125.97(18)	O2-C4-C5-C7	54.99(16)
C2-C1-C9-C10	120.99(19)	O1-C1-C9-C10	-58.11(16)
C2-C1-C9-C12	1.6(2)	O1-C1-C9-C12	-177.54(13)
C2-C1-C9-C11	-119.0(2)	O1-C1-C9-C11	61.90(18)
C18-C13-C14-C15	0.4(2)	N2-C13-C14-C15	-176.55(13)
C18-C13-C14-C20	179.34(15)	N2-C13-C14-C20	2.4(2)
C13-C14-C15-C16	1.3(2)	C20-C14-C15-C16	-177.71(15)
C14-C15-C16-C17	-2.4(2)	C14-C15-C16-C21	174.84(15)
C15-C16-C17-C18	1.9(2)	C21-C16-C17-C18	-175.26(15)
C16-C17-C18-C13	-0.3(2)	C16-C17-C18-C19	179.57(15)
C14-C13-C18-C17	-0.8(2)	N2-C13-C18-C17	176.08(13)
C14-C13-C18-C19	179.27(14)	N2-C13-C18-C19	-3.8(2)
C1-C2-N1-C3	-162.54(14)	C1-C2-N1-P1	-7.92(18)
C4-C3-N1-C2	166.77(14)	C4-C3-N1-P1	12.02(17)
C18-C13-N2-P1	85.04(17)	C14-C13-N2-P1	-97.99(16)
C2-C1-O1-P1	7.50(16)	C9-C1-O1-P1	-173.23(10)
C3-C4-O2-P1	-12.20(15)	C5-C4-O2-P1	167.03(9)
C13-N2-P1-N1	79.71(15)	C13-N2-P1-O1	-10.69(14)
C13-N2-P1-O2	167.46(14)	C2-N1-P1-N2	-83.92(13)
C3-N1-P1-N2	74.23(13)	C2-N1-P1-O1	10.05(11)
C3-N1-P1-O1	168.19(11)	C2-N1-P1-O2	-173.73(12)
C3-N1-P1-O2	-15.58(11)	C1-O1-P1-N2	113.36(10)
C1-O1-P1-N1	-9.92(10)	C1-O1-P1-O2	-48.8(5)
C4-O2-P1-N2	-107.58(10)	C4-O2-P1-N1	15.74(10)
C4-O2-P1-O1	54.6(5)		

II. Kinetics Data.

All kinetics experiments were conducted on the oxidative addition reaction of *n*-propylamine to **2.3** (**Figure A1**). Compound **2.3** was recrystallized from pentane three times then stored in a nitrogen-filled glovebox before use. *n*-Propylamine was distilled twice from zinc dust then stored in a nitrogen-filled glovebox before use. Benzene and pentane were dried by passage over an activated alumina column.

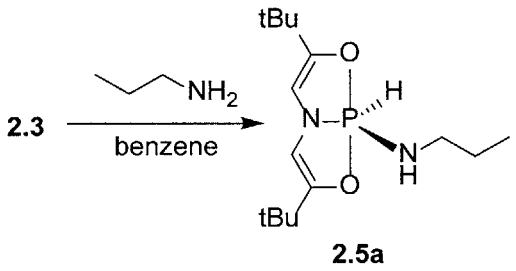

2.5a

Figure A1. Oxidative addition of *n*-propylamine to **2.3**.

Time-stacked UV-vis spectra (Figure 2.15A). Measurements were performed on a Hewlett-Packard 8453 spectrophotometer with a Hewlett-Packard 8909DA peltier-thermostatted cuvette holder. A stock solution of compound **1** (3 mL, 0.27 mM in pentane) was added to a screw-top quartz cuvette (1 cm pathlength) fitted with a threaded septum. An initial UV-vis absorbance spectrum (225 nm < λ < 400 nm) was recorded. *n*-Propylamine (0.2 mL, 2250 equiv.) was then added via syringe and spectra were collected at 30 s intervals over the course of 5 min. The spectra (Figure 12A) show the consumption of **1** (λ_{max} = 313 nm) and an increase in absorbance at lower wavelengths consistent with the formation of **1**•[H][NH^{n}Pr] (the absorbance maximum of **1**•[H][NH^{n}Pr] (λ_{max} = 239 nm) is obscured by the tail from the excess *n*-PrNH$_2$). An isosbestic point is evident at λ = 272 nm.

Pseudo-first order kinetics (Figure 2.15B). Measurements were performed on a Hitachi Digilab U-3010 spectrophotometer equipped with a cuvette holder thermostatted by a VWR 1140S water circulator. A stock solution of compound **1** (3 mL, 0.31 mM in benzene) was added to a screw-top quartz cuvette (1 cm pathlength) fitted with a threaded septum. The cuvette was placed in the temperature controlled spectrometer cell holder (25 °C) and allowed to thermally equilibrate for 10 min. Absorbance data were then collected at λ = 314 nm for ca. 15 seconds to establish a t = 0 baseline value. *n*-Propylamine (0.2 mL, 2250 equiv.) was then added via syringe and spectra were collected at 0.2 s intervals over the course of 500 s.

Determination of reaction order in amine (Figure 2.16). Measurements were performed on a Hitachi Digilab U-3010 spectrophotometer equipped with a cuvette holder thermostatted by a VWR 1140S water circulator. A stock solution of compound **1** (3 mL, 0.31 mM in benzene) was added to a screw-top quartz cuvette (1 cm pathlength) fitted with a threaded septum. The cuvette was placed in the temperature controlled spectrometer cell holder (25 °C) and allowed to thermally equilibrate for 10 min. Absorbance data were then collected at λ = 314 nm for ca. 15 seconds to establish a t = 0 baseline value. *n*-Propylamine solutions of varying concentrations (0.2 mL, 0.06 to 10.33 M, 14 to 2222 equiv.) were then added via syringe and spectra were collected at 0.2 s intervals over the course of 500 s. The observed pseudo-first order rate constant (k_{obs}) was extracted from an average of three independent runs at each concentration.

Table A5. Effect of amine concentration on observed rate.

[*n*-PrNH$_2$] (M)	[*n*-PrNH$_2$]^2 (M^2)	[*n*-PrNH$_2$]^3 (M^3)	k_{obs} (s^{-1})
6.46E-01	4.17E-01	2.69E-01	0.002920
3.23E-01	1.04E-01	3.37E-02	0.000319
1.61E-01	2.61E-02	4.21E-03	0.000064
8.07E-02	6.52E-03	5.26E-04	0.000017

4.04E-02	1.63E-03	6.57E-05	0.000014
4.03E-03	1.63E-05	6.56E-08	0.000012

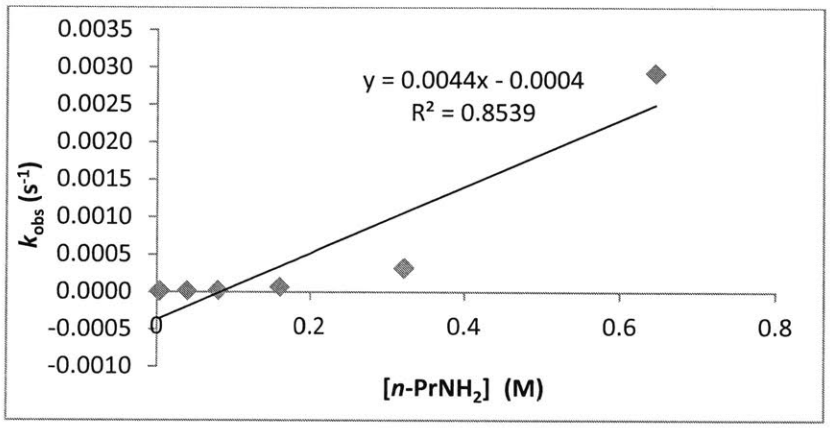

Figure A

Figure A2. Plot of k_{obs} vs. [n-PrNH$_2$] with attempted linear fit.

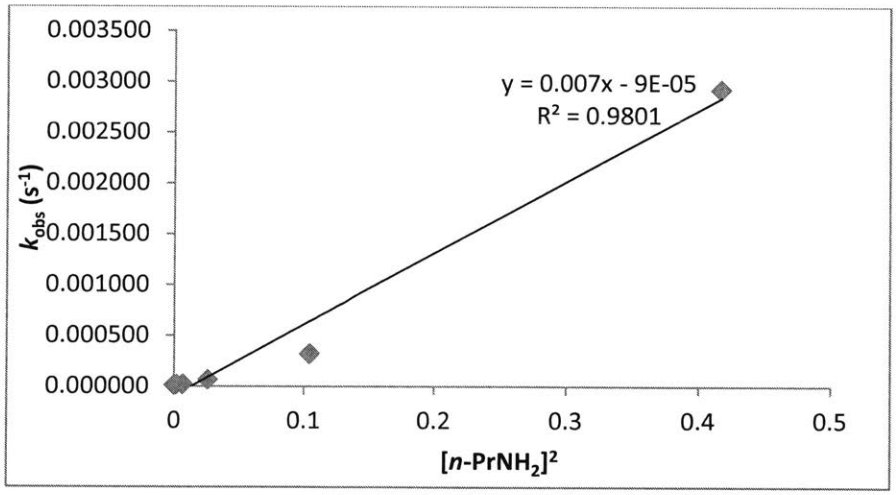

Figure A4

Figure A3. Plot of k_{obs} vs. [n-PrNH$_2$]^2 with attempted linear fit.

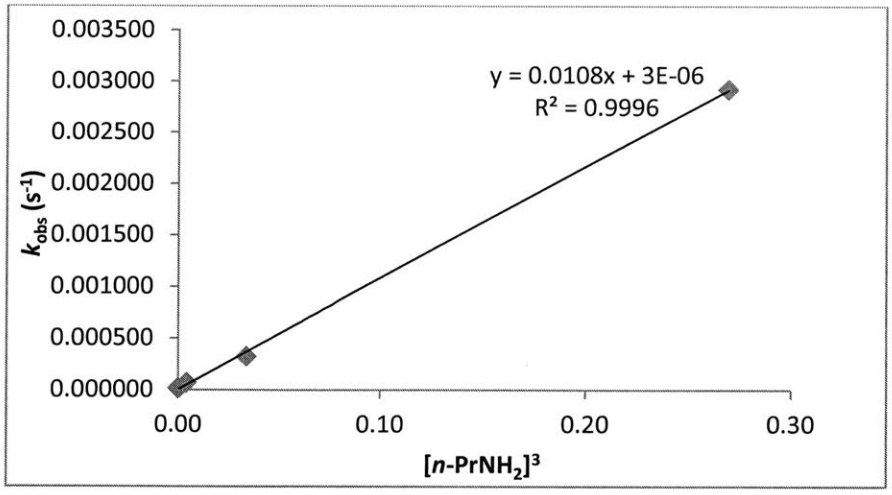

Figure A4. Plot of k_{obs} vs. $[n\text{-PrNH}_2]^3$ with attempted linear fit.

Eyring kinetics. Measurements were performed on a Hitachi Digilab U-3010 spectrophotometer equipped with a cuvette holder thermostatted by a VWR 1140S water circulator. A stock solution of compound **1** (3 mL, 0.31 mM in benzene) was added to a screw-top quartz cuvette (1 cm pathlength) fitted with a threaded septum. The cuvette was placed in the temperature controlled spectrometer cell holder and allowed to thermally equilibrate for 10 min to a series of temperatures (10 to 70 °C). Absorbance data were then collected at $\lambda = 314$ nm for ca. 15 seconds to establish a $t = 0$ baseline value. *n*-Propylamine (0.2 mL, 2613 equiv.) was then added via syringe and spectra were collected at 0.2 s intervals over the course of 500 s. The observed pseudo-first order rate constant (k_{obs}) was extracted from an average of three to six independent runs at each temperature.

Table A6. Eyring data.

Temp (K)	1/T (K^{-1})	k ($s^{-1}M^{-3}$)	ln(k/T)
283	0.00353	0.00601	-10.75911
293	0.00341	0.00576	-10.83640
303	0.00330	0.00533	-10.94803
313	0.00319	0.00577	-10.90111
323	0.00310	0.00522	-11.03209
333	0.00300	0.00568	-10.97830
343	0.00292	0.00558	-11.02609

III. Computational Details.

Cartesian coordinates of the M062X/6-311++G(2d,2p) stationary points in Å units and the absolute thermochemical data in Hartrees.

1

Temperature = 298.150 K
Pressure = 1.00000 Atm
Electronic Energy = -1015.81586866
Electronic and Zero-Point Energy = -1015.507997
Enthalpy = -1015.489590
Free Energy = -1015.552288

C	9.346105000	1.798568000	16.136273000
C	10.399565000	1.895505000	17.206779000
C	10.145468000	0.793260000	18.244389000
H	9.174406000	0.927523000	18.722117000
H	10.916555000	0.830132000	19.014417000
H	10.169645000	-0.190332000	17.777292000
C	11.775606000	1.685262000	16.560024000
H	11.826556000	0.715913000	16.066079000
H	12.550422000	1.724782000	17.326195000
H	11.979833000	2.462364000	15.822740000
C	10.347334000	3.265540000	17.881902000
H	10.530828000	4.067184000	17.165640000
H	11.115596000	3.319122000	18.652997000
H	9.380186000	3.436577000	18.355929000
C	8.441533000	2.732958000	15.757361000
H	8.293952000	3.725888000	16.141104000
C	6.628029000	2.980160000	14.136629000
H	6.413973000	3.981998000	14.461468000
C	6.024895000	2.251288000	13.167017000
C	4.882369000	2.647340000	12.271011000
C	3.723319000	1.665873000	12.493031000
H	4.035611000	0.644486000	12.279899000
H	2.895576000	1.920388000	11.830488000
H	3.367739000	1.712951000	13.522850000
C	5.353799000	2.564450000	10.812566000
H	6.174113000	3.259542000	10.630551000
H	4.530028000	2.821071000	10.145896000
H	5.692367000	1.557452000	10.572653000
C	4.425384000	4.070618000	12.588550000
H	4.079122000	4.154536000	13.619267000
H	3.598983000	4.340795000	11.931473000
H	5.230633000	4.789182000	12.431863000
N	7.642984000	2.259668000	14.734890000
O	9.240796000	0.680200000	15.441291000
O	6.551399000	1.046813000	13.037047000

P	7.929904000	0.676850000	14.172497000

NH_2Me

Temperature = 298.150 K
Pressure = 1.00000 Atm
Electronic Energy = -95.8441525997
Electronic and Zero-Point Energy = -95.779583
Enthalpy = -95.775209
Free Energy = -95.802517

N	8.188222000	-0.620279000	13.559196000
H	8.936118000	-0.957612000	12.965325000
C	6.932375000	-1.280868000	13.190073000
H	6.669365000	-1.006591000	12.170141000
H	6.963864000	-2.371676000	13.252255000
H	6.135944000	-0.926617000	13.841887000
H	8.446670000	-0.885761000	14.501810000

$3NH_2Me$ (trimer of NH_2Me)

Temperature = 298.150 K
Pressure = 1.00000 Atm
Electronic Energy = -287.544286153
Electronic and Zero-Point Energy = -287.346594
Enthalpy = -287.332973
Free Energy = -287.386037

N	0.083833000	-2.031697000	-2.168579000
H	0.539419000	-2.851691000	-1.771800000
N	0.984756000	-4.247418000	-0.132720000
H	0.052778000	-4.648728000	-0.185193000
C	0.972400000	-0.872436000	-2.046003000
H	1.150777000	-0.668794000	-0.990878000
H	1.942846000	-0.998593000	-2.534182000
H	0.490410000	0.005358000	-2.473766000
C	0.971598000	-3.172227000	0.863836000
H	0.251963000	-2.414853000	0.552329000
H	0.704251000	-3.499783000	1.871963000
H	1.952153000	-2.699888000	0.906822000
N	-2.014082000	-4.036259000	-0.908425000
H	-2.999906000	-3.937113000	-0.698579000
C	-1.850438000	-4.720484000	-2.195158000
H	-0.786508000	-4.843637000	-2.399702000
H	-2.293232000	-5.713646000	-2.139881000
H	-2.297827000	-4.192321000	-3.041759000
H	-0.073329000	-2.237633000	-3.148271000
H	1.613690000	-4.984405000	0.161081000
H	-1.638865000	-3.096128000	-1.001563000

TS-conc

Lowest Frequency Vibration = -1751.2854 cm**-1
Temperature = 298.150 K
Pressure = 1.00000 Atm
Electronic Energy = -1111.57601961
Electronic and Zero-Point Energy = -1111.206498
Enthalpy = -1111.184742
Free Energy = -1111.254176

C	9.542820000	1.496687000	15.792882000
C	10.454202000	1.369818000	16.979245000
C	10.611501000	-0.118630000	17.322924000
H	9.648718000	-0.555437000	17.591671000
H	11.291698000	-0.236090000	18.167469000
H	11.016935000	-0.670265000	16.475200000
C	11.827701000	1.959164000	16.628398000
H	12.258514000	1.449289000	15.767692000
H	12.507405000	1.844342000	17.473735000
H	11.743199000	3.021187000	16.395220000
C	9.865260000	2.113887000	18.177040000
H	9.751702000	3.177287000	17.963630000
H	10.530273000	2.009098000	19.034439000
H	8.890663000	1.709107000	18.452280000
C	8.374070000	2.135307000	15.672543000
H	7.849227000	2.710563000	16.414391000
C	6.585251000	2.364422000	13.923484000
H	5.942710000	2.980310000	14.527318000
C	6.361304000	1.891467000	12.692442000
C	5.180671000	2.088999000	11.785684000
C	4.626168000	0.720757000	11.365743000
H	5.384046000	0.141670000	10.838800000
H	3.774150000	0.856349000	10.698415000
H	4.296453000	0.151978000	12.236197000
C	5.633282000	2.856279000	10.534438000
H	6.011797000	3.842926000	10.803571000
H	4.791221000	2.983332000	9.852779000
H	6.420466000	2.313889000	10.012217000
C	4.093194000	2.882560000	12.509263000
H	3.752546000	2.359235000	13.403431000
H	3.237877000	3.015970000	11.846794000
H	4.452689000	3.869963000	12.800668000
N	7.861926000	2.016471000	14.375358000
O	9.944662000	0.907401000	14.629189000
O	7.425659000	1.195440000	12.195157000
P	8.727671000	0.971112000	13.351076000
N	8.271488000	-0.757364000	13.666836000
H	9.226351000	-0.349979000	12.669212000
C	6.966765000	-1.360711000	13.405944000
H	6.655823000	-1.108778000	12.395948000
H	7.036174000	-2.441305000	13.501123000
H	6.217054000	-0.982102000	14.103026000
H	8.767118000	-1.131698000	14.469849000

1•[H][NHMe]

Temperature = 298.150 K
Pressure = 1.00000 Atm
Electronic Energy = -1111.67775110
Electronic and Zero-Point Energy = -1111.303351
Enthalpy = -1111.281476
Free Energy = -1111.351831

C	1.172924000	1.316257000	1.670353000
C	2.282551000	1.115890000	2.659438000
C	1.705837000	0.480640000	3.933842000
H	0.960101000	1.134849000	4.386724000
H	2.504210000	0.313260000	4.657950000
H	1.236876000	-0.476863000	3.710689000
C	3.339035000	0.176692000	2.061328000
H	2.893761000	-0.777516000	1.781110000
H	4.124861000	-0.010336000	2.794285000
H	3.794110000	0.621147000	1.175207000
C	2.924104000	2.460034000	3.001601000
H	3.340712000	2.935171000	2.112763000
H	3.733316000	2.306157000	3.715563000
H	2.199842000	3.139821000	3.451563000
C	0.680533000	2.436193000	1.138341000
H	1.006955000	3.449037000	1.293038000
C	-0.968564000	2.990328000	-0.681300000
H	-0.738563000	4.040558000	-0.702350000
C	-1.751016000	2.294972000	-1.508476000
C	-2.542950000	2.737047000	-2.702295000
C	-4.028573000	2.427223000	-2.467884000
H	-4.178451000	1.362815000	-2.291559000
H	-4.610543000	2.717153000	-3.343669000
H	-4.405390000	2.977845000	-1.605243000
C	-2.051050000	1.966161000	-3.936044000
H	-1.000434000	2.183921000	-4.132291000
H	-2.633389000	2.254831000	-4.811988000
H	-2.160642000	0.891978000	-3.789296000
C	-2.359026000	4.237470000	-2.925083000
H	-2.705430000	4.808966000	-2.063296000
H	-2.937086000	4.550803000	-3.794528000
H	-1.312177000	4.483411000	-3.106527000
N	-0.433133000	2.160082000	0.322366000
O	0.484045000	0.197858000	1.271908000
O	-1.828878000	0.968365000	-1.168641000
P	-0.629062000	0.510476000	-0.005974000
N	0.289035000	-0.234681000	-1.162472000
C	1.534642000	-0.968994000	-0.971766000
H	1.422462000	-1.789234000	-0.264698000
H	1.832172000	-1.380276000	-1.932999000
H	2.328826000	-0.315483000	-0.618242000
H	-1.567605000	-0.290565000	0.624293000
H	-0.136480000	-0.291944000	-2.072101000

INT1

Temperature = 298.150 K
Pressure = 1.00000 Atm
Electronic Energy = -1303.36787014
Electronic and Zero-Point Energy = -1302.860338
Enthalpy = -1302.828591
Free Energy = -1302.922291

C	1.269999000	0.653833000	1.875773000
C	2.377242000	0.707325000	2.893585000
C	1.814445000	0.295990000	4.262034000
H	1.025407000	0.981052000	4.575132000
H	2.606047000	0.315377000	5.012595000
H	1.400681000	-0.710951000	4.220611000
C	3.482078000	-0.279229000	2.488426000
H	3.072229000	-1.279545000	2.344309000
H	4.244088000	-0.327251000	3.267687000
H	3.963192000	0.037590000	1.561888000
C	2.958553000	2.117592000	2.981803000
H	3.366542000	2.436210000	2.021787000
H	3.764647000	2.137322000	3.715927000
H	2.199952000	2.837456000	3.291150000
C	0.785319000	1.627980000	1.099662000
H	1.101173000	2.655439000	1.047734000
C	-0.634241000	1.786699000	-0.926001000
H	-0.253474000	2.764530000	-1.165391000
C	-1.428466000	1.004447000	-1.668631000
C	-1.965667000	1.240593000	-3.054212000
C	-3.498175000	1.160710000	-3.026091000
H	-3.825638000	0.194908000	-2.643043000
H	-3.898679000	1.287982000	-4.032976000
H	-3.912446000	1.943494000	-2.389267000
C	-1.417988000	0.142037000	-3.977425000
H	-0.328369000	0.189553000	-4.026991000
H	-1.812995000	0.265343000	-4.986898000
H	-1.707398000	-0.844651000	-3.614776000
C	-1.531944000	2.609917000	-3.574926000
H	-1.903951000	3.410254000	-2.934083000
H	-1.930816000	2.765549000	-4.577812000
H	-0.445127000	2.685656000	-3.626698000
N	-0.285636000	1.186332000	0.297070000
O	0.628249000	-0.529748000	1.716460000
O	-1.748160000	-0.159920000	-1.056381000
P	-0.680104000	-0.483548000	0.431103000
N	0.600308000	-1.273491000	-0.833888000
H	0.759421000	-2.254490000	-0.483359000
N	1.041550000	-3.875518000	0.250085000
H	0.559637000	-4.564342000	-0.324968000
C	1.913571000	-0.626331000	-1.030575000
H	2.459192000	-0.669900000	-0.093843000
H	2.471689000	-1.154093000	-1.801850000
H	1.770092000	0.409667000	-1.321742000
C	0.440497000	-3.890929000	1.590617000

H	-0.619543000	-3.653106000	1.501359000
H	0.534902000	-4.853755000	2.096975000
H	0.897323000	-3.116440000	2.203368000
N	-1.418452000	-5.186025000	-1.065338000
H	-2.072743000	-5.474665000	-0.347771000
C	-1.723068000	-3.815290000	-1.489420000
H	-1.018057000	-3.518102000	-2.265675000
H	-2.735405000	-3.679097000	-1.877435000
H	-1.591714000	-3.138402000	-0.644515000
H	0.093453000	-1.330496000	-1.714296000
H	2.015482000	-4.149067000	0.303187000
H	-1.556415000	-5.823129000	-1.840533000

TS1

Lowest Frequency Vibration = -810.8210 cm**-1
Temperature = 298.150 K
Pressure = 1.00000 Atm
Electronic Energy = -1303.36091642
Electronic and Zero-Point Energy = -1302.856909
Enthalpy = -1302.826134
Free Energy = -1302.917631

C	1.266362000	0.618639000	1.868401000
C	2.376205000	0.673522000	2.884942000
C	1.821825000	0.245938000	4.251783000
H	1.030649000	0.923926000	4.575123000
H	2.615741000	0.260461000	5.000300000
H	1.411875000	-0.762187000	4.200098000
C	3.487619000	-0.301615000	2.469716000
H	3.084938000	-1.304722000	2.324762000
H	4.256362000	-0.346423000	3.242850000
H	3.957115000	0.021449000	1.539354000
C	2.950761000	2.085690000	2.985616000
H	3.355024000	2.415459000	2.027750000
H	3.758520000	2.103249000	3.718242000
H	2.189060000	2.798952000	3.302565000
C	0.782411000	1.597728000	1.097407000
H	1.106212000	2.623990000	1.057970000
C	-0.616596000	1.769874000	-0.937708000
H	-0.197858000	2.729784000	-1.188823000
C	-1.434270000	1.012595000	-1.681406000
C	-1.946570000	1.269886000	-3.074186000
C	-3.481412000	1.251196000	-3.064336000
H	-3.850864000	0.300666000	-2.681552000
H	-3.866611000	1.390843000	-4.075811000
H	-3.871437000	2.051819000	-2.434137000
C	-1.434359000	0.151061000	-3.993327000
H	-0.343365000	0.157382000	-4.033866000
H	-1.817059000	0.287086000	-5.006212000
H	-1.761518000	-0.823349000	-3.630105000
C	-1.456236000	2.620336000	-3.594223000
H	-1.802634000	3.436005000	-2.958269000

H	-1.839603000	2.789332000	-4.601240000
H	-0.366863000	2.654422000	-3.635949000
N	-0.304237000	1.180477000	0.301970000
O	0.632400000	-0.568590000	1.711547000
O	-1.808115000	-0.137577000	-1.072403000
P	-0.690324000	-0.512943000	0.404672000
N	0.478202000	-1.314352000	-0.758820000
H	0.722128000	-2.561770000	-0.269259000
N	0.968306000	-3.675598000	0.210720000
H	0.449962000	-4.377330000	-0.340048000
C	1.805290000	-0.715366000	-0.986761000
H	2.385471000	-0.787854000	-0.070586000
H	2.317266000	-1.271894000	-1.771675000
H	1.731306000	0.331043000	-1.277653000
C	0.511048000	-3.747300000	1.613549000
H	-0.562681000	-3.571206000	1.629351000
H	0.722361000	-4.723544000	2.042936000
H	0.993904000	-2.962853000	2.187968000
N	-1.215214000	-5.166738000	-1.025723000
H	-1.780967000	-5.595591000	-0.302797000
C	-1.829930000	-3.904744000	-1.458031000
H	-1.246274000	-3.488803000	-2.278261000
H	-2.864831000	-4.005972000	-1.789760000
H	-1.803203000	-3.187228000	-0.636274000
H	-0.022250000	-1.384570000	-1.640511000
H	1.961467000	-3.872657000	0.142798000
H	-1.197739000	-5.824293000	-1.795752000

INT2

Temperature = 298.150 K
Pressure = 1.00000 Atm
Electronic Energy = -1303.36342597
Electronic and Zero-Point Energy = -1302.855662
Enthalpy = -1302.824774
Free Energy = -1302.915828

C	1.041790000	0.397912000	1.843590000
C	2.054981000	0.464037000	2.957080000
C	1.473604000	-0.214840000	4.205576000
H	0.568254000	0.296537000	4.535907000
H	2.200012000	-0.190152000	5.019591000
H	1.224324000	-1.254342000	3.995118000
C	3.326977000	-0.283183000	2.530903000
H	3.092505000	-1.307656000	2.242244000
H	4.040225000	-0.312633000	3.356397000
H	3.801995000	0.214541000	1.684245000
C	2.408848000	1.914331000	3.284136000
H	2.831925000	2.421791000	2.416270000
H	3.148679000	1.940765000	4.085126000
H	1.530269000	2.469736000	3.614091000
C	0.500273000	1.403779000	1.148333000
H	0.700281000	2.456339000	1.260014000

C	-0.734604000	1.674045000	-0.975441000
H	-0.398030000	2.691940000	-1.081215000
C	-1.408225000	0.939387000	-1.872206000
C	-1.824208000	1.322008000	-3.269753000
C	-3.342965000	1.153077000	-3.414387000
H	-3.638288000	0.129838000	-3.185800000
H	-3.652997000	1.383295000	-4.435207000
H	-3.870886000	1.824167000	-2.735161000
C	-1.117558000	0.385502000	-4.260942000
H	-0.034358000	0.505567000	-4.195902000
H	-1.427697000	0.609776000	-5.283055000
H	-1.363365000	-0.654704000	-4.047149000
C	-1.442106000	2.768789000	-3.579064000
H	-1.926456000	3.460066000	-2.888206000
H	-1.756431000	3.025372000	-4.591592000
H	-0.363203000	2.914338000	-3.512139000
N	-0.468238000	0.976875000	0.218839000
O	0.575867000	-0.827559000	1.497146000
O	-1.710678000	-0.306284000	-1.440655000
P	-0.632586000	-0.757701000	0.073001000
N	0.662171000	-1.263941000	-1.054623000
H	0.944360000	-2.882121000	-0.599979000
N	1.034583000	-3.855107000	-0.153641000
H	0.044306000	-4.132138000	0.104435000
C	1.964724000	-0.586057000	-1.039486000
H	2.465064000	-0.786383000	-0.094794000
H	2.582096000	-0.980425000	-1.847032000
H	1.874364000	0.495465000	-1.160180000
C	1.889092000	-3.788881000	1.053764000
H	1.483359000	-3.017279000	1.702208000
H	1.890901000	-4.752086000	1.554182000
H	2.901307000	-3.522949000	0.763563000
N	-1.687621000	-4.171594000	0.383665000
H	-1.862839000	-3.324543000	0.915470000
C	-2.241492000	-4.011965000	-0.968172000
H	-2.019681000	-4.900963000	-1.555470000
H	-3.319695000	-3.846167000	-0.978787000
H	-1.761364000	-3.155595000	-1.442546000
H	0.258575000	-1.214141000	-1.984027000
H	1.399226000	-4.512703000	-0.836608000
H	-2.143834000	-4.935155000	0.867643000

Note: Though the amidophosphoranide/ammonium ion pair intermediate is slightly more unstable than TS2 on the entropy and free energy surface, it is more stable by 1.5 kcal/mol on the SCF energy surface. This indicates the shallow nature of the energy surface connecting TS2 and TS3 and also consistent with the experimentally unobservable intermediate.

TS2

Lowest Frequency Vibration = -1101.3360 cm**-1
Temperature = 298.150 K
Pressure = 1.00000 Atm
Electronic Energy = -1303.35265214
Electronic and Zero-Point Energy = -1302.849415
Enthalpy = -1302.818762
Free Energy = -1302.909067

C	1.110560000	1.168381000	1.712706000
C	2.267075000	1.024981000	2.664287000
C	1.736533000	0.553278000	4.027397000
H	1.054325000	1.291476000	4.450438000
H	2.564821000	0.408787000	4.722926000
H	1.202499000	-0.392216000	3.933730000
C	3.251873000	-0.019606000	2.121851000
H	2.755760000	-0.980175000	1.976379000
H	4.072238000	-0.158415000	2.827468000
H	3.668365000	0.299894000	1.165792000
C	2.984824000	2.362924000	2.839154000
H	3.376546000	2.725433000	1.888108000
H	3.820226000	2.244113000	3.529885000
H	2.314637000	3.119811000	3.248163000
C	0.592511000	2.274486000	1.171027000
H	0.936926000	3.287490000	1.290970000
C	-1.006923000	2.828611000	-0.645586000
H	-0.686241000	3.854683000	-0.703657000
C	-1.828480000	2.180855000	-1.479116000
C	-2.515082000	2.678286000	-2.720877000
C	-4.032995000	2.509013000	-2.563366000
H	-4.286616000	1.466326000	-2.375984000
H	-4.542345000	2.830844000	-3.473064000
H	-4.402687000	3.109301000	-1.730938000
C	-2.034941000	1.842743000	-3.916612000
H	-0.962061000	1.971629000	-4.069041000
H	-2.551342000	2.154244000	-4.825897000
H	-2.236479000	0.784470000	-3.751794000
C	-2.187592000	4.151005000	-2.962835000
H	-2.522410000	4.770780000	-2.130209000
H	-2.691309000	4.495709000	-3.866517000
H	-1.115178000	4.299539000	-3.094757000
N	-0.568159000	2.012676000	0.415726000
O	0.424083000	0.036280000	1.390325000
O	-2.052393000	0.886338000	-1.114168000
P	-0.829648000	0.328508000	0.102700000
N	0.181347000	-0.240581000	-1.157758000
H	0.462139000	-1.859815000	2.405977000
N	0.173994000	-2.821186000	2.248570000
H	-1.723618000	-2.346562000	1.897483000
C	1.638990000	-0.265441000	-1.106383000
H	1.971635000	-0.888004000	-0.280399000
H	2.012860000	-0.699867000	-2.032751000
H	2.082194000	0.726389000	-0.982600000

C	0.656228000	-3.226721000	0.923189000
H	1.745922000	-3.229531000	0.832350000
H	0.289885000	-4.225077000	0.687763000
H	0.262369000	-2.532995000	0.179127000
N	-2.461799000	-1.842269000	1.386127000
H	-1.849064000	-0.819255000	0.869385000
C	-2.982890000	-2.639180000	0.266038000
H	-3.362005000	-3.604171000	0.593428000
H	-3.778594000	-2.087551000	-0.227956000
H	-2.175411000	-2.795858000	-0.447237000
H	-0.174367000	0.060270000	-2.053557000
H	0.598326000	-3.392441000	2.968540000
H	-3.195399000	-1.573768000	2.032677000

NBO Analysis. Calculations were carried out using the Gaussian09 (rev b1) suite of programs[1] running on Intel X5670 2.93 GHz processors located at the Research Computing and Cyberinfrastructure Unit of Information Technology Services at the Pennsylvania State University. With the M06-2X functional and 6-31G** basis set, NBO analysis[2] of isolated gas phase **2.5e** was performed using coordinates obtained from the crystallographically determined structure. Orbital surfaces (isovalue 0.04) were plotted with Gaussview 5.

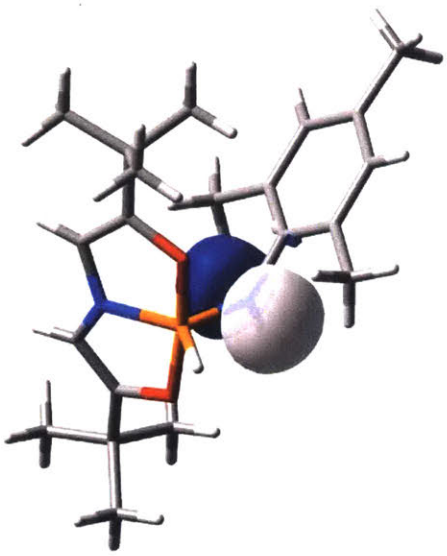

Lone pair: n(N2)
Occupancy: 1.85883
s(0.33%) p99.99(99.66%) d 0.02 (0.01%)

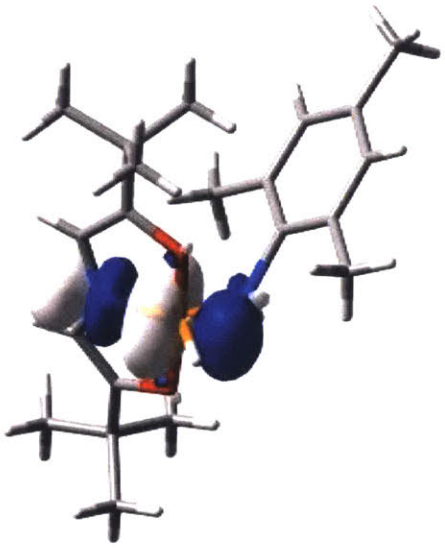

Antibonding: σ*(N1 — P1)
Occupancy: 0.16586
(25.03%) 0.5003* N1 s(30.15%)p 2.32(69.84%)d 0.00(0.01%)
(74.97%) -0.8659* P1 s(33.06%)p 1.97(65.27%)d 0.05(1.67%)

Donor NBO (i)		Acceptor NBO (j)	E(2) kcal/mol	E(j)-E(i) a.u.	F(i,j) a.u.
n(N2)	→	σ*(N1 — P1)	18.61	0.59	0.094

[1] Gaussian 09, Revision B.1, Frisch, M. J.; Trucks, G. W.; Schlegel, H. B.; Scuseria, G. E.; Robb, M. A.; Cheeseman, J. R.; Scalmani, G.; Barone, V.; Mennucci, B.; Petersson, G. A.; Nakatsuji, H.; Caricato, M.; Li, X.; Hratchian, H. P.; Izmaylov, A. F.; Bloino, J.; Zheng, G.; Sonnenberg, J. L.; Hada, M.; Ehara, M.; Toyota, K.; Fukuda, R.; Hasegawa, J.; Ishida, M.; Nakajima, T.; Honda, Y.; Kitao, O.; Nakai, H.; Vreven, T.; Montgomery, Jr., J. A.; Peralta, J. E.; Ogliaro, F.; Bearpark, M.; Heyd, J. J.; Brothers, E.; Kudin, K. N.; Staroverov, V. N.; Kobayashi, R.; Normand, J.; Raghavachari, K.; Rendell, A.; Burant, J. C.; Iyengar, S. S.; Tomasi, J.; Cossi, M.; Rega, N.; Millam, J. M.; Klene, M.; Knox, J. E.; Cross, J. B.; Bakken, V.; Adamo, C.; Jaramillo, J.; Gomperts, R.; Stratmann, R. E.; Yazyev, O.; Austin, A. J.; Cammi, R.; Pomelli, C.; Ochterski, J. W.; Martin, R. L.; Morokuma, K.; Zakrzewski, V. G.; Voth, G. A.; Salvador, P.; Dannenberg, J. J.; Dapprich, S.; Daniels, A. D.; Farkas, Ö.; Foresman, J. B.; Ortiz, J. V.; Cioslowski, J.; Fox, D. J. Gaussian, Inc., Wallingford CT, 2009.

[2] Weinhold, F.; Landis, C. *Valency and Bonding. A Natural Bond Orbital Donor-Acceptor Perspective*, University Press, Cambridge, 2005.

IV. Spectral Data.

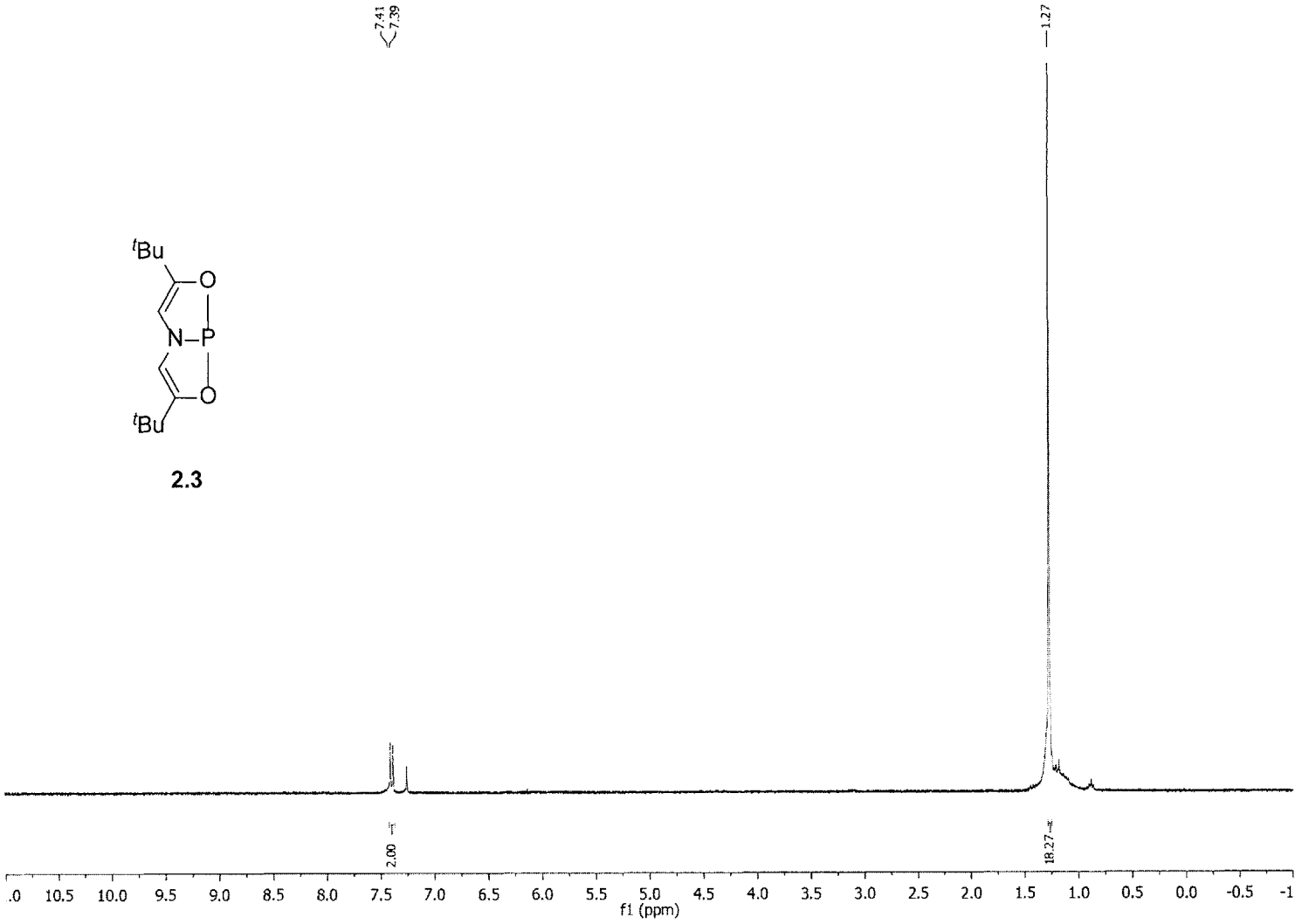

2.3

Figure A5. ^{1}H NMR of 2.3.

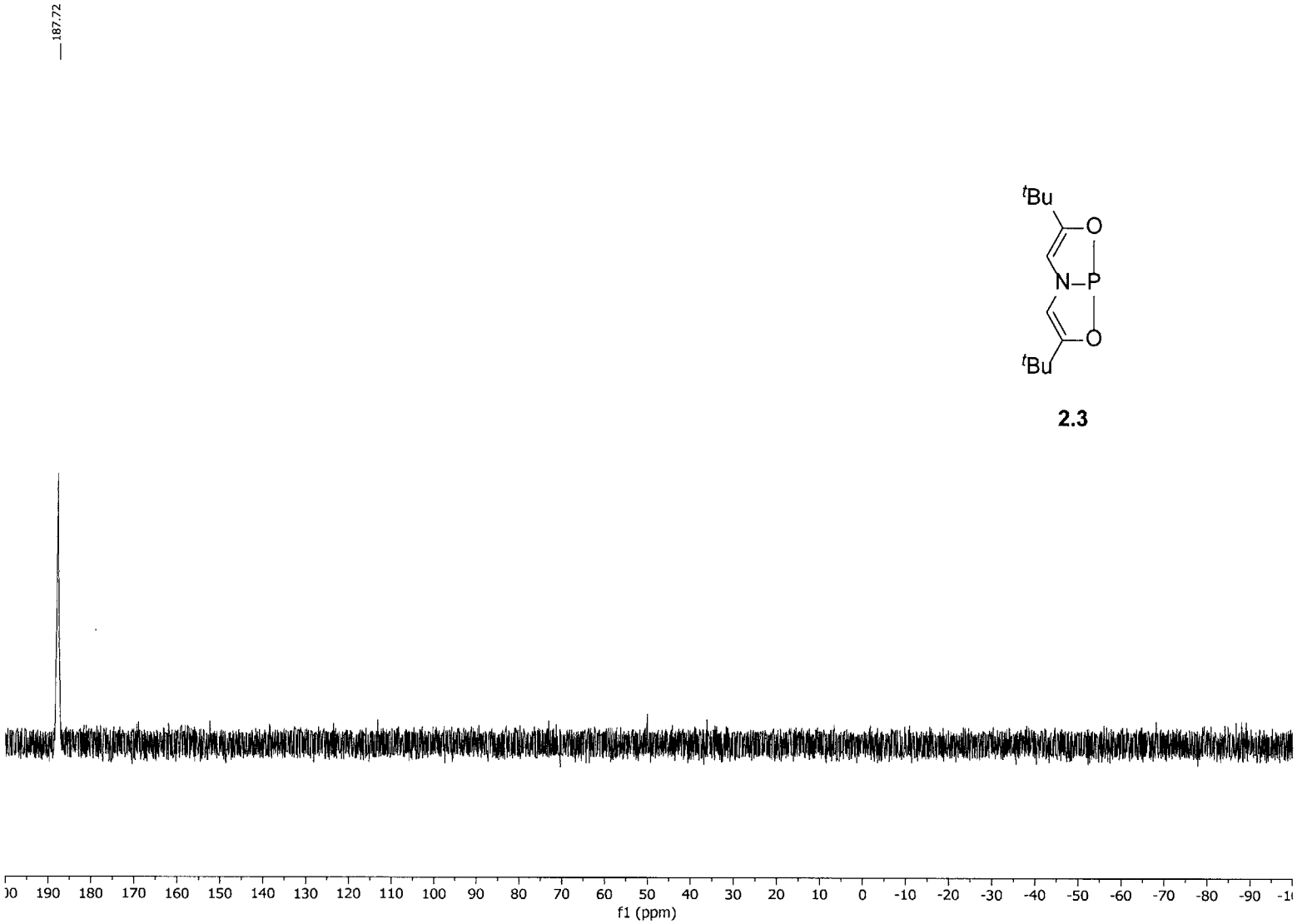

Figure A6. ^{31}P NMR of 2.3.

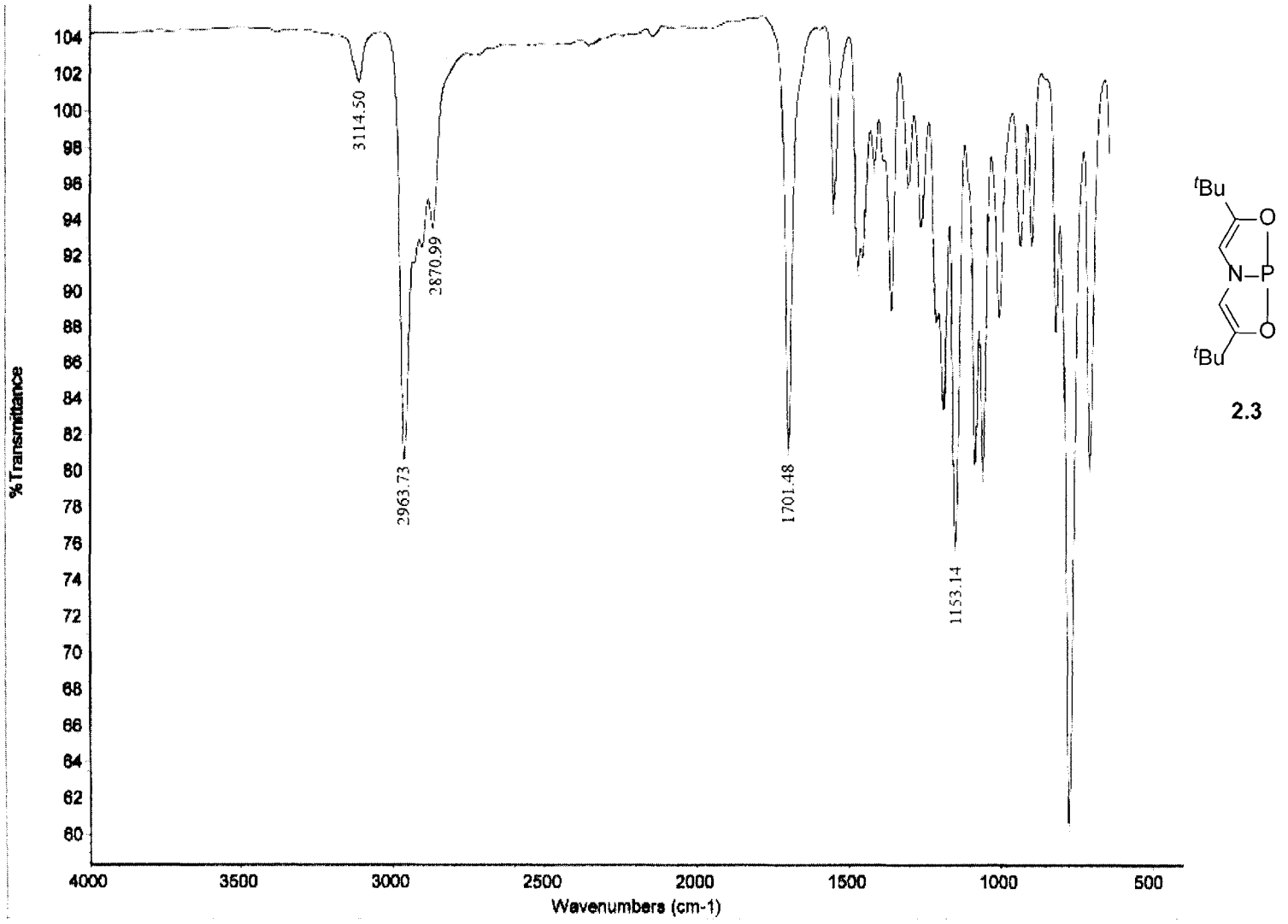

Figure A7. IR of 2.3.

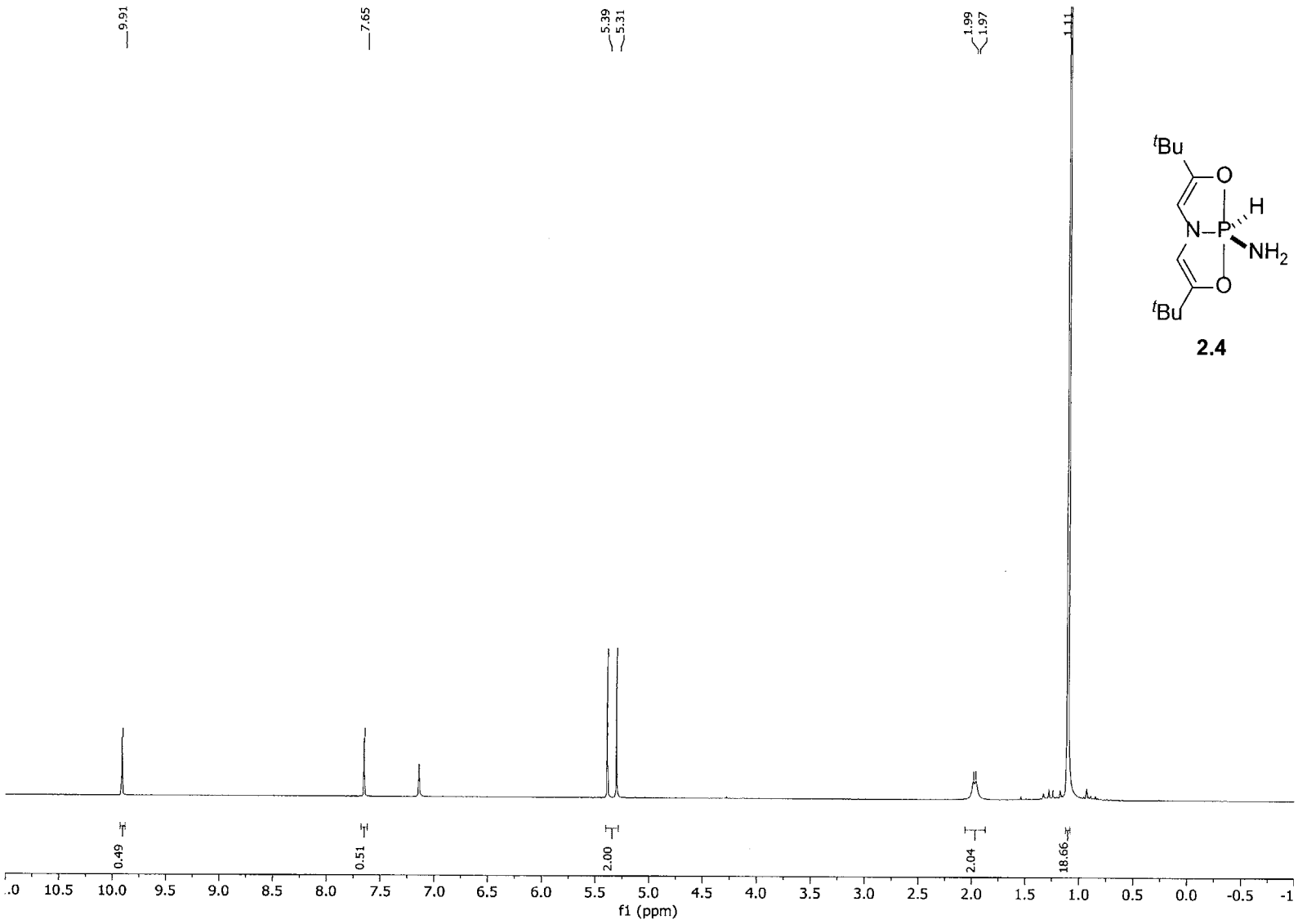

Figure A8. ^{1}H NMR of 2.4.

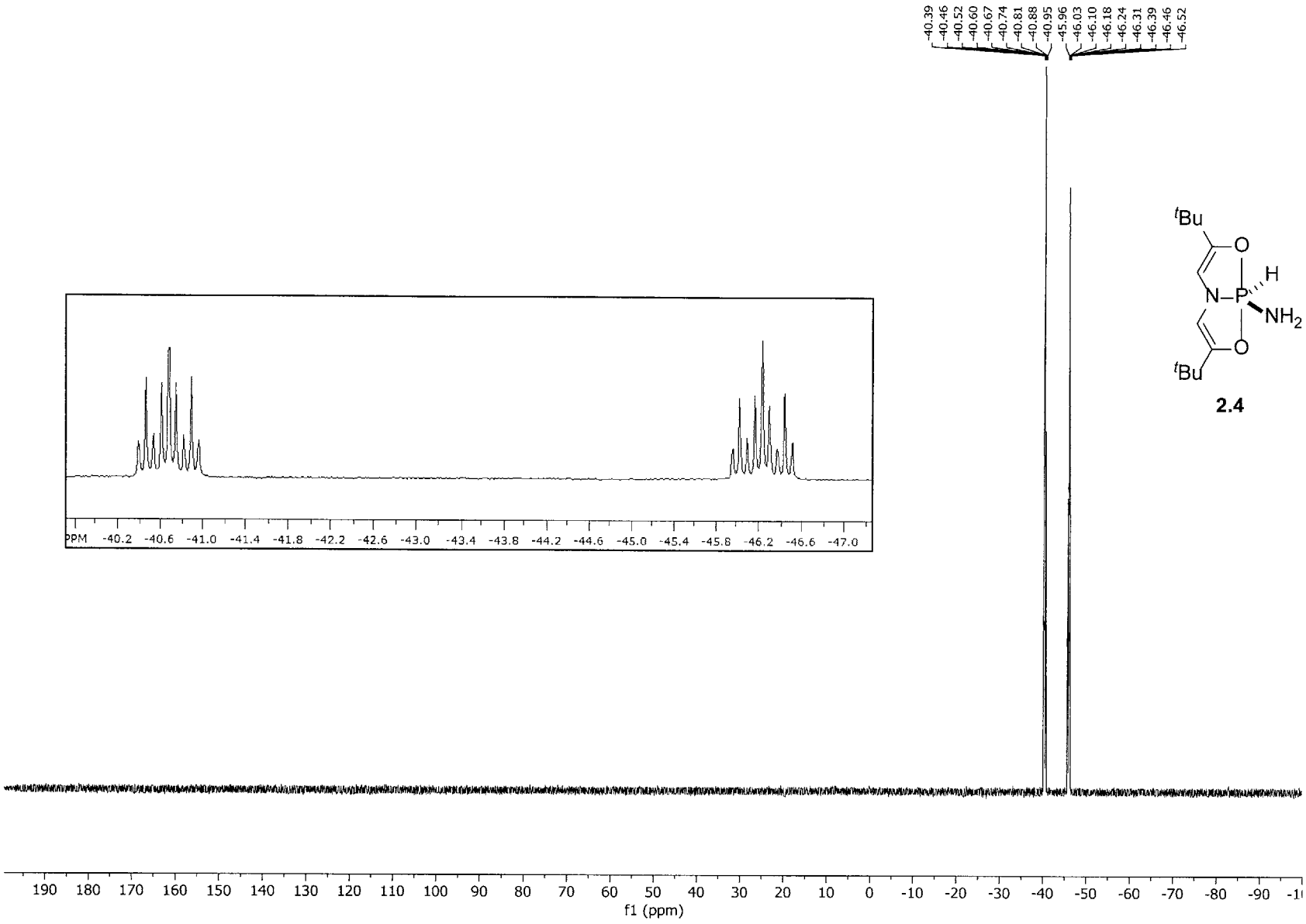

Figure A9. ^{31}P NMR of 2.4. Inset: expansion of signal.

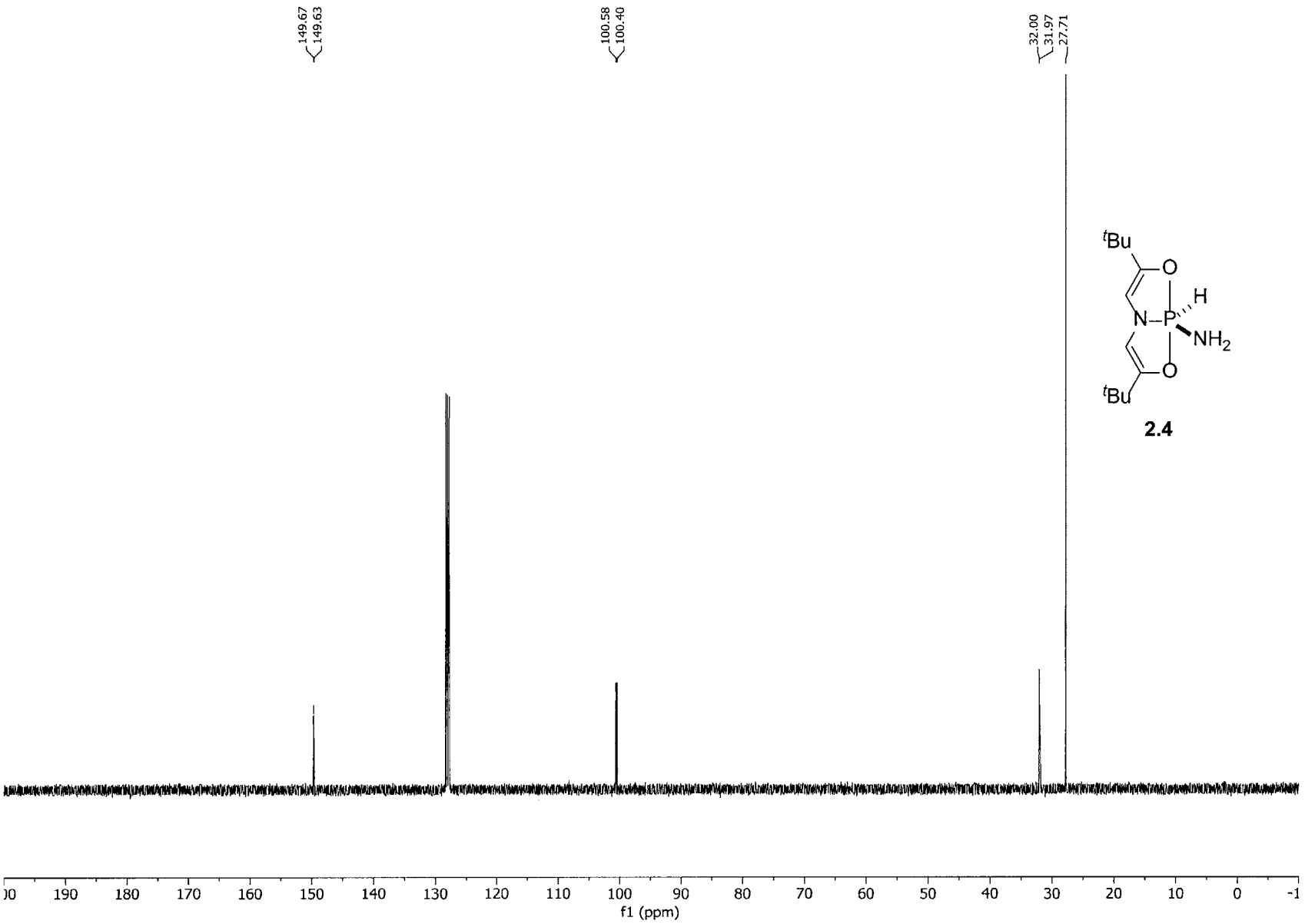

Figure A10. ^{13}C NMR of 2.4.

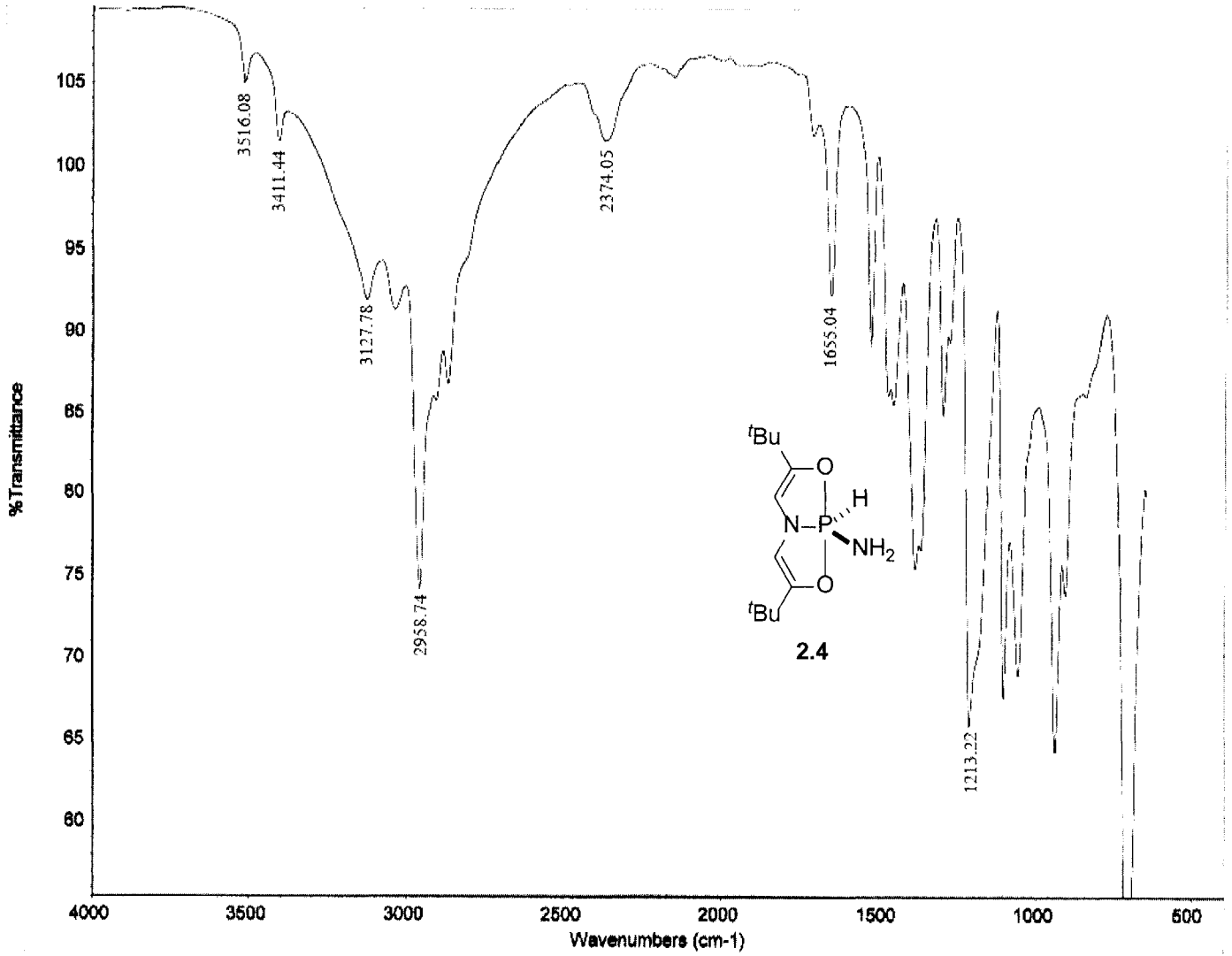

Figure A11. IR of 2.4.

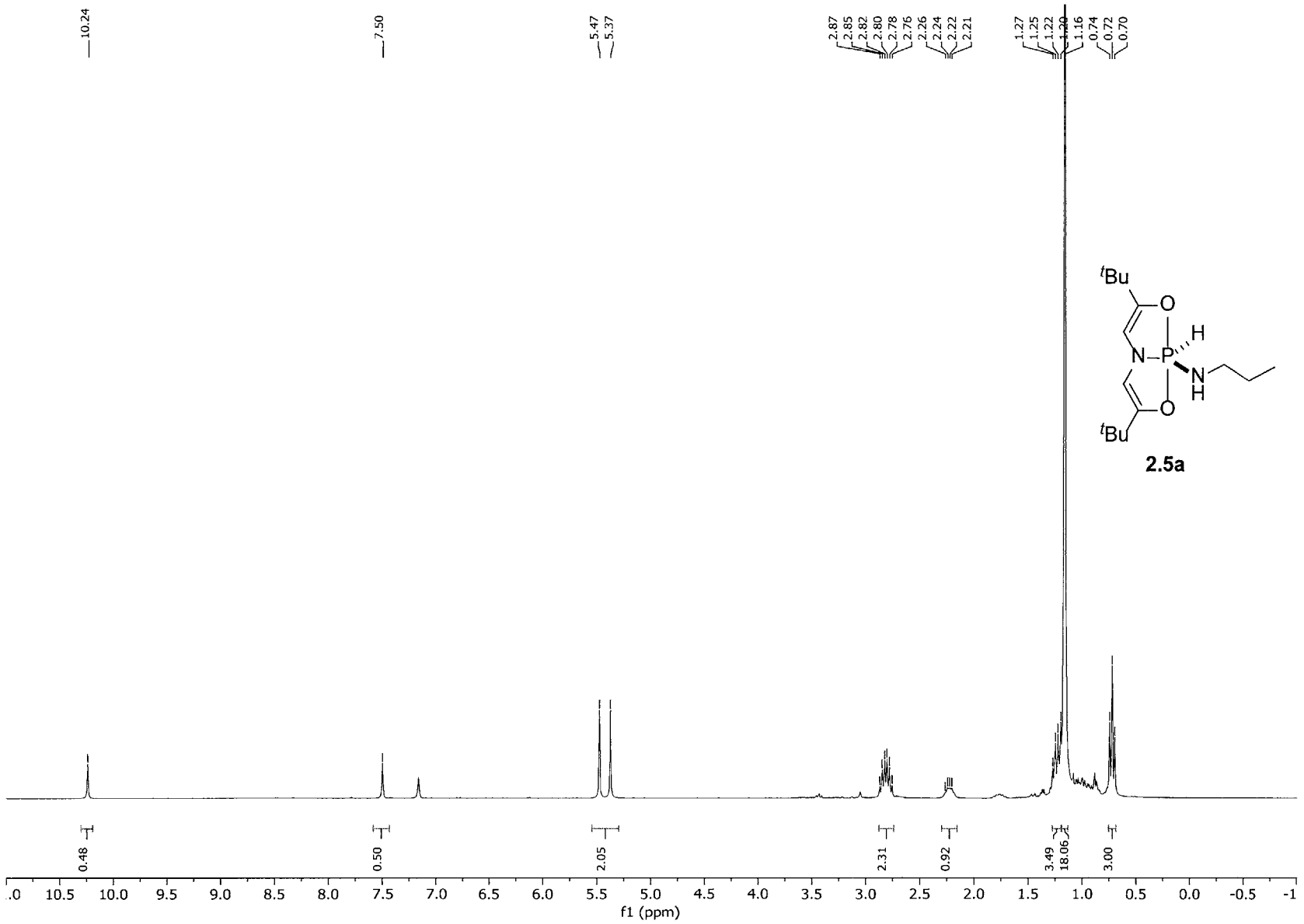

Figure A12. ^{1}H NMR of 2.5a.

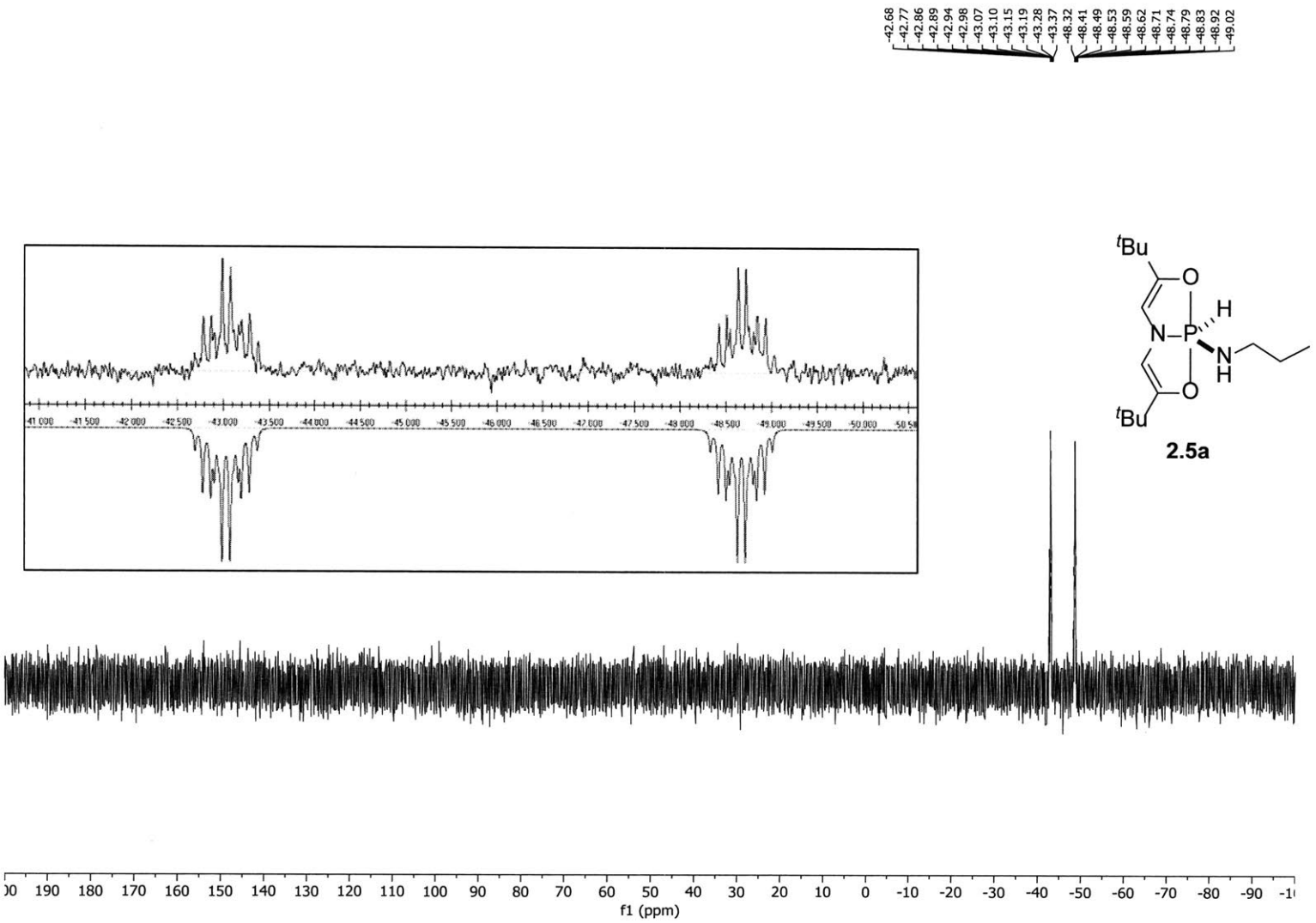

Figure A13. ^{31}P NMR of 2.5a. Inset: (*top*) experimental spectrum; (*bottom*) simulated spectrum (parameters: δ –45.85, *J*=821.3, 30.6, 12.5 Hz, linewidth 4.22 Hz).

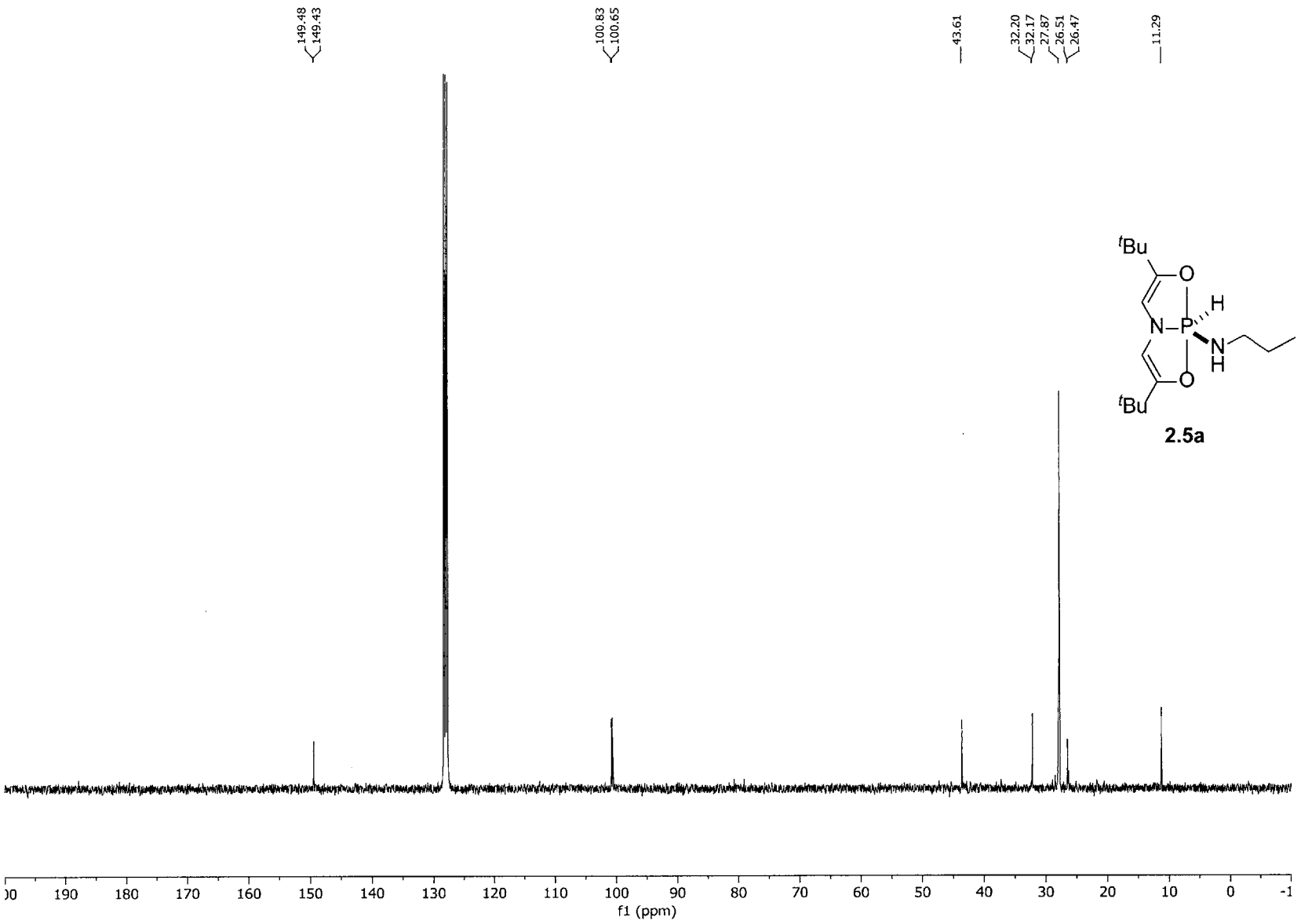

Figure A14. ^{13}C NMR of 2.5a.

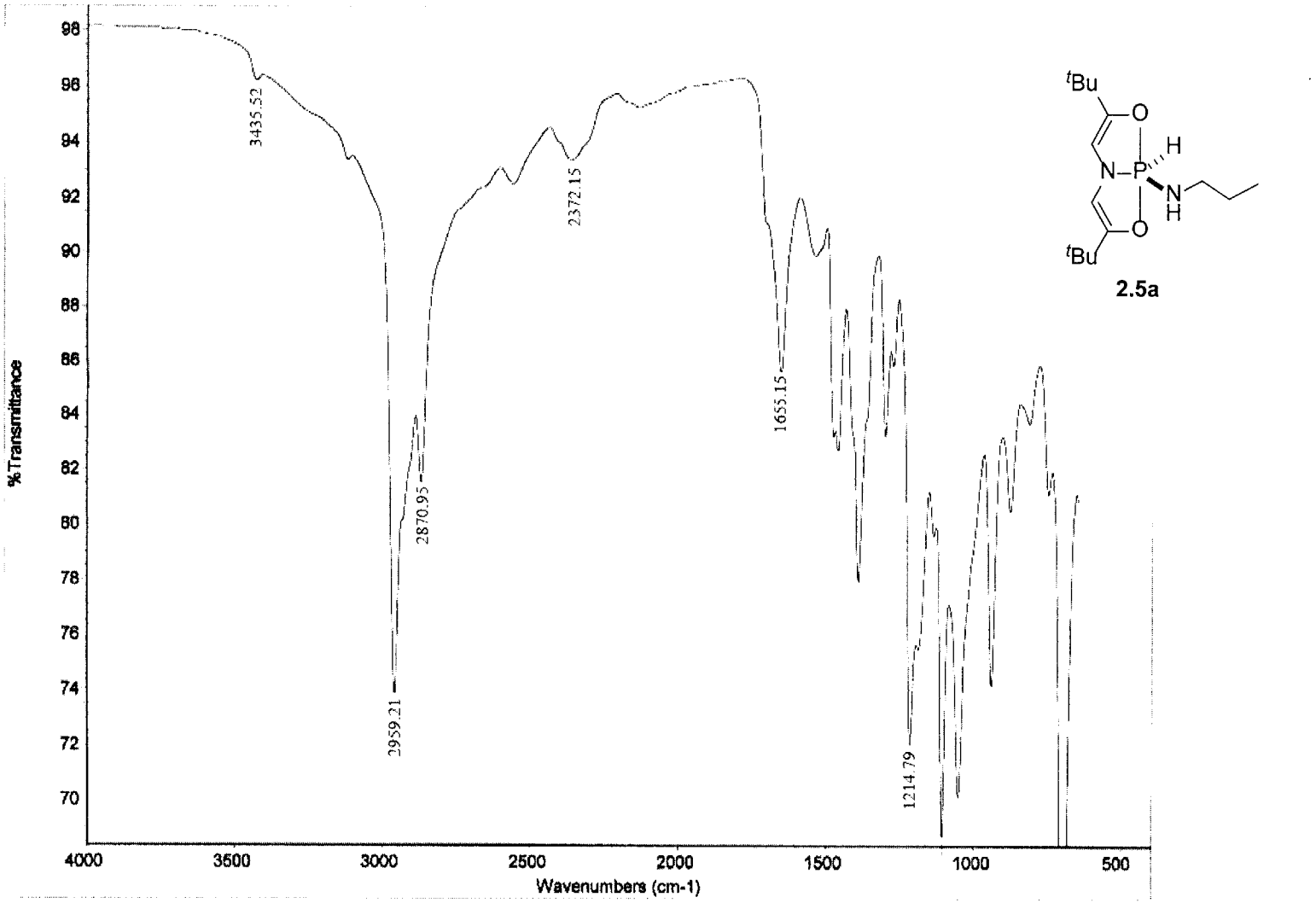

Figure A15. IR of 2.5a.

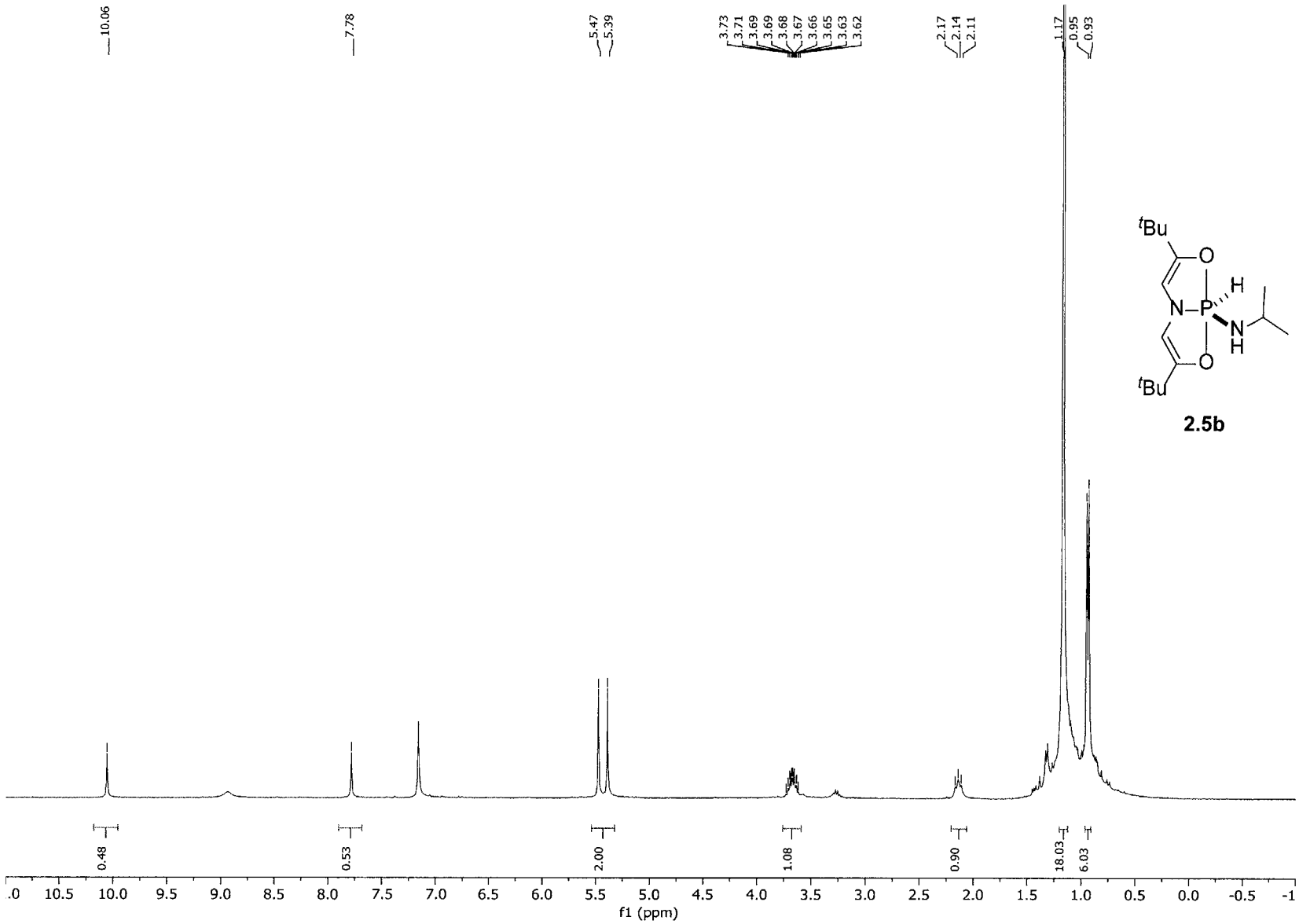

Figure A16. ^{1}H NMR of 2.5b.

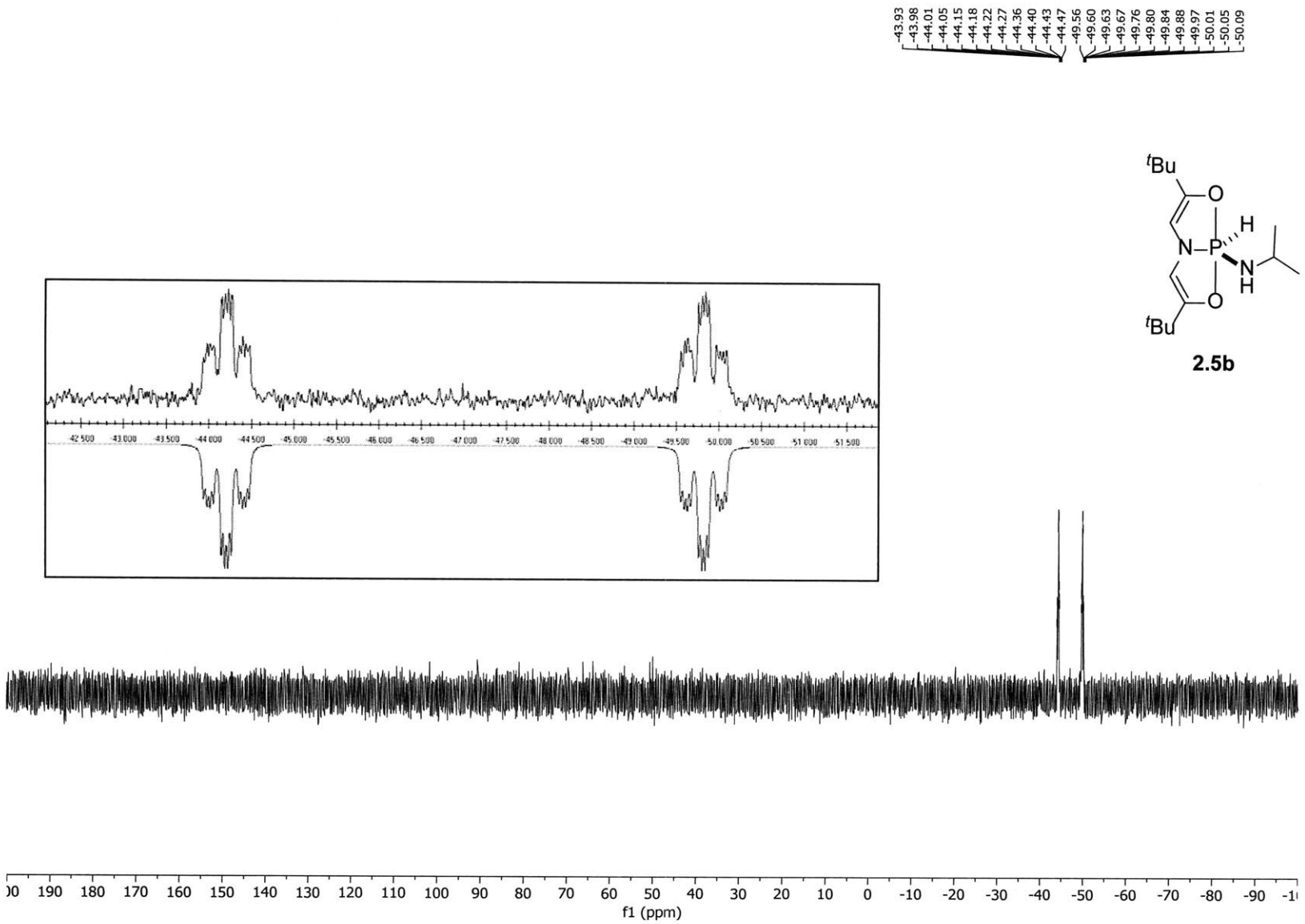

Figure A17. ^{31}P NMR of 2.5b. Inset (*top*) experimental spectrum; (*bottom*) simulated spectrum (parameters: δ –47.0, *J*=819.4, 30.6, 11.2, 5.9 Hz, linewidth 5.12 Hz).

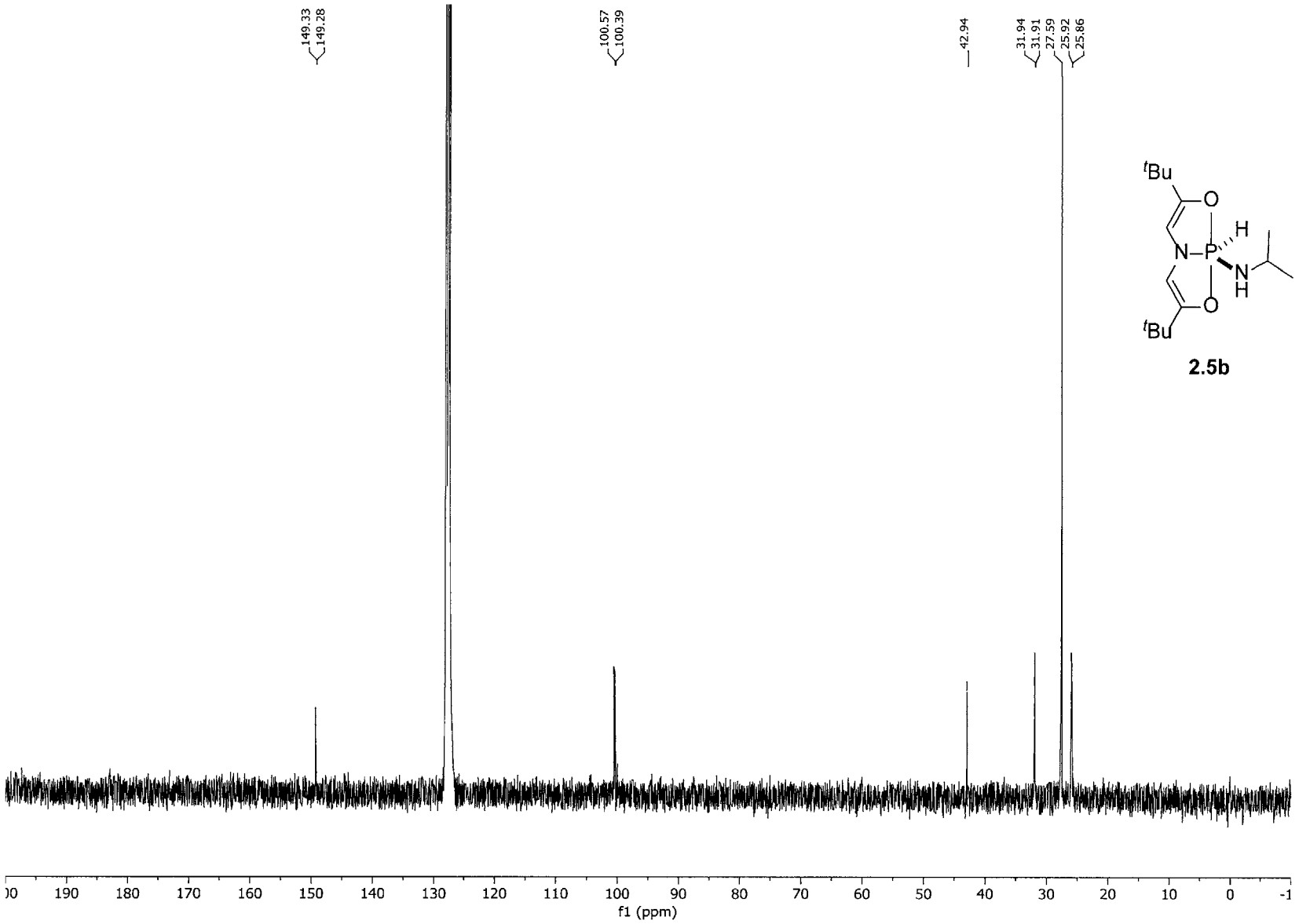

Figure A18. ^{13}C NMR of 2.5b.

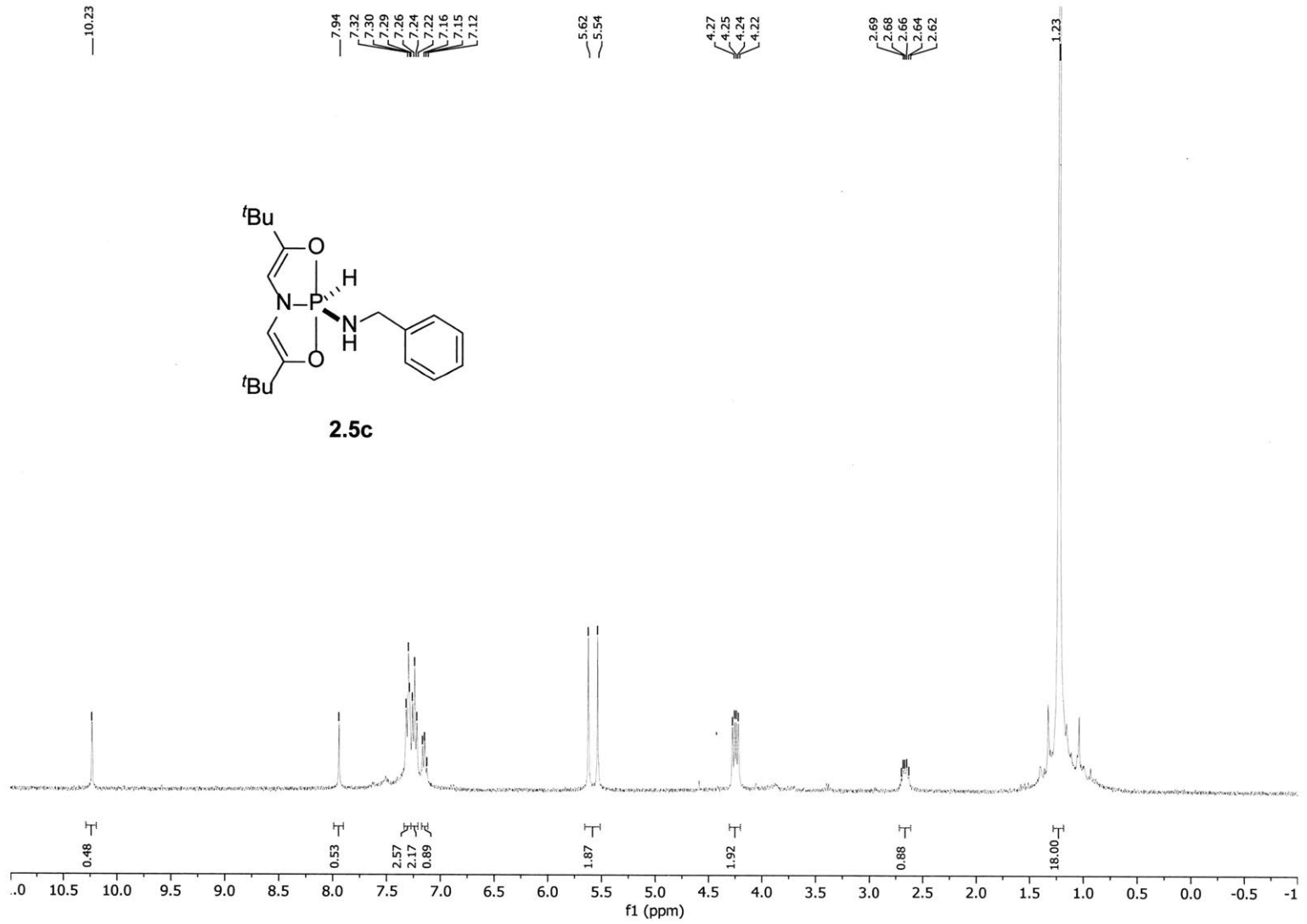

Figure A19. ^{1}H NMR of 2.5c.

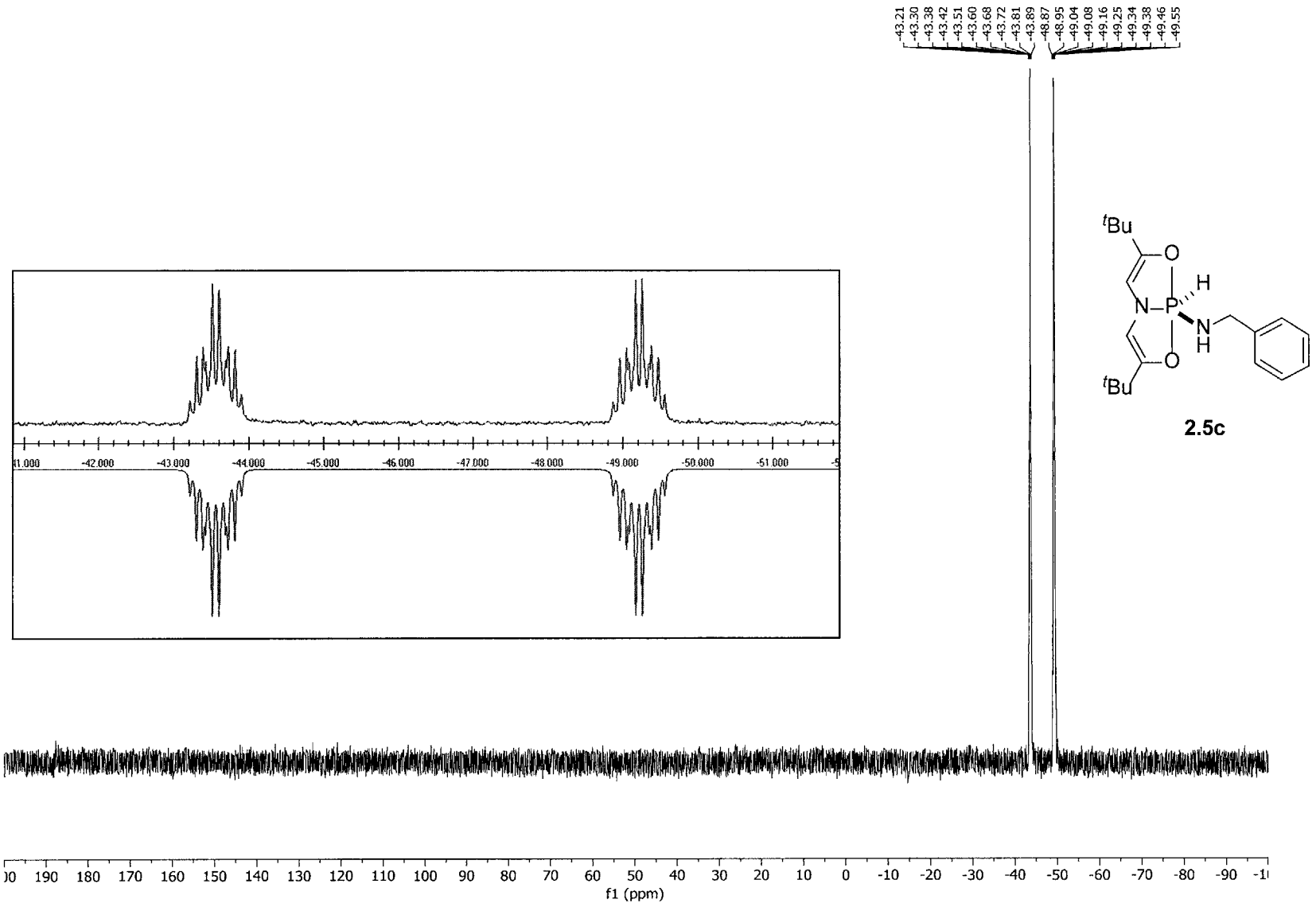

Figure A20. ^{31}P NMR of 2.5c. Inset (*top*) experimental spectrum; (*bottom*) simulated spectrum (parameters: δ –46.4, *J*=823.6, 30.8, 13.3, 12.7 Hz, linewidth 4.59 Hz).

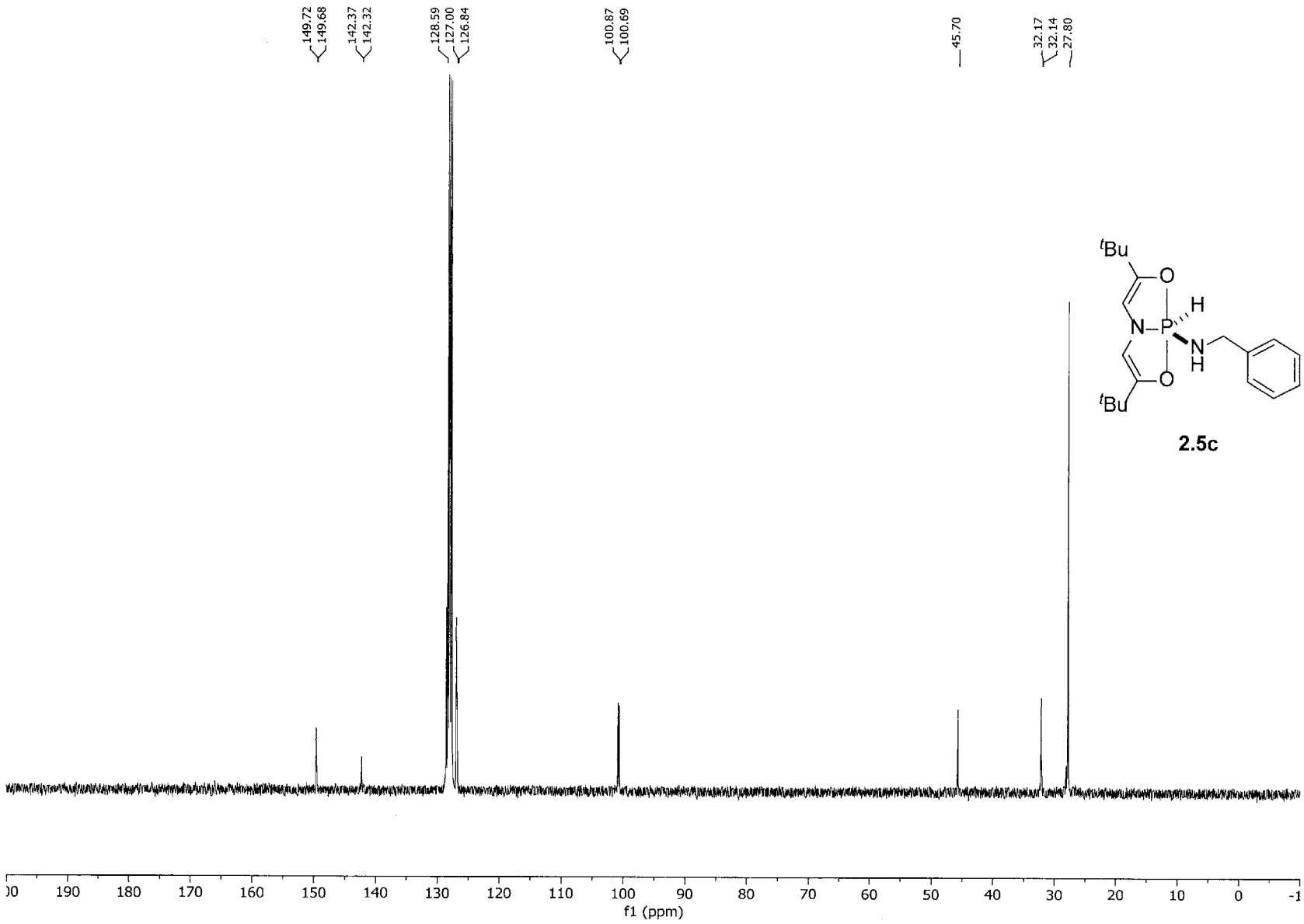

Figure A21. ^{13}C NMR of 2.5c.

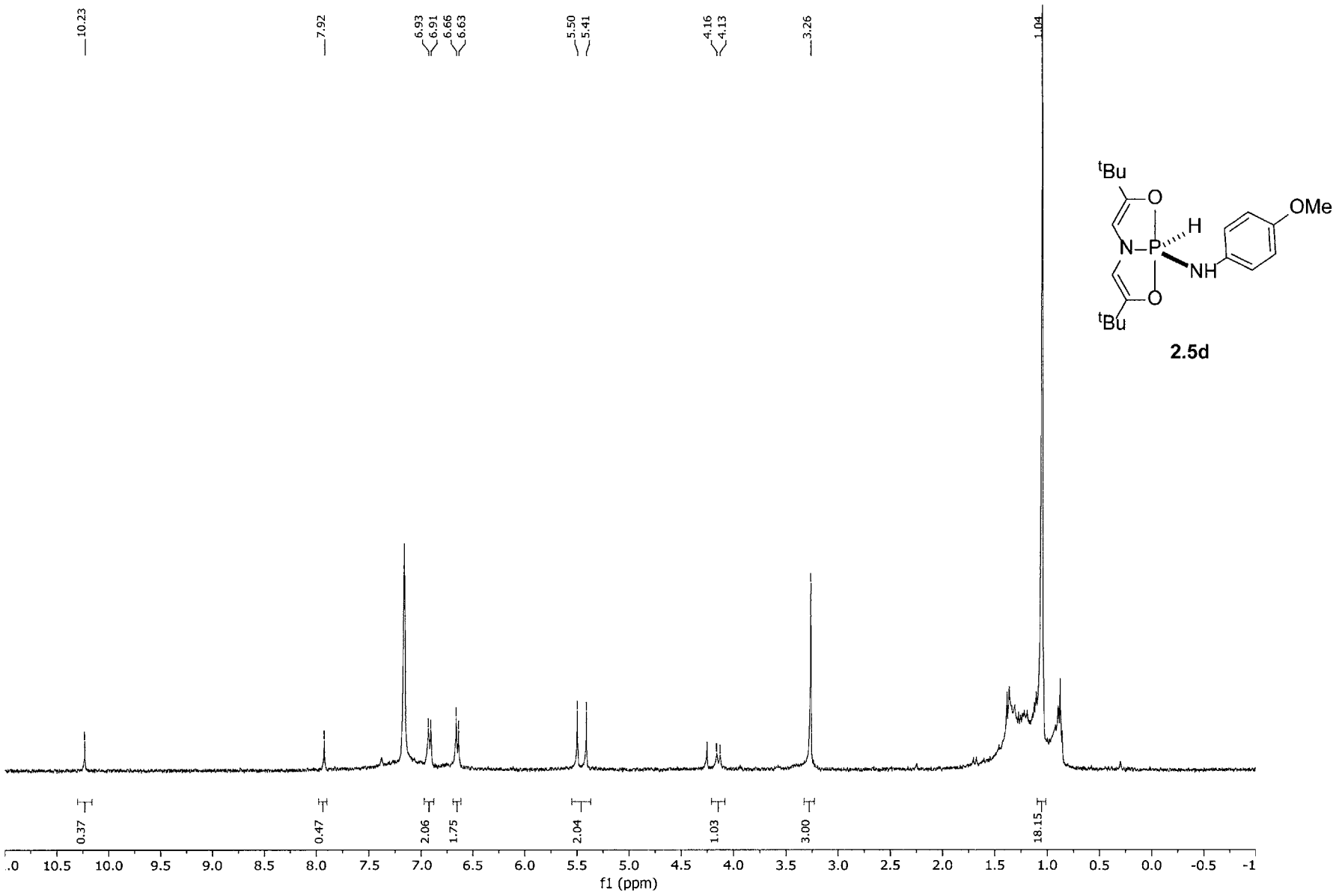

Figure A22. ^{1}H NMR of 2.5d.

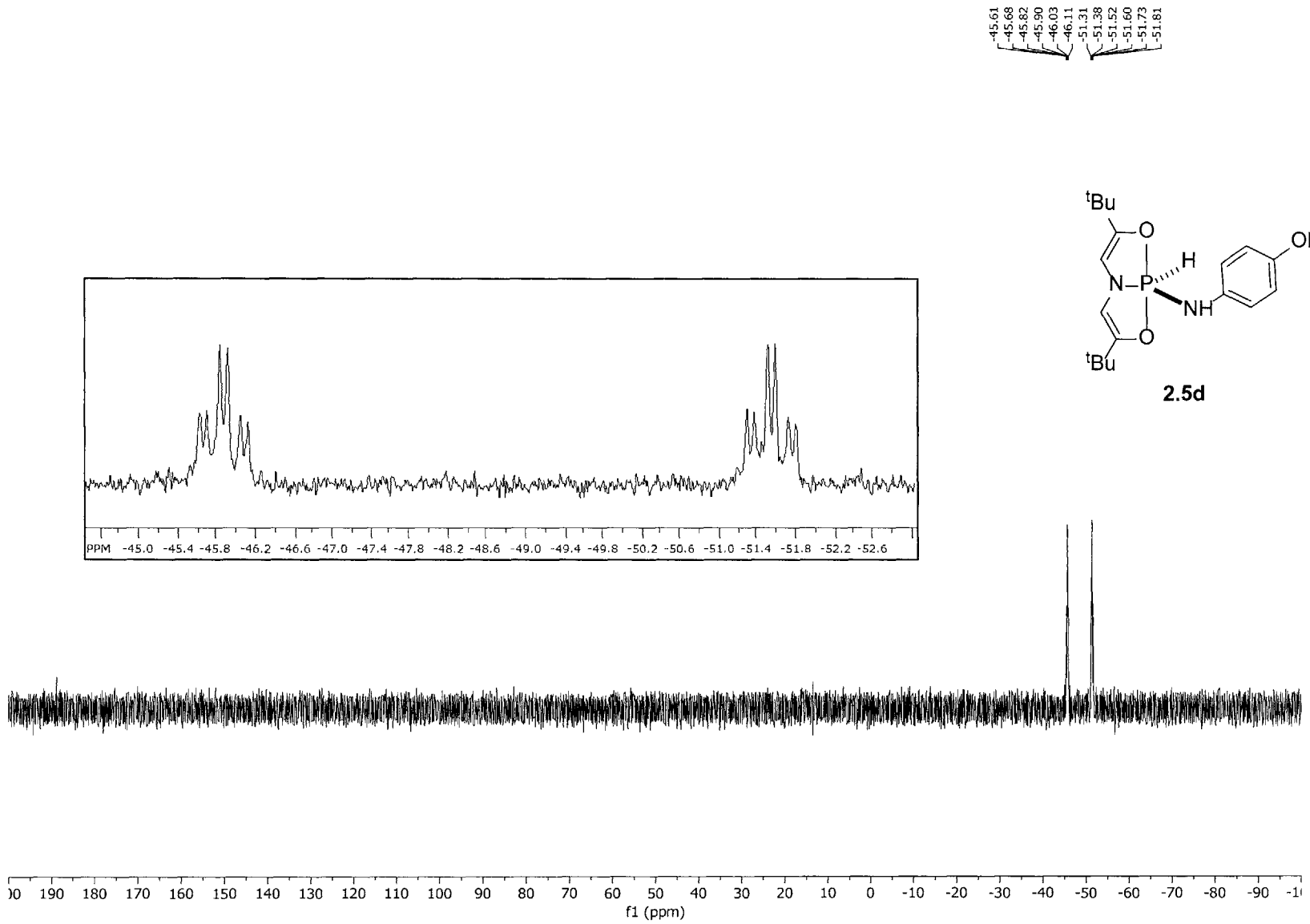

Figure A23. ^{31}P NMR of 2.5d. Inset: expansion of signal.

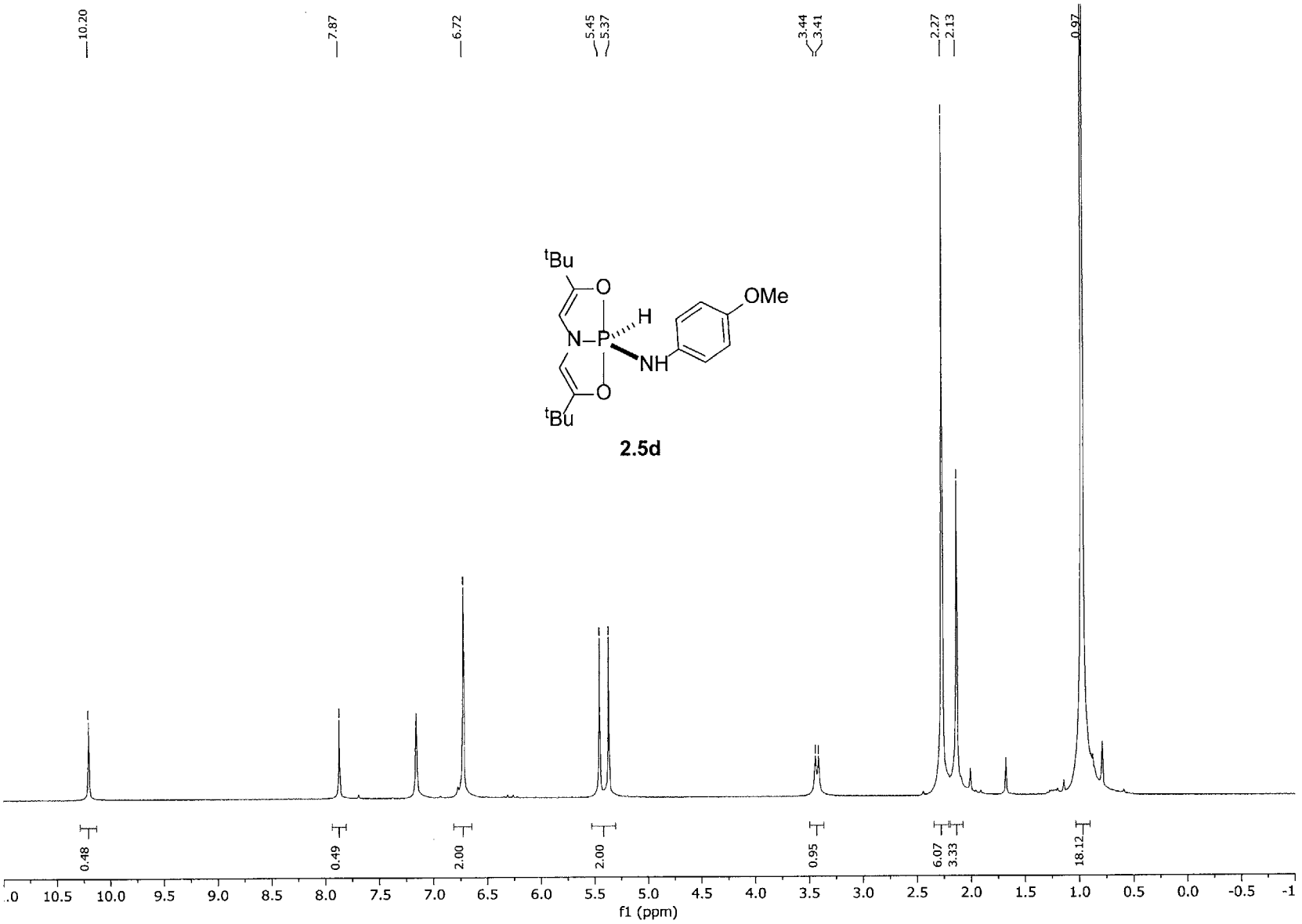

Figure A24. ^{1}H NMR of 2.5d.

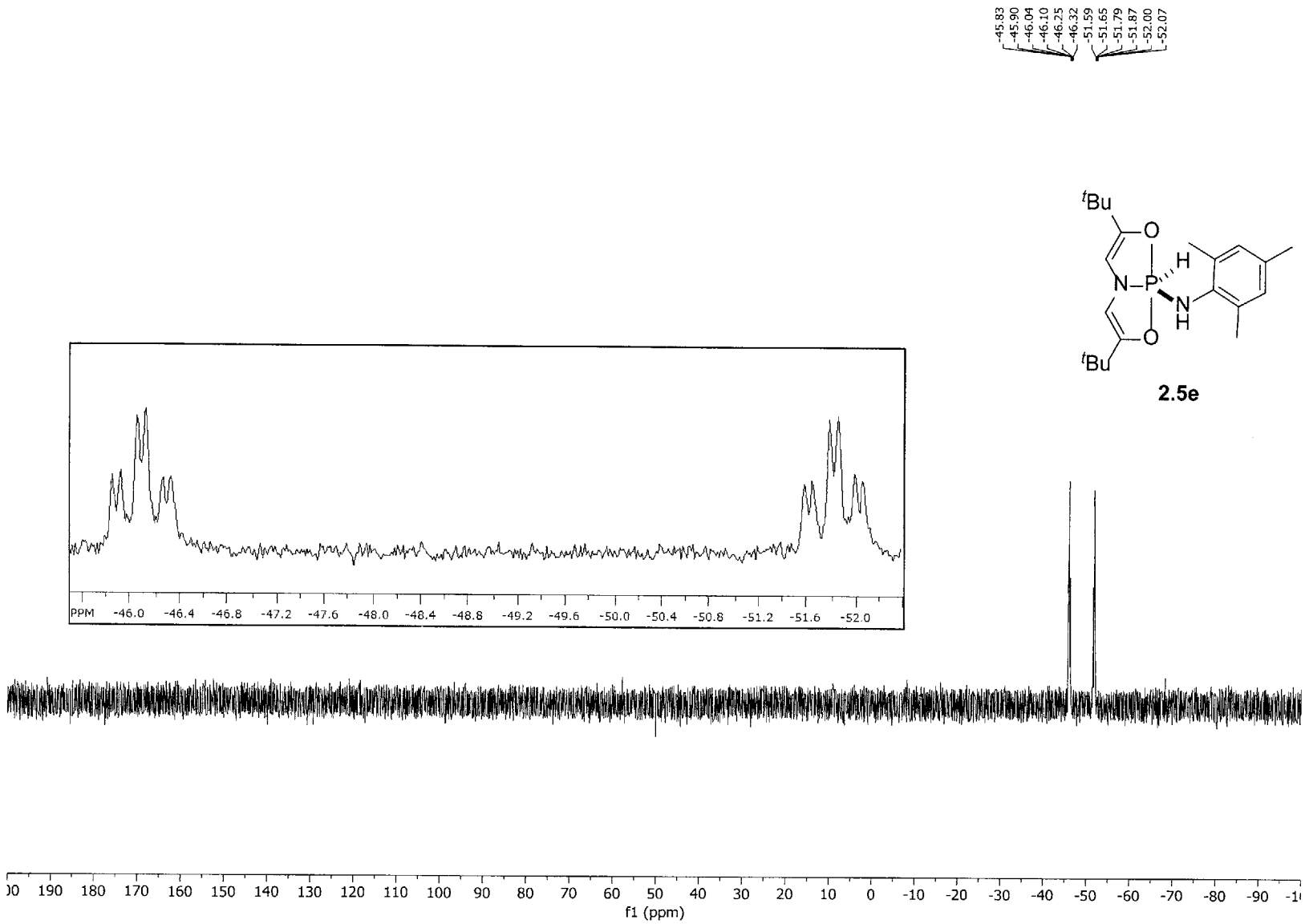

Figure A25. ^{31}P NMR of 2.5e. Inset: expansion of signal.

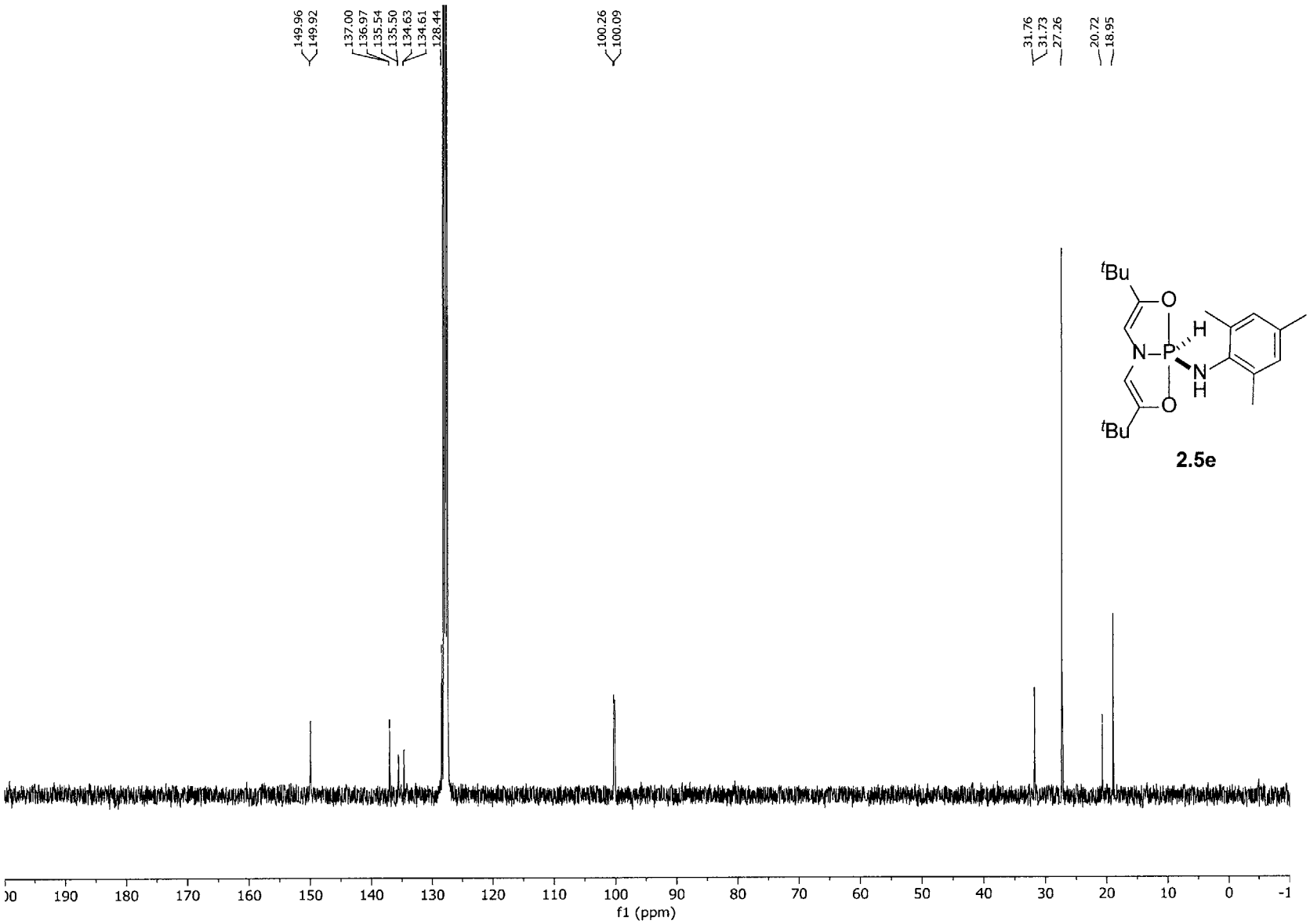

Figure A26. ^{13}C NMR of 2.5e.

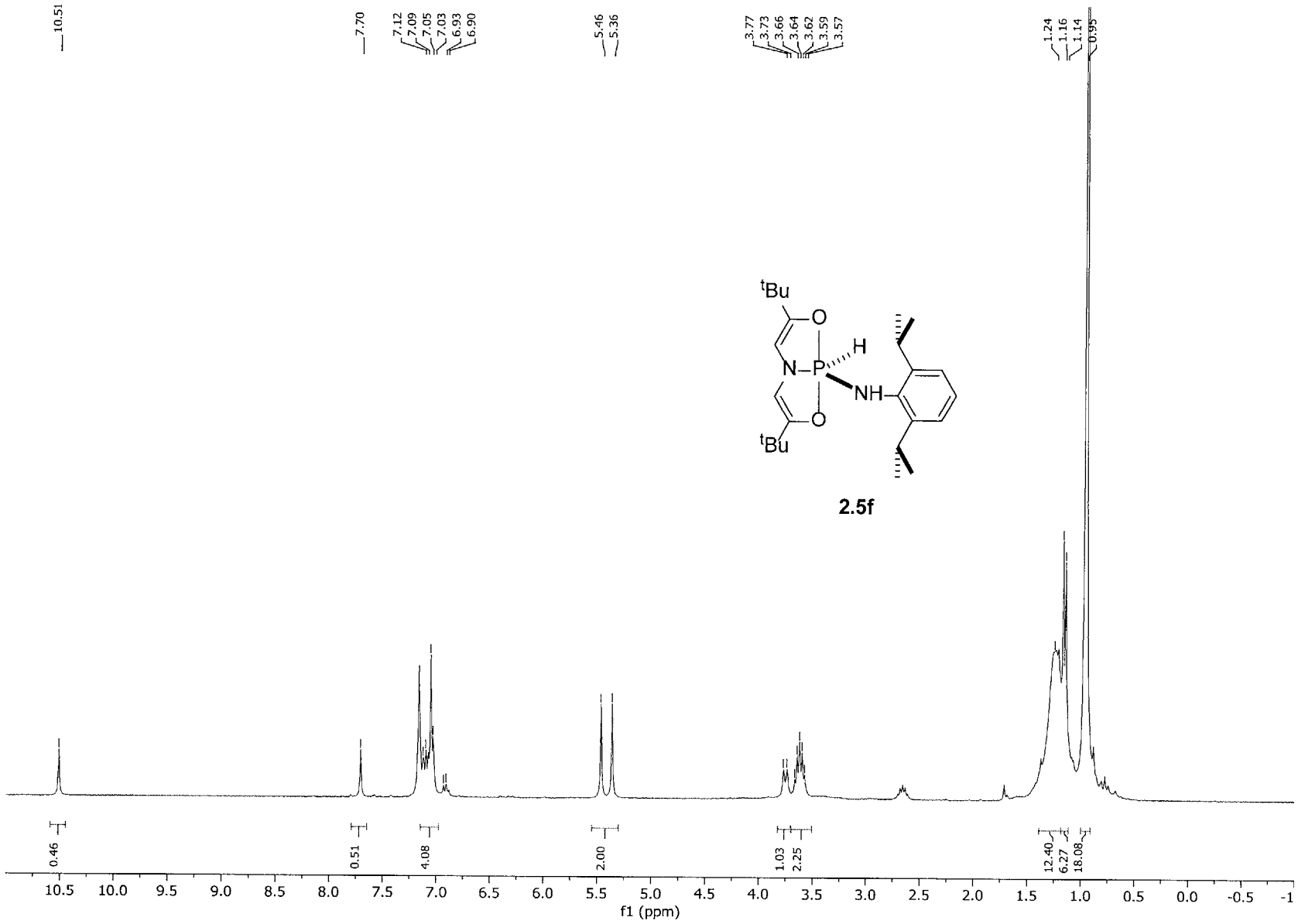

Figure A27. ^{1}H NMR of 2.5f.

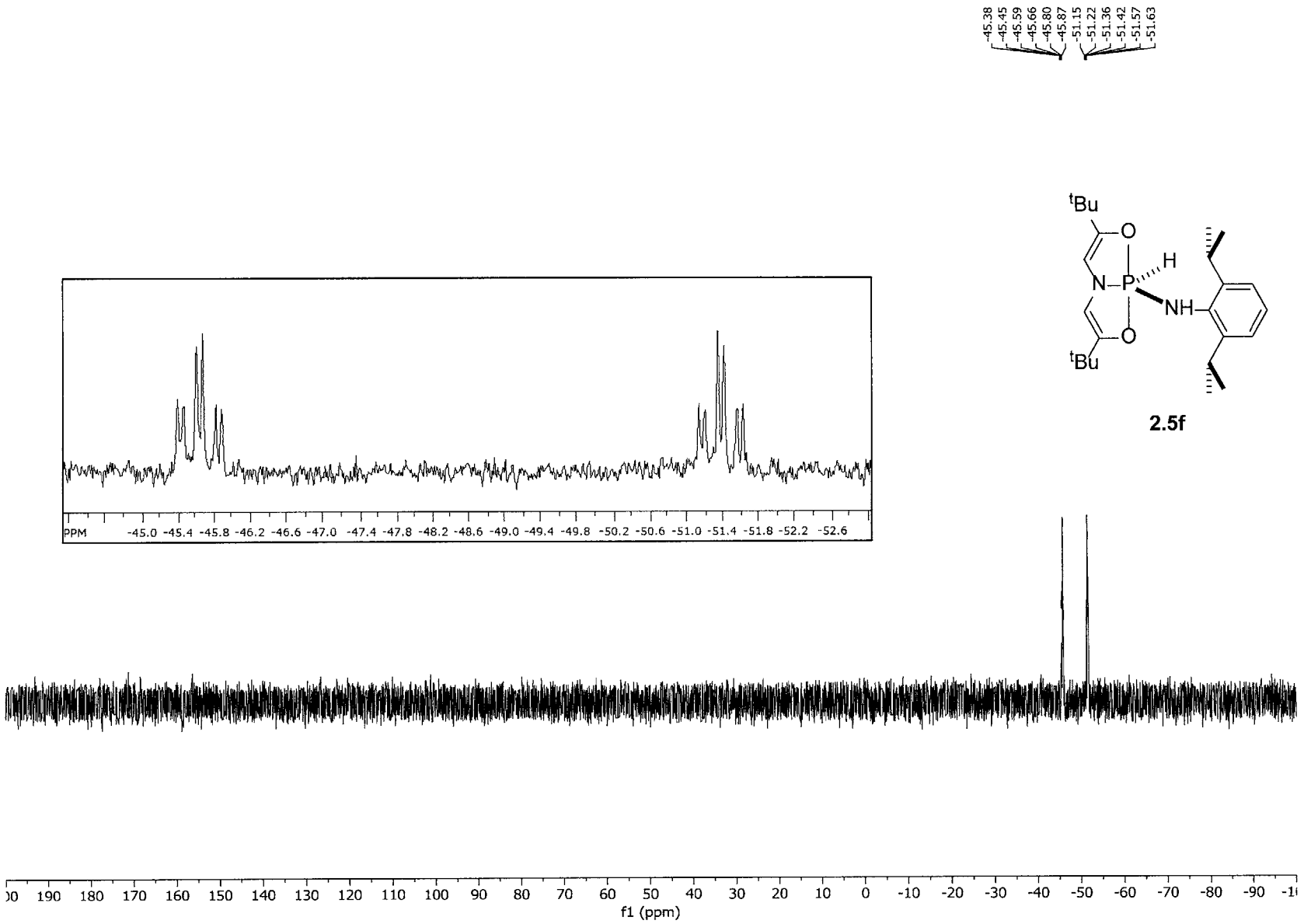

Figure A28. ^{31}P NMR of 2.5f. Inset: expansion of signal.

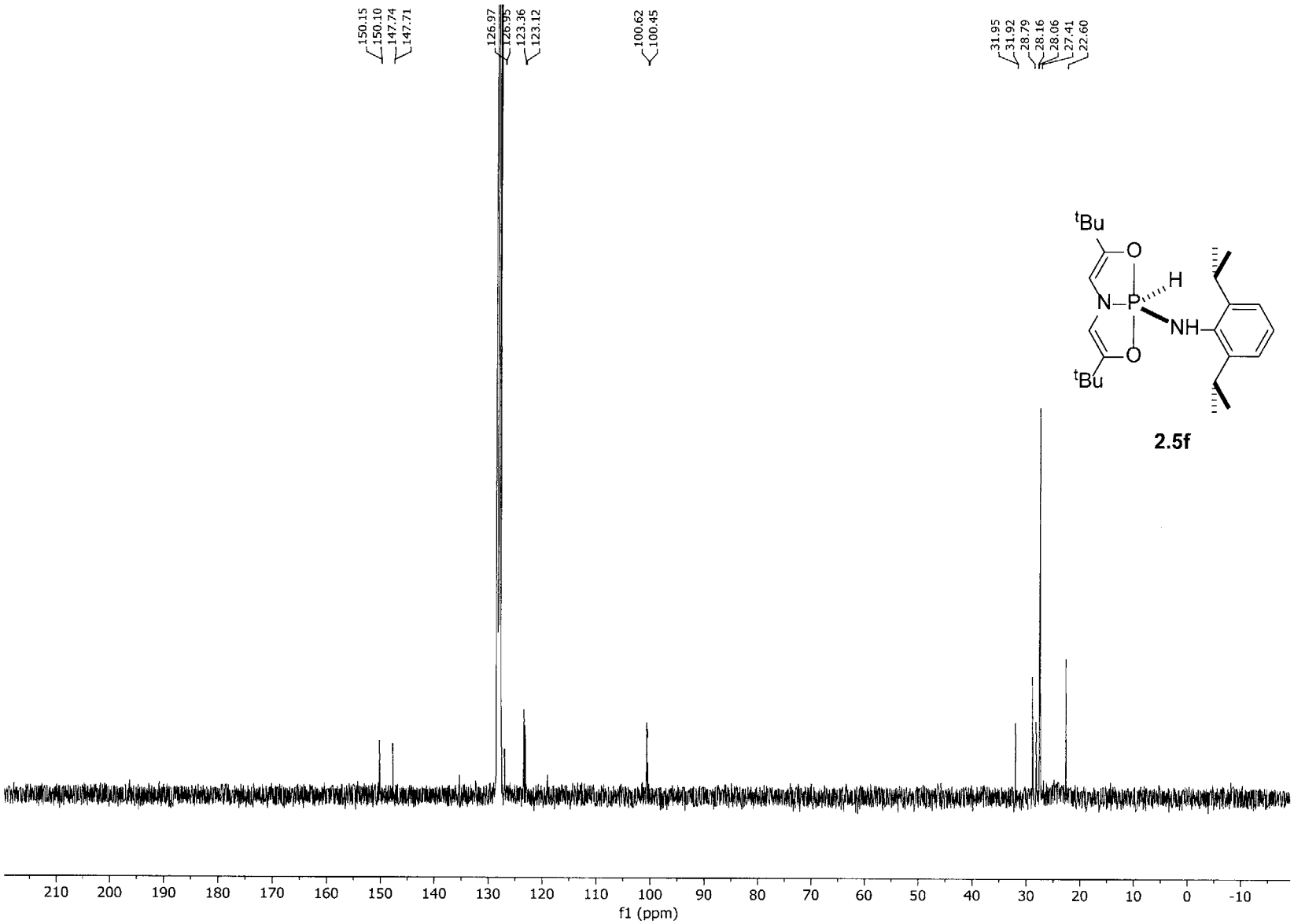

Figure A29. ^{13}C NMR of 2.5f.

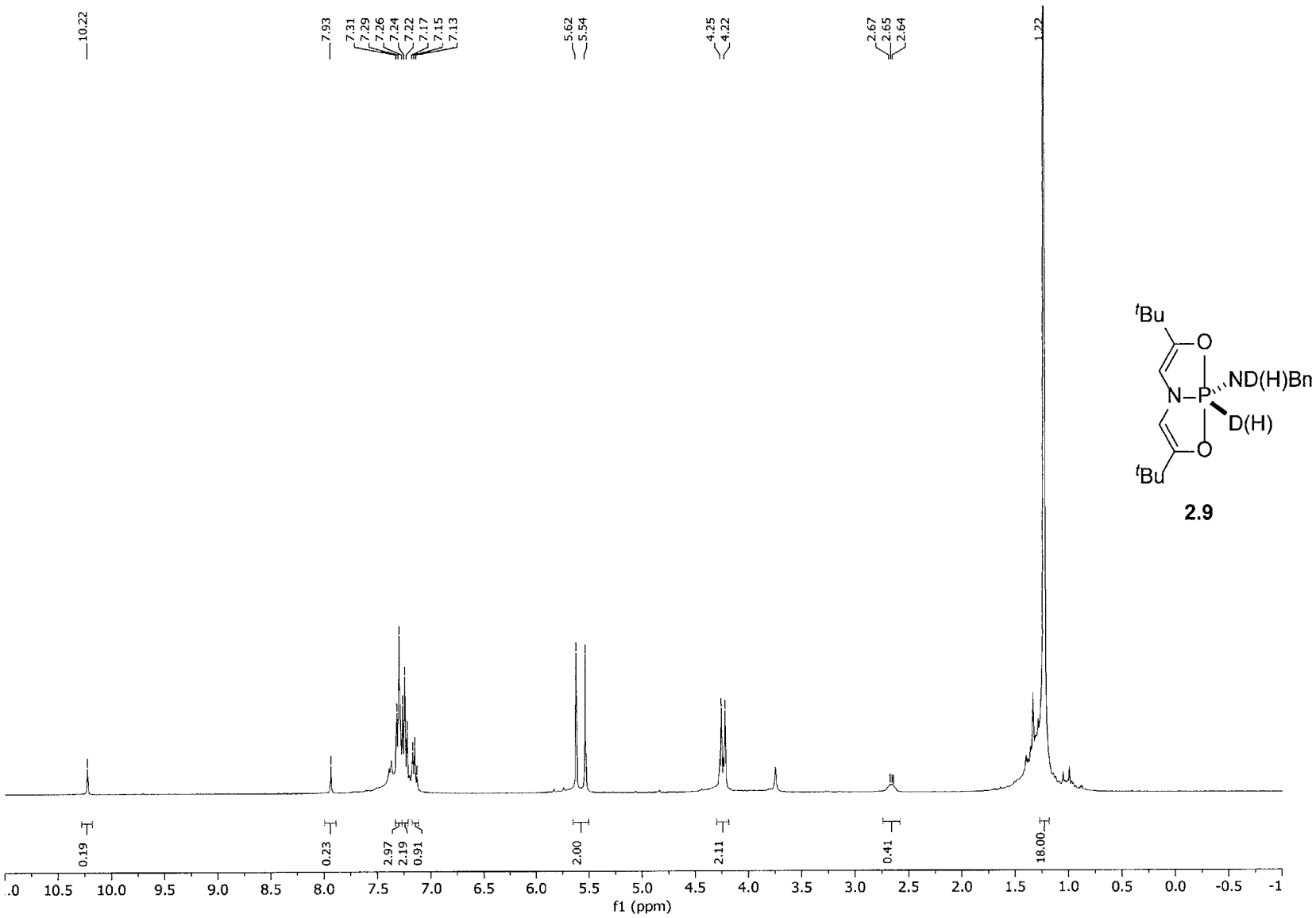

Figure A30. ^{1}H NMR of 2.9.

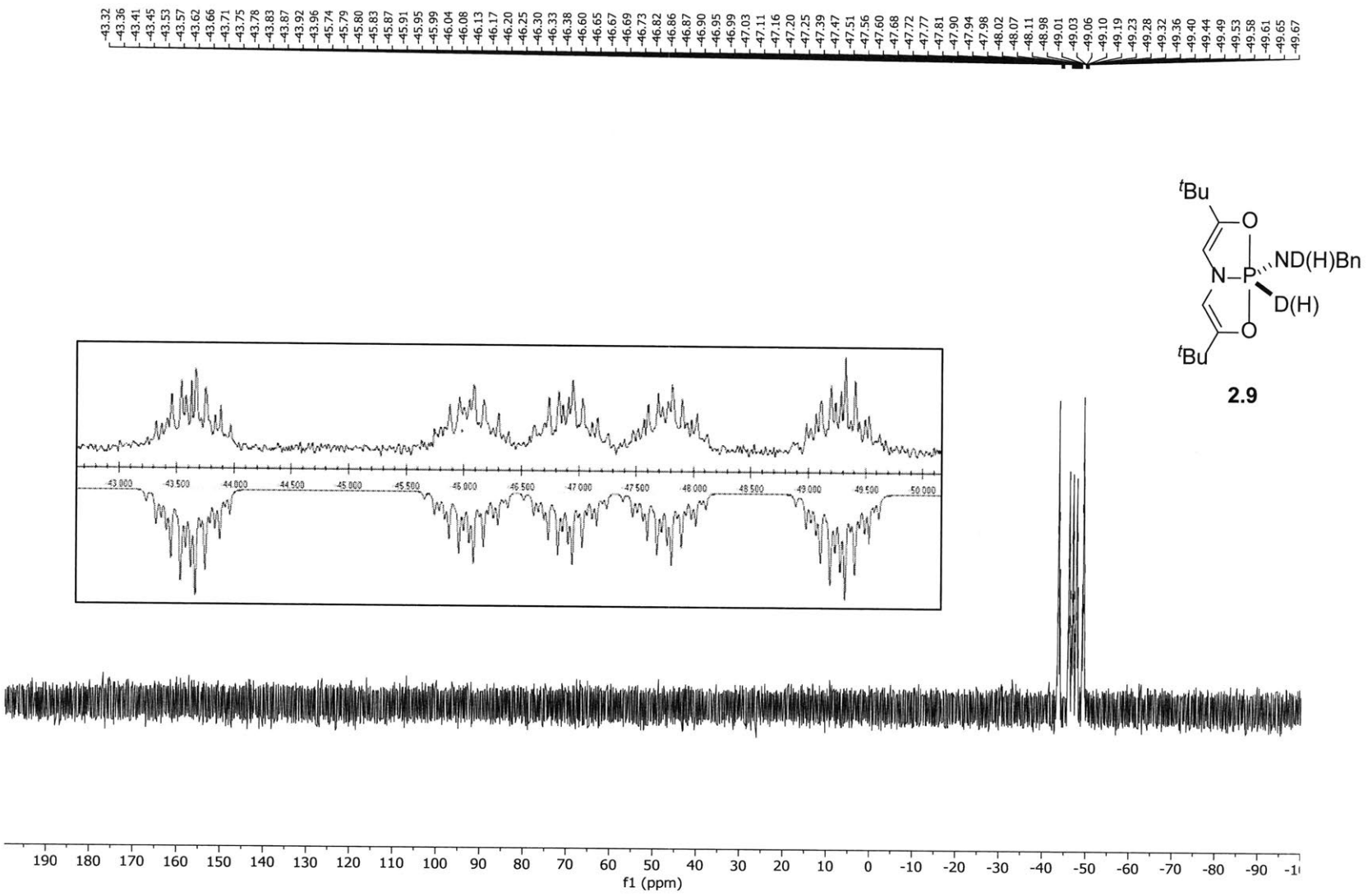

Figure A31. ^{31}P NMR of 2.9 and isotopologues. Inset: (*top*) experimental spectrum; (*bottom*) simulated spectrum with superposition of isotopologues 2.3•[D][NDBn] (δ -46.95, *J*=125.8, 30.8, 12.6 Hz); 2.3•[D][NHBn] (δ -46.87, *J*=125.8, 30.8, 12.6, 13.3 Hz); 2.3•[H][NDBn] (δ -46.50, *J*=824.7, 30.8, 12.6 Hz); 2.3•[H][NHBn] (δ -46.41, *J*=824.7, 30.8, 12.6, 13.3 Hz), linewidth 3.50 Hz.

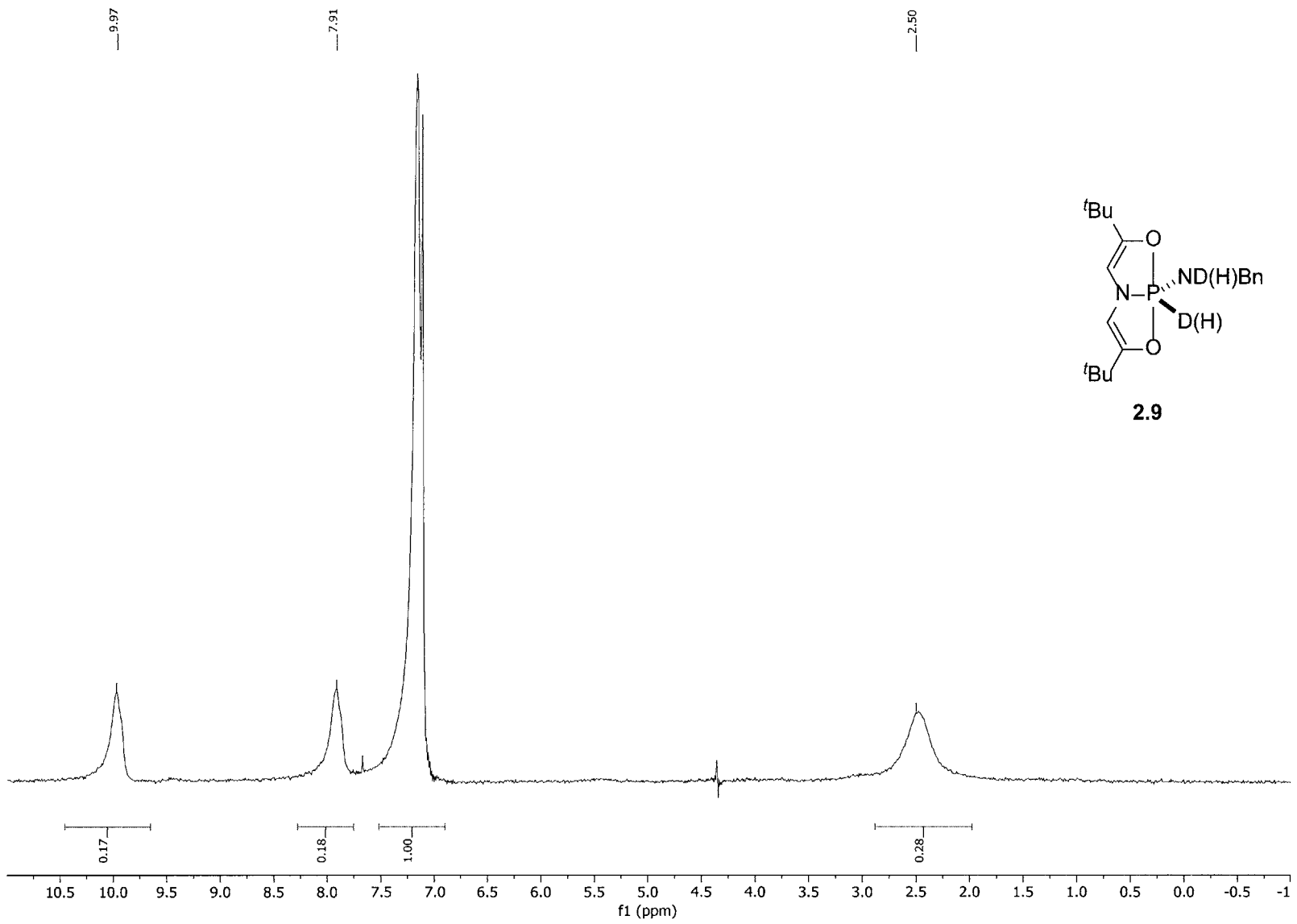

Figure A32. ^{2}H NMR of 2.9. Note the absence of vinylic ^{2}H NMR resonance at ca. 5.4 ppm.

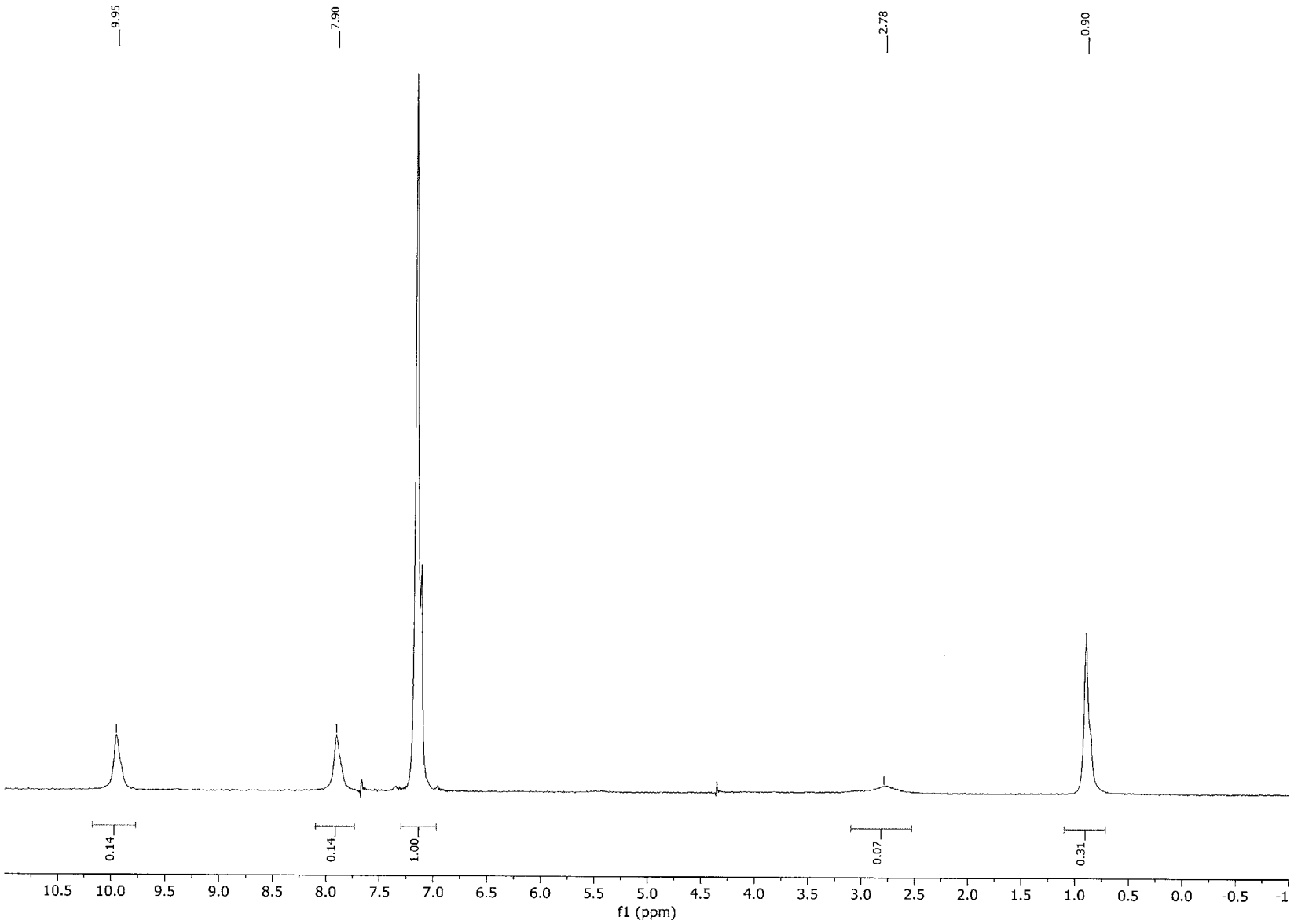

Figure A33. ^{2}H NMR of **2.9** after addition of $^{n}PrNH_2$, rt, 10 min. Exchange at the N–D, and to a lesser extent P–D, site is evident.

Appendix B

Supplemental Data for Chapters Three

Table of Contents

I. NOESY Experiments for Characterization of Compound 3.6

All NOE NMR spectra were obtained on a Bruker Avance 500 MHz NMR spectrometer equipped with a 5mm broadband, BBFO Z-gradient probe. The samples were *in situ* generated **3.6** from compound **3.2** and pinacolborane in C_6D_6 ($1.3x10^{-2}$ M).

Full spectrum:

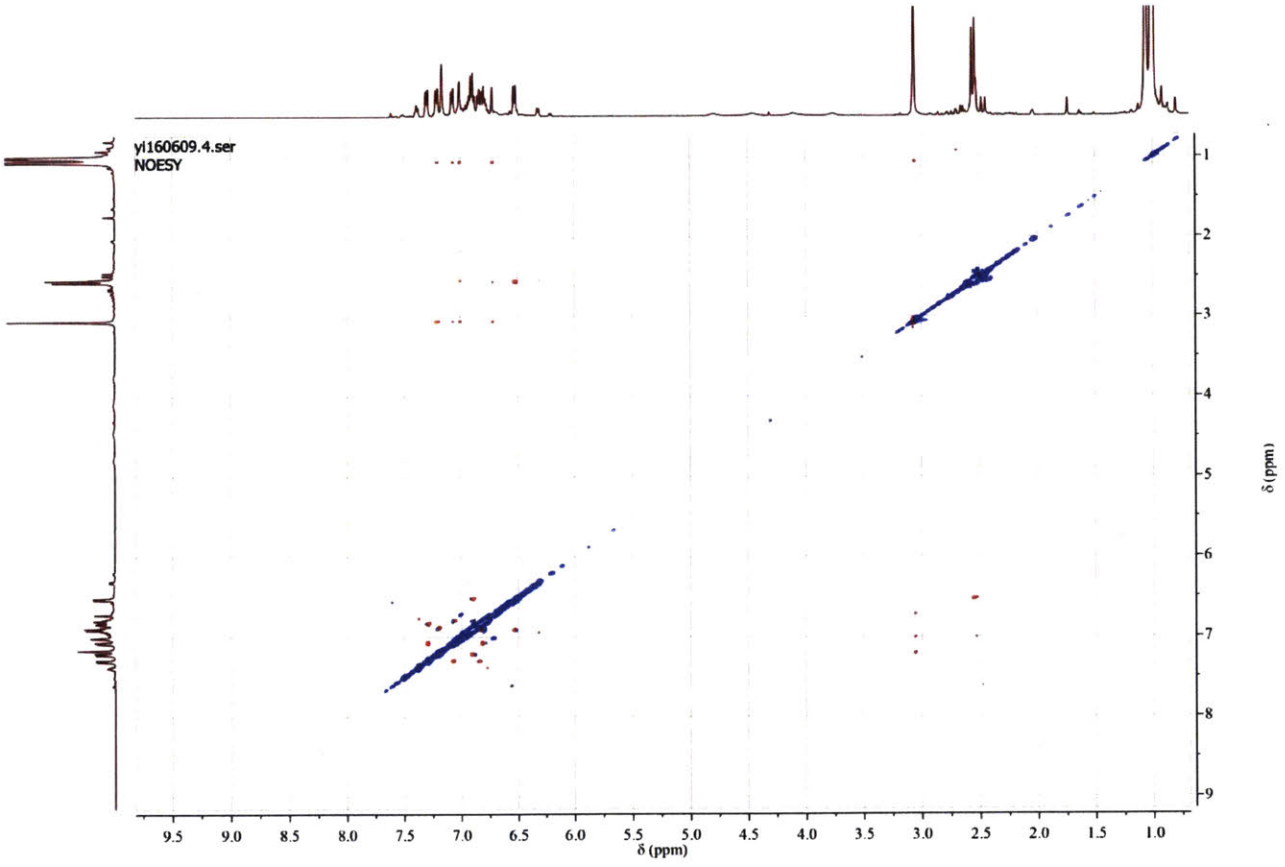

Correlation signals between aliphatic protons:

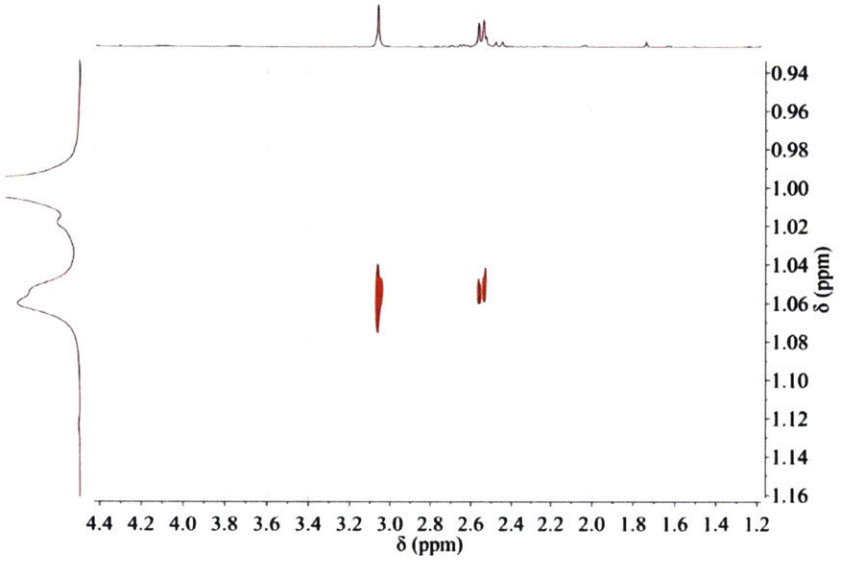

Correlation signals between aliphatic protons and aromatic protons:

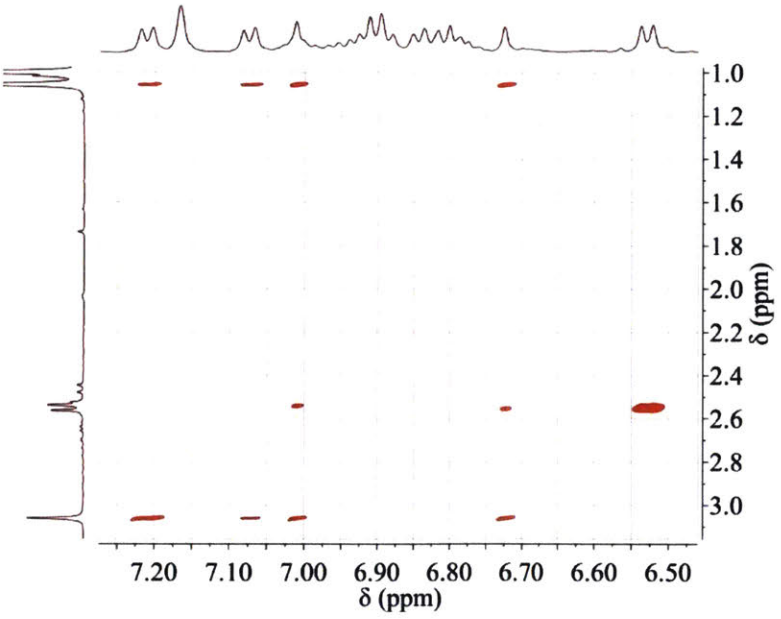

II. *In Situ* ^{31}P NMR for the Reaction of Compound 3.6 with chloroform

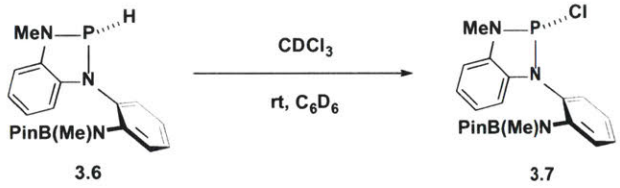

3.6 3.7

Under nitrogen atmosphere, pinacolborane (10 mg, 0. 08 mmol) was mixed with a C_6D_6 solution (0.6 mL) of compound **3.6** (20 mg, 0.08 mmol) in a J-Young NMR tube. The mixture was kept at 50 °C for 12 h to generate crude **3.7**. A C_6D_6 solution of $CDCl_3$ (0.2 ml, 42 mM) was then added. The reaction mixture was then monitored by ^{31}P NMR after 15 min, 2 h and 4h under ambient temperature.

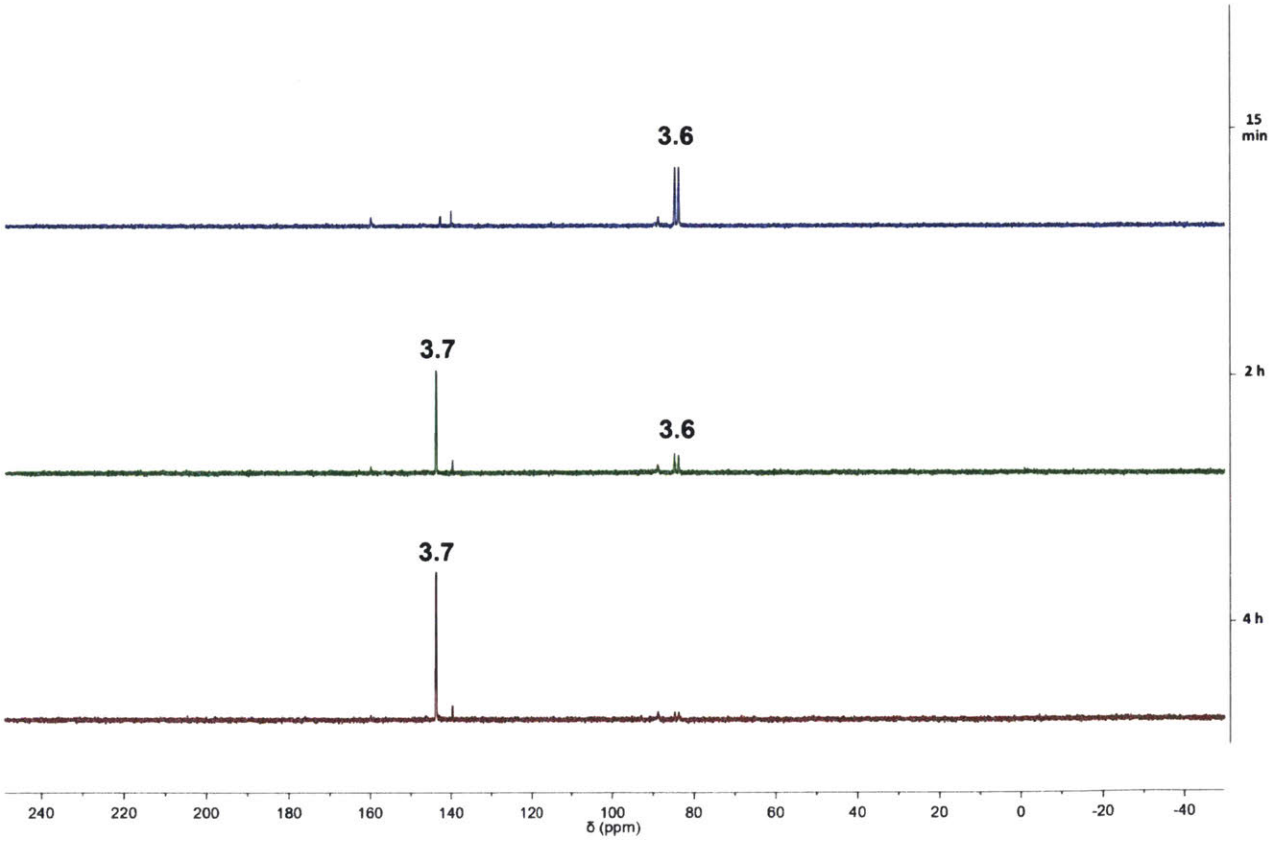

III. Kinetic Study of the B-H Activation Reaction

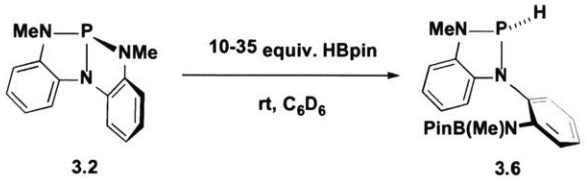

3.2 3.6

Pseudo-first order kinetics. Experiments were conducted with varying equivalent of HBPin with at least 10-fold excess. Measurements were performed on a Bruker AV-400 NMR spectrometer. A stock solution of compound **3.2** (0.6 ml, 13 mM in C_6D_6 containing 0.06 mmol 1,3,5-trimethoxybenzene as the internal standard) and HBpin were added to a volumetric flask and the resulting mixture was diluted to 1 ml with C_6D_6. The diluted solution was then transferred to a J-Young NMR tube and the conversion of **3.2** to **3.6** was monitored with ^{1}H NMR at ambient temperature. The concentrations of **3.2** were obtained from the NMR signal integral ratios between **3.2** and the internal standard. The error bars on the plot are generated from variability of ^{1}H NMR integrals.

Table B1. Pseudo-first order rate constant in varying equivalent of HBpin.

HBpin equiv.	[HBpin]	k_{obs} (s^{-1})
10	0.78	0.002228
15	1.17	0.002440
20	1.56	0.002875
25	1.95	0.003072
30	2.34	0.003427
35	2.73	0.003733

Determination of reaction order in HBpin. The observed pseudo-first order rate constants (k_{obs}) were plotted against the corresponding HBpin concentrations (0.78 M – 2.73 M).

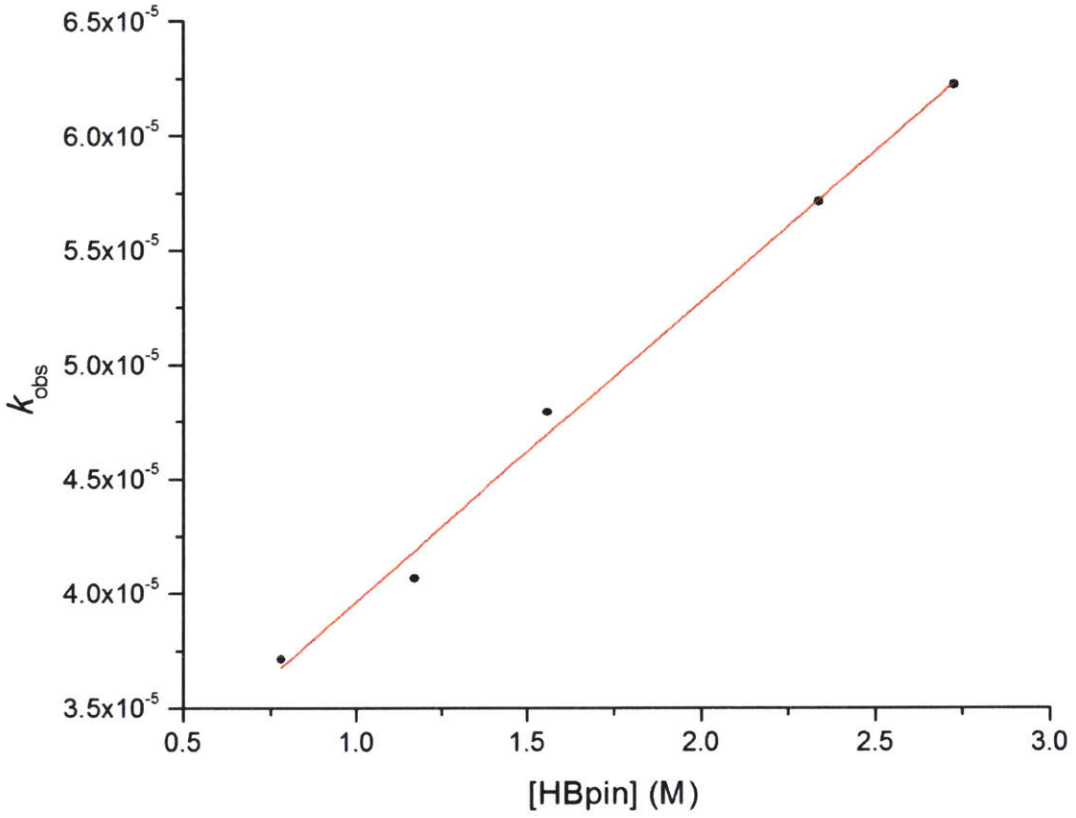

IV. Kinetic Study of the B-N Elimination Reaction

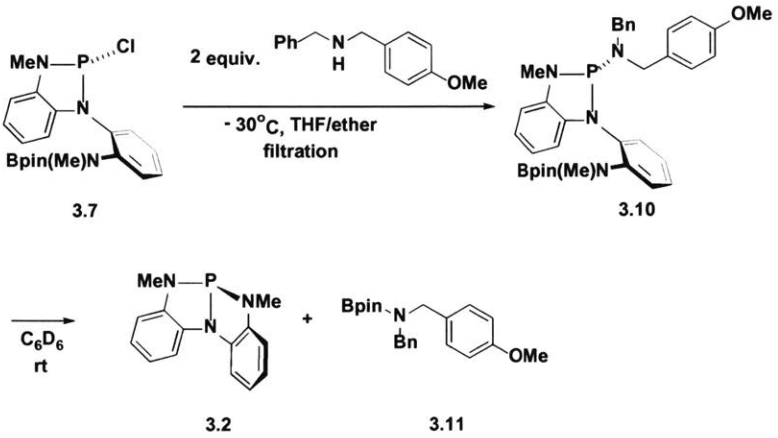

3.7 3.10

3.2 3.11

In a nitrogen-filled glovebox, a 1:1 THF/ether solution (2 ml) of **3.7** (10 mg, 2.39×10^{-2} mmol) and an ether solution (1 ml) of *N*-benzyl-1-(4-methoxyphenyl)methanamine (12 mg, 4.79×10^{-2} mmol) were both cooled to –30 °C and then mixed together. The resulting cloudy mixture was quickly filtered through Celite and all volatiles were removed in vacuo to afford crude **3.10**. (NMR yield 82 %). The crude product was dissolved in 1 mL of C_6D_6 containing 1,3,5-trimethoxybenzene (2 mg, 1.9×10^{-2} mmol) and the conversion of **3.10** to **3.2** and the *N*-borylamine **7** was monitored by ^{1}H NMR spectroscopy, with the varying concentrations of **3.10** and **3.2** determined at regular time intervals by ^{1}H NMR integration relative to internal standard. The error bars on the plot are generated from variability of ^{1}H NMR integrals.

V. General Synthetic Procedure for Imines[1]

Aldimines. In a two-neck round-bottom flask equipped with Dean-Stark apparatus, a toluene solution (20 ml) of the aldehyde (0.02 mol) was added the amine (0.02 mol). The mixture was refluxed and the reaction progress was monitored by thin layer chromatography. Upon completion, the solution was filtered through Celite and all volatiles were removed *in vacuo*. The resulting solid product was purified by recrystallization from ethanol.

Ketimines. In a two-neck round-bottom flask equipped with Dean-Stark apparatus, a toluene solution (20 ml) of the ketone (0.02 mol) was added the amine (0.02 mol) and sodium bicarbonate (0.02 mol). The mixture was refluxed and the reaction progress was monitored by thin layer chromatography. Upon completion, the solution was filtered through Celite and all volatiles were removed *in vacuo*. The resulting solid product was purified by recrystallization from ethanol.

VI. Catalytic Experiments and Characterization Data

A C_6D_6 solution (0.6 ml) of compound **3.2** ($1.50x10^{-2}$ mmol) was added the imine (0.15 mmol) and HBpin (0.19 mmol). The mixture was then added 10 mg of *1,3,5*-trimethoxybenzene as the internal standard and transferred to a J-Young NMR tube. The reaction solution was kept under 50 °C for 24 hours and the conversion of was monitored by ^{1}H NMR. The concentrations and yields of the product borylamine were obtained from the NMR signal integral ratios between the botylamine and the internal standard.

3.11. ^{1}H NMR (360 MHz, C_6D_6) δ 7.93, 7.43 (d, 2H, J = 7.6 Hz), 7.38 – 7.20 (m, 6H), 6.94 (d, 2H, J = 7.6 Hz), 5.37, 4.30 (s, 2H), 4.25 (s, 2H), 3.46 (s, 3H), 1.32(s, 12H). MS (ESI+) calcd for C21H28BNO3 (M) 353.2162 found 353.2165.

3.15a. ^{1}H NMR (360 MHz, C_6D_6): δ 7.49 (d, 2H, J = 7.9 Hz); 7.23 (d, 2H, J = 7.4 Hz); 7.14-7.09(m, 6H); 4.78(s, 2H); 1.08(s, 12H) ppm. MS (ESI+) calcd for C13H12N (M-Bpin) 182.0970 found 182.0968.

3.16a. ^{1}H NMR (360 MHz, C_6D_6): δ 7.25(d, 2H, J = 7.2 Hz); 7.19-7.09 (m, 5H); 6.87(d, 2H, J = 7.2 Hz); 4.03(s, 2H); 3.93(s, 2H); 1.15(s, 12H) ppm. MS (ESI+) calcd for C20H25NO2BBr (M) 401.1162 found 401.1166.

3.17a. ^{1}H NMR (360 MHz, C_6D_6): δ 7.40(d, 2H, J = 7.2 Hz); 7.20(d, 2H, J = 7.2 Hz); 7.01-6.91(m, 4H); 4.79(s, 2H); 2.07(s, 3H); 2.05(s, 3H); 1.10(s, 12H) ppm. MS (ESI+) calcd for C15H16N (M-Bpin) 210.1283 found 210.1285.

---

[1] Pham, N. N.; Dang, T. T.; Ngo, N. T.; Villinger, A.; Ehlers, P.; Langer, P. *Org. Biomol. Chem.* **2015**, *13*, 6047.

3.18a. ^{1}H NMR (360 MHz, C_6D_6): δ 7.32-6.13(m, 7H); 6.68(d, 2H, *J* = 9.1 Hz); 4.76(s, 2H); 3.26(s, 3H); 1.11(s, 12H) ppm. MS (EI+) calcd for C14H14NO (M-Bpin) 212.1075 found 212.1081.

3.19a. ^{1}H NMR (360 MHz, C_6D_6): δ 7.23(d, 2H, *J* = 9.0 Hz); 7.07-7.03(m, 2H); 6.80-6.76(m, 2H); 6.70(d, 2H, *J* = 9.0 Hz); 4.61(s, 2H); 3.27(s, 3H); 1.11(s, 12H) ppm. MS (ESI+) calcd for C14H13FNO (M-Bpin) 230.0981 found 230.0981.

3.20a. ^{1}H NMR (360 MHz, C_6D_6): δ 8.20(d, 1H, *J* = 8.1 Hz); 7.78(d, 1H, *J* = 7.6 Hz); 7.65(d, 1H, *J* = 8.1 Hz); 7.57(d, 1H, *J* = 6.9 Hz); 7.45-7.29(m, 5H); 6.75(d, 2H, *J* = 8.9 Hz); 5.33(s, 2H); 3.36(s, 3H); 1.24(s, 12H) ppm. MS (ESI+) calcd for C18H17NO (M-Bpin) 263.1310 found 263.1305.

3.21a. ^{1}H NMR (360 MHz, C_6D_6): δ 7.69(d, 1H, *J* = 7.8 Hz); 7.52(d, 1H, *J* = 7.8 Hz); 7.45(d, 2H, *J* = 9.0 Hz); 7.19-7.17(m, 1H); 6.93-6.88(m, 1H); 6.78(d, 2H, *J* = 9.0 Hz); 5.26(s, 2H); 3.38(s, 3H)); 1.20(s, 12H) ppm. MS (ESI+) calcd for C15H13F3NO (M-Bpin) 280.0949 found 280.0953.

3.22a. ^{1}H NMR (360 MHz, C_6D_6): δ 7.32(d, 1H, *J* = 9.1 Hz); 7.20(d, 1H, *J* = 8.7 Hz); 6.75 (d, 2H, *J* = 8.7 Hz); 6.71(d, 2H, *J* = 9.1 Hz); 4.72(s, 2H); 3.28(s, 3H); 3.27(s, 3H); 1.13(s, 12H) ppm. MS (ESI+) calcd for C15H17O2N (M-Bpin) 243.1259 found 243.1262.

3.23a. ^{1}H NMR (360 MHz, C_6D_6): δ 7.31(d, 2H, *J* = 8.0 Hz); 7.22(d, 2H, *J* = 9.0 Hz); 7.13-7.07(m, 3H); 6.70(d, 2H, *J* = 9.0 Hz); 4.62(s, 2H); 3.27(s, 3H); 1.10(s, 12H) ppm.MS (ESI+) calcd for C15H14F3NO (M-Bpin) 250.0844 found 250.0842.

3.24a. ^{1}H NMR (360 MHz, C_6D_6): δ 6.92(d, 2H, *J* = 8.9 Hz); 6.70(s, 2H); 6.55(d, 2H, *J* = 8.9 Hz); 4.71(s, 2H); 3.14(s, 3H); 2.26(s, 6H); 2.09(s, 3H); 1.14(s, 12H) ppm. MS (ESI+) calcd for C17H21NO (M-Bpin) 255.1623 found 255.1629.

3.25a. ^{1}H NMR (360 MHz, C_6D_6): δ 7.37-7.23(m, 7H); 6.88-6.83(m, 2H); 4.78(s, 2H); 1.20(s, 12H) ppm. MS (ESI+) calcd for C13H11FN (M-Bpin) 200.0876 found 200.0874.

3.26a. ^{1}H NMR (360 MHz, C_6D_6): δ 7.42 (d, 2H, *J* = 8.0 Hz); 7.22-7.02(m, 7H); 6.88(t, 1H, *J* = 6.5 Hz); 5.16 (q, 1H, *J* = 7.1 Hz); 1.58(d, 3H, *J* = 7.1 Hz); 1.05 (s, 12H) ppm. MS (EI+) calcd for C14H15N (M-Bpin) 197.1204 found 197.1210.

3.27a. ^{1}H NMR (360 MHz, C_6D_6): δ 7.27(d, 4H, *J* = 7.5 Hz); 7.22-7.04(m, 11H); 5.70(s, 1H); 4.32 (s, 2H); 1.04(s, 12H) ppm. MS (EI+) calcd for C20H18N (M-Bpin) 272.1439 found 272.1441.

3.28a. ^{1}H NMR (360 MHz, C_6D_6): δ 7.37 (d, 2H, *J* = 7.3 Hz); 7.29 (d, 2H, *J* = 7.2 Hz); 7.24-7.18(m, 6H); 4.50(q, 1H, *J* = 7.1 Hz); 4.24 (d, 1H, *J* = 15.6 Hz); 4.04 (d, 1H, *J* = 15.6 Hz); 1.47 (d, 3H, *J* = 7.0 Hz); 3.55(s, 2H); 1.15 (s, 12H) ppm. MS (EI+) calcd for C15H16N (M-Bpin) 210.1283 found 210.1286.

VII. Crystallographic Procedures and Data

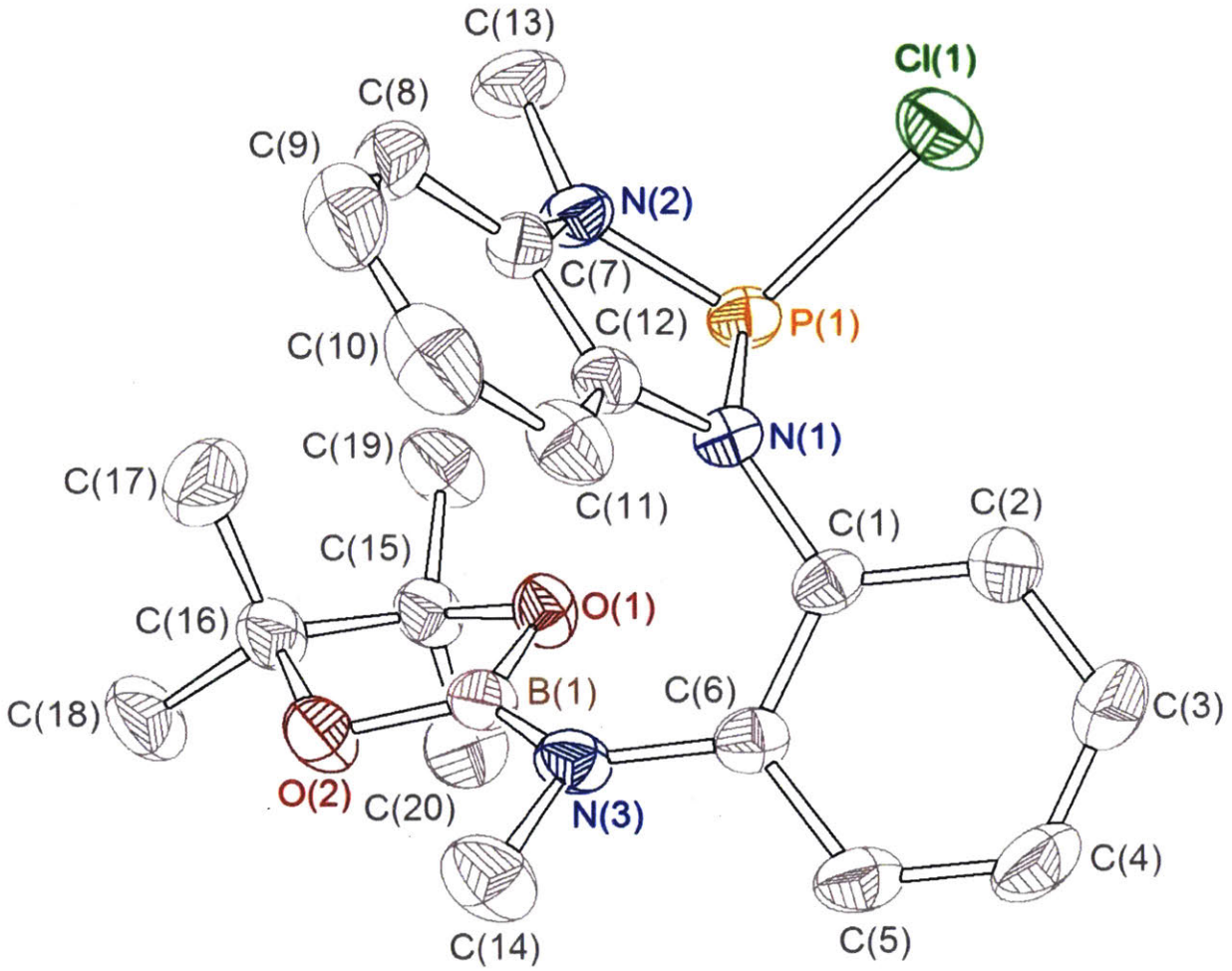

A colorless block shaped crystal of **3.7** (C20 H26 B Cl N3 O2 P) with approximate dimensions 0.29 × 0.25 × 0.24 mm, was used for the X-ray crystallographic analysis. The X-ray intensity data were measured at 213(2) K, cooled by Rigaku-MSC X-Stream 2000, on a Bruker SMART APEX CCD area detector system equipped with a graphite monochromator and a MoK fine-focus sealed tube (= 0.71073Å) operated at 1600 watts power (50 kV, 32 mA). The detector was placed at a distance of 5.82 cm from the crystal.

A total of 1850 frames were collected with a scan width of 0.3° in ω and an exposure time of 10 seconds/frame. The total data collection time was about 8 hours. The frames were integrated with the Bruker SAINT software package using a narrow-frame integration algorithm. The integration of the data using a Triclinic unit cell yielded a total of 10199 reflections to a maximum angle of

28.398 (0.90 Å resolution), of which 5223 were independent, completeness = 98.6%, R_{int} = 0.0163, R_{sigma} = 0.0372 and 4276 were greater than 2δ(I). The final cell constants: a = 8.197(4) Å, b = 9.932(4) Å, c = 15.016(7) Å, α = 90°, β = 93.531(2)°, γ = 68.269(11) °, volume = 1084.8(8) $Å^3$, are based upon the refinement of the XYZ-centroids of 4359 reflections above 20δ(I) with 4.496° ≤ 2θ ≤ 56.796°. Analysis of the data showed negligible decay during data collection. Data were corrected for absorption effects using the multiscan technique (SADABS). The ratio of minimum to maximum apparent transmission was 0.3144.

The structure was solved and refined using the Bruker SHELXTL (Version 6.1) Software Package, using the space group P-1, with Z = 2 for the formula unit, C20 H26 B Cl N3 O2 P. The final anisotropic full-matrix least-squares refinement on F^2 with 259 variables converged at R1 = 5.71%, for the observed data and wR2 = 15.86% for all data. The goodness-of-fit was 1.131. The largest peak on the final difference map was 0.342 $e^-/Å^3$ and the largest hole was -0.255 $e^-/Å^3$. Based on the final model, the calculated density of the crystal is 1.279 g/cm^3 and F(000) amounts to 440 electrons.

Table B2. Fractional Atomic Coordinates ($\times 10^4$) and Equivalent Isotropic Displacement Parameters ($Å^2 \times 10^3$) for 3.7. U_{eq} is defined as 1/3 of the trace of the orthogonalised U_{IJ} tensor.

Atom	*x*	*y*	*z*	U (eq)
P1	4014.3(9)	917.0(7)	3636.6(4)	31.81(17)
Cl1	4471.7(11)	-1533.9(8)	4180.9(5)	49.7(2)
N1	3584(3)	1177(2)	2551.8(13)	27.8(4)
O1	3938(2)	3969.7(19)	2533.9(12)	34.7(4)
O2	1942(3)	5863(2)	1691.4(13)	41.1(5)
N3	3545(3)	3651(2)	1024.2(14)	33.6(5)
C7	782(3)	1700(3)	3379(2)	36.3(6)
C12	1786(3)	1501(3)	2508.4(18)	31.2(5)
N2	1849(3)	1559(2)	4025.4(15)	37.2(5)
C6	4874(3)	2248(3)	1004.4(17)	31.4(5)
C1	4915(3)	1040(3)	1744.9(16)	30.0(5)
C2	6236(4)	-314(3)	1702(2)	40.0(6)
C15	3470(4)	5269(3)	2957.7(18)	37.5(6)
C11	1017(4)	1615(3)	1753(2)	41.9(6)
C5	6177(4)	2011(3)	219.7(19)	41.7(6)
C8	-1038(4)	2011(3)	3516(3)	54.1(9)
B1	3145(4)	4462(3)	1743.3(19)	32.0(6)
C10	-808(5)	1941(4)	1889(3)	59.9(9)

C3	7523(4)	-508(4)	921(2)	51.9(8)
C13	1154(5)	1620(4)	5006(2)	57.5(9)
C19	3387(5)	4770(4)	4009(2)	54.5(8)
C14	2708(5)	4366(4)	176(2)	51.6(8)
C16	1672(4)	6239(3)	2611.1(19)	41.1(6)
C20	4937(5)	5946(4)	2558(2)	51.6(8)
C17	110(5)	5796(4)	3176(3)	60.1(9)
C4	7475(4)	657(4)	182(2)	50.7(8)
C18	1294(5)	7883(3)	2497(2)	57.9(9)
C9	-1812(4)	2132(4)	2755(3)	63.7(11)

Table B3. Anisotropic Displacement Parameters ($Å^2 \times 10^3$) for 3.7. The Anisotropic displacement factor exponent takes the form: $-2\pi^2[h^2a^{*2}U_{11}+2hka^*b^*U_{12}+...]$.

Atom	U_{11}	U_{22}	U_{33}	U_{23}	U_{13}	U_{12}
P1	35.7(3)	35.8(4)	26.3(3)	-6.2(3)	-3.1(2)	-15.2(3)
Cl1	68.3(5)	36.4(4)	39.1(4)	-1.8(3)	-10.8(3)	-13.4(3)
N1	27.9(10)	31.1(10)	25.3(9)	-5.9(8)	-1.5(7)	-11.9(8)
O1	42(1)	28.4(9)	33.9(9)	-10.8(7)	-8.6(7)	-7.0(7)
O2	54.7(12)	30.4(10)	34.6(10)	-4.7(8)	-11.8(8)	-7.8(8)
N3	45.0(12)	32.2(11)	23.7(10)	-3.3(8)	-5.5(8)	-14.1(9)
C7	30.9(12)	27.5(12)	46.4(15)	-4.7(11)	2.7(11)	-11.5(10)
C12	30.2(12)	25.1(12)	38.9(13)	-2.6(10)	-5.3(10)	-12.2(9)
N2	40.6(12)	36.1(12)	31.3(11)	-9.2(9)	8.0(9)	-14.7(10)
C6	37.4(13)	34.0(13)	27.1(11)	-9.5(10)	-2.1(9)	-15.9(10)
C1	30.7(12)	35.3(13)	27.5(11)	-11.3(10)	0.4(9)	-14.3(10)
C2	44.5(15)	34.3(14)	38.5(14)	-9.6(11)	-1.2(11)	-11.2(11)
C15	51.8(16)	28.3(13)	33.0(13)	-9(1)	-7.4(11)	-11.0(11)
C11	44.8(15)	35.1(14)	51.8(17)	-0.7(12)	-18.5(13)	-18.1(12)
C5	51.8(16)	47.4(16)	27.9(12)	-8.5(11)	3.7(11)	-23.5(13)
C8	32.4(14)	40.2(16)	79(2)	-6.5(15)	9.5(15)	-14.2(12)
B1	37.2(14)	30.5(14)	28.4(13)	-3.2(11)	-2.9(11)	-14.0(11)
C10	49.6(18)	47.1(18)	92(3)	3.1(18)	-36.5(19)	-21.5(15)
C3	48.4(17)	48.8(18)	51.0(18)	-23.2(15)	7.4(14)	-7.4(14)
C13	73(2)	57(2)	37.8(16)	-17.0(14)	21.4(15)	-28.5(17)
C19	87(2)	41.4(17)	34.2(15)	-9.2(13)	-14.9(15)	-15.1(16)
C14	74(2)	48.3(18)	33.7(15)	-3.1(13)	-21.1(14)	-16.7(16)
C16	53.3(17)	27.5(13)	37.0(14)	-9.4(11)	-3.1(12)	-7.2(11)

C20	61.0(19)	48.1(18)	56.0(19)	-18.0(15)	-7.3(15)	-25.2(15)
C17	55.1(19)	50.4(19)	68(2)	-22.6(17)	10.8(16)	-14.0(15)
C4	50.7(17)	62(2)	36.1(15)	-22.6(14)	13.2(12)	-17.8(15)
C18	80(2)	27.7(15)	55.8(19)	-6.8(13)	-10.8(17)	-6.9(15)
C9	30.3(15)	45.0(18)	115(3)	-3.7(19)	-16.6(18)	-15.7(13)

Table B4. Bond Lengths for 3.7.

Atom	Atom	Length/Å	Atom	Atom	Length/Å
P1	Cl1	2.2756(14)	N2	C13	1.459(3)
P1	N1	1.681(2)	C6	C1	1.406(4)
P1	N2	1.665(2)	C6	C5	1.400(3)
N1	C12	1.401(3)	C1	C2	1.385(4)
N1	C1	1.428(3)	C2	C3	1.385(4)
O1	C15	1.470(3)	C15	C19	1.521(4)
O1	B1	1.376(3)	C15	C16	1.555(4)
O2	B1	1.370(3)	C15	C20	1.522(4)
O2	C16	1.469(3)	C11	C10	1.385(4)
N3	C6	1.418(3)	C5	C4	1.377(4)
N3	B1	1.418(3)	C8	C9	1.389(6)
N3	C14	1.475(3)	C10	C9	1.386(6)
C7	C12	1.393(4)	C3	C4	1.378(5)
C7	N2	1.400(4)	C16	C17	1.509(5)
C7	C8	1.383(4)	C16	C18	1.516(4)
C12	C11	1.382(4)			

Table B5. Bond Angles for 3.7.

Atom	Atom	Atom	Angle/°	Atom	Atom	Atom	Angle/°
N1	P1	Cl1	103.19(8)	C2	C1	C6	120.7(2)
N2	P1	Cl1	98.62(9)	C3	C2	C1	120.5(3)
N2	P1	N1	90.41(11)	O1	C15	C19	108.8(2)
C12	N1	P1	113.74(16)	O1	C15	C16	101.4(2)
C12	N1	C1	122.3(2)	O1	C15	C20	106.8(2)
C1	N1	P1	123.92(16)	C19	C15	C16	115.7(3)
B1	O1	C15	106.0(2)	C19	C15	C20	110.3(3)
B1	O2	C16	106.0(2)	C20	C15	C16	113.1(2)

C6	N3	B1	124.4(2)	C12	C11	C10	117.5(3)
C6	N3	C14	116.3(2)	C4	C5	C6	121.3(3)
B1	N3	C14	118.8(2)	C7	C8	C9	117.6(3)
C12	C7	N2	111.3(2)	O1	B1	N3	124.7(2)
C8	C7	C12	120.5(3)	O2	B1	O1	113.4(2)
C8	C7	N2	128.1(3)	O2	B1	N3	121.9(2)
C7	C12	N1	109.7(2)	C11	C10	C9	120.8(3)
C11	C12	N1	128.5(2)	C4	C3	C2	119.4(3)
C11	C12	C7	121.9(2)	O2	C16	C15	101.8(2)
C7	N2	P1	113.24(17)	O2	C16	C17	106.3(3)
C7	N2	C13	122.7(2)	O2	C16	C18	109.3(2)
C13	N2	P1	122.5(2)	C17	C16	C15	113.6(3)
C1	C6	N3	122.3(2)	C17	C16	C18	111.1(3)
C5	C6	N3	120.2(2)	C18	C16	C15	113.8(3)
C5	C6	C1	117.5(2)	C5	C4	C3	120.6(3)
C6	C1	N1	120.8(2)	C10	C9	C8	121.7(3)
C2	C1	N1	118.5(2)				

Table B6. Torsion Angles for 3.7.

A	B	C	D	Angle/°	A	B	C	D	Angle/°
P1	N1	C12	C7	7.2(3)	C1	N1	C12	C7	-174.5(2)
P1	N1	C12	C11	-172.3(2)	C1	N1	C12	C11	6.0(4)
P1	N1	C1	C6	-119.3(2)	C1	C6	C5	C4	-1.4(4)
P1	N1	C1	C2	61.6(3)	C1	C2	C3	C4	-0.5(5)
Cl1	P1	N1	C12	87.99(17)	C2	C3	C4	C5	1.0(5)
Cl1	P1	N1	C1	-90.22(19)	C15	O1	B1	O2	-11.7(3)
Cl1	P1	N2	C7	-91.60(18)	C15	O1	B1	N3	166.2(3)
Cl1	P1	N2	C13	74.4(2)	C11	C10	C9	C8	0.2(5)
N1	P1	N2	C7	11.81(19)	C5	C6	C1	N1	-177.2(2)
N1	P1	N2	C13	177.8(2)	C5	C6	C1	C2	1.9(4)
N1	C12	C11	C10	179.6(3)	C8	C7	C12	N1	-179.1(2)
N1	C1	C2	C3	178.1(3)	C8	C7	C12	C11	0.5(4)
O1	C15	C16	O2	-33.0(2)	C8	C7	N2	P1	170.8(2)
O1	C15	C16	C17	80.9(3)	C8	C7	N2	C13	4.8(4)
O1	C15	C16	C18	-150.6(2)	B1	O1	C15	C19	149.9(3)
N3	C6	C1	N1	1.0(4)	B1	O1	C15	C16	27.5(3)

N3	C6	C1	C2	-179.9(2)	B1	O1	C15	C20	-91.1(3)
N3	C6	C5	C4	-179.6(3)	B1	O2	C16	C15	27.2(3)
C7	C12	C11	C10	0.1(4)	B1	O2	C16	C17	-92.0(3)
C7	C8	C9	C10	0.4(5)	B1	O2	C16	C18	147.9(3)
C12	N1	C1	C6	62.6(3)	B1	N3	C6	C1	54.8(4)
C12	N1	C1	C2	-116.5(3)	B1	N3	C6	C5	-127.1(3)
C12	C7	N2	P1	-9.9(3)	C19	C15	C16	O2	-150.5(2)
C12	C7	N2	C13	-175.9(2)	C19	C15	C16	C17	-36.6(3)
C12	C7	C8	C9	-0.7(4)	C19	C15	C16	C18	92.0(3)
C12	C11	C10	C9	-0.5(5)	C14	N3	C6	C1	-133.3(3)
N2	P1	N1	C12	-10.97(18)	C14	N3	C6	C5	44.8(3)
N2	P1	N1	C1	170.8(2)	C14	N3	B1	O1	-174.6(3)
N2	C7	C12	N1	1.6(3)	C14	N3	B1	O2	3.1(4)
N2	C7	C12	C11	-178.9(2)	C16	O2	B1	O1	-10.9(3)
N2	C7	C8	C9	178.5(3)	C16	O2	B1	N3	171.1(2)
C6	N3	B1	O1	-2.9(4)	C20	C15	C16	O2	81.0(3)
C6	N3	B1	O2	174.8(2)	C20	C15	C16	C17	-165.1(3)
C6	C1	C2	C3	-1.0(4)	C20	C15	C16	C18	-36.6(3)
C6	C5	C4	C3	0.0(5)					

Table B7. Hydrogen Atom Coordinates (Å×10^4) and Isotropic Displacement Parameters (Å^2×10^3) for 3.7.

Atom	*x*	*y*	*z*	U (eq)
H2	6258	-1107	2206	48
H11	1707	1476	1169	50
H5	6167	2792	-292	50
H8	-1727	2137	4102	65
H10	-1373	2033	1388	72
H3	8423	-1426	896	62
H13A	716	800	5292	86
H13B	190	2543	5055	86
H13C	2092	1557	5323	86
H19A	2531	4252	4246	82
H19B	3027	5624	4298	82
H19C	4549	4115	4152	82
H14A	3503	4788	-298	77
H14B	1602	5142	322	77

H14C	2469	3640	-53	77
H20A	6077	5202	2661	77
H20B	4738	6755	2864	77
H20C	4929	6314	1895	77
H17A	-901	6268	2843	90
H17B	-190	6103	3774	90
H17C	416	4733	3276	90
H4	8336	525	-353	61
H18A	2205	8171	2033	87
H18B	1292	8111	3088	87
H18C	143	8418	2298	87
H9	-3048	2349	2830	76

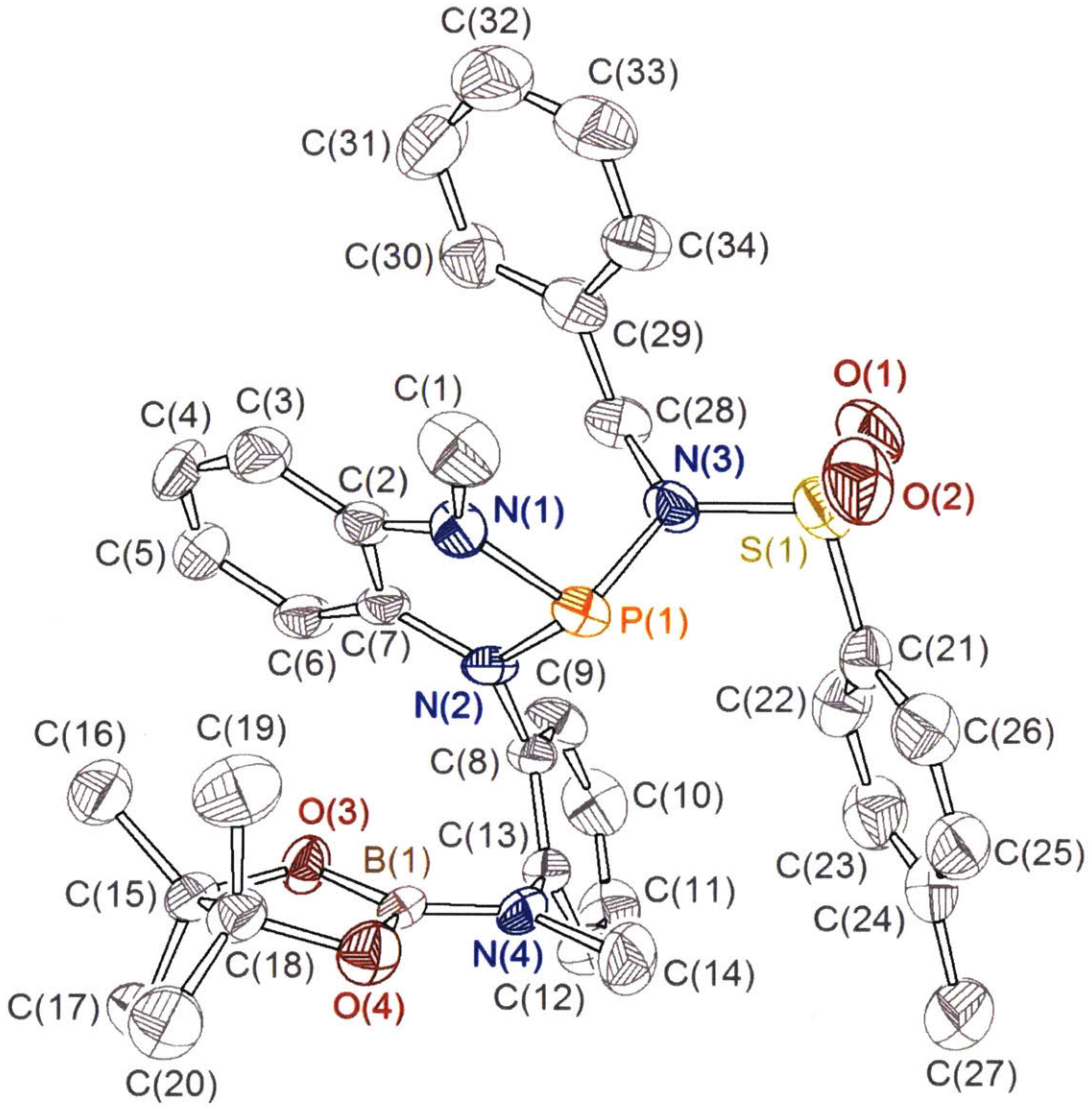

A colorless block shaped crystal of **3.8** (C34 H40 B N4 O4 P S) with approximate dimensions 0.15 × 0.14 × 0.11 mm, was used for the X-ray crystallographic analysis. The X-ray intensity data were measured at 298(2) K on a Bruker SMART APEX CCD area detector system equipped with a graphite monochromator and a MoK fine-focus sealed tube (= 0.71073Å) operated at 1600 watts power (50 kV, 32 mA). The detector was placed at a distance of 5.82 cm from the crystal.

A total of 1850 frames were collected with a scan width of 0.3° in ω and an exposure time of 10 seconds/frame. The total data collection time was about 8 hours. The frames were integrated with the Bruker SAINT software package using a narrow-frame integration algorithm. The integration of the data using a Triclinic unit cell yielded a total of 12176 reflections to a maximum angle of 28.41 (0.90 Å resolution), of which 7324 were independent, completeness = 92.3%, R_{int} = 0.0349,

R_{sigma} = 0.0778 and 5319 were greater than 2δ(I). The final cell constants: a = 10.580(2) Å, b = 10.675(2) Å, c = 15.627(4) Å, α = 108.388(5), β = 92.418(3)°, γ = 90.015(4) °, volume = 1673.2(6) $Å^3$, are based upon the refinement of the XYZ-centroids of 2764 reflections above 20δ(I) with 2.316° ≤ θ ≤ 26.603°. Analysis of the data showed negligible decay during data collection. Data were corrected for absorption effects using the multiscan technique (SADABS). The ratio of minimum to maximum apparent transmission was 0.1257.

The structure was solved and refined using the Bruker SHELXTL (Version 6.1) Software Package, using the space group P1, with Z = 2 for the formula unit, C34 H40 B N4 O4 P S. The final anisotropic full-matrix least-squares refinement on F^2 with 392 variables converged at R1 = 8.79%, for the observed data and wR2 = 26.02% for all data. The goodness-of-fit was 1.453. The largest peak on the final difference map was 0.715 $e^-/Å^3$ and the largest hole was -0.403 $e^-/Å^3$. Based on the final model, the calculated density of the crystal is 1.275 g/cm^3 and F(000) amounts to 680 electrons.

Table B8. Fractional Atomic Coordinates ($\times 10^4$) and Equivalent Isotropic Displacement Parameters ($Å^2 \times 10^3$) for 3.8. U_{eq} is defined as 1/3 of of the trace of the orthogonalised U_{IJ} tensor.

Atom	*x*	*y*	*z*	U(eq)
S1	377(2)	8667(2)	5613.3(14)	56.1(5)
P1	1807.3(16)	8953.3(16)	4120.1(11)	7.5(2)
O1	-41(5)	9498(6)	6463(4)	82(2)
O2	-518(5)	7757(6)	5030(4)	79(2)
O3	5165(4)	9275(4)	2917(3)	44.6(12)
O4	4696(4)	7128(4)	2080(3)	52.5(13)
N1	1288(5)	9744(5)	3395(3)	45.1(15)
N2	3129(5)	9950(5)	4327(3)	41.9(14)
N3	954(5)	9712(5)	5113(3)	43.2(14)
N4	4733(5)	7698(5)	3711(3)	45.7(14)
C1	98(6)	9387(8)	2839(5)	66(3)
C2	1928(6)	10888(7)	3454(4)	45.2(19)
C3	1672(7)	11819(9)	3038(5)	62(2)
C4	2515(8)	12909(8)	3187(5)	62(2)
C5	3579(8)	12987(7)	3718(5)	62(2)
C6	3857(6)	12058(7)	4151(4)	52.0(19)
C7	3056(5)	10997(6)	4011(4)	37.4(15)
C8	4181(5)	9736(6)	4878(4)	38.9(15)
C9	4427(6)	10655(7)	5731(4)	54(2)
C10	5396(7)	10467(8)	6279(4)	59(2)
C11	6181(7)	9454(8)	5993(5)	58(2)

C12	5960(6)	8511(7)	5128(5)	51.4(19)
C13	4948(5)	8669(6)	4589(4)	39.5(16)
C14	4397(8)	6366(6)	3664(5)	61(2)
C15	5425(6)	9217(7)	1992(4)	48.6(18)
C16	4968(8)	10450(7)	1840(5)	65(2)
C17	6860(7)	9101(8)	1937(5)	66(2)
C18	4711(6)	7869(7)	1431(4)	49.2(19)
C19	3338(7)	8107(8)	1183(5)	74(3)
C20	5389(8)	7089(8)	603(5)	69(3)
C21	1643(3)	7752(4)	5817(3)	49.5(19)
C22	2675(4)	8403(4)	6367(2)	55(2)
C23	3696(4)	7683(5)	6539(3)	69(3)
C24	3712(4)	6319(5)	6156(3)	68(3)
C25	2713(5)	5686(4)	5610(3)	74(3)
C26	1656(5)	6401(4)	5425(4)	61(2)
C27	4865(5)	5516(6)	6274(5)	99(4)
C28	780(6)	11081(5)	5483(4)	49.5(19)
C29	-327.9(14)	11631.5(13)	5089.0(9)	45.5(18)
C34	-1502.5(13)	10941.8(15)	4850.7(9)	61(2)
C33	-2498.8(15)	11487.9(19)	4509.7(12)	82(3)
C32	-2396.2(18)	12716(2)	4409.0(13)	81(3)
C31	-1263.9(19)	13407.8(17)	4662.6(13)	90(3)
C30	-247.7(17)	12849.9(14)	4964.5(11)	58(2)
B1	4861.1(18)	8049(2)	2915.6(13)	38.9(18)
S2	2942.4(13)	4412.8(15)	8043.7(11)	56.3(5)
P2	1496.6(15)	4167.7(15)	9560.7(11)	97.5(10)
O6	3389.6(16)	3575.5(15)	7210.5(12)	79(2)
O5	3812.5(11)	5313.3(18)	8645.9(12)	80(2)
O7	-1392.7(19)	5944(2)	11600.9(10)	51.4(13)
O8	-1860.7(19)	3801.7(19)	10739.7(12)	44.9(12)
N5	2061.8(18)	3344.8(19)	10250.7(13)	47.0(16)
N6	170.7(17)	3169.6(14)	9323.9(12)	35.0(12)
N7	2308.2(16)	3519.0(15)	8594.0(12)	40.2(14)
N8	-1419.4(14)	5391.3(15)	9947.7(9)	41.4(14)
C35	3208.0(19)	3741(2)	10811.6(14)	75(3)
C36	1372(2)	2195.2(19)	10201.0(14)	41.9(17)
C37	288(2)	2075.4(16)	9660.4(14)	41.9(17)
C38	-554(2)	1038.6(16)	9512.0(15)	49.0(18)

C39	-292(3)	88.1(18)	9931.1(17)	65(2)
C40	830(3)	221(2)	10450.9(17)	71(3)
C41	1649(2)	1240(2)	10584.5(16)	55(2)
C42	-863.6(16)	3339.4(12)	8764.5(11)	38.5(15)
C43	-1645.1(14)	4450.0(13)	9085.7(10)	43.2(17)
C44	-2624.9(13)	4592.5(14)	8500.7(11)	63(2)
C45	-2847.3(15)	3728.9(14)	7677.5(12)	73(3)
C46	-2107.9(18)	2619.2(11)	7368.7(12)	67(2)
C47	-1099.5(19)	2440.5(10)	7918.2(12)	48.5(18)
C48	-1090.8(13)	6719.0(14)	9946.3(7)	73(3)
C49	-1385(2)	5177(2)	12209.7(11)	47.1(18)
C50	-2(2)	4958(2)	12417.9(11)	80(3)
C51	-1985(2)	6016(2)	13066.2(11)	67(3)
C52	-2123(2)	3920(2)	11656.1(13)	41.9(17)
C53	-1625(2)	2678(2)	11836.8(15)	65(3)
C54	-3534(2)	4001(2)	11759.6(15)	60(2)
C55	1647(4)	5321(4)	7839(3)	50.4(19)
C56	633(4)	4692(4)	7262(3)	62(2)
C57	-353(5)	5413(5)	7108(4)	72(3)
C58	-432(4)	6766(5)	7498(3)	72(3)
C59	622(5)	7398(4)	8031(3)	73(3)
C60	1644(5)	6692(4)	8202(4)	65(2)
C61	-1565(5)	7474(6)	7328(5)	115(4)
C62	2529(7)	2001(5)	8181(5)	54(2)
C63	3661(3)	1495(4)	8591.2(18)	49.7(19)
C64	3549(3)	252(3)	8699(3)	66(2)
C65	4583(4)	-285(4)	9037(3)	74(3)
C66	5730(3)	400(5)	9224(2)	87(3)
C67	5813(3)	1634(5)	9145(3)	69(2)
C68	4776(3)	2173(4)	8822(3)	59(2)
B2	-1533(4)	5044(6)	10732(4)	39.3(18)

Table B9. Anisotropic Displacement Parameters ($Å^2 \times 10^3$) for 3.8. The Anisotropic displacement factor exponent takes the form: $-2\pi^2[h^2a^{*2}U_{11}+2hka^*b^*U_{12}+\ldots]$.

Atom	U_{11}	U_{22}	U_{33}	U_{23}	U_{13}	U_{12}
S1	50.9(11)	56.3(14)	61.6(11)	18.2(10)	11.0(9)	-7.7(10)
O1	80(5)	93(5)	78(4)	28(4)	52(4)	24(4)

O2	59(4)	90(5)	95(5)	40(4)	-5(3)	-28(4)
O3	56(3)	35(3)	40(2)	9(2)	7(2)	-6(2)
O4	58(3)	43(3)	51(3)	7(2)	5(2)	-4(3)
N1	58(4)	47(4)	33(3)	15(3)	7(2)	-7(3)
N2	37(3)	36(3)	46(3)	3(3)	5(2)	12(3)
N3	49(3)	29(3)	46(3)	-1(2)	36(2)	13(3)
N4	59(4)	33(4)	49(3)	17(3)	9(3)	-1(3)
C1	39(4)	84(7)	61(5)	6(5)	2(3)	-3(4)
C2	37(4)	58(5)	35(3)	5(3)	3(3)	16(4)
C3	51(5)	86(7)	51(4)	24(4)	12(4)	29(5)
C4	75(6)	51(6)	72(5)	36(4)	25(4)	20(5)
C5	70(6)	32(5)	85(6)	20(4)	14(5)	4(4)
C6	42(4)	51(5)	60(4)	14(4)	3(3)	11(4)
C7	26(3)	35(4)	51(4)	14(3)	8(3)	3(3)
C8	31(3)	37(4)	49(4)	13(3)	11(3)	5(3)
C9	47(4)	53(5)	52(4)	1(4)	14(3)	8(4)
C10	49(4)	70(6)	45(4)	2(4)	-3(3)	-20(4)
C11	50(4)	77(6)	58(4)	35(4)	-6(4)	4(4)
C12	42(4)	52(5)	68(5)	29(4)	11(3)	9(4)
C13	35(4)	41(4)	42(3)	11(3)	7(3)	-3(3)
C14	88(7)	26(4)	78(5)	25(4)	27(5)	5(4)
C15	58(5)	45(5)	45(4)	17(3)	3(3)	1(4)
C16	81(6)	51(6)	69(5)	28(4)	9(5)	12(5)
C17	52(5)	71(6)	72(5)	18(5)	17(4)	-3(4)
C18	55(4)	56(5)	32(3)	8(3)	0(3)	9(4)
C19	68(6)	75(7)	69(5)	12(5)	-16(4)	2(5)
C20	74(6)	72(6)	50(4)	1(4)	13(4)	12(5)
C21	54(4)	58(5)	33(3)	7(3)	10(3)	-4(4)
C22	73(5)	47(5)	44(4)	12(3)	1(4)	-10(4)
C23	63(5)	92(8)	62(5)	40(5)	-2(4)	-6(5)
C24	67(6)	64(6)	86(6)	37(5)	31(5)	1(5)
C25	81(7)	45(5)	98(7)	22(5)	32(5)	3(5)
C26	71(6)	41(5)	67(5)	12(4)	11(4)	-8(4)
C27	70(7)	130(11)	127(9)	78(9)	26(6)	17(7)
C28	31(3)	61(5)	44(4)	0(3)	-3(3)	-5(3)
C29	42(4)	50(5)	37(3)	2(3)	7(3)	-2(3)
C34	47(5)	47(5)	83(6)	10(4)	4(4)	0(4)
C33	43(5)	105(8)	85(6)	12(6)	1(4)	10(5)

C32	67(6)	97(8)	88(6)	43(6)	-8(5)	17(6)
C31	83(7)	95(9)	106(8)	52(7)	-8(6)	4(7)
C30	46(4)	69(6)	59(5)	18(4)	2(3)	-4(4)
B1	32(4)	39(5)	47(4)	14(3)	10(3)	12(3)
S2	48.8(11)	60.6(14)	58.2(11)	15.6(10)	13.0(8)	-3.8(10)
P2	87.8(19)	95(2)	96.5(19)	10.8(16)	14.9(15)	-20.6(16)
O6	87(5)	74(5)	76(4)	21(3)	45(4)	15(4)
O5	62(4)	78(5)	98(5)	28(4)	-12(3)	-35(4)
O7	70(4)	31(3)	51(3)	9(2)	5(2)	4(3)
O8	62(3)	32(3)	43(2)	15(2)	5(2)	5(2)
N5	27(3)	66(5)	45(3)	16(3)	-10(2)	-2(3)
N6	26(3)	30(3)	52(3)	18(2)	-2(2)	-1(2)
N7	47(3)	47(4)	36(3)	29(3)	-20(2)	-22(3)
N8	44(3)	25(3)	52(3)	7(3)	11(3)	12(3)
C35	68(6)	103(8)	53(5)	29(5)	-31(4)	-22(5)
C36	52(4)	36(4)	41(3)	16(3)	14(3)	7(3)
C37	47(4)	31(4)	48(4)	12(3)	10(3)	12(3)
C38	51(4)	23(4)	70(5)	10(3)	12(3)	0(3)
C39	64(6)	47(5)	91(6)	29(5)	26(5)	13(4)
C40	93(7)	64(6)	73(5)	44(5)	12(5)	30(6)
C41	57(5)	52(5)	60(4)	25(4)	1(4)	8(4)
C42	30(3)	40(4)	45(3)	14(3)	1(3)	2(3)
C43	32(3)	45(4)	58(4)	24(3)	5(3)	8(3)
C44	57(5)	69(6)	73(5)	39(5)	-1(4)	19(4)
C45	47(5)	106(8)	69(5)	34(5)	-20(4)	-11(5)
C46	61(5)	86(7)	53(4)	22(5)	-14(4)	-2(5)
C47	47(4)	46(5)	47(4)	6(3)	-1(3)	-12(3)
C48	93(7)	55(6)	68(5)	15(4)	21(5)	-10(5)
C49	52(4)	37(4)	55(4)	18(3)	3(3)	9(3)
C50	57(6)	92(8)	89(7)	29(6)	-16(5)	6(5)
C51	92(7)	54(6)	52(4)	12(4)	1(4)	4(5)
C52	45(4)	40(4)	39(3)	9(3)	11(3)	16(3)
C53	79(6)	65(6)	59(5)	29(5)	6(4)	15(5)
C54	52(5)	62(6)	64(5)	14(4)	15(4)	9(4)
C55	67(5)	32(4)	53(4)	14(3)	9(3)	-13(4)
C56	84(6)	45(5)	57(5)	15(4)	0(4)	-4(5)
C57	77(6)	78(7)	69(5)	37(5)	-16(5)	-9(5)
C58	69(6)	83(7)	81(6)	50(6)	9(5)	-2(5)

C59	86(7)	54(6)	85(6)	28(5)	20(5)	7(5)
C60	65(6)	57(6)	72(5)	17(4)	4(4)	-16(5)
C61	94(9)	108(10)	178(12)	96(10)	19(8)	25(8)
C62	56(5)	44(5)	54(4)	4(4)	10(3)	4(4)
C63	49(4)	47(5)	48(4)	6(3)	10(3)	7(4)
C64	69(6)	66(6)	67(5)	29(5)	-7(4)	-9(5)
C65	84(7)	61(6)	86(6)	36(5)	-1(5)	6(5)
C66	68(6)	105(9)	85(7)	25(6)	2(5)	16(6)
C67	43(5)	79(7)	82(6)	23(5)	-1(4)	-7(5)
C68	39(4)	81(6)	61(5)	26(4)	10(3)	3(4)
B2	43(4)	30(4)	46(4)	15(3)	0(3)	3(3)

Table B10. Bond Lengths for 3.8.

Atom	Atom	Length/Å	Atom	Atom	Length/Å
S1	O1	1.432(5)	S2	O6	1.4269
S1	O2	1.428(5)	S2	O5	1.4188
S1	N3	1.679(5)	S2	N7	1.6329
S1	C21	1.736(4)	S2	C55	1.755(4)
P1	N1	1.688(5)	P2	N5	1.6839
P1	N2	1.713(5)	P2	N6	1.7166
P1	N3	1.790(4)	P2	N7	1.7172
O3	C15	1.465(7)	O7	C49	1.4373
O3	B1	1.347(5)	O7	B2	1.395(6)
O4	C18	1.470(7)	O8	C52	1.4364
O4	B1	1.368(5)	O8	B2	1.374(7)
N1	C1	1.478(8)	N5	C35	1.4471
N1	C2	1.372(8)	N5	C36	1.4069
N2	C7	1.358(8)	N6	C37	1.4277
N2	C8	1.441(7)	N6	C42	1.4191
N3	C28	1.407(6)	N7	C62	1.565(5)
N4	C13	1.443(7)	N8	C43	1.4142
N4	C14	1.444(8)	N8	C48	1.4600
N4	B1	1.419(5)	N8	B2	1.398(7)
C2	C3	1.370(10)	C36	C37	1.3768
C2	C7	1.430(8)	C36	C41	1.3623
C3	C4	1.420(10)	C37	C38	1.3754

C4	C5	1.356(10)	C38	C39	1.3927
C5	C6	1.392(9)	C39	C40	1.3906
C6	C7	1.370(9)	C40	C41	1.3491
C8	C9	1.398(8)	C42	C43	1.4147
C8	C13	1.366(8)	C42	C47	1.3797
C9	C10	1.363(9)	C43	C44	1.3933
C10	C11	1.336(10)	C44	C45	1.3365
C11	C12	1.418(9)	C45	C46	1.3856
C12	C13	1.378(8)	C46	C47	1.3922
C15	C16	1.487(9)	C49	C50	1.5204
C15	C17	1.527(9)	C49	C51	1.5205
C15	C18	1.599(9)	C49	C52	1.5393
C18	C19	1.530(9)	C52	C53	1.5295
C18	C20	1.510(8)	C52	C54	1.5073
C21	C22	1.3987	C55	C56	1.3959
C21	C26	1.3773	C55	C60	1.3933
C22	C23	1.3916	C56	C57	1.3549
C23	C24	1.3898	C57	C58	1.3833
C24	C25	1.3642	C58	C59	1.3991
C24	C27	1.5290	C58	C61	1.4769
C25	C26	1.4242	C59	C60	1.3826
C28	C29	1.505(5)	C62	C63	1.513(6)
C29	C34	1.4187	C63	C64	1.3956
C29	C30	1.3776	C63	C68	1.3577
C34	C33	1.3726	C64	C65	1.3955
C33	C32	1.3735	C65	C66	1.3885
C32	C31	1.3830	C66	C67	1.3638
C31	C30	1.3668	C67	C68	1.3879

Table B11. Bond Angles for 3.8.

Atom	Atom	Atom	Angle/°	Atom	Atom	Atom	Angle/°
O1	S1	N3	104.9(3)	O6	S2	N7	109.8
O1	S1	C21	108.4(3)	O6	S2	C55	110.07(14)
O2	S1	O1	117.8(4)	O5	S2	O6	118.2
O2	S1	N3	111.4(3)	O5	S2	N7	107.8
O2	S1	C21	107.1(3)	O5	S2	C55	107.66(14)

N3	S1	C21	106.7(2)	N7	S2	C55	102.08(13)
N1	P1	N2	87.4(3)	N5	P2	N6	89.4
N1	P1	N3	103.5(2)	N5	P2	N7	103.8
N2	P1	N3	100.9(2)	N6	P2	N7	101.2
B1	O3	C15	108.3(4)	B2	O7	C49	106.3(3)
B1	O4	C18	105.8(4)	B2	O8	C52	106.6(2)
C1	N1	P1	123.3(5)	C35	N5	P2	122.8
C2	N1	P1	115.6(4)	C36	N5	P2	114.7
C2	N1	C1	120.3(5)	C36	N5	C35	122.4
C7	N2	P1	115.6(4)	C37	N6	P2	112.8
C7	N2	C8	123.5(5)	C42	N6	P2	122.9
C8	N2	P1	120.7(4)	C42	N6	C37	123.9
S1	N3	P1	115.1(3)	S2	N7	P2	123.7
C28	N3	S1	120.5(4)	C62	N7	S2	114.3(3)
C28	N3	P1	124.3(4)	C62	N7	P2	121.9(3)
C13	N4	C14	118.5(5)	C43	N8	C48	115.3
B1	N4	C13	120.4(4)	B2	N8	C43	120.9(3)
B1	N4	C14	121.0(5)	B2	N8	C48	123.8(3)
N1	C2	C7	109.7(6)	C37	C36	N5	111.2
C3	C2	N1	130.1(6)	C41	C36	N5	129.4
C3	C2	C7	120.0(7)	C41	C36	C37	119.4
C2	C3	C4	119.5(7)	C36	C37	N6	110.8
C5	C4	C3	119.3(7)	C38	C37	N6	126.9
C4	C5	C6	122.4(7)	C38	C37	C36	122.3
C7	C6	C5	119.0(6)	C37	C38	C39	118.2
N2	C7	C2	109.6(5)	C40	C39	C38	117.9
N2	C7	C6	130.6(6)	C41	C40	C39	123.1
C6	C7	C2	119.8(6)	C40	C41	C36	119.1
C9	C8	N2	118.8(5)	C43	C42	N6	119.0
C13	C8	N2	122.0(5)	C47	C42	N6	120.6
C13	C8	C9	119.2(5)	C47	C42	C43	120.5
C10	C9	C8	120.4(6)	N8	C43	C42	121.6
C11	C10	C9	121.0(6)	C44	C43	N8	121.6
C10	C11	C12	119.7(6)	C44	C43	C42	116.7
C13	C12	C11	119.2(6)	C45	C44	C43	122.8
C8	C13	N4	121.1(5)	C44	C45	C46	120.7
C8	C13	C12	120.3(5)	C45	C46	C47	118.9
C12	C13	N4	118.5(5)	C42	C47	C46	120.3

O3	C15	C16	108.6(5)	O7	C49	C50	106.2
O3	C15	C17	105.2(5)	O7	C49	C51	106.9
O3	C15	C18	100.8(5)	O7	C49	C52	102.5
C16	C15	C17	111.6(6)	C50	C49	C51	109.5
C16	C15	C18	117.3(6)	C50	C49	C52	114.5
C17	C15	C18	112.0(5)	C51	C49	C52	116.2
O4	C18	C15	103.2(4)	O8	C52	C49	103.4
O4	C18	C19	107.8(6)	O8	C52	C53	107.2
O4	C18	C20	109.8(5)	O8	C52	C54	109.0
C19	C18	C15	111.6(6)	C53	C52	C49	112.7
C20	C18	C15	113.3(6)	C54	C52	C49	114.2
C20	C18	C19	110.7(5)	C54	C52	C53	109.8
C22	C21	S1	119.31(18)	C56	C55	S2	120.6(2)
C26	C21	S1	120.78(18)	C60	C55	S2	120.73(19)
C26	C21	C22	119.9	C60	C55	C56	118.5
C23	C22	C21	120.1	C57	C56	C55	119.7
C24	C23	C22	120.5	C56	C57	C58	123.7
C23	C24	C27	121.5	C57	C58	C59	116.2
C25	C24	C23	119.4	C57	C58	C61	120.5
C25	C24	C27	118.9	C59	C58	C61	123.3
C24	C25	C26	121.1	C60	C59	C58	121.5
C21	C26	C25	119.0	C59	C60	C55	120.2
N3	C28	C29	115.7(5)	C63	C62	N7	114.6(5)
C34	C29	C28	121.9(2)	C64	C63	C62	117.5(3)
C30	C29	C28	121.0(2)	C68	C63	C62	123.0(3)
C30	C29	C34	117.1	C68	C63	C64	119.5
C33	C34	C29	120.2	C65	C64	C63	119.8
C34	C33	C32	121.3	C66	C65	C64	119.5
C33	C32	C31	118.8	C67	C66	C65	119.9
C30	C31	C32	120.4	C66	C67	C68	120.2
C31	C30	C29	122.0	C63	C68	C67	120.9
O3	B1	O4	115.3(3)	O7	B2	N8	123.5(5)
O3	B1	N4	123.7(4)	O8	B2	O7	112.3(5)
O4	B1	N4	121.0(4)	O8	B2	N8	124.2(5)

Table B12. Hydrogen Atom Coordinates (Å×10^4) and Isotropic Displacement Parameters (Å^2×10^3) for 3.8.

Atom	*x*	*y*	*z*	U(eq)
H1A	-119	8482	2756	98
H1B	208	9503	2262	98
H1C	-568	9945	3138	98
H3	952	11737	2661	75
H4	2340	13562	2924	74
H5	4142	13687	3795	74
H6	4576	12156	4531	62
H9	3927	11399	5926	65
H10	5512	11052	6861	70
H11	6870	9368	6359	70
H12	6492	7794	4926	62
H14A	5112	5959	3863	92
H14B	4151	5869	3053	92
H14C	3705	6385	4046	92
H16A	4079	10537	1941	97
H16B	5113	10415	1231	97
H16C	5416	11195	2251	97
H17A	7258	9880	2349	99
H17B	7093	9010	1333	99
H17C	7132	8341	2094	99
H19A	2926	7277	872	111
H19B	3321	8654	799	111
H19C	2904	8539	1723	111
H20A	6202	6832	782	104
H20B	5497	7624	219	104
H20C	4897	6314	282	104
H22	2678	9317	6617	66
H23	4374	8119	6913	83
H25	2722	4773	5354	89
H26	984	5963	5046	73
H27A	5405	5404	5777	149
H27B	4591	4667	6290	149
H27C	5322	5974	6829	149
H28A	1543	11530	5407	59
H28B	677	11286	6127	59
H34	-1598	10117	4926	73
H33	-3258	11017	4344	98

H32	-3076	13075	4175	97
H31	-1193	14258	4627	108
H30	522	13307	5090	70
H35A	3650	4401	10636	112
H35B	3738	2989	10739	112
H35C	2996	4098	11432	112
H38	-1278	974	9142	59
H39	-849	-613	9865	78
H40	1024	-423	10719	85
H41	2393	1290	10933	66
H44	-3147	5320	8691	75
H45	-3505	3874	7308	88
H46	-2282	2004	6804	81
H47	-582	1712	7714	58
H48A	-260	6718	9722	109
H48B	-1103	7320	10550	109
H48C	-1693	6992	9566	109
H50A	367	4395	11884	120
H50B	59	4549	12884	120
H50C	443	5791	12617	120
H51A	-1481	6801	13337	101
H51B	-2029	5522	13482	101
H51C	-2822	6255	12920	101
H53A	-2142	1932	11501	98
H53B	-1651	2789	12470	98
H53C	-768	2534	11653	98
H54A	-3828	4824	11705	90
H54B	-3726	3947	12342	90
H54C	-3945	3284	11298	90
H56	635	3782	6985	75
H57	-1015	4973	6719	87
H59	634	8313	8276	88
H60	2331	7134	8560	78
H61A	-1682	7336	6692	172
H61B	-1457	8401	7642	172
H61C	-2294	7146	7540	172
H62A	1778	1532	8258	64
H62B	2636	1795	7539	64

H64	2788	-218	8546	79
H65	4505	-1095	9137	89
H66	6442	19	9402	104
H67	6566	2116	9309	82
H68	4846	3009	8762	71

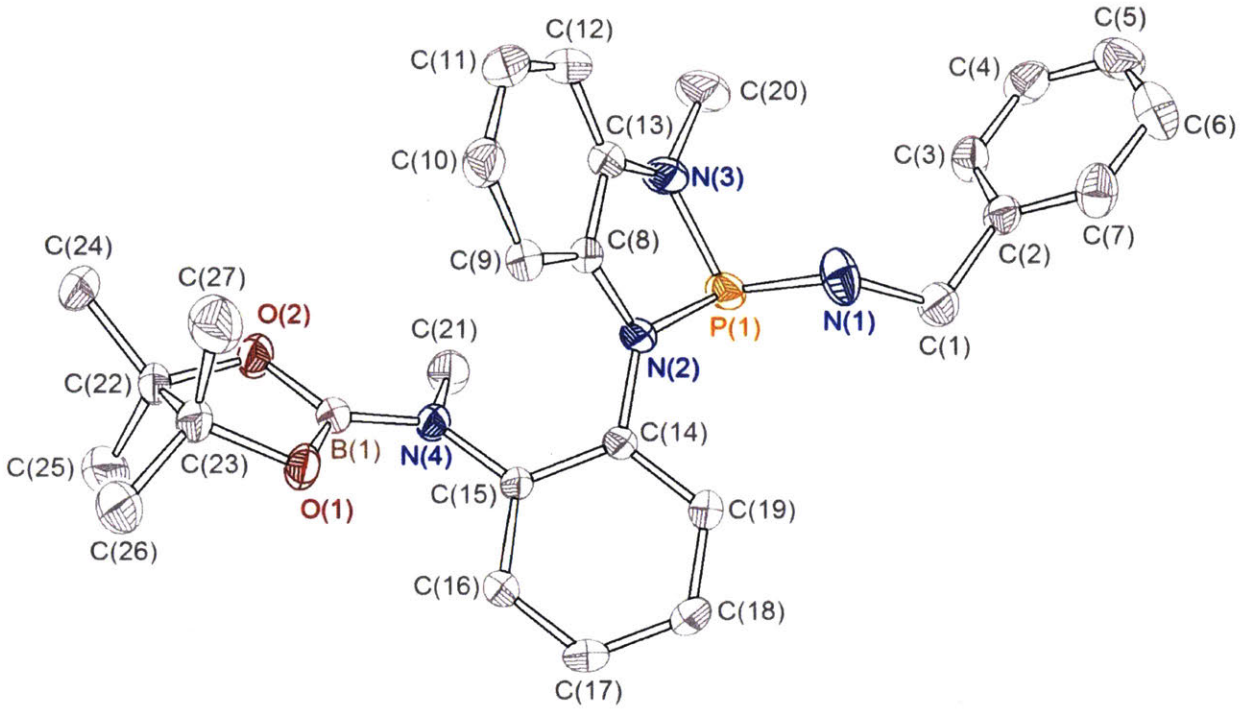

A colorless block shaped crystal of **3.12** (C27 H34 B N4 O2 P) with approximate dimensions 0.22 × 0.17 × 0.11 mm, was used for the X-ray crystallographic analysis. The X-ray intensity data were measured at 213(2) K, cooled by Rigaku-MSC X-Stream 2000, on a Bruker SMART APEX CCD area detector system equipped with a graphite monochromator and a MoK fine-focus sealed tube (= 0.71073Å) operated at 1600 watts power (50 kV, 32 mA). The detector was placed at a distance of 5.82 cm from the crystal.

A total of 1440 frames were collected with a scan width of 0.3° in ω and an exposure time of 10 seconds/frame. The total data collection time was about 6 hours. The frames were integrated with the Bruker SAINT software package using a narrow-frame integration algorithm. The integration of the data using a Triclinic unit cell yielded a total of 9853 reflections to a maximum angle of 28.323 (0.90 Å resolution), of which 6281 were independent, completeness = 98.9%, R_{int} = 0.0144, R_{sigma} = 0.0299 and 5520 were greater than 2δ(I). The final cell constants: a = 10.7971(12) Å, b = 11.4825(13) Å, c = 12.3601(14) Å, α = 89.490(2)°, β = 65.116(2)°, γ = 71.217(2)°, volume = 1301.7(3) $Å^3$, are based upon the refinement of the XYZ-centroids of 4458 reflections above 20δ(I) with 2.436° ≤ θ ≤ 28.278°. Analysis of the data showed negligible decay during data collection. Data were corrected for absorption effects using the multiscan technique (SADABS). The ratio of minimum to maximum apparent transmission was 0.8553.

The structure was solved and refined using the Bruker SHELXTL (Version 6.1) Software Package, using the space group P-1, with Z = 2 for the formula unit, C27 H34 B N4 O2 P. The

final anisotropic full-matrix least-squares refinement on F^2 with 326 variables converged at R1 = 5.89%, for the observed data and wR2 = 17.01% for all data. The goodness-of-fit was 1.267. The largest peak on the final difference map was 0.432 $e^-/Å^3$ and the largest hole was -0.269 $e^-/Å^3$. Based on the final model, the calculated density of the crystal is 1.246 g/cm^3 and F(000) amounts to 520 electrons.

Table B13. Fractional Atomic Coordinates ($\times 10^4$) and Equivalent Isotropic Displacement Parameters ($Å^2 \times 10^3$) for 3.12. U_{eq} is defined as 1/3 of of the trace of the orthogonalised U_{IJ} tensor.

Atom	*x*	*y*	*z*	U(eq)
B1	-940(2)	6739.6(17)	7567.9(16)	25.8(4)
C1	3383(2)	11029(2)	8071.1(19)	42.1(5)
C2	3773.8(18)	12107.4(17)	7501.9(15)	28.7(4)
C3	4471(2)	12025.1(18)	6258.5(16)	33.6(4)
C4	4884(2)	12982(2)	5718.1(17)	38.6(4)
C5	4602(2)	14039(2)	6425(2)	44.6(5)
C6	3899(2)	14147(2)	7657(2)	48.1(5)
C7	3479(2)	13184.0(19)	8198.4(17)	39.1(4)
C8	-302.9(17)	9809.8(15)	7653.9(14)	24.1(3)
C9	-1720.6(18)	9864.0(16)	8313.8(15)	28.7(4)
C10	-2788(2)	10631.0(18)	8012.0(18)	36.6(4)
C11	-2437(2)	11320.9(19)	7080(2)	42.6(5)
C12	-1010(2)	11262.3(18)	6409.3(18)	39.8(5)
C13	58.2(19)	10500.5(16)	6700.8(15)	28.8(4)
C14	967.1(16)	8251.8(14)	8589.6(13)	21.8(3)
C15	559.9(16)	7228.8(14)	8457.1(13)	21.6(3)
C16	488.5(19)	6410.5(16)	9301.1(15)	28.7(4)
C17	907(2)	6531.6(17)	10197.4(16)	32.4(4)
C18	1411.3(19)	7483.5(16)	10270.6(15)	30.6(4)
C19	1414.6(18)	8345.5(16)	9480.0(14)	27.1(3)
C20	2129(2)	11029(2)	5237.4(18)	46.3(5)
C21	1451(2)	6927.7(19)	6260.9(15)	33.9(4)
C22	-2325(2)	6025.2(18)	6990.6(17)	35.2(4)
C23	-3207(2)	6638.9(18)	8332.6(17)	34.7(4)
C24	-3142(3)	6393(2)	6222(2)	55.0(6)
C25	-1644(3)	4614(2)	6829(2)	52.2(6)
C26	-4037(2)	5899(2)	9170(2)	49.8(6)
C27	-4218(2)	7970(2)	8491(2)	51.4(6)
N1	2194.7(18)	10830.9(17)	7924.3(17)	40.2(4)

N2	943.5(15)	9169.5(13)	7817.4(12)	25.3(3)
N3	1544.3(17)	10301.8(15)	6158.4(13)	34.1(4)
N4	295.9(15)	6997.5(13)	7465.0(11)	24.3(3)
O1	-2055.7(13)	6697.3(12)	8635(1)	31.9(3)
O2	-1127.6(14)	6500.4(12)	6567.6(11)	34.1(3)
P1	2407.9(5)	9643.4(4)	7020.5(4)	27.98(15)

Table B14. Anisotropic Displacement Parameters ($Å^2 \times 10^3$) for 3.12. The Anisotropic displacement factor exponent takes the form: $-2\pi^2[h^2a^{*2}U_{11}+2hka^*b^*U_{12}+...]$.

Atom	U_{11}	U_{22}	U_{33}	U_{23}	U_{13}	U_{12}
B1	33.4(10)	26.4(9)	26.8(9)	8.6(7)	-17.4(7)	-16.2(8)
C1	53.6(12)	52.7(12)	46.7(11)	25.1(9)	-31.7(10)	-39(1)
C2	26.3(8)	36.3(9)	32.9(8)	10.8(7)	-16.6(7)	-18.0(7)
C3	34.5(9)	39.5(10)	32.3(9)	3.7(7)	-15.1(7)	-19.4(8)
C4	37.5(10)	55.0(12)	34.3(9)	17.7(8)	-19.0(8)	-25.7(9)
C5	43.9(11)	40.5(11)	60.3(13)	23.1(10)	-26.6(10)	-23.7(9)
C6	46.4(12)	35.8(11)	58.3(13)	-3.2(9)	-16.4(10)	-18.8(9)
C7	37.1(10)	49.2(12)	31.7(9)	0.0(8)	-10.2(7)	-22.9(9)
C8	29.2(8)	21.7(8)	29.0(8)	5.7(6)	-18.0(6)	-11.3(6)
C9	32.8(9)	27.8(9)	31.8(8)	6.3(7)	-17.2(7)	-14.5(7)
C10	31.5(9)	34.7(10)	48.9(11)	4.1(8)	-22.5(8)	-11.9(7)
C11	42.5(11)	34.8(10)	61.6(13)	12.8(9)	-36.1(10)	-9.7(8)
C12	54.0(12)	35.4(10)	44.9(11)	20.3(8)	-33.1(9)	-19.2(9)
C13	37.0(9)	28.1(9)	31.5(8)	10.4(7)	-20.4(7)	-16.9(7)
C14	23.7(7)	22.8(8)	24.1(7)	7.9(6)	-12.9(6)	-11.4(6)
C15	24.4(7)	23.7(8)	21.4(7)	6.7(6)	-12.2(6)	-11.5(6)
C16	37.1(9)	28.6(9)	31.2(8)	11.8(7)	-19.7(7)	-18.9(7)
C17	43(1)	33.3(9)	30.9(8)	16.4(7)	-22.9(8)	-17.0(8)
C18	37.7(9)	33.5(9)	30.0(8)	7.6(7)	-23.3(7)	-12.6(7)
C19	31.9(8)	28.0(8)	30.5(8)	6.3(6)	-18.6(7)	-15.2(7)
C20	55.0(12)	49.7(12)	42.6(11)	27.4(9)	-21.0(9)	-29.8(10)
C21	37.0(9)	43.6(10)	23.7(8)	6.7(7)	-11.2(7)	-20.5(8)
C22	52.0(11)	42.3(10)	38.8(9)	18.6(8)	-32.0(9)	-34.4(9)
C23	38.8(10)	44.9(11)	41.1(10)	19.4(8)	-26.3(8)	-29.1(8)
C24	82.4(17)	72.1(16)	65.1(14)	41.8(12)	-61.2(14)	-56.5(14)
C25	81.9(17)	41.9(12)	56.7(13)	13.1(10)	-43.3(13)	-34.1(12)
C26	52.3(12)	68.6(15)	56.0(13)	32.6(11)	-31.4(10)	-45.6(12)

C27	40.7(11)	49.1(13)	70.5(15)	13.8(11)	-26.8(11)	-20.4(10)
N1	29.6(8)	38.6(9)	54.8(10)	0.8(8)	-14.8(7)	-19.9(7)
N2	28.4(7)	26.2(7)	30.7(7)	12.8(5)	-16.9(6)	-16.1(6)
N3	40.1(8)	38.1(9)	33.1(8)	19.4(6)	-18.5(6)	-22.0(7)
N4	29.0(7)	29.3(7)	21.1(6)	6.4(5)	-13.2(5)	-15.7(6)
O1	35.5(7)	47.3(8)	28.4(6)	11.8(5)	-18.8(5)	-27.5(6)
O2	46.7(7)	46.4(8)	28.2(6)	12.7(5)	-23.3(5)	-30.7(6)
P1	26.8(2)	28.3(3)	32.4(2)	11.11(17)	-12.79(18)	-14.49(18)

Table B15. Bond Lengths for 3.12.

Atom	Atom	Length/Å	Atom	Atom	Length/Å
B1	N4	1.413(2)	C14	C19	1.393(2)
B1	O1	1.375(2)	C14	N2	1.4168(19)
B1	O2	1.377(2)	C15	C16	1.392(2)
C1	C2	1.509(2)	C15	N4	1.4156(19)
C1	N1	1.454(2)	C16	C17	1.384(2)
C2	C3	1.386(2)	C17	C18	1.388(2)
C2	C7	1.381(3)	C18	C19	1.384(2)
C3	C4	1.380(3)	C20	N3	1.452(2)
C4	C5	1.374(3)	C21	N4	1.467(2)
C5	C6	1.371(3)	C22	C23	1.554(3)
C6	C7	1.390(3)	C22	C24	1.522(3)
C8	C9	1.379(2)	C22	C25	1.524(3)
C8	C13	1.402(2)	C22	O2	1.457(2)
C8	N2	1.408(2)	C23	C26	1.514(3)
C9	C10	1.395(2)	C23	C27	1.523(3)
C10	C11	1.381(3)	C23	O1	1.461(2)
C11	C12	1.387(3)	N1	P1	1.6640(18)
C12	C13	1.386(2)	N2	P1	1.7320(14)
C13	N3	1.392(2)	N3	P1	1.7160(16)
C14	C15	1.413(2)			

Table B16. Bond Angles for 3.12.

Atom	Atom	Atom	Angle/°	Atom	Atom	Atom	Angle/°
O1	B1	N4	125.07(15)	C19	C18	C17	119.22(15)

O1	B1	O2	113.40(15)	C18	C19	C14	121.29(16)
O2	B1	N4	121.53(15)	C24	C22	C23	115.07(18)
N1	C1	C2	113.92(17)	C24	C22	C25	109.89(17)
C3	C2	C1	120.35(17)	C25	C22	C23	113.46(16)
C7	C2	C1	121.26(17)	O2	C22	C23	102.01(13)
C7	C2	C3	118.38(17)	O2	C22	C24	108.98(15)
C4	C3	C2	121.41(18)	O2	C22	C25	106.73(17)
C5	C4	C3	119.44(18)	C26	C23	C22	114.67(17)
C6	C5	C4	120.19(19)	C26	C23	C27	110.22(17)
C5	C6	C7	120.24(19)	C27	C23	C22	112.59(16)
C2	C7	C6	120.34(18)	O1	C23	C22	101.85(14)
C9	C8	C13	120.94(15)	O1	C23	C26	109.72(15)
C9	C8	N2	129.14(15)	O1	C23	C27	107.21(16)
C13	C8	N2	109.85(14)	C1	N1	P1	124.01(15)
C8	C9	C10	118.19(16)	C8	N2	C14	122.57(13)
C11	C10	C9	120.98(18)	C8	N2	P1	113.56(10)
C10	C11	C12	120.98(17)	C14	N2	P1	123.85(11)
C13	C12	C11	118.46(17)	C13	N3	C20	120.35(16)
C12	C13	C8	120.46(17)	C13	N3	P1	113.54(11)
C12	C13	N3	128.27(16)	C20	N3	P1	121.62(14)
N3	C13	C8	111.27(15)	B1	N4	C15	124.07(13)
C15	C14	N2	120.73(13)	B1	N4	C21	119.11(14)
C19	C14	C15	119.39(14)	C15	N4	C21	116.62(13)
C19	C14	N2	119.88(14)	B1	O1	C23	105.93(13)
C14	C15	N4	121.43(13)	B1	O2	C22	105.83(13)
C16	C15	C14	118.26(14)	N1	P1	N2	105.37(8)
C16	C15	N4	120.24(14)	N1	P1	N3	105.24(9)
C17	C16	C15	121.43(15)	N3	P1	N2	87.57(7)
C16	C17	C18	120.11(15)				

Table B17. Torsion Angles for 3.12.

A	B	C	D	Angle/°	A	B	C	D	Angle/°
C1	C2	C3	C4	-177.76(18)	C16	C15	N4	C21	-123.91(17)
C1	C2	C7	C6	177.5(2)	C16	C17	C18	C19	3.5(3)
C1	N1	P1	N2	139.38(16)	C17	C18	C19	C14	-2.1(3)
C1	N1	P1	N3	-128.94(16)	C19	C14	C15	C16	6.0(2)

C2	C1	N1	P1	108.4(2)	C19	C14	C15	N4	-170.99(15)
C2	C3	C4	C5	0.1(3)	C19	C14	N2	C8	-126.76(17)
C3	C2	C7	C6	-1.1(3)	C19	C14	N2	P1	51.4(2)
C3	C4	C5	C6	-0.9(3)	C20	N3	P1	N1	70.24(17)
C4	C5	C6	C7	0.7(3)	C20	N3	P1	N2	175.51(17)
C5	C6	C7	C2	0.4(3)	C22	C23	O1	B1	26.44(17)
C7	C2	C3	C4	0.8(3)	C23	C22	O2	B1	27.11(18)
C8	C9	C10	C11	-0.2(3)	C24	C22	C23	C26	91.2(2)
C8	C13	N3	C20	-173.26(17)	C24	C22	C23	C27	-35.9(2)
C8	C13	N3	P1	-16.67(19)	C24	C22	C23	O1	-150.42(15)
C8	N2	P1	N1	87.75(13)	C24	C22	O2	B1	149.21(18)
C8	N2	P1	N3	-17.39(12)	C25	C22	C23	C26	-36.6(2)
C9	C8	C13	C12	0.5(3)	C25	C22	C23	C27	-163.69(17)
C9	C8	C13	N3	-179.69(15)	C25	C22	C23	O1	81.81(19)
C9	C8	N2	C14	12.9(3)	C25	C22	O2	B1	-92.16(17)
C9	C8	N2	P1	-165.43(14)	C26	C23	O1	B1	148.33(17)
C9	C10	C11	C12	0.6(3)	C27	C23	O1	B1	-91.97(18)
C10	C11	C12	C13	-0.4(3)	N1	C1	C2	C3	-71.4(2)
C11	C12	C13	C8	-0.1(3)	N1	C1	C2	C7	110.1(2)
C11	C12	C13	N3	-179.84(18)	N2	C8	C9	C10	176.18(16)
C12	C13	N3	C20	6.5(3)	N2	C8	C13	C12	-176.63(15)
C12	C13	N3	P1	163.07(16)	N2	C8	C13	N3	3.1(2)
C13	C8	C9	C10	-0.4(2)	N2	C14	C15	C16	-174.83(14)
C13	C8	N2	C14	-170.22(14)	N2	C14	C15	N4	8.1(2)
C13	C8	N2	P1	11.44(17)	N2	C14	C19	C18	178.17(15)
C13	N3	P1	N1	-86.02(14)	N4	B1	O1	C23	169.50(17)
C13	N3	P1	N2	19.25(13)	N4	B1	O2	C22	168.27(16)
C14	C15	C16	C17	-4.8(2)	N4	C15	C16	C17	172.31(16)
C14	C15	N4	B1	-132.04(17)	O1	B1	N4	C15	1.1(3)
C14	C15	N4	C21	53.1(2)	O1	B1	N4	C21	175.84(16)
C14	N2	P1	N1	-90.57(14)	O1	B1	O2	C22	-11.7(2)
C14	N2	P1	N3	164.29(14)	O2	B1	N4	C15	-178.86(15)
C15	C14	C19	C18	-2.7(2)	O2	B1	N4	C21	-4.1(2)
C15	C14	N2	C8	54.1(2)	O2	B1	O1	C23	-10.6(2)
C15	C14	N2	P1	-127.71(14)	O2	C22	C23	C26	-151.01(16)
C15	C16	C17	C18	0.0(3)	O2	C22	C23	C27	81.91(18)
C16	C15	N4	B1	51.0(2)	O2	C22	C23	O1	-32.59(16)

Table B18. Hydrogen Atom Coordinates (Å×10^4) and Isotropic Displacement Parameters (Å^2×10^3) for 3.12.

Atom	*x*	*y*	*z*	U(eq)
H1A	4238	10278	7719	51
H1B	3114	11172	8925	51
H3	4665	11310	5778	40
H4	5348	12912	4882	46
H5	4889	14683	6067	54
H6	3702	14868	8132	58
H7	2998	13265	9034	47
H9	-1959	9402	8943	34
H10	-3750	10679	8445	44
H11	-3168	11832	6899	51
H12	-776	11724	5779	48
H16	152	5769	9262	34
H17	850	5974	10752	39
H18	1743	7542	10844	37
H19	1722	9000	9545	33
H20A	1711	11892	5577	70
H20B	1894	10922	4586	70
H20C	3169	10753	4940	70
H21A	1341	7750	6051	51
H21B	1384	6429	5682	51
H21C	2385	6558	6261	51
H24A	-3452	7279	6241	82
H24B	-3978	6141	6536	82
H24C	-2510	5992	5406	82
H25A	-952	4307	6001	78
H25B	-2393	4258	7047	78
H25C	-1157	4387	7335	78
H26A	-3364	5108	9162	75
H26B	-4707	5771	8904	75
H26C	-4567	6348	9974	75
H27A	-4558	8373	9292	77
H27B	-5036	7964	8366	77
H27C	-3699	8413	7915	77
H1	1440(30)	11390(30)	8290(30)	78(10)

VIII. Multinuclear NMR Spectra

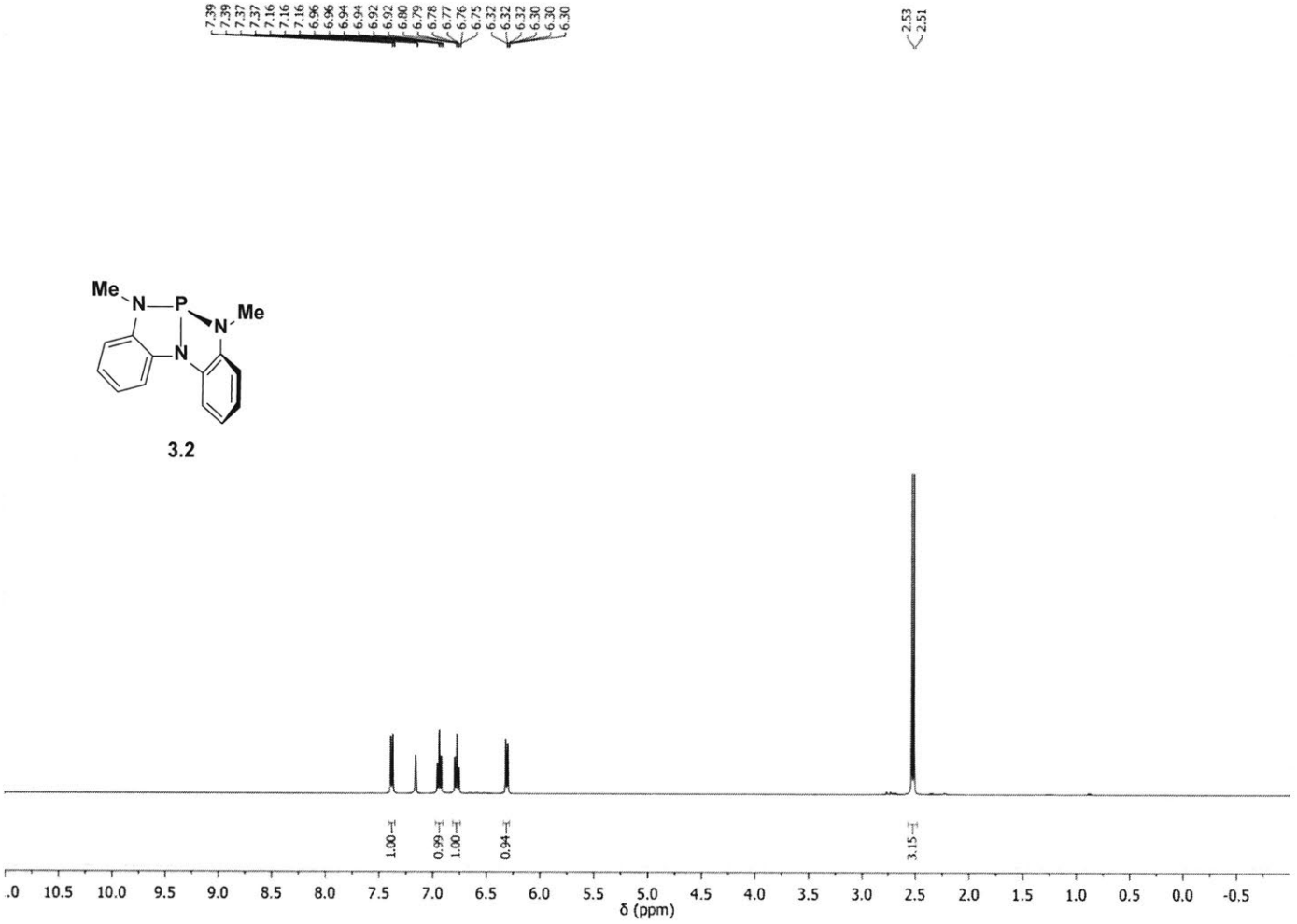

Figure B1. ^{1}H NMR of **3.2**.

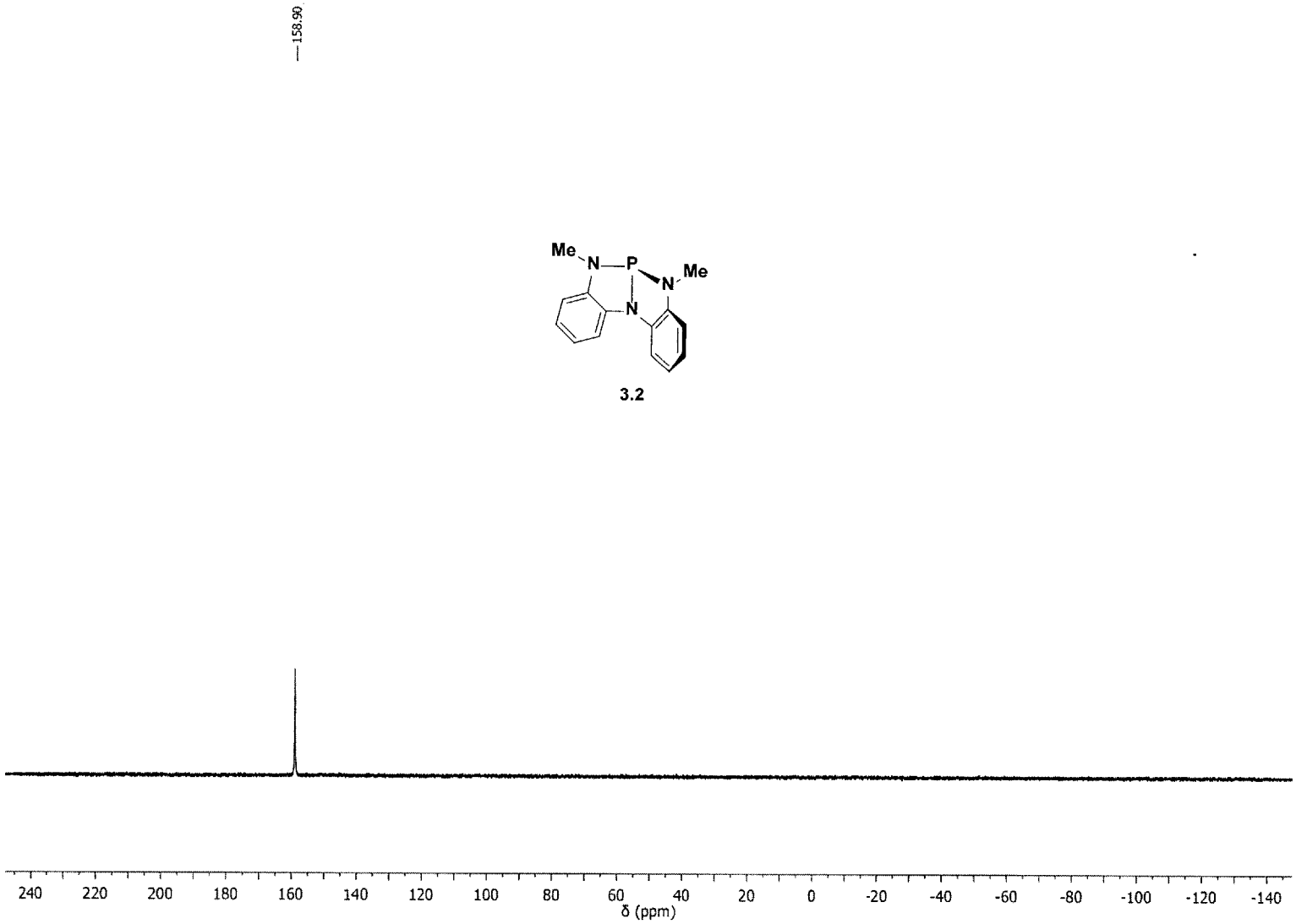

Figure B2. ^{31}P NMR of **3.2.**

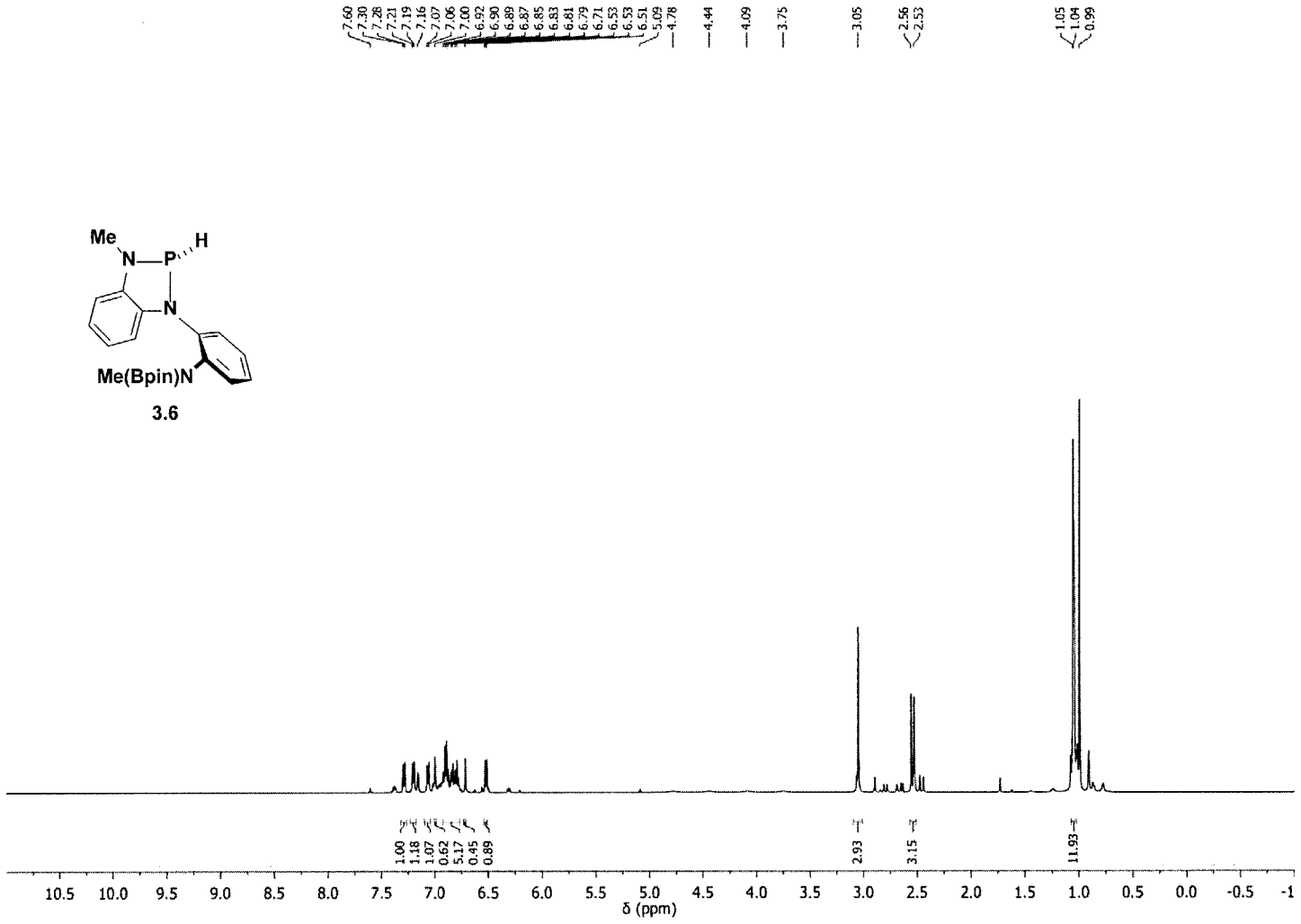

Figure B3. ^{1}H NMR of 3.6.

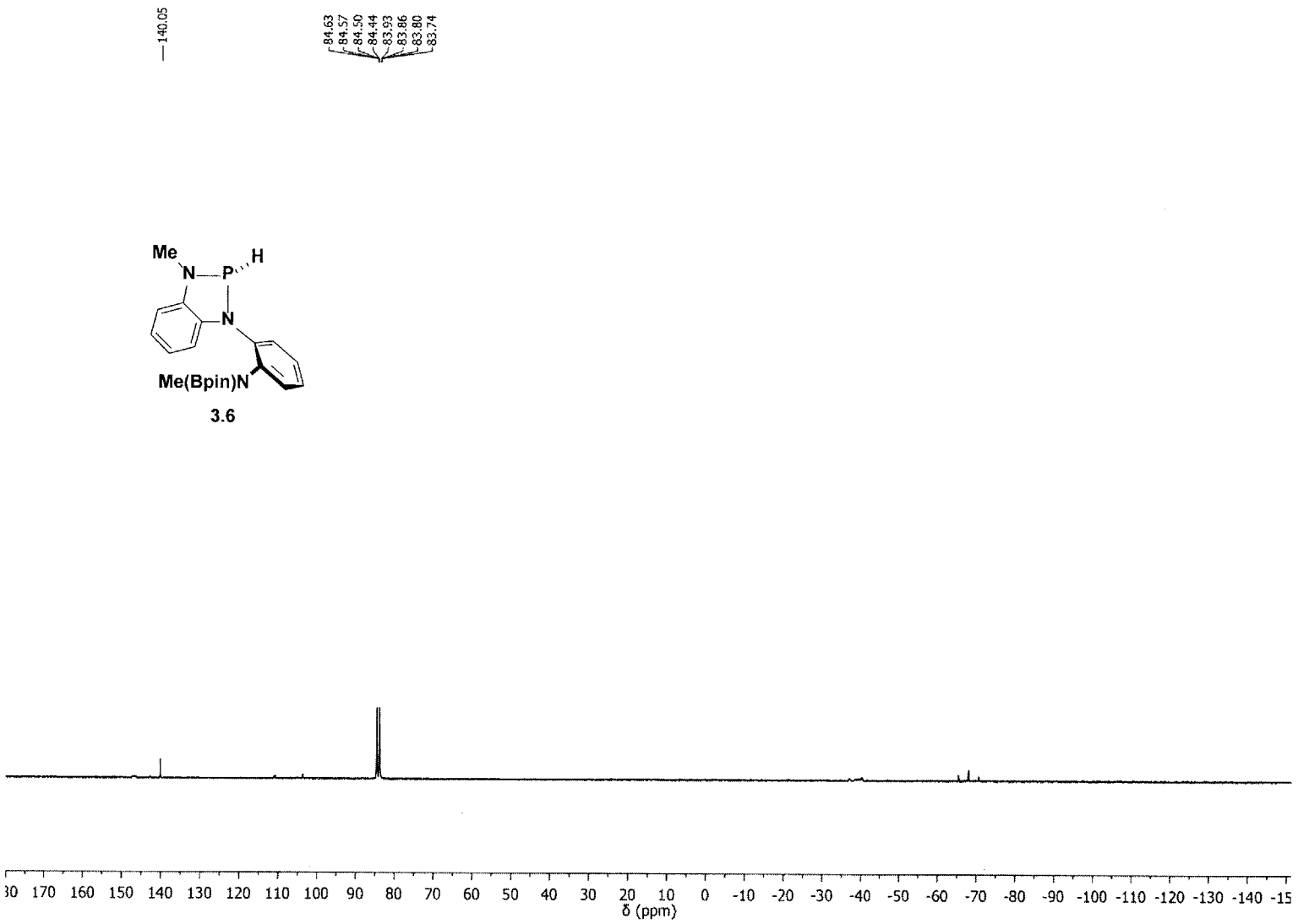

Figure B4. ^{31}P NMR of **3.6.**

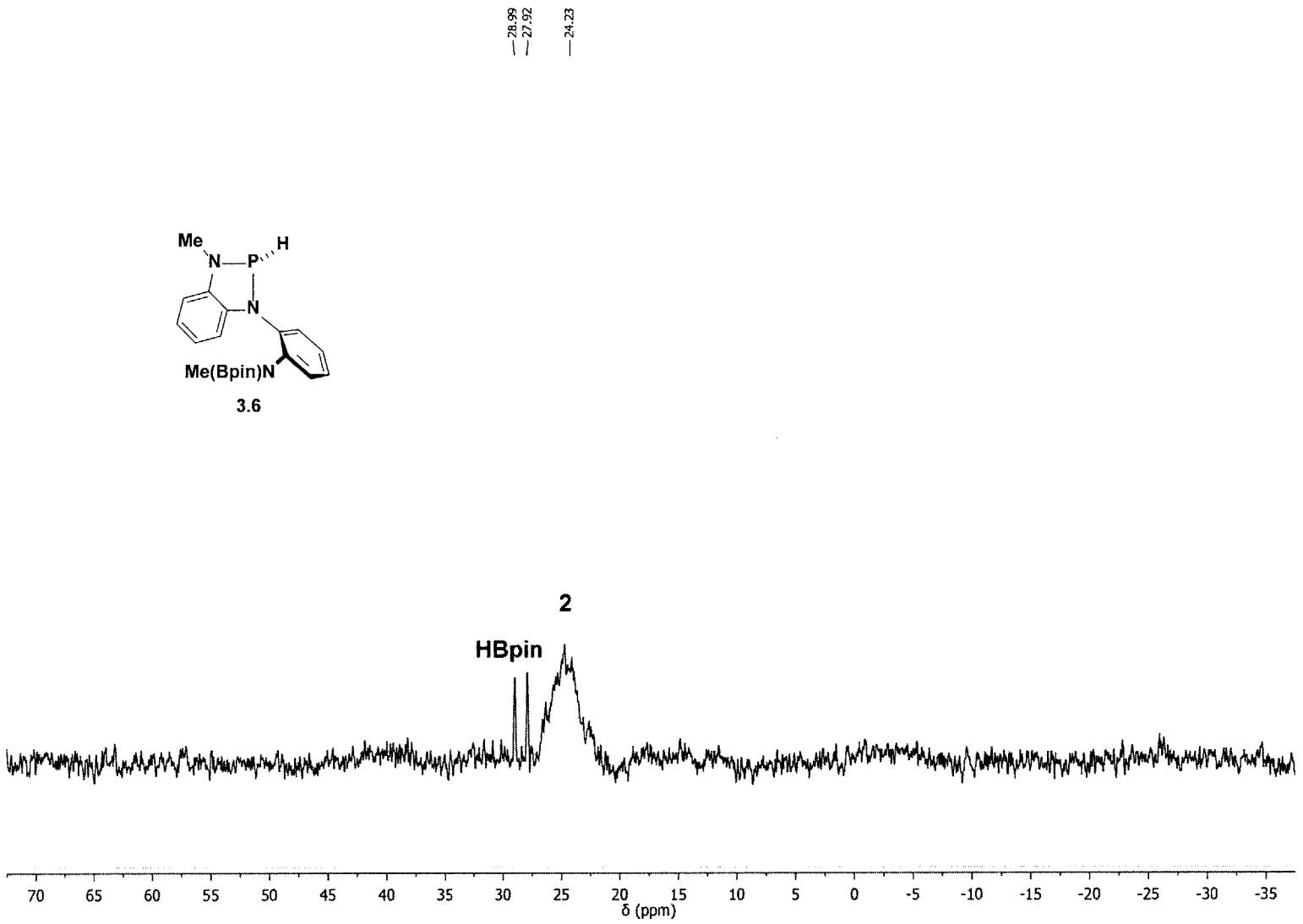

Figure B5. ^{11}B NMR of **3.6.**

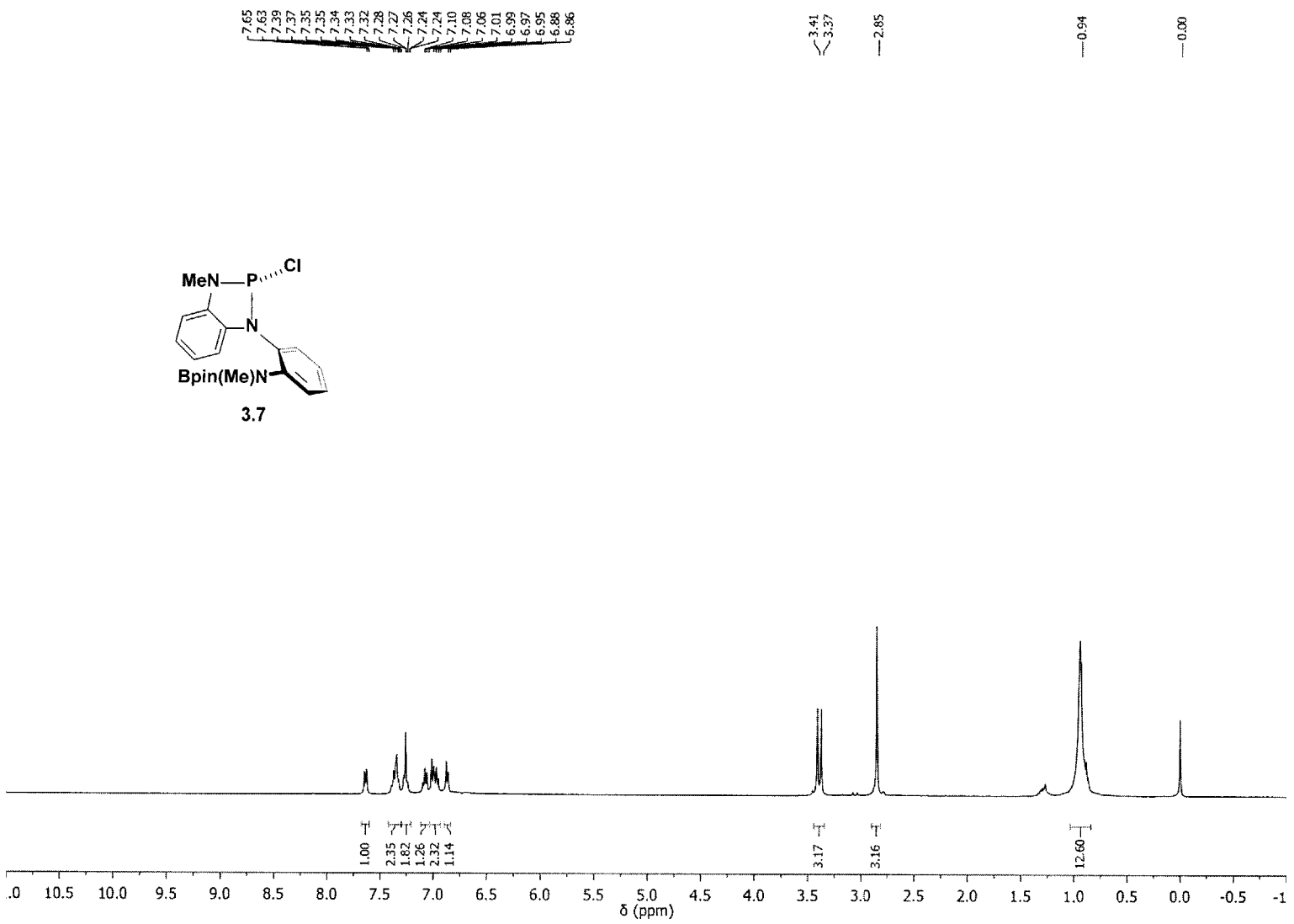

Figure B6. ^{1}H NMR of 3.7.

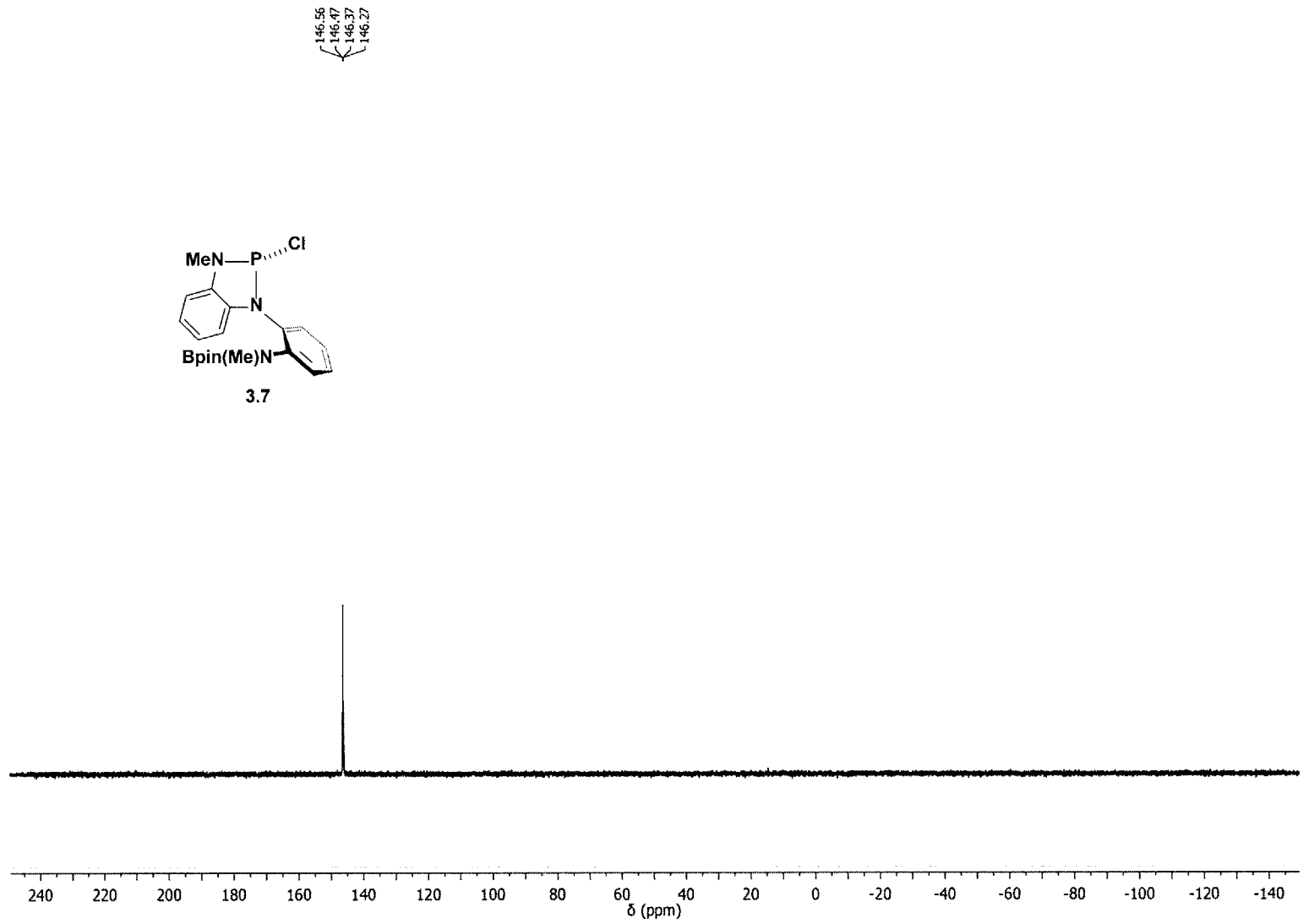

Figure B7. ^{31}P NMR of **3.7**.

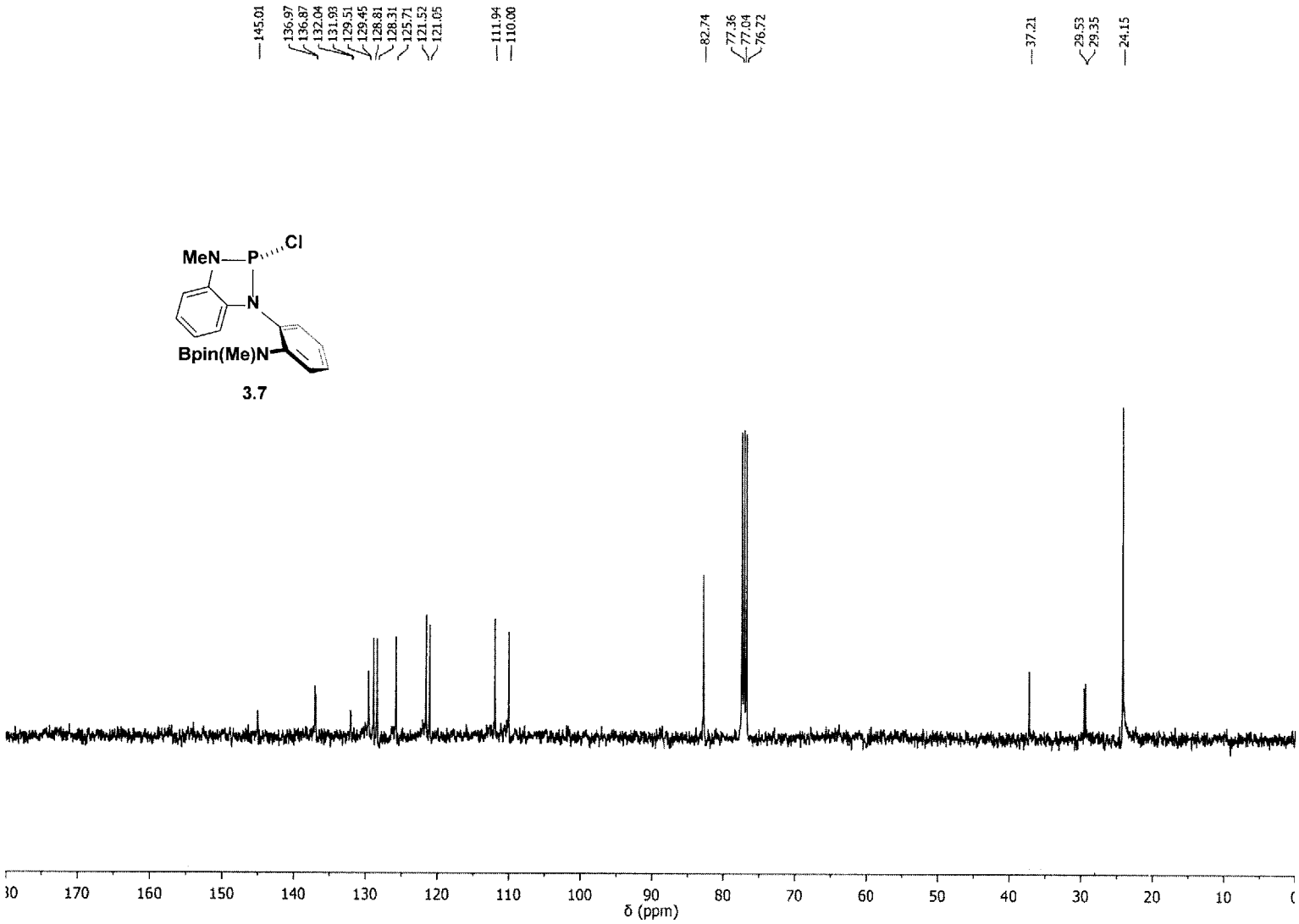

Figure B8. ^{13}C NMR of **3.7.**

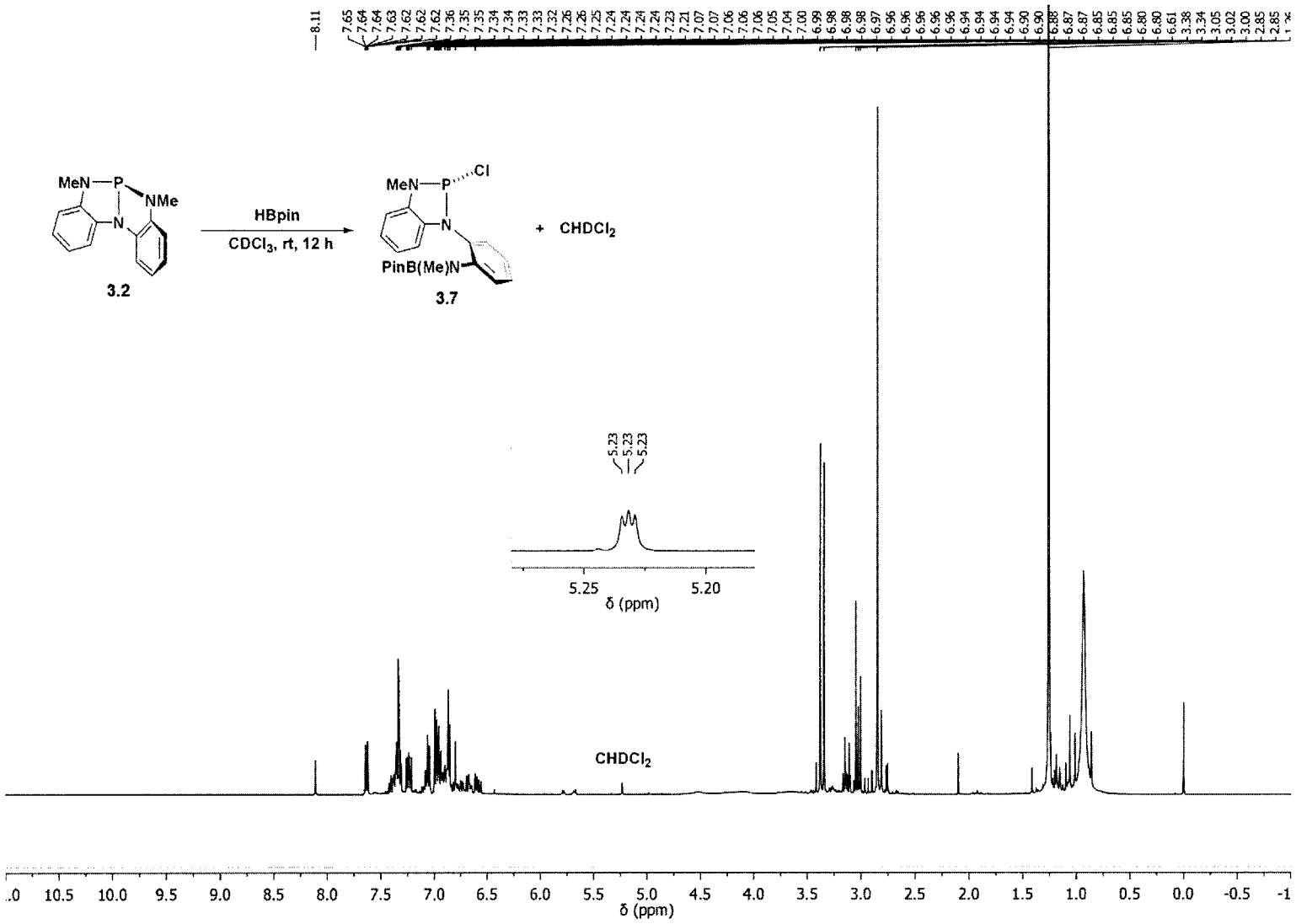

Figure B9. ^{1}H NMR monitoring of the hydrodechlorination of $CDCl_3$.

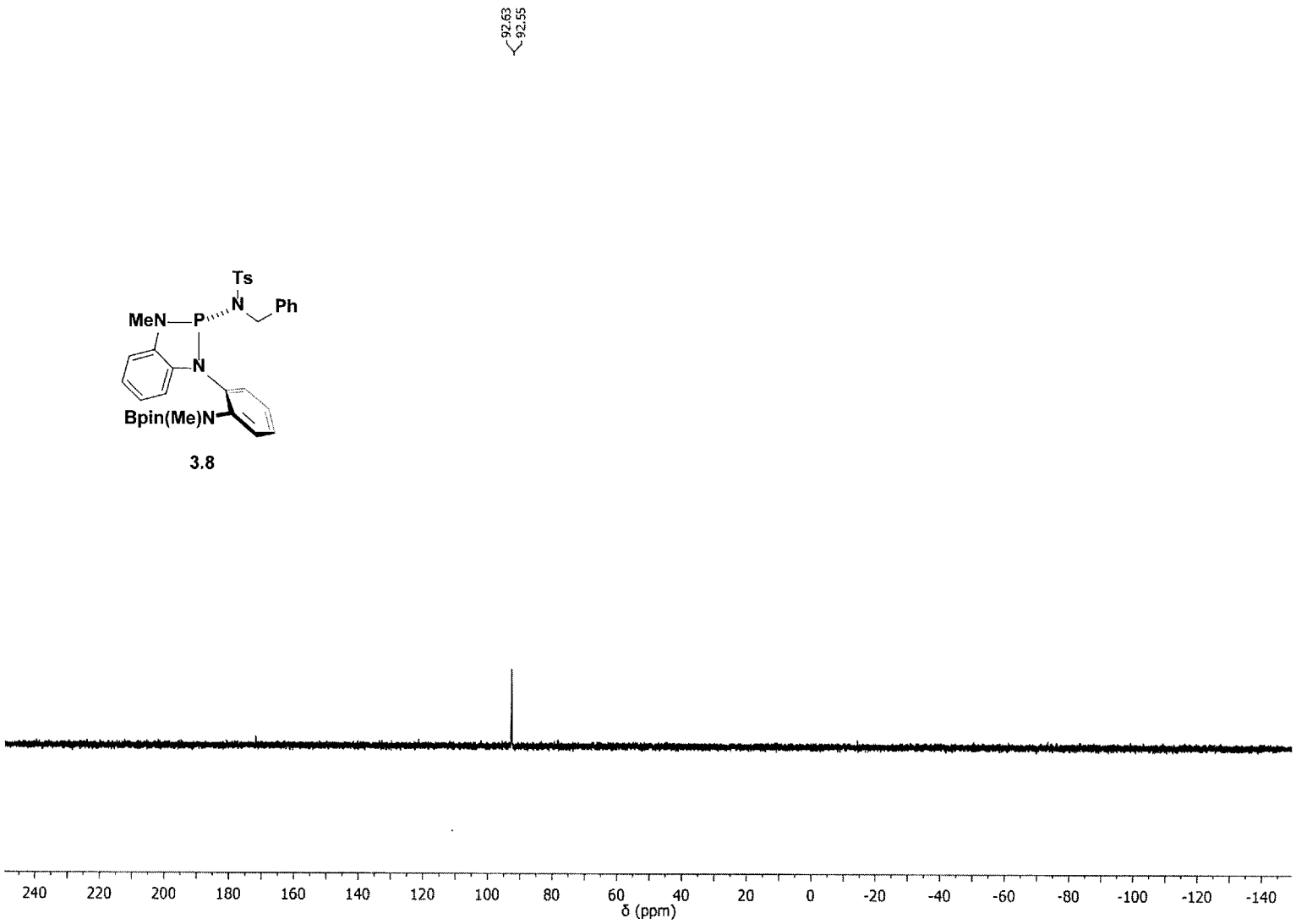

Figure B10. ^{31}P NMR of **3.8.**

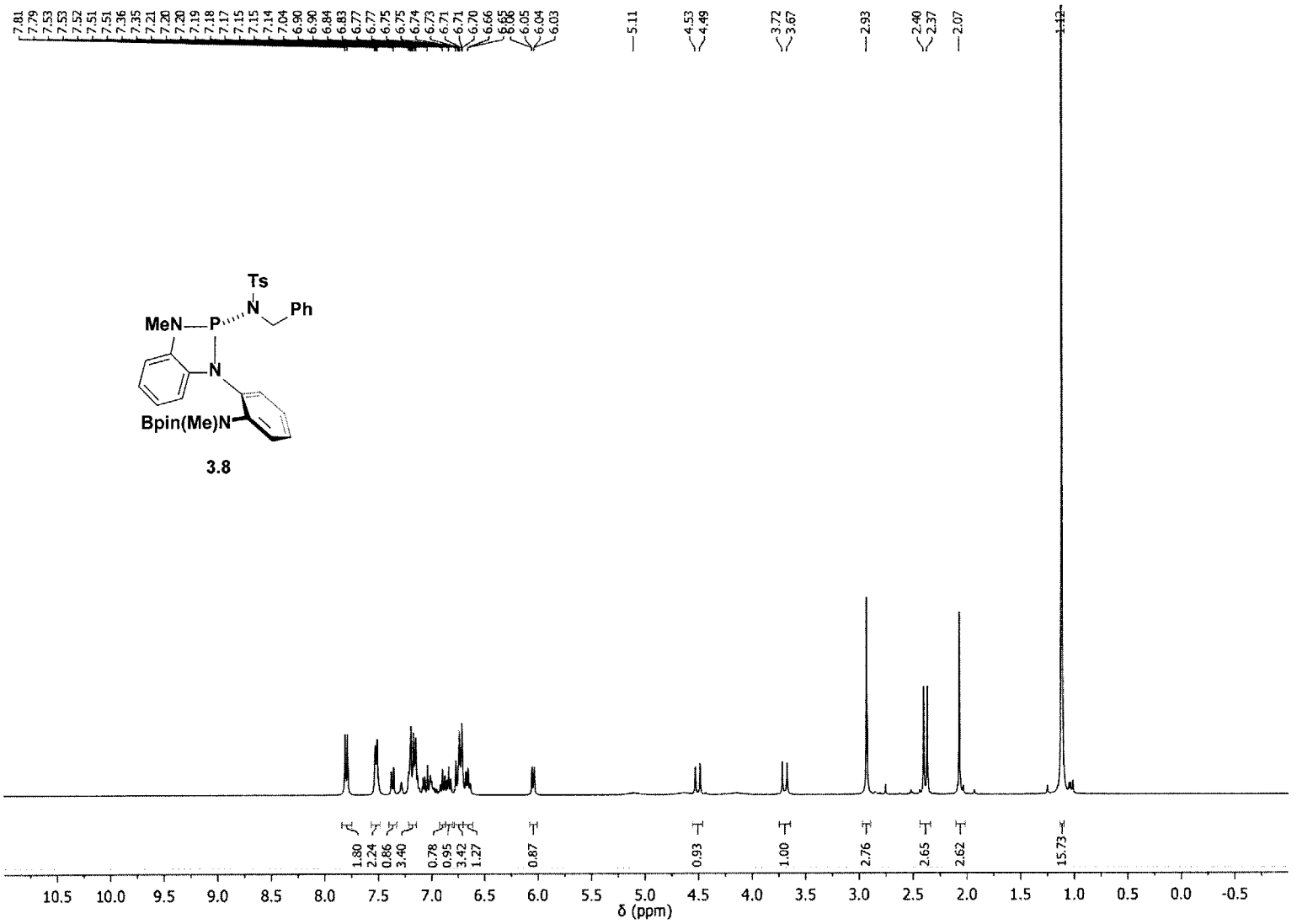

Figure B11. ^{1}H NMR of **3.8.**

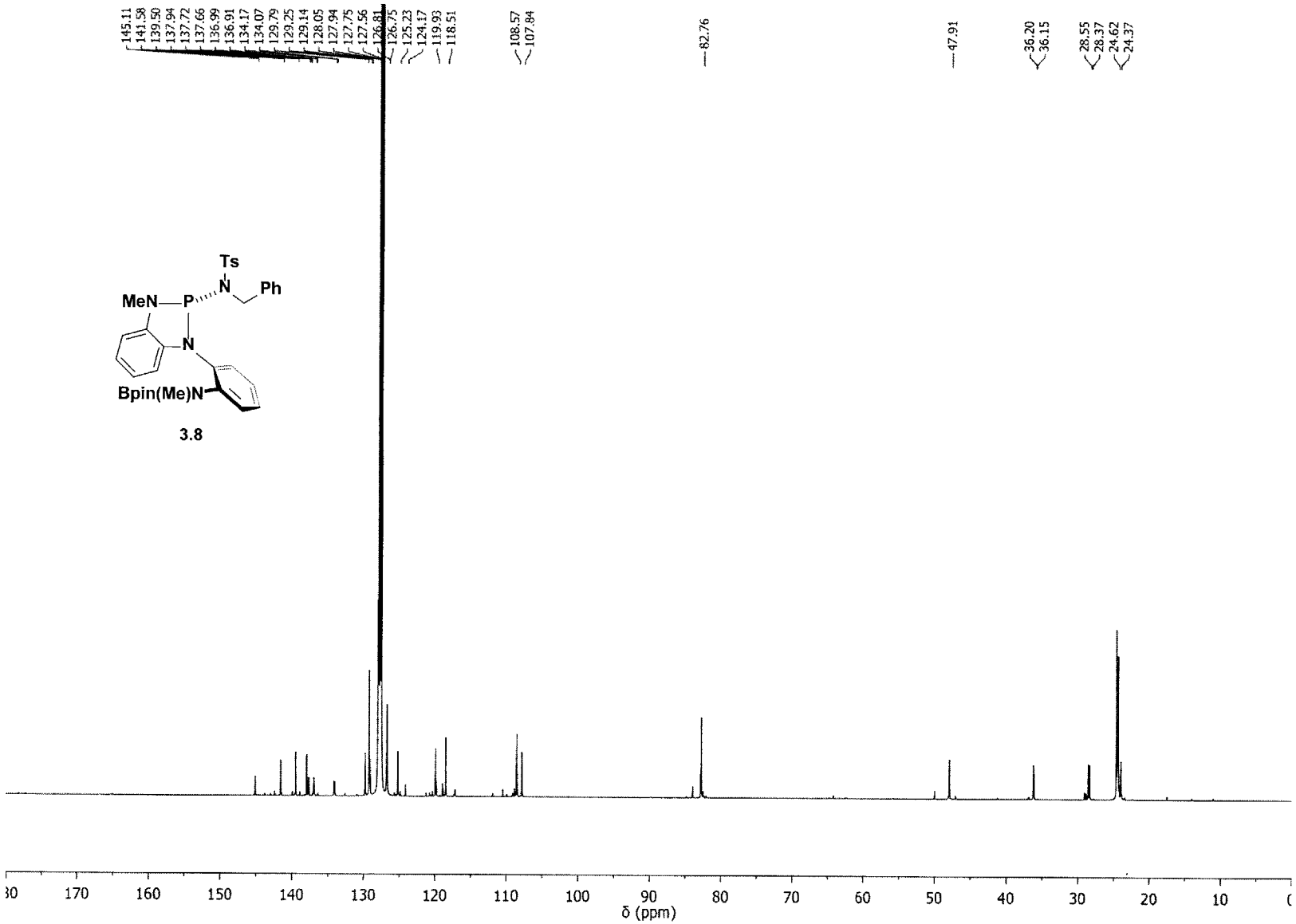

Figure B12. ^{13}C NMR of **3.8.**

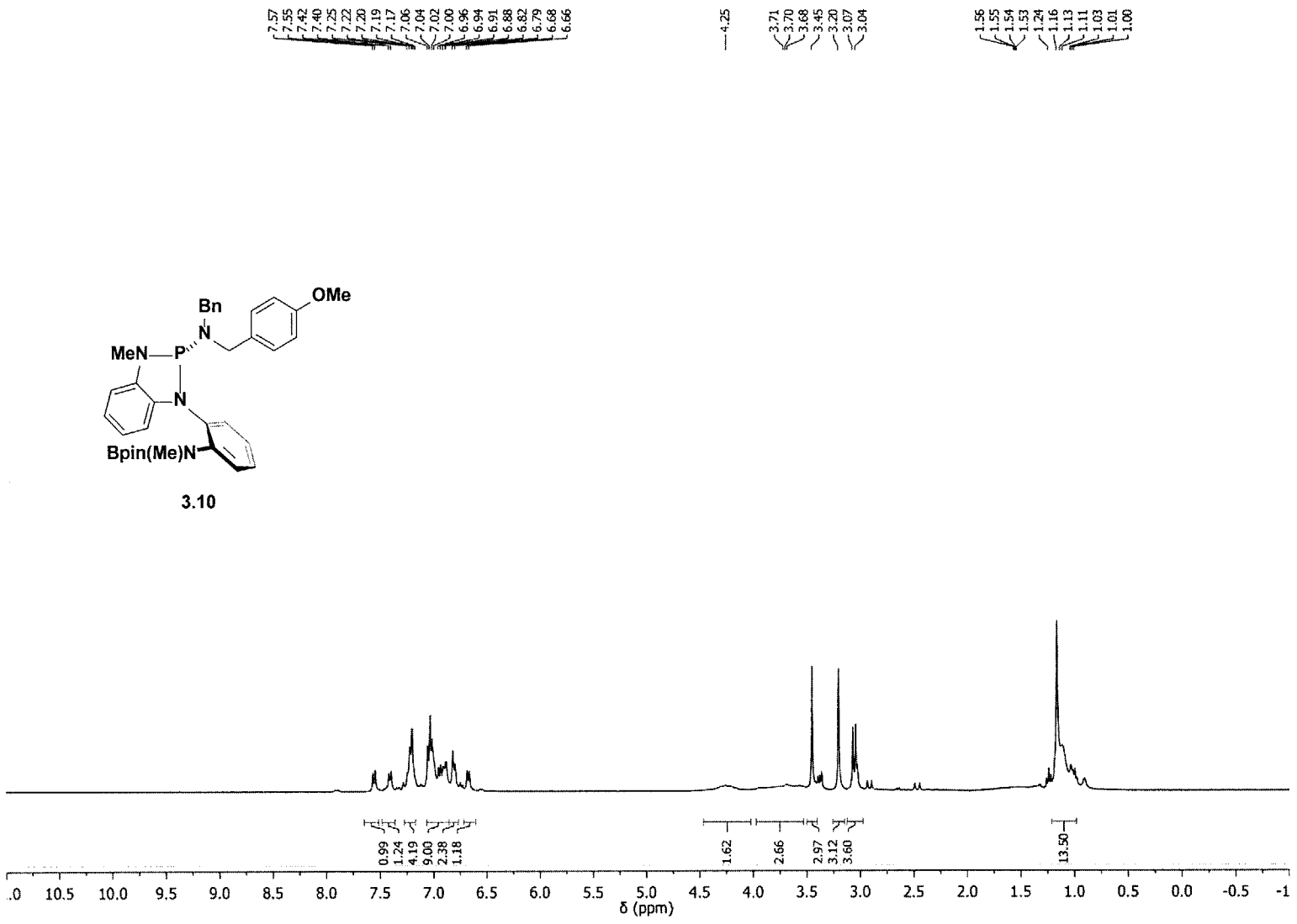

Figure B13. ^{1}H NMR of **3.10.**

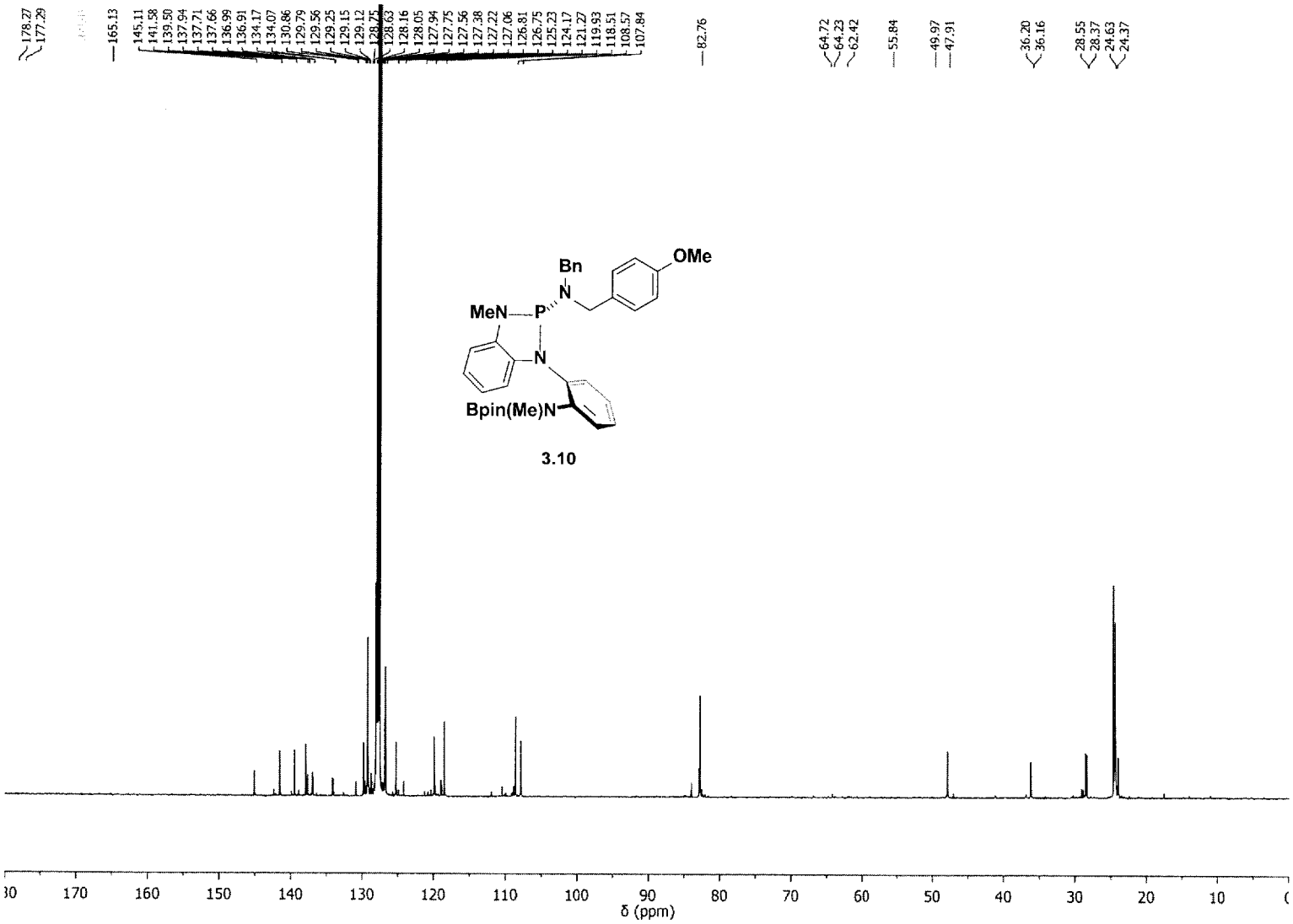

Figure B14. ^{13}C NMR of **3.10**.

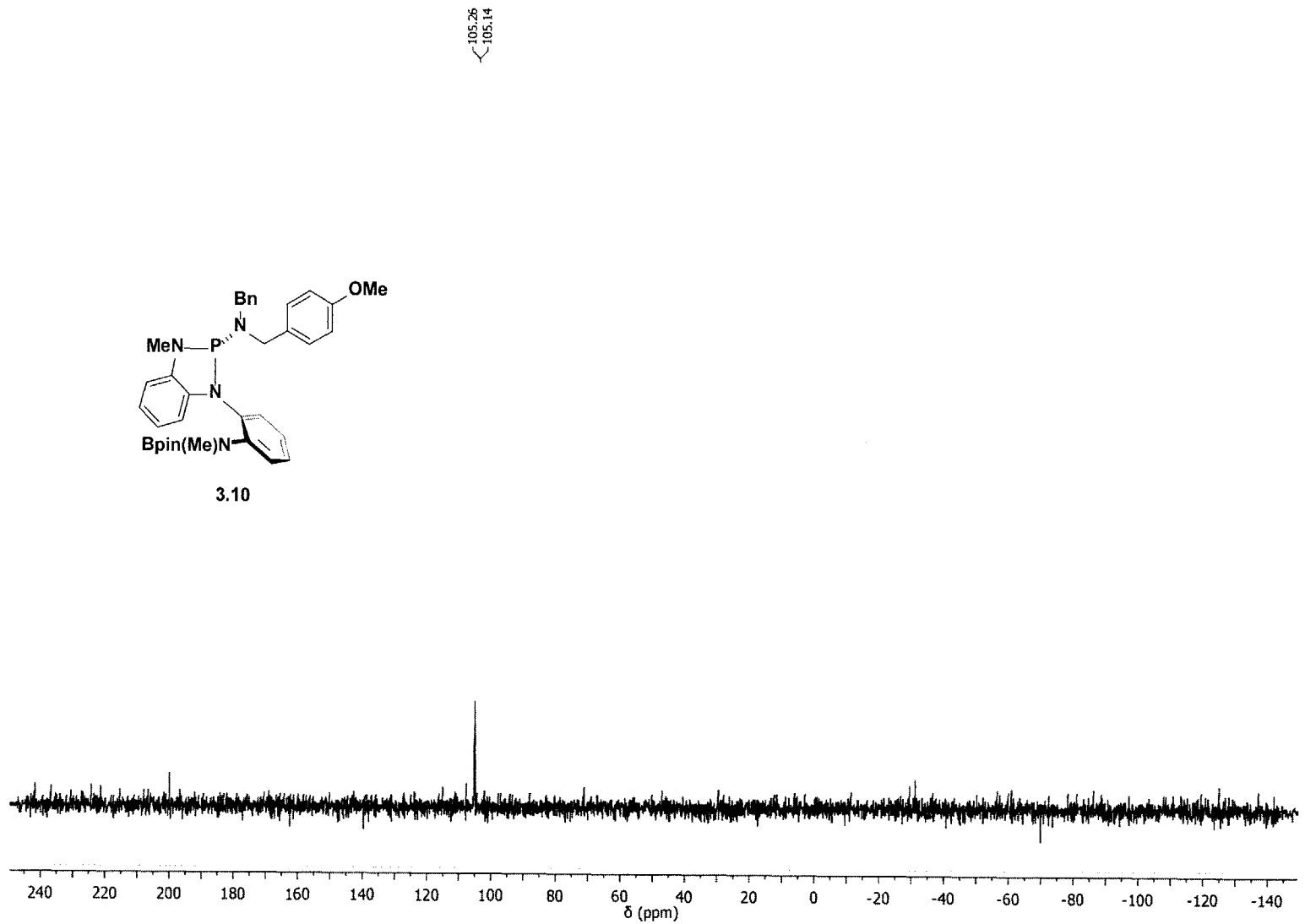

Figure B15. ^{31}P NMR of **3.10**.

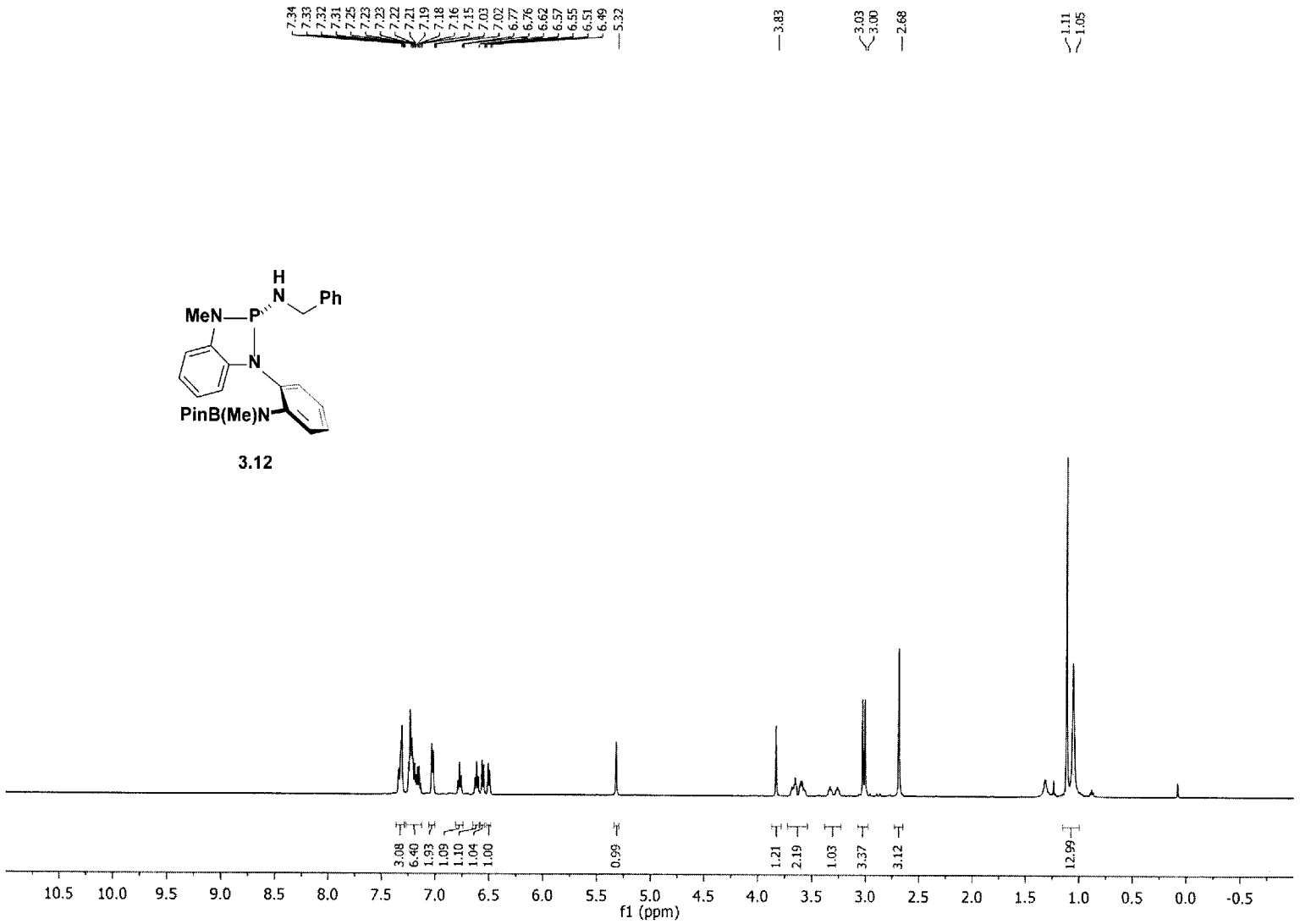

Figure B16. ^{1}H NMR of **3.12.**

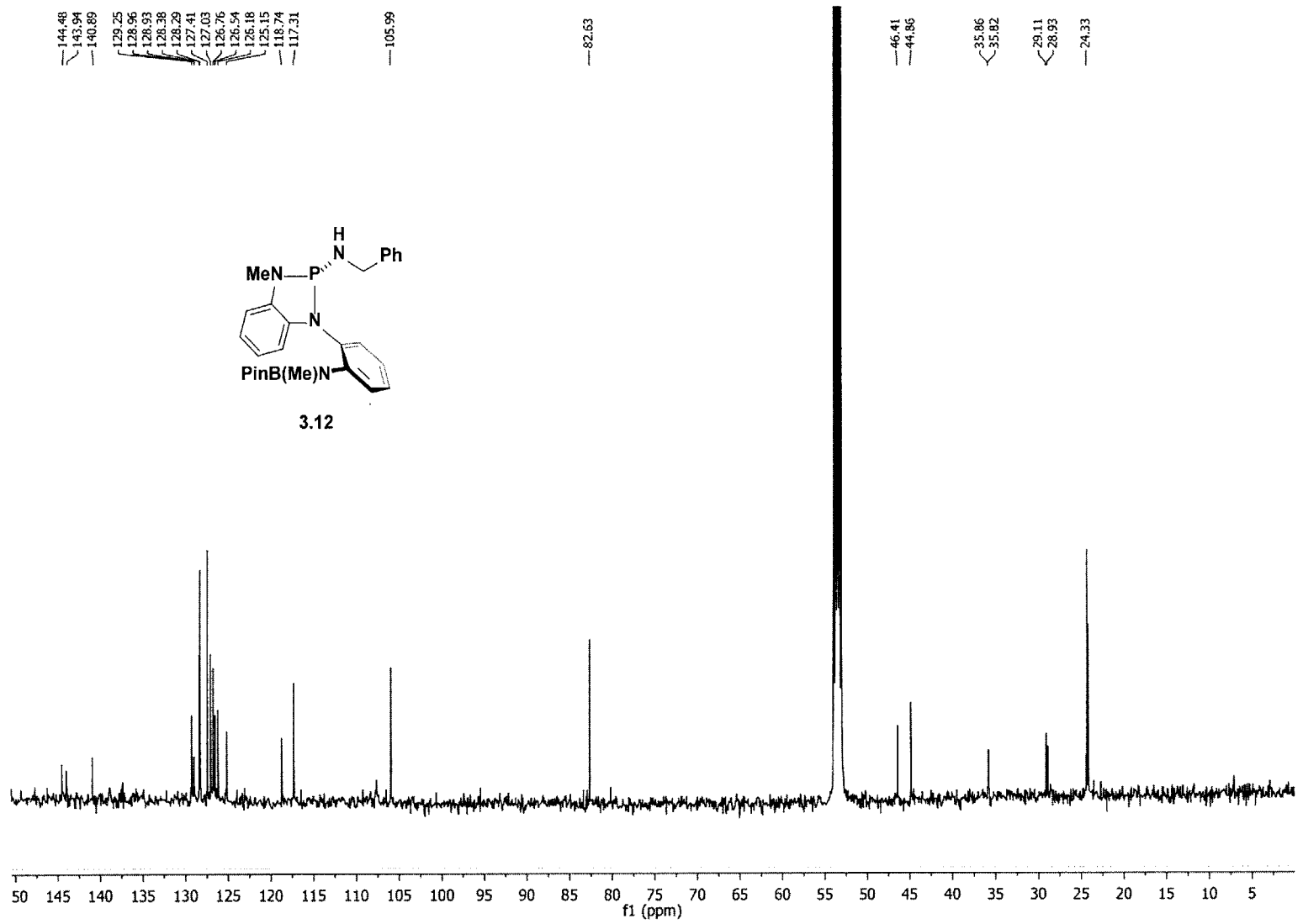

Figure B17. ^{13}C NMR of **3.12.**

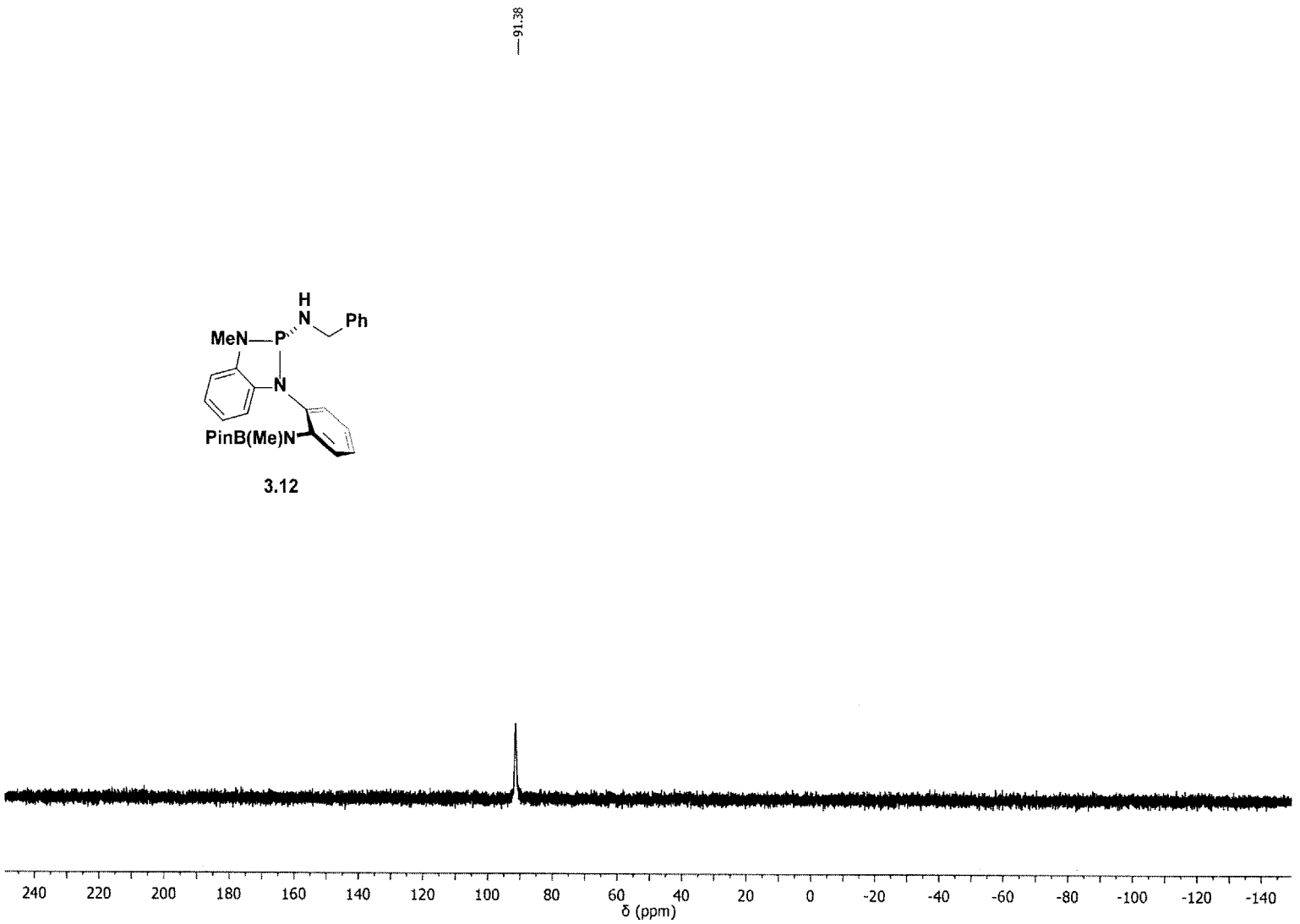

Figure B18. ^{13}P NMR of **3.12.**

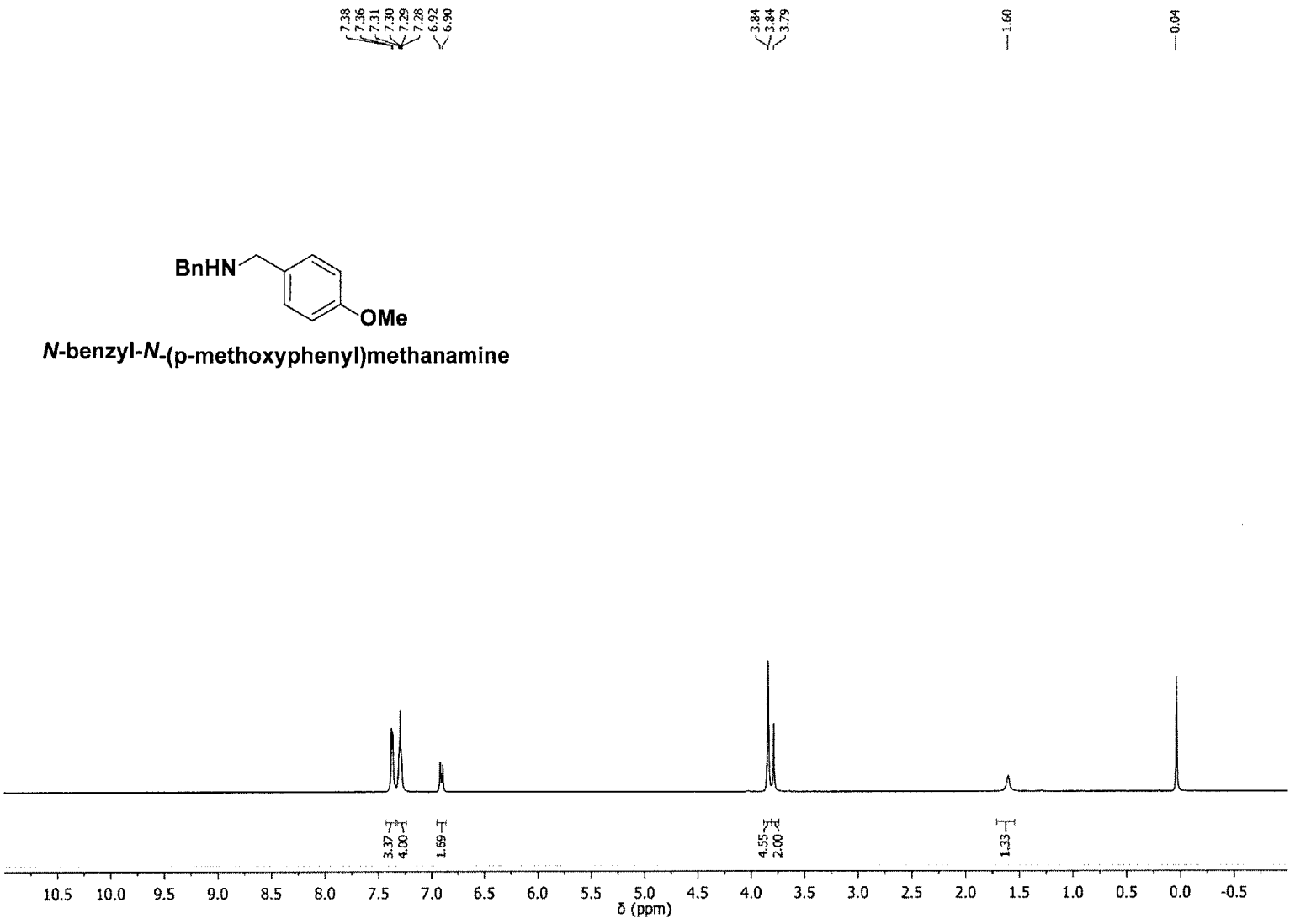

Figure B19. ^{1}H NMR of *N*-benzyl-*N*-(*p*-methoxyphenyl)methanamine

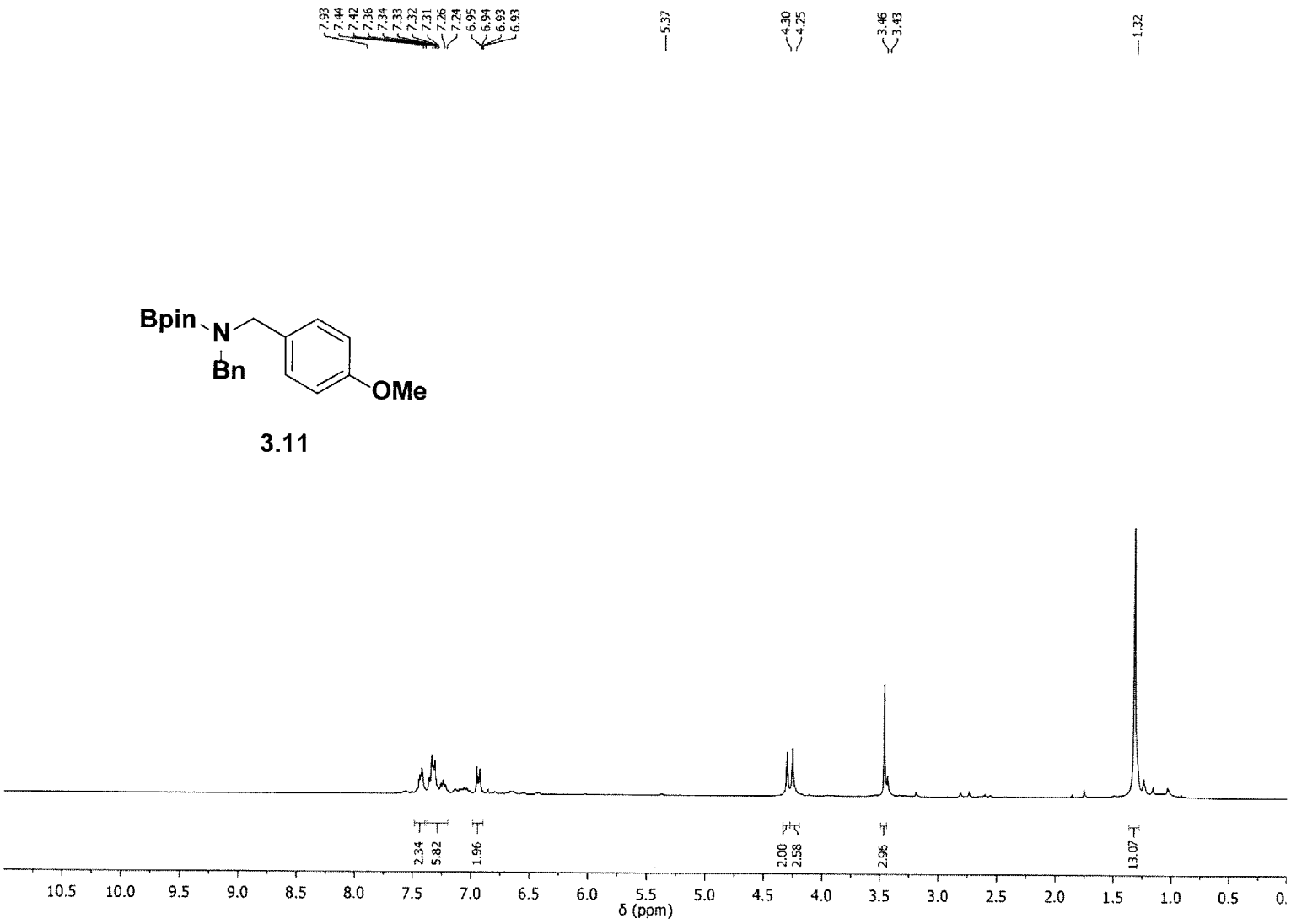

Figure B20. ^{1}H NMR of **3.11**.

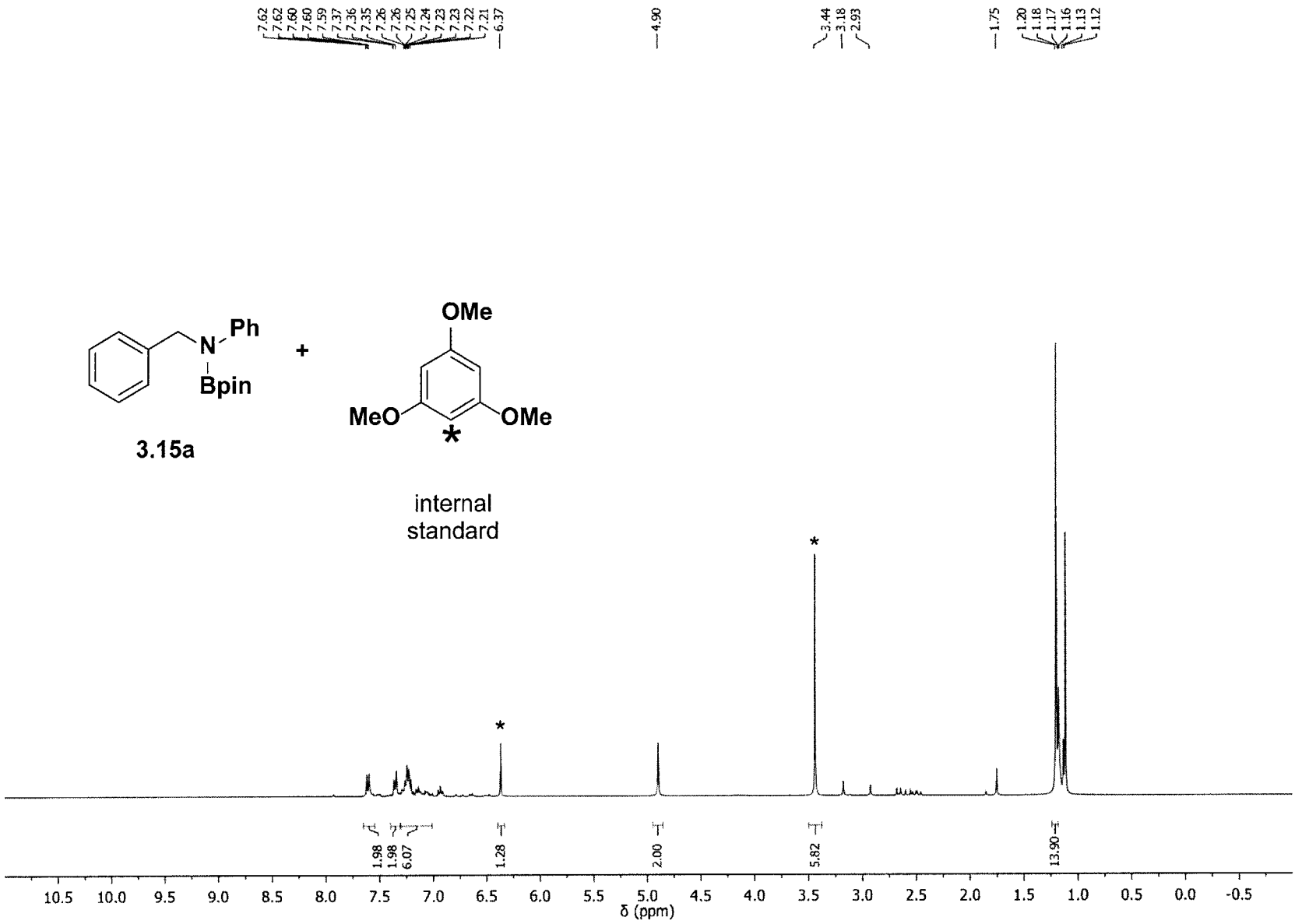

Figure B21. ^{1}H NMR of **3.15a.**

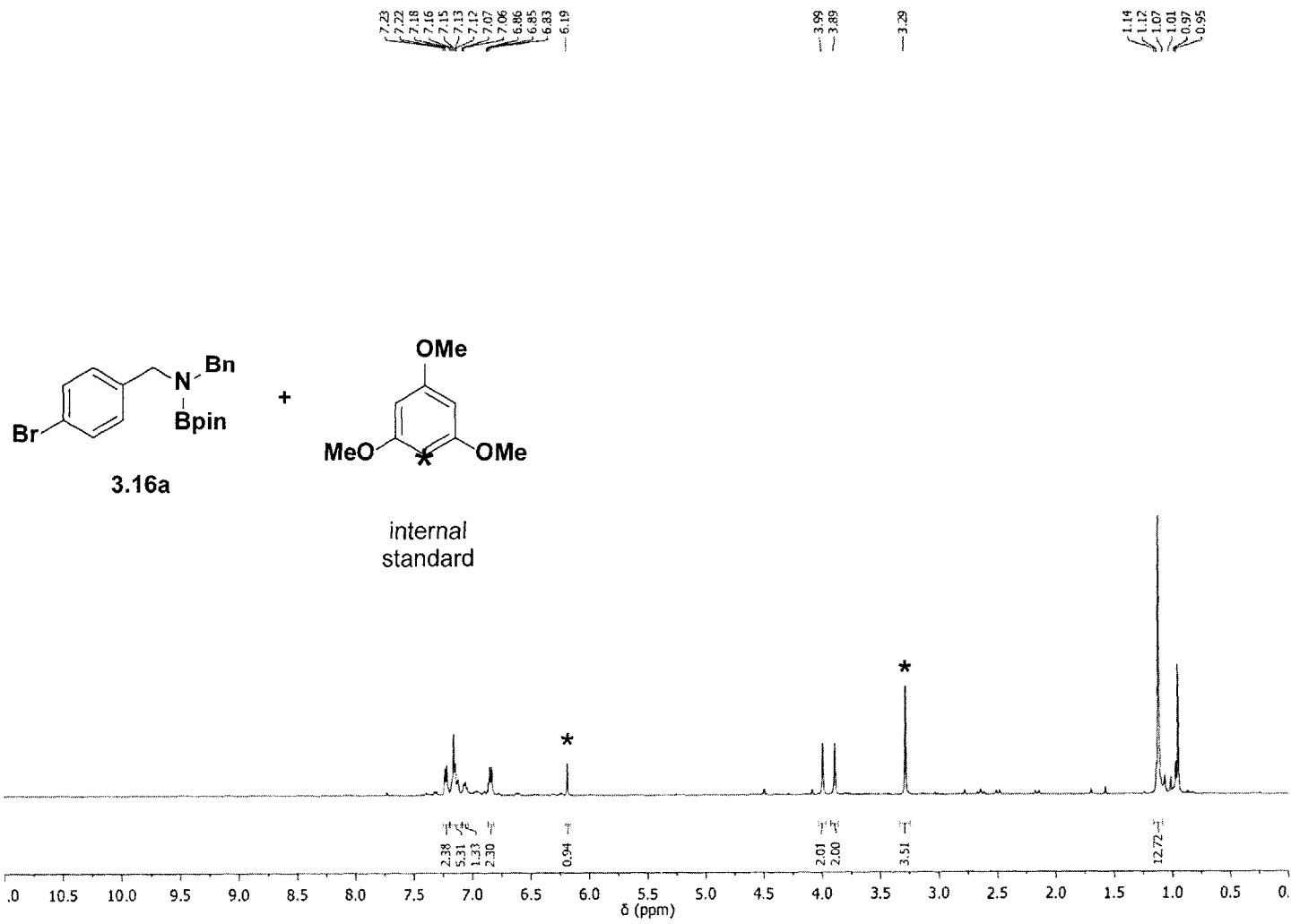

Figure B22. ^{1}H NMR of **3.16a.**

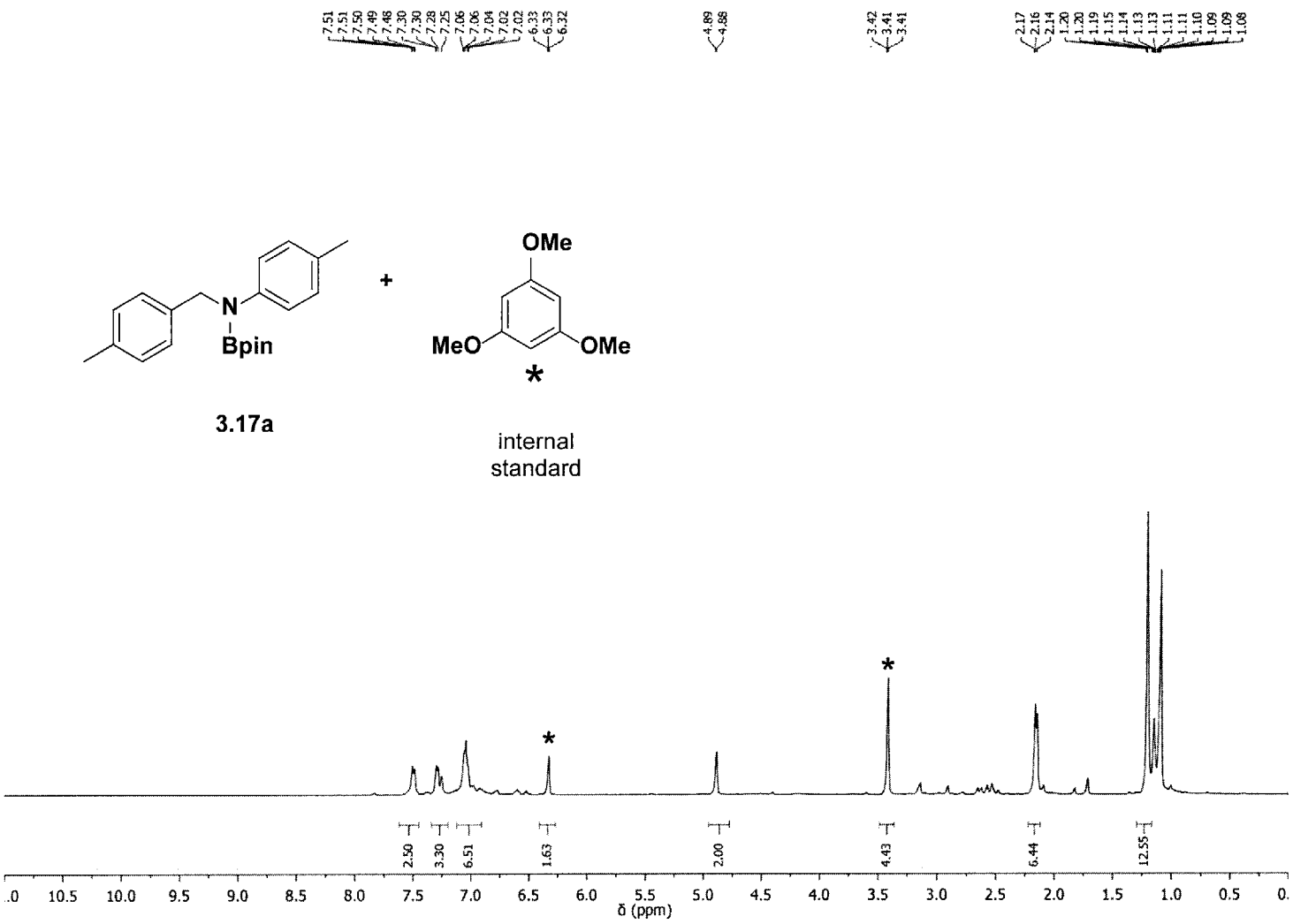

Figure B23. ^{1}H NMR of **3.17a.**

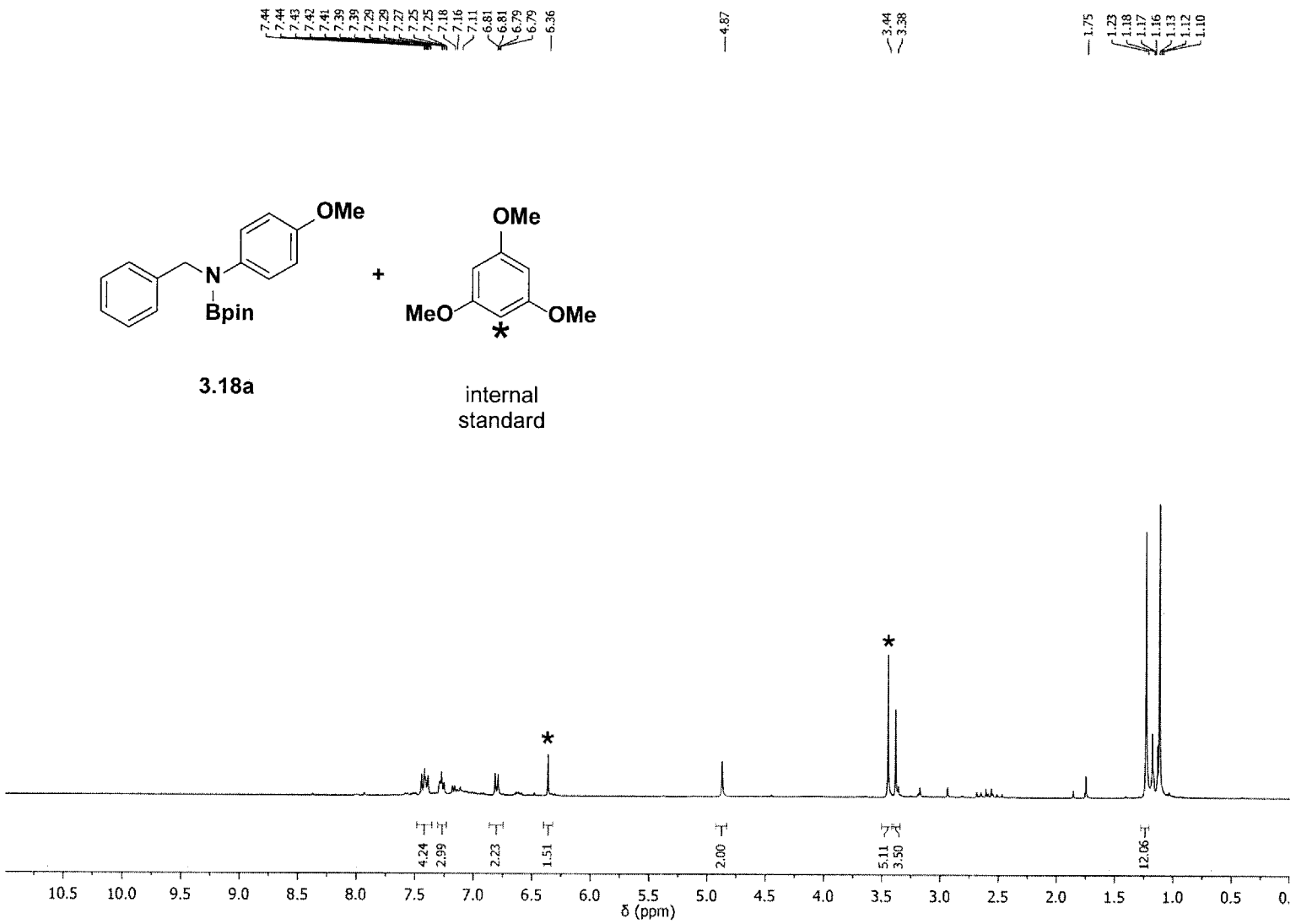

Figure B24. ^{1}H NMR of **3.18a.**

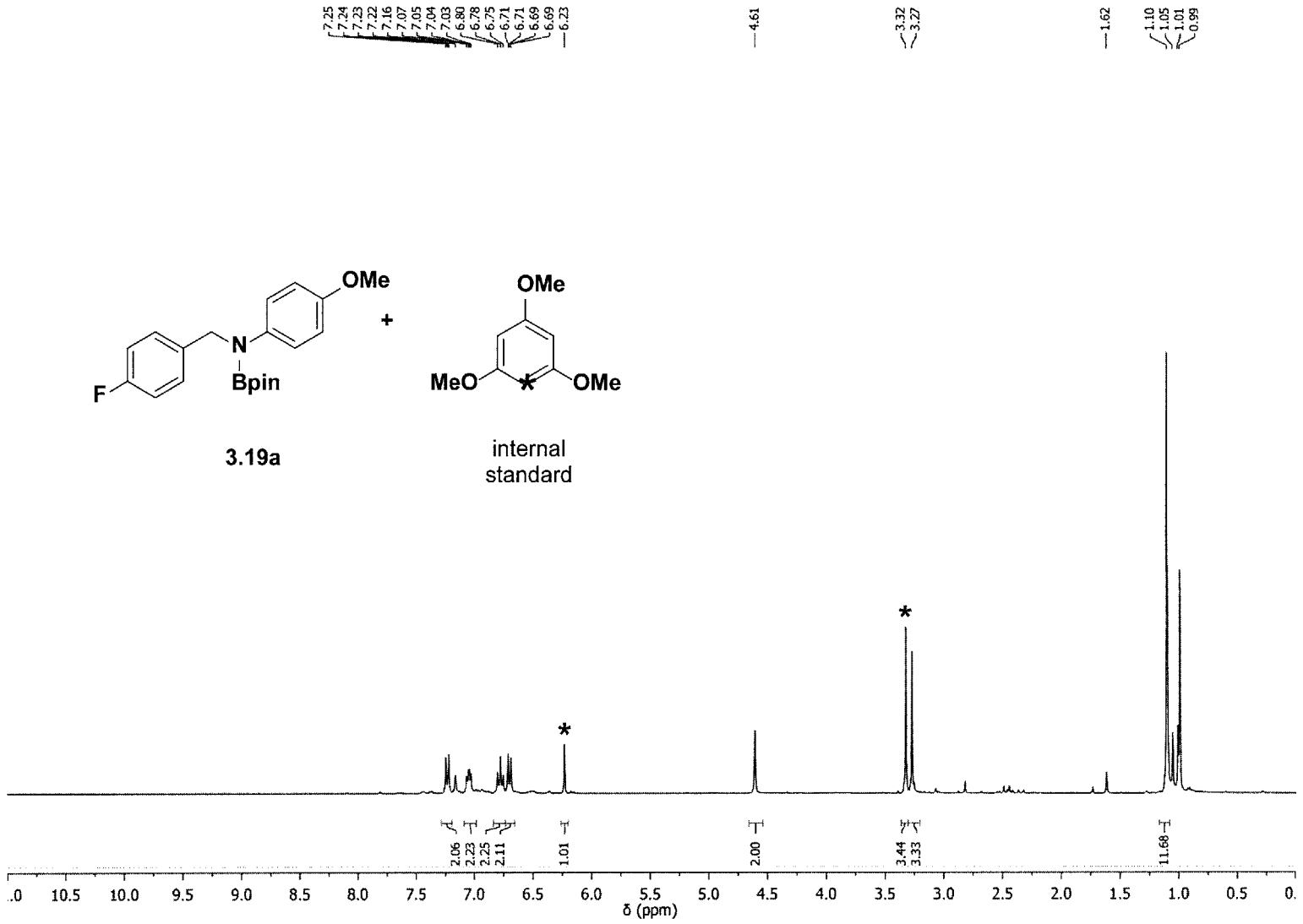

Figure B25. ^{1}H NMR of **3.19a.**

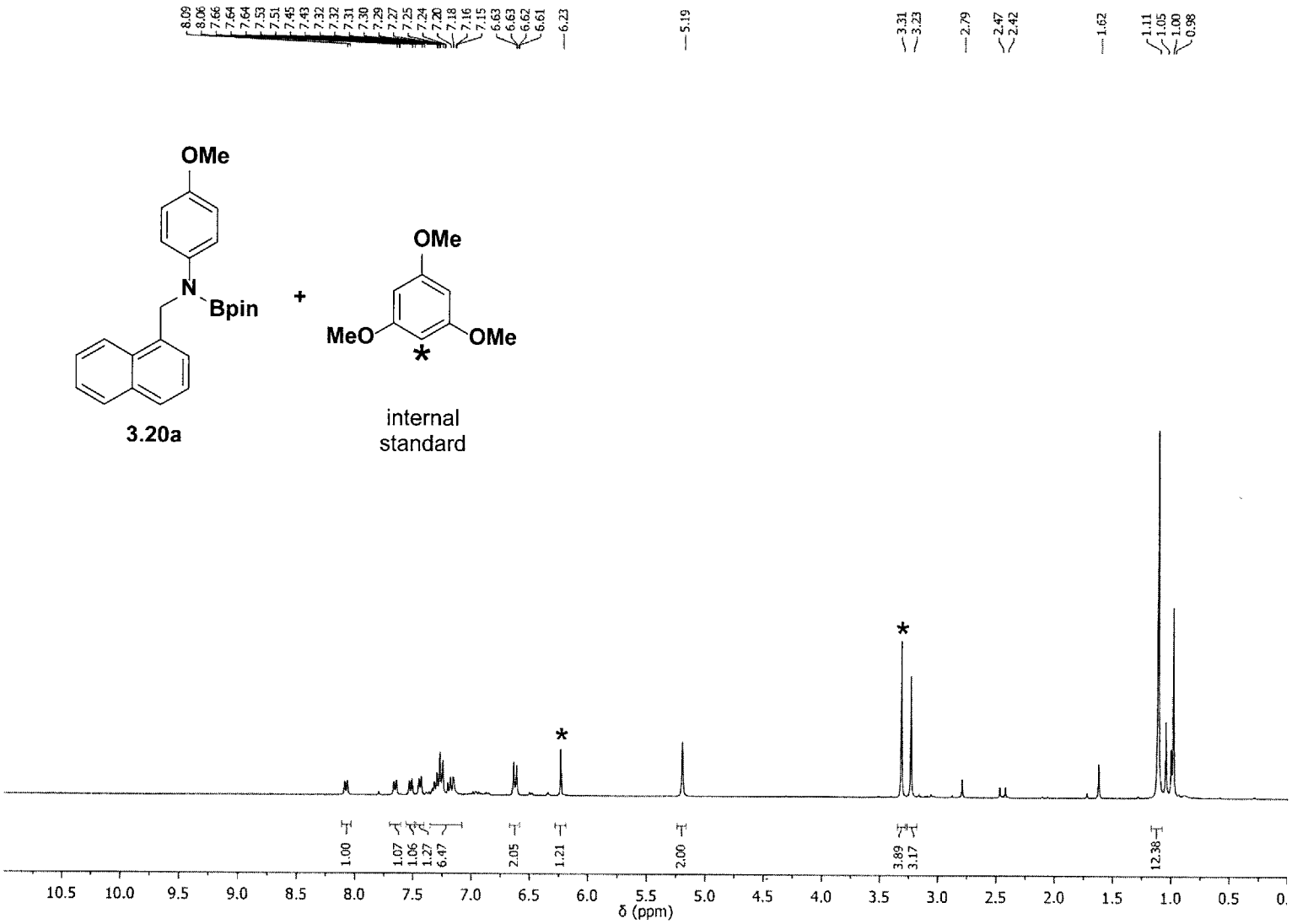

Figure B26. ^{1}H NMR of **3.20a.**

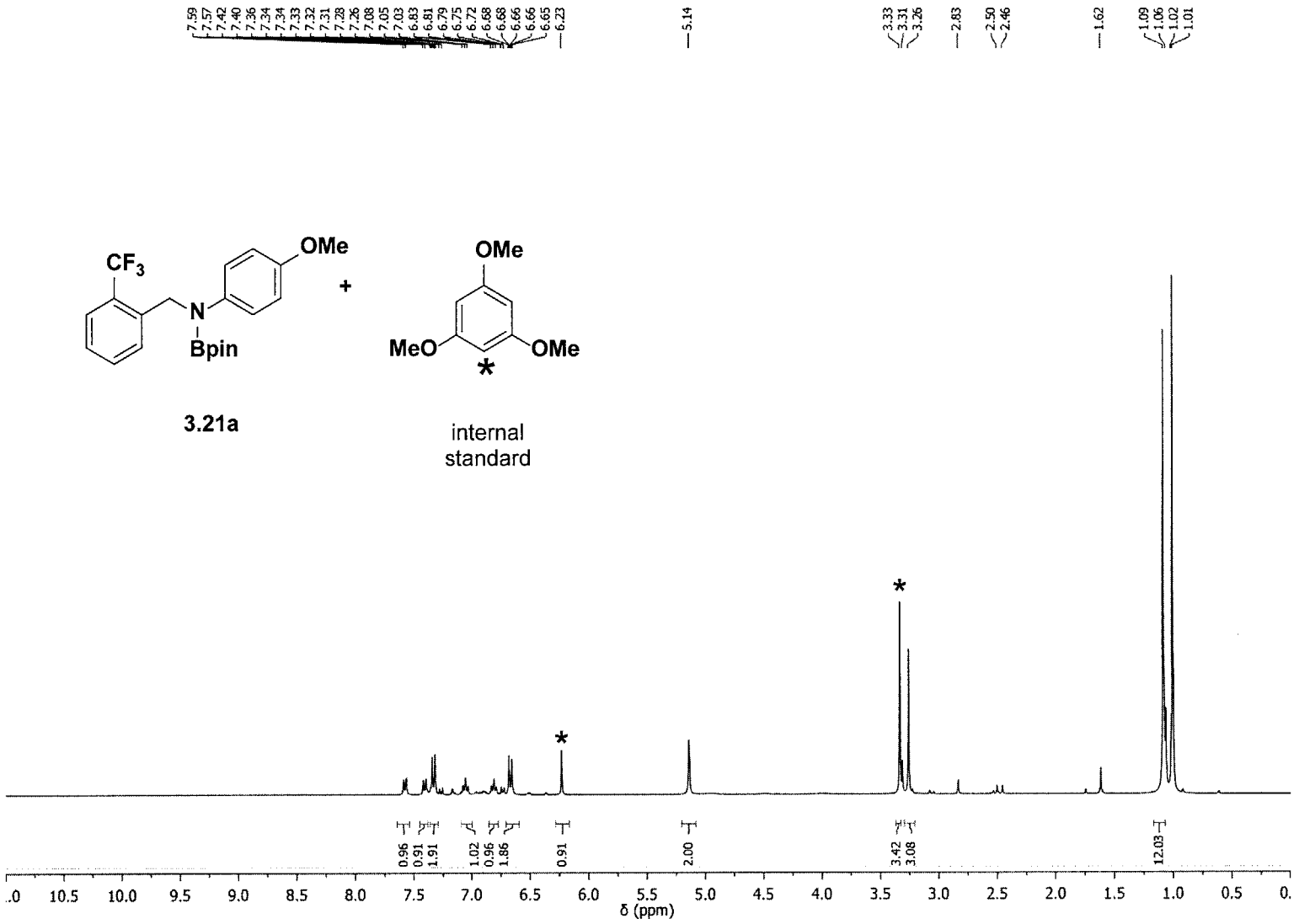

Figure B27. ^{1}H NMR of **3.21a**.

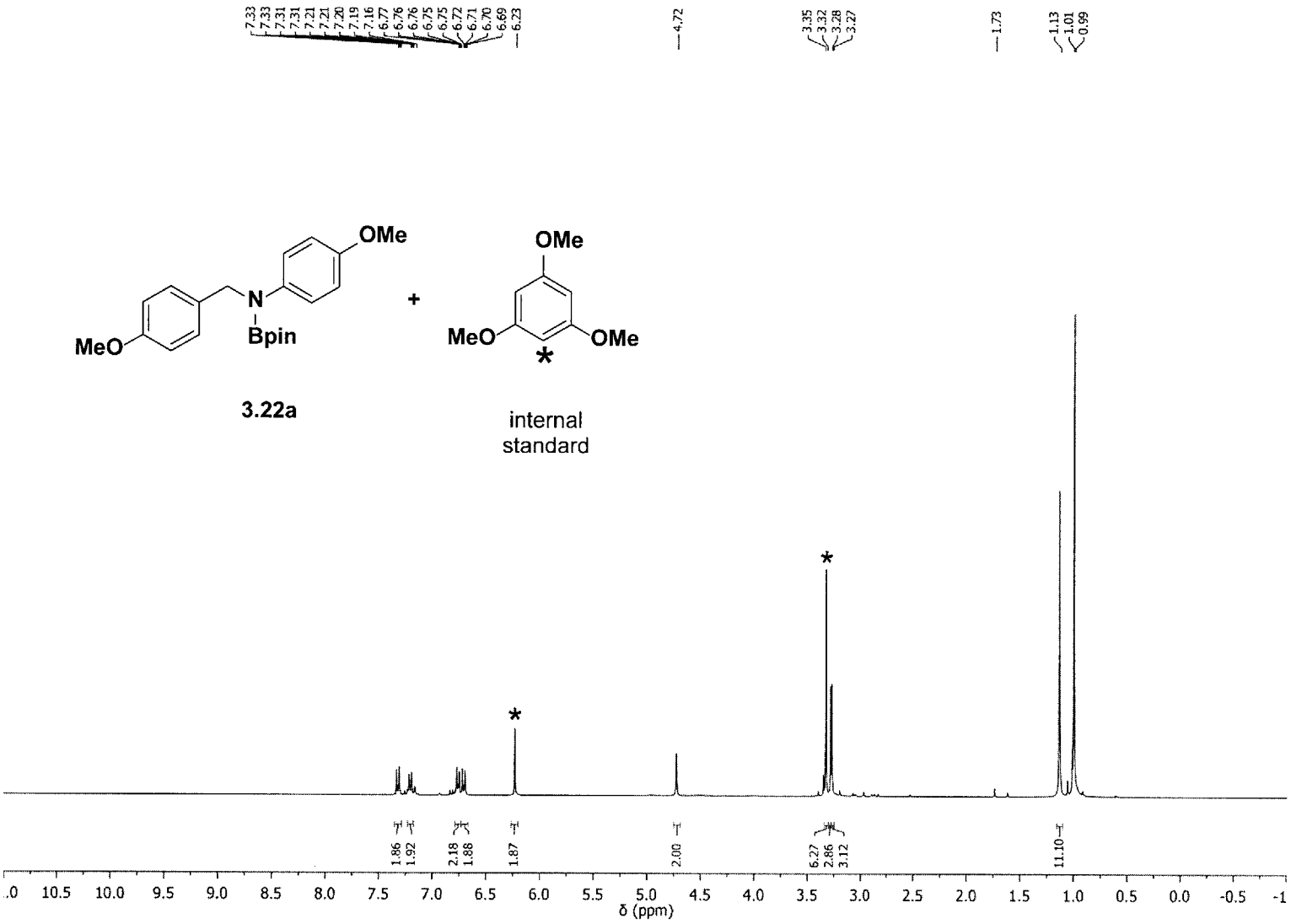

Figure B28. ^{1}H NMR of **3.22a.**

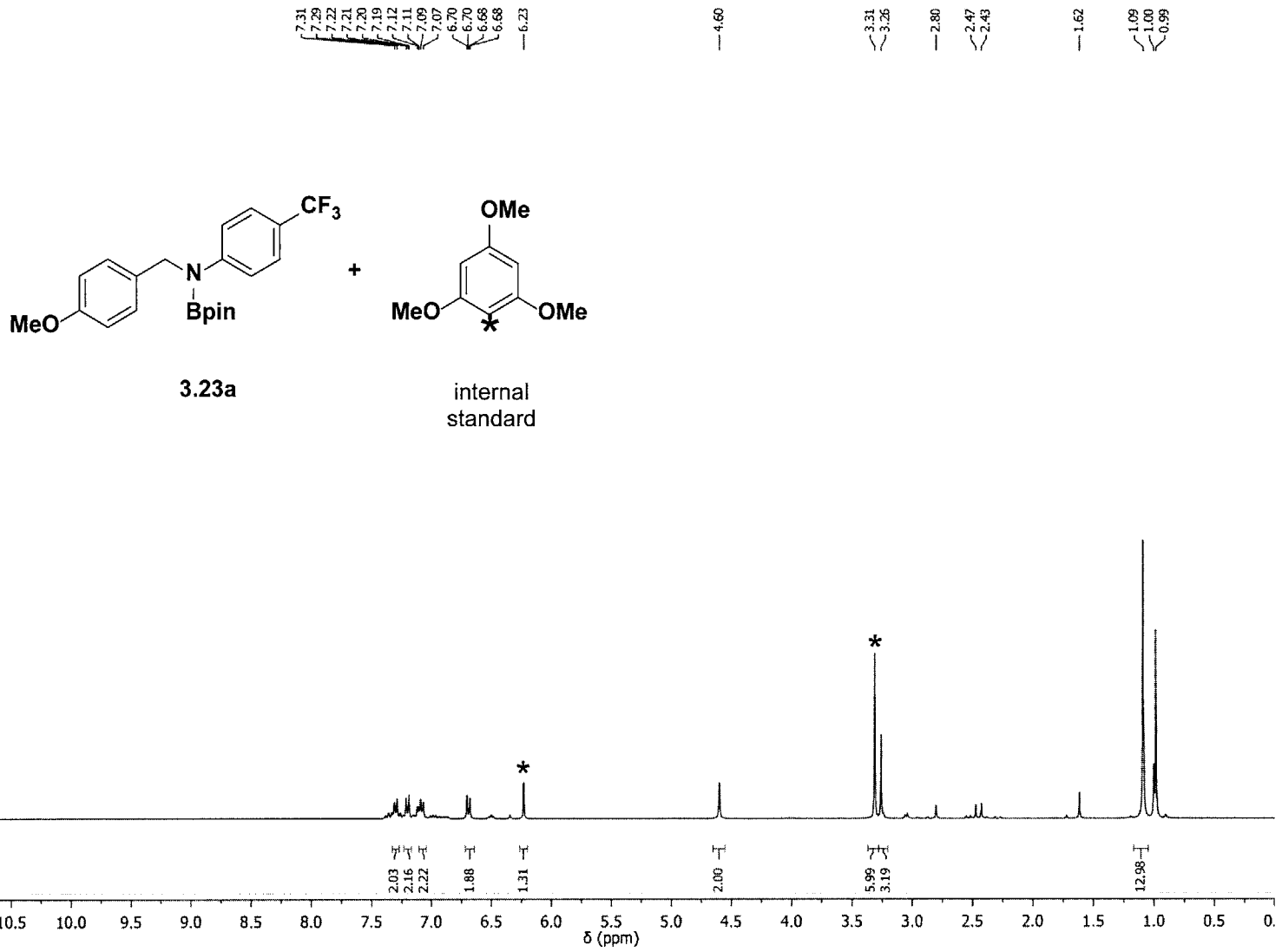

Figure B29. ^{1}H NMR of **3.23a.**

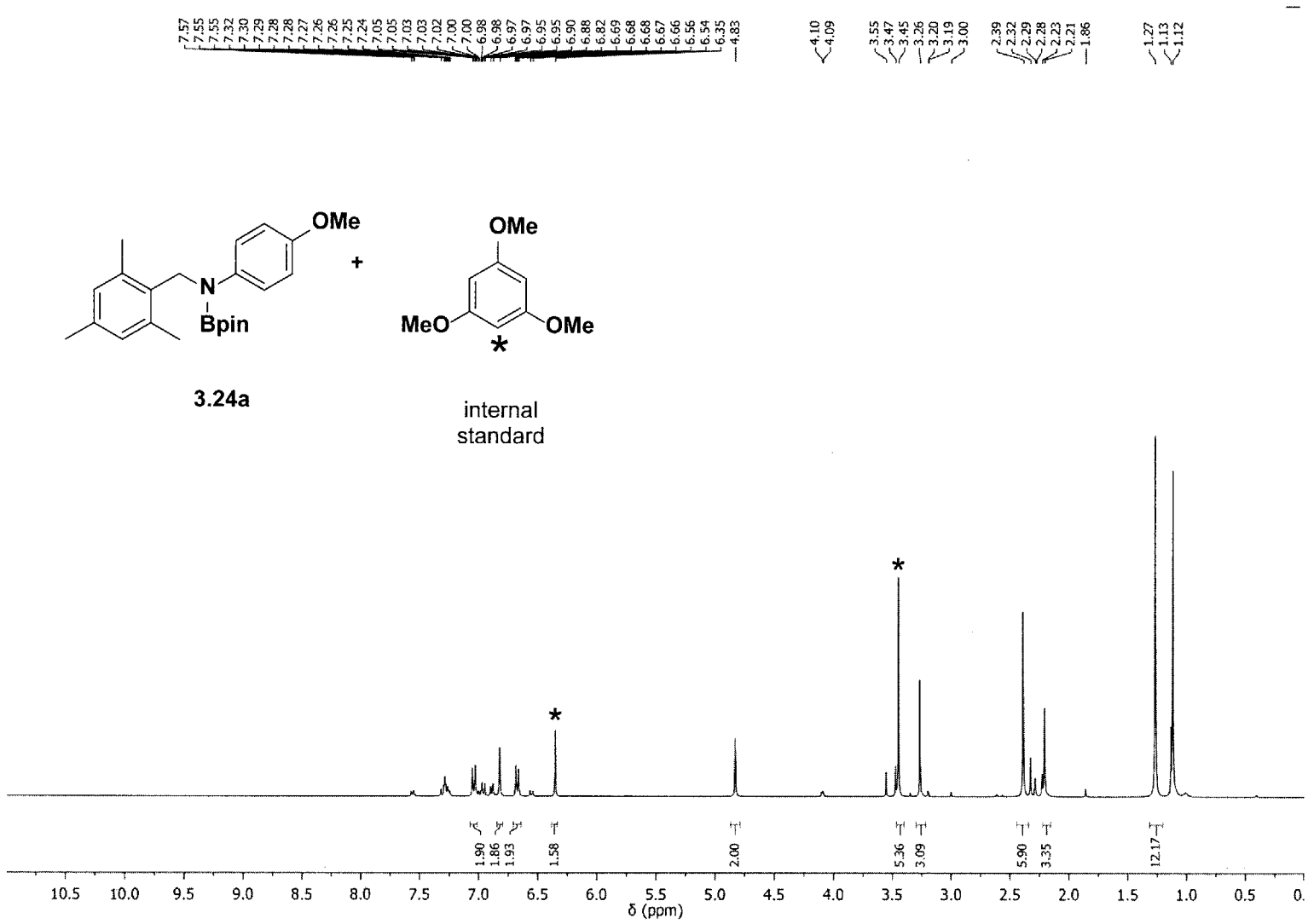

Figure B30. ^{1}H NMR of **3.24a.**

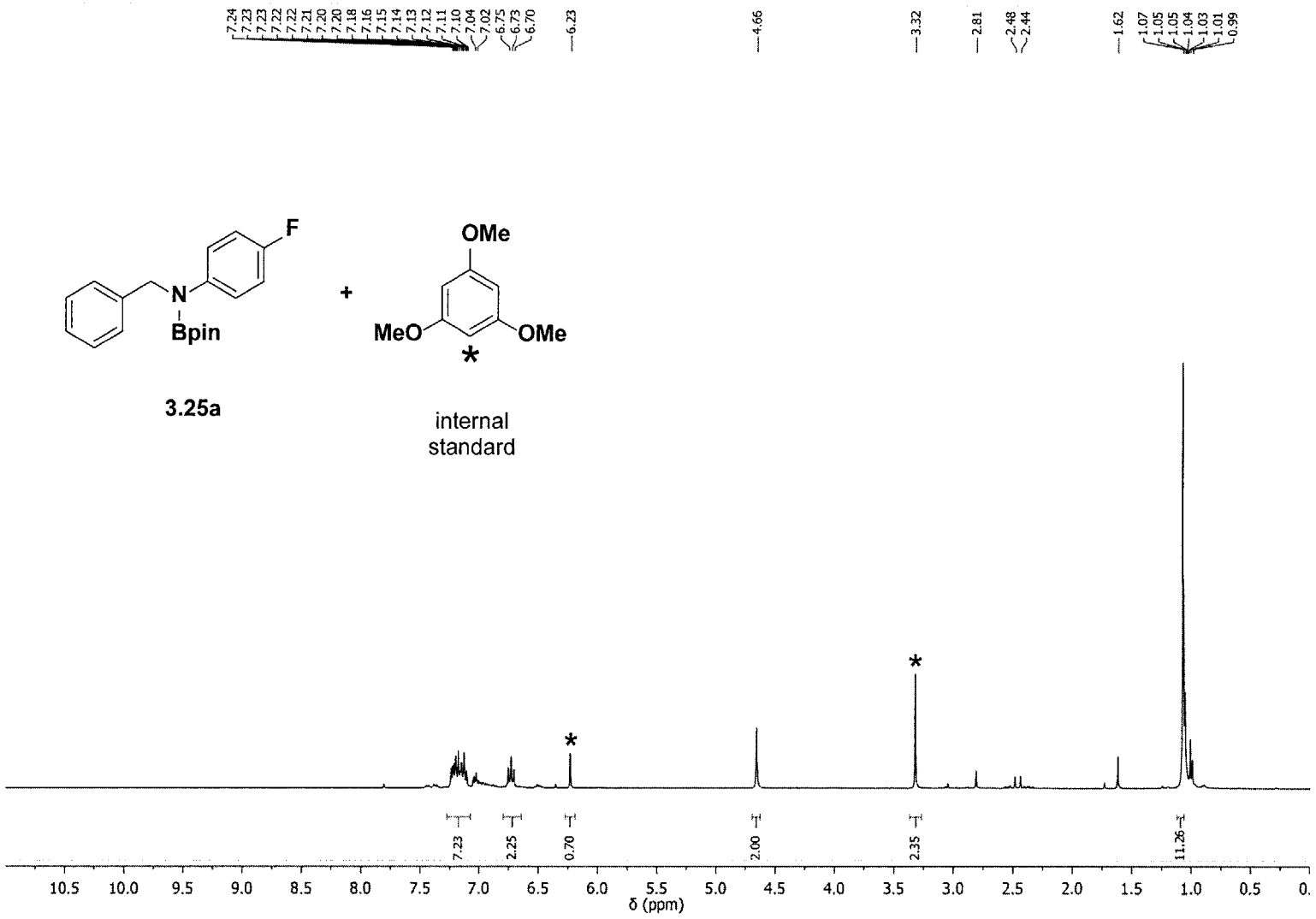

Figure B31. ^{1}H NMR of **3.25a**.

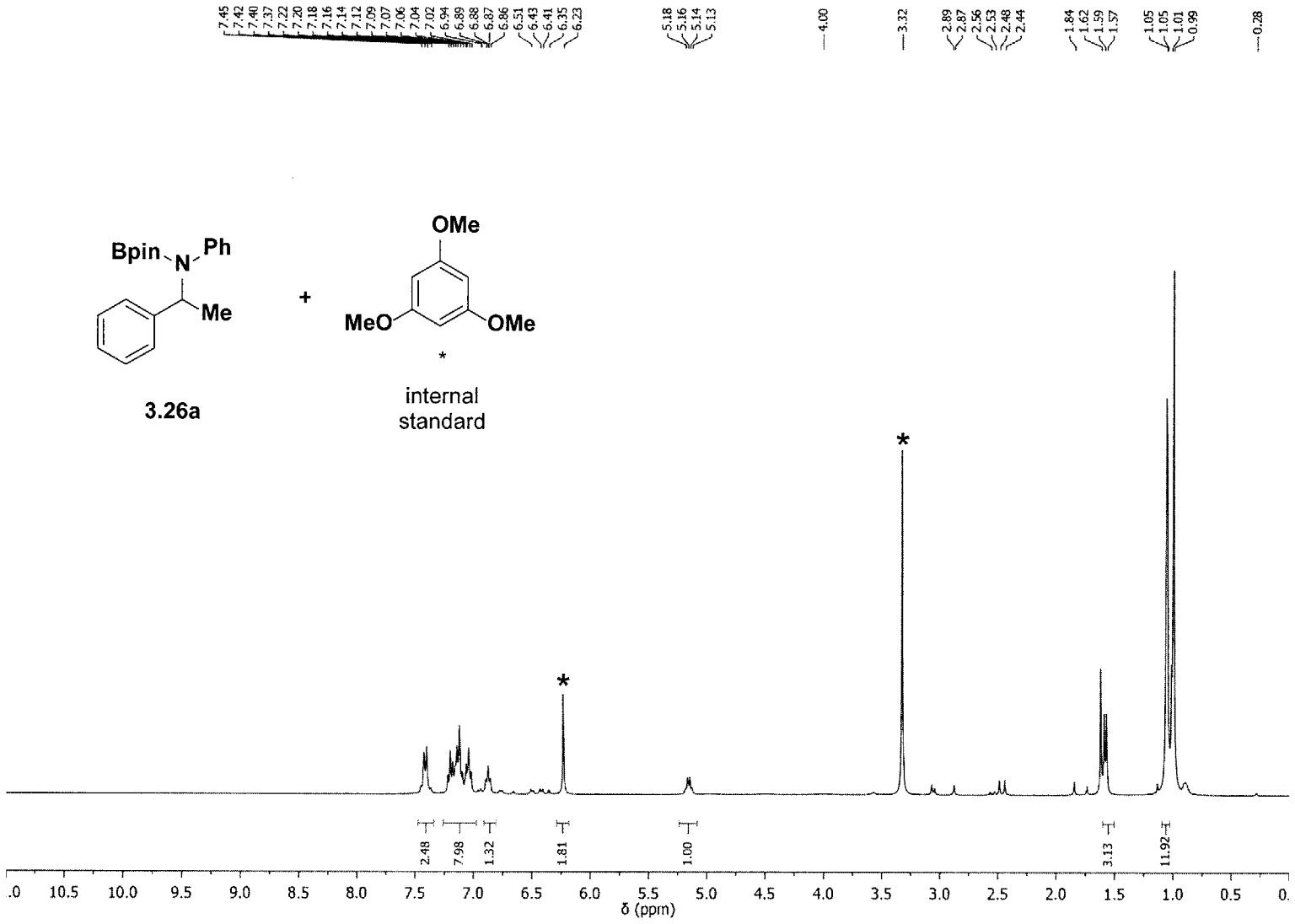

Figure B32. ^{1}H NMR of **3.26a.**

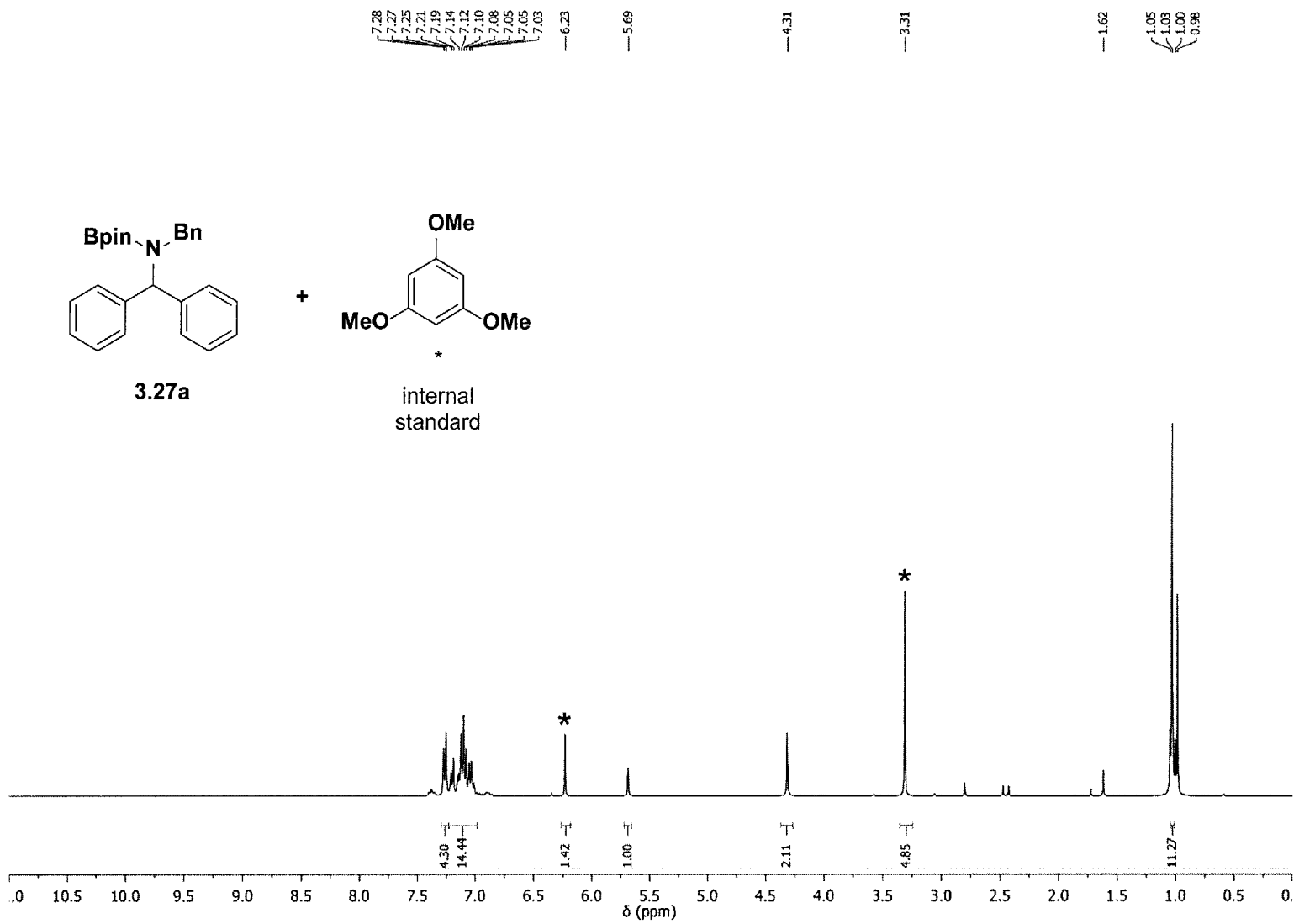

Figure B33. ^{1}H NMR of **3.27a.**

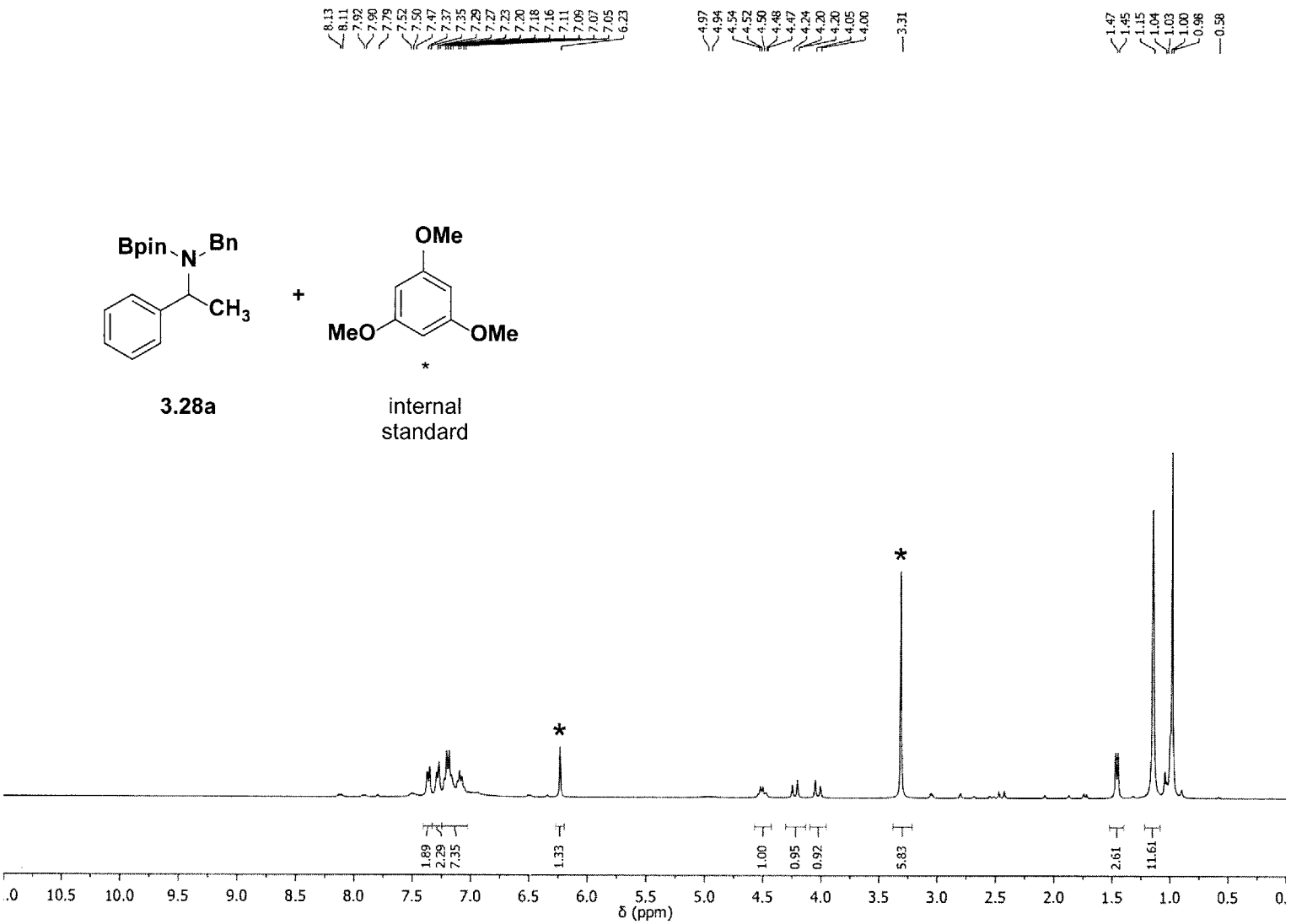

Figure B34. ^{1}H NMR of **3.28a.**

Appendix C

Supplemental Data for Chapters Four

Table of Contents

I. General Synthetic Procedure for Azides[1]

A mixture of amine (5 mmol) and $NaNO_2$ (5.5 mmol) were added to a cooled (−30 °C) acidic (5 mL of concentrated HCl and 5 mL of distilled H_2O) solution of $NaBF_4$ (10 mmol). A yellow precipitate was gradually formed after several minutes of stirring. The mixture was then stirred at −30 °C for additional 30 min. The resulting intermediate diazonium tetrafluoroborate salt was filtered quickly in air and washed with cold water. This yellow sticky powder was added to a cooled (0 °C) aqueous solution (10 mL) of NaN_3. After vigorous gas evolution, the orange mixture was stirred overnight at 25 °C. The product was extracted from the aqueous layer with diethyl ether and dried with $MgSO_4$. The solution was filtered, and the solvent was removed to give the crude azide product. The crude product was dissolved in 10 ml of hexane and further purified by passing through a plug of silica gel. Hexane was removed *in vacuo* from the collected solution to afford the pure azide product.

[1] Spencer, L. P.; Altwer, R.; Wei, P.; Gelmini, L.; Gauld, J.; Stephan, D. W. *Organometallics* **2003**, *22* , 3841.

II. Crystallographic Procedures and Data

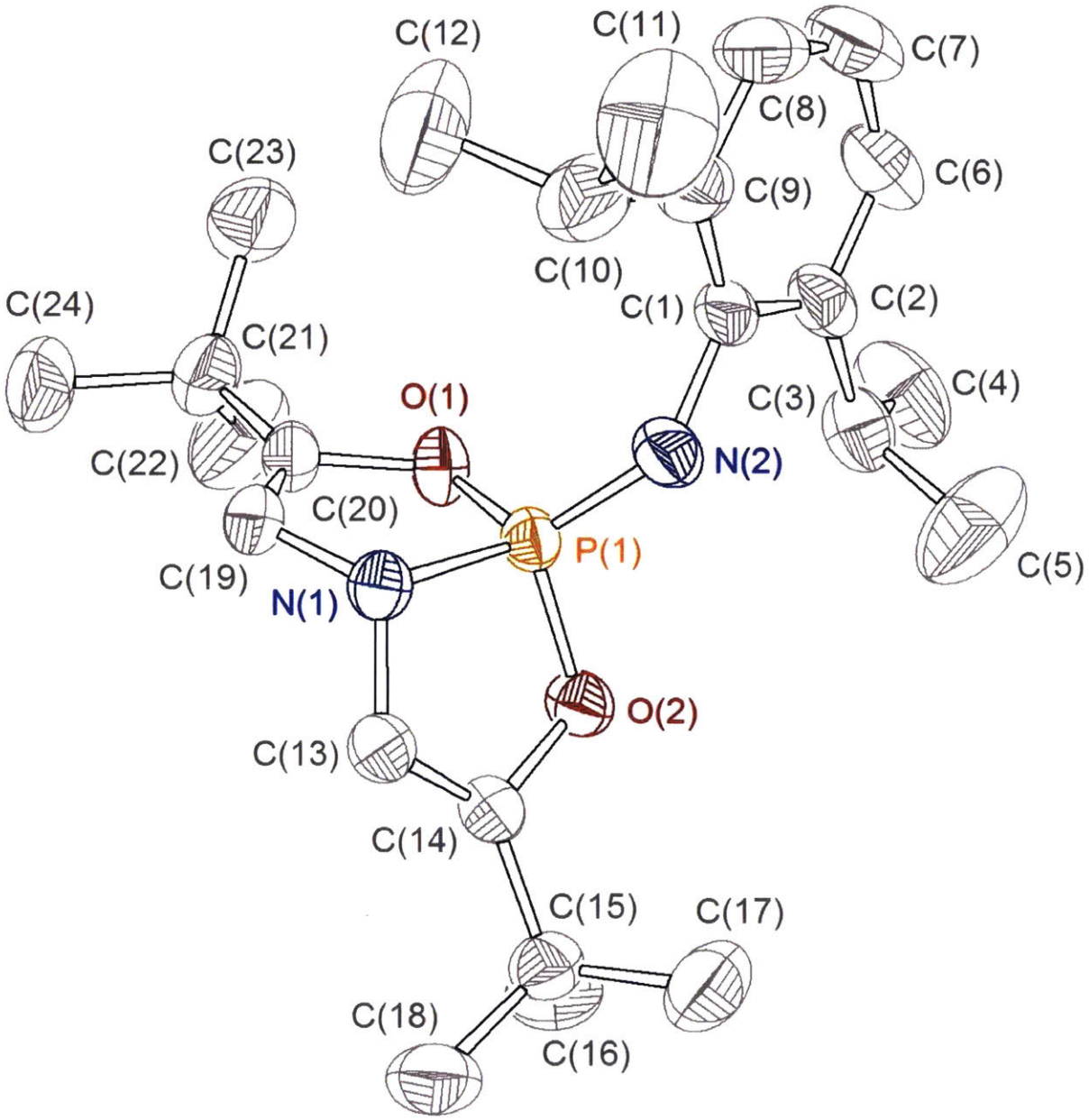

Table C1. Crystal data and structure refinement for 4.2.

Identification code	yzl18m
Empirical formula	$C_{25}H_{38}NO_2P$

Formula weight	415.53
Temperature/K	198(2)
Crystal system	monoclinic
Space group	C2/c
a/Å	19.931(8)
b/Å	12.616(8)
c/Å	21.565(12)
α/°	90.00
β/°	109.346(14)
γ/°	90.00
Volume/Å^3	5116(5)
Z	8
ρ_{calc}g/cm^3	1.079
μ/mm^{-1}	0.126
F(000)	1808.0
Crystal size/mm^3	0.2 × 0.15 × 0.12
Radiation	MoKα (λ = 0.71073)
2Θ range for data collection/°	3.88 to 56.76
Index ranges	-26 ≤ h ≤ 26, -16 ≤ k ≤ 11, -28 ≤ l ≤ 28
Reflections collected	18786
Independent reflections	6358 [R_{int} = 0.0309, R_{sigma} = 0.0263]
Data/restraints/parameters	6358/0/272
Goodness-of-fit on F^2	1.055
Final R indexes [I>=2σ (I)]	R_1 = 0.0579, wR_2 = 0.1718
Final R indexes [all data]	R_1 = 0.0667, wR_2 = 0.1819
Largest diff. peak/hole / e Å^{-3}	0.70/-0.69

Table C2. Fractional Atomic Coordinates (×10^4) and Equivalent Isotropic Displacement Parameters (Å^2×10^3) for 4.2. U_{eq} is defined as 1/3 of the trace of the orthogonalised U_{IJ} tensor.

Atom	*x*	*y*	*z*	U(eq)
C1	2364.0(9)	4646.3(12)	3038.1(7)	35.8(3)
C2	2821.3(9)	5049.4(13)	3629.6(8)	41.1(4)
C3	2537.0(11)	5695.5(15)	4014.6(9)	47.6(4)
C4	1747.2(12)	5933.9(18)	3794.6(11)	57.0(5)

C5	1543.3(17)	6749(3)	3247(2)	108.0(13)
C6	1466.6(18)	6236(3)	4346.7(18)	92.1(10)
C7	3000.5(14)	6127.2(19)	4586.9(11)	63.1(6)
C8	3721.2(15)	5950(2)	4776.7(11)	72.1(7)
C9	3994.1(12)	5326(2)	4394.2(11)	66.0(6)
C10	3557.8(11)	4869.7(16)	3811.4(10)	51.6(5)
C11	3866.1(13)	4198(2)	3388.4(14)	67.7(6)
C12	4476(2)	4752(3)	3247(2)	112.9(13)
C13	4092(2)	3105(3)	3684(2)	112.4(13)
C14	1512.9(9)	2714.9(14)	1738.0(8)	39.6(4)
C15	1013.9(9)	3421.0(13)	1724.3(8)	37.1(3)
C16	359(1)	3787.2(15)	1197.2(9)	43.6(4)
C17	-267.0(11)	3733(2)	1457.2(12)	61.4(6)
C18	459.3(14)	4927(2)	1005.5(14)	71.1(7)
C19	211.3(14)	3068(2)	595.8(11)	69.6(7)
C20	2175.8(9)	1734.4(14)	2738.9(8)	41.9(4)
C21	2067.5(9)	1857.9(13)	3303.8(9)	41.2(4)
C22	2139.0(12)	1123.4(16)	3871.6(11)	54.1(5)
C23	1467.4(17)	1185(3)	4058.4(18)	93.3(10)
C24	2775.8(17)	1462(2)	4459.1(11)	74.5(7)
C25	2271.5(19)	-7.8(18)	3666.9(14)	82.3(9)
N1	2082.8(7)	2687.2(11)	2354.0(7)	38.2(3)
O1	1871.9(7)	2915.0(9)	3408.3(6)	41.1(3)
O2	1155.9(6)	3977.3(10)	2323.0(6)	41.4(3)
P1	1919.6(2)	3662.7(3)	2822.85(19)	33.17(14)

Table C3. Anisotropic Displacement Parameters ($Å^2 \times 10^3$) for 4.2. The Anisotropic displacement factor exponent takes the form: $-2\pi^2[h^2a^{*2}U_{11}+2hka^*b^*U_{12}+\ldots]$.

Atom	U_{11}	U_{22}	U_{33}	U_{23}	U_{13}	U_{12}
C1	42.0(8)	28.8(7)	32.6(7)	0.6(6)	6.9(6)	-9.4(6)
C2	45.7(9)	32.4(8)	40.3(8)	5.2(6)	7.4(7)	-11.3(7)
C3	56.6(11)	39.7(9)	45.4(9)	-1.2(7)	15.6(8)	-18.2(8)
C4	59.8(12)	48.4(11)	69.3(13)	-6.7(10)	30.1(10)	-12.9(9)
C5	69.7(18)	105(2)	157(3)	61(3)	48(2)	26.0(17)
C6	91(2)	89(2)	115(2)	-42.9(18)	59(2)	-23.9(16)
C7	82.0(16)	59.1(13)	48.1(10)	-11.5(9)	21.4(10)	-31.4(12)
C8	78.7(16)	78.6(16)	43.8(10)	2.5(11)	0.2(10)	-37.4(14)

C9	50.5(11)	74.6(15)	55.7(12)	20.1(11)	-5.5(9)	-16.1(11)
C10	47.3(10)	46.2(10)	52.4(10)	13.9(8)	4.7(8)	-5.2(8)
C11	49.2(11)	67.0(15)	82.7(16)	9.4(12)	16.2(11)	7.7(10)
C12	104(3)	103(3)	159(4)	14(3)	81(3)	1(2)
C13	113(3)	66.5(19)	164(4)	23(2)	54(3)	19.6(18)
C14	43.6(9)	39.7(8)	36.0(8)	-4.4(6)	13.8(6)	2.8(7)
C15	36.8(8)	36.6(8)	38.1(8)	-4.2(6)	12.7(6)	-2.4(6)
C16	38.8(9)	46(1)	43.5(9)	0.5(7)	10.2(7)	4.2(7)
C17	36.1(9)	82.8(16)	61.6(12)	2.2(11)	11.3(8)	1.3(9)
C18	64.1(14)	57.4(13)	83.6(16)	22.3(12)	13.6(12)	6.6(11)
C19	66.5(14)	81.2(17)	46.7(11)	-11.7(11)	-0.7(9)	16.1(12)
C20	44.8(9)	32.5(8)	45.3(9)	-3.4(7)	11.0(7)	8.3(7)
C21	43.5(9)	30.4(8)	48.7(9)	-1.8(7)	13.7(7)	1.8(6)
C22	67.2(13)	41(1)	56.4(11)	10.0(8)	23.7(10)	8.2(9)
C23	88(2)	87(2)	121(3)	50.8(19)	57.1(19)	10.6(16)
C24	96(2)	74.8(16)	47.4(11)	1.8(11)	16.0(12)	17.3(14)
C25	127(2)	38.9(11)	67.9(15)	8.9(10)	15.1(15)	14.6(13)
N1	37.6(7)	37.1(7)	40.2(7)	-5.0(6)	13.6(5)	5.0(6)
O1	50.8(7)	31.2(6)	48.0(6)	-2.4(5)	25.6(5)	1.2(5)
O2	34.2(6)	41.7(6)	45.7(6)	-12.2(5)	9.8(5)	5.3(5)
P1	32.4(2)	29.4(2)	38.1(2)	-3.88(14)	12.11(16)	-0.54(14)

Table C4. Bond Lengths for 4.2

Atom	Atom	Length/Å	Atom	Atom	Length/Å
C1	C2	1.395(2)	C15	C16	1.492(2)
C1	P1	1.5058(17)	C15	O2	1.413(2)
C2	C3	1.409(3)	C16	C17	1.529(3)
C2	C10	1.406(3)	C16	C18	1.527(3)
C3	C4	1.516(3)	C16	C19	1.529(3)
C3	C7	1.385(3)	C20	C21	1.315(3)
C4	C5	1.516(4)	C20	N1	1.437(2)
C4	C6	1.522(3)	C21	C22	1.504(3)
C7	C8	1.375(4)	C21	O1	1.428(2)
C8	C9	1.376(4)	C22	C23	1.522(4)
C9	C10	1.394(3)	C22	C24	1.528(4)
C10	C11	1.516(3)	C22	C25	1.542(3)

C11	C12	1.518(4)	N1	P1	1.6914(15)
C11	C13	1.524(4)	O1	P1	1.6038(14)
C14	C15	1.328(2)	O2	P1	1.5966(14)
C14	N1	1.434(2)			

Table C5. Bond Angles for 4.2.

Atom	Atom	Atom	Angle/°	Atom	Atom	Atom	Angle/°
C2	C1	P1	136.19(13)	C15	C16	C19	109.67(16)
C1	C2	C3	118.76(17)	C18	C16	C17	109.68(18)
C1	C2	C10	120.09(18)	C18	C16	C19	109.5(2)
C10	C2	C3	121.01(17)	C19	C16	C17	109.48(18)
C2	C3	C4	120.58(17)	C21	C20	N1	114.00(15)
C7	C3	C2	118.2(2)	C20	C21	C22	132.91(17)
C7	C3	C4	121.2(2)	C20	C21	O1	113.20(15)
C3	C4	C6	114.7(2)	O1	C21	C22	113.83(15)
C5	C4	C3	111.15(19)	C21	C22	C23	109.24(18)
C5	C4	C6	111.5(3)	C21	C22	C24	109.35(19)
C8	C7	C3	121.6(2)	C21	C22	C25	108.42(18)
C7	C8	C9	119.7(2)	C23	C22	C24	109.2(2)
C8	C9	C10	121.6(2)	C23	C22	C25	111.8(2)
C2	C10	C11	121.06(18)	C24	C22	C25	108.8(2)
C9	C10	C2	117.8(2)	C14	N1	C20	117.81(14)
C9	C10	C11	121.1(2)	C14	N1	P1	106.61(11)
C10	C11	C12	112.0(2)	C20	N1	P1	106.06(11)
C10	C11	C13	112.1(3)	C21	O1	P1	109.55(11)
C12	C11	C13	110.9(3)	C15	O2	P1	110.54(10)
C15	C14	N1	113.23(14)	C1	P1	N1	125.02(9)
C14	C15	C16	133.17(16)	C1	P1	O1	115.10(8)
C14	C15	O2	113.02(15)	C1	P1	O2	109.58(9)
O2	C15	C16	113.71(14)	O1	P1	N1	96.66(8)
C15	C16	C17	108.72(16)	O2	P1	N1	96.11(7)
C15	C16	C18	109.75(17)	O2	P1	O1	112.69(7)

Table C6. Torsion Angles for 4.2.

A	B	C	D	Angle/°	A	B	C	D	Angle/°

C1	C2	C3	C4	0.9(2)	C15	C14	N1	C20	114.88(17)
C1	C2	C3	C7	-177.34(17)	C15	C14	N1	P1	-4.06(18)
C1	C2	C10	C9	177.42(17)	C15	O2	P1	C1	123.93(12)
C1	C2	C10	C11	-2.8(3)	C15	O2	P1	N1	-6.66(12)
C2	C1	P1	N1	-110.8(2)	C15	O2	P1	O1	-106.51(12)
C2	C1	P1	O1	8.2(2)	C16	C15	O2	P1	-171.49(12)
C2	C1	P1	O2	136.5(2)	C20	C21	C22	C23	-131.2(3)
C2	C3	C4	C5	-76.0(3)	C20	C21	C22	C24	109.4(3)
C2	C3	C4	C6	156.4(2)	C20	C21	C22	C25	-9.1(3)
C2	C3	C7	C8	0.9(3)	C20	C21	O1	P1	-5.53(18)
C2	C10	C11	C12	129.8(3)	C20	N1	P1	C1	120.73(13)
C2	C10	C11	C13	-104.9(3)	C20	N1	P1	O1	-6.38(12)
C3	C2	C10	C9	1.8(3)	C20	N1	P1	O2	-120.16(11)
C3	C2	C10	C11	-178.39(18)	C21	C20	N1	C14	-115.12(17)
C3	C7	C8	C9	-0.3(4)	C21	C20	N1	P1	4.11(18)
C4	C3	C7	C8	-177.3(2)	C21	O1	P1	C1	-126.94(13)
C7	C3	C4	C5	102.2(3)	C21	O1	P1	N1	6.91(12)
C7	C3	C4	C6	-25.4(3)	C21	O1	P1	O2	106.41(11)
C7	C8	C9	C10	0.5(4)	C22	C21	O1	P1	171.98(14)
C8	C9	C10	C2	-1.2(3)	N1	C14	C15	C16	175.39(18)
C8	C9	C10	C11	179.0(2)	N1	C14	C15	O2	-0.5(2)
C9	C10	C11	C12	-50.5(3)	N1	C20	C21	C22	-176.19(19)
C9	C10	C11	C13	74.9(3)	N1	C20	C21	O1	0.7(2)
C10	C2	C3	C4	176.58(17)	O1	C21	C22	C23	51.9(3)
C10	C2	C3	C7	-1.7(3)	O1	C21	C22	C24	-67.5(2)
C14	C15	C16	C17	129.4(2)	O1	C21	C22	C25	174.05(19)
C14	C15	C16	C18	-110.6(2)	O2	C15	C16	C17	-54.7(2)
C14	C15	C16	C19	9.7(3)	O2	C15	C16	C18	65.3(2)
C14	C15	O2	P1	5.27(18)	O2	C15	C16	C19	-174.37(17)
C14	N1	P1	C1	-112.94(13)	P1	C1	C2	C3	-90.1(2)
C14	N1	P1	O1	119.95(12)	P1	C1	C2	C10	94.2(2)
C14	N1	P1	O2	6.18(12)					

Table C7. Hydrogen Atom Coordinates (Å×10^4) and Isotropic Displacement Parameters (Å^2×10^3) for 4.2.

Atom	*x*	*y*	*z*	U(eq)
H1	2323	5100	2688	43

H4	1504	5276	3604	68
H5A	1801	7393	3399	162
H5B	1042	6886	3118	162
H5C	1658	6482	2877	162
H6A	1565	5675	4665	138
H6B	962	6349	4170	138
H6C	1695	6875	4554	138
H7	2820	6547	4849	76
H8	4023	6251	5162	86
H9	4482	5206	4528	79
H11	3488	4093	2966	81
H12A	4331	5453	3084	169
H12B	4607	4357	2925	169
H12C	4877	4798	3645	169
H13A	4434	3179	4116	169
H13B	4299	2716	3411	169
H13C	3683	2730	3712	169
H14	1495	2282	1384	48
H17A	-301	3031	1616	92
H17B	-699	3903	1110	92
H17C	-194	4232	1810	92
H18A	533	5382	1379	107
H18B	43	5152	657	107
H18C	865	4963	860	107
H19A	616	3069	449	104
H19B	-197	3326	250	104
H19C	122	2360	711	104
H20	2301	1088	2601	50
H23A	1391	1904	4164	140
H23B	1519	741	4433	140
H23C	1068	949	3696	140
H24A	3207	1334	4365	112
H24B	2782	1062	4840	112
H24C	2739	2204	4542	112
H25A	1867	-237	3307	123
H25B	2343	-481	4032	123
H25C	2686	-9	3534	123

Experimental

Single crystals of $C_{25}H_{38}NO_2P$ [**4.2**] were [yzl18m]. A suitable crystal was selected and [] on a CCD area detector diffractometer. The crystal was kept at 198(2) K during data collection. Using Olex2 [1], the structure was solved with the ShelXS-1997 [2] structure solution program using Direct Methods and refined with the XL [3] refinement package using Least Squares minimisation.

Crystal Data for $C_{25}H_{38}NO_2P$ (M =415.53 g/mol): monoclinic, space group C2/c (no. 15), a = 19.931(8) Å, b = 12.616(8) Å, c = 21.565(12) Å, β = 109.346(14)°, V = 5116(5) Å^3, Z = 8, T = 198(2) K, μ(MoKα) = 0.126 mm^{-1}, *Dcalc* = 1.079 g/cm^3, 18786 reflections measured (3.88° ≤ 2Θ ≤ 56.76°), 6358 unique (R_{int} = 0.0309, R_{sigma} = 0.0263) which were used in all calculations. The final R_1 was 0.0579 (>2sigma(I)) and wR_2 was 0.1819 (all data).

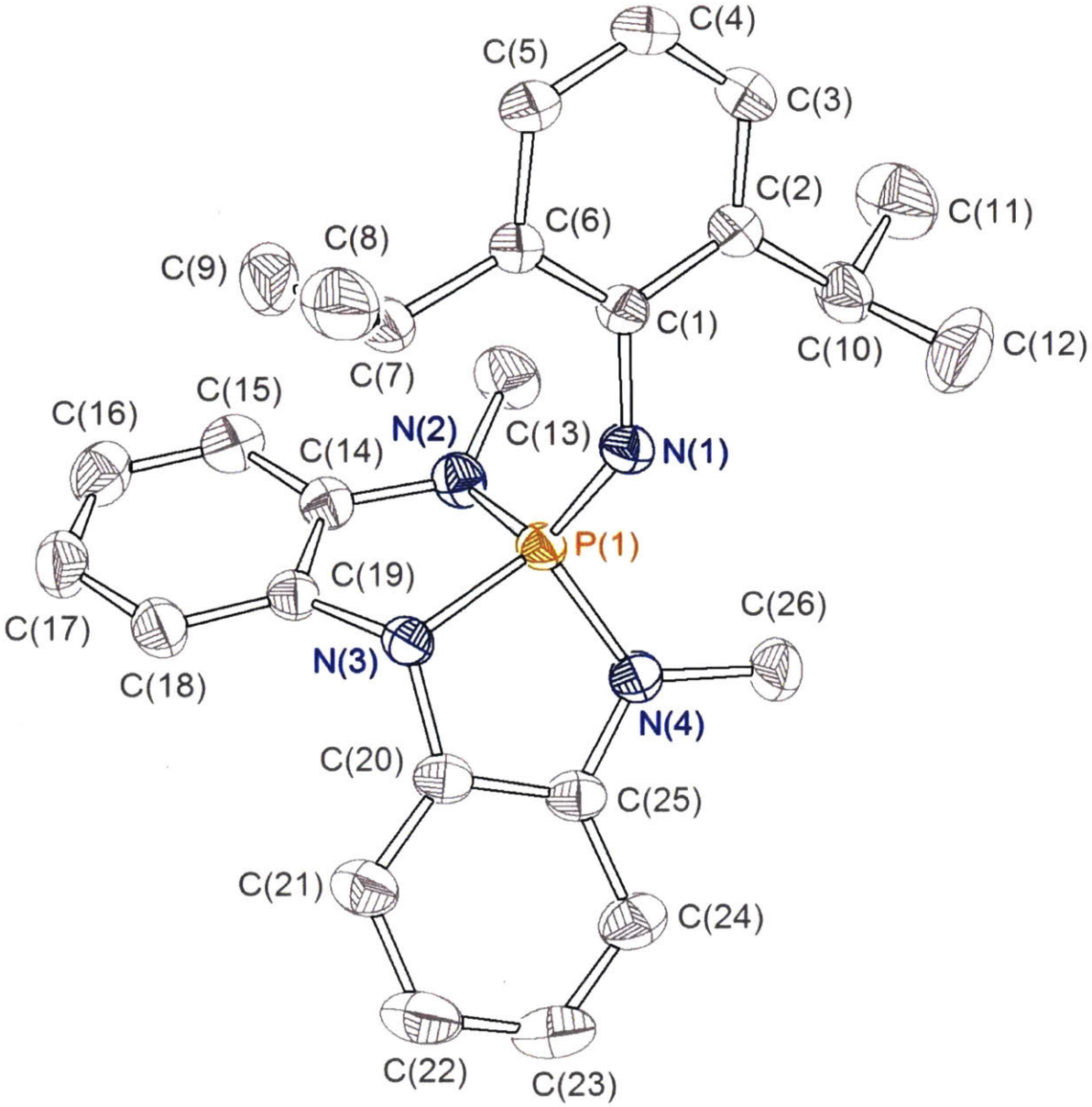

Table C8. Crystal data and structure refinement for 4.4.	
Identification code	yzl19s
Empirical formula	$C_{26}H_{31}N_4P$
Formula weight	430.52
Temperature/K	223.15
Crystal system	monoclinic
Space group	$P2_1/n$

a/Å	12.8565(18)
b/Å	9.4531(13)
c/Å	19.152(3)
α/°	90.00
β/°	96.382(4)
γ/°	90.00
Volume/Å^3	2313.2(6)
Z	4
ρ_{calc}g/cm^3	1.236
μ/mm^{-1}	0.140
F(000)	920.0
Crystal size/mm^3	0.22 × 0.2 × 0.16
Radiation	MoKα (λ = 0.71073)
2Θ range for data collection/°	4.04 to 56.6
Index ranges	$-11 \leq h \leq 17$, $-12 \leq k \leq 12$, $-25 \leq l \leq 21$
Reflections collected	15190
Independent reflections	5662 [R_{int} = 0.0172, R_{sigma} = 0.0208]
Data/restraints/parameters	5662/0/286
Goodness-of-fit on F^2	1.035
Final R indexes [I>=2σ (I)]	R_1 = 0.0432, wR_2 = 0.1188
Final R indexes [all data]	R_1 = 0.0489, wR_2 = 0.1248
Largest diff. peak/hole / e Å^{-3}	0.29/-0.35

Table C9. Fractional Atomic Coordinates (×10^4) and Equivalent Isotropic Displacement Parameters (Å^2×10^3) for 4.4. U_{eq} is defined as 1/3 of of the trace of the orthogonalised U_{IJ} tensor.

Atom	*x*	*y*	*z*	U(eq)
C1	6466.9(9)	8157.5(13)	1254.6(6)	27.3(2)
C2	5609.3(10)	9024.5(13)	1386.5(7)	31.6(3)
C3	4596.1(10)	8532.6(16)	1218.1(8)	37.6(3)
C4	4401.9(11)	7219.7(17)	916.6(8)	41.2(3)
C5	5235.7(11)	6394.2(16)	770.3(8)	39.2(3)
C6	6272.5(10)	6833.6(14)	929.7(7)	32.0(3)
C7	7141.9(11)	5881.7(15)	727.7(9)	43.1(4)
C8	7021.8(14)	4343.5(18)	943.5(12)	58.3(5)

C9	7194.5(14)	5971(2)	-68.6(11)	58.7(5)
C10	5795.7(12)	10458.2(16)	1729.2(9)	42.7(3)
C11	4989.3(16)	11573.2(19)	1460.5(13)	66.2(5)
C12	5870.0(19)	10311(2)	2522.9(10)	70.8(6)
C13	7488.2(13)	10474.5(17)	101.8(9)	46.1(4)
C14	8900.6(10)	8741.1(13)	-47.8(7)	30.3(3)
C15	8786.8(12)	8724.7(15)	-773.2(7)	38.5(3)
C16	9357.8(13)	7737.6(17)	-1112.2(8)	43.9(3)
C17	10032.3(13)	6806.4(17)	-740.1(8)	44.7(4)
C18	10144.7(11)	6815.0(15)	-7.2(8)	37.3(3)
C19	9575.4(10)	7779.0(13)	332.7(6)	28.2(2)
C20	10398.3(10)	8154.5(13)	1563.4(7)	29.7(3)
C21	11336.8(11)	7434.4(16)	1642.9(8)	41.1(3)
C22	12104.2(12)	7863.1(19)	2173.3(10)	52.9(4)
C23	11917.6(13)	8958.8(19)	2614.7(10)	52.2(4)
C24	10969.1(12)	9683.4(16)	2541.8(8)	41.2(3)
C25	10216.3(10)	9287.9(14)	2006.1(7)	30.9(3)
C26	8822.7(13)	10981.0(17)	2268.9(9)	46.1(4)
N1	7473.3(8)	8610.0(11)	1517.6(6)	30.4(2)
N2	8350.2(9)	9573.5(11)	392.8(6)	32.6(2)
N3	9512.5(8)	7903.9(11)	1065.0(5)	27.3(2)
N4	9225.5(8)	9888.5(11)	1835.7(6)	31.8(2)
P1	8496.5(2)	8982.8(3)	1220.95(16)	25.94(10)

Table C10. Anisotropic Displacement Parameters ($Å^2 \times 10^3$) for 4.4. The Anisotropic displacement factor exponent takes the form: $-2\pi^2[h^2a^{*2}U_{11}+2hka^*b^*U_{12}+\ldots]$.

Atom	U_{11}	U_{22}	U_{33}	U_{23}	U_{13}	U_{12}
C1	24.3(6)	30.8(6)	27.1(6)	-0.8(5)	3.3(4)	-1.1(5)
C2	28.0(6)	33.6(6)	33.2(6)	-2.7(5)	3.8(5)	1.9(5)
C3	25.6(6)	45.2(7)	42.1(7)	-2.8(6)	3.8(5)	5.4(5)
C4	24.3(6)	50.3(8)	47.9(8)	-7.1(6)	-1.6(6)	-3.3(6)
C5	29.1(7)	42.8(7)	44.7(8)	-13.0(6)	-0.3(6)	-4.9(6)
C6	25.8(6)	35.4(6)	34.7(6)	-7.2(5)	2.1(5)	-0.4(5)
C7	26.4(6)	38.4(7)	64.4(10)	-21.6(7)	4.8(6)	-3.4(5)
C8	45.1(9)	41.0(8)	87.2(14)	-14.9(9)	0.2(9)	5.9(7)
C9	44.7(9)	62.4(11)	73.6(12)	-32.6(9)	26.8(8)	-17.8(8)
C10	35.3(7)	37.0(7)	56.6(9)	-12.9(6)	8.8(6)	3.5(6)

C11	58.9(11)	39.2(8)	100.2(16)	-6.9(9)	7.7(11)	11.9(8)
C12	85.7(15)	69.4(13)	55.5(11)	-28.8(10)	-0.2(10)	9.0(11)
C13	44.6(8)	43.7(8)	49.0(8)	10.5(7)	1.2(7)	15.6(7)
C14	30.0(6)	27.7(5)	33.6(6)	1.9(5)	6.1(5)	-4.3(5)
C15	41.7(8)	40.1(7)	33.8(7)	6.8(5)	4.7(6)	-5.9(6)
C16	49.6(8)	52.1(8)	31.8(7)	-2.6(6)	12.4(6)	-11.4(7)
C17	45.5(8)	47.9(8)	43.5(8)	-12.2(6)	17.2(7)	-3.1(7)
C18	34.5(7)	35.3(6)	43.0(7)	-4.7(6)	8.3(6)	2.0(5)
C19	26.0(6)	28.0(5)	31.1(6)	-0.8(5)	5.0(5)	-3.6(4)
C20	26.1(6)	29.4(6)	33.1(6)	4.6(5)	1.3(5)	-3.1(5)
C21	33.0(7)	40.0(7)	49.3(8)	3.0(6)	-0.4(6)	4.7(6)
C22	32.3(7)	55.4(9)	67.3(11)	3.8(8)	-10.6(7)	5.0(7)
C23	38.2(8)	58.2(10)	55.9(10)	2.1(8)	-14.1(7)	-7.2(7)
C24	38.0(7)	43.4(8)	40.7(7)	-2.3(6)	-1.2(6)	-10.9(6)
C25	26.5(6)	31.9(6)	34.2(6)	3.7(5)	2.4(5)	-5.8(5)
C26	39.4(8)	48.1(8)	52.3(9)	-22.7(7)	11.6(7)	-6.1(6)
N1	23.8(5)	31.5(5)	36.1(5)	-5.4(4)	4.5(4)	-2.2(4)
N2	33.2(6)	29.3(5)	35.0(6)	3.5(4)	2.3(5)	5.7(4)
N3	23.3(5)	27.4(5)	31.1(5)	-0.3(4)	3.1(4)	0.9(4)
N4	27.1(5)	32.0(5)	36.4(6)	-7.6(4)	4.1(4)	-3.5(4)
P1	23.34(17)	23.84(16)	30.70(17)	-2.10(11)	3.28(12)	-0.64(11)

Table C11. Bond Lengths for 4.4.

Atom	Atom	Length/Å	Atom	Atom	Length/Å
C1	C2	1.4189(17)	C16	C17	1.377(2)
C1	C6	1.4076(17)	C17	C18	1.395(2)
C1	N1	1.4021(16)	C18	C19	1.3769(18)
C2	C3	1.3870(19)	C19	N3	1.4187(16)
C2	C10	1.5133(19)	C20	C21	1.3790(19)
C3	C4	1.380(2)	C20	C25	1.4019(18)
C4	C5	1.380(2)	C20	N3	1.4222(16)
C5	C6	1.3972(18)	C21	C22	1.395(2)
C6	C7	1.5181(18)	C22	C23	1.375(3)
C7	C8	1.524(2)	C23	C24	1.392(2)
C7	C9	1.536(3)	C24	C25	1.3815(19)
C10	C11	1.527(2)	C25	N4	1.3997(17)

C10	C12	1.519(3)	C26	N4	1.4555(17)
C13	N2	1.4584(17)	N1	P1	1.5309(11)
C14	C15	1.3809(19)	N2	P1	1.6723(12)
C14	C19	1.4037(18)	N3	P1	1.7095(10)
C14	N2	1.4016(16)	N4	P1	1.6591(11)
C15	C16	1.392(2)			

Table C12. Bond Angles for 4.4.

Atom	Atom	Atom	Angle/°	Atom	Atom	Atom	Angle/°
C6	C1	C2	119.27(11)	C18	C19	N3	127.90(12)
N1	C1	C2	117.65(11)	C21	C20	C25	120.89(12)
N1	C1	C6	122.79(11)	C21	C20	N3	128.12(13)
C1	C2	C10	120.39(12)	C25	C20	N3	110.98(11)
C3	C2	C1	119.55(12)	C20	C21	C22	118.43(15)
C3	C2	C10	120.03(12)	C23	C22	C21	120.59(15)
C4	C3	C2	121.36(13)	C22	C23	C24	121.32(15)
C5	C4	C3	119.03(13)	C25	C24	C23	118.36(15)
C4	C5	C6	122.10(13)	C24	C25	C20	120.37(13)
C1	C6	C7	122.68(11)	C24	C25	N4	127.42(13)
C5	C6	C1	118.63(12)	N4	C25	C20	112.20(11)
C5	C6	C7	118.66(12)	C1	N1	P1	137.19(10)
C6	C7	C8	113.38(13)	C13	N2	P1	123.92(10)
C6	C7	C9	109.60(14)	C14	N2	C13	120.73(12)
C8	C7	C9	109.78(14)	C14	N2	P1	111.86(9)
C2	C10	C11	113.77(14)	C19	N3	C20	123.23(10)
C2	C10	C12	109.97(14)	C19	N3	P1	110.55(8)
C12	C10	C11	111.42(15)	C20	N3	P1	110.72(8)
C15	C14	C19	120.36(12)	C25	N4	C26	121.82(12)
C15	C14	N2	127.43(13)	C25	N4	P1	112.56(9)
N2	C14	C19	112.06(11)	C26	N4	P1	124.19(10)
C14	C15	C16	118.32(14)	N1	P1	N2	114.72(6)
C17	C16	C15	121.43(13)	N1	P1	N3	129.22(6)
C16	C17	C18	120.38(14)	N1	P1	N4	107.24(6)
C19	C18	C17	118.59(14)	N2	P1	N3	92.35(5)
C14	C19	N3	111.06(11)	N4	P1	N2	119.73(6)
C18	C19	C14	120.91(12)	N4	P1	N3	92.84(5)

Table C13. Torsion Angles for 4.4.

A	B	C	D	Angle/°	A	B	C	D	Angle/°
C1	C2	C3	C4	-0.7(2)	C19	C14	C15	C16	-0.16(19)
C1	C2	C10	C11	145.00(15)	C19	C14	N2	C13	-169.95(12)
C1	C2	C10	C12	-89.22(17)	C19	C14	N2	P1	-10.24(14)
C1	C6	C7	C8	133.57(15)	C19	N3	P1	N1	111.98(9)
C1	C6	C7	C9	-103.39(15)	C19	N3	P1	N2	-13.03(9)
C1	N1	P1	N2	27.48(16)	C19	N3	P1	N4	-132.96(8)
C1	N1	P1	N3	-88.25(15)	C20	C21	C22	C23	1.4(3)
C1	N1	P1	N4	163.08(13)	C20	C25	N4	C26	173.44(12)
C2	C1	C6	C5	-2.28(19)	C20	C25	N4	P1	6.53(14)
C2	C1	C6	C7	176.02(13)	C20	N3	P1	N1	-107.88(9)
C2	C1	N1	P1	-120.93(13)	C20	N3	P1	N2	127.10(9)
C2	C3	C4	C5	-1.1(2)	C20	N3	P1	N4	7.17(9)
C3	C2	C10	C11	-36.9(2)	C21	C20	C25	C24	-1.5(2)
C3	C2	C10	C12	88.88(18)	C21	C20	C25	N4	179.26(12)
C3	C4	C5	C6	1.2(2)	C21	C20	N3	C19	-50.82(19)
C4	C5	C6	C1	0.5(2)	C21	C20	N3	P1	175.03(12)
C4	C5	C6	C7	-177.90(15)	C21	C22	C23	C24	-0.8(3)
C5	C6	C7	C8	-48.1(2)	C22	C23	C24	C25	-0.8(3)
C5	C6	C7	C9	74.90(17)	C23	C24	C25	C20	2.0(2)
C6	C1	C2	C3	2.43(19)	C23	C24	C25	N4	-178.88(14)
C6	C1	C2	C10	-179.46(13)	C24	C25	N4	C26	-5.8(2)
C6	C1	N1	P1	65.28(19)	C24	C25	N4	P1	-172.69(11)
C10	C2	C3	C4	-178.85(14)	C25	C20	C21	C22	-0.2(2)
C13	N2	P1	N1	36.63(14)	C25	C20	N3	C19	129.51(12)
C13	N2	P1	N3	172.33(12)	C25	C20	N3	P1	-4.64(13)
C13	N2	P1	N4	-93.05(13)	C25	N4	P1	N1	124.83(9)
C14	C15	C16	C17	-0.8(2)	C25	N4	P1	N2	-102.22(10)
C14	C19	N3	C20	-124.86(12)	C25	N4	P1	N3	-7.88(9)
C14	C19	N3	P1	9.35(12)	C26	N4	P1	N1	-41.72(13)
C14	N2	P1	N1	-122.31(9)	C26	N4	P1	N2	91.23(13)
C14	N2	P1	N3	13.38(10)	C26	N4	P1	N3	-174.43(12)
C14	N2	P1	N4	108.00(10)	N1	C1	C2	C3	-171.58(12)
C15	C14	C19	C18	0.79(19)	N1	C1	C2	C10	6.53(18)
C15	C14	C19	N3	-175.40(11)	N1	C1	C6	C5	171.41(13)

C15	C14	N2	C13	5.5(2)	N1	C1	C6	C7	-10.3(2)
C15	C14	N2	P1	165.16(11)	N2	C14	C15	C16	-175.22(13)
C15	C16	C17	C18	1.2(2)	N2	C14	C19	C18	176.56(12)
C16	C17	C18	C19	-0.5(2)	N2	C14	C19	N3	0.37(15)
C17	C18	C19	C14	-0.4(2)	N3	C20	C21	C22	-179.86(14)
C17	C18	C19	N3	175.06(12)	N3	C20	C25	C24	178.24(11)
C18	C19	N3	C20	59.29(18)	N3	C20	C25	N4	-1.04(15)
C18	C19	N3	P1	-166.50(11)					

Table C14. Hydrogen Atom Coordinates (Å×10^4) and Isotropic Displacement Parameters (Å^2×10^3) for 4.4.

Atom	*x*	*y*	*z*	U(eq)
H3	4030	9105	1311	45
H4	3712	6893	812	49
H5	5102	5508	556	47
H7	7813	6238	967	52
H8A	7010	4290	1448	87
H8B	7606	3795	810	87
H8C	6373	3966	709	87
H9A	6561	5573	-314	88
H9B	7796	5443	-190	88
H9C	7260	6953	-204	88
H10	6485	10795	1614	51
H11A	4921	11592	951	99
H11B	5216	12494	1641	99
H11C	4318	11342	1618	99
H12A	5195	10029	2658	106
H12B	6073	11211	2740	106
H12C	6389	9600	2677	106
H13A	7746	11171	-209	69
H13B	7190	10953	481	69
H13C	6955	9899	-160	69
H15	8335	9364	-1032	46
H16	9281	7706	-1606	53
H17	10419	6161	-981	54
H18	10600	6176	249	45
H21	11457	6673	1347	49

H22	12755	7399	2229	63
H23	12441	9224	2973	63
H24	10844	10423	2849	49
H26A	8769	10608	2735	69
H26B	8136	11278	2059	69
H26C	9294	11785	2301	69

Experimental

Single crystals of $C_{26}H_{31}N_4P$ [**4.4**] were [yzl19s]. A suitable crystal was selected and [] on a CCD area detector diffractometer. The crystal was kept at 223.15 K during data collection. Using Olex2 [1], the structure was solved with the ShelXS-1997 [2] structure solution program using Direct Methods and refined with the XL [3] refinement package using Least Squares minimisation.

Crystal Data for $C_{26}H_{31}N_4P$ (M =430.52 g/mol): monoclinic, space group $P2_1/n$ (no. 14), a = 12.8565(18) Å, b = 9.4531(13) Å, c = 19.152(3) Å, β = 96.382(4)°, V = 2313.2(6) Å^3, Z = 4, T = 223.15 K, μ(MoKα) = 0.140 mm^{-1}, *Dcalc* = 1.236 g/cm^3, 15190 reflections measured (4.04° ≤ 2Θ ≤ 56.6°), 5662 unique (R_{int} = 0.0172, R_{sigma} = 0.0208) which were used in all calculations. The final R_1 was 0.0432 (>2sigma(I)) and wR_2 was 0.1248 (all data).

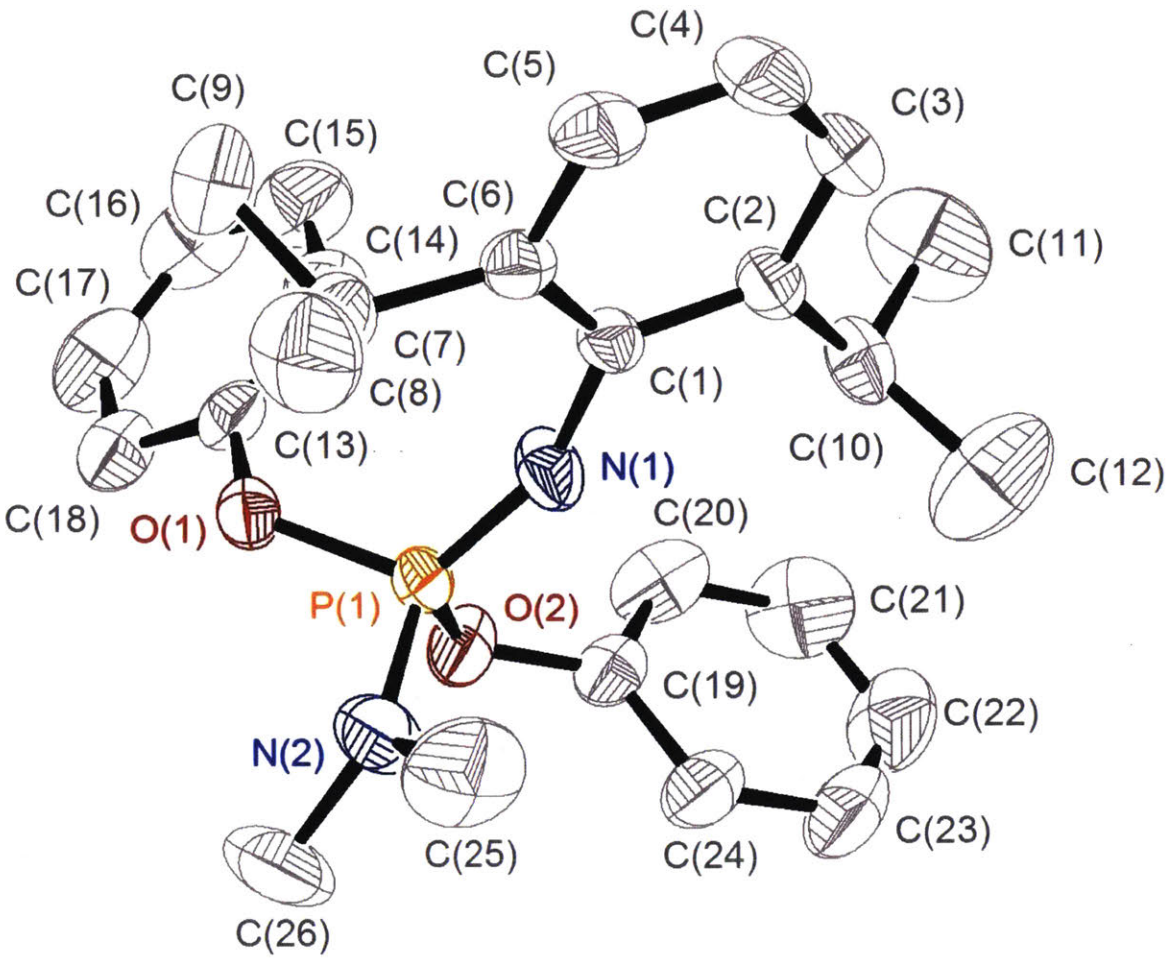

Table C15. Crystal data and structure refinement for 4.5.	
Identification code	yzl21m
Empirical formula	$C_{26}H_{33}N_2O_2P$
Formula weight	436.51
Temperature/K	213(2)
Crystal system	monoclinic
Space group	$P2_1/n$
a/Å	8.587(2)
b/Å	17.687(5)
c/Å	16.430(5)
α/°	90.00
β/°	99.539(6)
γ/°	90.00

Volume/Å^3	2460.9(12)
Z	4
ρ_{calc}g/cm^3	1.178
μ/mm^{-1}	0.136
F(000)	936.0
Crystal size/mm^3	0.2 × 0.17 × 0.08
Radiation	MoKα (λ = 0.71073)
2Θ range for data collection/°	3.4 to 56.6
Index ranges	$-8 \leq h \leq 11$, $-16 \leq k \leq 23$, $-21 \leq l \leq 21$
Reflections collected	14030
Independent reflections	5863 [R_{int} = 0.0291, R_{sigma} = 0.0310]
Data/restraints/parameters	5863/0/286
Goodness-of-fit on F^2	1.123
Final R indexes [I>=2σ (I)]	R_1 = 0.0679, wR_2 = 0.1670
Final R indexes [all data]	R_1 = 0.0810, wR_2 = 0.1747
Largest diff. peak/hole / e Å^{-3}	0.46/-0.24

Table C16. Fractional Atomic Coordinates (×10^4) and Equivalent Isotropic Displacement Parameters (Å^2×10^3) for 4.5. U_{eq} is defined as 1/3 of of the trace of the orthogonalised U_{IJ} tensor.

Atom	*x*	*y*	*z*	U(eq)
C1	5172(2)	2850.3(11)	6199.9(11)	30.7(4)
C2	5931(2)	3558.6(12)	6213.6(13)	36.4(4)
C3	6864(3)	3712.1(14)	5619.6(16)	51.0(6)
C4	7075(3)	3183.7(15)	5030.6(16)	54.4(6)
C5	6366(3)	2491.5(15)	5033.2(14)	46.1(5)
C6	5407(2)	2301.2(12)	5608.8(13)	35.4(4)
C7	4700(3)	1517.2(13)	5582.6(15)	45.9(6)
C8	3831(4)	1305.0(19)	4730(2)	75.9(9)
C9	5964(4)	930.1(15)	5885(2)	73.2(9)
C10	5687(3)	4147.8(13)	6846.2(14)	45.9(5)
C11	7195(4)	4516(2)	7276(2)	91.5(12)
C12	4517(5)	4742(2)	6487(2)	97.1(13)
C13	5068(3)	1366.2(12)	8205.7(13)	38.3(5)
C14	6468(3)	1746.6(15)	8183.8(18)	55.1(6)
C15	7694(4)	1652.5(19)	8821(2)	70.6(8)
C16	7547(4)	1196(2)	9469(2)	75.9(10)
C17	6155(4)	809.1(19)	9484.1(17)	71.9(9)

C18	4891(3)	891.7(14)	8842.4(15)	50.6(6)
C19	3004(3)	3386.3(13)	8252.7(13)	40.8(5)
C20	4236(4)	3679.0(17)	8787.2(15)	60.0(7)
C21	4238(4)	4446(2)	8971.4(19)	77.8(10)
C22	3005(5)	4897.7(18)	8621(2)	78.2(10)
C23	1796(4)	4596.8(17)	8095(2)	70.4(8)
C24	1765(3)	3837.7(15)	7903.7(17)	54.1(6)
C25	847(4)	2367(2)	5936(2)	83.3(10)
C26	244(4)	1744(2)	7183(3)	88.8(12)
N1	4196(2)	2731.7(10)	6779.8(12)	44.5(5)
N2	1436(2)	2072.2(13)	6747.5(15)	56.2(6)
O1	3786.8(17)	1440.6(8)	7569.2(9)	37.9(3)
O2	2996(2)	2615.0(9)	8102.0(9)	45.5(4)
P1	3187.8(6)	2259.3(3)	7228.6(3)	33.08(16)

Table C17. Anisotropic Displacement Parameters ($Å^2 \times 10^3$) for 4.5. The Anisotropic displacement factor exponent takes the form: $-2\pi^2[h^2a^{*2}U_{11}+2hka^*b^*U_{12}+\ldots]$.

Atom	U_{11}	U_{22}	U_{33}	U_{23}	U_{13}	U_{12}
C1	30.3(10)	32.5(9)	29.9(9)	4.7(7)	7.0(8)	-0.3(8)
C2	35.3(11)	35.8(10)	38.3(10)	4.7(8)	6.5(9)	-4.8(8)
C3	49.0(14)	46.1(13)	61.9(15)	9.6(11)	21.0(12)	-11.5(11)
C4	51.4(15)	65.6(16)	53.5(14)	9.8(12)	29.8(12)	-3.4(12)
C5	46.3(14)	56.6(13)	39.5(11)	-2.4(10)	18.8(10)	5.0(11)
C6	33.2(11)	38.3(11)	35.5(10)	1.0(8)	8.1(8)	2.4(8)
C7	52.7(14)	37.0(11)	51.8(13)	-11.0(9)	19.5(11)	-3.5(10)
C8	80(2)	70(2)	75(2)	-24.4(16)	4.9(17)	-16.6(17)
C9	84(2)	40.5(14)	96(2)	6.9(14)	18.2(19)	6.5(14)
C10	55.3(15)	36.5(11)	46.6(12)	-3.3(9)	10.3(11)	-15.3(10)
C11	84(3)	108(3)	76(2)	-29(2)	-6.1(19)	-29(2)
C12	121(3)	77(2)	86(2)	-35.1(19)	-2(2)	33(2)
C13	39.8(12)	31.4(10)	42.7(11)	-6.3(8)	4.1(9)	8.2(9)
C14	43.2(14)	54.9(15)	64.8(16)	-2.9(12)	1.8(12)	-2.1(11)
C15	52.6(18)	74(2)	79(2)	-17.3(17)	-7.2(16)	1.3(14)
C16	73(2)	86(2)	57.8(17)	-20.9(16)	-19.1(16)	19.8(18)
C17	96(3)	71.2(19)	45.0(14)	5.3(13)	0.9(16)	25.4(18)
C18	58.9(16)	44.3(13)	49.2(13)	3.7(10)	10.9(12)	11.2(11)
C19	50.3(14)	42.9(11)	33.4(10)	5.8(8)	19.6(10)	11.7(10)

C20	65.3(18)	74.6(18)	38.8(12)	-4.8(12)	4.4(12)	20.7(14)
C21	90(2)	85(2)	57.3(17)	-31.5(16)	6.9(16)	-2.2(19)
C22	104(3)	51.7(16)	84(2)	-18.4(16)	30(2)	10.8(17)
C23	80(2)	50.3(15)	82(2)	1.7(15)	17.5(17)	25.6(15)
C24	52.0(16)	51.1(14)	59.7(15)	3.5(11)	11.2(12)	14.5(12)
C25	71(2)	105(3)	65.1(19)	13.7(18)	-15.4(17)	10.7(19)
C26	40.6(16)	102(3)	125(3)	40(2)	16.3(18)	-15.5(16)
N1	59.3(13)	32.9(9)	48.3(10)	-4.4(8)	29.8(10)	-8.4(8)
N2	37.6(12)	62.8(13)	66.0(14)	25.5(11)	2.2(10)	-5.2(10)
O1	36.6(8)	29.9(7)	46.1(8)	5.2(6)	3.4(7)	-2.2(6)
O2	63.9(11)	39.0(8)	40.1(8)	10.0(6)	27.2(8)	11.2(7)
P1	34.8(3)	30.4(3)	36.4(3)	6.51(19)	12.7(2)	-0.9(2)

Table C18. Bond Lengths for 4.5.

Atom	Atom	Length/Å	Atom	Atom	Length/Å
C1	C2	1.411(3)	C15	C16	1.360(5)
C1	C6	1.412(3)	C16	C17	1.381(5)
C1	N1	1.385(2)	C17	C18	1.390(4)
C2	C3	1.388(3)	C19	C20	1.360(4)
C2	C10	1.511(3)	C19	C24	1.377(3)
C3	C4	1.379(4)	C19	O2	1.386(3)
C4	C5	1.368(4)	C20	C21	1.390(4)
C5	C6	1.394(3)	C21	C22	1.374(5)
C6	C7	1.512(3)	C22	C23	1.346(5)
C7	C8	1.521(4)	C23	C24	1.378(4)
C7	C9	1.525(4)	C25	N2	1.443(4)
C10	C11	1.516(4)	C26	N2	1.463(3)
C10	C12	1.506(4)	N1	P1	1.4845(17)
C13	C14	1.383(3)	N2	P1	1.613(2)
C13	C18	1.369(3)	O1	P1	1.6060(15)
C13	O1	1.393(3)	O2	P1	1.5999(16)
C14	C15	1.366(4)			

Table C19. Bond Angles for 4.5.

Atom	Atom	Atom	Angle/°	Atom	Atom	Atom	Angle/°

C2	C1	C6	120.22(17)	C15	C16	C17	120.1(3)
N1	C1	C2	117.01(17)	C16	C17	C18	120.3(3)
N1	C1	C6	122.77(18)	C13	C18	C17	118.2(3)
C1	C2	C10	120.48(18)	C20	C19	C24	120.8(2)
C3	C2	C1	118.8(2)	C20	C19	O2	118.0(2)
C3	C2	C10	120.7(2)	C24	C19	O2	121.0(2)
C4	C3	C2	121.3(2)	C19	C20	C21	119.0(3)
C5	C4	C3	119.6(2)	C22	C21	C20	120.2(3)
C4	C5	C6	122.1(2)	C23	C22	C21	119.9(3)
C1	C6	C7	123.23(18)	C22	C23	C24	121.0(3)
C5	C6	C1	118.0(2)	C19	C24	C23	119.1(3)
C5	C6	C7	118.80(19)	C1	N1	P1	153.66(16)
C6	C7	C8	112.7(2)	C25	N2	C26	115.4(3)
C6	C7	C9	110.8(2)	C25	N2	P1	122.3(2)
C8	C7	C9	110.3(2)	C26	N2	P1	120.9(2)
C2	C10	C11	114.3(2)	C13	O1	P1	120.96(13)
C12	C10	C2	111.8(2)	C19	O2	P1	123.29(12)
C12	C10	C11	110.2(3)	N1	P1	N2	116.45(12)
C14	C13	O1	121.1(2)	N1	P1	O1	120.07(10)
C18	C13	C14	121.7(2)	N1	P1	O2	112.30(10)
C18	C13	O1	117.2(2)	O1	P1	N2	101.80(10)
C15	C14	C13	118.9(3)	O2	P1	N2	107.10(11)
C16	C15	C14	120.8(3)	O2	P1	O1	96.69(8)

Table C20. Torsion Angles for 4.5.

A	B	C	D	Angle/°	A	B	C	D	Angle/°
C1	C2	C3	C4	-0.9(4)	C15	C16	C17	C18	-0.8(5)
C1	C2	C10	C11	133.2(3)	C16	C17	C18	C13	-0.4(4)
C1	C2	C10	C12	-100.7(3)	C18	C13	C14	C15	-0.9(4)
C1	C6	C7	C8	129.2(3)	C18	C13	O1	P1	132.36(18)
C1	C6	C7	C9	-106.7(3)	C19	C20	C21	C22	0.5(5)
C1	N1	P1	N2	-77.8(5)	C19	O2	P1	N1	31.5(2)
C1	N1	P1	O1	45.7(5)	C19	O2	P1	N2	-97.53(19)
C1	N1	P1	O2	158.2(4)	C19	O2	P1	O1	157.91(18)
C2	C1	C6	C5	-1.9(3)	C20	C19	C24	C23	0.9(4)
C2	C1	C6	C7	176.9(2)	C20	C19	O2	P1	-112.8(2)

C2	C1	N1	P1	-171.6(4)	C20	C21	C22	C23	-0.3(5)
C2	C3	C4	C5	-0.6(4)	C21	C22	C23	C24	0.5(5)
C3	C2	C10	C11	-48.9(3)	C22	C23	C24	C19	-0.7(5)
C3	C2	C10	C12	77.2(3)	C24	C19	C20	C21	-0.7(4)
C3	C4	C5	C6	1.0(4)	C24	C19	O2	P1	70.3(3)
C4	C5	C6	C1	0.3(4)	C25	N2	P1	N1	-2.1(3)
C4	C5	C6	C7	-178.5(2)	C25	N2	P1	O1	-134.6(3)
C5	C6	C7	C8	-52.1(3)	C25	N2	P1	O2	124.5(3)
C5	C6	C7	C9	72.0(3)	C26	N2	P1	N1	-167.8(2)
C6	C1	C2	C3	2.2(3)	C26	N2	P1	O1	59.7(3)
C6	C1	C2	C10	-179.8(2)	C26	N2	P1	O2	-41.2(3)
C6	C1	N1	P1	9.0(6)	N1	C1	C2	C3	-177.2(2)
C10	C2	C3	C4	-178.9(2)	N1	C1	C2	C10	0.8(3)
C13	C14	C15	C16	-0.3(4)	N1	C1	C6	C5	177.5(2)
C13	O1	P1	N1	67.44(18)	N1	C1	C6	C7	-3.8(3)
C13	O1	P1	N2	-162.26(16)	O1	C13	C14	C15	-179.7(2)
C13	O1	P1	O2	-53.18(16)	O1	C13	C18	C17	180.0(2)
C14	C13	C18	C17	1.2(3)	O2	C19	C20	C21	-177.6(2)
C14	C13	O1	P1	-48.8(3)	O2	C19	C24	C23	177.6(2)
C14	C15	C16	C17	1.1(5)					

Table C21. Hydrogen Atom Coordinates (Å×10^4) and Isotropic Displacement Parameters (Å^2×10^3) for 4.5.

Atom	*x*	*y*	*z*	U(eq)
H3	7362	4185	5619	61
H4	7702	3298	4629	65
H5	6530	2133	4634	55
H7	3923	1510	5965	55
H8A	4582	1263	4351	114
H8B	3059	1692	4535	114
H8C	3300	824	4759	114
H9A	5486	432	5868	110
H9B	6446	1047	6448	110
H9C	6765	937	5533	110
H10	5218	3883	7278	55
H11A	7691	4788	6874	137
H11B	7910	4130	7538	137

H11C	6949	4866	7691	137
H12A	4933	5018	6059	146
H12B	4336	5090	6918	146
H12C	3529	4502	6251	146
H14	6573	2065	7738	66
H15	8652	1907	8810	85
H16	8394	1143	9908	91
H17	6062	489	9930	86
H18	3940	629	8846	61
H20	5073	3367	9028	72
H21	5086	4657	9337	93
H22	3006	5416	8748	94
H23	959	4909	7854	85
H24	910	3631	7540	65
H25A	281	1972	5599	125
H25B	1725	2540	5682	125
H25C	139	2786	5981	125
H26A	-590	2109	7204	133
H26B	728	1609	7740	133
H26C	-197	1295	6893	133

Experimental

Single crystals of $C_{26}H_{33}N_2O_2P$ [**4.5**]. A suitable crystal was selected on a 'CCD area detector' diffractometer. The crystal was kept at 213(2) K during data collection. Using Olex2 [1], the structure was solved with the XS [2] structure solution program using Direct Methods and refined with the XL [3] refinement package using CGLS minimisation.

1. Dolomanov, O.V., Bourhis, L.J., Gildea, R.J, Howard, J.A.K. & Puschmann, H. (2009), J. Appl. Cryst. 42, 339-341.
2. Sheldrick, G.M. (2008). Acta Cryst. A64, 112-122.
3. Sheldrick, G.M. (2008). Acta Cryst. A64, 112-122.

Crystal structure determination of [**4.5**]

Crystal Data for $C_{26}H_{33}N_2O_2P$ (M =436.51 g/mol): monoclinic, space group $P2_1/n$ (no. 14), a = 8.587(2) Å, b = 17.687(5) Å, c = 16.430(5) Å, β = 99.539(6)°, V = 2460.9(12) Å^3, Z = 4, T = 213(2) K, μ(MoKα) = 0.136 mm^{-1}, *Dcalc* = 1.178 g/cm^3, 14030 reflections measured (3.4° ≤ 2Θ ≤ 56.6°), 5863 unique (R_{int} = 0.0291, R_{sigma} = 0.0310) which were used in all calculations. The final R_1 was 0.0679 (>2sigma(I)) and wR_2 was 0.1747 (all data).

Refinement model description

Number of restraints - 0, number of constraints - unknown.

Details:

```
1. Fixed Uiso
 At 1.2 times of:
  All C(H) groups
 At 1.5 times of:
  All C(H,H,H) groups
2.a Ternary CH refined with riding coordinates:
 C7(H7), C10(H10)
2.b Aromatic/amide H refined with riding coordinates:
 C3(H3), C4(H4), C5(H5), C14(H14), C15(H15), C16(H16), C17(H17), C18(H18),
 C20(H20), C21(H21), C22(H22), C23(H23), C24(H24)
2.c Idealised Me refined as rotating group:
 C8(H8A,H8B,H8C), C9(H9A,H9B,H9C), C11(H11A,H11B,H11C), C12(H12A,H12B,H12C),
 C25(H25A,H25B,H25C), C26(H26A,H26B,H26C)
```

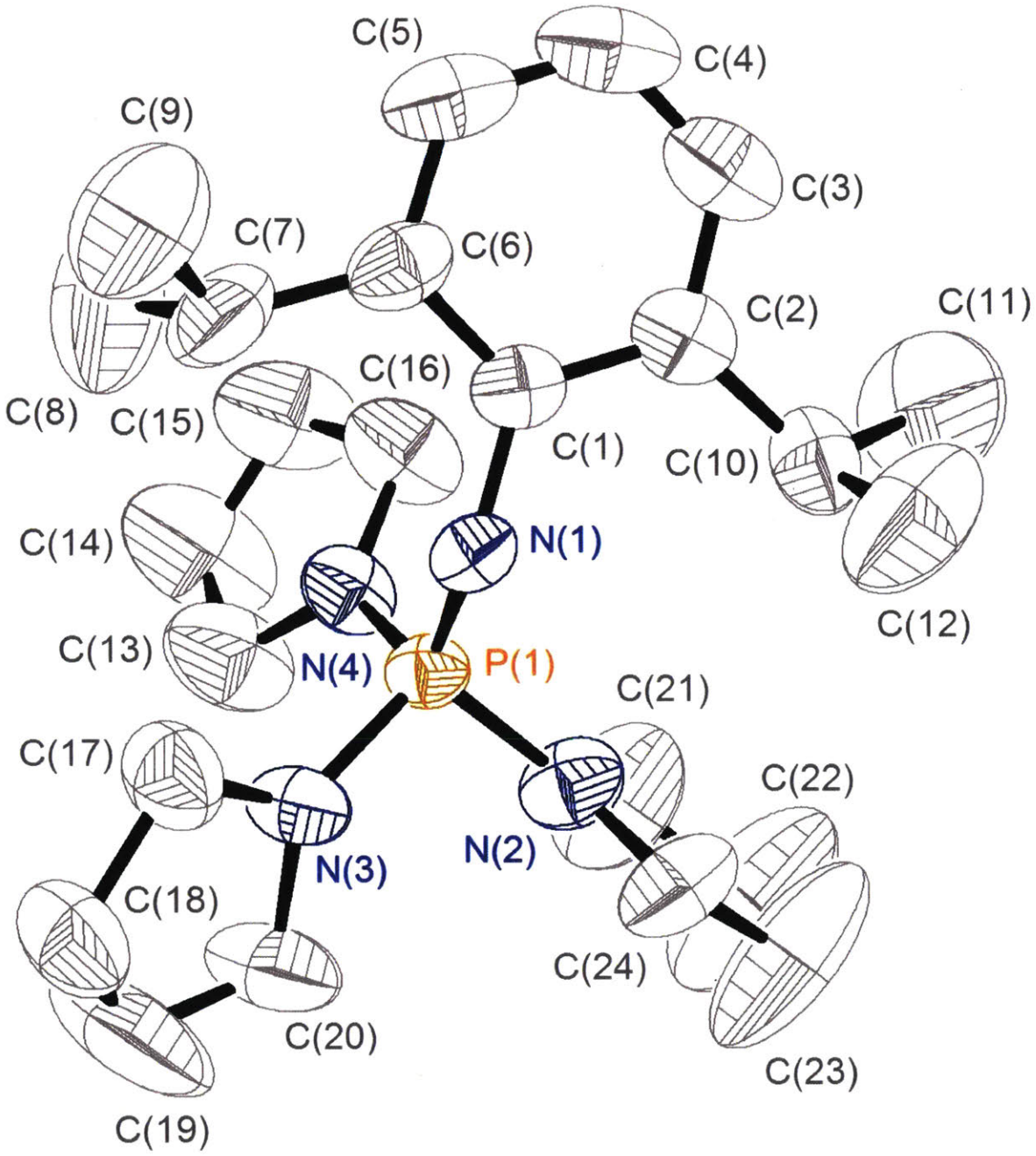

Table C22. Crystal data and structure refinement for 4.6.	
Identification code	yzl22s
Empirical formula	$C_{24}H_{41}N_4P$
Formula weight	416.58
Temperature/K	298(2)

Crystal system	monoclinic
Space group	$P2_1/c$
a/Å	8.3589(18)
b/Å	16.491(4)
c/Å	18.049(4)
α/°	90
β/°	93.767(5)
γ/°	90
Volume/Å^3	2482.6(9)
Z	4
ρ_{calc}g/cm^3	1.115
μ/mm^{-1}	0.127
F(000)	912.0
Crystal size/mm^3	0.24 × 0.19 × 0.13
Radiation	MoKα (λ = 0.71073)
2Θ range for data collection/°	3.348 to 56.66
Index ranges	$-10 \leq h \leq 11$, $-19 \leq k \leq 21$, $-23 \leq l \leq 23$
Reflections collected	19629
Independent reflections	6112 [R_{int} = 0.0377, R_{sigma} = 0.0479]
Data/restraints/parameters	6112/0/266
Goodness-of-fit on F^2	1.042
Final R indexes [I>=2σ (I)]	R_1 = 0.1261, wR_2 = 0.2434
Final R indexes [all data]	R_1 = 0.1627, wR_2 = 0.2627
Largest diff. peak/hole / e Å^{-3}	0.40/-0.46

Table C23. Fractional Atomic Coordinates (×10^4) and Equivalent Isotropic Displacement Parameters (Å^2×10^3) for 4.6. U_{eq} is defined as 1/3 of of the trace of the orthogonalised U_{IJ} tensor.

Atom	*x*	*y*	*z*	U(eq)
C1	3156(4)	3982(2)	7301(2)	48.0(9)
C2	3479(5)	3603(3)	7998(3)	60.9(11)
C3	3780(6)	2771(3)	8015(4)	79.6(15)
C4	3794(7)	2314(3)	7385(4)	91.3(19)
C5	3552(7)	2687(3)	6717(4)	83.6(17)
C6	3229(5)	3513(3)	6647(3)	61.7(12)

C7	2992(7)	3904(4)	5893(3)	80.5(15)
C8	1304(9)	3833(6)	5576(4)	144(3)
C9	4144(9)	3615(5)	5332(4)	127(3)
C10	3587(6)	4097(3)	8702(3)	71.4(13)
C11	2969(13)	3679(6)	9365(4)	166(4)
C12	5282(8)	4388(5)	8874(4)	134(3)
C13	-1670(7)	5399(4)	6782(4)	108(2)
C14	-2979(8)	4816(5)	6721(6)	150(4)
C15	-2363(7)	4032(4)	6979(5)	117(3)
C16	-794(6)	4191(3)	7385(4)	86.8(17)
C17	2418(7)	6113(3)	6071(3)	76.2(15)
C18	2304(8)	6960(4)	5757(3)	96.1(19)
C19	1248(14)	7388(4)	6214(5)	177(5)
C20	989(8)	6974(3)	6868(4)	99(2)
C21	33(9)	5839(6)	8611(4)	129(3)
C22	621(15)	6276(8)	9282(5)	214(6)
C23	2186(14)	6542(8)	9204(5)	202(6)
C24	2702(8)	6279(4)	8498(3)	96.4(19)
N2	2875(4)	4814.4(19)	7247.3(17)	47.0(8)
N3	1337(5)	5832(2)	8142(2)	65.9(11)
N4	-307(4)	4989(2)	7143(2)	59.7(9)
N5	1669(5)	6159(2)	6774(2)	60.4(10)
P1	1467.2(12)	5389.4(6)	7329.2(6)	44.6(3)

Table C24. Anisotropic Displacement Parameters ($Å^2 \times 10^3$) for 4.6. The Anisotropic displacement factor exponent takes the form: $-2\pi^2[h^2a^{*2}U_{11}+2hka^*b^*U_{12}+\ldots]$.

Atom	U_{11}	U_{22}	U_{33}	U_{23}	U_{13}	U_{12}
C1	30.4(18)	50(2)	64(3)	-5.5(19)	4.4(17)	-2.8(16)
C2	43(2)	62(3)	78(3)	6(2)	10(2)	-2(2)
C3	66(3)	66(3)	107(4)	21(3)	6(3)	6(3)
C4	83(4)	49(3)	144(6)	-1(4)	17(4)	1(3)
C5	75(4)	60(3)	117(5)	-30(3)	12(3)	-5(3)
C6	46(2)	62(3)	76(3)	-20(2)	1(2)	-2(2)
C7	94(4)	82(4)	65(3)	-29(3)	2(3)	3(3)
C8	92(5)	244(11)	94(5)	1(6)	-16(4)	14(6)
C9	128(6)	163(7)	93(5)	-27(5)	30(4)	-2(5)
C10	74(3)	82(3)	59(3)	12(3)	4(2)	11(3)

C11	251(11)	165(8)	87(5)	15(5)	63(6)	-37(8)
C12	100(5)	170(8)	128(6)	-60(6)	-12(4)	-6(5)
C13	69(4)	89(4)	162(7)	22(4)	-18(4)	3(3)
C14	60(4)	128(6)	255(11)	59(7)	-37(5)	-23(4)
C15	55(3)	92(5)	202(8)	9(5)	-7(4)	-18(3)
C16	53(3)	80(4)	129(5)	28(3)	9(3)	-12(3)
C17	92(4)	76(3)	62(3)	13(3)	17(3)	7(3)
C18	120(5)	84(4)	84(4)	32(3)	8(4)	-9(4)
C19	311(13)	83(5)	149(7)	57(5)	100(8)	87(7)
C20	124(5)	51(3)	126(5)	10(3)	34(4)	12(3)
C21	105(5)	187(8)	100(5)	-41(5)	51(4)	-4(5)
C22	210(12)	313(16)	129(8)	-128(9)	77(8)	-32(11)
C23	190(11)	301(15)	117(7)	-136(9)	29(7)	-34(10)
C24	114(5)	88(4)	87(4)	-38(3)	2(4)	-8(4)
N2	48.1(18)	47.1(19)	46.2(18)	-8.6(14)	6.9(14)	-4.0(14)
N3	69(2)	68(3)	63(2)	-14.3(19)	23.0(19)	1(2)
N4	41.0(18)	59(2)	79(3)	10.5(19)	-1.7(17)	0.8(16)
N5	69(2)	42.1(19)	72(2)	2.5(17)	18.4(19)	1.6(17)
P1	45.5(5)	40.8(5)	48.5(6)	-2.5(5)	10.2(4)	-1.1(4)

Table C25. Bond Lengths for 4.6.

Atom	Atom	Length/Å	Atom	Atom	Length/Å
C1	C2	1.415(6)	C15	C16	1.483(8)
C1	C6	1.415(6)	C16	N4	1.453(6)
C1	N2	1.395(5)	C17	C18	1.509(7)
C2	C3	1.394(7)	C17	N5	1.453(6)
C2	C10	1.508(7)	C18	C19	1.432(9)
C3	C4	1.366(8)	C19	C20	1.394(8)
C4	C5	1.355(8)	C20	N5	1.474(6)
C5	C6	1.393(7)	C21	C22	1.466(11)
C6	C7	1.508(7)	C21	N3	1.424(6)
C7	C8	1.492(8)	C22	C23	1.395(13)
C7	C9	1.520(8)	C23	C24	1.439(9)
C10	C11	1.501(8)	C24	N3	1.470(7)
C10	C12	1.509(8)	N2	P1	1.526(3)
C13	C14	1.455(8)	N3	P1	1.648(4)

C13	N4	1.443(6)	N4	P1	1.638(4)
C14	C15	1.456(9)	N5	P1	1.633(4)

Table C26. Bond Angles for 4.6.

Atom	Atom	Atom	Angle/°	Atom	Atom	Atom	Angle/°
C6	C1	C2	118.9(4)	C19	C18	C17	105.4(5)
N2	C1	C2	121.2(4)	C20	C19	C18	112.6(6)
N2	C1	C6	119.8(4)	C19	C20	N5	105.4(5)
C1	C2	C10	120.5(4)	N3	C21	C22	105.5(7)
C3	C2	C1	118.6(5)	C23	C22	C21	109.7(7)
C3	C2	C10	120.8(5)	C22	C23	C24	109.4(7)
C4	C3	C2	122.4(6)	C23	C24	N3	105.6(6)
C5	C4	C3	118.8(5)	C1	N2	P1	137.1(3)
C4	C5	C6	122.7(5)	C21	N3	C24	109.8(5)
C1	C6	C7	120.5(4)	C21	N3	P1	129.1(4)
C5	C6	C1	118.6(5)	C24	N3	P1	121.1(3)
C5	C6	C7	120.9(5)	C13	N4	C16	109.4(4)
C6	C7	C9	114.6(5)	C13	N4	P1	125.5(4)
C8	C7	C6	112.2(5)	C16	N4	P1	124.8(3)
C8	C7	C9	110.1(5)	C17	N5	C20	109.9(4)
C2	C10	C12	110.4(4)	C17	N5	P1	124.3(3)
C11	C10	C2	114.8(5)	C20	N5	P1	125.5(3)
C11	C10	C12	110.5(6)	N2	P1	N3	117.2(2)
N4	C13	C14	107.0(5)	N2	P1	N4	115.01(19)
C13	C14	C15	108.3(5)	N2	P1	N5	108.17(18)
C14	C15	C16	106.5(5)	N4	P1	N3	104.5(2)
N4	C16	C15	105.5(5)	N5	P1	N3	102.6(2)
N5	C17	C18	105.0(4)	N5	P1	N4	108.4(2)

Table C27. Torsion Angles for 4.6.

A	B	C	D	Angle/°	A	B	C	D	Angle/°
C1	C2	C3	C4	0.9(7)	C16	N4	P1	N3	-86.7(5)
C1	C2	C10	C11	145.3(6)	C16	N4	P1	N5	164.4(4)
C1	C2	C10	C12	-89.0(6)	C17	C18	C19	C20	13.9(11)
C1	C6	C7	C8	-95.7(6)	C17	N5	P1	N2	31.1(5)

C1	C6	C7	C9	137.8(5)	C17	N5	P1	N3	155.7(4)
C1	N2	P1	N3	95.6(4)	C17	N5	P1	N4	-94.2(4)
C1	N2	P1	N4	-27.7(5)	C18	C17	N5	C20	4.8(6)
C1	N2	P1	N5	-149.1(4)	C18	C17	N5	P1	179.2(4)
C2	C1	C6	C5	2.6(6)	C18	C19	C20	N5	-10.9(11)
C2	C1	C6	C7	-176.3(4)	C19	C20	N5	C17	3.3(8)
C2	C1	N2	P1	-81.3(5)	C19	C20	N5	P1	-171.0(6)
C2	C3	C4	C5	1.9(9)	C20	N5	P1	N2	-155.3(5)
C3	C2	C10	C11	-38.2(8)	C20	N5	P1	N3	-30.8(5)
C3	C2	C10	C12	87.5(6)	C20	N5	P1	N4	79.4(5)
C3	C4	C5	C6	-2.4(9)	C21	C22	C23	C24	-1.4(17)
C4	C5	C6	C1	0.2(8)	C21	N3	P1	N2	-125.3(6)
C4	C5	C6	C7	179.1(5)	C21	N3	P1	N4	3.2(6)
C5	C6	C7	C8	85.4(7)	C21	N3	P1	N5	116.3(6)
C5	C6	C7	C9	-41.1(7)	C22	C21	N3	C24	-1.8(10)
C6	C1	C2	C3	-3.1(6)	C22	C21	N3	P1	176.2(7)
C6	C1	C2	C10	173.4(4)	C22	C23	C24	N3	0.2(14)
C6	C1	N2	P1	103.0(5)	C23	C24	N3	C21	1.1(9)
C10	C2	C3	C4	-175.7(5)	C23	C24	N3	P1	-177.2(7)
C13	C14	C15	C16	15.0(11)	C24	N3	P1	N2	52.5(5)
C13	N4	P1	N2	-143.6(5)	C24	N3	P1	N4	-178.9(4)
C13	N4	P1	N3	86.5(5)	C24	N3	P1	N5	-65.8(5)
C13	N4	P1	N5	-22.4(5)	N2	C1	C2	C3	-178.8(4)
C14	C13	N4	C16	-6.6(8)	N2	C1	C2	C10	-2.3(6)
C14	C13	N4	P1	179.3(5)	N2	C1	C6	C5	178.4(4)
C14	C15	C16	N4	-18.6(8)	N2	C1	C6	C7	-0.5(6)
C15	C16	N4	C13	15.7(7)	N3	C21	C22	C23	2.0(15)
C15	C16	N4	P1	-170.2(4)	N4	C13	C14	C15	-5.4(10)
C16	N4	P1	N2	43.2(5)	N5	C17	C18	C19	-10.9(8)

Table C28. Hydrogen Atom Coordinates (Å×10^4) and Isotropic Displacement Parameters (Å^2×10^3) for 4.6.

Atom	*x*	*y*	*z*	U(eq)
H3	3977	2518	8473	96
H4	3967	1758	7412	110
H5	3603	2378	6288	100
H7	3199	4485	5967	97

H8A	1053	3273	5482	216
H8B	1183	4132	5119	216
H8C	591	4049	5922	216
H9A	5220	3626	5553	190
H9B	4067	3965	4906	190
H9C	3873	3071	5182	190
H10	2922	4580	8608	86
H11A	1858	3546	9264	248
H11B	3084	4032	9788	248
H11C	3571	3191	9466	248
H12A	5959	3934	9008	201
H12B	5304	4766	9279	201
H12C	5662	4650	8444	201
H13A	-1419	5586	6294	129
H13B	-1964	5864	7073	129
H14A	-3402	4776	6209	179
H14B	-3837	4990	7021	179
H15A	-2231	3674	6561	140
H15B	-3096	3781	7305	140
H16A	-899	4184	7917	104
H16B	-14	3784	7263	104
H17A	1855	5730	5739	91
H17B	3529	5945	6147	91
H18A	3351	7216	5778	115
H18B	1873	6951	5245	115
H19A	1702	7916	6336	212
H19B	228	7472	5936	212
H20A	-149	6941	6942	119
H20B	1522	7246	7292	119
H21A	-276	5290	8732	154
H21B	-886	6114	8371	154
H22A	-67	6737	9361	257
H22B	599	5921	9710	257
H23A	2894	6322	9601	242
H23B	2228	7128	9234	242
H24A	3635	5930	8566	116
H24B	2972	6741	8198	116

Experimental

Single crystals of $C_{24}H_{41}N_4P$ [**4.6**] . A suitable crystal was selected on a 'CCD area detector' diffractometer. The crystal was kept at 298(2) K during data collection. Using Olex2 [1], the structure was solved with the olex2.solve [2] structure solution program using Charge Flipping and refined with the ShelXL [3] refinement package using Least Squares minimisation.

1. Dolomanov, O.V., Bourhis, L.J., Gildea, R.J, Howard, J.A.K. & Puschmann, H. (2009), J. Appl. Cryst. 42, 339-341.
2. Bourhis, L.J., Dolomanov, O.V., Gildea, R.J., Howard, J.A.K., Puschmann, H. (2015). Acta Cryst. A71, 59-75.
3. Sheldrick, G.M. (2008). Acta Cryst. A64, 112-122.

Crystal structure determination of [yzl22s]

Crystal Data for $C_{24}H_{41}N_4P$ (M =416.58 g/mol): monoclinic, space group $P2_1/c$ (no. 14), a = 8.3589(18) Å, b = 16.491(4) Å, c = 18.049(4) Å, β = 93.767(5)°, V = 2482.6(9) Å^3, Z = 4, T = 298(2) K, μ(MoKα) = 0.127 mm^{-1}, *Dcalc* = 1.115 g/cm^3, 19629 reflections measured (3.348° ≤ 2Θ ≤ 56.66°), 6112 unique (R_{int} = 0.0377, R_{sigma} = 0.0479) which were used in all calculations. The final R_1 was 0.1261 (I > 2σ(I)) and wR_2 was 0.2627 (all data).

Refinement model description

Number of restraints - 0, number of constraints - unknown.

Details:

```
1. Fixed Uiso
 At 1.2 times of:
  All C(H) groups, All C(H,H) groups
 At 1.5 times of:
  All C(H,H,H) groups
2.a Ternary CH refined with riding coordinates:
 C7(H7), C10(H10)
2.b Secondary CH2 refined with riding coordinates:
 C13(H13A,H13B), C14(H14A,H14B), C15(H15A,H15B), C16(H16A,H16B), C17(H17A,
 H17B), C18(H18A,H18B), C19(H19A,H19B), C20(H20A,H20B), C21(H21A,H21B),
 C22(H22A,H22B), C23(H23A,H23B), C24(H24A,H24B)
2.c Aromatic/amide H refined with riding coordinates:
 C3(H3), C4(H4), C5(H5)
2.d Idealised Me refined as rotating group:
 C8(H8A,H8B,H8C), C9(H9A,H9B,H9C), C11(H11A,H11B,H11C), C12(H12A,H12B,H12C)
```

This report has been created with Olex2, compiled on 2015.01.26 svn.r3150 for OlexSys. Please let us know if there are any errors or if you would like to have additional features.

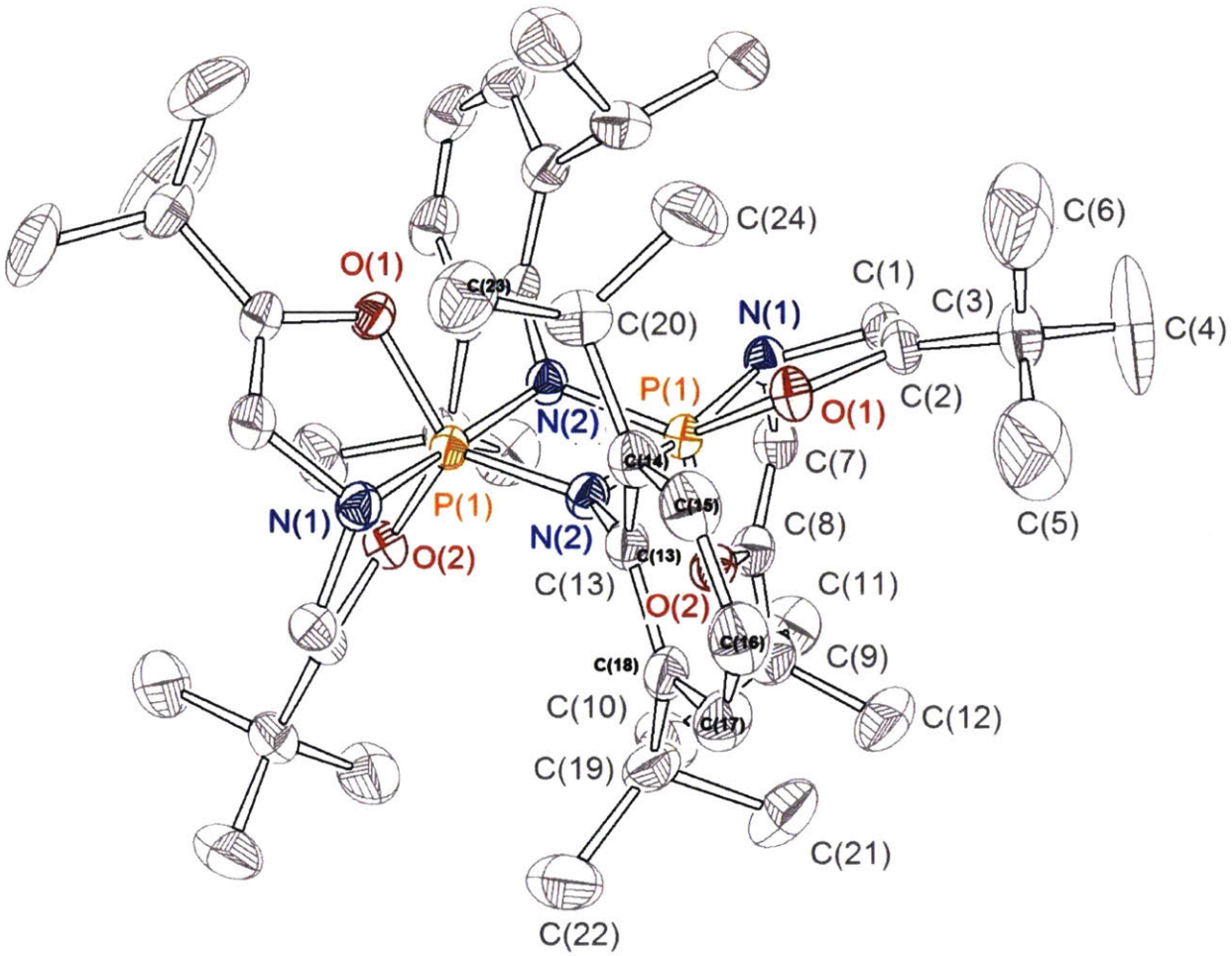

A colorless block shaped crystal of 4.2a (C24 H37 N2 O2 P) with approximate dimensions 0.15 x 0.18 x 0.21 mm, was used for the X-ray crystallographic analysis. The X-ray intensity data were measured at 273(2) K, on a Bruker SMART APEX CCD area detector system equipped with a graphite monochromator and a MoKα fine-focus sealed tube (λ = 0.71073Å) operated at 1600 watts power (50 kV, 32 mA). The detector was placed at a distance of 5.8 cm from the crystal.

A total of 1650 frames were collected with a scan width of 0.3° in ω and an exposure time of 20 seconds/frame. The total data collection time was about 12 hours. The frames were integrated with the Bruker SAINT software package using a narrow-frame integration algorithm. The integration of the data using a Monoclinic unit cell yielded a total of 24852 reflections to a

maximum θ angle of 28.35° (0.90 Å resolution), of which 5968 were independent, completeness = 98.0%, R_{int} = 0.0528, R_{sig} = 0.0487 and 4575 were greater than 2σ(I). The final cell constants: a = 27.535(11)Å, b = 11.390(5)Å, c = 20.157(8)Å, α = 90°, β = 129.447(7)°, γ = 90°, volume = 4882(3)Å^3, are based upon the refinement of the XYZ-centroids of 1808 reflections above 20σ(I) with 2.274° <θ <23.213°. Analysis of the data showed negligible decay during data collection. Data were corrected for absorption effects using the multiscan technique (SADABS). The ratio of minimum to maximum apparent transmission was 0.3627.

The structure was solved and refined using the Bruker SHELXTL (Version 6.1) Software Package, using the space group C2/c, with Z = 8 for the formula unit, C24 H37 N2 O2 P. The final anisotropic full-matrix least-squares refinement on F^2 with 272 variables converged at R1 = 7.86%, for the observed data and wR2 = 23.34% for all data. The goodness-of-fit was 1.049. The largest peak on the final difference map was 0.608 e$^-$/Å^3 and the largest hole was -0.334 e$^-$/Å^3. Based on the final model, the calculated density of the crystal is 1.133 g/cm^3 and F(000) amounts to 1808 electrons.

Table C29. Sample and crystal data for 4.2a.

Identification code	yzl5	
Empirical formula	C24 H37 N2 O2 P	
Formula weight	416.53	
Temperature	273(2) K	
Wavelength	0.71073 Å	
Crystal size	0.21 x 0.18 x 0.15 mm	
Crystal habit	colorless block	
Crystal system	Monoclinic	
Space group	C2/c	
Unit cell dimensions	a = 27.535(11) Å	α= 90°
	b = 11.390(5) Å	β= 129.447(7)°
	c = 20.157(8) Å	γ = 90°
Volume	4882(3) Å^3	
Z	8	
Density (calculated)	1.133 g/cm^3	

Absorption coefficient	0.133 mm^{-1}
F(000)	1808

Table C30. Data collection and structure refinement for 4.2a.

Diffractometer	CCD area detector
Radiation source	fine-focus sealed tube, MoKα
Generator power	1600 watts (50 kV, 32mA)
Detector distance	5.8 cm
Data collection method	phi and omega scans
Theta range for data collection	1.92 to 28.35°
Index ranges	$-30 \leq h \leq 36, -14 \leq k \leq 15, -26 \leq l \leq 26$

Table C31. Atomic coordinates and equivalent isotropic atomic displacement parameters ($Å^2$) for 4.2a.

U(eq) is defined as one third of the trace of the orthogonalized U_{ij} tensor.

	x	y	z	U(eq)
P1	0.04603(3)	0.44120(6)	0.74602(4)	0.0276(2)
N1	0.05306(11)	0.4540(2)	0.66438(15)	0.0326(5)
N2	-0.03219(10)	0.4463(2)	0.67892(14)	0.0290(5)
O2	0.07392(9)	0.30607(17)	0.76864(13)	0.0344(5)
O1	0.10123(9)	0.54063(17)	0.80291(13)	0.0344(5)
C14	-0.07959(14)	0.5953(3)	0.56443(19)	0.0378(6)
C7	0.05874(14)	0.3372(3)	0.6442(2)	0.0384(7)
C1	0.10827(14)	0.5193(3)	0.6977(2)	0.0396(7)
C13	-0.07571(13)	0.4779(3)	0.58904(18)	0.0332(6)
C2	0.13525(14)	0.5655(3)	0.7741(2)	0.0379(7)
C8	0.07235(14)	0.2588(3)	0.7022(2)	0.0370(6)
C20	-0.03387(17)	0.6913(3)	0.6244(2)	0.0459(8)
C9	0.09205(16)	0.1325(3)	0.7133(2)	0.0464(8)
C19	-0.11150(16)	0.2630(3)	0.5467(2)	0.0465(8)
C18	-0.11591(13)	0.3928(3)	0.52742(19)	0.0389(7)
C15	-0.12651(16)	0.6258(3)	0.4788(2)	0.0484(8)

C3	0.19605(16)	0.6314(3)	0.8350(2)	0.0514(9)
C16	-0.16852(16)	0.5437(4)	0.4183(2)	0.0534(9)
C10	0.0591(2)	0.0572(3)	0.7372(3)	0.0692(12)
C12	0.16379(19)	0.1259(4)	0.7855(3)	0.0705(12)
C11	0.0771(2)	0.0859(4)	0.6309(3)	0.0666(11)
C17	-0.16239(16)	0.4294(4)	0.4422(2)	0.0506(9)
C4	0.2353(3)	0.6162(7)	0.8073(4)	0.135(3)
C6	0.1848(3)	0.7609(5)	0.8350(5)	0.137(3)
C5	0.2297(3)	0.5851(7)	0.9241(4)	0.142(3)
C23	0.0016(2)	0.7402(4)	0.5949(3)	0.0624(10)
C21	-0.1716(2)	0.2208(4)	0.5292(3)	0.0720(13)
C22	-0.0996(2)	0.1897(4)	0.4944(3)	0.0721(12)
C24	-0.0663(2)	0.7909(4)	0.6333(3)	0.0712(12)

Table C32. Bond lengths (Å) for 4.2a.

P1-O1	1.641(2)	P1-O2	1.650(2)
P1-N2	1.664(2)	P1-N1	1.781(2)
P1-N2#1	1.780(2)	P1-P1#1	2.6395(17)
N1-C1	1.420(4)	N1-C7	1.428(4)
N2-C13	1.446(4)	N2-P1#1	1.780(2)
O2-C8	1.417(3)	O1-C2	1.410(3)
C14-C15	1.391(4)	C14-C13	1.406(4)
C14-C20	1.520(5)	C7-C8	1.322(4)
C7-H7	0.9300	C1-C2	1.321(5)
C1-H1	0.9300	C13-C18	1.400(4)
C2-C3	1.504(4)	C8-C9	1.504(4)
C20-C24	1.522(5)	C20-C23	1.535(5)
C20-H20	0.9800	C9-C11	1.530(5)
C9-C12	1.540(5)	C9-C10	1.531(5)
C19-C18	1.514(5)	C19-C21	1.534(5)
C19-C22	1.534(5)	C19-H19	0.9800
C18-C17	1.403(5)	C15-C16	1.381(5)
C15-H15	0.9300	C3-C4	1.509(6)
C3-C5	1.499(7)	C3-C6	1.507(7)
C16-C17	1.360(5)	C16-H16	0.9300
C10-H10A	0.9600	C10-H10B	0.9600
C10-H10C	0.9600	C12-H12A	0.9600
C12-H12B	0.9600	C12-H12C	0.9600
C11-H11A	0.9600	C11-H11B	0.9600
C11-H11C	0.9600	C17-H17	0.9300

C4-H4A	0.9600	C4-H4B	0.9600
C4-H4C	0.9600	C6-H6A	0.9600
C6-H6B	0.9600	C6-H6C	0.9600
C5-H5A	0.9600	C5-H5B	0.9600
C5-H5C	0.9600	C23-H23A	0.9600
C23-H23B	0.9600	C23-H23C	0.9600
C21-H21A	0.9600	C21-H21B	0.9600
C21-H21C	0.9600	C22-H22A	0.9600
C22-H22B	0.9600	C22-H22C	0.9600
C24-H24A	0.9600	C24-H24B	0.9600
C24-H24C	0.9600		

Symmetry transformations used to generate equivalent atoms (if any):
#1 -x,y,-z+3/2

Table C33. Bond angles (°) for 4.2a.

O1-P1-O2	112.88(11)	O1-P1-N2	133.62(11)
O2-P1-N2	113.06(11)	O1-P1-N1	89.59(11)
O2-P1-N1	91.55(11)	N2-P1-N1	95.19(12)
O1-P1-N2#1	89.27(11)	O2-P1-N2#1	96.24(10)
N2-P1-N2#1	79.88(12)	N1-P1-N2#1	171.94(11)
O1-P1-P1#1	117.16(8)	O2-P1-P1#1	106.24(7)
N2-P1-P1#1	41.63(8)	N1-P1-P1#1	136.76(9)
N2#1-P1-P1#1	38.38(7)	C1-N1-C7	110.1(2)
C1-N1-P1	108.53(19)	C7-N1-P1	106.38(19)
C13-N2-P1	129.90(18)	C13-N2-P1#1	128.20(18)
P1-N2-P1#1	99.99(12)	C8-O2-P1	111.32(18)
C2-O1-P1	114.43(18)	C15-C14-C13	118.5(3)
C15-C14-C20	117.0(3)	C13-C14-C20	124.4(3)
C8-C7-N1	113.5(3)	C8-C7-H7	123.3 N1-
C7-H7	123.3	C2-C1-N1	113.6(3)
C2-C1-H1	123.2	N1-C1-H1	123.2 C18-
C13-C14	120.3(3)	C18-C13-N2	119.9(3)
C14-C13-N2	119.7(3)	C1-C2-O1	111.8(3)
C1-C2-C3	131.4(3)	O1-C2-C3	116.7(3)
C7-C8-O2	113.6(3)	C7-C8-C9	130.6(3)
O2-C8-C9	115.6(3)	C14-C20-C24	112.3(3)
C14-C20-C23	111.2(3)	C24-C20-C23	109.9(3)
C14-C20-H20	107.8	C24-C20-H20	107.8 C23-
C20-H20	107.8	C8-C9-C11	110.4(3)
C8-C9-C12	108.1(3)	C11-C9-C12	108.0(3)
C8-C9-C10	110.6(3)	C11-C9-C10	110.0(3)

C12-C9-C10	109.7(4)	C18-C19-C21	110.3(3)
C18-C19-C22	111.8(3)	C21-C19-C22	110.0(3)
C18-C19-H19	108.2	C21-C19-H19	108.2 C22-
C19-H19	108.2	C17-C18-C13	118.2(3)
C17-C18-C19	117.8(3)	C13-C18-C19	124.0(3)
C16-C15-C14	121.5(3)	C16-C15-H15	119.2 C14-
C15-H15	119.2	C2-C3-C4	109.1(3)
C2-C3-C5	108.8(3)	C4-C3-C5	111.1(5)
C2-C3-C6	111.5(3)	C4-C3-C6	107.9(5)
C5-C3-C6	108.4(6)	C17-C16-C15	119.3(3)
C17-C16-H16	120.4	C15-C16-H16	120.4 C9-
C10-H10A	109.5	C9-C10-H10B	109.5 H10A-
C10-H10B	109.5	C9-C10-H10C	109.5 H10A-
C10-H10C	109.5	H10B-C10-H10C	109.5 C9-
C12-H12A	109.5	C9-C12-H12B	109.5 H12A-
C12-H12B	109.5	C9-C12-H12C	109.5 H12A-
C12-H12C	109.5	H12B-C12-H12C	109.5 C9-
C11-H11A	109.5	C9-C11-H11B	109.5 H11A-
C11-H11B	109.5	C9-C11-H11C	109.5 H11A-
C11-H11C	109.5	H11B-C11-H11C	109.5 C16-
C17-C18	122.0(3)	C16-C17-H17	119.0 C18-
C17-H17	119.0	C3-C4-H4A	109.5 C3-C4-
H4B	109.5	H4A-C4-H4B	109.5 C3-C4-
H4C	109.5	H4A-C4-H4C	109.5 H4B-
C4-H4C	109.5	C3-C6-H6A	109.5 C3-C6-
H6B	109.5	H6A-C6-H6B	109.5 C3-C6-
H6C	109.5	H6A-C6-H6C	109.5 H6B-
C6-H6C	109.5	C3-C5-H5A	109.5 C3-C5-
H5B	109.5	H5A-C5-H5B	109.5 C3-C5-
H5C	109.5	H5A-C5-H5C	109.5 H5B-
C5-H5C	109.5	C20-C23-H23A	109.5 C20-
C23-H23B	109.5	H23A-C23-H23B	109.5 C20-
C23-H23C	109.5	H23A-C23-H23C	109.5 H23B-
C23-H23C	109.5	C19-C21-H21A	109.5 C19-
C21-H21B	109.5	H21A-C21-H21B	109.5 C19-
C21-H21C	109.5	H21A-C21-H21C	109.5 H21B-
C21-H21C	109.5	C19-C22-H22A	109.5 C19-
C22-H22B	109.5	H22A-C22-H22B	109.5 C19-
C22-H22C	109.5	H22A-C22-H22C	109.5 H22B-
C22-H22C	109.5	C20-C24-H24A	109.5 C20-
C24-H24B	109.5	H24A-C24-H24B	109.5 C20-
C24-H24C	109.5	H24A-C24-H24C	109.5 H24B-
C24-H24C	109.5		

Symmetry transformations used to generate equivalent atoms (if any):

#1 -x,y,-z+3/2

Table C34. Torsion angles (°) for 4.2a.

O1-P1-N1-C1	12.0(2)	O2-P1-N1-C1	-100.9(2)
N2-P1-N1-C1	145.8(2)	N2#1-P1-N1-C1	93.9(8)
P1#1-P1-N1-C1	143.23(16)	O1-P1-N1-C7	130.52(19)
O2-P1-N1-C7	17.64(19)	N2-P1-N1-C7	-95.68(19)
N2#1-P1-N1-C7	-147.6(7)	P1#1-P1-N1-C7	-98.28(19)
O1-P1-N2-C13	82.1(3)	O2-P1-N2-C13	-106.2(2)
N1-P1-N2-C13	-12.3(3)	N2#1-P1-N2-C13	161.2(2)
P1#1-P1-N2-C13	165.0(3)	O1-P1-N2-P1#1	-82.93(17)
O2-P1-N2-P1#1	88.76(13)	N1-P1-N2-P1#1	-177.33(11)
N2#1-P1-N2-P1#1	-3.76(15)	O1-P1-O2-C8	-106.19(19)
N2-P1-O2-C8	80.3(2)	N1-P1-O2-C8	-15.98(19)
N2#1-P1-O2-C8	161.97(18)	P1#1-P1-O2-C8	124.10(17)
O2-P1-O1-C2	78.0(2)	N2-P1-O1-C2	-110.3(2)
N1-P1-O1-C2	-13.5(2)	N2#1-P1-O1-C2	174.5(2)
P1#1-P1-O1-C2	-158.10(17)	C1-N1-C7-C8	102.1(3)
P1-N1-C7-C8	-15.3(3)	C7-N1-C1-C2	-124.1(3)
P1-N1-C1-C2	-8.0(3)	C15-C14-C13-C18	3.8(4)
C20-C14-C13-C18	-173.2(3)	C15-C14-C13-N2	-173.0(3)
C20-C14-C13-N2	9.9(4)	P1-N2-C13-C18	113.3(3)
P1#1-N2-C13-C18	-85.6(3)	P1-N2-C13-C14	-69.9(3)
P1#1-N2-C13-C14	91.2(3)	N1-C1-C2-O1	-1.5(4)
N1-C1-C2-C3	174.4(3)	P1-O1-C2-C1	11.6(3)
P1-O1-C2-C3	-165.0(2)	N1-C7-C8-O2	4.3(4)
N1-C7-C8-C9	-169.3(3)	P1-O2-C8-C7	10.0(3)
P1-O2-C8-C9	-175.4(2)	C15-C14-C20-C24	63.8(4)
C13-C14-C20-C24	-119.1(4)	C15-C14-C20-C23	-59.8(4)
C13-C14-C20-C23	117.3(3)	C7-C8-C9-C11	-16.8(5)
O2-C8-C9-C11	169.7(3)	C7-C8-C9-C12	101.1(4)
O2-C8-C9-C12	-72.4(4)	C7-C8-C9-C10	-138.8(4)
O2-C8-C9-C10	47.8(4)	C14-C13-C18-C17	-4.1(4)
N2-C13-C18-C17	172.7(3)	C14-C13-C18-C19	174.6(3)
N2-C13-C18-C19	-8.6(4)	C21-C19-C18-C17	-64.1(4)
C22-C19-C18-C17	58.7(4)	C21-C19-C18-C13	117.2(3)
C22-C19-C18-C13	-120.0(3)	C13-C14-C15-C16	-0.4(5)
C20-C14-C15-C16	176.8(3)	C1-C2-C3-C4	-13.9(6)
O1-C2-C3-C4	161.9(4)	C1-C2-C3-C5	-135.3(5)
O1-C2-C3-C5	40.5(5)	C1-C2-C3-C6	105.3(5)
O1-C2-C3-C6	-79.0(5)	C14-C15-C16-C17	-2.6(5)
C15-C16-C17-C18	2.3(6)	C13-C18-C17-C16	1.0(5)
C19-C18-C17-C16	-177.8(3)		

Symmetry transformations used to generate equivalent atoms (if any):
#1 -x,y,-z+3/2

Table C35. Anisotropic atomic displacement parameters (Å^2) for 4.2a.
The anisotropic atomic displacement factor exponent takes the form: $-2\pi^2 [h^2a^{*2} U_{11} + ... + 2hka^* b^* U_{12}]$

	U_{11}	U_{22}	U_{33}	U_{23}	U_{13}
	U_{12}				
P1	0.0232(3)	0.0308(3)	0.0283(4)	-0.0010(3)	0.0161(3)
	-0.0006(2)				
N1	0.0305(12)	0.0393(13)	0.0310(12)	-0.0026(9)	0.0209(10)
	-0.0035(9)				
N2	0.0251(11)	0.0351(12)	0.0257(11)	-0.0003(9)	0.0156(10)
	-0.0009(8)				
O2	0.0341(10)	0.0346(10)	0.0378(11)	0.0010(8)	0.0244(9)
	0.0049(8)				
O1	0.0300(10)	0.0397(11)	0.0362(11)	-0.0070(8)	0.0223(9)
	-0.0086(8)				
C14	0.0359(15)	0.0460(16)	0.0333(15)	0.0029(12)	0.0228(13)
	0.0046(12)				
C7	0.0370(15)	0.0447(16)	0.0389(16)	-0.0094(13)	0.0267(14)
	-0.0049(12)				
C1	0.0370(15)	0.0438(16)	0.0476(18)	-0.0007(13)	0.0314(15)
	-0.0034(13)				
C13	0.0256(13)	0.0424(15)	0.0301(14)	-0.0011(11)	0.0170(12)
	0.0025(11)				
C2	0.0312(14)	0.0399(15)	0.0477(18)	-0.0035(13)	0.0274(14)
	-0.0059(12)				
C8	0.0345(15)	0.0377(15)	0.0421(17)	-0.0076(12)	0.0259(14)
	-0.0008(11)				
C20	0.0527(19)	0.0396(16)	0.0396(17)	0.0034(13)	0.0265(16)
	-0.0001(14)				
C9	0.0467(18)	0.0404(17)	0.059(2)	-0.0041(15)	0.0369(17)
	0.0037(13)				
C19	0.0383(16)	0.0523(19)	0.0376(17)	-0.0106(14)	0.0189(14)
	-0.0110(14)				
C18	0.0253(13)	0.0526(18)	0.0347(16)	-0.0047(13)	0.0171(12)
	-0.0008(12)				
C15	0.0446(18)	0.057(2)	0.0384(18)	0.0129(15)	0.0237(15)
	0.0136(15)				
C3	0.0368(17)	0.060(2)	0.058(2)	-0.0140(17)	0.0303(17)
	-0.0156(15)				

C16	0.0378(17)	0.081(3)	0.0282(16)	0.0064(16)	0.0149(14)
	0.0142(17)				
C10	0.087(3)	0.0374(18)	0.107(4)	0.001(2)	0.073(3)
	-0.0006(18)				
C12	0.052(2)	0.069(3)	0.081(3)	0.003(2)	0.038(2)
	0.019(2)				
C11	0.080(3)	0.053(2)	0.076(3)	-0.014(2)	0.054(3)
	0.006(2)				
C17	0.0338(16)	0.073(2)	0.0315(16)	-0.0059(16)	0.0143(14)
	-0.0005(15)				
C4	0.077(3)	0.223(8)	0.146(6)	-0.114(6)	0.090(4)
	-0.094(5)				
C6	0.079(4)	0.071(3)	0.230(8)	-0.058(4)	0.084(5)
	-0.039(3)				
C5	0.060(3)	0.208(8)	0.068(4)	0.013(4)	-0.002(3)
	-0.060(4)				
C23	0.060(2)	0.058(2)	0.069(3)	0.0064(19)	0.040(2)
	-0.0039(18)				
C21	0.054(2)	0.086(3)	0.065(3)	-0.010(2)	0.033(2)
	-0.030(2)				
C22	0.076(3)	0.065(3)	0.066(3)	-0.022(2)	0.040(2)
	-0.004(2)				
C24	0.089(3)	0.050(2)	0.093(3)	-0.005(2)	0.067(3)
	0.002(2)				

Table C36. Hydrogen atom coordinates and isotropic atomic displacement parameters (Å^2) for 4.2a.

	x/a	y/b	z/c	U
H7	0.0534	0.3181	0.5951	0.046
H1	0.1239	0.5286	0.6686	0.048
H20	-0.0028	0.6564	0.6814	0.055
H19	-0.0761	0.2510	0.6078	0.056
H15	-0.1297	0.7033	0.4619	0.058
H16	-0.2006	0.5662	0.3618	0.064
H10A	0.0676	0.0886	0.7878	0.104
H10B	0.0744	-0.0219	0.7480	0.104
H10C	0.0145	0.0578	0.6906	0.104
H12A	0.1844	0.1713	0.7696	0.106
H12B	0.1773	0.0457	0.7943	0.106
H12C	0.1745	0.1568	0.8376	0.106
H11A	0.0325	0.0892	0.5848	0.100
H11B	0.0912	0.0061	0.6395	0.100
H11C	0.0982	0.1332	0.6166	0.100
H17	-0.1898	0.3740	0.4008	0.061
H4A	0.2735	0.6604	0.8448	0.203
H4B	0.2122	0.6438	0.7495	0.203
H4C	0.2452	0.5346	0.8101	0.203
H6A	0.1651	0.7737	0.8602	0.205
H6B	0.1579	0.7897	0.7771	0.205
H6C	0.2243	0.8019	0.8679	0.205
H5A	0.2031	0.5932	0.9394	0.213
H5B	0.2678	0.6286	0.9639	0.213
H5C	0.2396	0.5037	0.9261	0.213
H23A	0.0172	0.6764	0.5821	0.094
H23B	0.0361	0.7877	0.6397	0.094
H23C	-0.0265	0.7872	0.5443	0.094
H21A	-0.1793	0.2684	0.5610	0.108
H21B	-0.1667	0.1404	0.5466	0.108
H21C	-0.2065	0.2274	0.4689	0.108
H22A	-0.1357	0.1942	0.4345	0.108
H22B	-0.0923	0.1094	0.5129	0.108
H22C	-0.0634	0.2198	0.5029	0.108
H24A	-0.0993	0.8226	0.5776	0.107
H24B	-0.0362	0.8514	0.6692	0.107
H24C	-0.0837	0.7615	0.6588	0.107

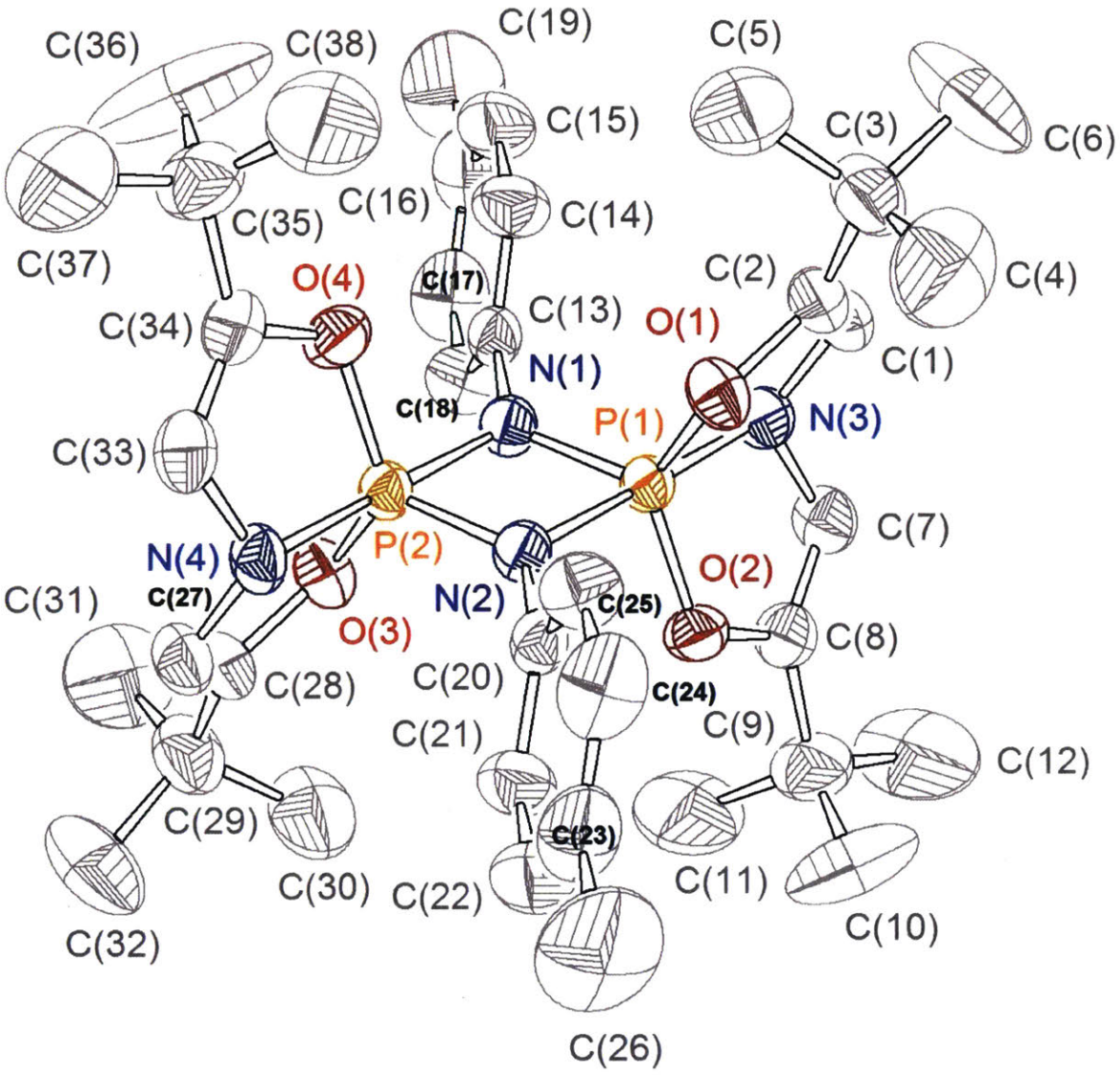

A colorless block shaped crystal of **4.7a** (C38 H54 N4 O4 P2) with approximate dimensions 0.21 x 0.26 x 0.32 mm, was used for the X-ray crystallographic analysis. The X-ray intensity data were measured at 298(2) K, on a Bruker SMART APEX CCD area detector system equipped with a graphite monochromator and a MoKα fine-focus sealed tube (λ = 0.71073Å) operated at 1600 watts power (50 kV, 32 mA). The detector was placed at a distance of 5.8 cm from the crystal.

A total of 1850 frames were collected with a scan width of 0.3° in ω and an exposure time of 10 seconds/frame. The total data collection time was about 8 hours. The frames were integrated with

the Bruker SAINT software package using a narrow-frame integration algorithm. The integration of the data using a Monoclinic unit cell yielded a total of 30213 reflections to a maximum θ angle of 28.42° (0.90 Å resolution), of which 10085 were independent, completeness = 98.5%, R_{int} = 0.0337, R_{sig} = 0.0450 and 7052 were greater than 2σ(I). The final cell constants: a = 9.2449(12)Å, b = 21.052(3)Å, c = 20.977(3)Å, α = 90°, β = 94.271(2)°, γ = 90°, volume = 4071.3(10)Å^3, are based upon the refinement of the XYZ-centroids of 5650 reflections above 20σ(I) with 2.411° <θ <25.944°. Analysis of the data showed negligible decay during data collection. Data were corrected for absorption effects using the multiscan technique (SADABS). The ratio of minimum to maximum apparent transmission was 0.7582.

The structure was solved and refined using the Bruker SHELXTL (Version 6.1) Software Package, using the space group P2(1)/n, with Z = 4 for the formula unit, C38 H54 N4 O4 P2. The final anisotropic full-matrix least-squares refinement on F^2 with 447 variables converged at R1 = 8.05%, for the observed data and wR2 = 23.90% for all data. The goodness-of-fit was 1.100. The largest peak on the final difference map was 0.764 e$^-$/Å^3 and the largest hole was -0.286 e$^-$/Å^3. Based on the final model, the calculated density of the crystal is 1.130 g/cm^3 and F(000) amounts to 1488 electrons.

Table C37. Sample and crystal data for 4.7a.

Identification code	yzl1	
Empirical formula	C38 H54 N4 O4 P2	
Formula weight	692.79	
Temperature	298(2) K	
Wavelength	0.71073 Å	
Crystal size	0.32 x 0.26 x 0.21 mm	
Crystal habit	colorless block	
Crystal system	Monoclinic	
Space group	P2(1)/n	
Unit cell dimensions	a = 9.2449(12) Å	α= 90°
	b = 21.052(3) Å	β= 94.271(2)°
	c = 20.977(3) Å	γ = 90°
Volume	4071.3(10) Å^3	
Z	4	
Density (calculated)	1.130 g/cm^3	

Absorption coefficient	0.147 mm^{-1}
F(000)	1488

Table C38. Data collection and structure refinement for 4.7a.

Diffractometer	CCD area detector
Radiation source	fine-focus sealed tube, MoKα
Generator power	1600 watts (50 kV, 32mA)
Detector distance	5.8 cm
Data collection method	phi and omega scans
Theta range for data collection	1.93 to 28.42°
Index ranges	$-12 \leq h \leq 12, -27 \leq k \leq 28, -28 \leq l \leq 25$

Table C39. Atomic coordinates and equivalent isotropic atomic displacement parameters ($Å^2$) for 4.7a.

U(eq) is defined as one third of the trace of the orthogonalized U_{ij} tensor.

	x	y	z	U(eq)
C1	0.8485(4)	0.05685(19)	0.30448(19)	0.0498(9)
C2	0.7411(4)	0.03179(18)	0.33420(19)	0.0480(9)
C3	0.7363(5)	-0.0020(2)	0.3970(2)	0.0664(12)
C4	0.6435(11)	-0.0601(4)	0.3882(4)	0.183(5)
C5	0.6736(11)	0.0411(4)	0.4448(3)	0.157(4)
C6	0.8882(7)	-0.0206(4)	0.4217(3)	0.141(3)
C7	0.8590(4)	0.07653(18)	0.18970(19)	0.0486(9)
C8	0.7577(4)	0.06303(19)	0.14421(19)	0.0487(9)
C9	0.7631(5)	0.0504(2)	0.0738(2)	0.0663(12)
C10	0.7216(9)	-0.0184(3)	0.0603(3)	0.116(2)
C11	0.6569(7)	0.0941(3)	0.0357(3)	0.099(2)
C12	0.9172(6)	0.0632(4)	0.0545(3)	0.103(2)
C13	0.6759(3)	0.21678(15)	0.25968(18)	0.0391(7)
C14	0.7031(4)	0.24214(19)	0.3201(2)	0.0540(10)
C15	0.7962(5)	0.2935(2)	0.3293(3)	0.0706(13)
C16	0.8639(5)	0.3197(2)	0.2809(3)	0.0708(14)

C17	0.8388(5)	0.2935(2)	0.2212(3)	0.0752(15)
C18	0.7437(5)	0.24304(19)	0.2097(2)	0.0573(10)
C19	0.9695(7)	0.3753(3)	0.2910(4)	0.124(3)
C20	0.3217(3)	0.03646(15)	0.22495(17)	0.0387(7)
C21	0.2845(5)	0.0084(2)	0.1663(2)	0.0570(10)
C22	0.1911(5)	-0.0430(2)	0.1629(3)	0.0745(14)
C23	0.1339(5)	-0.0673(2)	0.2159(3)	0.0744(15)
C24	0.1715(5)	-0.0396(2)	0.2727(3)	0.0720(14)
C25	0.2659(5)	0.01208(19)	0.2781(2)	0.0580(10)
C26	0.0287(7)	-0.1235(3)	0.2109(4)	0.131(3)
C27	0.1488(4)	0.19786(18)	0.17552(18)	0.0466(8)
C28	0.2564(4)	0.22347(19)	0.14625(18)	0.0477(9)
C29	0.2622(5)	0.2587(2)	0.0844(2)	0.0677(12)
C30	0.3316(9)	0.2157(4)	0.0365(3)	0.127(3)
C31	0.3504(9)	0.3186(3)	0.0940(3)	0.127(3)
C32	0.1082(7)	0.2737(5)	0.0584(3)	0.149(4)
C33	0.1385(4)	0.17662(18)	0.28945(18)	0.0468(9)
C34	0.2382(4)	0.18945(18)	0.33535(18)	0.0463(8)
C35	0.2338(5)	0.2005(2)	0.4057(2)	0.0641(12)
C36	0.2963(9)	0.2657(3)	0.4230(3)	0.114(2)
C37	0.0766(7)	0.1958(5)	0.4233(3)	0.138(3)
C38	0.3238(7)	0.1508(3)	0.4426(2)	0.0873(16)
N1	0.5777(3)	0.16457(12)	0.24902(14)	0.0370(6)
N2	0.4204(3)	0.08903(13)	0.23025(14)	0.0377(6)
N3	0.7990(3)	0.08971(14)	0.24818(15)	0.0417(7)
N4	0.1971(3)	0.16365(14)	0.23108(14)	0.0404(6)
O1	0.6061(3)	0.04270(12)	0.30189(12)	0.0467(6)
O2	0.6170(3)	0.06251(12)	0.16589(12)	0.0459(6)
O3	0.3913(2)	0.21294(11)	0.17887(12)	0.0435(6)
O4	0.3792(2)	0.18998(12)	0.31397(12)	0.0439(6)
P1	0.60954(8)	0.08889(4)	0.23921(4)	0.0336(2)
P2	0.38774(8)	0.16499(4)	0.24049(4)	0.0332(2)

Table C40. Bond lengths (Å) for 4.7a.

C1-C2	1.321(5)	C1-N3	1.415(5)
C1-H1	0.9300	C2-O1	1.395(4)
C2-C3	1.500(6)	C3-C4	1.497(8)
C3-C5	1.501(8)	C3-C6	1.512(7)
C4-H4A	0.9600	C4-H4B	0.9600
C4-H4C	0.9600	C5-H5A	0.9600
C5-H5B	0.9600	C5-H5C	0.9600
C6-H6A	0.9600	C6-H6B	0.9600

C6-H6C	0.9600	C7-C8	1.317(5)
C7-N3	1.411(5)	C7-H7	0.9300
C8-O2	1.409(4)	C8-C9	1.506(6)
C9-C10	1.519(8)	C9-C11	1.527(7)
C9-C12	1.533(7)	C10-H10A	0.9600
C10-H10B	0.9600	C10-H10C	0.9600
C11-H11A	0.9600	C11-H11B	0.9600
C11-H11C	0.9600	C12-H12A	0.9600
C12-H12B	0.9600	C12-H12C	0.9600
C13-C18	1.377(5)	C13-C14	1.382(5)
C13-N1	1.433(4)	C14-C15	1.386(6)
C14-H14	0.9300	C15-C16	1.351(7)
C15-H15	0.9300	C16-C17	1.371(7)
C16-C19	1.528(6)	C17-C18	1.388(6)
C17-H17	0.9300	C18-H18	0.9300
C19-H19A	0.9600	C19-H19B	0.9600
C19-H19C	0.9600	C20-C25	1.363(5)
C20-C21	1.385(5)	C20-N2	1.433(4)
C21-C22	1.383(6)	C21-H21	0.9300
C22-C23	1.365(7)	C22-H22	0.9300
C23-C24	1.349(7)	C23-C26	1.531(6)
C24-C25	1.394(6)	C24-H24	0.9300
C25-H25	0.9300	C26-H26A	0.9600
C26-H26B	0.9600	C26-H26C	0.9600
C27-C28	1.322(5)	C27-N4	1.414(4)
C27-H27	0.9300	C28-O3	1.395(4)
C28-C29	1.500(5)	C29-C31	1.506(8)
C29-C32	1.519(7)	C29-C30	1.527(8)
C30-H30A	0.9600	C30-H30B	0.9600
C30-H30C	0.9600	C31-H31A	0.9600
C31-H31B	0.9600	C31-H31C	0.9600
C32-H32A	0.9600	C32-H32B	0.9600
C32-H32C	0.9600	C33-C34	1.310(5)
C33-N4	1.402(5)	C33-H33	0.9300
C34-O4	1.410(4)	C34-C35	1.497(5)
C35-C38	1.514(7)	C35-C36	1.522(8)
C35-C37	1.530(7)	C36-H36A	0.9600
C36-H36B	0.9600	C36-H36C	0.9600
C37-H37A	0.9600	C37-H37B	0.9600
C37-H37C	0.9600	C38-H38A	0.9600
C38-H38B	0.9600	C38-H38C	0.9600
N1-P1	1.636(3)	N1-P2	1.752(3)
N2-P2	1.644(3)	N2-P1	1.745(3)
N3-P1	1.748(3)	N4-P2	1.759(3)
O1-P1	1.638(3)	O2-P1	1.642(3)
O3-P2	1.642(2)	O4-P2	1.636(3)

Table C41. Bond angles (°) for 4.7a.

C2-C1-N3	112.4(3)	C2-C1-H1	123.8 N3-
C1-H1	123.8	C1-C2-O1	112.5(3)
C1-C2-C3	132.6(4)	O1-C2-C3	114.9(3)
C4-C3-C2	109.5(4)	C4-C3-C5	109.3(7)
C2-C3-C5	109.7(4)	C4-C3-C6	109.9(6)
C2-C3-C6	109.6(4)	C5-C3-C6	108.8(6)
C3-C4-H4A	109.5	C3-C4-H4B	109.5 H4A-
C4-H4B	109.5	C3-C4-H4C	109.5 H4A-
C4-H4C	109.5	H4B-C4-H4C	109.5 C3-C5-
H5A	109.5	C3-C5-H5B	109.5 H5A-
C5-H5B	109.5	C3-C5-H5C	109.5 H5A-
C5-H5C	109.5	H5B-C5-H5C	109.5 C3-C6-
H6A	109.5	C3-C6-H6B	109.5 H6A-
C6-H6B	109.5	C3-C6-H6C	109.5 H6A-
C6-H6C	109.5	H6B-C6-H6C	109.5 C8-C7-
N3	111.6(3)	C8-C7-H7	124.2 N3-
C7-H7	124.2	C7-C8-O2	113.0(3)
C7-C8-C9	132.5(4)	O2-C8-C9	114.5(3)
C8-C9-C10	108.9(4)	C8-C9-C11	109.9(4)
C10-C9-C11	109.4(5)	C8-C9-C12	109.1(4)
C10-C9-C12	110.2(5)	C11-C9-C12	109.3(5)
C9-C10-H10A	109.5	C9-C10-H10B	109.5 H10A-
C10-H10B	109.5	C9-C10-H10C	109.5 H10A-
C10-H10C	109.5	H10B-C10-H10C	109.5 C9-
C11-H11A	109.5	C9-C11-H11B	109.5 H11A-
C11-H11B	109.5	C9-C11-H11C	109.5 H11A-
C11-H11C	109.5	H11B-C11-H11C	109.5 C9-
C12-H12A	109.5	C9-C12-H12B	109.5 H12A-
C12-H12B	109.5	C9-C12-H12C	109.5 H12A-
C12-H12C	109.5	H12B-C12-H12C	109.5 C18-
C13-C14	118.8(3)	C18-C13-N1	120.6(3)
C14-C13-N1	120.6(3)	C13-C14-C15	119.8(4)
C13-C14-H14	120.1	C15-C14-H14	120.1 C16-
C15-C14	122.2(5)	C16-C15-H15	118.9 C14-
C15-H15	118.9	C15-C16-C17	117.7(4)
C15-C16-C19	122.4(6)	C17-C16-C19	119.8(5)
C16-C17-C18	121.9(4)	C16-C17-H17	119.0 C18-
C17-H17	119.0	C13-C18-C17	119.5(4)

C13-C18-H18	120.2	C17-C18-H18	120.2 C16-
C19-H19A	109.5	C16-C19-H19B	109.5 H19A-
C19-H19B	109.5	C16-C19-H19C	109.5 H19A-
C19-H19C	109.5	H19B-C19-H19C	109.5 C25-
C20-C21	118.8(3)	C25-C20-N2	120.3(3)
C21-C20-N2	120.9(3)	C22-C21-C20	119.6(4)
C22-C21-H21	120.2	C20-C21-H21	120.2 C23-
C22-C21	121.9(5)	C23-C22-H22	119.0 C21-
C22-H22	119.0	C24-C23-C22	117.9(4)
C24-C23-C26	121.0(6)	C22-C23-C26	121.1(6)
C23-C24-C25	121.8(5)	C23-C24-H24	119.1 C25-
C24-H24	119.1	C20-C25-C24	120.0(4)
C20-C25-H25	120.0	C24-C25-H25	120.0 C23-
C26-H26A	109.5	C23-C26-H26B	109.5 H26A-
C26-H26B	109.5	C23-C26-H26C	109.5 H26A-
C26-H26C	109.5	H26B-C26-H26C	109.5 C28-
C27-N4	112.9(3)	C28-C27-H27	123.6 N4-
C27-H27	123.6	C27-C28-O3	112.6(3)
C27-C28-C29	132.9(4)	O3-C28-C29	114.5(3)
C28-C29-C31	110.6(4)	C28-C29-C32	108.6(4)
C31-C29-C32	111.0(6)	C28-C29-C30	108.6(4)
C31-C29-C30	109.5(5)	C32-C29-C30	108.4(6)
C29-C30-H30A	109.5	C29-C30-H30B	109.5 H30A-
C30-H30B	109.5	C29-C30-H30C	109.5 H30A-
C30-H30C	109.5	H30B-C30-H30C	109.5 C29-
C31-H31A	109.5	C29-C31-H31B	109.5 H31A-
C31-H31B	109.5	C29-C31-H31C	109.5 H31A-
C31-H31C	109.5	H31B-C31-H31C	109.5 C29-
C32-H32A	109.5	C29-C32-H32B	109.5 H32A-
C32-H32B	109.5	C29-C32-H32C	109.5 H32A-
C32-H32C	109.5	H32B-C32-H32C	109.5 C34-
C33-N4	112.7(3)	C34-C33-H33	123.7 N4-
C33-H33	123.7	C33-C34-O4	112.6(3)
C33-C34-C35	133.4(4)	O4-C34-C35	113.9(3)
C34-C35-C38	110.1(4)	C34-C35-C36	109.7(4)
C38-C35-C36	108.5(5)	C34-C35-C37	108.9(4)
C38-C35-C37	109.0(5)	C36-C35-C37	110.6(5)
C35-C36-H36A	109.5	C35-C36-H36B	109.5 H36A-
C36-H36B	109.5	C35-C36-H36C	109.5 H36A-
C36-H36C	109.5	H36B-C36-H36C	109.5 C35-
C37-H37A	109.5	C35-C37-H37B	109.5 H37A-
C37-H37B	109.5	C35-C37-H37C	109.5 H37A-
C37-H37C	109.5	H37B-C37-H37C	109.5 C35-
C38-H38A	109.5	C35-C38-H38B	109.5 H38A-
C38-H38B	109.5	C35-C38-H38C	109.5 H38A-
C38-H38C	109.5	H38B-C38-H38C	109.5 C13-

N1-P1	130.4(2)	C13-N1-P2	129.1(2)
P1-N1-P2	100.41(14)	C20-N2-P2	129.7(2)
C20-N2-P1	129.4(2)	P2-N2-P1	100.36(14)
C7-N3-C1	120.4(3)	C7-N3-P1	111.1(2)
C1-N3-P1	110.1(2)	C33-N4-C27	120.1(3)
C33-N4-P2	110.3(2)	C27-N4-P2	109.7(2)
C2-O1-P1	114.7(2)	C8-O2-P1	113.8(2)
C28-O3-P2	114.4(2)	C34-O4-P2	114.1(2)
N1-P1-O1	117.57(15)	N1-P1-O2	117.90(15)
O1-P1-O2	123.78(14)	N1-P1-N2	79.83(13)
O1-P1-N2	90.46(13)	O2-P1-N2	90.66(13)
N1-P1-N3	99.52(14)	O1-P1-N3	89.93(13)
O2-P1-N3	89.56(13)	N2-P1-N3	179.34(14)
O4-P2-O3	123.30(14)	O4-P2-N2	117.25(14)
O3-P2-N2	118.71(14)	O4-P2-N1	91.36(13)
O3-P2-N1	90.26(13)	N2-P2-N1	79.40(13)
O4-P2-N4	89.57(13)	O3-P2-N4	90.02(13)
N2-P2-N4	99.33(14)	N1-P2-N4	178.67(15)

Table C42. Torsion angles (°) for 4.7a.

N3-C1-C2-O1	1.4(5)	N3-C1-C2-C3	-174.2(4)
C1-C2-C3-C4	-134.5(7)	O1-C2-C3-C4	50.0(7)
C1-C2-C3-C5	105.6(7)	O1-C2-C3-C5	-69.9(6)
C1-C2-C3-C6	-13.8(8)	O1-C2-C3-C6	170.7(5)
N3-C7-C8-O2	-2.5(5)	N3-C7-C8-C9	175.0(4)
C7-C8-C9-C10	113.4(6)	O2-C8-C9-C10	-69.0(5)
C7-C8-C9-C11	-126.7(5)	O2-C8-C9-C11	50.8(6)
C7-C8-C9-C12	-6.9(7)	O2-C8-C9-C12	170.6(4)
C18-C13-C14-C15	0.6(6)	N1-C13-C14-C15	-178.7(4)
C13-C14-C15-C16	-0.8(7)	C14-C15-C16-C17	-0.6(7)
C14-C15-C16-C19	-178.5(5)	C15-C16-C17-C18	2.2(7)
C19-C16-C17-C18	-179.9(5)	C14-C13-C18-C17	0.9(6)
N1-C13-C18-C17	-179.8(4)	C16-C17-C18-C13	-2.4(7)
C25-C20-C21-C22	0.6(6)	N2-C20-C21-C22	178.8(4)
C20-C21-C22-C23	0.0(7)	C21-C22-C23-C24	-0.2(8)
C21-C22-C23-C26	178.9(5)	C22-C23-C24-C25	-0.1(8)
C26-C23-C24-C25	-179.3(5)	C21-C20-C25-C24	-0.9(6)
N2-C20-C25-C24	-179.1(4)	C23-C24-C25-C20	0.7(7)
N4-C27-C28-O3	-2.7(5)	N4-C27-C28-C29	174.3(4)
C27-C28-C29-C31	131.9(6)	O3-C28-C29-C31	-51.2(6)

C27-C28-C29-C32	9.8(8)	O3-C28-C29-C32	-173.2(5)
C27-C28-C29-C30	-107.9(6)	O3-C28-C29-C30	69.1(6)
N4-C33-C34-O4	2.8(5)	N4-C33-C34-C35	-173.8(4)
C33-C34-C35-C38	118.7(5)	O4-C34-C35-C38	-57.9(5)
C33-C34-C35-C36	-122.0(6)	O4-C34-C35-C36	61.4(5)
C33-C34-C35-C37	-0.9(8)	O4-C34-C35-C37	-177.4(5)
C18-C13-N1-P1	78.5(4)	C14-C13-N1-P1	-102.3(4)
C18-C13-N1-P2	-99.4(4)	C14-C13-N1-P2	79.9(4)
C25-C20-N2-P2	-77.2(4)	C21-C20-N2-P2	104.7(4)
C25-C20-N2-P1	92.4(4)	C21-C20-N2-P1	-85.7(4)
C8-C7-N3-C1	126.9(4)	C8-C7-N3-P1	-4.0(4)
C2-C1-N3-C7	-128.5(4)	C2-C1-N3-P1	2.7(4)
C34-C33-N4-C27	-126.0(4)	C34-C33-N4-P2	3.1(4)
C28-C27-N4-C33	127.4(4)	C28-C27-N4-P2	-2.0(4)
C1-C2-O1-P1	-5.4(4)	C3-C2-O1-P1	171.1(3)
C7-C8-O2-P1	8.6(4)	C9-C8-O2-P1	-169.5(3)
C27-C28-O3-P2	6.7(4)	C29-C28-O3-P2	-170.9(3)
C33-C34-O4-P2	-8.1(4)	C35-C34-O4-P2	169.2(3)
C13-N1-P1-O1	96.8(3)	P2-N1-P1-O1	-84.87(17)
C13-N1-P1-O2	-92.7(3)	P2-N1-P1-O2	85.60(16)
C13-N1-P1-N2	-178.0(3)	P2-N1-P1-N2	0.29(14)
C13-N1-P1-N3	1.9(3)	P2-N1-P1-N3	-179.81(15)
C2-O1-P1-N1	-94.9(3)	C2-O1-P1-O2	95.2(3)
C2-O1-P1-N2	-173.7(3)	C2-O1-P1-N3	5.8(3)
C8-O2-P1-N1	91.6(3)	C8-O2-P1-O1	-98.5(3)
C8-O2-P1-N2	170.5(2)	C8-O2-P1-N3	-8.9(3)
C20-N2-P1-N1	-172.2(3)	P2-N2-P1-N1	-0.31(15)
C20-N2-P1-O1	-54.2(3)	P2-N2-P1-O1	117.65(16)
C20-N2-P1-O2	69.5(3)	P2-N2-P1-O2	-118.56(16)
C20-N2-P1-N3	179(100)	P2-N2-P1-N3	-9(13)
C7-N3-P1-N1	-110.8(3)	C1-N3-P1-N1	113.2(3)
C7-N3-P1-O1	131.2(3)	C1-N3-P1-O1	-4.8(3)
C7-N3-P1-O2	7.4(3)	C1-N3-P1-O2	-128.6(3)
C7-N3-P1-N2	-102(13)	C1-N3-P1-N2	122(13)
C34-O4-P2-O3	97.9(3)	C34-O4-P2-N2	-92.1(3)
C34-O4-P2-N1	-170.9(2)	C34-O4-P2-N4	8.1(2)
C28-O3-P2-O4	-96.0(3)	C28-O3-P2-N2	94.2(3)
C28-O3-P2-N1	172.2(3)	C28-O3-P2-N4	-6.5(3)
C20-N2-P2-O4	86.1(3)	P1-N2-P2-O4	-85.74(16)
C20-N2-P2-O3	-103.4(3)	P1-N2-P2-O3	84.71(17)
C20-N2-P2-N1	172.1(3)	P1-N2-P2-N1	0.29(14)
C20-N2-P2-N4	-8.3(3)	P1-N2-P2-N4	179.90(14)
C13-N1-P2-O4	-64.5(3)	P1-N1-P2-O4	117.18(15)
C13-N1-P2-O3	58.8(3)	P1-N1-P2-O3	-119.51(15)
C13-N1-P2-N2	178.0(3)	P1-N1-P2-N2	-0.31(15)
C13-N1-P2-N4	161(6)	P1-N1-P2-N4	-17(7) C33-

N4-P2-O4	-6.4(2)	C27-N4-P2-O4	128.1(3)
C33-N4-P2-O3	-129.7(2)	C27-N4-P2-O3	4.8(3)
C33-N4-P2-N2	111.1(3)	C27-N4-P2-N2	-114.3(3)
C33-N4-P2-N1	128(6)	C27-N4-P2-N1	-98(7)

Table C43. Anisotropic atomic displacement parameters (Å^2) for 4.7a.

The anisotropic atomic displacement factor exponent takes the form: $-2\pi^2 [h^2a^{*2} U_{11} + ... + 2hka^* b^* U_{12}]$

	U_{11}	U_{22}	U_{33}	U_{23}	U_{13} U_{12}
C1	0.0354(18)	0.057(2)	0.055(2)	-0.0018(18)	-0.0086(16) 0.0104(16)
C2	0.046(2)	0.046(2)	0.051(2)	0.0034(16)	-0.0040(17) 0.0094(16)
C3	0.067(3)	0.074(3)	0.056(3)	0.017(2)	-0.007(2) 0.005(2)
C4	0.263(11)	0.132(7)	0.139(7)	0.093(6)	-0.084(7) -0.099(7)
C5	0.231(10)	0.176(8)	0.071(4)	0.031(5)	0.061(5) 0.079(7)
C6	0.098(5)	0.225(9)	0.097(5)	0.080(5)	-0.010(4) 0.053(5)
C7	0.0323(17)	0.053(2)	0.061(2)	-0.0003(18)	0.0082(16) 0.0055(15)
C8	0.043(2)	0.053(2)	0.052(2)	-0.0029(17)	0.0157(17) 0.0077(16)
C9	0.067(3)	0.078(3)	0.056(3)	-0.010(2)	0.017(2) 0.013(2)
C10	0.161(7)	0.107(5)	0.081(4)	-0.038(4)	0.015(4) -0.008(5)
C11	0.097(4)	0.143(6)	0.058(3)	0.013(3)	0.012(3) 0.031(4)
C12	0.081(4)	0.158(6)	0.075(4)	-0.022(4)	0.034(3) 0.007(4)
C13	0.0266(15)	0.0333(16)	0.057(2)	0.0037(14)	0.0011(14) 0.0014(12)
C14	0.049(2)	0.055(2)	0.057(2)	-0.0018(19)	-0.0015(18) -0.0082(18)
C15	0.063(3)	0.059(3)	0.085(3)	-0.015(2)	-0.021(3)

	-0.005(2)				
C16	0.047(2)	0.045(2)	0.120(4)	-0.004(3)	-0.001(3)
	-0.0109(19)				
C17	0.065(3)	0.054(3)	0.111(4)	0.010(3)	0.035(3)
	-0.011(2)				
C18	0.059(2)	0.047(2)	0.068(3)	0.0001(19)	0.024(2)
	-0.0083(18)				
C19	0.094(5)	0.073(4)	0.202(8)	-0.008(4)	-0.008(5)
	-0.042(3)				
C20	0.0302(15)	0.0331(16)	0.053(2)	0.0004(14)	0.0046(14)
	-0.0002(13)				
C21	0.055(2)	0.061(2)	0.055(2)	-0.0066(19)	0.0016(19)
	-0.0117(19)				
C22	0.066(3)	0.064(3)	0.091(4)	-0.021(3)	-0.014(3)
	-0.012(2)				
C23	0.045(2)	0.049(2)	0.129(5)	-0.013(3)	0.011(3)
	-0.0105(19)				
C24	0.066(3)	0.056(3)	0.098(4)	0.008(3)	0.031(3)
	-0.013(2)				
C25	0.065(3)	0.050(2)	0.061(3)	-0.0008(19)	0.019(2)
	-0.0114(19)				
C26	0.102(5)	0.082(4)	0.211(9)	-0.023(5)	0.016(5)
	-0.050(4)				
C27	0.0329(17)	0.059(2)	0.047(2)	0.0028(17)	-0.0047(15)
	0.0040(16)				
C28	0.0416(19)	0.054(2)	0.047(2)	0.0078(17)	0.0005(16)
	0.0081(16)				
C29	0.063(3)	0.079(3)	0.060(3)	0.025(2)	-0.001(2)
	0.004(2)				
C30	0.187(8)	0.135(6)	0.064(4)	0.013(4)	0.051(4)
	0.011(5)				
C31	0.181(8)	0.086(4)	0.111(5)	0.055(4)	-0.012(5)
	-0.034(5)				
C32	0.086(5)	0.248(10)	0.111(5)	0.105(6)	-0.012(4)
	0.031(5)				
C33	0.0309(17)	0.059(2)	0.052(2)	0.0068(17)	0.0093(15)
	0.0089(15)				
C34	0.0422(19)	0.052(2)	0.046(2)	0.0027(16)	0.0119(16)
	0.0104(16)				
C35	0.058(3)	0.088(3)	0.047(2)	-0.002(2)	0.0113(19)
	0.019(2)				
C36	0.177(7)	0.092(4)	0.073(4)	-0.029(3)	0.003(4)
	0.023(5)				
C37	0.077(4)	0.276(11)	0.064(4)	-0.003(5)	0.030(3)
	0.038(5)				
C38	0.098(4)	0.105(4)	0.059(3)	0.014(3)	0.000(3)

	0.010(3)				
N1	0.0269(13)	0.0321(13)	0.0518(17)	0.0031(12)	0.0025(11)
	-0.0020(10)				
N2	0.0294(13)	0.0332(13)	0.0506(17)	0.0003(12)	0.0028(12)
	-0.0024(11)				
N3	0.0261(13)	0.0447(16)	0.0538(18)	0.0006(13)	-0.0005(12)
	0.0052(12)				
N4	0.0286(14)	0.0446(16)	0.0478(17)	0.0050(13)	0.0006(12)
	0.0004(12)				
O1	0.0409(13)	0.0442(13)	0.0543(15)	0.0141(11)	-0.0006(11)
	-0.0004(11)				
O2	0.0355(12)	0.0527(15)	0.0498(15)	-0.0084(12)	0.0048(11)
	0.0010(11)				
O3	0.0351(12)	0.0462(13)	0.0493(14)	0.0153(11)	0.0036(10)
	0.0012(10)				
O4	0.0322(12)	0.0539(14)	0.0456(14)	-0.0048(11)	0.0033(10)
	0.0037(10)				
P1	0.0264(4)	0.0329(4)	0.0412(5)	0.0013(3)	0.0012(3)
	0.0009(3)				
P2	0.0266(4)	0.0339(4)	0.0392(5)	0.0026(3)	0.0023(3)
	0.0010(3)				

Table C44. Hydrogen atom coordinates and isotropic atomic displacement parameters (Å^2) for 4.7a.

	x/a	y/b	z/c	U
H1	0.9457	0.0533	0.3189	0.060
H4A	0.5486	-0.0482	0.3705	0.274
H4B	0.6358	-0.0804	0.4288	0.274
H4C	0.6865	-0.0890	0.3597	0.274
H5A	0.7249	0.0808	0.4462	0.235
H5B	0.6828	0.0216	0.4862	0.235
H5C	0.5730	0.0486	0.4324	0.235
H6A	0.9321	-0.0454	0.3900	0.211
H6B	0.8841	-0.0451	0.4601	0.211
H6C	0.9448	0.0171	0.4307	0.211
H7	0.9578	0.0773	0.1840	0.058
H10A	0.7871	-0.0458	0.0850	0.174
H10B	0.7271	-0.0271	0.0156	0.174
H10C	0.6244	-0.0256	0.0718	0.174
H11A	0.5609	0.0876	0.0491	0.148
H11B	0.6579	0.0846	-0.0090	0.148
H11C	0.6850	0.1375	0.0431	0.148
H12A	0.9419	0.1069	0.0629	0.155

H12B	0.9217	0.0546	0.0098	0.155
H12C	0.9844	0.0362	0.0788	0.155
H14	0.6590	0.2248	0.3546	0.065
H15	0.8126	0.3104	0.3702	0.085
H17	0.8870	0.3100	0.1875	0.090
H18	0.7259	0.2271	0.1685	0.069
H19A	0.9237	0.4091	0.3126	0.186
H19B	0.9969	0.3901	0.2503	0.186
H19C	1.0544	0.3615	0.3164	0.186
H21	0.3220	0.0240	0.1295	0.068
H22	0.1666	-0.0616	0.1233	0.089
H24	0.1335	-0.0554	0.3093	0.086
H25	0.2909	0.0299	0.3180	0.070
H26A	0.0815	-0.1623	0.2190	0.197
H26B	-0.0195	-0.1248	0.1688	0.197
H26C	-0.0419	-0.1187	0.2419	0.197
H27	0.0517	0.2019	0.1611	0.056
H30A	0.4290	0.2056	0.0524	0.190
H30B	0.3333	0.2373	-0.0037	0.190
H30C	0.2762	0.1773	0.0309	0.190
H31A	0.3074	0.3454	0.1244	0.191
H31B	0.3526	0.3406	0.0540	0.191
H31C	0.4476	0.3079	0.1097	0.191
H32A	0.0534	0.2350	0.0538	0.224
H32B	0.1101	0.2940	0.0175	0.224
H32C	0.0637	0.3015	0.0875	0.224
H33	0.0396	0.1762	0.2950	0.056
H36A	0.3914	0.2693	0.4078	0.171
H36B	0.3024	0.2709	0.4685	0.171
H36C	0.2344	0.2980	0.4034	0.171
H37A	0.0196	0.2282	0.4012	0.207
H37B	0.0732	0.2014	0.4686	0.207
H37C	0.0382	0.1548	0.4113	0.207
H38A	0.2814	0.1096	0.4347	0.131
H38B	0.3262	0.1601	0.4875	0.131
H38C	0.4207	0.1511	0.4291	0.131

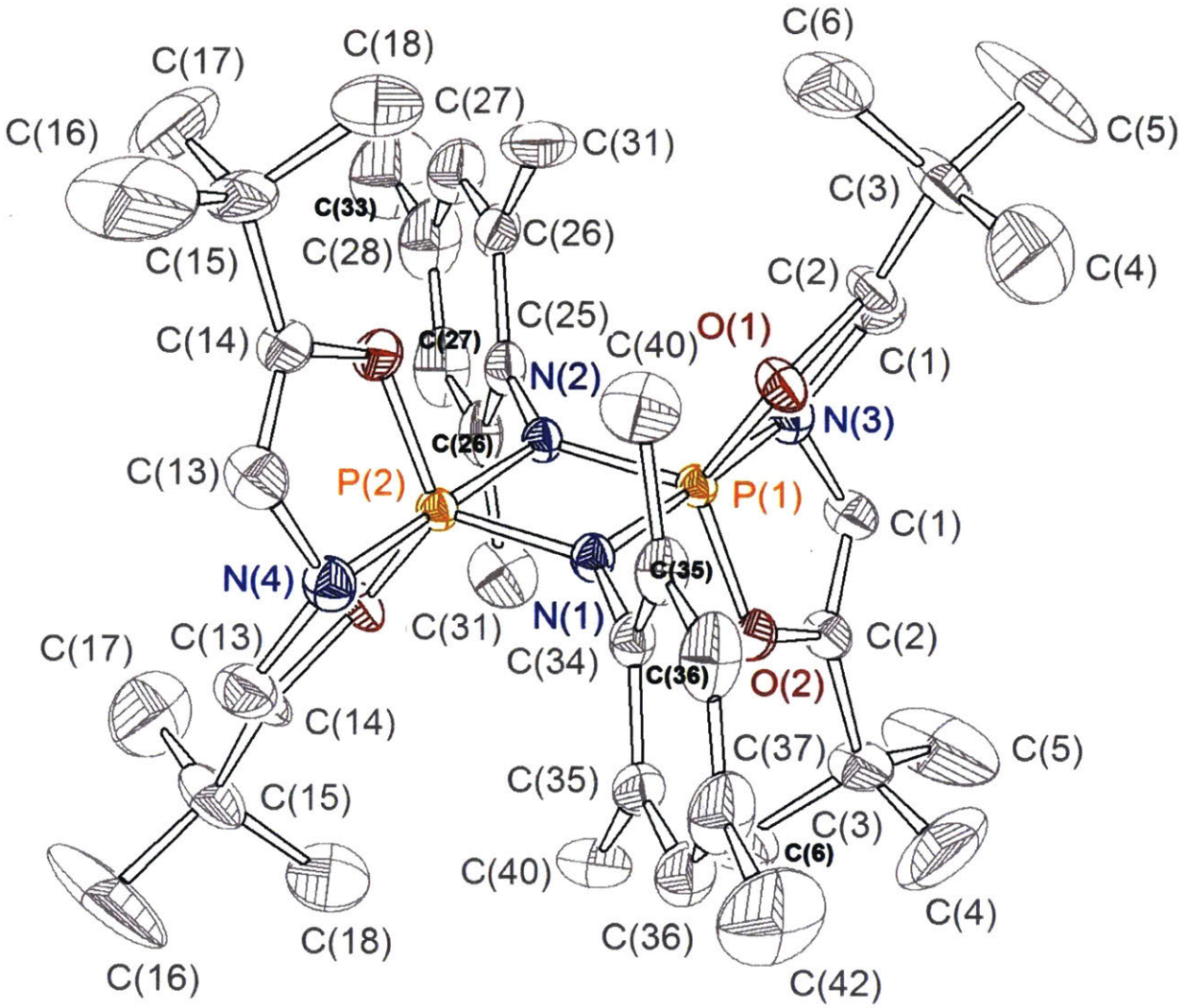

Table C45. Crystal data and structure refinement for 4.8a.	
Identification code	yzl3s
Empirical formula	$C_{42}H_{62}ClN_4O_4P_2$
Formula weight	784.35
Temperature/K	293(2)
Crystal system	N/A
Space group	Pnma
a/Å	20.913(3)
b/Å	21.309(3)

c/Å	9.4587(14)
α/°	90.00
β/°	90.00
γ/°	90.00
Volume/Å^3	4215.1(11)
Z	4
ρ_{calc}g/cm^3	1.236
μ/mm^{-1}	0.211
F(000)	1684.0
Crystal size/mm^3	0.22 × 0.14 × 0.13
Radiation	MoKα (λ = 0.71073)
2Θ range for data collection/°	3.9 to 56.74
Index ranges	$-27 \leq h \leq 27$, $-28 \leq k \leq 27$, $-11 \leq l \leq 12$
Reflections collected	33490
Independent reflections	5364 [R_{int} = 0.0944, R_{sigma} = N/A]
Data/restraints/parameters	5364/0/261
Goodness-of-fit on F^2	1.332
Final R indexes [I>=2σ (I)]	R_1 = 0.1691, wR_2 = 0.3562
Final R indexes [all data]	R_1 = 0.2023, wR_2 = 0.3906
Largest diff. peak/hole / e Å^{-3}	5.86/-0.68

Table C46. Fractional Atomic Coordinates (×10^4) and Equivalent Isotropic Displacement Parameters (Å^2×10^3) for 4.8a. Ueq is defined as 1/3 of of the trace of the orthogonalised UIJ tensor.

Atom	*x*	*y*	*z*	U(eq)
P1	1658.0(6)	2500	6187.3(14)	22.0(4)
P2	878.7(6)	2500	4033.2(13)	22.3(4)
O1	2028.7(13)	3174.5(13)	6221(3)	33.6(7)
O2	501.5(13)	1826.5(13)	4001(3)	30.9(7)
N1	1654.7(18)	2500	4317(5)	24.9(9)
N2	881.9(17)	2500	5903(4)	23.0(9)
N3	1634(2)	2500	8055(5)	36.1(11)
N4	892(2)	2500	2175(5)	33.4(11)
C2	2098(2)	3443.7(19)	7574(4)	33.5(10)
C3	2364(3)	4092(2)	7604(5)	52.4(14)

C4	3021(3)	4094(4)	6846(12)	124(4)
C5	2427(6)	4310(3)	9148(8)	152(5)
C6	1936(3)	4548(2)	6833(7)	72.9(18)
C13	639(2)	1942(2)	1641(5)	43.1(11)
C14	423(2)	1557(2)	2647(4)	34.6(10)
C15	151(3)	910(2)	2636(5)	53.4(14)
C16	93(6)	682(4)	1129(9)	146(5)
C17	-496(3)	915(3)	3405(11)	102(3)
C18	590(3)	450(2)	3433(8)	76.7(19)
C25	355(2)	2500	6887(6)	32.9(12)
C26	97(2)	1935(2)	7394(5)	40.4(11)
C27	-428(2)	1948(3)	8257(6)	58.6(15)
C28	-695(3)	2500	8714(9)	71(3)
C31	394(3)	1313(2)	7047(6)	58.8(14)
C33	-1264(4)	2500	9723(11)	105(4)
C34	2174(2)	2500	3315(6)	28.6(11)
C35	2418.3(19)	3066(2)	2809(5)	36.6(10)
C36	2935(2)	3053(3)	1886(5)	50.6(13)
C37	3196(3)	2500	1397(8)	55.3(19)
C40	2132(2)	3687(2)	3178(6)	52.5(13)
C42	3746(4)	2500	319(11)	91(3)
C1	1889(2)	3068(2)	8634(5)	37.1(10)

Table C47. Anisotropic Displacement Parameters ($Å^2 \times 10^3$) for 4.8a. The Anisotropic displacement factor exponent takes the form: $-2\pi^2[h^2a^{*2}U_{11}+2hka^*b^*U_{12}+\ldots]$.

Atom	U_{11}	U_{22}	U_{33}	U_{23}	U_{13}	U_{12}
P1	23.7(6)	22.1(7)	20.1(7)	0	-2.0(4)	0
P2	24.2(6)	21.8(7)	20.8(7)	0	-2.2(5)	0
O1	41.0(15)	32.0(16)	27.8(15)	-3.9(11)	-7.4(11)	-5.6(12)
O2	38.5(14)	29.9(15)	24.4(14)	-5.0(11)	-6.3(11)	-7.4(11)
N1	23.8(19)	31(2)	20(2)	0	-1.3(16)	0
N2	22.5(19)	27(2)	20(2)	0	-2.4(15)	0
N3	35(2)	41(3)	33(3)	0	-6(2)	0
N4	35(2)	38(3)	27(2)	0	0.0(19)	0
C2	49(2)	23(2)	28(2)	-4.9(14)	-13.2(17)	-2.3(17)
C3	87(4)	29(3)	41(3)	-1.8(19)	-22(2)	-20(3)
C4	74(5)	74(5)	224(12)	-7(6)	-19(6)	-41(4)

C5	326(14)	48(4)	81(6)	-4(4)	-90(7)	-57(6)
C6	112(5)	31(3)	76(4)	5(3)	-12(4)	-5(3)
C13	56(3)	39(3)	34(2)	-4.6(18)	-3(2)	4(2)
C14	50(2)	25(2)	29(2)	-9.6(15)	-7.4(17)	-5.7(18)
C15	85(4)	31(3)	45(3)	-3(2)	-13(3)	-21(3)
C16	298(14)	63(5)	78(5)	-27(4)	-38(7)	-67(7)
C17	59(4)	66(5)	181(9)	-7(5)	-18(4)	-25(3)
C18	97(5)	31(3)	103(5)	2(3)	-6(4)	-7(3)
C25	27(2)	45(3)	26(3)	0	-4(2)	0
C26	32(2)	55(3)	34(2)	8.5(19)	-4.3(16)	-11(2)
C27	42(2)	91(4)	42(3)	15(3)	5(2)	-16(3)
C28	39(4)	119(8)	54(5)	0	15(3)	0
C31	72(3)	43(3)	61(3)	15(2)	4(3)	-18(3)
C33	71(6)	150(12)	93(8)	0	40(6)	0
C34	24(2)	40(3)	23(3)	0	-0.6(19)	0
C35	29.9(19)	46(3)	33(2)	8.3(18)	-0.8(16)	-5.9(18)
C36	33(2)	82(4)	37(3)	15(2)	3.8(18)	-11(2)
C37	32(3)	92(6)	42(4)	0	10(3)	0
C40	65(3)	39(3)	54(3)	14(2)	6(2)	-7(2)
C42	59(5)	122(10)	91(7)	0	43(5)	0
C1	45(2)	31(2)	35(2)	2.8(17)	-1.8(18)	3.6(17)

Table C48. Bond Lengths for 4.8a.

Atom	Atom	Length/Å	Atom	Atom	Length/Å
P1	O1	1.633(3)	C3	C5	1.538(8)
P1	O1[1]	1.633(3)	C3	C4	1.551(10)
P1	N2	1.645(4)	C13	C14	1.335(6)
P1	N3	1.767(5)	C14	C15	1.491(6)
P1	N1	1.769(4)	C15	C16	1.510(9)
P2	O2	1.638(3)	C15	C18	1.542(8)
P2	O2[1]	1.638(3)	C15	C17	1.536(9)
P2	N1	1.645(4)	C25	C26[1]	1.403(5)
P2	N4	1.758(5)	C25	C26	1.403(5)
P2	N2	1.769(4)	C26	C27	1.367(6)
O1	C2	1.410(5)	C26	C31	1.501(7)
O2	C14	1.413(4)	C27	C28	1.371(6)

N1	C34	1.442(6)	C28	C27[1]	1.371(6)
N2	C25	1.443(6)	C28	C33	1.525(10)
N3	C1	1.433(5)	C34	C35	1.394(5)
N3	C1[1]	1.433(5)	C34	C35[1]	1.394(5)
N4	C13	1.395(5)	C35	C36	1.389(6)
N4	C13[1]	1.395(5)	C35	C40	1.495(6)
C2	C1	1.355(6)	C36	C37	1.380(6)
C2	C3	1.489(6)	C37	C36[1]	1.380(6)
C3	C6	1.508(8)	C37	C42	1.537(9)

[1]+X,1/2-Y,+Z

Table C49. Bond Angles for 4.8a.

Atom	Atom	Atom	Angle/°	Atom	Atom	Atom	Angle/°
O1	P1	O1[1]	123.3(2)	C2	C3	C6	111.5(4)
O1	P1	N2	118.12(10)	C2	C3	C5	109.3(5)
O1[1]	P1	N2	118.12(10)	C6	C3	C5	108.4(6)
O1	P1	N3	89.68(12)	C2	C3	C4	108.9(5)
O1[1]	P1	N3	89.68(12)	C6	C3	C4	107.5(5)
N2	P1	N3	97.7(2)	C5	C3	C4	111.2(6)
O1	P1	N1	91.22(12)	C14	C13	N4	113.2(4)
O1[1]	P1	N1	91.22(12)	C13	C14	O2	110.9(4)
N2	P1	N1	80.36(19)	C13	C14	C15	133.8(4)
N3	P1	N1	178.1(2)	O2	C14	C15	115.2(4)
O2	P2	O2[1]	122.4(2)	C14	C15	C16	109.5(5)
O2	P2	N1	118.57(10)	C14	C15	C18	110.9(4)
O2[1]	P2	N1	118.57(10)	C16	C15	C18	107.7(6)
O2	P2	N4	89.36(12)	C14	C15	C17	109.1(5)
O2[1]	P2	N4	89.36(12)	C16	C15	C17	112.3(7)
N1	P2	N4	98.5(2)	C18	C15	C17	107.3(5)
O2	P2	N2	91.18(11)	C26[1]	C25	C26	118.1(6)
O2[1]	P2	N2	91.18(11)	C26[1]	C25	N2	121.0(3)
N1	P2	N2	80.4(2)	C26	C25	N2	121.0(3)
N4	P2	N2	178.9(2)	C27	C26	C25	119.7(5)
C2	O1	P1	115.1(3)	C27	C26	C31	118.7(4)
C14	O2	P2	115.4(3)	C25	C26	C31	121.6(4)
C34	N1	P2	129.5(4)	C26	C27	C28	122.2(5)

C34	N1	P1	130.9(3)	C27[1]	C28	C27	118.0(6)
P2	N1	P1	99.6(2)	C27[1]	C28	C33	121.0(3)
C25	N2	P1	130.4(3)	C27	C28	C33	121.0(3)
C25	N2	P2	130.0(3)	C35	C34	C35[1]	119.8(5)
P1	N2	P2	99.6(2)	C35	C34	N1	120.1(3)
C1	N3	C1[1]	115.5(5)	C35[1]	C34	N1	120.1(3)
C1	N3	P1	111.8(3)	C36	C35	C34	118.9(4)
C1[1]	N3	P1	111.8(3)	C36	C35	C40	118.4(4)
C13	N4	C13[1]	116.8(5)	C34	C35	C40	122.6(4)
C13	N4	P2	110.8(3)	C35	C36	C37	122.4(5)
C13[1]	N4	P2	110.8(3)	C36	C37	C36[1]	117.5(6)
C1	C2	O1	113.5(4)	C36	C37	C42	121.2(3)
C1	C2	C3	130.8(4)	C36[1]	C37	C42	121.2(3)
O1	C2	C3	115.7(4)	C2	C1	N3	109.6(4)

[1]+X,1/2-Y,+Z

Table C50. Torsion Angles for 4.8a.

A	B	C	D	Angle/°	A	B	C	D	Angle/°
O1[1]	P1	O1	C2	-94.4(3)	O2	P2	N4	C13[1]	126.9(3)
N2	P1	O1	C2	93.6(3)	O2[1]	P2	N4	C13[1]	4.5(3)
N3	P1	O1	C2	-5.0(3)	N1	P2	N4	C13[1]	-114.3(3)
N1	P1	O1	C2	173.3(3)	N2	P2	N4	C13[1]	-114.3(3)
O2[1]	P2	O2	C14	94.0(3)	P1	O1	C2	C1	5.1(5)
N1	P2	O2	C14	-94.1(3)	P1	O1	C2	C3	-172.9(3)
N4	P2	O2	C14	5.2(3)	C1	C2	C3	C6	-115.8(6)
N2	P2	O2	C14	-173.8(3)	O1	C2	C3	C6	61.8(6)
O2	P2	N1	C34	93.92(15)	C1	C2	C3	C5	4.0(9)
O2[1]	P2	N1	C34	-93.92(15)	O1	C2	C3	C5	-178.4(6)
N4	P2	N1	C34	0.0	C1	C2	C3	C4	125.7(6)
N2	P2	N1	C34	180.0	O1	C2	C3	C4	-56.7(6)
O2	P2	N1	P1	-86.08(15)	C13[1]	N4	C13	C14	-125.4(5)
O2[1]	P2	N1	P1	86.08(15)	P2	N4	C13	C14	2.8(5)
N4	P2	N1	P1	180.0	N4	C13	C14	O2	0.9(6)
N2	P2	N1	P1	0.0	N4	C13	C14	C15	-176.1(5)
O1	P1	N1	C34	61.67(11)	P2	O2	C14	C13	-4.6(5)
O1[1]	P1	N1	C34	-61.67(10)	P2	O2	C14	C15	173.0(3)

N2	P1	N1	C34	180.0	C13	C14	C15	C16	-3.1(9)
N3	P1	N1	C34	180.000(7)	O2	C14	C15	C16	179.9(6)
O1	P1	N1	P2	-118.33(11)	C13	C14	C15	C18	115.6(6)
O1[1]	P1	N1	P2	118.33(11)	O2	C14	C15	C18	-61.3(6)
N2	P1	N1	P2	0.0	C13	C14	C15	C17	-126.4(7)
N3	P1	N1	P2	0.000(7)	O2	C14	C15	C17	56.7(6)
O1	P1	N2	C25	-93.80(15)	P1	N2	C25	C26[1]	89.2(4)
O1[1]	P1	N2	C25	93.80(15)	P2	N2	C25	C26[1]	-90.8(4)
N3	P1	N2	C25	0.0	P1	N2	C25	C26	-89.2(4)
N1	P1	N2	C25	180.0	P2	N2	C25	C26	90.8(4)
O1	P1	N2	P2	86.20(15)	C26[1]	C25	C26	C27	5.6(8)
O1[1]	P1	N2	P2	-86.20(15)	N2	C25	C26	C27	-175.9(4)
N3	P1	N2	P2	180.0	C26[1]	C25	C26	C31	-172.5(3)
N1	P1	N2	P2	0.0	N2	C25	C26	C31	5.9(7)
O2	P2	N2	C25	-61.21(10)	C25	C26	C27	C28	-3.6(8)
O2[1]	P2	N2	C25	61.21(10)	C31	C26	C27	C28	174.6(6)
N1	P2	N2	C25	180.0	C26	C27	C28	C27[1]	1.3(11)
N4	P2	N2	C25	180.001(15)	C26	C27	C28	C33	-177.6(7)
O2	P2	N2	P1	118.79(10)	P2	N1	C34	C35	88.8(4)
O2[1]	P2	N2	P1	-118.79(10)	P1	N1	C34	C35	-91.2(4)
N1	P2	N2	P1	0.0	P2	N1	C34	C35[1]	-88.8(4)
N4	P2	N2	P1	0.001(15)	P1	N1	C34	C35[1]	91.2(4)
O1	P1	N3	C1	4.0(3)	C35[1]	C34	C35	C36	-4.8(8)
O1[1]	P1	N3	C1	127.3(3)	N1	C34	C35	C36	177.6(4)
N2	P1	N3	C1	-114.4(3)	C35[1]	C34	C35	C40	172.9(3)
N1	P1	N3	C1	-114.4(3)	N1	C34	C35	C40	-4.7(7)
O1	P1	N3	C1[1]	-127.3(3)	C34	C35	C36	C37	3.2(8)
O1[1]	P1	N3	C1[1]	-4.0(3)	C40	C35	C36	C37	-174.6(5)
N2	P1	N3	C1[1]	114.4(3)	C35	C36	C37	C36[1]	-1.5(10)
N1	P1	N3	C1[1]	114.4(3)	C35	C36	C37	C42	176.9(6)
O2	P2	N4	C13	-4.5(3)	O1	C2	C1	N3	-1.7(5)
O2[1]	P2	N4	C13	-126.9(3)	C3	C2	C1	N3	175.9(5)
N1	P2	N4	C13	114.3(3)	C1[1]	N3	C1	C2	127.5(4)
N2	P2	N4	C13	114.3(3)	P1	N3	C1	C2	-1.9(5)

[1]+X,1/2-Y,+Z

Table C51. Hydrogen Atom Coordinates (Å×10^4) and Isotropic Displacement Parameters (Å^2×10^3) for 4.8a.

Atom	*x*	*y*	*z*	U(eq)
H4A	3313	3826	7346	186
H4B	3188	4513	6826	186
H4C	2970	3943	5896	186
H5A	2017	4290	9601	228
H5B	2582	4734	9169	228
H5C	2723	4042	9637	228
H6A	1846	4390	5903	109
H6B	2146	4947	6759	109
H6C	1543	4596	7345	109
H13	623	1848	682	52
H16A	-211	937	632	220
H16B	-48	254	1127	220
H16C	502	711	673	220
H17A	-443	1090	4333	153
H17B	-655	494	3481	153
H17C	-796	1165	2880	153
H18A	1003	441	2989	115
H18B	406	37	3409	115
H18C	635	583	4397	115
H27	-609	1571	8543	70
H31A	562	1127	7893	88
H31B	734	1373	6379	88
H31C	76	1041	6645	88
H33A	-1141	2690	10602	126
H33B	-1399	2076	9889	126
H33C	-1609	2734	9311	126
H36	3111	3432	1587	61
H40A	2455	3954	3577	79
H40B	1794	3628	3854	79
H40C	1961	3879	2341	79
H42A	3852	2925	73	109
H42B	3616	2276	-514	109
H42C	4114	2299	726	109

Table C52. Atomic Occupancy for 4.8a.

Atom	*Occupancy*	Atom	*Occupancy*	Atom	*Occupancy*
H33A	0.50	H33B	0.50	H33C	0.50
H42A	0.50	H42B	0.50	H42C	0.50

Experimental

Single crystals of $C_{42}H_{62}ClN_4O_4P_2$ [yzl3s] were []. A suitable crystal was selected and [] on a diffractometer. The crystal was kept at 293(2) K during data collection. Using Olex2 [1], the structure was solved with the ShelXS-1997 [2] structure solution program using Direct Methods and refined with the XL [3] refinement package using Least Squares minimisation.

Crystal structure determination of [yzl3s]

Crystal Data for $C_{42}H_{62}ClN_4O_4P_2$ (M=784.35 g/mol): , space group Pnma (no. 62), a = 0.913(3) Å, b = 21.309(3) Å, c = 9.4587(14) Å, V = 4215.1(11) Å^3, Z = 4, T = 293(2) K, μ(MoKα) = 0.211 mm^{-1}, *Dcalc* = 1.236 g/cm^3, 33490 reflections measured ($3.9° \leq 2\Theta \leq 56.74°$), 5364 unique ($R_{int}$ = 0.0944, R_{sigma} = N/A) which were used in all calculations. The final R_1 was 0.1691 (>2sigma(I)) and wR_2 was 0.3906 (all data).

Refinement model description

Number of restraints - 0, number of constraints - unknown.

III. Multinuclear NMR Spectra

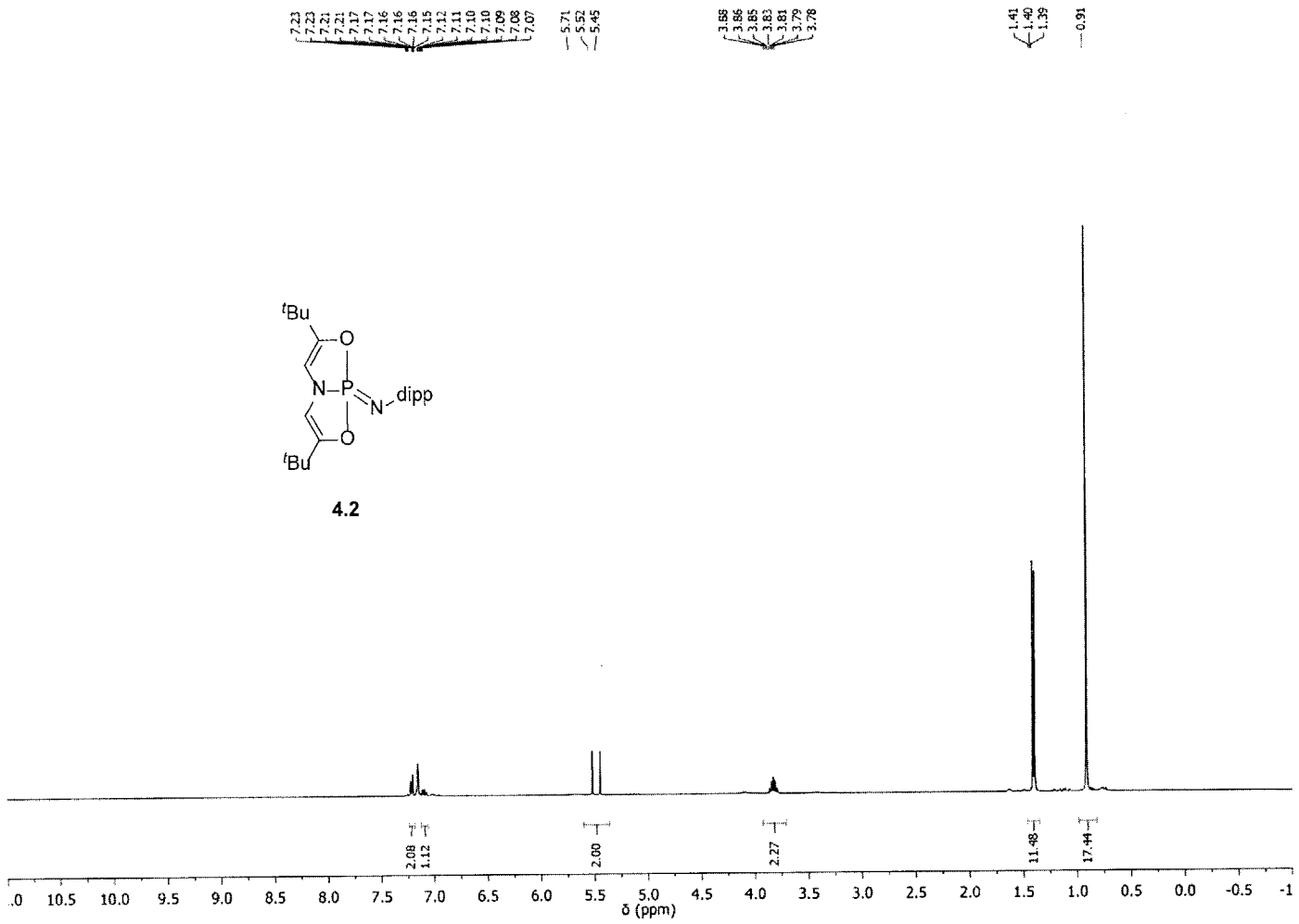

Figure C1. ^{1}H NMR of **4.2**.

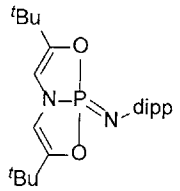

4.2

Figure C2. ^{31}P NMR of **4.2**.

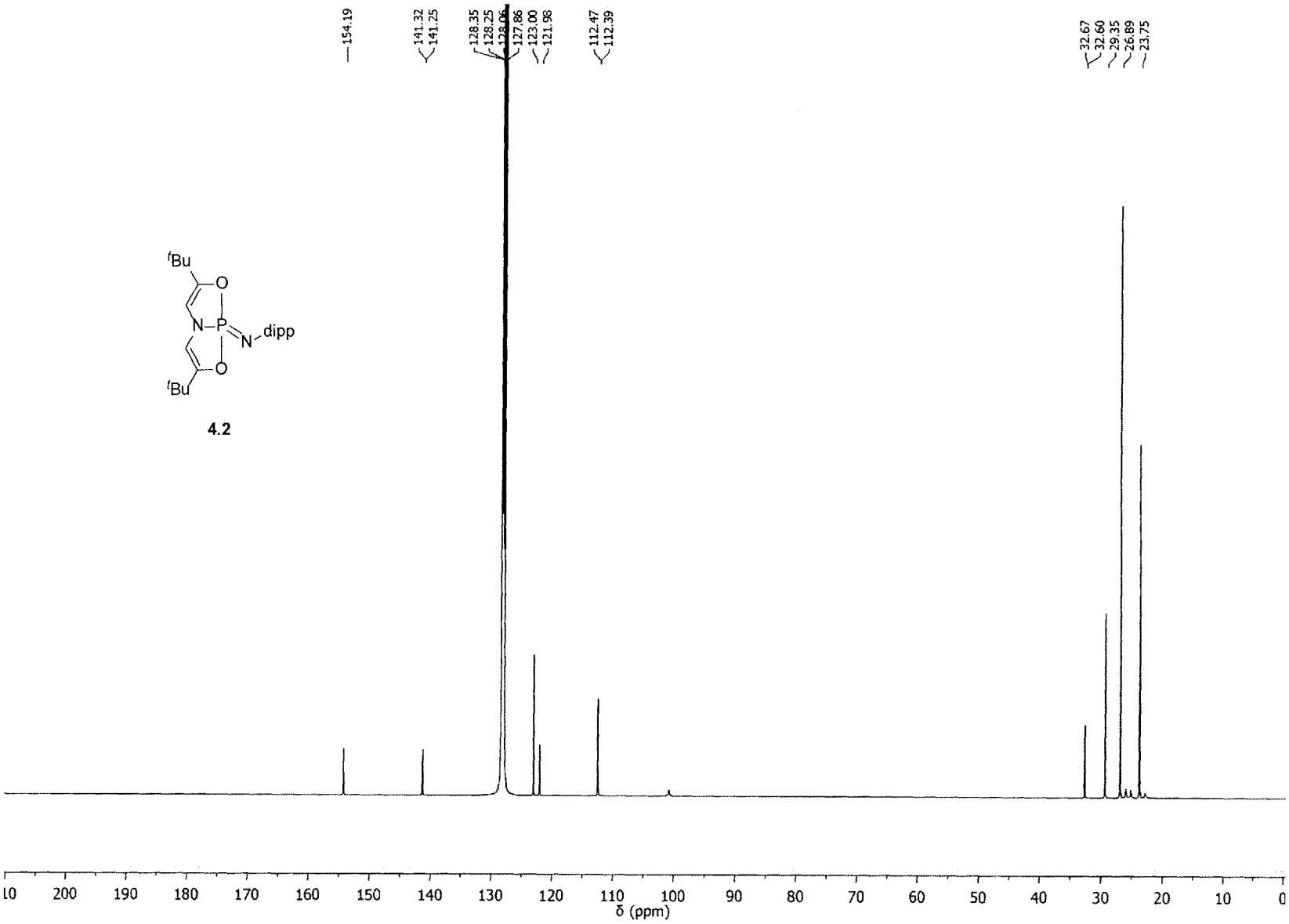

Figure C3. ^{13}C NMR of **4.2**.

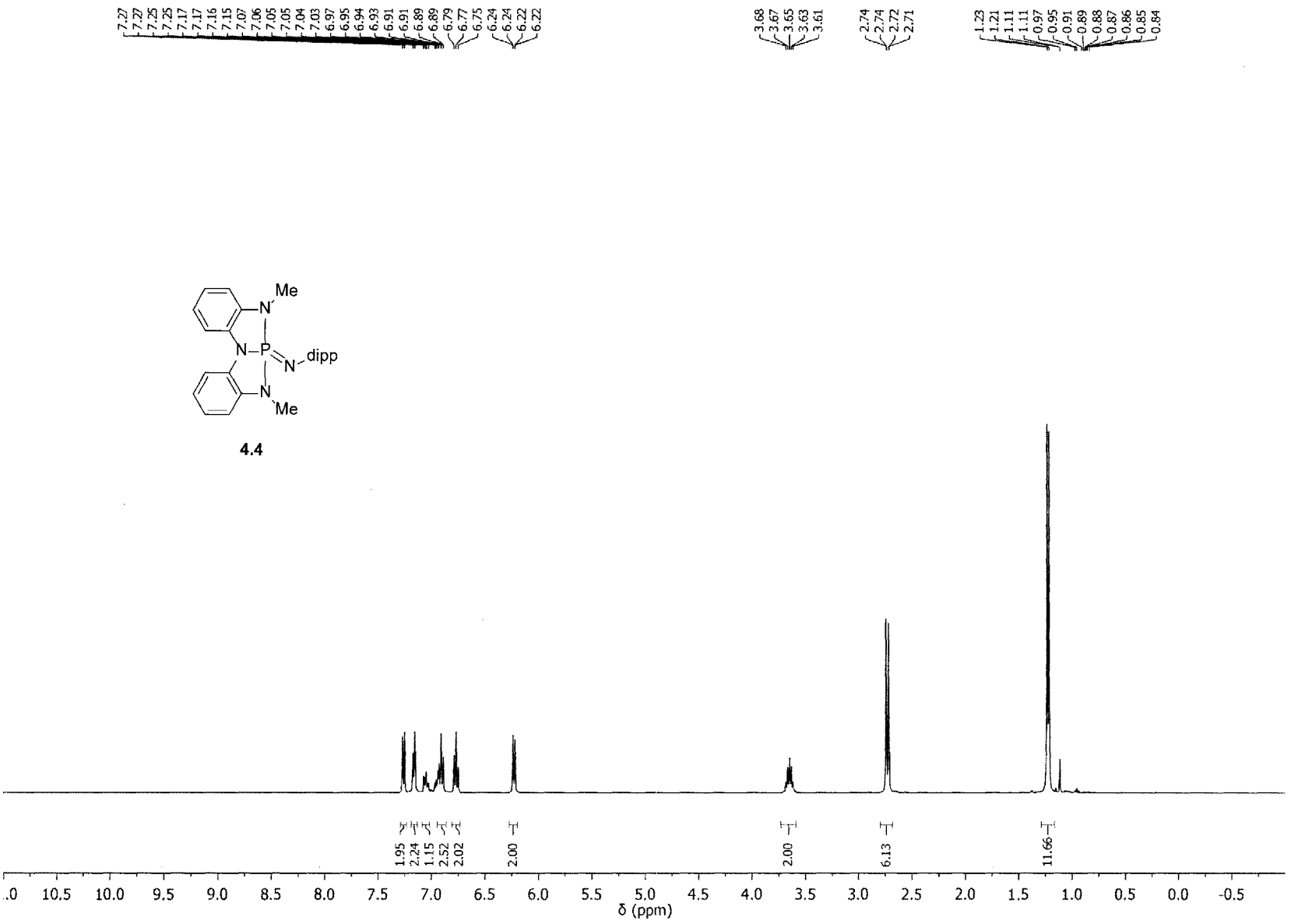

Figure C4. ^{1}H NMR of **4.4**.

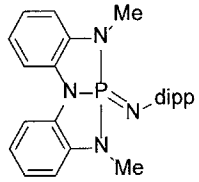

4.4

Figure C5. ^{31}P NMR of **4.4**.

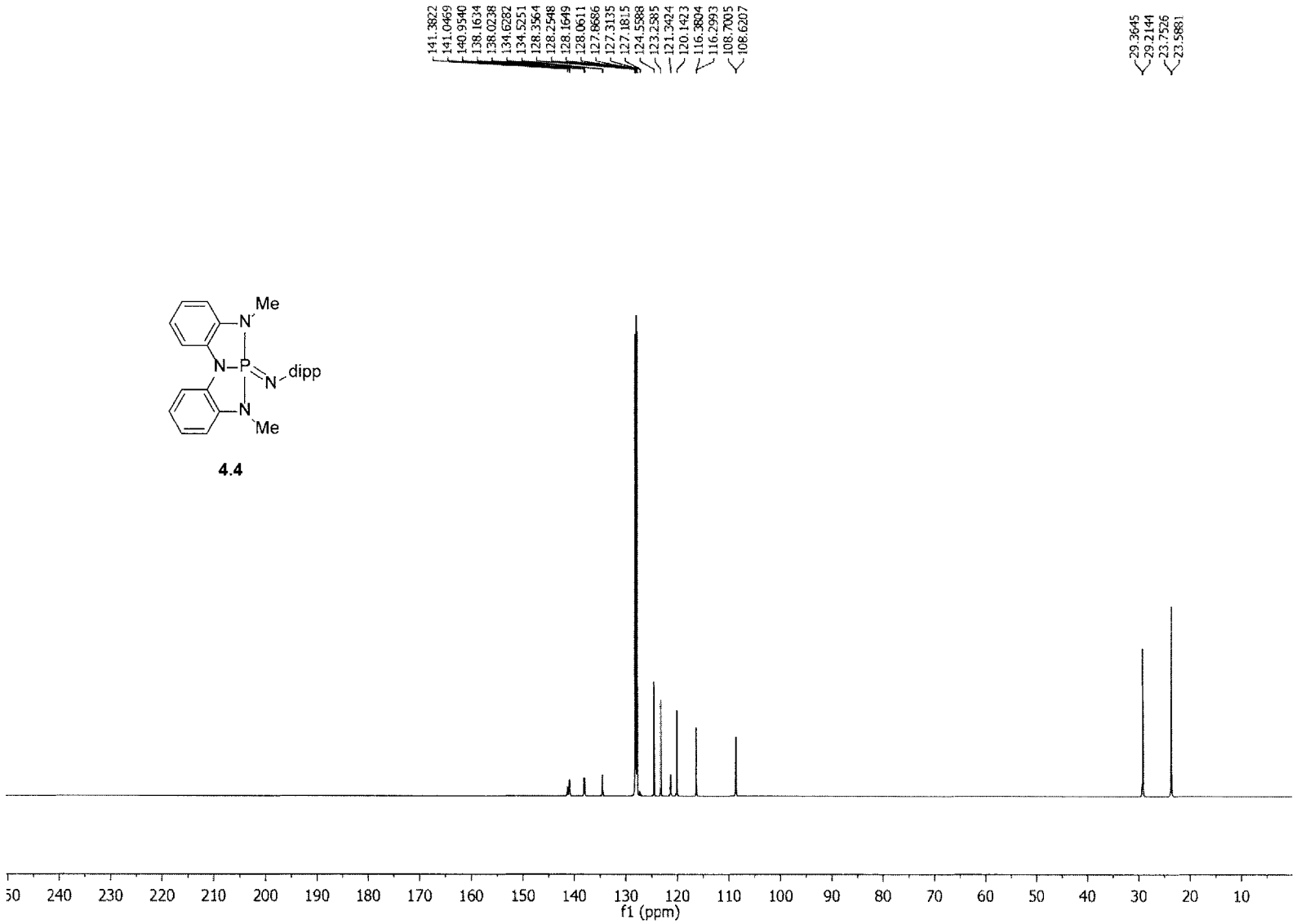

Figure C6. ^{13}C NMR of **4.4**.

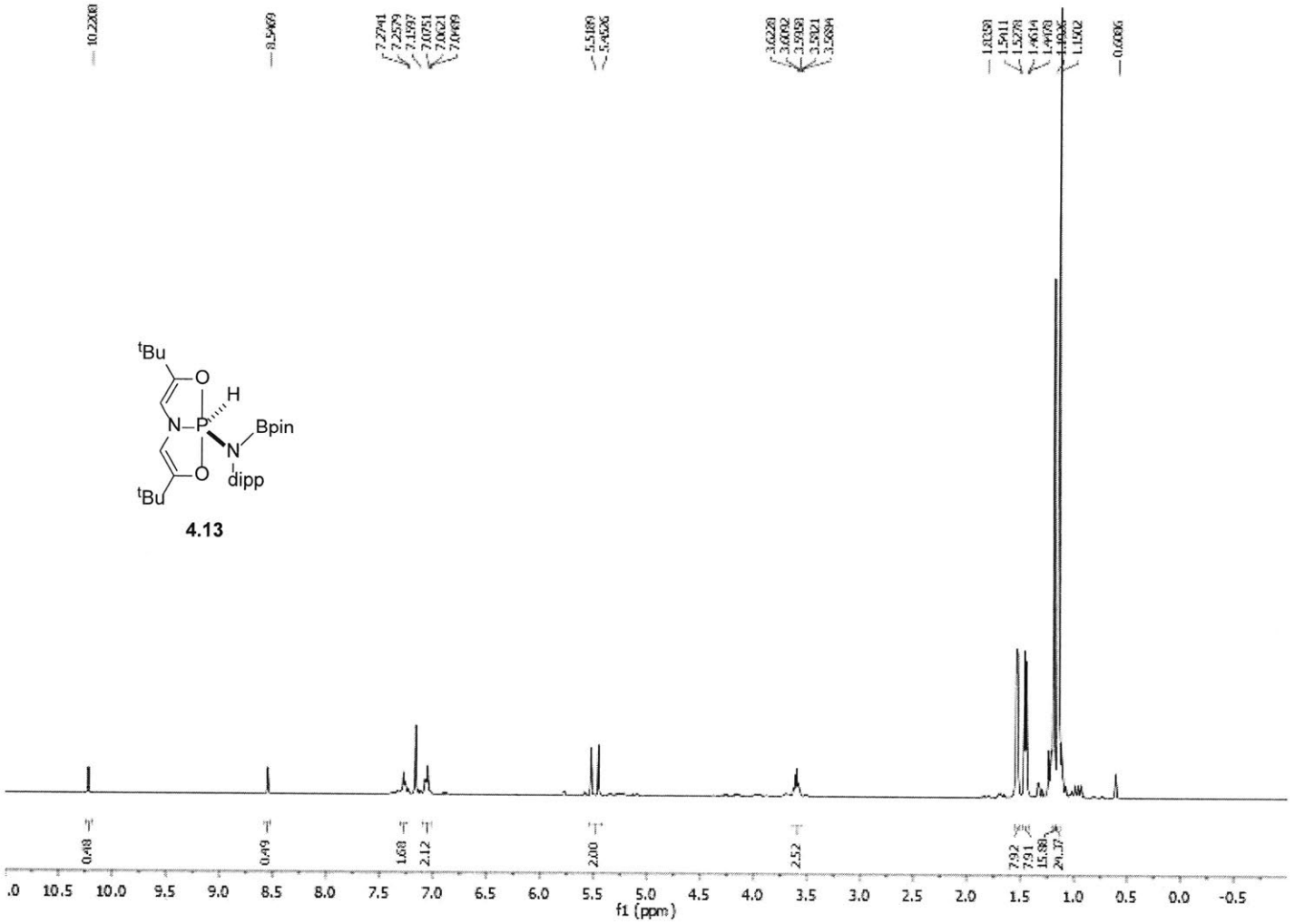

Figure C7. ^{1}H NMR of **4.13**.

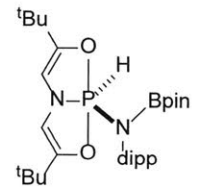

4.13

Figure C8. ^{31}P NMR of **4.13**.

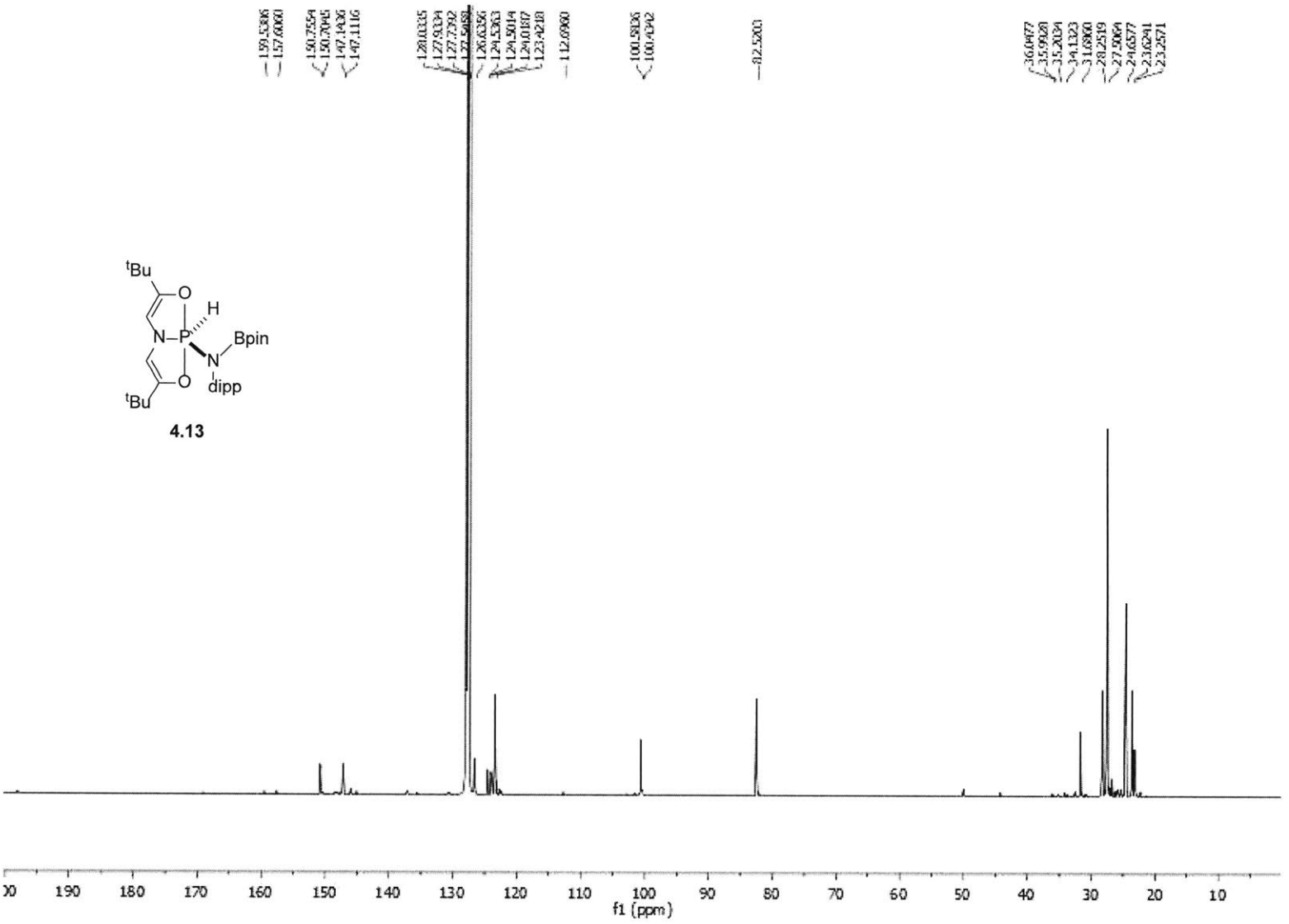

Figure C9. ^{13}C NMR of **4.13**.

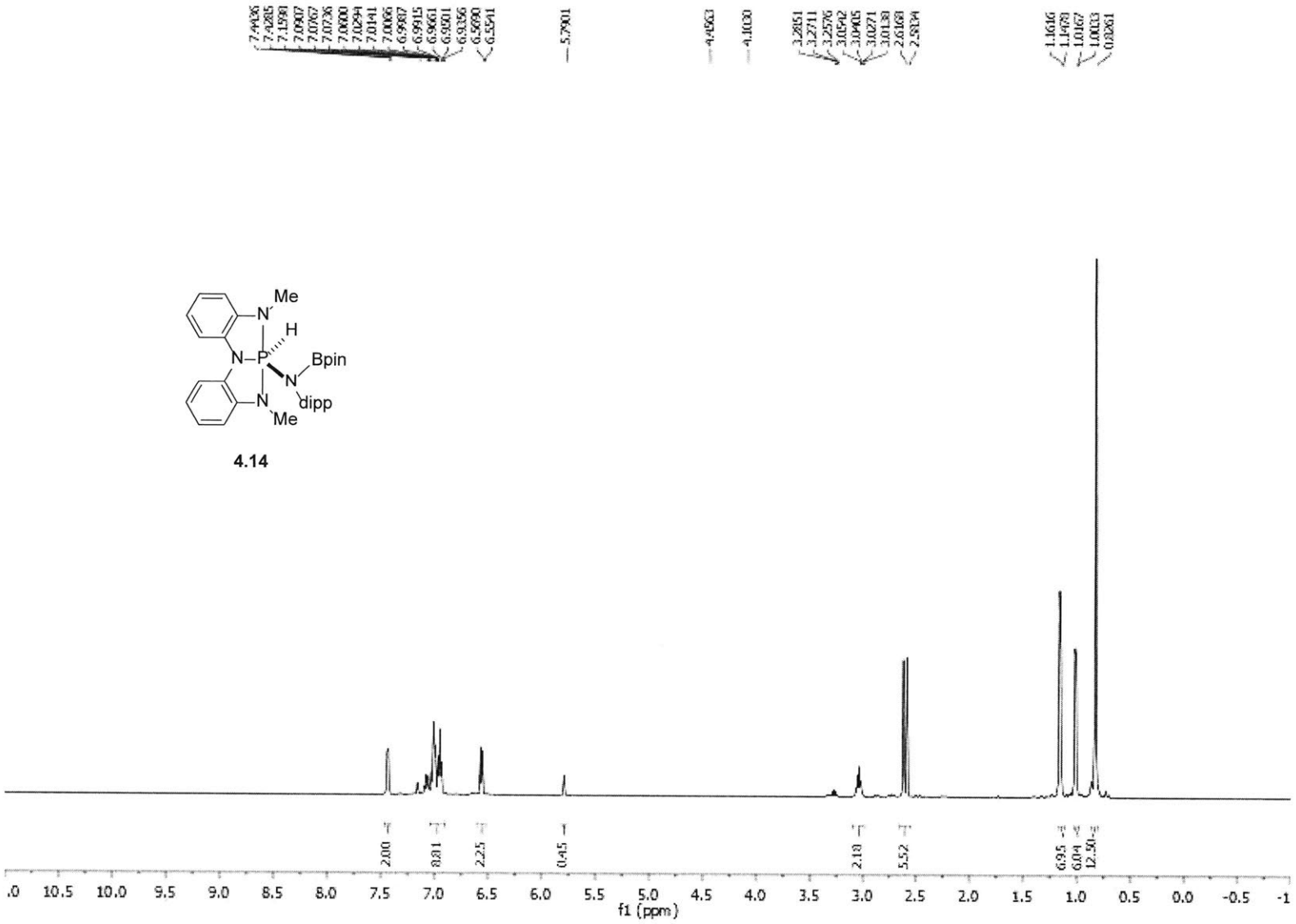

Figure C10. ^{1}H NMR of **4.14**.

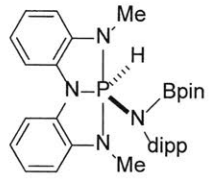

4.14

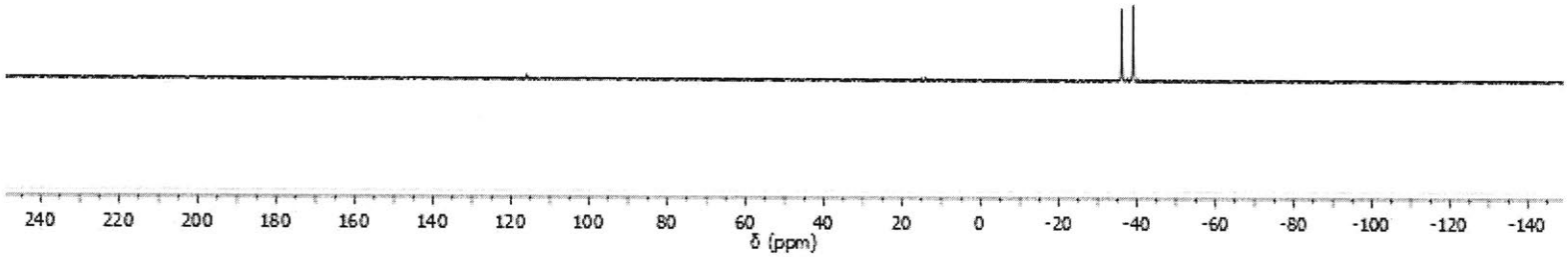

Figure C11. ^{31}P NMR of **4.14**.

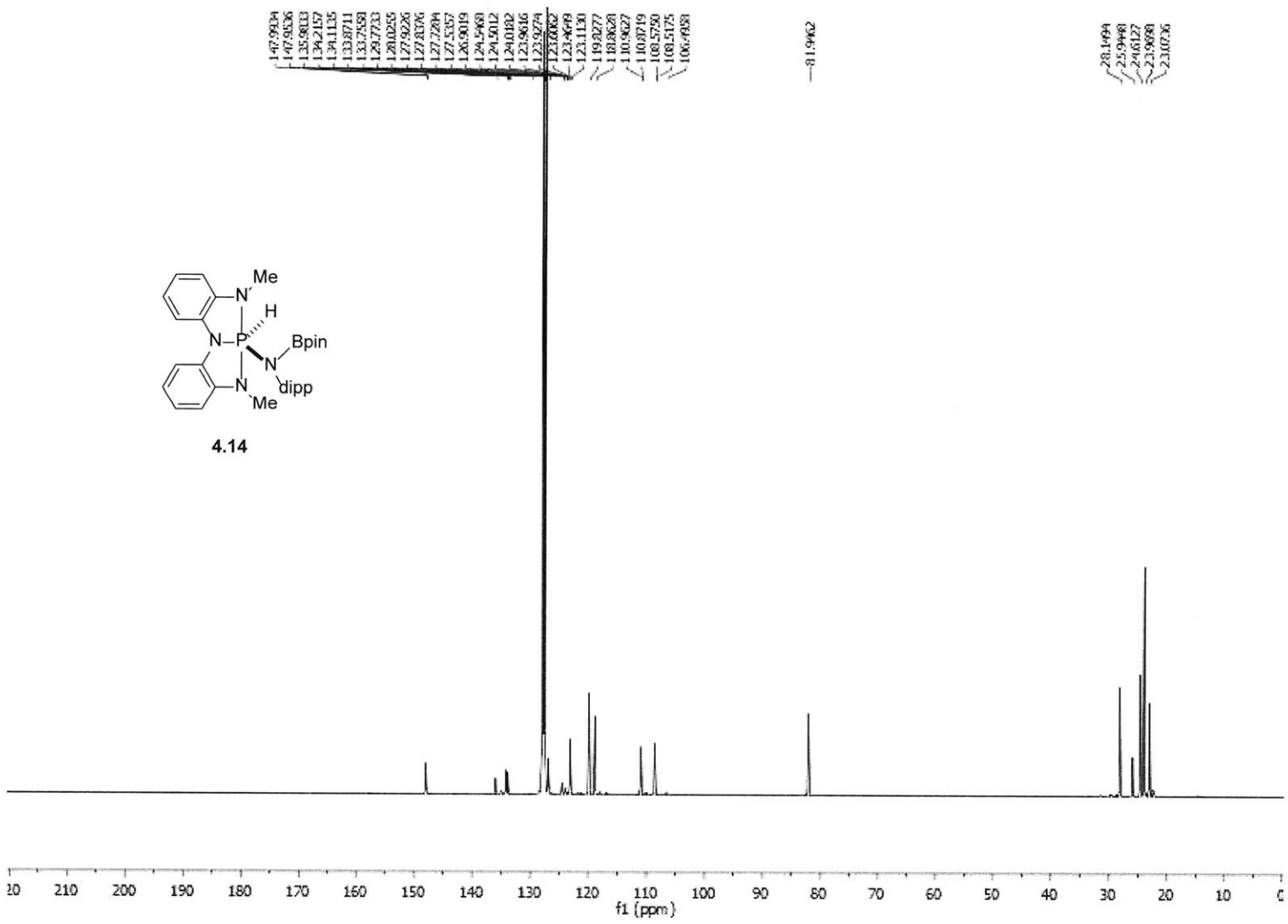

Figure C12. ^{13}C NMR of **4.14**.

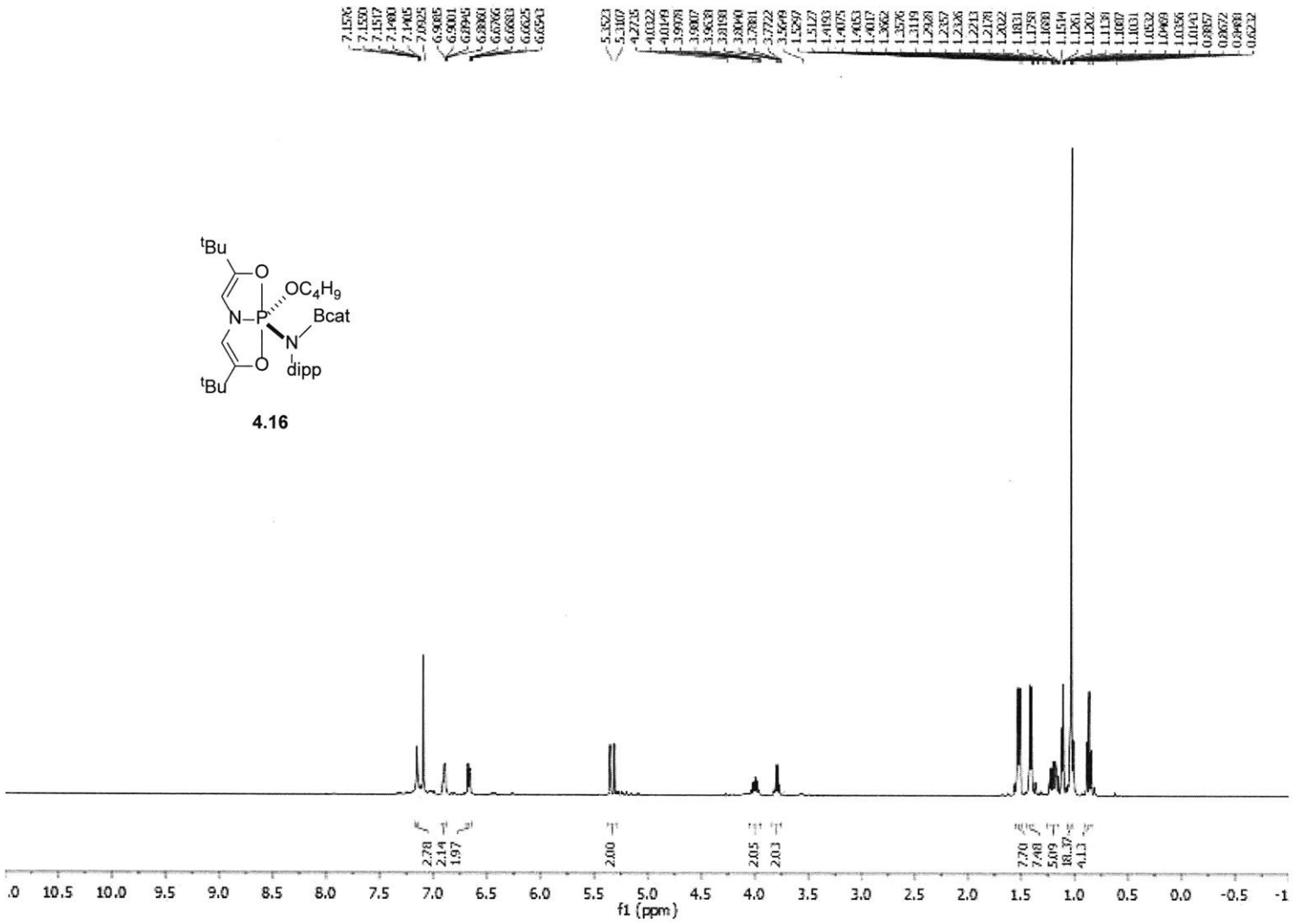

Figure C13. ^{1}H NMR of **4.16**.

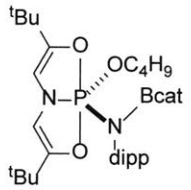

4.16

Figure C14. ^{31}P NMR of **4.16**.

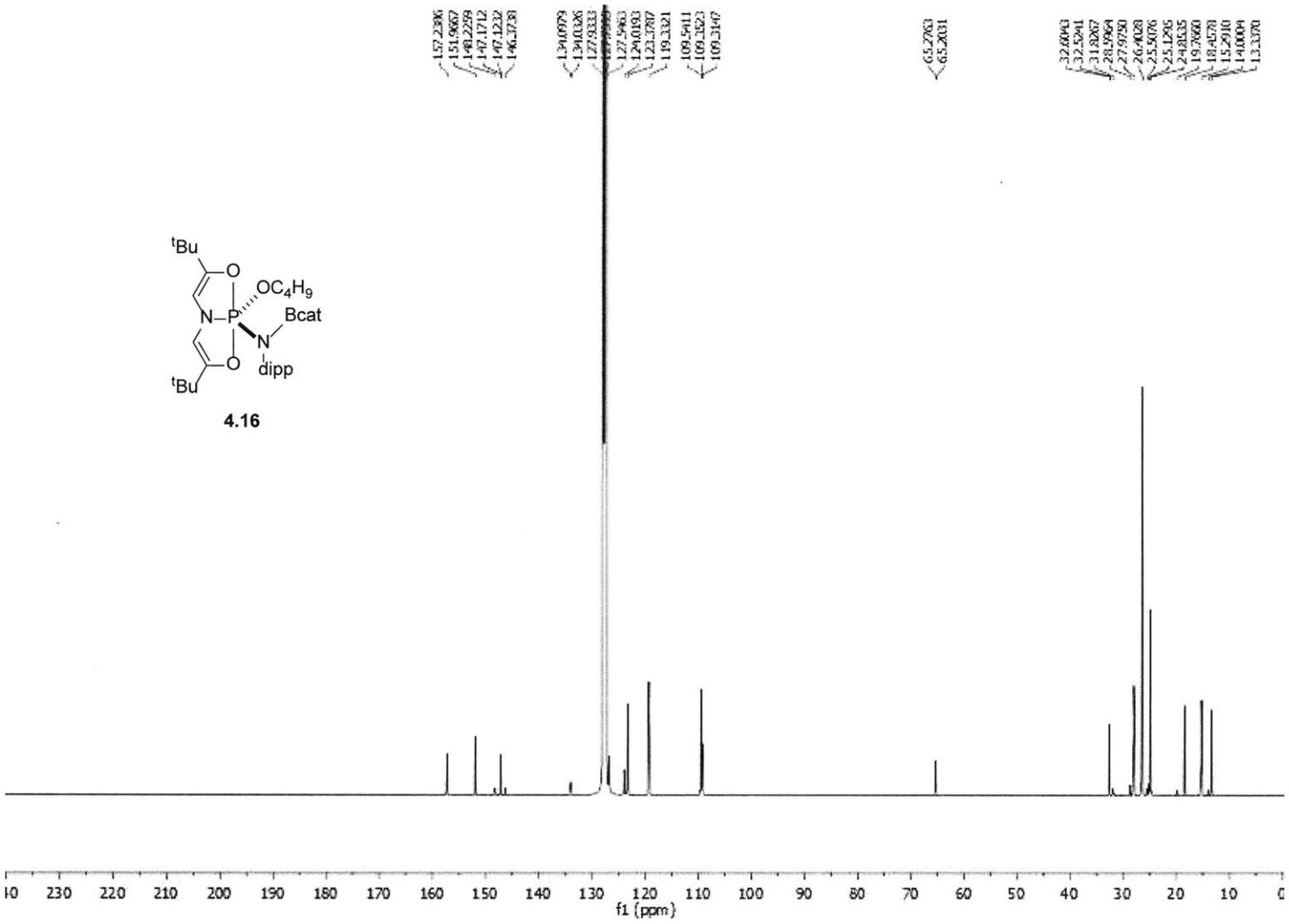

Figure C15. ^{13}C NMR of **4.16**.

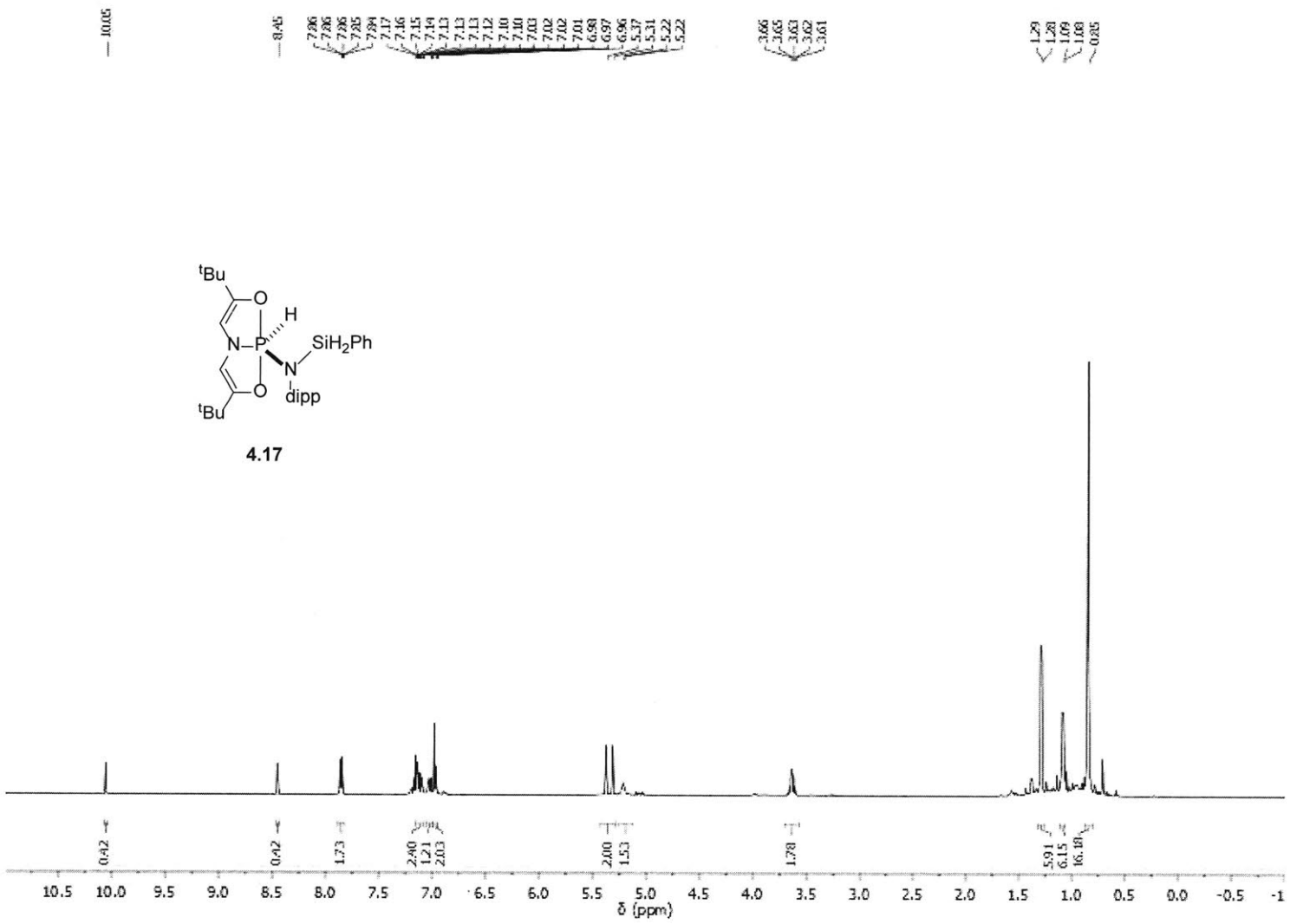

Figure C16. ^{1}H NMR of **4.17**.

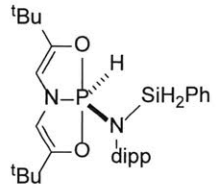

4.17

Figure C17. ^{31}P NMR of **4.17**.

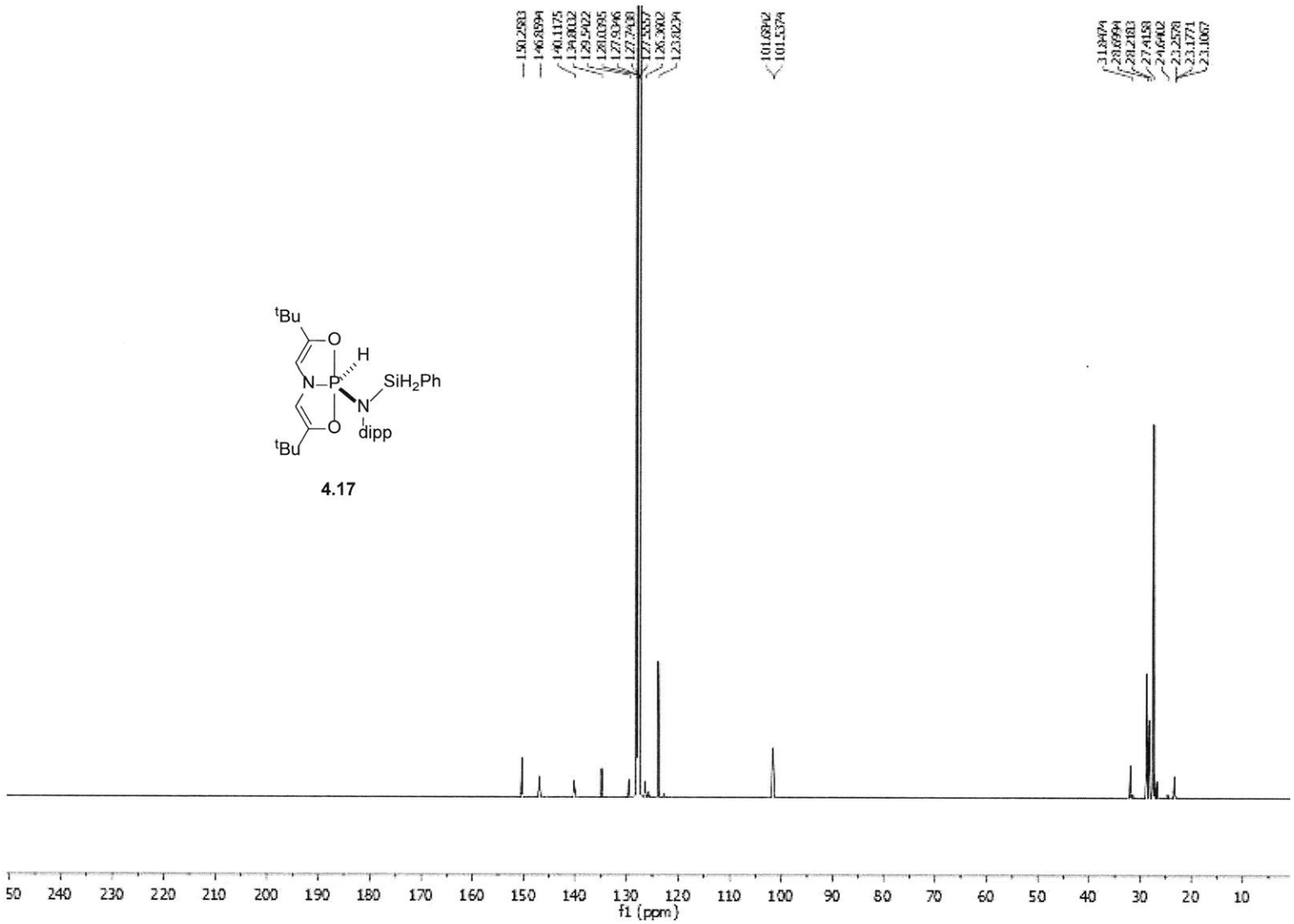

Figure C18. ^{13}C NMR of **4.17**.

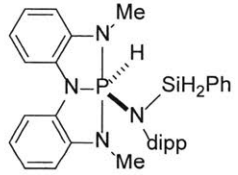

4.18

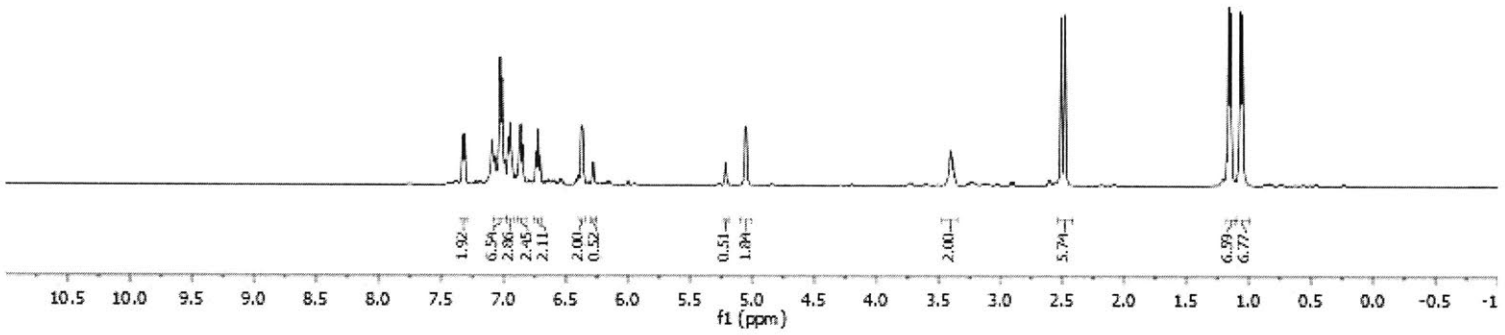

Figure C19. ^{1}H NMR of **4.18**.

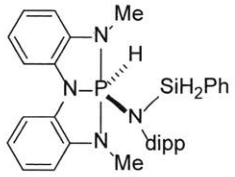

4.18

Figure C20. ^{31}P NMR of **4.18**.

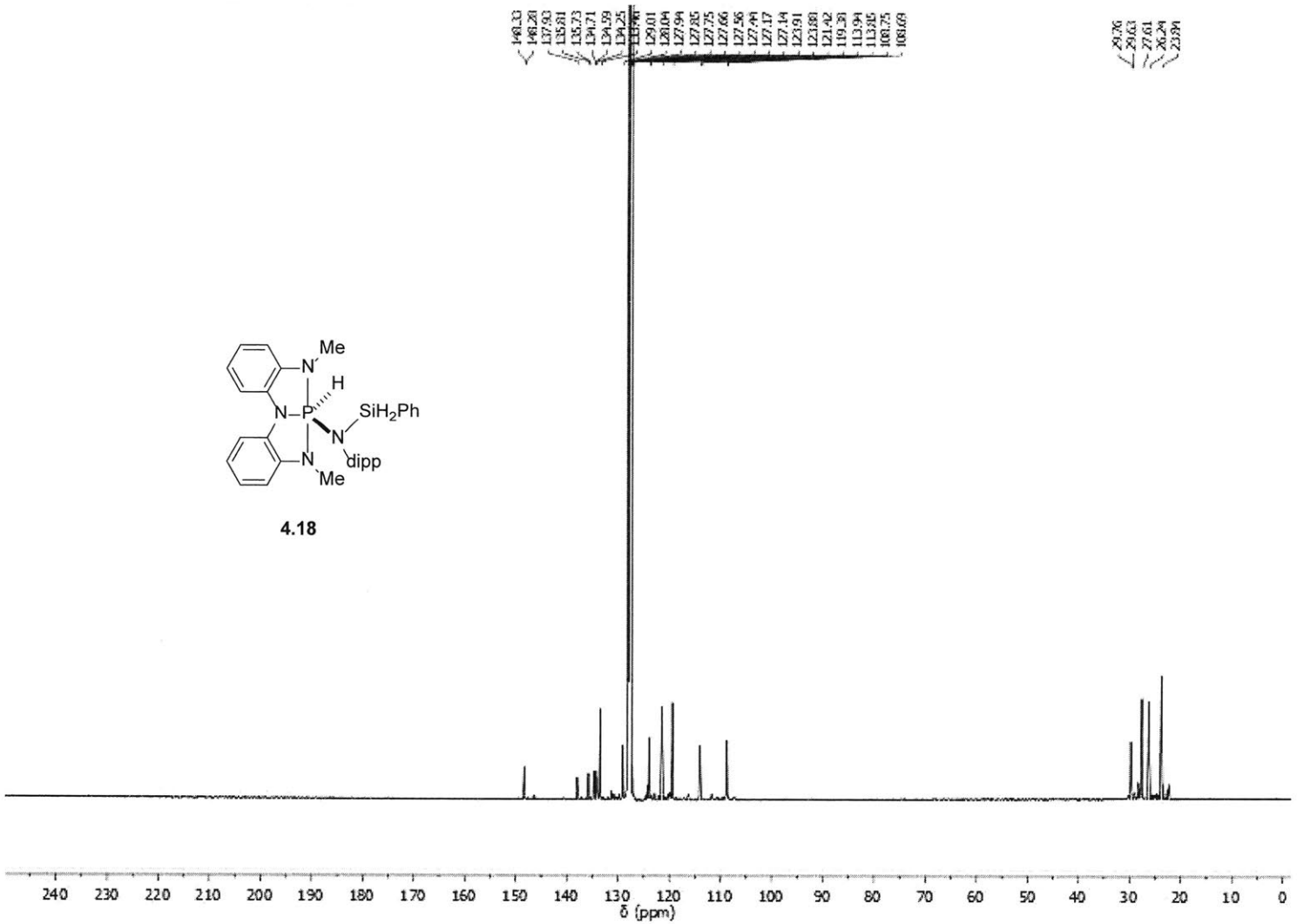

Figure C21. ^{13}C NMR of **4.18**.

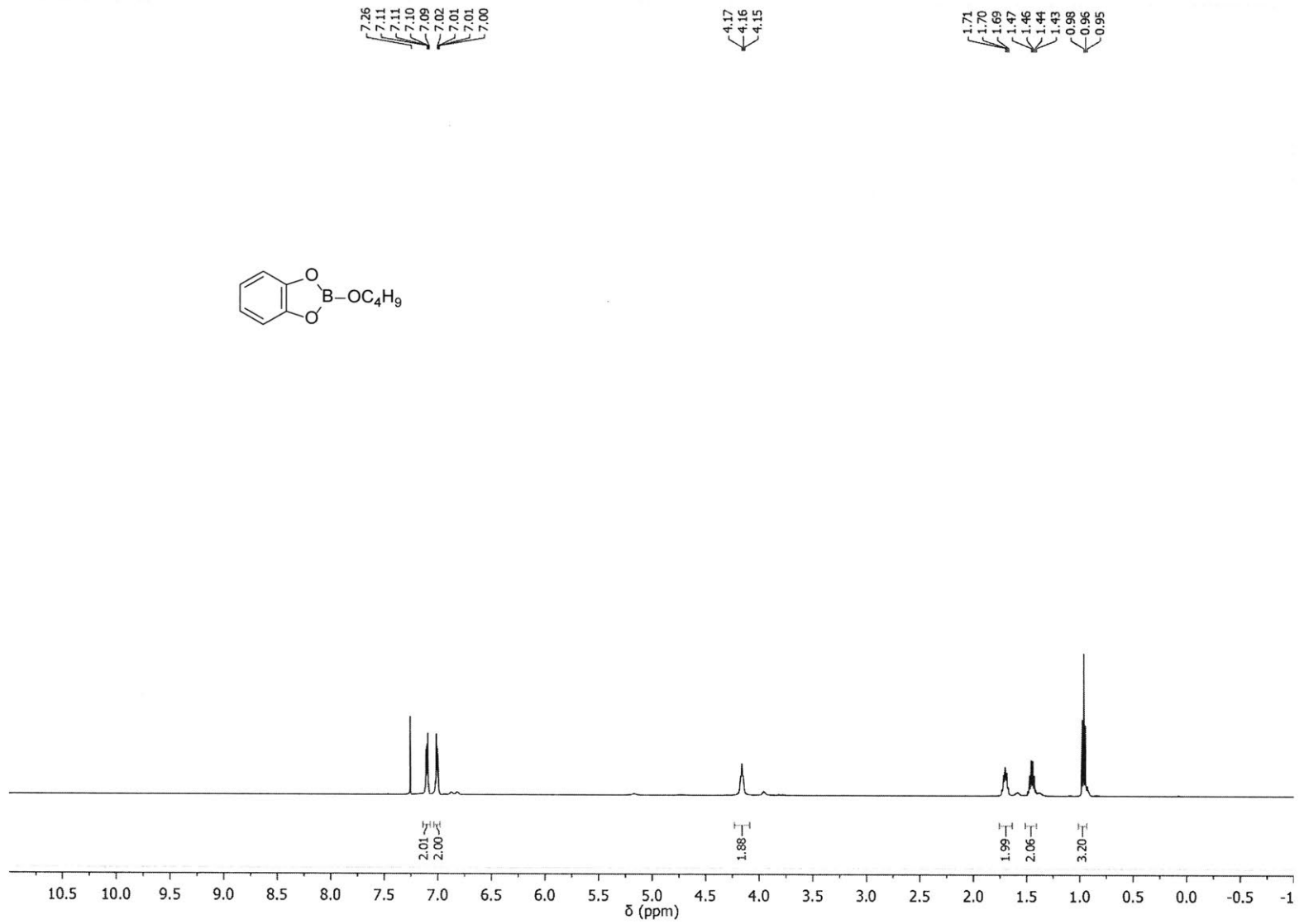

Figure C22. ^{1}H NMR of butoxy catecholborane.

Appendix D

ACS Publications
Most Trusted. Most Cited. Most Read.

Title:	The shapes and other properties of non-transition element complexes. 2. AB4
Author:	Benjamin M. Gimarc, Shakil A. Khan
Publication:	Journal of the American Chemical Society
Publisher:	American Chemical Society
Date:	Apr 1, 1978

LOGIN

If you're a copyright.com user, you can login to RightsLink using your copyright.com credentials. Already a RightsLink user or want to learn more?

PERMISSION/LICENSE IS GRANTED FOR YOUR ORDER AT NO CHARGE

This type of permission/license, instead of the standard Terms & Conditions, is sent to you because no fee is being charged for your order. Please note the following:

- Permission is granted for your request in both print and electronic formats, and translations.
- If figures and/or tables were requested, they may be adapted or used in part.
- Please print this page for your records and send a copy of it to your publisher/graduate school.
- Appropriate credit for the requested material should be given as follows: "Reprinted (adapted) with permission from (COMPLETE REFERENCE CITATION). Copyright (YEAR) American Chemical Society." Insert appropriate information in place of the capitalized words.
- One-time permission is granted only for the use specified in your request. No additional uses are granted (such as derivative works or other editions). For any other uses, please submit a new request.

If credit is given to another source for the material you requested, permission must be obtained from that source.

BACK CLOSE WINDOW

Title: Intermolecular N–H Oxidative Addition of Ammonia, Alkylamines, and Arylamines to a Planar σ3-Phosphorus Compound via an Entropy-Controlled Electrophilic Mechanism

Author: Sean M. McCarthy, Yi-Chun Lin, Deepa Devarajan, et al

Publication: Journal of the American Chemical Society

Publisher: American Chemical Society

Date: Mar 1, 2014

PERMISSION/LICENSE IS GRANTED FOR YOUR ORDER AT NO CHARGE

This type of permission/license, instead of the standard Terms & Conditions, is sent to you because no fee is being charged for your order. Please note the following:

- Permission is granted for your request in both print and electronic formats, and translations.
- If figures and/or tables were requested, they may be adapted or used in part.
- Please print this page for your records and send a copy of it to your publisher/graduate school.
- Appropriate credit for the requested material should be given as follows: "Reprinted (adapted) with permission from (COMPLETE REFERENCE CITATION). Copyright (YEAR) American Chemical Society." Insert appropriate information in place of the capitalized words.
- One-time permission is granted only for the use specified in your request. No additional uses are granted (such as derivative works or other editions). For any other uses, please submit a new request.

If credit is given to another source for the material you requested, permission must be obtained from that source.

BACK CLOSE WINDOW

Title: P-N Cooperative Borane Activation and Catalytic Hydroboration by a Distorted Phosphorous Triamide Platform

Author: Yi-Chun Lin, Emmanuel Hatzakis, Sean M. McCarthy, et al

Publication: Journal of the American Chemical Society

Publisher: American Chemical Society

Date: Apr 1, 2017

PERMISSION/LICENSE IS GRANTED FOR YOUR ORDER AT NO CHARGE

This type of permission/license, instead of the standard Terms & Conditions, is sent to you because no fee is being charged for your order. Please note the following:

- Permission is granted for your request in both print and electronic formats, and translations.
- If figures and/or tables were requested, they may be adapted or used in part.
- Please print this page for your records and send a copy of it to your publisher/graduate school.
- Appropriate credit for the requested material should be given as follows: "Reprinted (adapted) with permission from (COMPLETE REFERENCE CITATION). Copyright (YEAR) American Chemical Society." Insert appropriate information in place of the capitalized words.
- One-time permission is granted only for the use specified in your request. No additional uses are granted (such as derivative works or other editions). For any other uses, please submit a new request.

If credit is given to another source for the material you requested, permission must be obtained from that source.

BACK CLOSE WINDOW

Curriculum Vitae

for

Yi-Chun Lin

Education

PhD in chemistry September 2017
Massachusetts Institute of Technology
Cambridge, MA, USA

MSc in chemistry (July 2006)
National Tsing Hua University
Hsinchu, Taiwan ROC

BSc in chemistry (June 2003)
National Dong Hwa University
Hualien, Taiwan ROC

Experience

The Pennsylvania State University
Graduate Research and Teaching Assistant, 2011 – 2016.

Institute of Chemistry, Academia Sinica, Taiwan
Research Assistant, 2006 – 2011.

Publications

Lin, Y.-C.; Hatzakis, E.; McCarthy, S. M.; Reichl, K. D.; Lai, T.-Y.; Yennawar, H. P.; Radosevich, A. T. *J. Am. Chem. Soc.* **2017**. 139, 6008.

McCarthy, S. M.; Lin, Y.-C.; Devarajan, D.; Chang, J. W.; Yennawar, H. P.; Rioux, R. M.; Ess, D. H.; Radosevich, A. T. *J. Am. Chem. Soc.* **2014**, 136, 4640.

Liu, Y.-M.; Lin, Y.-C.; Chen, W.-C.; Cheng, J.-H.; Chen, Y.-L.; Yap, G. P. A.; Sun, S.-S.; Ong, T.-G. *Dalton Trans.* **2012**, 41 (24), 7382.

Lin, Y.-C.; Lin, C.-H.; Chen, C.-Y.; Sun, S.-S.; Pal, B. *Org. Biomol. Chem.* **2011**, 9, 4507.

Lin, Y.-C.; Lin, C.-H. *Org. Lett.* **2007**, 9, 2075.